Vol. 154, November 1, 1983
Complete in one issue

ISSN 0003-2670

ANALYTICA CHIMICA ACTA

International journal devoted to all branches of analytical chemistry

ELSEVIER

ANALYTICA CHIMICA ACTA

International journal devoted to all branches of analytical chemistry
Revue internationale consacrée à tous les domaines de la chimie analytique
Internationale Zeitschrift für alle Gebiete der analytischen Chemie

PUBLICATION SCHEDULE FOR 1983

	J	F	M	A	M	J	J	A	S	O	N	D
Analytica Chimica Acta	145	146	147	148	149	150/1 150/2	151/1	151/2	152	153	154	155

Scope. *Analytica Chimica Acta* publishes original papers, short communications, and reviews dealing with ever aspect of modern chemical analysis, both fundamental and applied.

Submission of Papers. Manuscripts (three copies) should be submitted as designated below for rapid and efficien handling:

Papers from the Americas to: Professor Harry L. Pardue, Department of Chemistry, Purdue University, West Lafayette IN 47907, U.S.A.

Papers from all other countries to: Dr. A. M. G. Macdonald, Department of Chemistry, The University, P.O. Box 363 Birmingham B15 2TT, England. Papers dealing particularly with computer techniques to: Professor J. T. Clerc Universität Bern, Pharmazeutisches Institut, Baltzerstrasse 5, CH-3012 Bern, Switzerland.

Submission of an article is understood to imply that the article is original and unpublished and is not being considere for publication elsewhere. Upon acceptance of an article by the journal, authors will be asked to transfer the copyrigh of the article to the publisher. This transfer will ensure the widest dissemination of information.

Information for Authors. Papers in English, French and German are published. There are no page charges Manuscripts should conform in layout and style to the papers published in this Volume. Authors should consul Vol. 132, p. 239 for detailed information. Reprints of this information are available from the Editors or from: Elsevie Editorial Services Ltd., Mayfield House, 256 Banbury Road, Oxford OX2 7DH (Great Britain).

Reprints. Fifty reprints will be supplied free of charge. Additional reprints (minimum 100) can be ordered. An orde form containing price quotations will be sent to the authors together with the proofs of their article.

Advertisements. Advertisement rates are available from the publisher.

Subscriptions. Subscriptions should be sent to: Elsevier Science Publishers B.V., Journals Department, P.O. Bo 211, 1000 AE Amsterdam, The Netherlands. Tel: 5803 911, Telex: 18582.

Publication. *Analytica Chimica Acta* appears in 11 volumes in 1983. The subscription for 1983 (Vols. 145–155) i Dfl. 1980.00 plus Dfl. 220.00 (p.p.h.) (total approx. U.S. $880.00). All earlier volumes (Vols. 1–144) except Vols. 2 and 28 are available at Dfl. 200.00 (U.S. $80.00), plus Dfl. 15.00 (U.S. $6.00) p.p.h., per volume.

Our p.p.h. (postage, packing and handling) charge includes surface delivery of all issues, except to subscribers in th U.S.A., Canada and India who receive all issues by air delivery (S.A.L. — Surface Air Lifted) at no extra cost. For th rest of the world, airmail and S.A.L. charges are available upon request.

Claims for issues not received should be made within three months of publication of the issues. If not they cannot b honoured free of charge.

For further information, or a free sample copy of this or any other Elsevier Science Publishers journal, readers in th U.S.A. and Canada can contact the following address: Elsevier Science Publishing Co., Inc., Journal Informatio Center, 52 Vanderbilt Avenue, New York, NY 10017, U.S.A., Tel: (212) 867-9040.

ANALYTICA CHIMICA ACTA
VOL. 154 (1983)

ANALYTICA CHIMICA ACTA

International journal devoted to all branches of analytical chemistry

ELSEVIER Amsterdam–Oxford–New York–Tokyo

Anal. Chim. Acta, Vol. 154 (1983)

0003-2670/83/$03.0

Printed in The Netherlands

Analytica Chimica Acta, 154 (1983) 1—16
Elsevier Science Publishers B.V., Amsterdam — Printed in The Netherlands

Review

DISPERSION IN CONTINUOUS-FLOW SAMPLE PROCESSING

C. C. PAINTON and HORACIO A. MOTTOLA*
Department of Chemistry, Oklahoma State University, Stillwater, OK 74078 (U.S.A.)
(Received 21st February 1983)

SUMMARY

The shape and quality of the analytical signal acquired after continuous-flow sample processing is directly influenced by dispersion. Dispersion in such procedures occurs as a result of mass transfer and mixing during sample transport by the carrier stream to a detector. The occurrence of chemical reactions during the transport can alter diffusion and convection processes. This review covers dispersion in fields such as physiological circulation research, chemical reactor engineering, and chromatography. The physical description in these fields has, to a large extent, influenced the views of those concerned with dispersion in continuous-flow sample processing. Views of dispersion in segmented and unsegmented continuous-flow situations are also considered and the limited attention given to chemical kinetics in these approaches to sample handling in chemical analysis is noted.

Continuous-flow sample processing is commonly considered to be comprised of two branches: (1) continuous-flow analysis as the air-segmented version of the approach, and (2) flow injection analysis as the unsegmented version. Both procedures introduce the sample by discrete injection or intercalation into a continuous flowing stream which transports the sample plug to the detection area. Mixing of chemical species occurs during sample transport, and kinetics is at the heart of these types of sample treatment. Direct attention to the formulation of kinetic models, however, has received limited consideration by practitioners in these fields. Some exceptions can be cited such as the consecutive-reaction model advanced for direct sample injection into the detection chamber [1] and the variable-time kinetic model that Pardue and Fields developed to describe the case of flow injection with large dispersion (use of gradient mixing chambers in the manifold) [2]. The insight gained by kinetic modeling is illustrated by Pardue and Fields [3] who showed their variable-time model [2] to be superior to the "titration" models proposed previously [4]. Indirectly, the effect of kinetic processes on the shape and quality of the signal in flow injection systems is reflected in the use of the practical dispersion value [5] which, however, fails to convey information about the distribution of residence times and, by ignoring chemical kinetics, introduces confusing situations in its evaluation [6].

In its physico-chemical context, the word dispersion characterizes the distribution (scattering) of matter or radiation in a dispersing medium; a

0003-2670/83/$04.80

typical example is a colloidal system consisting of a dispersed phase in a dispersion medium. Although many colloidal systems are formed as a result of chemical reactions, the term dispersion is commonly considered to involve a physical process only. A purely physical view of dispersion has permeated in flow injection systems. The occurrence of chemical reactions, however, can alter both the spontaneous process of concentration equalization, described as diffusion, and mass transfer by movement of the system as a whole, known as convection. In actuality, chemical reactions can alter the concentration profile which in turn leads to changed diffusion and convection and these then affect the collisional frequency that governs chemical reactions. This interdependence defines the complexity of the actual situation and points to the incompleteness of the description of dispersion in flow injection in purely physical terms. The impact of this chemical omission on the air-segmented version of continuous-flow sample processing is not as serious because measurements are usually acquired when the chemistry has reached equilibrium. In unsegmented flow systems, however, all measurements must be made under non-equilibrium (kinetic) conditions.

The dominance of a purely physical description of dispersion is the result of overlapping developments from different fields which have preceded the description of dispersion in a continuous-flow sample processing but which have directly influenced the views of analytical chemists concerned with its description in this field. This paper is offered as a concise review in the hope that it will help to correlate developments in other areas that have contributed to current understanding of dispersion. The fields of physiological circulation research, chemical reactor engineering, and chromatography were selected for review because the physical description of dispersion in these fields has, to a large extent, influenced the present appreciation of dispersion in the continuous-flow sample processing. The most representative models in continuous-flow methods (based on Poisson distribution) and in flow-injection methods (based on the Taylor model, the "dispersion equation", the tanks-in-series model, and Pungor's model for mixing chambers) are also discussed. Selection of typical examples such as the indicator dilution theory provided by physiologists and the tank-in-series model developed by chemical engineers are used to illustrate the transfer of purely physical concepts and their mathematical formulation into the description of dispersion in continuous-flow sample treatment. The overlap of developments and concepts can be recognized by the realization that, for instance, the tanks-in-series model is intimately related to the plate theory of chromatography. Peak broadening in chromatography as well as peak shape in flow injection are, however, the result of dynamic situations, with the distinct difference that phase partition and random walk caused by the packing are commoner in the chromatographic separations.

Without being comprehensive, this paper also tries to project a dominating omission: the failure to recognize that chemical reactions that commonly occur during transport of samples to detectors introduce chemical kinetic complications in the description of dispersion.

DISPERSION IN PHYSIOLOGY: THE INDICATOR DILUTION TECHNIQUE

About eighty-five years ago, Stewart [7] introduced the indicator dilution technique to estimate the quantity of blood put out by the heart and lungs from the dilution of known amounts of an injected, easily detected, and nontoxic substance by the blood that passes through the heart during a known period of time. The possibility of determining the time of transport of blood from one part of the cardiovascular system to another by injection of chemical species has been known, however, for about 150 years [8]. Figure 1 illustrates representative curves of the first published indicator–dilution curves by Hamilton et al. [8]. These authors proposed an exponential decay formulation to describe the descending portion of these curves [9]. The proposed expression was $C = C_0[\exp(-Ft/\alpha V]$, where C_0 is the original concentration of injected indicator, C is the concentration of indicator in the blood sample at time t, F is the volumetric flow rate, α is an experimentally determined factor to correct for non-instantaneous mixing, and V is the volume of the flow system. This kinetic description by a first-order process is similar to the exponential decay formulation of the contribution to signal deformation from unsegmented portions of the flow in air-segmented continuous flow systems [10] for the decreasing portion of the signal in the series reaction model of Mottola and Hanna [1], and for the same portion of the signal in kinetically-assisted equilibrium-based repetitive determinations

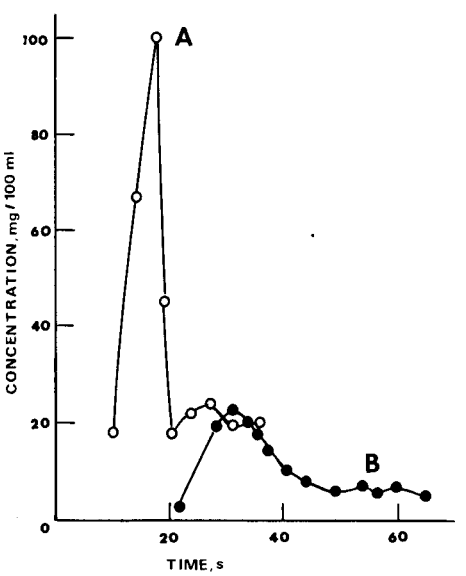

Fig. 1. Concentration–time profiles for the injection of a chemical indicator into blood. The transported indicator (sodium phenoltetraiodophthalein) was injected in the jugular vein. A, Subject weighed 75 kg, pulse 124, 700 mg of indicator injected; B, Subject weighed 85 kg, pulse 72, 300 mg of indicator injected.

[11]. These observations point again to the kinetic component of all these signals.

Several mathematical models for simulating concentration–time curves have been proposed; a critical review has been provided by Harris and Newman [12]. They classified the available models in two major categories: (1) the compartmental (multicompartment) model, and (2) the distributive model. The compartmental model assumes that mixing in the system is limited to certain regions between the injection and measuring sites, and some imprecision has limited its use. In contrast, the distributive model assumes uniform mixing between the injection and detection sites and has been more widely adopted. Table 1 lists typical mathematical formulations used in distributive models. Because of its impact on the description of dispersion in flow injection techniques, the model introduced by Taylor to represent laminar dispersion in cylindrical channels [13] deserves some detailed attention. The addition of a diffusion term in the radial direction to the conventional distributive model is the salient characteristic of Taylor's formulation. Under laminar flow in a cylindrical tube of radius a, the flow velocity at a radial distance r is given by the Poiseuille–Hagen [17] relation

$$u = U_{max}[1 - (r^2/a^2)] \tag{1}$$

where U_{max} is the maximum velocity at the center of the axis of the tube. (Symbols are defined in Table 2.) Combining the effects of velocity profile and diffusion gives the following partial differential equation

$$dC/dt = D[(d^2C/dr^2) + (dC/r\,dr) + (d^2C/dx^2)] - 2\bar{u}(1 - r^2/a^2)(dC/dx) \tag{2}$$

where C is the instantaneous concentration of a given solute. Taylor provided simple solutions of Eqn. (2) for two extreme conditions: (1) when changes in concentration caused by convective transport take place so rapidly that molecular diffusion can be neglected and dispersion is determined by convective transport alone; and (2) when convective transport is slow compared with the "decay" of the radial variation of concentration to a fraction of the initial value by molecular diffusion (i.e., molecular diffusion dominates). Other than for these two extreme conditions, Eqn. (2) can be solved only by numerical methods.

The work of Bate et al. [18] is representative of efforts to provide numerical solutions to Eqn. (2). Two situations can be considered: (1) continuous injection, and (2) bolus injection. The continuous injection approach can be illustrated by assuming that originally the tube is filled with colored solution of concentration C_0. An uncolored solution is then allowed to flow, and at the solution interface, the colored solution is displaced by the uncolored one. If what is monitored is the cross-sectional mean concentration, C_m, at a fixed distance downstream, the value of C_m/C_0 will decrease from 1 to 0 as time progresses. Figure 2 illustrates the concentration profiles under four different experimental conditions. In curve A, convection is the only mode of mass transfer (first case in Taylor's solution). Curve D represents diffusion-dominated dispersion (second case in Taylor's solution). Curves B and C

TABLE 1

Distributive models for the circulatory indicator-dilution curve

Formula[a]	Comment(s)	Ref.
$\frac{dC}{dt} + \frac{u}{L}\frac{dC}{dx'} = \frac{D}{L^2}\frac{d^2C}{dx'^2}$ (1)	Diffusion and convection were both considered	13
$x' = \frac{x}{L}$		
$\frac{dC}{dt} + u\frac{dC}{dx} = D\frac{d^2C}{dx^2} + \frac{R_i}{V}$ (2)[b]	More general than Eqn. (1). A source term representing the rate of injection, R_i, is included.	14
$\frac{dC}{dt} + \frac{F}{A'}\frac{dC}{dx} = 0$ (3)[c]	Dispersion is not accounted for as a part of the flow. Dispersion was considered to be accomplished only by flow through a number of vessels of various lengths. No mixing parameter is shown. It can be used as a comparison for concentration curves for diffusible and nondiffusible samples.	15
$\frac{dC}{dt} = D\frac{d^2C}{dx^2} - \frac{FL}{\lambda V}\frac{dC}{dx}$ (4)[d]	This model has the mathematical form of the time-dependent Fick's diffusion equation to which a convection term has been added. It is just a diffusional interpretation of Eqn. (1).	16

[a]For definition of symbols, see Table 2. [b]V = Volume of the system between the injection and detection points (ml). [c]A' = cross-sectional area of the tubing (cm^2). [d]λ = partition coefficient between extra- and intra-vascular spaces.

represent intermediate flow conditions in which Taylor's solutions do not apply. A parameter, A_x, defined as $A_x = (a)^2\bar{u}/Dx$, is used to characterize the different flow conditions. The "dispersion" curve is then the result of the following combined effects: mean flow velocity $\bar{u}$, tube radius a, tube length x, and diffusion coefficient D.

Bolus injection applies to the injection of a finite volume of indicator solution to produce two concentration profiles. This is the type of profile typical of unsegmented continuous-flow procedures with discrete sample injection. In these cases, dispersion can be treated by combining the results for uncolored displaced by colored solution with the results for colored displaced by uncolored solution. The concentrations (normalized) obtained are then

$$C_m/C_0 = (C_m/C_0)_{\text{trailing}} - (C_m/C_0)_{\text{leading}} \quad (3)$$

The concentration—time curves are illustrated in Fig. 3.

The numerical method used by Bate et al. is an explicit finite-difference replacement method requiring considerable computation time [19].

TABLE 2

List of frequently used symbols

a	Reactor tube radius (cm)
C	Concentration (M)
C_0	Original concentration (M)
C_m	Mean concentration (M)
C^*	Normalized concentration, $C^* = C/C_0$ (dimensionless)
D	Molecular diffusion coefficient ($cm^2\ s^{-1}$)
D	Practical dispersion number, $D = C_0/C_{max}$ (dimensionless)
D_{eff}	Effective diffusion coefficient ($cm^2\ s^{-1}$)
F	Volumetric flow rate ($ml\ min^{-1}$)
H	Height equivalent to a theoretical plate (cm)
H_{max}	Signal height measured at the peak maximum (cm)
H_0	Signal height obtained with an undispersed sample (cm)
L	Length of reactor tube (cm)
M	Mass of solute in the injected sample plug (g)
N	Number of mixing tanks (dimensionless)
R_i	Rate of sample injection ($ml\ s^{-1}$)
r	Radial distance from the tube axis (cm)
t	Time (s)
t_A	Time for first appearance of signal (s)
Δt_B	Time for appearance of the entire concentration—time curve = t_{bas} (s)
t_m	Mean residence time (s)
U_{max}	Maximum velocity in the center axis of the tube ($cm\ s^{-1}$)
u	Linear velocity of flow ($cm\ s^{-1}$)
$\bar{u}$	Mean velocity of flow in axial direction ($cm\ s^{-1}$)
V	Volume of reactor vessel (ml)
V_m	Volume of mixing chamber (ml)
V_s	Volume of each liquid segment (for segmented flow); or volume of an injected sample (for unsegmented flow) (ml)
X	Reduced distance, $X = (xD)/(a)^2U_{max}$ (dimensionless)
x	Axial distance (cm)
η	Dynamic viscosity (poise)
ν	Kinematic viscosity ($cm^2\ s^{-1}$)
γ	Liquid surface tension ($dyn\ cm^{-1}$)
γ'	Tortuosity factor (dimensionless)
σ^2	Variance (dimensionless)
$(\sigma_t)^2$	Variance in time units (min^2)
τ	Reduced time, $\tau = (tD)/a^2$ (dimensionless)
τ_m	Reduced mean residence time, $\tau_m = (t_m)D/a^2$ (dimensionless)

DISPERSION IN CHEMICAL REACTOR ENGINEERING

Many papers devoted to the description of dispersion in chemical reactor engineering are available. This is not surprising because of the role that transport phenomena play in the design, analysis, and simulation of such reactors. Selected methods of particular interest are: (1) the velocity profile model, (2) the dispersion model, and (3) the tanks-in-series model.

In the velocity profile model (also called the convective model), flow velocity is used to characterize three possibilities. First, in a high velocity

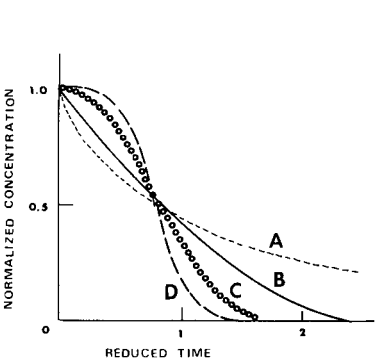

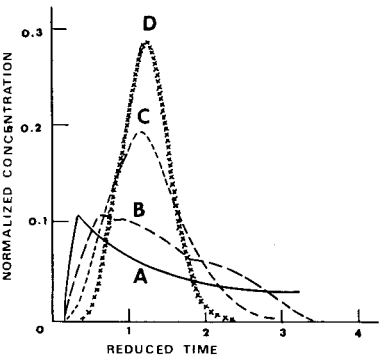

Fig. 2. Dispersion curves for an injected sample considering a single interface boundary. The magnitudes of A_x values ($A_x = \bar{u}a^2/Dx$) for the curves are in the following order: Curve A > Curve B > Curve C > Curve D.

Fig. 3. Dispersion curves for an injected sample considering two interface boundaries. The magnitudes of A_x values for the curves are in the following order: Curve A > Curve B > Curve C > Curve D.

mode when dispersion is the result of convection, and second in a moderate velocity mode, when dispersion of the sample solute results from both convection and diffusion. The effect of velocity profile still dominates over the effect of molecular diffusion in the longitudinal direction so that

$$U_{max}(1 - r^2/a^2)\mathrm{d}C/\mathrm{d}x \gg D(\mathrm{d}^2C/\mathrm{d}x^2) \tag{4}$$

and the dispersion equation (Eqn. 2) reduces to

$$\mathrm{d}C/\mathrm{d}t = D[(\mathrm{d}^2C/\mathrm{d}r^2) + (\mathrm{d}C/r\,\mathrm{d}r)] - U_{max}(1 - r^2/a^2)(\mathrm{d}C/\mathrm{d}x) \tag{5}$$

which can be solved numerically or analytically. Third, in a low velocity mode, convection resulting from the velocity profile is much smaller than longitudinal molecular diffusion, which therefore controls the dispersion of the solute. The dispersion equation is simplified further to

$$D(\mathrm{d}^2C/\mathrm{d}x^2) = \mathrm{d}C/\mathrm{d}t \tag{6}$$

which is Fick's second law of diffusion.

In the dispersion model, a dimensionless term, D/uL, called the reactor dispersion number [20] is used to describe the variance (a measure of dispersion) for the concentration profile curves. The dispersion number, which is the reciprocal of the Peclet number, N_{pe}, defined as $N_{pe} = a(U_{max})/D$, has values from zero for plug flow to infinity for completely mixed flow. The relationship between dispersion expressed as the variance of the concentration—time profile and the dispersion number can be summarized as follows. First, for a closed vessel which has no dispersion at either end of the vessel,

$$\sigma^2 = (\sigma_t)^2/(t_m)^2 = (2D/\bar{u}L) - 2(D/\bar{u}L)^2\{1 - \exp(-\bar{u}L/D)\} \tag{7}$$

Second, for an open vessel which exhibits no discontinuity of dispersion at any point

$$\sigma^2 = (\sigma_t)^2/(t_m)^2 = (2D/\bar{u}L) + 8(D/\bar{u}L)^2 \quad (8)$$

Third, for an "open—closed" vessel representing an intermediate case between an open and closed vessel

$$\sigma^2 = (\sigma_t)^2/(t_m)^2 = 2(D/\bar{u}L) + 3(D/\bar{u}L)^2 \quad (9)$$

An alternative approach to the dispersion model for dealing with small deviation from plug flow is the tanks-in-series model. It assumes that the liquid flows through a series of well-stirred tanks of equal size [20]. If the number of tanks in series is j, the normalized concentration profile is described by

$$C^* = C/C_0 = [(j)^j(\theta)^{j-1}/(j-1)!] \exp(-j\theta) \quad (10)$$

where θ is the reduced time (actual time/residence time); the variance in this case is $1/j$. The model assumes instantaneous mixing and although it can be successfully applied to some continuous-flow sample systems in which a single tank can be assumed [3], its use in flow injection situations in which the number of tanks is small is open to criticism.

DISPERSION IN OPEN-TUBE (COLUMN) CHROMATOGRAPHY

Chromatography involves partition and dispersion processes and open columns provide a close analogy to flow injection techniques. Band broadening in chromatography as well as in flow injection techniques, however, is also caused by extra-column components (e.g., connections, injection loops, post-column reactors, flow cells, etc.) These contributions to band broadening have been discussed in detail in the pertinent literature [21—24].

In chromatography, the relative band broadening (a measure of dispersion) is generally discussed in terms of the height equivalent to a theoretical plate, H. Starting with Taylor's solution to the dispersion equation (Eqn. 2) as modified by Aris by taking into consideration axial dispersion [25], Golay [26, 27] derived an equation for calculating H for a chromatographic process in an ideal open tube. Such a tube, as defined by Halasz [28], is a straight one with a constant circular cross-section, a smooth inner wall, and smooth inlet and outlet surfaces. Assuming that the diffusion time in the stationary phase is not negligible, Golay's equation states

$$H = (K_1/u) + K_m u + K_s u \quad (11)$$

where $K_1 = 2\gamma' D$,

$K_m = [1 + 6k' + 11(k')^2/(1 + k')^2](a^2/24D)$

$K_s = 2(k')^3/3(1 + k')^2$

and $k' = (V_R)'/(V_A)$. In these equations, γ' is the tortuosity factor (approximately 1 for an open column), k' is the capacity factor, V'_R represents an adjusted retention volume, V_A represents the reference retention volume, K_1

is the longitudinal diffusion term, K_m is the resistance to mass transfer term in the mobile phase, and K_s measures the diffusion effect of the time lag between the sample concentration at the mobile—stationary interface and within the stationary phase.

Differentiating Golay's equation and setting the result equal to zero provides the optimum velocity for minimizing the value of H,

$$U_{opt} = (13.86D/2a)\{[1 + 6k' + 11(k')^2]/[1 + (k')]^2\}^{1/2} \quad (12)$$

The impact of H on band spreading (peak width) is seen in the expression $\sigma^2 = HL$, in which L is the column length.

If the roughness of the tubing wall is not negligible, Golay's equation needs modification. In a small-diameter, rough-wall tubing, laminar flow is destroyed and radial mass transfer is enhanced, facilitating partition. For a roughened surface with an effective area Q times the area of the smooth walls, Golay suggested that the K_s term is diminished by a factor of Q^2.

Slug flow is a hypothetical analog of bolus in segmented continuous-flow systems. Giddings [29] provided an expression for H for an analogous case in coated tubes,

$$H = (1 - R)^2 a^2 u/4D \quad (13)$$

in which R is the retention factor representing the fraction of total sample within the column that is not present in the mobile phase. Equation (13) has been used by Snyder and Adler [30] in developing a dispersion model for air-segmented continuous-flow analysis.

The most recent chromatographic descriptions of axial and radial dispersion phenomena in flow injection techniques are well exemplified by the efforts of Tijssen [31]. Tijssen asserts that there is no need to define a separate dispersion parameter for flow injection techniques, because the general dispersion definition is well accepted in other sciences based on flowing systems such as reactor engineering, hydrology, and chromatography. Tijssen [31] recommended that the vast amount of published data in the chromatographic and technological literature should be consulted in the study of axial dispersion because the flow injection reactor can be regarded as a (chromatographic) tubular reactor. The advantages of miniaturization and of using tightly coiled reactors emanates from Tijssen's considerations. He indicates that for optimal work in flow injection systems, instrumental designs should match those of present day chromatography. Such a move would remove the pronounced asymmetry (ascribed to large extra-reactor effects), and the standard deviation (in time units) or the plate height would be all that would be required to describe the dispersion. Such a description would replace Růžička and Hansen's practical dispersion parameter, which is a measure of dilution rather than of residence time distribution. Some limitations of this parameter have been exposed recently in connection with the effect of chemical kinetics on peak profiles typical of flow injection responses [6].

DISPERSION IN SEGMENTED, CONTINUOUS-FLOW SYSTEMS

Sample dispersion in segmented continuous-flow processes is conceptually like processes such as countercurrent distribution and chromatography. Early attempts to describe dispersion in this form of sample processing were limited to empirical relationships with limited insight into the dispersion process itself [32—35]. Mathematical models have been developed to predict concentration distributions along a line of sample segments which are the fundamental basis of segmented-flow procedures; they are known as the linear and the nonlinear models [36—39].

In the linear model, it is assumed that the first segment contains an undiluted sample of concentration, C_0, the next segment a concentration, $C_1 (C_1 < C_0)$, and all following segments contain no sample. By integrating the mass transfer process occurring in each segment over the entire length of the tubing, the resulting concentration can be described by a Poisson distribution

$$C_{n+1}/C = 1 - e^{-q}\left[1 + q + \frac{q^2}{2!} + \frac{q^3}{3!} + \ldots + \frac{q^n}{n!}\right] \tag{14}$$

where q is a constant defined as $q = (R_\alpha t/V_s) = (V_f/V_s)$ where V_s is the volume of each liquid segment, R_α is the rate of the wall deposit influxes and effluxes into and out of each segment, and V_f is the total volume of liquid film deposited from any segment during its passage through a given tube.

The linear model assumes that the rate at which liquid films enter and leave each segment, R_α, is constant and independent of concentration; this assumption limits the usefulness of the model. More general is the nonlinear model, in which the rate of the liquid film transfer between liquid segments is not a constant and depends on sample concentration.

In the nonlinear model, R_α is given by $R_\alpha = k_1 + k_2 C$, where k_1 and k_2 are constants. The model for predicting concentrations along a line of segments is then expressed by

$$(R_{n+1}t/L) - (R_n t/L) = \mathrm{d}(V_s)_{n+1}/\mathrm{d}l \tag{15}$$

in which L is the length of the tube and l the distance that a liquid segment has travelled. Then

$$C_{n+1}(R_{n+1}t/L) - C_n(R_n t/L) = \mathrm{d}[(V_s)_{n+1}C_{n+1}]/\mathrm{d}l \tag{16}$$

which can only be solved by numerical integration.

Neither linear nor nonlinear models can predict dispersion as a function of experimental parameters. To compensate for this shortcoming, Snyder and co-workers have developed two models based on the ones just discussed, which are known as the ideal and the nonideal models for use particularly in the design of high-speed continuous-flow systems [22, 30, 40, 41]. The ideal model was derived from Begg's linear model but ruled out the nonlinear dispersion arising from a change in liquid surface tension as the sample

concentration varies, because such effects are counteracted in normal practice by the addition of a surfactant. By assuming that there is perfect mixing within each moving liquid segment, and using Eqn. (14), the following is obtained

$$C_k/C_0 = e^{-q} q^k/k! \tag{17}$$

where $q = V_f/V_s = 2\pi a\phi L/\pi a^2 Ls = 2L\phi/aLs$

and where C_k is the concentration of sample in the kth segment, L_s is the length of a liquid segment, and ϕ is the average thickness of the liquid film. For a Poisson distribution model, q represents the retardation of the center of the original sample distribution for a single sample segment; thus q equals the variance, σ_i^2, of the resulting dispersed sample concentration distribution. As the mixing within the liquid segments slows down, the sample displacement, equal to q, is expected to remain constant. Sample dispersion and variance, however, do increase and $\sigma^2 > \sigma_i^2$ (σ^2 is the variance resulting from slow mixing). This problem leads to a more generalized model, the nonideal one.

In a segmented continuous-flow system, transport of the sample analyte in discrete sample zones is commonly referred to as a bolus flow. Mixing in a bolus flow has a unique pattern; the sample starts from the center axis and immediately disperses along the edge of the liquid segment, slowly moving into adjacent regions of streamlines [30]. Because bolus circulation limits diffusion, radial mass transfer (by convection) is rapid, while mass transfer perpendicular to streamlines is slow. Because radial mass transfer is fast, it does not alter the part of dispersion that is predicted by the ideal model. However, the predicted dispersion value increases so that the total variance is given by $\sigma^2 = \sigma_i^2 + \sigma_p^2$, in which σ_p^2 is the variance caused by mass transfer perpendicular to streamlines. The hypothetical analog of bolus flow in chromatography is the so-called slug flow for which Eqn. (13) does apply. Assuming the validity of this equation in bolus flow under the following conditions: (1) an effective diffusion coefficient, D', including additional mass transfer between streamlines replaces the conventional diffusion coefficient, and (2) only one of the two symmetrical lobes is compared with slug flow so that the effective radius, a', is approximately equal to $(2/3)a$, and with appropriate modifications from Snyder and Adler [30], can be obtained the following equation

$$\sigma^2 = \{[\pi a^4 u^{5/3} \eta^{7/3}/1.71 \times 10^{-3} D'_{w,25} V_s \gamma^{2/3}] + 1\} \left[2\pi L a^2 \left(\frac{u\eta}{\gamma}\right)^{2/3} \left(\frac{1}{V_s}\right)\right] \tag{18}$$

which describes dispersion according to the nonideal model. The term, $D'_{w,25}$, refers to the value of D' at 25°C with water as reference and $D' = D'_{w,25} (\eta/0.0089)^{-1.7}$. This equation predicts dispersion in continuous-flow over a broad range of experimental conditions.

DISPERSION IN UNSEGMENTED CONTINUOUS-FLOW SYSTEMS

The dynamic concepts in unsegmented continuous-flow systems can be traced back to the belief that turbulent flow was needed to preserve sample

integrity as well as provide efficient mixing. The need for turbulent mixing was correctly realized in unsegmented sample processing systems designed around a mixing chamber constituting the detection area and into which the sample is directly injected [42], but turbulent mixing was initially also considered necessary when injection takes place away from the detection area and mixing coils are used [43]. This interpretation was based on the belief that the parabolic flow profile typical of laminar flow would rapidly lead to axial mixing and result in peak broadening. The contradictory experimental fact that dilution decreased with decreasing pumping rates, however, drew attention to laminar flow [44] and its beneficial characteristics for unsegmented continuous-flow systems. Laminar flow is preferable not just because it can provide a well-defined sample zone, but because it also provides the advantages of reducing reagent consumption and eliminating the need for high pumping pressure.

The two dispersion models commonly adopted by those who study flow-injection systems are the Taylor model and the tanks-in-series model discussed earlier. Both models apply under laminar-flow conditions and for injection of the sample plug at a distance from the detection point. Pungor et al. [45] have developed a model for use in systems in which a mixing chamber is the primary contributor to dispersion. This model is based on injection at a distance from the detection point and primarily electrochemical detection. As stated earlier, the kinetic description of direct injection into the detection area consisting of a mixing chamber and involving turbulent flow has been given in an earlier paper [1]. All these models provide mathematical tools for dealing with signal-time distributions that result from concentration—time profiles under particular conditions.

A discussion of Taylor's model as applied to flow-injection situations is given by Růžička and Hansen [5]. Taylor's model is an analog of the differential equation describing diffusion in the presence of convection. For large tubing lengths and small mean flow velocity, the solution of the concentration—time curve is a Gaussian-type function

$$C = (M/\pi a^2)(4\pi Dt)^{-\frac{1}{2}} \exp\left[-(x - L)^2/4Dt\right] \tag{19}$$

Taylor's solution requires long residence times in order to stabilize radial concentration changes, i.e., $(t_m) \gg (a^2/14.4D)$, or expressed as reduced time, $(\tau_m) \gg 0.07$ with $(\tau_m) = (t_m)D/a^2$. Lighthill [46], Ananthakrishnan et al. [47], and Golay and Atwood [23] have all indicated that Taylor's effect develops if τ_m is larger than 0.8. In a typical flow injection system in which $D = 0.5 \times 10^{-5}$ cm^2 s^{-1} and radius equal to 0.025 cm, the mean residence time has to be 100 s or more to satisfy this criterion.

Aris's modification of Taylor's solution [25] describes well the simple case of homogeneous flow in a straight tubular channel; this is the only type of dispersion that can be accounted for from first principles. Flow conditions in several cases of unsegmented, continuous-flow sample processing lie outside the region in which Taylor's solution or even the Aris—Taylor model applies [48].

The tanks-in-series model embodies a conceptual approach parallel to the height equivalent to a theoretical plate model in chromatography [49]. It assumes that the concentration of the monitored species is constant throughout each tank. The model is questionable if mixing chambers are not used or if the hypothetical situation represents a rather small number of tanks. However, Ramsing et al. [50] used a single-tank model to describe unsegmented sample processing in short, straight, open tubes representing large dispersion on a short time-scale. Applicability of the model in such a case seems questionable; success of the same model in the description of a large-dispersion system generated by a well-stirred mixing chamber, however, is not surprising [2, 3]. A small number of tanks should result in skewed concentration—time profiles while very large number of tanks should produce near Gaussian curves with a variance $(\sigma_t)^2 = (t_m)^2/N$ [51]. The longer a sample zone has traveled (large mean residence times), the more dispersed the sample zone becomes, and the resulting concentration—time curve is more Gaussian in shape, conforming to the predictions of the tanks-in-series model.

Comparing Taylor's model and the tanks-in-series model shows that Taylor's model provides an appropriate approximation only for narrow and long reactor tubing and low flow rate values. For other conditions, the tanks-in-series model would seem better, particularly in reactors with a uniform pattern of structure such as the single-bead-string reactor [52].

For the model of Pungor et al. [45], in which dispersion is due mainly to the presence of a mixing chamber at a point relatively close to the detector or in the detection area itself, the following mathematical model is proposed

$$\frac{d\Delta C}{dt} = (F/V_m)\{[M/2A'(\pi D_{eff}t)^{\frac{1}{2}}] \exp [-(1/4D_{eff})[(L/t^{\frac{1}{2}}) - (Ft^{\frac{1}{2}}/A')]^2] - \Delta C\} \quad (20)$$

in which V_m is the volume of the mixing chamber, and D_{eff} is an effective diffusion coefficient that is not a simple physical constant but a composite parameter including several processes. It depends on the radius of the transporting tubing, the flow rate, and microscopic properties of the injected and carrier solutions.

All foregoing discussions center on mathematical equations used to predict the concentration—time profiles generated in different unsegmented situations of continuous-flow sample processing. These equations are quite involved because several parameters have to be included in the description. Use of a single parameter related to dispersion would be a valuable tool, particularly for method development and optimization. In 1977 Růžička et al. [44] proposed such a parameter called the dilution factor, taken as the ratio of the peak heights obtained at the detector and at the point of injection. Later, Růžička and Hansen [5] introduced the reciprocal of this factor and called it dispersion. It is formulated as follows

$$D = C_0/C_{max} = [AH_0]/[BH_{max}] \quad (21)$$

in which A and B are proportionality constants. This parameter describes the degree of dilution of an unreactive sample species responsible for the signal and the ratio in which this sample component has been mixed with the carrier stream solution. It does not provide any information about the shape of the signal because it does not reflect a distribution of residence times; its designation as a dispersion parameter is open to criticism. From a practical viewpoint, the lack of information regarding time for returning to baseline and its limited physical dilution nature restricts its usefulness [6].

Using the numerical solution of Ananthakrishnan et al. [47] for the dispersion equation (Eqn. 2), Vanderslice et al. [48] proposed the time taken from injection to initial appearance of the peak at the detector, t_A, and the total time for the observation of the peak, Δt_B, as measures of dispersion. Their mathematical expressions are

$$t_A = (109\, a^2 D^{0.025}/f)(L/F)^{1.025} \tag{22}$$

$$\Delta t_B = (35.4\, a^2 f/D^{0.36})(L/F)^{0.64} \tag{23}$$

in which f is a correction factor. A somewhat surprising finding by Vanderslice et al. is that Δt_B was found insensitive to sample size variations. The sample sizes used by Vanderslice et al., however, were less than 20% of the total reactor volume so that there was little contribution to axial molecular diffusion when the sample size varied between 5 and 20% of the reactor volume.

Růžička and Hansen's D measures mainly the degree of radial dispersion and Δt_B is a more direct measurement of the degree of axial spreading; neither is capable of describing the overall complexity of the dispersion process. This, however, is the trade-off faced in dealing with signal profiles; a reasonable description of all mass transfer processes and chemical collisions requires complex models lacking the simplicity of these empirical parameters, which are inadequate to describe the complexity of the dispersion as a whole but are relatively easy to extract from experimental data, and despite their inadequacies, may be used as practical guiding points in method development.

CHEMICAL KINETICS AND DISPERSION IN UNSEGMENTED CONTINUOUS-FLOW SYSTEMS

Although it has been pointed out that "... the comprehensive theory of the flow injection method will eventually combine the theory of mixing of liquids in continuous moving streams with the theory of chemical kinetics" [5], the effect of chemical kinetics has been practically ignored in the relatively few papers devoted to fundamental aspects of these approaches. As far as the authors of this contribution are concerned, only three documented studies have directly considered chemical kinetics. Selecting as a model a chemical reaction of moderate speed (the oxidation of L-ascorbic acid by dichromate ion), we have analyzed the effect that chemical kinetics may have in obscuring the significance of Růžička and Hansen's practical dispersion

parameter [6]. Haagensen [53] has proposed a semi-empirical model based on the time-dependence of the practical dispersion parameter and rate expressions for chemical reactions involved. The model considers a second-order reaction taking place in the presence of a moderate excess of reagent and the following differential expression is proposed for the product formation, P, in A + R → P,

$$d[P] = k\{([A]_0/D) - [P]\}\{(D-1)/D)[R]_0 - [P]\}dT - ([P]/D)(\partial D/\partial T)dT \quad (24)$$

in which k is the second-order rate constant for the chemical reaction, D is the practical dispersion parameter, and T the residence time. Computation of the product formation curve and comparison with experimentally obtained curves were not attempted because k values and the time dependence of D are not available. Reasonable prediction of peak height trends, however, were possible in the determination of some amino acids with *o*-phthaldehyde [53]. Using as model reaction the complex formation between chromium(III) and EDTA, Reijn [54] considered chemical kinetic effects in a single-bead-string reactor. Assuming that the tanks-in-series model applies to this reactor, that the number of tanks is constant for a given reactor, that the chemical reaction is pseudo-first-order, and that adequate mixing is ensured, Reijn concluded that "no great influence of the chemical reaction on the dispersion is to be expected in FIA".

This work was supported by the National Science Foundation (Grant No. CHE-7923956).

REFERENCES

1 H. A. Mottola and A. Hanna, Anal. Chim. Acta, 100 (1978) 167.
2 H. L. Pardue and B. Fields, Anal. Chim. Acta, 124 (1981) 39.
3 H. L. Pardue and B. Fields, Anal. Chim. Acta, 124 (1981) 65.
4 J. Růžička, E. H. Hansen and H. Mosbaek, Anal. Chim. Acta, 92 (1977) 235.
5 J. Růžička and E. H. Hansen, Anal. Chim. Acta, 99 (1978) 37.
6 C. C. Painton and H. A. Mottola, Anal. Chem., 53 (1981) 1713.
7 G. N. Stewart, J. Physiol., 22 (1897) 159.
8 W. F. Hamilton, J. W. Moore, J. M. Kinsman and R. G. Spurling, Am. J. Physiol., 84 (1928) 338.
9 W. F. Hamilton, J. W. Moore, J. M. Kinsman and R. G. Spurling, Am. J. Physiol., 99 (1932) 534.
10 W. H. C. Walker, in William B. Furman (Ed.), Continuous Flow Analysis: Theory and Practice, M. Dekker, New York, 1976, Ch. 7.
11 V. V. S. Eswara Dutt, A. Eskander-Hanna and H. A. Mottola, Anal. Chem., 48 (1976) 1207.
12 T. R. Harris and E. V. Newman, J. Appl. Physiol., 28 (1970) 840.
13 G. Taylor, Proc. R. Soc. London, Ser. A, 219 (1953) 186; 223 (1954) 446.
14 O. Levenspiel and K. B. Bischoff, Adv. Chem. Eng., 4 (1963) 95.
15 C. A. Goresky, Am. J. Physiol., 204 (1963) 626.
16 W. Perl and F. P. Chinard, Circulation Res., 22 (1968) 273.

17 C. G. Caro, J. Physiol., 185 (1966) 501.
18 H. Bate, S. Rowlands, J. A. Sirs and H. W. Thomas, J. Appl. Phys. (J. Phys. D), Ser. 2, 2 (1969) 1447.
19 B. Carnahan, H. A. Luther and J. O. Wilkers, Applied Numerical Methods, Wiley, New York, 1969, p. 431.
20 O. Levenspiel, Chemical Reaction Engineering, 2nd edn., Wiley, New York, 1972.
21 J. C. Sternberg, in J. C. Giddings and R. A. Keller (Eds.), Advances in Chromatography, 2nd edn., M. Dekker, New York, 1966, pp. 205—207.
22 L. R. Snyder, J. Chromatogr., 125 (1976) 287.
23 M. J. E. Golay and J. G. Atwood, J. Chromatogr., 186 (1979) 353.
24 J. G. Atwood and M. J. E. Golay, J. Chromatogr., 218 (1981) 97.
25 R. Aris, Proc. Roy. Soc. London, Ser. A, 235 (1956) 67; 252 (1959) 538.
26 M. J. E. Golay, Anal. Chem., 29 (1957) 928; Nature, 180 (1957) 435.
27 M. J. E. Golay, in D. H. Desty (Ed.), Gas Chromatography 1958, Butterworths, London, 1958, pp. 36—55.
28 I. Halasz, J. Chromatogr., 173 (1979) 229.
29 J. C. Giddings, Dynamics of Chromatography, Part 1, Principles and Theory, M. Dekker, New York, 1965.
30 L. R. Snyder and H. J. Adler, Anal. Chem., 48 (1976) 1022.
31 R. Tijssen, Anal. Chim. Acta, 114 (1980) 71.
32 R. E. Thiers, A. H. Reed and K. Delander, Clin. Chem., 17 (1971) 42.
33 M. E. Evenson, G. P. Hicks and R. E. Thiers, Clin. Chem., 16 (1970) 606.
34 R. E. Thiers, R. R. Cole and W. J. Kirsch, Clin. Chem., 13 (1967) 451.
35 R. E. Thiers, M. Jeyn and R. F. Wildermann, Clin. Chem., 16 (1970) 832.
36 W. H. C. Walker, C. A. Pennock and G. K. McGowan, Clin. Chim. Acta, 27 (1970) 421.
37 G. Ertingshausen, H. J. Adler and A. S. Reichler, J. Chromatogr., 42 (1969) 355.
38 R. D. Begg, Anal. Chem., 43 (1971) 854; 44 (1972) 631.
39 W. H. C. Walker and K. R. Andrew, Clin. Chim. Acta, 57 (1974) 181.
40 L. R. Snyder, J. Levine, R. Stoy and A. Conetta, Anal. Chem., 48 (1976) 942A.
41 L. R. Snyder and H. J. Adler, Anal. Chem., 48 (1976) 1017.
42 V. V. S. Eswara-Dutt and H. A. Mottola, Anal. Chem., 47 (1975) 357.
43 J. Růžička and E. H. Hansen, Anal. Chim. Acta, 78 (1975) 145.
44 J. Růžička, E. H. Hansen and E. A. Zagatto, Anal. Chim. Acta, 88 (1977) 1.
45 E. Pungor, Z. Fehér, G. Nagy, K. Toth, G. Horvai and M. Gratzl, Anal. Chim. Acta, 109 (1979) 1.
46 M. J. Lighthill, J. Inst. Math. Its Appl., 2 (1966) 97.
47 V. Ananthakrishnan, W. N. Gill and A. J. Barduhn, Am. Inst. Chem. Eng. J., 11 (1965) 1063.
48 J. T. Vanderslice, K. K. Stewart, A. G. Rosenfeld and D. J. Higgs, Talanta, 28 (1981) 11.
49 D. Betteridge, Anal. Chem., 50 (1978) 832A.
50 A. U. Ramsing, J. Růžička and E. H. Hansen, Anal. Chim. Acta, 129 (1981) 1.
51 J. H. M. van den Berg, R. S. Deelder and H. G. M. Egberink, Anal. Chim. Acta, 114 (1980) 91.
52 J. M. Reijn, W. E. van der Linden and H. Poppe, Anal. Chim. Acta, 123 (1981) 229.
53 P. Haagensen, cited in J. Růžička and E. H. Hansen, Flow Injection Analysis, Wiley, New York, 1981, pp. 26—29.
54 J. M. Reijn, Ph.D. Thesis, University of Amsterdam, The Netherlands, 1982, pp. 77—91.

Analytica Chimica Acta, 154 (1983) 17—31
Elsevier Science Publishers B.V., Amsterdam — Printed in The Netherlands

THEORETICAL PREDICTIONS ON THE RESPONSE PROPERTIES OF POTENTIOMETRIC GAS SENSORS BASED ON INTERNAL POLYMER MEMBRANE ELECTRODES

M. E. MEYERHOFF*, Y. M. FRATICELLI, W. N. OPDYCKE, L. G. BACHAS and A. D. GORDUS

Department of Chemistry, University of Michigan, Ann Arbor, MI 48109 (U.S.A.)

(Received 9th May 1983)

SUMMARY

The appropriate equilibrium expressions and known thermodynamic equilibrium constants are used in calculations on the expected response properties of polymer membrane electrode-based ammonia and carbon dioxide gas sensors. Slopes, detection limits, Nernstian response ranges and selectivities of such devices are shown to be a function of the initial pH, ionic strength and equilibrium constant of the internal electrolyte buffer used within these probes. Previously reported data for an ammonia sensor of this type correlate well with the theory. The poor response characteristics of carbon dioxide sensors based on internal carbonate-responsive membranes is also explained via the model presented. Future prospects and considerations for the development of other gas sensors of this type are discussed.

Potentiometric gas sensors based on internal glass pH electrodes (e.g., for CO_2, NH_3, NO_2, etc.) have become routinely used in numerous procedures for clinical and environmental analysis [1—3]. Measurements with these sensors are based on the diffusion of the analyte gas through a gas-permeable membrane into a thin film of electrolyte solution in contact with the glass pH electrode. The diffusing gas participates in an equilibrium reaction with the electrolyte in the thin film producing a pH change in this layer. Several workers have developed models for predicting the response properties of these sensors [4—7]. It has been shown that the detection limits and Nernstian response ranges of these devices are dependent on the composition and concentrations of the internal electrolytes used within these probes (e.g., NH_4Cl for the NH_3 sensor, $NaHCO_3$ for the CO_2 sensor, etc.).

Recently, in an attempt to overcome certain limitations of the conventional gas sensors, new types of potentiometric gas probes have been developed [8—12]. These new sensors utilize internal polymeric ion-selective membrane electrodes as internal sensing elements within the traditional gas-sensing configurations. In one case, the conventional glass pH electrode can be replaced by an inexpensive polymer pH-responsive membrane [11, 12], although for this approach, the response properties and selectivities of the resulting sensors are analogous to the conventional probes because the mechanism of response

0003-2670/83/$03.00

remains the same (i.e., a pH change in a thin electrolyte film). Alternatively, polymer ion-selective membranes responsive to equilibrium ionic forms of the analyte gases have been utilized in conjunction with internal electrolyte buffers to fabricate sensors which function via a buffer trap mechanism. For example, a nonactin-based ammonium ion-responsive polymer membrane electrode has been used as an internal element for the development of a new ammonia sensor [8]. The resulting device had improved detection limits and selectivity when compared to the conventional ammonia probes [9, 13]. Similarly, attempts were made to develop a new carbon dioxide sensor through the use of an internal polymeric carbonate ion-selective membrane [10]. Both the ammonia and carbon dioxide sensors of this type exhibited sub-Nernstian responses and limited dynamic measuring ranges with the overall response properties being largely dependent on the choice of the internal electrolyte buffer.

The purpose of this paper is to present an equilibrium model which can be used to predict accurately the response properties of these new types of sensors with regard to expected slopes, detection limits, Nernstian response ranges, etc. Calculations are made for a variety of internal electrolyte buffers that have been used in the past as well as for some not previously evaluated. For carbon dioxide and ammonia sensors, it will be shown that the choice of internal electrolyte buffer dramatically affects the behavior of the sensors and that predicted response properties for each buffer correlate with previously reported observations. Prospects for improving the response of the carbon dioxide sensor as well as for preparing other sensors of this type will also be discussed.

THE EQUILIBRIUM MODEL

Figure 1(a) shows a general schematic view of the type of gas sensor for which calculations are made. Figure 1(b) shows expanded views of the CO_2 and NH_3 sensors along with the pertinent reactions which take place within the sensing tips of these probes. These sensors initially contain an internal electrolyte buffer system, B/BH^+ (referring to the free base form, B, and the protonated form, BH^+, of the buffer reagent, e.g., tris(hydroxymethyl)-aminomethane (Tris), etc.). The ratio of these two species in the thin film electrolyte controls the initial pH of the buffer in the sensing layer.

In order to predict the Nernstian response ranges, slopes, selectivities, and detection limits of these sensors, it is necessary to derive expressions which will evaluate the pH of the thin buffer film as a function of the dissolved gas concentration in the sample. Alternatively, an expression which evaluates the concentration of gas required in the sample to attain a given pH in the thin film could also be used. To derive the required expressions, it is necessary to make the following five assumptions about the equilibrium models shown in Fig. 1(b). First, it is assumed that the rate of species exchange between the bulk reservoir of internal electrolyte buffer and the thin film is very slow

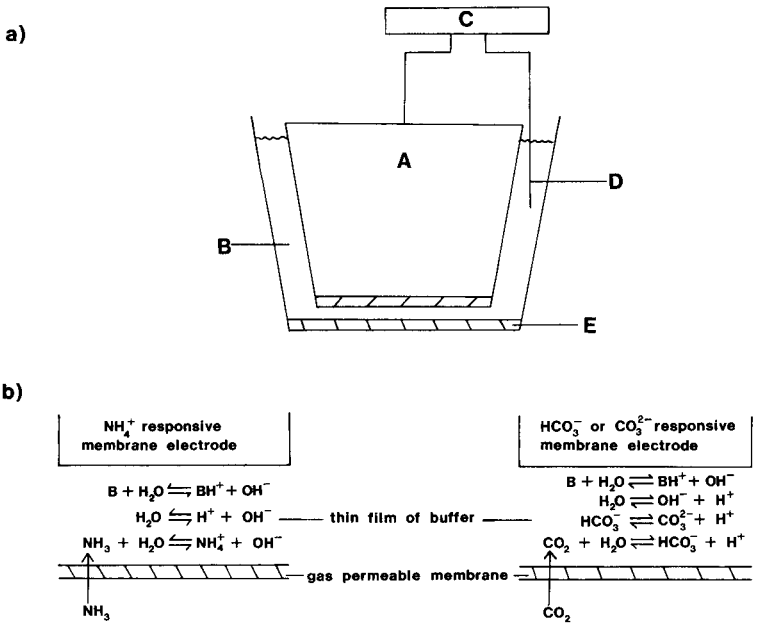

Fig.1. (a) Schematic diagram of polymer membrane electrode-based potentiometric gas sensor: (A) internal polymer membrane ion-selective electrode; (B) reservoir of internal electrolyte buffer; (C) pH meter; (D) Ag/AgCl reference electrode; (E) outer gas-permeable membrane (silicone rubber for CO_2 sensor, polytetrafluoroethylene for NH_3 sensor). (b) Expanded views of new ammonia and carbon dioxide sensors and their associated chemical equilibria.

relative to the rate of gas diffusion into the thin film of buffer and the rates associated with equilibrium reactions in that layer. Thus the thin film is considered to be an essentially isolated small volume of buffer with which the sample gas is in equilibrium, the junction between the internal reservoir of buffer and the thin film merely serving as a point of electrolytic contact between the two solutions.

Second, the Henry constants (K_H) for the dissolved gases are assumed to be equal on both sides of the gas-permeable membrane so that at equilibrium, i.e., when the partial pressure of gas is equal on both sides of the gas-permeable membrane, the concentration of dissolved gas will be equal. This will be true if the sample and internal buffer solutions have similar ionic strengths and osmolarities. Third, it is assumed that the osmolarities of the sample and internal buffer solutions are indeed very similar so that diffusion of water vapor across the gas-permeable membrane will not dilute or concentrate the ionic strength of the internal electrolyte buffer film.

Fourth, the thin film of buffer is assumed to be an extremely small volume relative to the possible sample volumes into which these sensors are placed. Therefore, the sample can be considered an unlimited sink of analyte gas, and, at equilibrium, the concentration of gas in the thin film will be exactly

the same as in the sample volume. Thus, in setting up equilibrium expressions regarding the hydrolysis of the analyte gas, the sample gas concentration value is used, not that value minus the amount ionized by the hydrolysis reaction.

The fifth assumption is that for any sample gas concentration, equilibration of the gas with the thin film buffer does not significantly alter the total ionic strength of this aqueous layer. Consequently, the same conditional equilibrium constants can be utilized throughout the gas concentration range considered. It will be shown that this assumption is not always valid for the CO_2 sensor.

For the ammonia sensor model depicted in Fig. 1(b), the pH of the buffer film is initially governed by the buffer equilibrium reaction and the dissociation of water:

$$B + H_2O \rightleftharpoons BH^+ + OH^-; H_2O \rightleftharpoons H^+ + OH^-$$

At equilibrium,

$$K_{b(B)} = (([BH^+]_s + [BH^+]_{ioniz})[OH^-])/([B]_s - [BH^+]_{ioniz}) \quad (1)$$

where $K_{b(B)}$ is the conditional ionization constant for the weak base buffer reagent B, $[BH^+]_s$ and $[B]_s$ are the starting concentrations of the protonated buffer and free base buffer reagent, respectively, $[BH^+]_{ioniz}$ is the concentration of protonated buffer formed from hydrolysis of the given starting concentration of B, and $[OH^-]$ represents the hydroxide ion concentration in the thin film at equilibrium.

Solving Eqn. (1) for $[BH^+]_{ioniz}$ yields

$$[BH^+]_{ioniz} = ([B]_s K_{b(B)} - [BH^+]_s[OH^-])/(K_{b(B)} + [OH^-]) \quad (2)$$

In the presence of ammonia gas, a simultaneous weak base hydrolysis reaction occurs in the buffer film: $NH_3 + H_2O \rightleftharpoons NH_4^+ + OH^-$. Because at equilibrium, $[NH_3]_{sample} = [NH_3]_{film}$ (as assumed above), the equilibrium constant for this reaction can be written as follows

$$K_{b(NH_3)} = ([NH_4^+][OH^-])/[NH_3]_{sample} \quad (3)$$

If, for example, hydrochloric acid is used initially to prepare the buffer reagent, then the charge-balance equation for these simultaneous hydrolysis reactions can be implemented as follows:

$$[H^+] + [NH_4^+] + [BH^+]_s + [BH^+]_{ioniz} = [Cl^-]_s + [OH^-] \quad (4)$$

Because $[BH^+]_s = [Cl^-]_s$, Eqn. (4) can be written as

$$[OH^-] - [H^+] = [BH^+]_{ioniz} + [NH_4^+] \quad (5)$$

Solving Eqn. (3) for $[NH_4^+]$ and substituting that expression along with $[B^+]_{ioniz}$ (Eqn. 2) into Eqn. (5) (also for notational simplicity, writing $[BH^+] = [BH^+]_s$ and $K_w/[OH^-] = [H^+]$) yields

$$[OH^-] - (K_w/[OH^-]) = \{([B]K_{b(B)} - [BH^+][OH^-])/(K_{b(B)} + [OH^-])\} + \{([NH_3]_{sample}K_{b(NH_3)})/[OH^-]\} \quad (6)$$

It is much easier to solve Eqn. (6) for $[NH_3]_{sample}$ as a function of $[OH^-]$ rather than for $[OH^-]$ as a function of $[NH_3]_{sample}$. Such treatment results in

$$[NH_3]_{sample} = \{[OH^-]^3 + [OH^-]^2(K_{b(B)} + [BH^+]) - [OH^-](K_w + [B]K_{b(B)}) - K_wK_{b(B)}\}/\{[OH^-]K_{b(NH_3)} + K_{b(B)}K_{b(NH_3)}\} \quad (7)$$

In an analogous manner, the model depicted in Fig. 1(b) for the carbon dioxide sensor can be utilized to derive the expression necessary to determine the sample CO_2 concentration required to attain a given pH value in the thin buffer film of the new probe. Equation (8) is the result of such a derivation:

$$[CO_2]_{sample} = \{[H^+] - (K_w/[H^+]) + ((K_{b(B)}[B][H^+] - [BH^+]K_w)/(K_w + K_{b(B)}[H^+]))\}/\{(K_1/[H^+]) + (2K_1K_2/[H^+]^2)\} \quad (8)$$

where K_1 and K_2 are first and second conditional dissociation constants of carbonic acid. For a given sample CO_2 concentration and thin-film pH value, the equilibrium thin-film concentrations of hydrogencarbonate and carbonate ions can be calculated from the following equations:

$$[CO_3^{2-}]_{film} = K_1K_2[CO_2]_{sample}/[H^+]^2 \quad (9)$$

and

$$[HCO_3^-]_{film} = K_1[CO_2]_{sample}/[H^+] \quad (10)$$

In order to evaluate Eqns. (7) and (8) for various buffer reagents, each having different initial pH values and ionic strengths, it is necessary to use conditional equilibrium constants in the calculations, because Eqns. (7) and (8) are derived in concentration terms rather than activities. In general, for any equilibrium reaction, e.g., $A + H_2O \rightleftharpoons B + C$, the conditional constant can be readily determined from the known thermodynamic constant via the equation $K_{cond} = K_{therm}/K_\gamma$, where $K_{therm} = a_Ba_C/a_A = \gamma_B[B]\gamma_C[C]/\gamma_A[A]$, and $K_\gamma = \gamma_B\gamma_C/\gamma_A$; here a represents activities of species and γ is the activity coefficient for the species. Therefore, for each internal buffer solution considered, activity coefficients for all species must be calculated by the extended Debye–Hückel equation [14] before evaluating the conditional equilibrium constants for the buffer system as well as for the dissolved analyte gases (i.e., K_1 and K_2 for the CO_2 sensor, and $K_{b(NH_3)}$ for the NH_3 probe). Similarly, the dissociation constant for water (K_w) must also be corrected for ionic strength effects. Table 1 summarizes some of the conditional constants utilized in this report for theoretical calculations involving different internal buffer reagents and their associated ionic strengths.

While assumptions could be made to simplify Eqns. (7) and (8), the use of a microcomputer (Commodore, model 8032) allows for the strict evaluation of each equation. Programs were written which allowed conditional constants, initial pH values, ionic strengths, required activity coefficients, etc., to be

TABLE 1

Summary of conditional equilibrium constants used in theoretical calculations

Constant	K_{therm}[a]	Conditional constants[b]				
		0.01 M	0.04 M	0.05 M	0.14 M	0.2 M
$K_{b(NH_3)}$	1.79×10^{-5}	2.21×10^{-5}	—	2.75×10^{-5}	—	4.47×10^{-5}
$K_{b(Tris)}$	1.20×10^{-6}	1.47×10^{-6}	1.70×10^{-6}	1.78×10^{-6}	2.14×10^{-6}	2.50×10^{-6}
$K_{b(Bis\text{-}Tris)}$	6.31×10^{-8}	—	—	—	—	1.32×10^{-7}
K_w	1.00×10^{-14}	1.21×10^{-14}	1.39×10^{-14}	1.45×10^{-14}	1.71×10^{-14}	1.98×10^{-14}
K_1 (K_a for H_2CO_3)	4.47×10^{-7}	—	6.17×10^{-7}	—	7.44×10^{-7}	—
K_2 (K_a for HCO_3^-)	4.68×10^{-11}	—	9.61×10^{-11}	—	1.29×10^{-10}	—

[a]Thermodynamic equilibrium constants at 25°C. [b]For the indicated initial ionic strength of the buffer system.

entered into the microcomputer. Based on these initial values for a given buffer reagent, the computer determined [B]. An iteration part of the program then evaluated Eqns. (7) or (8) for continuously increasing (for ammonia system) or decreasing (for carbon dioxide system) thin-film pH values and all concentration data were output to a printer (Centronics, model 739). For each iteration, the pH was changed by ±0.001 units to generate the theoretical plots.

RESULTS AND DISCUSSION

Ammonia sensor

Figure 2 shows the computer-generated plots of the thin-film pH as a function of sample ammonia concentration for five different internal Tris—HCl buffer reagents. It can be seen that the internal solutions in which the initial pH $\approx$ $pK_{a(B)}$ (i.e., pH 8.0 or pH 8.3) offer the best buffering ability towards increasing sample ammonia concentrations and allow the use of less concentrated (lower ionic strength) buffers. For solutions in which the initial pH differs significantly from the $pK_{a(B)}$ and $pK_{a(NH_3)}$ (i.e., pH 7.50 buffers), the ionic strength of the buffer has a greater effect on maintaining the initial pH of the thin-film electrolyte layer of the sensor. In previous work [13], experi-

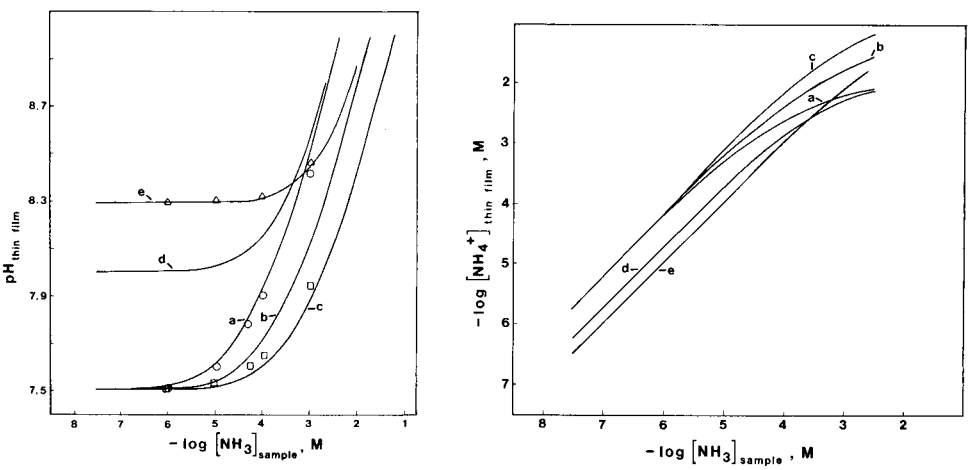

Fig. 2. Computer-generated plots of thin-film pH vs. sample ammonia concentration for new ammonia sensor prepared with various internal buffer solutions: (a) 0.01 M Tris—HCl, pH 7.50; (b) 0.05 M Tris—HCl, pH 7.50; (c) 0.20 M Tris—HCl, pH 7.50; (d) 0.01 M Tris—HCl, pH 8.00; (e) 0.05 M Tris—HCl, pH 8.30; (concentrations of buffers refer to total ionic strength of buffer solution which is due solely to the presence of $Tris^+$ and Cl^- ions.) Also shown are experimental results taken from [13]: (△) 0.05 M Tris—HCl, pH 8.30; (○) 0.01 M Tris—HCl, pH 7.50; (□) 0.1C M Tris—HCl, pH 7.50 (computer plot not shown).

Fig. 3. Computer plots of equilibrium thin-film ammonium ion concentration vs. sample ammonia concentration for the same five buffers (a—e) shown in Fig. 2.

ments were conducted actually to measure the thin-film pH as a function of the sample gas concentration for several of the buffers and the results of those experiments are also shown in Fig. 2. There is good correlation between the experimentally observed values and those predicted by the equilibrium model.

As can be seen in Fig. 3, the ability to maintain a constant pH in the thin film will ultimately determine the Nernstian response range of the sensor. This figure shows the plots of equilibrium thin-film ammonium ion concentration as a function of sample gas concentration for the same five Tris–HCl buffers considered in Fig. 2. It is apparent that for internal reagents with greater buffer capacity, an improved linear range of log $[NH_4^+]_{film}$ vs. log $[NH_3]_{sample}$ plots result. It is, however, evident that a lower initial pH value for the internal buffer reagent is desirable to improve detection limits because more ammonium ions are formed in the film for a given concentration of dissolved gas (i.e., improved buffer trap effect). It should be noted that Tris–HCl buffers were evaluated in these calculations because previous experiments [8, 9] demonstrated that this buffer is the optimum choice among common buffering systems. This is primarily because the internal nonactin-based polymer ammonium electrode lacks selectivity over many common cationic buffer components, e.g., potassium, sodium, etc., and the presence of these species in the internal electrolyte would diminish the detection capabilities of the sensor.

From Fig. 3, it is a simple matter to predict the slopes and logarithmic response ranges of ammonia gas sensors prepared with the various Tris–HCl buffers. Because the internal ammonium responsive electrode responds in a Nernstian fashion toward ammonium ion activity in the thin buffer film,

$$E_{cell} = K + 0.059 \log (\gamma_{NH_4^+}[NH_4^+]) \tag{11}$$

and because for a satisfactory ammonia gas sensor, the potentiometric response should be expressed by the equation

$$E_{cell} = K + S \log [NH_3]_{sample} \tag{12}$$

where S is the operational slope of the sensor, then for Eqns. (12) and (11), respectively,

$$S = dE_{cell}/d\log [NH_3]_{sample} \tag{13}$$

and

$$dE_{cell} = 0.059\ d\log (\gamma_{NH_4^+}[NH_4^+]) \tag{14}$$

Substitution of dE_{cell} in Eqn. (13) yields the following expression for the slope of the gas sensor:

$$S = 0.059\ d\log (\gamma_{NH_4^+}[NH_4^+])/d\log [NH_3]_{sample} \tag{15}$$

Because $\gamma_{NH_4^+}$ is constant for a given ionic strength internal buffer, the slopes of the curves shown in Fig. 3 multiplied by 0.059 V will give the theoretical

slopes of the gas sensors. As can be seen in Fig. 3, the log—log plots rapidly become non-linear at higher ammonia gas concentrations because of the pH change within the buffer film. Indeed, Table 2 lists the predicted slopes for decade ranges of sample ammonia concentrations. The sub-Nernstian response properties, even at extremely low concentrations of ammonia (i.e., 10^{-7} — 10^{-6} M), for gas sensors prepared with low ionic strength buffers (e.g., 0.01 M Tris—HCl) fit well with what has been observed experimentally [8, 9]. Perfectly Nernstian response slopes for low ammonia concentrations are predicted for the internal buffer solutions having greater buffer capacities, although in practice this is seldom the case because the internal nonactin polymer membrane electrode often exhibits slightly sub-Nernstian response (i.e., 55—58 mV/decade) toward ammonium ions. Indeed, the operational slopes of the final sensors can never exceed that of the internal sensing element. As can be seen in Table 2, near-Nernstian behavior can be extended up to 10^{-4} M ammonia when a 0.05 M Tris—HCl pH 8.30 buffer is used and even to higher sample ammonia concentrations when buffers with higher ionic strengths are used. In principle, it would take an extremely concentrated buffer reagent to obtain Nernstian response above 10^{-3} M ammonia. Therefore, conventional types of sensors are recommended for such measurements.

Whereas increasing the ionic strength of the internal buffer improves the Nernstian range for the new ammonia sensor, these improved slopes come at the expense of absolute detection limits. There are two reasons for this effect. First, the detection limits of the sensor will be partly dependent on the innate detection limits of the nonactin membrane electrode toward ammonium ions formed in the thin buffer film. Increasing the ionic strength of the buffer will also increase the concentration of protonated $Tris^+$ ions (BH^+) in the film. Although the nonactin-based membrane displays only

TABLE 2

Predicted slopes for new ammonia sensors prepared with Tris—HCl internal buffer solutions of different strengths and pH[a,b]

Sample NH_3 concentration range (M)	Slopes (mV/decade)				
	0.01 M pH 7.50	0.05 M pH 7.50	0.20 M pH 7.50	0.01 M pH 8.00	0.05 M pH 8.30
10^{-7}—10^{-6}	57	59	59	59	59
10^{-6}—10^{-5}	54	57	58	58	59
10^{-5}—10^{-4}	40	50	55	52	58
10^{-4}—10^{-3}	25	34	42	34	53

[a]Slopes determined from least-squares fit of computer-generated log $[NH_4^+]_{film}$ vs. log $[NH_3]_{sample}$ data points for given ammonia concentration range. [b]Values given assume that the internal nonactin polymer membrane electrode has Nernstian response of 59 mV/decade towards ammonium ion activities.

minimal response to $Tris^+$, there is indeed some finite response and the selectivity of the membrane over $Tris^+$ can be evaluated from the Nicolsky equation:

$$E = K + 0.059 \log (a_{NH_4^+} + ka_{Tris^+}) \quad (19)$$

The selectivity coefficient, k, was found to be about 10^{-5}; however, even with this high degree of selectivity, any increase in $Tris^+$ levels will diminish the ability to sense extremely low levels of ammonium ions in the buffer film. Secondly, because the nonactin polymer membrane electrode actually responds to the activity of ammonium ions in the thin film, any increase in the ionic strength of the buffer above 0.1 M will rapidly decrease the $a_{NH_4^+}$ for a given sample gas concentration, thereby reducing the detection capabilities of the sensor. In practice, when low ionic strength buffers with low initial pH values (pH 7.50) are used, atmospheric levels of ammonia and ammonia impurities in the reagents used to evaluate the sensors (e.g., sodium hydroxide sample solutions to generate ammonia gas) appear to determine the detection limits of the new ammonia sensor. For example, normal atmospheric levels of ammonia in equilibrium with a sodium hydroxide solution will produce a background level of 10^{-8}—5×10^{-7} M ammonia in the test solution [1, 15]. Thus, for an internal buffer of 0.01 M Tris—HCl, pH 7.50, examination of Fig. 3 shows that between 10^{-6} and 5×10^{-5} M ammonium ions are formed in the thin film when in total equilibrium with the atmosphere. These ammonium ion concentrations are well within the detection limits of the nonactin-based polymer electrode under these low ionic strength conditions [8].

The selectivity of the new ammonia sensor has previously been studied with regard to volatile amine interferences [13]. It was found experimentally that the degree of selectivity depends on the buffering strength of the internal buffer reagent. Indeed, these substances interfere with the response by diffusing across the gas-permeable membrane and altering the pH of the buffer film in much the same manner as high ammonia gas concentrations change the pH of the film (see Fig. 1). Because the internal nonactin-based membrane electrode has only minimal response to protonated forms of the amines [13], only a negative interference in the measurement of ammonia is possible when volatile amines are present in a sample (i.e., interfering amines make the film pH higher, thereby decreasing the equilibrium concentration of ammonium ions formed from the analyte). Thus, as is the case for improving slopes and linear response ranges, high ionic strength buffers with pH values at or near the pK_b of the buffer base are desirable for decreasing the negative interferences caused by volatile amines. To actually determine the effect of amine concentrations on the pH of the thin buffer film, Eqn. (7) can be evaluated using the appropriate K_b values for the given amines rather than K_b for ammonia.

Carbon dioxide sensors

Figure 4 shows the computer-generated data for thin-film pH values as a function of sample gas concentration for new CO_2 sensors depicted in

Fig. 1(b). Plots are presented for sensors prepared with three different internal buffer reagents. Figure 5 shows how equilibrium thin-film carbonate and hydrogencarbonate ion concentrations change as the sample CO_2 concentration increases for these three internal reagents. The same generalizations made for the ammonia sensor can also be made for the carbon dioxide sensor. As sample CO_2 concentrations increase, the pH of the buffer film decreases. If the buffer film has an initially high pH value (e.g., 8.75), which is required to produce significant quantities of carbonate from diffusing CO_2 (this is the case when a carbonate-selective polymer electrode is used as the internal sensing element), then the pH decreases rapidly over the entire CO_2 concentration range evaluated (see Fig. 4). This is because there is a relatively large difference between the initial buffer pH (8.75) and the acidity constant for carbonic acid (pK_a 6.6). Increasing the ionic strength of the internal buffer

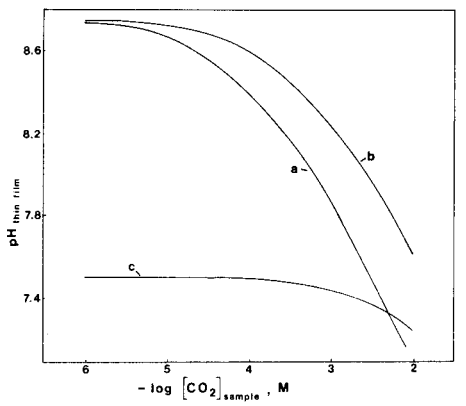

Fig. 4. Computer-generated plots of equilibrium thin-film pH vs. sample carbon dioxide concentration for new carbon dioxide sensors prepared with various internal buffer solutions: (a) 0.04 M Tris—H_2SO_4, pH 8.75; (b) 0.14 M Tris—H_2SO_4, pH 8.75; (c) 0.20 M Bis-Tris—HCl, pH 7.50 (concentrations of buffers refer to total ionic-strengths).

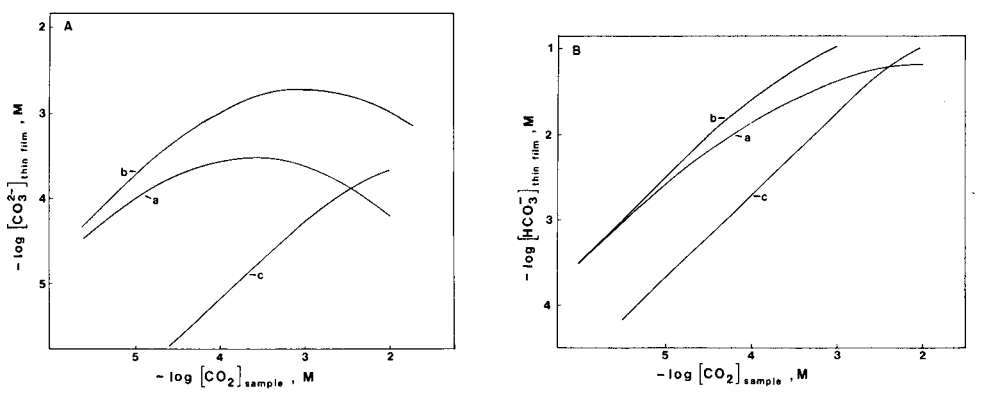

Fig. 5. Computer plots of equilibrium thin-film concentrations of (A) carbonate and (B) hydrogencarbonate vs. sample carbon dioxide concentration for the same three buffers shown in Fig. 4; (a—c) refer to Fig. 4.

(e.g., from 0.04 M to 0.14 M, decreases the degree of pH change in the film; however, even relatively high ionic strength buffers (e.g., 0.50 M) do not eliminate this effect over the typical concentration range of CO_2 measurements (data not shown in figures). If, however, the internal buffer system is changed to one with a lower pK_a value, e.g., 1,3-bis-[tris(hydroxymethyl)-methylamino]propane (Bis-Tris) and the initial pH of the buffer is lowered to 7.50, the magnitude of the pH change in the thin film is greatly reduced (see Fig. 4).

The data presented in Fig. 4 support the observations made previously when a carbonate-selective polymer membrane was utilized as an internal element for a new CO_2 sensor [10]. In that work, it was reported that such a sensor, when prepared with a Tris—H_2SO_4 buffer, pH 8.75 (0.1 M with regard to total Tris, 0.04 M ionic strength), as the internal solution, had negligible response toward dissolved CO_2. When the buffer capacity of the internal reagent was increased (0.5 M with respect to total Tris, 0.14 M ionic strength), logarithmic response toward CO_2 was obtained between 3×10^{-5} and 3×10^{-4} M CO_2, although the slope of this response was sub-Nernstian (15—20 mV/decade). Above 5×10^{-4} M CO_2, the response completely leveled off and actually reversed in direction [10]. Examination of Fig. 5A explains these results. Predicted slopes based on the log $[CO_3^{2-}]_{film}$ vs. log $[CO_2]_{sample}$ plots for both pH 8.75 buffers are sub-Nernstian over the 10^{-5}—10^{-4} M CO_2 concentration range (see Table 3). At higher analyte concentrations, equilibrium carbonate concentrations actually decrease in the thin film because of the large pH change. This fact is reflected in the positive slopes listed in Table 3 for the carbonate electrode-based CO_2 sensor at CO_2 concentrations $>10^{-3}$ M. As can be seen in Fig. 5A and Table 3, when a low initial pH buffer system (Bis-Tris, pH 7.50) with a relatively high ionic strength is utilized internally, the situation improves dramatically with regard to

TABLE 3

Predicted slopes for new carbon dioxide sensors prepared with various internal buffer solutions and polymer membrane electrodes[a]

Sample CO_2 concentration range (M)	Slopes (mV/decade)					
	Internal CO_3^{2-} electrode[b]			Internal HCO_3^- electrode[c]		
	Tris—SO_4, pH 8.75		Bis-Tris—HCl, pH 7.50, 0.20 M	Tris—SO_4, pH 8.75		Bis-Tris—HCl pH 7.50, 0.2(
	0.04 M	0.14 M		0.04 M	0.14 M	
10^{-5}—10^{-4}	−13	−21	−29	−43	−52	−58
10^{-4}—10^{-3}	+2	−7	−27	−28	−37	−56
10^{-3}—10^{-2}	+17	+8	−17	−12	−21	−47

[a]Slopes determined from least-squares fit of computer-generated log $[CO_3^{2-}]_{film}$ or log $[HCO_3^-]_{film}$ vs. log $[CO_2]_{sample}$ data points for each CO_2 concentration range. [b]Values given assume internal carbonate-responsive membrane electrode has Nernstian slope of 29.5 mV/decade. [c]Values given assume internal hydrogencarbonate-responsive membrane electrode has Nernstian slope of 59 mV/decade.

Nernstian response properties. However, at this lower initial pH, much lower equilibrium concentrations of carbonate ions are formed in the film and these levels are below the detection limits of the internal carbonate-responsive polymer membrane electrode [10]. Therefore, the Bis-Tris buffer cannot be utilized to prepare a carbonate membrane-based CO_2 sensor that possesses acceptable detection capabilities.

The data shown in Fig. 5B and Table 3 suggest that the potentiometric detection of hydrogencarbonate ion concentrations in the thin film would greatly improve the analytical performance of the new CO_2 sensor design. This would be particularly true when the Bis-Tris buffer system is used as the internal electrolyte. Use of such a buffer in conjunction with a hydrogencarbonate-responsive polymer membrane electrode would insure Nernstian detection of CO_2 to concentrations $\geqslant 10^{-3}$ M. Moreover, because a hydrogencarbonate membrane electrode would exhibit slopes of 59 mV/decade, the final gas sensor would be more sensitive to variations in CO_2 concentrations. This approach has recently been demonstrated in a Japanese patent [16] and further work in this direction is now in progress in this laboratory.

Regardless of the type of internal sensing element (carbonate or hydrogencarbonate), the theoretical detection limits of these new CO_2 sensors are determined by three parameters: (a) the initial pH of the buffer electrolyte, (b) the species composition of the buffer electrolyte, and (c) the ionic strength of the buffer. The initial pH of the buffer controls the equilibrium concentrations of carbonate and hydrogencarbonate in the thin film (see Fig. 5) and it is therefore desirable to utilize an initial pH which strongly favors the formation of the electro-detectable species (i.e., a good buffer trap effect). The anionic composition of the internal buffer also plays an important role in evaluating the theoretical detection limits for the CO_2 sensor. Indeed, selectivity coefficients for the carbonate and hydrogencarbonate membrane electrodes over common buffer anions (e.g., chloride, phosphates, etc.) determine how low the inner sensing element can detect the ionic forms of CO_2 in a given buffer reagent. It is for this reason that Tris—H_2SO_4 rather than Tris—HCl buffers were used in the development of carbonate electrode-based CO_2 sensor [10]. In addition, as mentioned earlier for the ammonia sensor, the total initial ionic strength of the internal buffer also affects detection limits by decreasing the activity coefficients of the measured thin-film species and consequently their activities. Therefore, while high ionic strength buffers are required for more favorable Nernstian response ranges, these buffers will decrease the theoretical detection limits of the sensor. In principle, the above parameters will determine the detection limits of the CO_2 sensors only when the sensors are used in a CO_2-free environment. In practice, under normal measurement conditions, ambient levels of CO_2 in equilibrium with the internal and sample solutions will dictate the lower limit of CO_2 response and it has been reported that this level is typically $1-3 \times 10^{-5}$ M [17]. Examination of Fig. 5A and the present observations with the carbonate membrane-based CO_2 sensor support this view. For example, from

Fig. 5A, the background level of CO_2 in solution originating from ambient levels will produce approximately 1×10^{-4} M carbonate in the thin film (for the 0.14 M Tris—H_2SO_4 buffer). This level is within the detection capabilities of the internal polymer carbonate electrode when evaluated separately in the same buffer reagent.

The selectivities of the new polymer membrane-based CO_2 sensors are also dependent on two parameters: (a) the selectivity of the internal carbonate or hydrogencarbonate membrane electrode over anionic forms of acidic molecules capable of diffusing through the outer gas-permeable membrane, and (b) the effect of diffusing acids on the pH of the thin-film buffer. The former mechanism yields positive errors in the measurement of CO_2 while the latter causes a negative interference in much the same way that volatile amines affect the new ammonia sensor [13]. The negative interference can be diminished to some degree by using higher ionic strength internal buffers. The positive interference can be overcome only through the development of more selective carbonate or hydrogencarbonate polymer membrane electrodes. For example, salicylic acid would be a major interferent for the carbon dioxide sensor prepared with the carbonate-responsive polymer membrane electrode. This is because the internal carbonate-responsive membrane lacks selectivity over salicylate and this anion would be formed in the thin film as salicylic acid permeates the outer gas-permeable membrane. Indeed, it has recently been shown that such nonvolatile acids can readily diffuse through the silicone rubber membranes often used to fabricate CO_2 sensors [18]. Therefore, a more selective internal electrode is needed to eliminate this problem.

CONCLUSIONS

It is clear from the models presented that the optimum internal buffer electrolyte used in polymer membrane electrode-based gas sensors will vary depending on the situation. For Nernstian response over a wide concentration range, the internal buffer must have high buffer capacity toward the diffusing analyte gas so that the pH of the thin sensing film remains essentially unchanged. Similarly, high ionic strength buffers are required to eliminate negative interferences caused by acidic or basic species which can diffuse through the outer gas-permeable membrane. Unfortunately, the use of these concentrated internal buffer reagents has adverse effects on the detection limits of the sensors. Absolute theoretical detection limits can be extended by using buffers with initial pH values that are significantly different from the pK_a of the analyte gas (large buffer-trap) although this approach often results in limited measurement ranges.

Aside from the CO_2 and NH_3 sensors modeled here, the development of other polymer membrane electrode-based probes seems highly probable. These may include: (a) a nitrogen dioxide sensor based on an internal polymeric nitrate-selective electrode, and (b) a sulfur dioxide sensor based on an

internal bisulfite-responsive polymer membrane. In each case, the internal buffer electrolyte will have to be judiciously chosen so that optimum performance is obtained. The models and discussions presented in this report should aid in the ultimate development of these new probes.

The authors gratefully acknowledge the National Institutes of Health (Grant GM 28882-01) for supporting this work.

REFERENCES

1 M. Riley, in A. K. Covington (Ed.), Ion-Selective Electrode Methodology, Vol. II, CRC Press, Boca Raton, FL, 1979, Ch. 1.
2 M. E. Meyerhoff and Y. M. Fraticelli, Anal. Chem., 54 (1982) 27R.
3 G. J. Moody and J. D. R. Thomas, in H. Freiser (Ed.), Ion-Selective Electrodes in Analytical Chemistry, Vol. I, Plenum, New York, 1978, Ch. 6.
4 M. Mascini and C. Cremisini, Anal. Chim. Acta, 97 (1978) 237.
5 E. H. Hansen and N. R. Larsen, Anal. Chim. Acta, 78 (1975) 459.
6 P. L. Bailey and M. Riley, Analyst, 102 (1977) 212.
7 J. W. Ross, J. H. Riseman and J. A. Krueger, Pure Appl. Chem., 35 (1973) 473.
8 M. E. Meyerhoff, Anal. Chem., 52 (1980) 1532.
9 M. E. Meyerhoff and R. H. Robins, Anal. Chem., 52 (1980) 2383.
10 J. Greenberg and M. E. Meyerhoff, Anal. Chim. Acta, 141 (1982) 57.
11 M. E. Meyerhoff, Y. M. Fraticelli, J. A. Greenberg, J. Rosen, S. J. Parks and W. N. Opdycke, Clin. Chem., 28 (1982) 1973.
12 W. N. Opdycke, S. J. Parks and M. E. Meyerhoff, Anal. Chim. Acta, (1983) in press.
13 Y. M. Fraticelli and M. E. Meyerhoff, Anal. Chem., 53 (1981) 1857.
14 D. G. Peters, J. M. Hayes and G. M. Hieftje, Chemical Separations and Measurements, Saunders, Philadelphia, PA, 1974, Ch. 3.
15 D. Midgley and K. Torrance, Analyst, 97 (1972) 626.
16 Agency of Industrial Sciences and Technology, Jpn. Pat. No. 57, 154, 048, Sept. 22, 1982.
17 U. Fiedler, E. H. Hansen and J. Růžička, Anal. Chim. Acta, 74 (1975) 423.
18 R. K. Kobos, S. J. Parks and M. E. Meyerhoff, Anal. Chem., 54 (1982) 1976.

Analytica Chimica Acta, 154 (1983) 33—39
Elsevier Science Publishers B.V., Amsterdam — Printed in The Netherlands

IMPROVED DYNAMIC RESPONSE OF POTENTIOMETRIC AMMONIA SENSORS USING PURE TEFLON MEMBRANES

MARK A. ARNOLD

Department of Chemistry, University of Iowa, Iowa City, IA 52242 (U.S.A.)

(Received 9th May 1983)

SUMMARY

Several microporous membrane parameters are investigated in an attempt to improve the dynamic response of ammonia gas-sensing electrodes. Parameters of interest include hydrophobic and support membrane porosities as well as support polymer composition. Results show that the electrode recovery process represents the major component of the total dynamic response and that, of the teflon membranes currently available, the 0.02-μm pure teflon membrane is the membrane of choice for these electrodes.

Potentiometric ammonia gas-sensors have been shown to possess a high degree of selectivity which makes them attractive for the quantitation of ammonia [1—3]. Unfortunately, poor dynamic response characteristics can limit the usefulness of these sensors in some cases. An attempt to improve the dynamic response is reported here, where several commercially available microporous membranes are evaluated with respect to dynamic behavior. Membrane compositions studied include pure porous teflon, nylon-supported teflon, and teflon laminated with either polyethylene, polypropylene, or polyester support polymers. Moreover, the effects of hydrophobic and support membrane pore sizes are examined. It will be shown that 0.02-μm pure teflon is the membrane of choice for optimal dynamic response.

For the most part, ammonia gas-sensing electrodes have been designed with some type of microporous teflon-based gas-permeable membrane owing to the rapid diffusion rate of ammonia across this membrane material [4]. Because the diffusion of ammonia across the gas-permeable membrane is an essential part of the electrode response mechanism [3], various membrane parameters such as pore size and composition might be expected to affect the dynamic response by altering the diffusion rate of ammonia into the internal electrolyte layer. Indeed, Mascini and Guilbault [5] have reported an improvement in the dynamic response of an ammonia sensor-based urea probe by changing the hydrophobic membrane of their ammonia sensor. The effects of teflon membrane pore size, support membrane composition, and support membrane porosity, however, have not been previously addressed with respect to dynamic responses of these electrodes.

0003-2670/83/$03.00

EXPERIMENTAL

Apparatus and reagents

All potentiometric measurements were made using an Altex 71 pH meter in conjunction with a Sargent-Welch strip-chart recorder. Measurements were made in thermostated cells controlled at 25°C with a Fisher Model 80 water-bath. The Orion 95-10 ammonia gas-sensor was used in all studies.

Unless otherwise noted, all teflon-based hydrophobic membranes were generously donated by W. L. Gore & Associates, Elkton, MD. Monofilament nylon mesh membranes (Small Parts, Miami, FL) were also tested.

All solutions were prepared from analytical-grade reagents and distilled, deionized water.

Procedures

Each sensor was prepared as suggested by the manufacturer, using the particular hydrophobic membrane of interest. For the nylon-supported membrane systems, the nylon-mesh membrane was positioned immediately adjacent to the teflon membrane in the electrode assembly such that the nylon membrane was in contact with the external solution and the teflon membrane was sandwiched between the nylon membrane and the internal electrolyte. For studies with the laminated membranes, electrodes were constructed with the polymer support layer in contact with the external solution.

All recovery and response-time measurements were made using the stopwatch function of the pH meter in conjunction with the auto-read function. The auto-read function served to flag a specified rate of potential change such that a rate of less than 0.4 mV s^{-1} represented the point at which the response and recovery times were measured. Although this rate of potential change differed considerably from the actual steady-state condition, the use of the auto-read function was quite convenient for objectively measuring long-time responses. Moreover, because the rate of potential change was constant for each response and recovery time, the measured dynamic responses for each membrane tested can be directly compared.

The following procedure was used to measure the dynamic and steady-state responses. After construction, the sensor was dipped in approximately 50 ml of fresh buffer (0.1 M potassium phosphate, pH 12.0) and allowed to equilibrate for 2—3 h. The baseline potential was then recorded and the electrode was dipped into a fresh 5 ml portion of the same buffer. The time necessary for the potential to reach a response rate of 0.4 mV s^{-1} and the corresponding potential were recorded. At this point, 30 μl of a 0.01 M ammonium chloride solution was added to the buffer, which resulted in an ammonia concentration of 6.5×10^{-5} M ($pNH_3 = 4.22$), and the response time and the corresponding potential were recorded. To this same solution, 30 μl of a 0.1 M ammonium chloride solution was added which resulted in a final ammonia concentration of 6.5×10^{-4} M ($pNH_3 = 3.19$). Once again the response time and the corresponding potential were recorded. At this point,

the sensor was removed from the ammonia solution, rinsed with water and placed into a fresh 50-ml portion of the buffer. This recovery time (i.e., the bulk recovery time) and the final baseline potential were recorded. Unless otherwise stated, this entire process was then repeated at the point starting with the 5-ml buffer solution for each sensor at least three times. In this way, at least three measurements of each potential, recovery time and response time were obtained.

Because the sensor displays a Nernstian response for ammonia concentrations down to about 1×10^{-5} M under the conditions used, the potential readings at pNH_3 values of 4.22 and 3.19 were used to calculate slopes of potential vs. log NH_3 concentration. Moreover, limits of detection [6] were calculated by using the baseline potentials for 5 ml of buffer and the corresponding potentials at pNH_3 values of 4.22 and 3.19.

RESULTS AND DISCUSSION

Figure 1 shows a typical potential vs. time trace for an ammonia sensor in which the hydrophobic membrane supplied by Orion was used. The potential change corresponds to the addition of ammonium chloride to 5 ml of the buffer so that the final ammonia concentration is 6.0×10^{-5} M. After the attainment of a steady-state potential (point C), the sensor is rinsed with water and placed in a 50-ml portion of fresh buffer. At a pH of 12.0, the response time is approximately 1 min. The recovery time, however, is about 8.5 min under these conditions. In general, the recovery process amounts to between 85 and 70% of the total dynamic response, defined as the time between points when one measurement is started and the next measurement can begin. For the most part, shorter recovery times are observed when

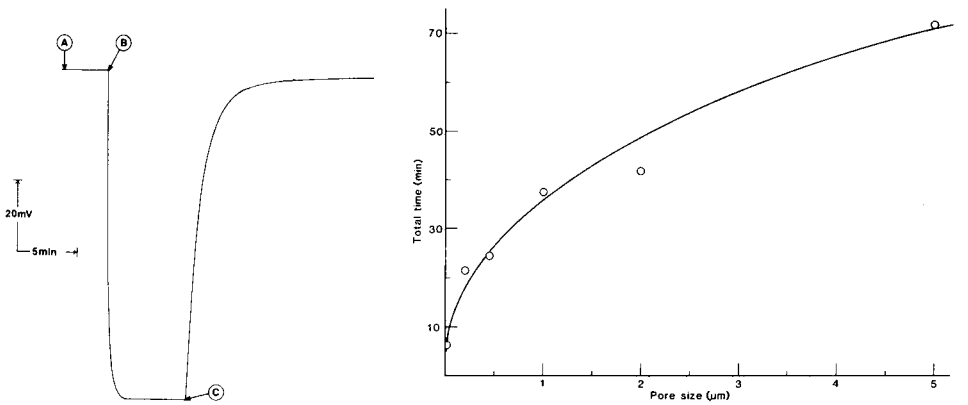

Fig. 1. Potential vs. time trace for the Orion ammonia gas sensor: (A) 5 ml of fresh buffer; (B) 30 μl of 0.01 M NH_4Cl; (C) 50 ml of fresh buffer.

Fig. 2. Total dynamic response for ammonia sensors with various teflon membrane pore sizes.

the recovery process starts at lower ammonia concentrations. In such a case, the percentage of the total dynamic response that can be attributed to the recovery process decreases because longer response times are generally observed at lower ammonia concentrations. These results emphasize the need to investigate the recovery process because it is the major component of the total dynamic response.

Effect of teflon membrane structure

Table 1 summarizes the steady-state and dynamic response characteristics observed when pure teflon membranes are used in the construction of the sensor. Average pore sizes ranging from 0.02 to 15 μm were tested. These data show that Nernstian slopes were observed until the larger pore size membranes were used. Moreover, similar limits of detection were obtained for the membranes with 0.02—3-μm pore size. The 5 and 10—15 μm membranes displayed significantly higher detection limits.

Figure 2 shows the total dynamic response time in relation to membrane pore size. As can be seen, the 0.02-μm pore size results in the fastest response. The slow dynamic response for the larger pore sizes can be explained by the resulting membrane geometry. For large pore sizes, the resulting membrane is observed to bulge away from the internal pH electrode owing to the weight of the internal electrolyte solution on the flexible teflon membrane; i.e., instead of a thin layer of internal electrolyte, there is a "pool" of internal electrolyte at the pH-sensing surface because of the greater flexibility of the membrane. As the volume of the internal electrolyte pool increases, so will the time necessary to establish the steady-state equilibria at the glass electrode surface. The greater porosity of the membrane alters the electrode dynamic response, not by affecting ammonia diffusion rates, but by altering the membrane geometry. Unfortunately, teflon membrane thickness is inversely related to pore size; thus, membrane thickness cannot be held constant while membrane porosity is varied.

TABLE 1

Effect of teflon membrane structure on the response of the ammonia sensor

Membrane pore size (μm)	Membrane thickness (μm)	Detection limit (10^{-6} M)	Recovery time (min)		Response time (min)[a]	
			Bulk	5 ml Buffer	4.22	3.19
0.02	90	1.78 ± 0.20	2.5 ± 0.5	2.2 ± 0.8	0.9 ± 0.1	0.6 ± 0.1
0.20	40	2.4 ± 0.7	11.3 ± 0.5	3.8 ± 1.7	3.6 ± 0.1	2.8 ± 0.1
0.45	25	2.9 ± 1.1	13.1 ± 1.5	2.9 ± 0.6	4.7 ± 0.2	3.8 ± 0.4
1.0	20	2.6 ± 0.2	17.2 ± 0.6	9.3 ± 0.3	6.2 ± 0.3	4.9 ± 0.2
3.0	8	2.9 ± 1.0	18.8 ± 0.1	10.2 ± 6.2	7.0 ± 0.2	5.9 ± 0.1
5.0[b]	5	8.7	36.1	10.9	13.9	11.2
10—15[b]	3	27.1	25.6	23.8	6.8	6.0

[a]At the pNH_3 values stated. [b]Only one measurement obtained.

Effect of mesh size of the nylon membrane

To provide support for the teflon membranes with large pores, monofilament nylon mesh membranes were added to the electrode surface. Nylon meshes ranging from 10 to 88 μm were studied in conjunction with a 1-μm pure teflon membrane.

Figure 3 shows the dynamic behavior for sensors with nylon-supported teflon membranes with different nylon mesh sizes. It can be seen that response times are independent of the nylon mesh size over the range from 20 to 74 μm. Moreover, the recovery times in 5 ml of buffer remain fairly constant at 3—4 min over this range of mesh sizes. The bulk recovery time, however, varies considerably with a minimum recovery time being obtained when the 53-μm nylon membrane is employed. Likewise, the total dynamic response shows a minimum when the 53-μm nylon membrane is used. These results show that an optimal support membrane pore size of 53 μm exists when a 1-μm membrane is used as the hydrophobic membrane. It is difficult to understand why the pore size of the nylon membrane affects the dynamic response properties of the ammonia sensor. Possible explanations may be that the small pore sizes reduce the effective surface area of the hydrophobic membrane and that the large pore sizes introduce eddy diffusion pockets at the gas electrode surface owing to the nylon mesh thickness.

Each of the nylon-supported teflon membranes results in near-Nernstian slopes with an average value of 59.8 ± 1.5 mV per decade of concentration change. Limits of detection are dependent on the nylon membrane mesh size, however (Fig. 4). In this case, the best limit of detection is obtained when a 53-μm nylon support membrane is used.

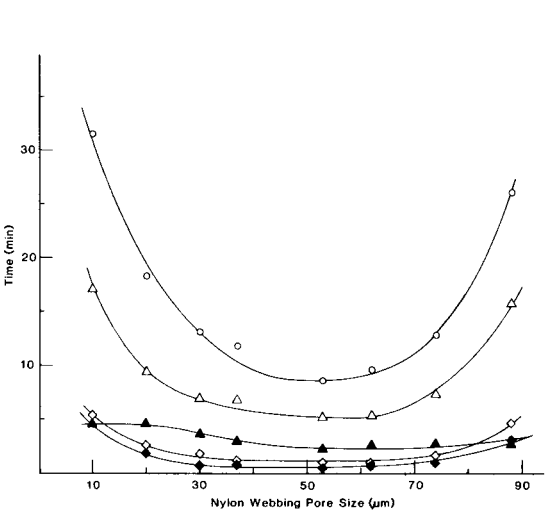

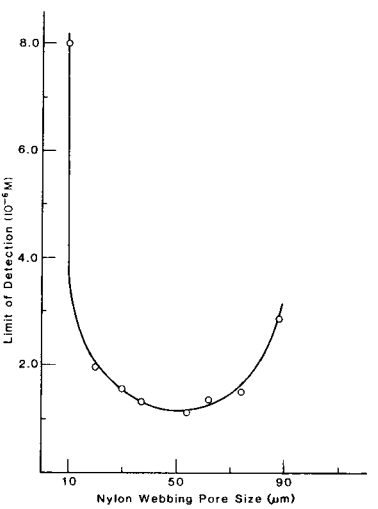

Fig. 3. Effect of nylon support mesh size on the dynamic behavior of ammonia sensors: (○) total dynamic response; (△) bulk recovery time; (▲) recovery time with 5 ml of buffer; (◇) response time at pNH_3 = 4.22; (◆) response time at pNH_3 = 3.19.

Fig. 4. Detection limits for various mesh sizes of the nylon support.

Effect of laminated support membranes

Table 2 summarizes the steady-state response characteristics for a variety of polymer support materials laminated onto 1-μm teflon membranes. Polymer supports tested were scrim polyester, scrim polypropylene, unwoven polypropylene and unwoven polyethylene. Near-Nernstian slopes were observed for each membrane tested with an average slope of 59.9 ± 0.7 mV per decade for all sensors. Moreover, detection limits were similar for each sensor with an average of 1.87 ± 0.45 × 10^{-6} M ammonia.

Figure 5 summarizes the dynamic behavior for the laminated membranes. The unwoven polyester-based membrane results in the fastest dynamic response. All membranes give similar response times but recovery times vary considerably. Because the composition of the support polymer would not be expected significantly to alter diffusion rates, the difference in dynamic behavior is more likely due to differences in porosity of the support polymer. Unfortunately, it is not possible to investigate the effect of laminated membrane pore size on dynamic response because manufacturers do not control or report pore sizes for support polymers. Figure 5 also emphasizes the large fraction of the total dynamic response which corresponds to the recovery process.

Comparison of membrane types

Figure 6 summarizes the overall dynamic response for sensors constructed with the best of each membrane class tested. The 0.02-μm pure teflon membrane is seen to result in the shortest total dynamic response time. Also shown in this figure is the total dynamic response for a sensor based on the hydrophobic membrane supplied with the Orion kit. Each of the membrane classes studied results in better dynamic behavior than the currently available Orion system. In addition, the pure teflon membranes seem to give better seals around the sensor body than the other membrane classes. This latter point provides further incentive to use the 0.02-μm pure teflon membrane in the construction of these sensors.

This study represents an attempt to obtain optimal dynamic response characteristics for ammonia sensors with currently available teflon membranes.

TABLE 2

Steady-state behavior of ammonia sensors made with laminated teflon membranes[a]

Laminated polymer	Slope (mV/decade)	Limit of detection (10^{-6} M)
Unwoven polyester	59.4 ± 0.8	2.1 ± 0.2
Unwoven polypropylene	60.4 ± 0.5	2.3 ± 0.4
Scrim polypropylene	60.4 ± 0.4	1.40 ± 0.13
Scrim polyethylene	59.4 ± 0.4	1.61 ± 0.19

[a] 1-μm teflon membrane pore size.

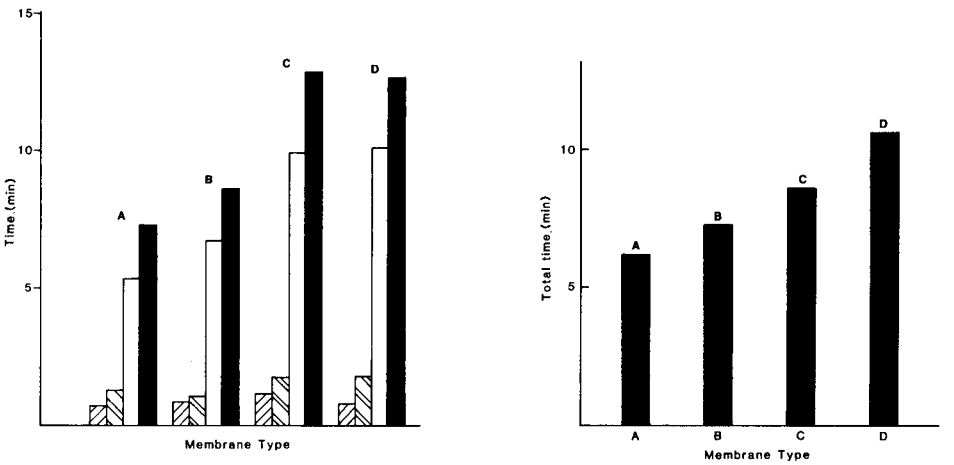

Fig. 5. Dynamic behavior for laminated teflon membranes: (A) unwoven polyester; (B) scrim polyethylene; (C) unwoven polypropylene; (D) scrim polypropylene. Filled blocks indicate the total recovery time with 5 ml of buffer plus bulk solution; open blocks are total dynamic response times; the larger and smaller hatched blocks are response times for pNH_3 values of 4.22 and 3.19, respectively.

Fig. 6. Comparison of total dynamic responses for sensors using the optimum of each membrane class: (A) 0.02-μm pure teflon; (B) 1.0-μm teflon, unwoven polyester; (C) 1.0-μm teflon, 53-μm nylon webbing; (D) Orion.

Limited availability of well-characterized hydrophobic membranes imposes significant restrictions on this effort. Restrictions such as porosity range and thickness of the teflon membrane, and pore size of the support membrane do not allow for a correlation of membrane parameters and dynamic response. Future studies must include pure teflon membranes with even smaller porosities as well as constant thickness, alternative membrane materials, and better characterized polymer support membranes.

REFERENCES

1 M. E. Meyerhoff and Y. M. Fraticelli, Anal. Chem., 54 (1982) 27R.
2 Handbook of Electrode Technology, Orion Research, Cambridge, MA, 1982, p. A1.
3 M. Riley, in A. K. Covington (Ed.), Ion-Selective Electrode Methodology, Vol. II, CRC Press, Boca Raton, FL, 1979, Ch. 1.
4 J. W. Ross, J. H. Riseman and J. A. Krueger, Pure Appl. Chem., 36 (1973) 473.
5 M. Mascini and G. G. Guilbault, Anal. Chem., 49 (1977) 795.
6 IUPAC Analytical Division, Pure Appl. Chem., 48 (1976) 127.

Analytica Chimica Acta, 154 (1983) 41—49
Elsevier Science Publishers B.V., Amsterdam — Printed in The Netherlands

AUTOMATED DETERMINATION OF DETECTION LIMITS AND SELECTIVITY COEFFICIENTS OF ION-SELECTIVE ELECTRODES BY USING A MICROCOMPUTER-CONTROLLED POTENTIOMETRIC SYSTEM

C. E. EFSTATHIOU

Laboratory of Analytical Chemistry, University of Athens, 104 Solonos Str., Athens 144 (Greece)

(Received 14th March 1983)

SUMMARY

The detection limit and the potentiometric selectivity coefficients of ion-selective electrodes are determined automatically with a microcomputer-controlled potentiometric system. Measurements of these parameters for three commercially available electrodes of the liquid membrane type (chloride, nitrate and calcium electrodes) gave results in good agreement with those reported in the literature. The non-linear least-squares fit evaluation of data (potential and activities) and the selection of the appropriate transfer functions are described. The reproducibility of the results is discussed.

Hitherto no significant attempts have been made to automate the evaluation of performance characteristics of ion-selective electrodes (i.s.e.). Many mini- or microcomputer-controlled potentiometric systems have been described but they were designed mainly for direct potentiometry [1—9] or potentiometric titrations [10—14]. A versatile system was described by Martin and Freiser [15] which was capable of obtaining i.s.e. calibration plots automatically and was claimed to be useful for evaluation of selectivity coefficients.

In this paper, a microcomputer-controlled potentiometric system is described which is easily programmed to prepare a series of solutions automatically and measure the potential of an i.s.e. in each of them. These measurements are treated mathematically and the results are presented in terms of detection limit or potentiometric selectivity coefficient. The system was tested for three commercially available, liquid-membrane electrodes and their performance characteristics (detection limits and selectivity coefficients) were found to agree well with literature data.

THEORY

All data obtained for evaluation of detection limits are in the form of pairs (E, a_A) and those for selectivity coefficients in the form of triplets (E, a_A, a_B); where E is the measured potential of the i.s.e. (vs. an appropriate refer-

0003-2670/83/$03.00

ence electrode), and a_A and a_B are the activities of the primary ion A and the secondary ion B, respectively. These data are fitted, by nonlinear regression to equations that fully describe the transfer functions of the transducer (i.s.e.) under the experimental conditions.

For evaluation of the detection limit of an i.s.e., E and a_A were fitted to

$$E = E' + S \ln (a_A + L) \quad (1)$$

where E' is a constant, S is the slope factor (ideally RT/z_AF in the Nernst equation), and L is the detection limit. Equation (1) is arbitrary in nature but offers the following advantages over other more precise functions [16, 17]: (i) it describes acceptably well the actual response of most i.s.e.'s; (ii) L is easily and reproducibly evaluated by nonlinear regression of experimental data; and (iii) L coincides with the IUPAC definition of detection limit [18], which states that the detection limit is taken as "the concentration at the point of intersection of the extrapolated linear segments of a graph of potential vs. the logarithm of concentration". A more rigorous and statistically correct definition of the detection limit which takes into account random errors of measurements has been presented by Midgley [19].

For the determination of the selectivity coefficients, $K^{pot}_{A,B}$, the experimental values of E, a_A, a_B were fitted to a modified Nikolskii—Eisenman equation:

$$E = E' + S \ln [a_A + K^{pot}_{A,B} (a_B)^{z_A/z_B} + L] \quad (2)$$

This equation is also arbitrary because there is some interaction between all terms in the brackets, but it describes well the actual response of the i.s.e.'s tested in the presence of secondary ions B and $K^{pot}_{A,B}$ is easily evaluated from experimental data. The only disadvantage is that L must be previously evaluated for pure solutions of A. Anyhow, L cannot be ignored, especially when selectivity measurements are made with activities of the primary ion A close to the detection limit of the i.s.e. [20].

The constant term E' and the slope factor S are essential characteristics of any i.s.e. The overall stability of response for an i.s.e. is assessed by periodic measurements of these parameters. They are evaluated along with L or $K^{pot}_{A,B}$ and will depend on the actual measurement conditions.

EXPERIMENTAL

Hardware design

The overall configuration of the microcomputer-controlled potentiometric system (microcomputer/electrometer/burette) has been described elsewhere [21].

The following electrodes were tested: (a) the Orion 92-17 chloride-selective electrode (liquid membrane type) in conjunction with the Orion 90-02-00 double-junction Ag/AgCl electrode with the external chamber filled with 0.01 M ammonium fluoride solution; (b) the Orion 92-07 nitrate-selective

electrode in conjunction with the Orion 90-01-00 single-junction Ag/AgCl (0.1 M KCl) electrode; and (c) the Orion 92-20 calcium ion-selective electrode used with the same single-junction reference electrode.

A double-walled 100-ml beaker kept at 25 ± 0.1°C was used as measurement cell with constant magnetic stirring. To reduce diffusion of the delivered solution into the test solution when the burette was not in the delivery mode, the tip of the glass delivery tube was blocked by melting gently in a flame and then filled back to provide an orifice diameter of 0.08—0.1 mm.

Software design

The control program is written in BASIC (16 K EXTENDED BASIC, version 4.1; Microsoft). Double-precision arithmetics were used. The operator inputs the following information: (a) the concentration and ionic strength of the solution of the primary ion to be delivered; (b) the concentration of the secondary ion B (if present), the volume and the ionic strength of the initial solution in the measurement cell; (c) the charges of the primary and secondary ions; (d) the detection limit of the i.s.e. tested (for evaluation of selectivity coefficients); (e) the maximum allowable standard deviation of potential measurements; and (f) the concentration range to be covered and the number, N, of solutions needed to cover this range. The computer calculates the amount of the stock solution needed to yield the concentrations that divide the required concentration range into $(N - 1)$ logarithmically equal subranges.

For one stock solution of the primary ion, the concentration range cannot exceed three decades, but this suffices for the present purposes provided that a nonlinear part of the response curve is included in the concentration range required.

Starting from the more dilute solution, the necessary amounts of stock solution are delivered to yield each concentration level. In each case, the actual activities of the primary and interfering ion are calculated, taking into consideration the actual ionic strength, I, and the charge, z, of ions of interest, using the equation $\log f_x = -0.51\, z_x^2\, I^{1/2}/(1 + I^{1/2})$ for the calculation of the activity coefficients.

The average of ten consecutive potential readings is taken as the potential of the i.s.e., provided that the standard deviation does not exceed a preset value. The acceptance criterion is dropped and the last average is accepted if the standard deviation remains larger than the preset value after five sequences of potential averaging. In this case, a question mark is printed along the potential as a prompt sign.

The experimental data E_i, $a_{A,i}$ for the evaluation of the detection limit, and E_i, $a_{A,i}$, $a_{B,i}$ $(i = 1,2, \ldots, N)$ for the evaluation of the selectivity coefficients, are subjected to nonlinear least-squares regression fitted to Eqns. (1) and (2), respectively (see Appendix). The activity of the secondary ion B varies over a limited range because of the gradual dilution and increase of the ionic strength during each measurement. This variation is usually

ignored when the graphical approach is followed to evaluate the selectivity coefficient but is taken into consideration in the present case.

Measurements

The burette is filled with the appropriate stock solution of the salt of the primary ion A (sodium chloride, sodium nitrate and calcium chloride for the electrodes considered here. Typical concentrations are 0.2—0.5 M). A known volume (typically 25—100 ml) of water or of an aqueous solution of ion B is transferred to the measurement cell for evaluation of the detection limit or of a selectivity coefficient, respectively. Sodium salts of the interfering anions and chloride salts of the interfering cations were used in the latter case.

The electrodes and the burette delivery tip are immersed in the solution and after the initial dialog of the operator with the computer has been completed, delivery of the stock solution and potential measurements are done automatically. The duration of the experiment in minutes is arithmetically about equal to the number of the solutions and measurements required (typically 8—12 min). It may last longer if exceptionally unstable potential readings are encountered.

RESULTS AND DISCUSSION

The electrodes tested were found to obey the described arbitrary transfer functions acceptably well. Average deviations between the experimental and theoretical values, through Eqns. (1) and (2) using the calculated values of E', S, L and $K^{pot}_{A,B}$, were less than 1 mV. The goodness of fit of the experimental data on the calculated transfer functions for the nitrate-selective electrode, in the absence and the presence of bromide as secondary ion, is shown in Fig. 1. The calculated results from the experimental data shown in Fig. 1 are summarized in Table 1.

Reproducibility of the evaluation of performance characteristics

The following observations were made on the reproducibility of the characteristics evaluated for the three i.s.e. tested.

Constant term, E'. The short-term (run-to-run or within-day) reproducibility of E' is generally within ±1 mV. The day-to-day reproducibility is rather inferior with a trend for upward (Ca^{2+}-i.s.e.) or downward (NO^-_3 and Cl^--i.s.e.) drift. The E' values depend strongly on the nature and the activity of the secondary ions, probably because all liquid junction potentials are affected in the absence of ionic strength adjustment buffer.

Slope, S. The short-term reproducibility of S values is generally good (within ±1%) whereas the long-term reproducibility is inferior with a trend toward absolutely smaller values. The presence of interfering ions affects the S values strongly. For instance, with the chloride and nitrate i.s.e.'s, S values decrease when the activity and the interfering action of other anions increase; this decrease can be (in extreme cases) about 40% of the

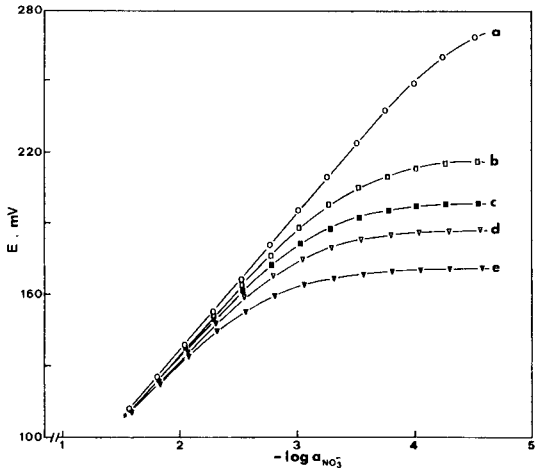

Fig. 1. Potential curves of the nitrate-selective electrode in the absence and the presence of bromide at various activity levels. The solid lines represent the theoretical potential curve, calculated from the data shown in Table 1. (a) No bromide present; (b) a_{Br^-} = 0.00202—0.00236 M; (c) a_{Br^-} = 0.00401—0.00463 M; (d) a_{Br^-} = 0.00988—0.0111 M; (e) a_{Br^-} = 0.0193—0.0213 M.

TABLE 1

Data calculated from the experimental curves shown in Fig. 1

Curve	Range of bromide activity (× 10^{-3} M)	E' (mV)	S (mV/log $a_{NO_3^-}$)	L (M)	$K^{pot}_{NO_3^-, Br^-}$
a	—	17.67	−59.72	2.59 × 10^{-5}	—
b	2.02—2.36	17.26	−59.57	—	0.163
c	4.01—4.63	17.49	−59.59	—	0.181
d	9.88—11.1	19.77	−58.21	—	0.111
e	19.3—21.3	22.03	−56.82	—	0.108

original S value for pure primary ion solutions. In contrast, with the calcium-i.s.e., increases up to 30% were noted.

Detection limit, L. The short-term reproducibility of L values, in the worst case, can amount to ±50%. During the evaluation of L, it is essential to avoid contamination of the initial solution in the measurement cell with the stock solution of the primary ion to be delivered; accordingly, the burette tip was immersed in the solution just before delivery of the stock solution was initiated. The long-term reproducibility of L shows a clear upward drift.

The L values for the three electrodes tested lay within the following ranges: (a) chloride-i.s.e., 3 × 10^{-5}—5 × 10^{-5} M; (b) nitrate-i.s.e., 3 × 10^{-5}—1.5 × 10^{-4} M; (c) calcium-i.s.e., 1.2 × 10^{-5}—3 × 10^{-5} M.

Ten consecutive measurements of E', S and L for the nitrate-i.s.e. (approximately 3 weeks old) gave the following average values (± standard deviation):

E' = 21.45 ± 0.81 mV, S = −57.02 ± 0.25 mV/activity decade, L = (1.08 ± 0.18) × 10^{-4} M.

Selectivity coefficients, $K^{pot}_{A,B}$. No significant difference was noticed between the short-term and long-term reproducibility of $K^{pot}_{A,B}$ values, unless the membrane of the i.s.e. had been poisoned by strong interfering ions. The reproducibility of $K^{pot}_{A,B}$ values, in terms of relative standard deviation, ranged between 1 and 30%, the extreme variations being observed in cases of very weak or very strong interfering actions; in the former case because the slightest fluctuation of the potential reading affects the final results and in the latter probably because of poisoning of the electrode membrane.

The activity level of secondary ion B affects the $K^{pot}_{A,B}$ values, especially in the case of strong interference, as has previously been noted [22—25]. Measurements of $K^{pot}_{A,B}$ values with extremely interfering species, such as perchlorate and tetraphenylborate for the anionic i.s.e.'s (expected $K^{pot}_{A,B}$ values of 100—1000) failed even at low activity levels of the secondary ions (10^{-6}—10^{-5} M) because of continuous potential drift.

The calculated selectivity coefficients for the three i.s.e.'s tested at various activities of interfering ion, are shown in Table 2, compared with those reported in the literature.

TABLE 2

Potentiometric selectivity coefficients determined automatically

Electrode	Interfering ion B	$K^{pot}_{A,B}$	Literature values[b]
Chloride	I^-	15.3 ± 1.6 (3.05)/5.3 ± 0.3 (3.57) 2.6 ± 0.3 (4.05)	17, 4.4—26.7, 6—23.9
	Br^-	1.86 ± 0.04 (2.58)/1.49 ± 0.06 (3.05) 1.50 ± 0.06 (3.57)/1.18 ± 0.02 (4.05)	1.6, 1.72—3.73, 2.58—3.42
	SCN^-	2.5 ± 0.7 (3.05)/1.04 ± 0.04 (3.57) 0.92 ± 0.07 (4.05)	—
	NO_3^-	1.40 ± 0.01 (2.58)/0.91 ± 0.03 (3.05) 0.57 ± 0.00 (3.57)/0.56 ± 0.00 (4.05)	4.2, 1.68—5.89, 2.62—4.34
	CH_3COO^-	0.27 ± 0.02 (2.07)/0.25 ± 0.03 (2.58) 0.21 ± 0.01 (3.05)/0.24 ± 0.04 (3.57)	0.32
	SO_4^{2-}	0.11 ± 0.02 (2.02)/0.100 ± 0.004 (2.34) 0.099 ± 0.012 (2.76)	0.14
Nitrate	I^-	10.6 ± 2.1 (3.34)/7.5 ± 0.8 (3.74) 6.0 ± 1.7 (4.03)	20, 2.7—22.2, 3.2—15.7
	ClO_3^-	1.58 ± 0.03 (3.04)/1.55 ± 0.13 (3.34) 1.34 ± 0.16 (3.74)/1.5 ± 0.5 (4.03)	1.14—1.21
	Br^-	0.113 ± 0.003 (1.78)/0.104 ± 0.007 (2.06) 0.125 ± 0.003 (2.36)/0.143 ± 0.017 (2.75)	0.09—0.24, 0.09—0.13
	Cl^-	(5.8 ± 0.5) × 10^{-3} (0.86)/(5.2 ± 0.2) × 10^{-3} (1.13) (5.3 ± 0.2) × 10^{-3} (1.40)/(6.0 ± 0.1) × 10^{-3} (1.78)	4 × 10^{-3}—6 × 10^{-3}
	SO_4^{2-}	(3.2 ± 0.4) × 10^{-4} (1.88)/(2.5 ± 0.5) × 10^{-4} (2.07) (2.8 ± 1.6) × 10^{-4} (2.34)	—
Calcium(II)	Zn^{2+}	1.4 ± 0.3 (2.82)/1.9 ± 0.4 (3.25) 3.2 ± 0.4 (3.75)	3.2
	Fe^{2+}	0.69 ± 0.09 (2.82)/0.81 ± 0.04 (3.25) 1.10 ± 0.12 (3.75)	0.80
	Mg^{2+}	0.032 ± 0.001 (1.88)/0.028 ± 0.003 (2.12) 0.026 ± 0.003 (2.33)/0.025 ± 0.001 (2.56) 0.028 ± 0.001 (2.90)	0.01—0.04

TABLE 2 (continued)

Electrode	Interfering ion B	$K^{pot}_{A,B}$	Literature values[b]
	Sr^{2+}	0.020 ± 0.002 (2.12)/0.024 ± 0.001 (2.33) 0.026 ± 0.003 (2.56)/0.025 ± 0.001 (2.90)	0.017—0.02, 0.07
	Ba^{2+}	0.022 ± 0.003 (1.88)/0.019 ± 0.001 (2.12) 0.015 ± 0.000 (2.33)/0.012 ± 0.000 (2.56) $(9.8 \pm 0.7) \times 10^{-3}$ (2.90)	0.01
	Na^{+}	$(3.2 \pm 0.6) \times 10^{-3}$ (1.14)/$(2.5 \pm 0.3) \times 10^{-3}$ (1.63) $(1.8 \pm 0.1) \times 10^{-3}$ (2.08)/$(1.6 \pm 0.1) \times 10^{-3}$ (2.60)	$(1.6—2.0) \times 10^{-3}$

[a]Average and standard deviation of 3 or 4 consecutive measurements; $-\log a_B$ in parentheses represents the mean activity level of secondary ion B tested.
[b]Values taken from [24] and [26]. Commas separate values from individual sources cited.

Conclusions

The procedure described for the automated determination of the detection limit and the selectivity coefficients should be useful in the development of new types of ion-selective electrodes because it allows fast and reliable comparison of many i.s.e.'s under the same experimental conditions.

The control programs may be improved in various respects (e.g., statistic weighting factors may be included) and more appropriate transfer functions may be tested. Also novel techniques for the determination of selectivity characteristics may be used [23]. Under development are control programs for the evaluation of other quality characteristics of i.s.e.'s, such as pH—potential and temperature—potential profiles, short-term and long-term potential reproducibility.

APPENDIX

Fitting of data to Eqn. (1)

The statistically correct values of E', S and L should satisfy the least-squares criterion:

$$G(E', S, L) = \sum_{i=1}^{N} [E_i - E' - S \ln(a_{A,i} + L)]^2 = \text{minimum} \quad \text{(A1)}$$

Evaluation of $G(E', S, L)$ gives

$$G(E', S, L) = E_{(2)} + NE'^2 + S^2 L_{(2)} - 2E'E_{(1)} - 2SP + 2SE'L_{(1)} \quad \text{(A2)}$$

where $E_{(1)} = \sum_{i=1}^{N} E_i$, $E_{(2)} = \sum_{i=1}^{N} E_i^2$, $L_{(1)} = \sum_{i=1}^{N} \ln(a_{A,i} + L)$, $L_{(2)} = \sum_{i=1}^{N} [\ln(a_{A,i} + L)]^2$,

and $P = \sum_{i=1}^{N} E_i \ln(a_{A,i} + L)$

When $G(E', S, L)$ is at a minimum, then

$$\partial G(E', S, L)/\partial E' = 2NE' - 2E_{(1)} + 2SL_{(1)} = 0 \quad \text{(A3)}$$

$$\partial G(E', S, L)/\partial S = 2SL_{(2)} - 2P + 2E'L_{(1)} = 0 \tag{A4}$$

$$\partial G(E', S, L)/\partial L = S^2(\partial L_{(2)}/\partial L) - 2S(\partial P/\partial L) + 2SE'(\partial L_{(1)}/\partial L) = 0 \tag{A5}$$

From Eqn. (A5), assuming that $S \neq 0$, and for simplicity writing Q_i for $(a_{A,i} + L)$, then

$$S \sum_{i=1}^{N} [(\ln Q_i)/Q_i] - \sum_{i=1}^{N} (E_i/Q_i) + E' \sum_{i=1}^{N} Q_i^{-1} = 0 \tag{A6}$$

Solving the system of Eqns. (A3) and (A4) then gives

$$E = [\sum_{i=1}^{N} E_i \ln Q_i \sum_{i=1}^{N} \ln Q_i - \sum_{i=1}^{N} E_i \sum_{i=1}^{N} (\ln Q_i)^2]/[(\sum_{i=1}^{N} \ln Q_i)^2 - N \sum_{i=1}^{N} (\ln Q_i^2)] \tag{A7}$$

and

$$S = [\sum_{i=1}^{N} \ln Q_i \sum_{i=1}^{N} E_i - N \sum_{i=1}^{N} E_i \ln Q_i]/[(\sum_{i=1}^{N} \ln Q_i)^2 - N \sum_{i=1}^{N} (\ln Q_i)^2] \tag{A8}$$

Therefore Eqn. (A6) is solely a function of L with $a_{A,1}, a_{A,2}, \ldots, a_{A,N}$ and $E_1, E_2, \ldots, E_N$ as parameters. Equation (A6) is solved numerically by using the Newton–Raphson iterative procedure [27]. Starting with an initial guess value of L and L_0, a new one, L_1, is calculated, and generally, L_{j+1} is calculated from L_j from $L_{j+1} = L_j - Y(L_j)/Y'(L_j)$, where $Y(L_j)$ is the arithmetic value of the left term of Eqn. (A6) for $L = L_j$, and $Y'(L_j)$ is the arithmetic value of the first derivative of this term with respect to L, for $L = L_j$. The first derivative is easily approximated numerically from

$$Y'(L_j) = [Y(L_j + 0.01\,L_j) - Y(L_j)]/0.01\,L_j$$

The iterations are continued until the following condition is met: $100|(L_{j+1} - L_j)/L_j| \leqslant 0.01$. Thus, L is obtained with an accuracy of about 0.01% which is better than is actually needed.

Equations (A7) and (A8) are used to calculate E' and S.

Fitting of data to Eqn. (2)

The procedure is the same as that outlined above. In this case, L must be known and is treated as a parameter along with the experimental data $(E_1, a_{A,1}, a_{B,1})$, $(E_2, a_{A,2}, a_{B,2}), \ldots, (E_N, a_{A,N}, a_{B,N})$. The respective G function, analogous to Eqn. (A1) is

$$G(E', S, K_{A,B}^{pot}) = \sum_{i=1}^{N} \{E_i - E' - S \ln [a_{A,i} + K_{A,B}^{pot} (a_{B,i})^{z_A/z_B} + L]\}^2 \tag{A9}$$

The equation analogous to Eqn. (A6) is

$$\partial G(E', S, K_{A,B}^{pot})/\partial K_{A,B}^{pot} = S \sum_{i=1}^{N} \{[(a_{B,i})^{z_A/z_B} \ln F_i]/F_i\} - \sum_{i=1}^{N} \{[E_i (a_{B,i})^{z_A/z_B}]/F_i\}$$

$$+ E' \sum_{i=1}^{N} [(a_{B,i})^{z_A/z_B}/F_i] = 0 \tag{A10}$$

where $F_i = a_{A,i} + K_{A,B}^{pot} (a_{B,i})^{z_A/z_B} + L$

$$E' = [\sum_{i=1}^{N} E_i \ln F_i \sum_{i=1}^{N} \ln F_i - \sum_{i=1}^{N} E_i \sum_{i=1}^{N} (\ln F_i)^2]/[(\sum_{i=1}^{N} \ln F_i)^2 - N \sum_{i=1}^{N} (\ln F_i)^2] \tag{A11}$$

$$S = [\sum_{i=1}^{N} \ln F_i \sum_{i=1}^{N} E_i - N \sum_{i=1}^{N} E_i \ln F_i]/[(\sum_{i=1}^{N} \ln F_i)^2 - N \sum_{i=1}^{N} (\ln F_i)^2] \tag{A12}$$

The same iterative procedure is used to solve Eqn. (A10) for $K^{pot}_{A,B}$. Equations (A11) and (A12) are used to calculate E' and S.

The author thanks T. P. Hadjiioannou for his valuable suggestions. This research was financially supported by the Greek National Institute of Research and by the University of Athens.

REFERENCES

1 I. Sekerka and J. F. Lechner, Anal. Lett., 7 (6) (1974) 399.
2 I. Sekerka and J. F. Lechner, Anal. Lett., 7 (7) (1974) 463.
3 J. J. Zipper, B. Fleet and S. P. Perone, Anal. Chem., 46 (1974) 2111.
4 P. D. Gaarenstroom, J. C. English, S. P. Perone and J. W. Bixter, Anal. Chem., 50 (1978) 811.
5 J. M. Ariano and W. F. Gutknecht, Anal. Chem., 48 (1976) 281.
6 L. P. Rigdon, G. J. Moody and J. W. Frazer, Anal. Chem., 50 (1978) 465.
7 J. Slanina, F. Bakker, J. J. Möls, J. E. Ordelman and A. G. M. Bruyn-Hes, Anal. Chim. Acta, 112 (1979) 45.
8 L. P. Rigdon, C. L. Pomernacki, D. J. Balaban and J. W. Frazer, Anal. Chim. Acta, 112 (1979) 397.
9 A. Gustavsson and P. Nylén, Anal. Chim. Acta, 125 (1981) 65.
10 D. Betteridge, E. L. Dagless, P. David, D. R. Deans, G. E. Penketh and P. Shawcross, Analyst, 101 (1976) 409.
11 J. W. Frazer, W. Selig and L. P. Rigdon, Anal. Chem., 49 (1977) 1250.
12 N. Busch, P. Freyer and H. Szameit, Anal. Chem., 50 (1978) 2166.
13 A. H. B. Wu and H. V. Malmstadt, Anal. Chem., 50 (1978) 2090.
14 O. Siroky, R. D. Werder, R. W. Arndt and P. Frueh, Fresenius Z. Anal. Chem., 297 (1979) 126.
15 C. R. Martin and H. Freiser, Anal. Chem., 51 (1979) 803.
16 D. Midgley, Anal. Chem., 49 (1977) 1211.
17 N. Kamo, N. Hazemoto and Y. Kobatake, Talanta, 24 (1977) 803.
18 International Union of Pure and Applied Chemistry, Pure Appl. Chem., 48 (1976) 127.
19 D. Midgley, Analyst, 104 (1979) 248.
20 E. Pungor and K. Tóth, Anal. Chim. Acta, 47 (1969) 291.
21 C. E. Efstathiou and T. P. Hadjiioannou, Talanta, 30 (1983) 145.
22 A. Hulanicki and Z. Augustowska, Anal. Chim. Acta, 78 (1975) 261.
23 M. S. Okunev, N. V. Khirova and O. I. Kornienko, Zh. Anal. Khim, 37 (1) (1982) 5.
24 K. Srinivasan and G. A. Rechnitz, Anal. Chem., 41 (1969) 1203.
25 R. P. Buck, Anal. Chim. Acta, 73 (1974) 321.
26 G. J. Moody and J. D. R. Thomas, Selective Ion-sensitive Electrodes, Merrow, Watford, 1970, p. 21.
27 J. B. Dence, Mathematical Techniques in Chemistry, Wiley, New York, 1975, p. 54.

Analytica Chimica Acta, 154 (1983) 51—60
Elsevier Science Publishers B.V., Amsterdam — Printed in The Netherlands

DETERMINATION OF SELECTIVITY COEFFICIENTS OF ION-SELECTIVE ELECTRODES BY MEANS OF LINEARIZED MULTIPLE STANDARD ADDITION TECHNIQUES

CARLO MACCÀ* and MIROSLAV ČAKRT[a]
Istituto di Chimica Analitica dell'Università, Via Marzolo 1, 35100 Padova (Italy)
(Received 16th March 1983)

SUMMARY

The application of multiple known-addition or dilution techniques to the evaluation of potentiometric selectivity coefficients of ion-selective electrodes is proposed. The validity of the common form of the Nikolskii—Eisenman equation is assumed and experimental data are processed by using Gran-type linear functions. Six possible methods are derived which make it possible to work under bi-ionic conditions for the electrode response. Optimization of the experimental procedures is discussed.

No ion-selective electrode responds exclusively to the ion which it is designed to measure. The ability of an ion-selective electrode to distinguish between the primary ion A and an interfering ion B in the same solution is defined [1] by its potentiometric selectivity coefficient, $k^{pot}_{A,B}$, which follows from the Nikolskii—Eisenman equation. Several experimental methods have been described [2—5] for the evaluation of selectivity coefficients. The methods can be classified in two categories: (a) separate solution methods, involving the measurement of the electrode response in two solutions, one containing the primary ion and the other the interfering ion; (b) mixed solution methods, with measurements of the electrode potential in solutions containing both ions. Whilst the first approach is considered as admissible only when the mixed solution method is not feasible, the fixed interference method involving e.m.f. measurements on solutions of constant level of interference and varying activity of the primary ion has been sanctioned by IUPAC [1]. However, changes of the surface of the electrode membrane in that part of the measurements, in which high ratios of concentration of the interfering ion to that of the primary ion are needed, can lower the reliability of the experimental values of selectivity coefficients so determined.

The aim of the present work is to propose a method for the determination of selectivity coefficients under experimental conditions such that it can be assumed that the membrane of the investigated electrode is not seriously

[a]On leave from the Faculty of Chemical Technology of Slovak Technical University, Bratislava, Czechoslovakia.

0003-2670/83/$03.00

affected by the presence of the interfering ion. Consequently, the e.m.f. values are measured in mixed solutions with a concentration ratio between the interfering and the primary ions high enough to have a measurable effect on the potential response, but not so high as to cause any modification in the membrane. Further, the concentration range of the primary ion is kept narrow enough to prevent any concentration-dependent change in the electrode behaviour. The results of the measurements are treated by linear equations that allow both a simple calculation of the selectivity coefficient and a direct check on the validity of the measurements. This approach leads to six different procedures. Their convenience depends on the particular characteristics of the system under study, namely on the value of the selectivity coefficient.

THEORY

The methods described below are based on the assumption that the measured electrode potential in the presence of both the primary ion A and an interfering ion B can be expressed by the equation

$$E = E^* + S \log \{ [A] + k^{pot}_{A,B} [B]^{z_A/z_B} \} \quad (1)$$

where E is the electrode potential as measured vs. an external reference electrode, E^* is a constant that includes the standard electrode potential, the junction potential and activity coefficient terms, S is the slope of the electrode potential response, [A] and [B] are the concentrations in the tested solution, and z_A and z_B are the charges of the ions. The experimental procedures consist essentially of stepwise additions either of a primary or interfering ion solution or of a mixed solution of ions A and B, into a solution containing either a mixture or one of the two kinds of ions. The corresponding mathematical treatment of data is related to the potentiometric multiple-addition method suggested earlier [6, 7] for the application of Gran's second method to the known addition procedure. As the response slope S is necessary in the calculations, its value must be determined experimentally for the same concentration range of the primary ion as that to be used in evaluation of the selectivity coefficient. A convenient method of determining the slope may involve readings of the potential during stepwise addition or stepwise dilution of primary ion solutions in the absence of interfering ions.

Method I. Multiple additions of primary ion solution

A solution of the primary ion A at the concentration C_A is added stepwise to a known initial volume V^0 of a solution of the interfering ion B at the concentration C_B. Both instantaneous concentrations of A and B vary during this procedure; [A] varies on additions of the solution of A, and [B] on dilution of the original solution. When a volume V has been added, the resulting concentrations are

$$[A] = C_A \; V/(V^0 + V) \tag{2}$$

$$[B] = C_B \; V^0/(V^0 + V) \tag{3}$$

Substitution of Eqns. (2) and (3) in Eqn. (1) and rearrangement gives

$$(V^0 + V)\, 10^{E/S} = 10^{E^*/S} \left[C_A \; V + k^{pot}_{A,B} \; (C_B \; V^0)^{z_A/z_B} \; (V^0 + V)^{(z_B - z_A)/z_B}\right] \tag{4}$$

If $z_A = z_B$, Eqn. (4) can be simplified to give

$$(V^0 + V)\, 10^{E/S} = 10^{E^*/S} \left[C_A \; V + k^{pot}_{A,B} \; C_B \; V^0\right] \tag{5}$$

It follows from Eqn. (5) that if $k^{pot}_{A,B}$, E^*, and S are constant, both sides of this equation represent linear functions of the added volume V. As the left side contains only experimentally accessible data, the values of the function

$$\phi = (V^0 + V)\, 10^{E/S} \tag{6}$$

can be calculated and plotted against V. A straight line is obtained, which on extrapolation intercepts the abscissa axis at the point where $\phi = 0$ and $V = V_x$. When $\phi = 0$, then $C_A \; V_x + k^{pot}_{A,B} \; C_B \; V^0 = 0$ and the selectivity coefficient can be calculated from the equation

$$k^{pot}_{A,B} = -C_A \; V_x / C_B \; V^0 \tag{7}$$

Although the function ϕ vs. V is linear only when $z_A = z_B$, according to Eqn. (4) one can obtain practically linear plots even when $z_A \neq z_B$, if it can be assumed that the maximum added volume remains negligible with respect to the initial volume V^0. In this case, the selectivity coefficient can be estimated by means of the expression

$$k^{pot}_{A,B} = -C_A \; V_x / C_B{}^{z_A/z_B} \; V^0 \tag{8}$$

The condition for linearity is more easily met when $z_B > z_A$.

Method II. Fixed interference method

A solution containing both A and B at concentrations C_A and C_B is added stepwise to the original volume of the solution of B with the same concentration C_B. In this case, the concentration of B is constant during the measurement procedure, $[B] = C_B$, and this method can be considered as a true "fixed interference method". [A] is still given by Eqn. (2). Substitution into Eqn. (1) gives the equation

$$(V^0 + V)\, 10^{E/S} = 10^{E^*/S} \left[k^{pot}_{A,B} \; C_B{}^{z_A/z_B} \; V^0 + (C_A + k^{pot}_{A,B} \; C_B{}^{z_A/z_B})\, V\right] \tag{9}$$

according to which the function ϕ vs. V is linear regardless of the ratio z_A/z_B. The value of the selectivity coefficient is calculated from the experimentally determined value of $V = V_x$ (for $\phi = 0$) as

$$k^{pot}_{A,B} = -C_A \; V_x / C_B{}^{z_A/z_B} \; (V^0 + V_x) \tag{10}$$

Method III. Multiple additions of interfering ion solutions

A solution of B is added incrementally to the solution containing A. The resulting concentrations, both varying during the measurement procedure, are

$$[A] = C_A V^0/(V^0 + V) \tag{11}$$

$$[B] = C_B V/(V^0 + V) \tag{12}$$

Combination of Eqns. (11), (12), and (1) gives

$$(V^0 + V)\,10^{E/S} = 10^{E^*/S}\,[C_A V^0 + k^{pot}_{A,B}\,(C_B V)^{z_A/z_B}\,(V^0 + V)^{(z_B - z_A)/z_B}] \tag{13}$$

When $z_A = z_B$, the right-hand side of Eqn. (13) becomes a linear function of the added volume and the value of the selectivity coefficient can be calculated by using the value of V_x found experimentally by linear extrapolation to $\phi = 0$:

$$k^{pot}_{A,B} = -C_A V^0/C_B V_x \tag{14}$$

Method IV. Fixed primary ion concentration

The procedure of method III can be modified to provide a fixed primary ion concentration during the measurements, $[A] = C_A$, by adding a mixed solution containing not only B but also A at the same concentration C_A. The resulting concentration of B is given by Eqn. (12). Substitution in Eqn. (1) gives the equation

$$(V^0 + V)\,10^{E/S} = 10^{E^*/S}\,[C_A\,(V^0 + V) + k^{pot}_{A,B}\,(C_B V)^{z_A/z_B}\,(V^0 + V)^{(z_B - z_A)/z_B}] \tag{15}$$

the right-hand side of which is linear (in contrast to the symmetric case of method II) only when $z_A = z_B$. The selectivity coefficient in this case can be evaluated from

$$k^{pot}_{A,B} = -C_A\,(V^0 + V_x)/C_B V_x \tag{16}$$

Methods III and IV can be applied when $z_B > z_A$, if the maximum added volume is negligible with respect to the initial volume V^0. V_x is obtained on extrapolation of ϕ vs. V^{z_A/z_B}, and the selectivity coefficient can be estimated from the expression

$$k^{pot}_{A,B} = -C_A\,(V^0/C_B V_x)^{z_A/z_B} \tag{17}$$

Method V. Stepwise dilution of primary ion solution at fixed interference

Two more possibilities have to be considered for the sake of completeness. Linear relationships, which are applicable even when $z_A \neq z_B$, are obtained when a solution of B is added to the mixed solution of both ions A and B with B at the same concentration in both solutions. Then, $[B] = C_B$ and [A] is given by Eqn. (11). The selectivity coefficient is calculated from the experimental data as

$$k^{pot}_{A,B} = -C_A V^0/C_B{}^{z_A/z_B}\,(V^0 + V_x) \tag{18}$$

Method VI. Stepwise dilution of interfering ion solution at fixed primary ion concentration

A fixed primary ion concentration method that is applicable only when $z_A = z_B$ is obtained when the solution of primary ion is added to the mixed solution of both ions, with A at the same concentration in both solutions. Then [A] = C_A, and [B] is given by Eqn. (3). One obtains

$$k^{pot}_{A,B} = -C_A\ (V^0 + V_x)/C_B\, V^0 \tag{19}$$

DISCUSSION

It is generally accepted that a mixed solution approach is to be preferred for the evaluation of selectivity coefficients, as it corresponds better to the real situation in which the electrodes are used. However, the mixed solution methods currently used do not always fulfil this demand. For instance, the application of the recommended "fixed interference method" [1], Fig. 1, may be considered. Selectivity coefficients are evaluated by extrapolating the linear branches of the response curve, which correspond to extreme ratios [A]/[B] where the responses are determined by only one of the two ions. Only experimental data corresponding to log [A] values lower than point a and higher than point c are used. When the effect of the interfering ion predominates, the electrode response mechanism can be seriously altered, and the reliability of the measurements can be affected similarly as in the separate solutions method. Moreover, as the concentration of A has to be varied over several decades in a single experiment, possible variations of slope S can affect results, and investigation of the dependence of the selectivity coefficients on concentration is made difficult. The part of the response curve between a and c, that represents the true bi-ionic response range where the selectivity coefficient is of practical importance, is apparently neglected.

Even the bi-ionic response range has to be narrowed to obtain the useful working interval, in order to avoid any attack by the interferent on the electrode surface that would modify its response behaviour. For example, the metathetic reaction of an isovalent ($z_A = z_B$) interfering ion with the electroactive component of a precipitate-based electrode membrane changes the response characteristics of the electrode if the concentration ratio [B]/[A] rises above a level dictated by the quotient of the solubility products of the corresponding precipitates, $K_{so}(B)/K_{so}(A)$, which according to the accepted theory of the response mechanism is equal to the reciprocal value of the selectivity coefficient [8]. Hence the interference potential [9]

$$\Delta E = S \log \{1 + k^{pot}_{A,B}\ [B]^{z_A/z_B}/[A]\} \tag{20}$$

must not exceed the absolute value of 17.8 mV. In general, though the maximum allowable [B]/[A] ratio depends on the mechanism of the potential-generating process, it seems reasonable to consider $17.8/z_A$ mV as the maximum admissible interference potential. This corresponds to the situation

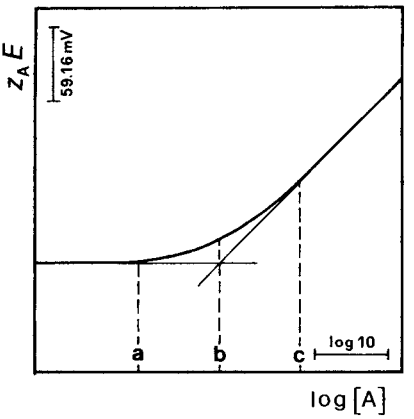

Fig. 1. Theoretical plot of the electrode response in the "fixed interference" method: a, lower limit of bi-ionic response; b, lower limit of the useful working range for the determination of the selectivity coefficient; c, higher limit of bi-ionic response.

at the point b in Fig. 1, where the response curve differs from the extrapolated Nernstian dependence by 17.8 mV.

On the other side, the minimum but still significant value of the interference potential, corresponding to a situation where the response just starts to deviate from the Nernstian behaviour, depends on the reproducibility of the electrode potential measurements; it can be arbitrarily taken as ±1 mV (point c, Fig. 1).

The known-addition or dilution methods described above, in contrast to the extrapolation methods, make it possible to restrict within the true bi-ionic response range defined above, the variation of the concentration either of the primary or of the interfering ion (the other one being at a constant or nearly constant concentration) in a single experiment for the determination of a selectivity coefficient. If $k^{pot}_{A,B}$ is constant in this range (i.e., the Nikolskii—Eisenman equation is obeyed), its value can be obtained by graphical or least-squares extrapolation of ϕ; if it is not, an apparent selectivity coefficient could be calculated from each step of the procedure.

Working procedures have to be optimized by adjusting the values of the experimental parameters, namely C_A, C_B, V^0, and the variation range of the experimental master variable V (i.e., the minimum and maximum added volumes, V_{min} and V_{max}, respectively), in order that the measurements cover the useful bi-ionic response range, the added volume V can be reliably measured, the ratio V/V^0 does not exceed a reasonable limit, and the resulting value of $-V_x$ is compatible with the reliability of measurements of V. Likewise, the choice of appropriate volumetric apparatus should be based on the expected value of $-V_x$ and on the necessary V range.

Preliminarily, an approximate value of the selectivity coefficient has to be evaluated on the basis either of theoretical predictions or of rough

measurements. Further considerations are simplified by expressing volumes as ratios to the initial volume V^0 and combining the other experimental parameters in the dimensionless parameter P:

$$P = k_{A,B}^{pot} C_B^{z_A/z_B}/C_A \quad (21)$$

On the assumption that values of selectivity coefficients range from 10^{-6} to 10^6 and that the ratio of reliably maintainable concentrations is restricted between 10^3 and 10^{-3} M, the significant values of P are between 10^{-3} and 10^3. The relationships between the experimental variables and P are summarized in Table 1. The expressions showing the dependence of the interference potential ΔE on the ratio between initial and added volume, V/V^0 (which for simplicity is indicated as v in these formulae), are obtained by substituting for concentrations in Eqn. (20) the expressions pertaining to each method. The equations for methods II and IV of course are valid for any z_A/z_B ratio, while the others are valid only when $z_A = z_B$, or when $V \gg V^0$ (i.e., whenever ϕ is a linear function of V).

The influence of P on the variation of the interference potential during the experimental procedure of method I is illustrated in Fig. 2. Horizontal

TABLE 1

Relationships between the experimental variables and parameters of known-addition or dilution methods for the determination of selectivity coefficients[a]

Method	$10^{\Delta E/S}$	$-V_x/V^0$	Method	$10^{\Delta E/S}$	$-V_x/V^0$
I	$1 + P/v$	P	IV	$1 + Pv/(1 + v)$	$1/(1 + P)$
II	$1 + P(1 + v)/v$	$P/(1 + P)$	V	$1 + P(1 + v)$	$(1 + P)/P$
III	$1 + Pv$	$1/P$	VI	$1 + P/(1 + v)$	$1 + P$

[a] $v = V/V^0$.

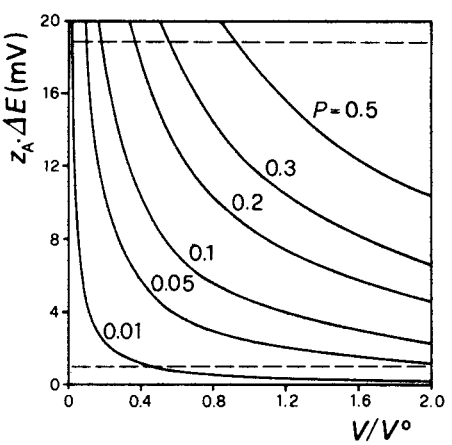

Fig. 2. Dependence of the interference potential on the added volume to initial volume ratio for method I. Dashed horizontal lines mark the limits of the useful bi-ionic response range.

dashed lines at 1 and 17.8 mV locate on each graph the values of V_{min}/V^0 and of V_{max}/V^0, respectively. It appears that P values lower than 0.1 to 0.2 have to be chosen in order to avoid excessive V/V^0 ratios (it is not necessary, though advisable, to cover the whole allowable ΔE range). Very low values of P are admissible only if microvolumetric apparatus is available. Of course, as the initial solution does not contain the primary ion, the electrode under investigation should not be immersed until V_{min} is added, to avoid meaningless readings of potential.

The variation of the interference potential ΔE with V/V^0 at a given value of P for all the proposed procedures is shown for comparison in Fig. 3.

The dependences on P of $-V_x/V^0$ and of the values of V/V^0 for which $z_A\ \Delta E = 17.8$ mV (corresponding to V_{min} for methods I, II, and VI, and to V_{max} for methods III, IV, and V) are shown in Figs. 4 and 5, respectively. The values of V/V^0 for which $z_A\ \Delta E = 1$ mV are simply obtained by shifting the corresponding curves horizontally by $\log P = -1.40$. These figures allow a direct comparison of working conditions for the proposed methods, and show the complementary character of methods I—III, II—IV, and V—VI. More important, the optimal working conditions for each method can be deduced. As an example, Fig. 6, from which V_{min} and V_{max} can be obtained together with V_x for any chosen value of P, shows that method II can be used only with P values lower than about 0.04; in the useful P range $-V_x$ is equal to V_{min}.

As an example of application of the proposed methods, the results obtained in a set of experiments for the determination of $k^{pot}_{Br,Cl}$ of a bromide electrode (Radiometer F1022) by method I are represented in Fig. 7. The

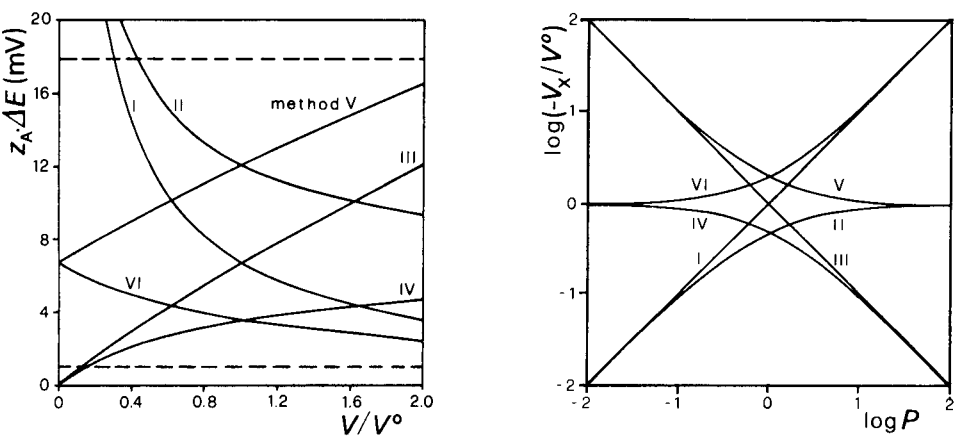

Fig. 3. Dependence of the interference potential on the ratio of added volume to initial volume; $P = 0.3$.

Fig. 4. Dependence on the parameter P of the intercept volume V_x, i.e., the volume for which ϕ extrapolates to 0.

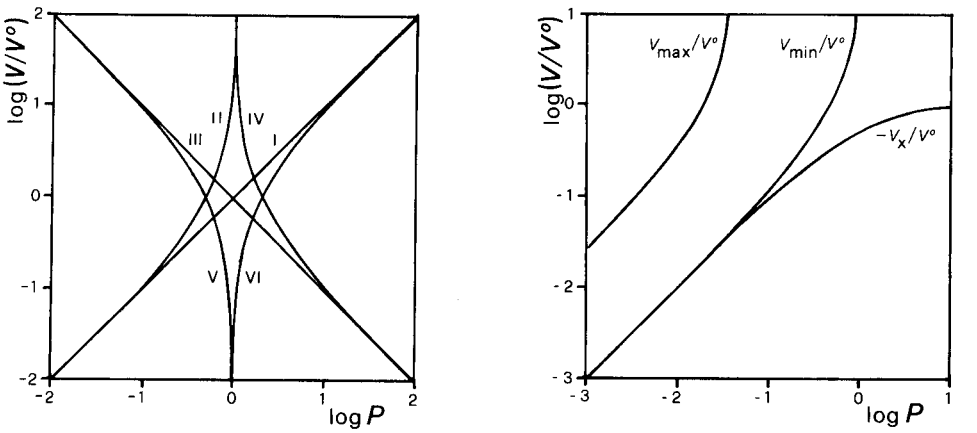

Fig. 5. Dependence on the parameter P of the added volume corresponding to the maximum admissible interference potential ($z_A\Delta E$ = 17.8 mV).

Fig. 6. Plot for the choice of optimal working conditions for method II.

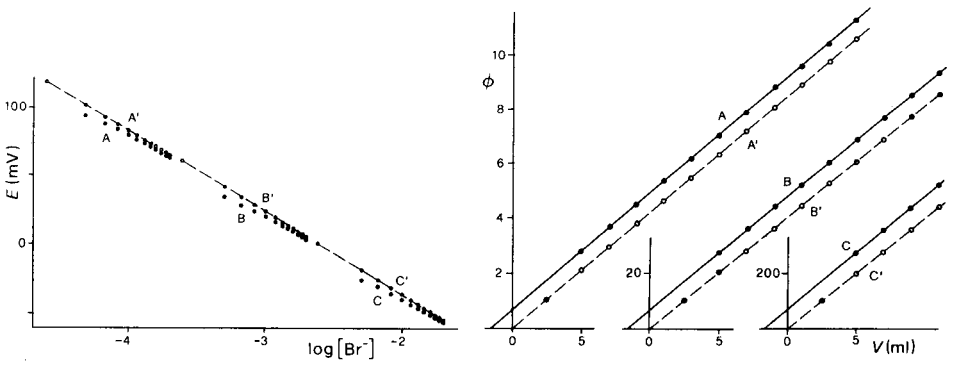

Fig. 7. Determination of $k^{pot}_{Br,Cl}$ of a bromide-selective electrode (Radiometer F1022) at 25°C (μ = 1.0 M (KNO_3), V^0 = 100 ml.) C_{Br}: (A, A') 1.00 × 10^{-3} M; (B, B') 1.00 × 10^{-2} M; (C, C') 1.00 × 10^{-1} M. C_{Cl}: (A) 1.00 × 10^{-2} M; (B) 1.00 × 10^{-1} M; (C) 1.00 M; (A', B', C') 0. $k^{pot}_{Br,Cl}$: (A) 1.60 × 10^{-3}; (B) 1.67 × 10^{-3}; (C) 1.65 × 10^{-3}. (Higher points in the B, B', C, C' ϕ plots have been omitted for scale requirements.)

measurements were made at three different initial values of interfering ion concentration C_{Cl}. For each C_{Cl}, a separate determination of the slope S was made by means of an identical series of additions of the primary ion solution to the supporting electrolyte in the absence of the interferent. Linear ϕ vs. V plots prove that response characteristics and $k^{pot}_{A,B}$ are constant (i.e., the Nikolskii—Eisenman equation is obeyed) in the concentration range of a single experiment. Plots of ϕ, also from the data for the determination of S, provide checks that supporting electrolyte interferences are absent (V_x = 0) and that experimental conditions and electrode response characteristics are

well reproduced in both series of additions (parallel straight lines). For the electrode under examination, $k^{pot}_{Br,Cl}$ was found to be constant in the whole experimental concentration range ($[Br^-] = 10^{-4.5}$—$10^{-1.5}$ M; $k^{pot}_{Br,Cl} = 1.64 \times 10^{-3}$).

Conclusions

The accurate determination of selectivity coefficients should be possible in principle in a very wide variety of cases by choosing the most appropriate method among those here described. The "continuous" procedures of methods I—IV are easily applicable with automatic apparatus, and directly utilizable with microcomputerized titrators that can handle Gran functions. Methods I and II are suitable for correcting the results of measurements of the primary ion by the multiple standard addition method [6] for the presence of a known amount of interferent. Methods V and VI are more conveniently applied with discontinuous procedures, in order to attain the high V^0/V ratios needed.

The experimental cooperation of Dr. Emanuela Fedeli is gratefully acknowledged. The Radiometer electrode was lent by A. De Mori, Divisione Strumenti, Milano. The stay of M. Č. was made possible by the thoughtful interest of Prof. M. Fiorani and by partial financial support by the University of Padova.

REFERENCES

1 IUPAC, Compendium of Analytical Nomenclature, Pergamon, Oxford, 1978, p. 168.
2 J. Koryta, Ion-selective Electrodes, Cambridge University Press, Cambridge, 1975, p. 65.
3 L. Bailey, Analysis with Ion-selective Electrodes, Heyden, London, 1976, p. 44.
4 T. Mussini, Chim. Ind. (Milan), 58 (1976) 179.
5 J. Veselý, D. Weiss and K. Štulík, Analysis with Ion-selective Electrodes, Horwood, Chichester, 1978, p. 28.
6 A. Liberti and M. Mascini, Anal. Chem., 41 (1969) 676.
7 M. Mascini, Ion-selective Electrodes Rev., 2 (1980) 17.
8 E. Pungor and K. Tóth, in H. Freiser (Ed.), Ion-selective Electrodes in Analytical Chemistry, Vol. 1, Plenum, New York, 1978, p. 147.
9 G. J. Moody, N. S. Nassory and J. D. R. Thomas, Talanta, 26 (1979) 873.

Analytica Chimica Acta, 154 (1983) 61—70
Elsevier Science Publishers B.V., Amsterdam — Printed in The Netherlands

VOLTAMMETRIC INSTRUMENTATION CONTROLLED BY TWO MICROCOMPUTERS

PER BAECKLUND and ROLF DANIELSSON*

Department of Analytical Chemistry, Institute of Chemistry, University of Uppsala, P.O. Box 531, S-752 25 Uppsala (Sweden)

(Received 25th April 1983)

SUMMARY

A voltammetric instrument with two microcomputers is described. An INTEL SYS 80/10A microcomputer, interfaced to the electrochemical cell, is provided with general machine-code routines in PROM for control and measurement. A personal computer (Luxor/Scandia Metric ABC 80) is used for control of the microcomputer and for evaluation of results. A list of machine-code routine addresses with parameters comprises a program. The parameters are selected at the personal computer which also loads the program into the SYS 80/10A and initiates the experiment. The use of two low-cost computers eliminates the need for a complex multi-task system or a remote host computer.

In voltammetric measurements, a varying potential is applied from a potentiostat to an electrochemical cell and the resulting current is recorded. The potentiostat is controlled by a potential programmer. The cell current is measured via an *I/E* (current-to-voltage) converter, and the resulting signal is fed to a unit for conditioning to give a suitable readout. The aspects of voltammetric instrumentation dealt with in this paper concern the programming and conditioning units, i.e., the generation of the input signal to the potentiostat and the processing of the output signal from the current-measuring device.

With the advent of transistors and integrated circuits, voltammetric instrumentation was considerably improved over earlier models, with more complex potential programs and signal conditioning. The two main lines followed for application of potentials are the a.c. methods, in which a sinusoidal or square wave component is superimposed on the potential ramp and the current is measured by rectification or phase-sensitive detection; and the pulse methods, in which the potential is changed abruptly in a preset manner and the current is sampled during the transient response [1]. With the electronic components now available, practically any potential program and signal conditioning requirement can be implemented. The latest commercially available voltammetric instruments involve microprocessors, which provide a greater degree of flexibility. Facilities for processing raw data and for automated chemical analysis can be included. However,

0003-2670/83/$03.00

the functions of a specific instrument remain fixed, determined by the resident microprocessor program. These functions are often hard to reveal [2], let alone modify, compared with conventional electronic circuitry.

A quite different way of implementing potential programming and signal conditioning is to use a computer connected to the instrument (Fig. 1). The basic functions then lie in alterable computer memory and much greater flexibility can be achieved. The potential program is generated by the computer and fed via a D/A (digital-to-analog) converter to the potentiostat. The current signal is read into the computer via an A/D (analog-to-digital) converter.

A computerized voltammetric instrument was first reported by Lauer et al. [3]; further contributions have been presented by Lauer and Osteryoung [4] and by Perone et al. [5]. With computerized equipment, the usual computer facilities for input, storage, processing and display of data can be used, giving a considerably enhanced flexibility in design of voltammetric experiments. However, even a minicomputer with the peripheral devices and system support necessary can be rather expensive and the benefits of the system will hardly match the total costs. Apart from research purposes and automatic routine analysis, the minicomputer has not become a commonly used part of voltammetric instrumentation.

Two-computer instrumentation

Microcomputers have decreased the cost of computer hardware markedly, but the capabilities of a microcomputer system are limited and probably suffice only for well defined voltammetric applications. A low-cost microcomputer can, however, be used simply as an interface to a larger host computer (Fig. 2). The host computer, usually in a multi-user environment,

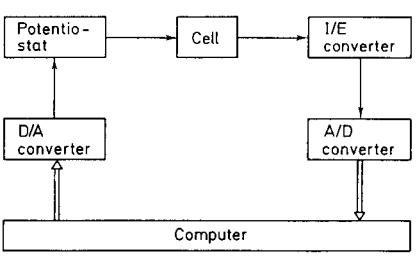

Fig. 1. Computer implementation of potential programming and signal conditioning.

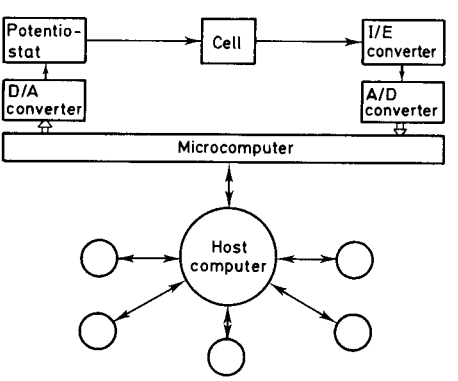

Fig. 2. A microcomputer used to interface the instrumentation to a multi-user host computer.

deals with experimental design and evaluation of results, while the microcomputer exerts the real-time control of the experiment. This configuration seems to give a cost-efficient solution [6—9], but such a system relies heavily on the maintenance of the host computer and demands sophisticated system software and reliable data communication facilities.

The computerized voltammetric instrumentation presented in this report also utilizes two computers, although in a single-user fashion. A "naked" microcomputer without peripheral units is used for potential control and data acquisition, while the data processing is handled by a personal computer (Fig. 3). The widespread use of personal computers has resulted in the availability of well documented system software including high-level programming language. Peripheral devices such as keyboard, floppy disc memory, cathode ray tube (CRT) display, printer and plotter are available at comparatively low prices. Moreover, the single user application gives the operator full control over the computer, which greatly facilitates system operations and adds to the user-orientated design. Personal computers, however, are not ideal for simultaneous measurement and control tasks and data processing. Their operating systems are directed towards interactive work with the operator rather than running real-time control and data acquisition routines. Accordingly, a second microcomputer is used as the signal-orientated part of the system. The necessary routines are resident in this computer, being activated and supervised via the personal computer.

Although the discussion and the solutions presented in this paper concern voltammetric instrumentation, the basic concepts are common to various kinds of equipment. A general-purpose laboratory computer system is not easy to achieve at reasonable cost. The dual microcomputer configuration

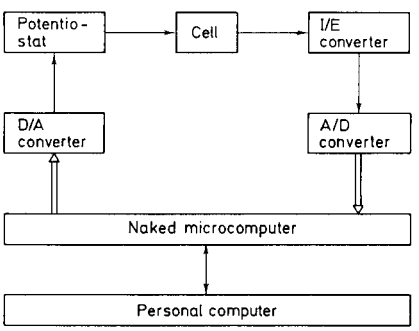

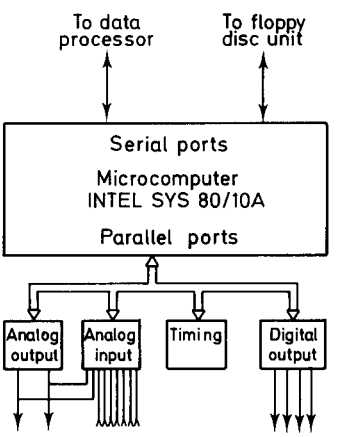

Fig. 3. A stand-alone dual microcomputer system using a "naked" microcomputer for signal control and a personal computer for data handling.

Fig. 4. The hardware configuration of the signal processing microcomputer.

should be favorable in many cases where a minicomputer system is not cost-effective. The choice of computers and the division of tasks between them depend on the nature of the problem. For the present application, the main point is the real-time operation, combining speed, high resolution and flexibility. A similar system for computerizing quality control tests in chromatography will be described elsewhere.

DESCRIPTION OF THE SYSTEM

The computerized voltammetric system described here, called LMY, is based on two microcomputers, one dealing with the instrumental signals (the signal processor) and the other dealing with control of the former and with storage and processing of raw data (the data processor).

The signal processor

The main tasks for the signal processor are generation of the potential program and acquisition of the current. In addition, some functions of the electrochemical cell can be controlled, e.g., mercury drop dislodge, nitrogen inlet and stirrer action. These tasks are done by the naked microcomputer with specially designed units for analog input and output. The hardware configuration of the system is shown in Fig. 4. The system software needed for running the system ranges over 7 kbytes and is resident in read-only memory. The main features of the signal processor are listed below; more detailed information is available elsewhere [10].

Microcomputer. The microcomputer INTEL SYS 80/10A with an expansion card SBC 108 provides an 8-bit processor (8080), 9 kbytes of read/write memory (RAM), 8 kbytes of read-only memory (PROM), 2 ports for serial data transfer and 12 ports (12*8 bits) for parallel input/output of digital signals.

Analog outputs. To achieve both high resolution and high speed, two D/A converters are used. A 16-bit converter is suitable for generation of a slowly varying potential and for large steps. An additional 12-bit converter (8 bits utilized) can be used to form small and fast superimposed steps.

Analog inputs. A 12-bit A/D converter is used together with an 8-channel multiplexer. Two channels are connected to the analog outputs, which leaves six channels for analog inputs. Thus, in addition to the cell current, five signals can be monitored during the experiment (from temperature sensors, etc.).

Digital signals. Four optocoupled outputs for ON/OFF signals are provided. Usual functions are control of mercury drop dislodge, nitrogen inlet and the relay function for cell connection. Other possibilities are stirring control in stripping voltammetry and control of pumps and valves in systems for automated analysis. Only six of the twelve parallel ports of the computer have been used, which leaves 48 digital input/output signals for future expansion.

Timing. For timing of the input and output events, a crystal-controlled oscillator is used. The time base (i.e., the smallest time unit) is 1 ms for general input/output routines, but it is possible to sample a single analog input channel at 0.1 ms intervals.

Data communication. The signal processor receives instructions and delivers results via a serial port (RS232C), connected to the data processor. It is also possible to direct data output to a second serial port, e.g., to a floppy disc unit for data dumping.

LMY monitor. The microcomputer is delivered with a system monitor for loading and execution of programs by simple commands from the data processor. The original INTEL monitor was modified and extended to simplify and speed up communication. This special version is called the LMY monitor.

LMY commands. The input and output of analog and digital signals with appropriate timing and storage of results is done by a set of machine code routines, the LMY SOFTPACK. Each routine evokes a specific action and is referred to as an LMY command. It is notified either by the memory address where the routine is located, or by a suitable three-character mnemonic. For most LMY commands, one or two parameters are needed to specify timing, channel selection, etc.

LMY programs. A list of LMY commands, together with appropriate parameters, forms an LMY program. The program may be written more legibly as a list of command labels, but it is loaded into the signal processor as two tables, one with the addresses of the routines and one with the parameter values. A system program called MAIN then extracts the address and the parameters of the routines and runs the LMY program by executing the commands in due order. When the LMY program is idle (i.e., awaiting the next event), control is returned to the LMY monitor. In this way, the LMY program is transparent to the data processor and data can be transferred while the LMY program is running. An indication of the progress of an experiment can thus be obtained at an early stage.

The data processor

For a particular experiment, the role of the data processor is to set up and load an LMY program (the address and parameter lists) into the signal processor and to collect the data. Other tasks, e.g., processing of raw data from previous experiments, can be done while the experiment is running. It is also possible to supervise the running experiment and to transfer the data obtained so far. The data processor deals only with data (no input/output signals related to the voltammetric instrumentation) and no real-time operations are involved. Any personal computer with standard peripherals can be chosen to match the specific needs for data processing. The only non-standard feature needed is the serial link to the signal processor.

Personal computer. The present system is based on an ABC 80 (Luxor, Sweden) with 32 kbyte RAM and resident BASIC. It is equipped with a dual floppy disc unit, providing 160 kbyte external memory on each disc.

A printer (Microline 80) and a plotter (Hiplot, Houston Instruments) are the peripherals for documentation of results. A serial I/O card (Databoard 4017) is used as the serial interface to the signal processor.

Utility programs. With a standard terminal routine, the ABC 80 can be used as an ordinary console unit for the signal processor. In this way the LMY monitor can be utilized to its full extent. Some BASIC programs are intended for general use in connection with development of LMY programs [11]. The LMY programs in the form of mnemonics with parameters and labels are created and stored on a file by use of an editor. This file is converted to address and parameter tables stored on another file by a compiling program. The tables are transferred to the signal processor by a loader, which also initiates the execution of the LMY program and collects the results. The dialogue with the LMY monitor is conducted by the loader, not the operator, which adds to the safety of the system. The loader also facilitates testing of LMY programs by step-wise execution and display of variables.

Voltammetric programs. A further step is the development of data processor programs for a certain type of voltammetric experiment. In this case, the structure of the LMY program is more or less fixed, while the operator may select the parameters in any convenient way. The voltammetric program loads and runs the LMY program and collects and processes the resulting data. A general program for several current variations of pulse voltammetric techniques has been developed [11] and is in use for determination of metals in studies of complexation [12]. A more elaborate program including multiple current sampling for each potential step and first drop measurements (no depletion) is under development for more fundamental studies.

SOME DESIGN CONSIDERATIONS OF THE LMY SYSTEM

The main idea of the two-computer approach is the separation of tasks: on one computer, the measurement and control tasks and on the other the data handling and man—machine communication. As far as possible, the standard software for each type of computer should be retained, the monitor for the naked microcomputer and the operative system and high-level programming language (usually BASIC) for the personal computer. Then programs for the two computers can be developed and tested independently. The crucial points are the choice of the level of the signal processor routines and the technique of information exchange between the computers.

A guiding principle in the design of the LMY system was the independent operation of the two computers. As many as possible of the instrumental functions are resident in the signal processor as preprogrammed machine code routines (LMY SOFTPACK). To maintain flexibility, these routines are not too complex, yet powerful enough to allow for a comprehensive combining program in the data processor. The use of the signal processor monitor for communication, even during a running experiment, also facilitates independent operation. As long as the data processor can act as a terminal

there are no instrumental considerations (e.g., interrupts, real-time clock) to be considered. Thus all normal capabilities of a personal computer can be utilized.

Some features of the LMY system and its operation will be discussed, while more detailed descriptions [10, 11] and program listings are available on request.

The structure of the LMY SOFTPACK

The tasks done by the LMY commands are often quite simple. Indeed, the machine instructions themselves have a suitable level of complexity for most of the commands. However, the LMY commands operate on different kinds of data, represented by data words of different length (one, two or four bytes). Instead of using internal CPU registers, the data words are stored as variables at fixed memory locations. The variables are used as general-purpose registers and for passing data to and from the parallel ports. There is also a data storage area where results can be stored for later retrieval and a buffer for data transfer to an optional floppy disc. The LMY commands are coded as subroutines, to which necessary parameters for register identification, immediate (fixed) data, etc., should be attached. A large group of LMY commands is intended for arithmetic and logic operations on the variables as well as for data transfer operations and conditional and unconditional jumps. These commands are similar to CPU instructions and the programming is similar to assembler programming. For timing reasons, the actual input and output of signals are done by interrupt routines, which can be enabled and disabled by special LMY commands. There are also more complex commands for analog input, which are described below. A special wait command is used to control the timing of the program.

LMY program execution

The execution of an LMY program is controlled by the resident program MAIN. This program extracts the addresses and the parameters of the LMY command routines from the tables forming the LMY program. These routines conduct data transfer, etc., until a wait command is encountered. For a specified time, control then passes to the LMY monitor. A scheme of the program execution, including the interrupt handling, is shown in Fig. 5.

The timing of the LMY systems is determined by a 1-kHz clock pulse generator. The clock pulse causes an interrupt of the current operation and interrupt routines are executed. Initially, a reserved variable, the real-time clock, is incremented. Then some input/output operations can be done, previously enabled by special LMY commands:

(i) Analog input via preselected channel. The result is stored as a variable.

(ii) Input/output via parallel ports. Data are exchanged between the ports and the reserved input/output variables.

(iii) Output to optional floppy disc unit. If the floppy disc buffer is not empty, the next character is sent to the serial output port.

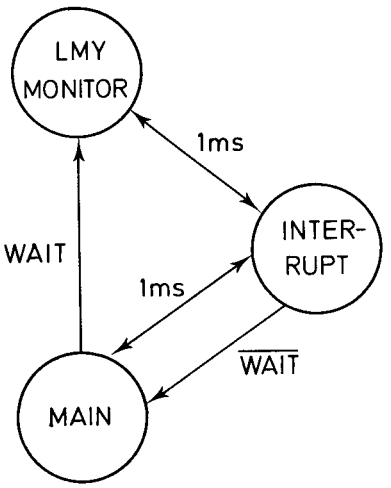

Fig. 5. The paths for program execution as determined by the interrupt signal (1 ms) and the WAIT condition (set by MAIN and reset by INTERRUPT).

The completion of the interrupt handling depends on the status of the running LMY program. Normally, control is passed back to the interrupted program. However, if a wait command is made, a comparison is made between the running clock and a selected variable. If a match occurs, the wait command is terminated and MAIN resumes operation.

The temporary return to the monitor during the wait command makes it possible for the data processor to follow the operations. All current information about variables, flags and pointers is accessible by use of the monitor commands for memory display. Data processor routines for such actions are incorporated in the loader.

Output and input of instrumental signals

The digital information to the D/A converters is transferred from three reserved variables via three parallel ports by one of the interrupt routines (I/O). The LMY program sequence for changing the analog outputs will typically include the following steps: (i) disable the I/O interrupt routine; (ii) determine the new digital values, e.g., by adding fixed values to the present content of the output variables; (iii) check current time and set an appropriate wait time; (iv) enable the I/O interrupt routine, which performs the output operation at the next clock pulse.

One output port is not affected by the I/O interrupt routine. This port partly controls the analog input channel and partly the four ON/OFF outputs. The latter are controlled by special LMY commands for changing the bit pattern, the specified action being taken at the next clock pulse.

The analog input operations are conducted by more complex routines. The five commands for different modes of operation are as follows.

(i) Fast serial. The selected input channel is measured a preset number of times. The interval time is an integer multiplied by 0.1 ms. The results are stored in the data storage area.

(ii) Slow serial. This acts in the same way as the fast serial, except that the result is taken as the median of three successive readings. The minimum time interval is now an integer multiplied by 1 ms.

(iii) Serial sum. Measurements are done according to slow serial, but the successive results are summed. The final sum is divided by the maximum power of two not exceeding the number of measurements (to reduce word length) and stored in the data storage area.

(iv) Parallel storage. The input channels are scanned once at an interval of 0.1 ms. The results selected by a channel mask are stored in the data storage area.

(v) Parallel input. Measurements are taken as in parallel storage, but the results are stored in reserved variables.

Further developments

Besides the possibilities for complex potential programs and for automation, the extended measurement capabilities should be recognized. Instead of sampling the current once after each potential step, the entire current transient can be recorded. The extensive amount of data obtained then becomes a problem. Although RAM is inexpensive and the data storage area can be made very large, the transfer of data to the data processor will make the system impractical. This problem might be solved by applying fast Fourier transform (FFT) [13] to the transient, by means of the signal processor. By using a number of low-frequency amplitudes, the transient could be represented economically and conveniently. Moreover, the transformed result should be useful in exploring the kinetic properties of the electrode reactions. In a similar way, FFT applied to continuous measurements in square-wave polarography would give results related to in-phase and quadrature components of a.c. harmonics. Work along these lines is now in progress.

The set of LMY commands implemented by the LMY SOFTPACK may turn out to be inadequate. Extensions can easily be made by loading assembled routines into memory space via the monitor. The corresponding address and parameter characteristics are then added to the compiler under a suitable mnemonic by means of a special editor. It is also possible to run other signal processor programs than MAIN from the monitor. In more complex experimental situations (e.g., with interactions between measurement and control based on calculations), the data processor could work in a quasi real-time mode. The LMY program and parameters are then changed during the course of the experiment according to the outcome of the processing of present data. Other cases where more permanent on-line operation of the data processor should be useful are automated analysis and serial experiments with the same sample. In this type of operation, the

signal processor can be regarded as an intelligent interface between the data processor and the voltammetric part of the instrumentation. The principal tasks are then done by the data processor, which may call for a personal computer of higher performance.

This work was financially supported by the Swedish National Science Research Council which is gratefully acknowledged.

REFERENCES

1 A. M. Bond, Modern Polarographic Methods in Analytical Chemistry, M. Dekker, New York, 1980.
2 T. Anfält and M. Strandberg, Anal. Chim. Acta, 103 (1978) 379.
3 G. Lauer, R. Abel and F. C. Anson, Anal. Chem., 39 (1967) 765.
4 G. Lauer and R. A. Osteryoung, Anal. Chem., 40 (1968) 30A.
5 S. P. Perone, J. E. Harrar, F. B. Stephens and R. E. Anderson, Anal. Chem., 40 (1968) 899.
6 H. J. Skov and L. Kryger, Anal. Chim. Acta, 122 (1980) 179.
7 H. C. Smit, Anal. Chim. Acta, 122 (1980) 201.
8 C-Y. Li, T. H. Barrett, Jr., D. Lunney and A. Salt, Anal. Chem., 134 (1982) 167.
9 R. P. J. Duursma, H. Steigstra, R. Logchies and H. C. Smit, Anal. Chim. Acta, 144 (1982) 13.
10 P. Baecklund, University of Uppsala, Institute of Chemistry, Publ. UUIC A82/02, 1982.
11 P. Baecklund and G. Wikmark, University of Uppsala, Institute of Chemistry, Publ. UUIC A82/03, 1982.
12 Å. Olin and G. Wikmark, Anal. Chem., 55 (1983) 1402.
13 D. E. Smith, Anal. Chem., 48 (1976) 221A.

Analytica Chimica Acta, 154 (1983) 71—78
Elsevier Science Publishers B.V., Amsterdam — Printed in The Netherlands

STRIPPING VOLTAMMETRY OF CHROMIUM(VI) AT A POLY(4-VINYLPYRIDINE)-COATED PLATINUM ELECTRODE

JAMES A. COX* and PAWEL J. KULESZA

Department of Chemistry and Biochemistry, Southern Illinois University, Carbondale, IL 62901 (U.S.A.)

(Received 23rd March 1983)

SUMMARY

By coating an electrode with a thin film of a polymer that has ion-exchange properties, the scope of stripping voltammetry can be extended to include electrochemically irreversible, ionic analytes. Such species are accumulated on the electrode by an ion-exchange reaction rather than by electrolysis. This approach was demonstrated by preconcentrating chromium(VI) in a protonated poly(4-vinylpyridine) film from a 0.15 M sodium fluoride electrolyte buffered at pH 3.5. The ion-exchange preconcentration required 60 s at 0.9 V vs. SCE. The stripping was effected by applying a 50 mV s^{-1} potential scan. The peak at 0.2 V vs. SCE, which was due to the reduction of Cr(VI) to Cr(III), was proportional to the Cr(VI) concentration over the 10^{-6}—10^{-8} M range. Because of the anion-exchange property of the film, cations such as Fe(III) and Cu(II) did not interfere. A 1000-fold excess of Cr(III) did not alter the peak current. Anions which are electroactive in the range 0.9—0.1 V vs. SCE will interfere. Because they can affect the partitioning of Cr(VI) into the film, interference will also be caused by high concentrations of multivalent and strong hydrogen-bonding anions. The electrode is simple to prepare and is stable.

Stripping voltammetry is one of the most sensitive methods available for the determination of ionic species in solution. The method requires that a representative fraction of the analyte first be accumulated on an electrode. Subsequently, it is stripped by scanning the potential through a region where the accumulated analyte is electrolyzed by effecting the electrolysis with a constant current or by using a chemical redox reaction. The recorded signal is a current—voltage curve in the former mode; a peak that can be related to the concentration of the analyte in solution is obtained. In the latter two modes, the time required to strip the accumulated analyte is determined from a potential—time curve and related to the sample concentration. In the determination of cations, the accumulation step is generally an electroreduction to the metal although certain cations can be deposited by oxidative electrolysis to sparingly soluble salts. Anions can be accumulated by oxidizing an electrode metal to a sparingly soluble salt of the analyte.

There is a need to devise alternative methods for the accumulation step. For example, the difference between the deposition and stripping potentials when anions are accumulated as sparingly soluble salts is so small that an

0003-2670/83/$03.00

uncertainty in the baseline is introduced which is deleterious to the detection limit. Several important ionic species cannot be accumulated by the classical approaches.

Modification of electrode surfaces can provide alternative approaches for the accumulation of ions. For example, an adsorbed layer of adenosine-5'-monophosphate on platinum can form a complex with Fe(III) [1]; the subsequent reduction to Fe(II), which is not held on the surface, allows Fe(III) to be quantified in a manner analogous to the classical stripping voltammetric method [2]. The dynamic range of the system is limited by the relatively small number of sites available to Fe(III). Similarly, ferrocenecarboxaldehyde was quantified at an allylamine-coated Pt electrode [3]; silver, at an amidized carbon paste electrode [4]; copper, at a carbon paste electrode that was modified with dithio-oxamide [5]; and U(VI) at a glassy carbon electrode that was modified by dip-coating with tri-n-octyl-phosphine oxide [6].

Recently, it has been demonstrated that the adsorption of polymers that contain ion-exchange sites provides an alternative to covalent functionalization and the adsorption of complexing agents as a means of modifying electrode surfaces. For example, an adsorbed film of poly(4-vinylpyridine), PVP, in an acidic solution acts as an anion-exchange layer on an electrode [7—10]. In the present study, a Pt/PVP system was used. The electrode is easier to prepare than those which require covalent attachment of the functional group. It is very stable as long as the film contains ions that can crosslink the polymeric chains [11]. Because the film contains more active sites than are present with other types of modified electrodes, it can be hypothesized that the Pt/PVP system will be well suited for experiments analogous to stripping voltammetry but with ion-exchange reactions as the accumulation step.

The present study tests the above suggestion with Cr(VI) as the analyte. The selection was based upon two considerations. First, classical stripping voltammetry of Cr(VI) by deposition of $Cr(OH)_3$ at a graphite electrode is possible [12], but the sensitivity and selectivity are not very satisfactory. In addition, the electrode passivation that will occur [13—15] undoubtedly limits the dynamic range. Second, Cr(VI) is toxic. There is a need to develop improved methods for that ion which can be extended to the concentration range below 10^{-7} M and which are selective for Cr(VI) in the presence of Cr(III). Voltammetric methods are applicable in these regards, but means must be developed to avoid the passivation effects of Cr(III).

EXPERIMENTAL

Equipment and chemicals

A Princeton Applied Research Model 174A Polarographic Analyzer was used. All potentials were recorded and reported vs. a saturated calomel reference electrode (SCE).

Solutions of poly(4-vinylpyridine) (Polysciences, lot 2108) were prepared by mixing 0.2 g of PVP in 50 ml of methanol. All other chemicals were ACS

Reagent Grade and were used without further purification. The water was distilled and doubly deionized with Cole-Parmer research grade cartridges. The standard solutions were freshly prepared for each use by dilution of a 0.1 M stock.

Preparation of electrodes

The modified electrode substrate was a platinum disk (electrode area, 4.5 mm^2) heat-sealed into soft glass tubing. Based on previous reports, [15—17] the platinum was cleaned by first polishing with Fisher Gamal 0.1 μm alumina on a Gamal cloth with distilled water as the lubricant. The electrode was rinsed and transferred to deaerated 1 M sulfuric acid where it was cycled at 50 mV s^{-1} between 1.4 and —0.2 V about 50—100 times. The pretreatment was completed by reduction of the surface at 0.4 V until the current decayed to a constant low value (2—3 min). The pretreated electrode was rinsed, dried, and immediately placed into a 0.4% solution of PVP in methanol for 25 min. During this simple dipping step the polymer strongly adsorbs on the platinum surface [18].

To obtain the thin films that are necessary, the electrodes were subsequently washed repeatedly with methanol and soaked for 2 min in that solvent. Any adherent solvent was removed with a soft tissue. The electrodes were air-dried and subsequently immersed in 1 M sulfuric acid solution for 5 min. This step protonates the pyridine sites and makes the film more uniform, thinner, and more conductive.

To incorporate Cr(VI) anions initially into a PVP coating, the electrode was placed in a mixture of 1 mM dichromate and 0.15 M sodium fluoride which was adjusted with dilute hydrochloric acid to pH 3.5. The electrode potential was cycled continuously at 50 mV s^{-1} between 0.9 and 0 V; each time the scan was stopped at 0.9 V for about 1 min. The voltammogram reached a steady state after 30—40 cycles.

During the positive-going potential excursion and at the 0.9 V rest potential, cations, including the majority of Cr(III)-species, are ejected from the film. The Cr(III) is not electroactive in this range of potentials.

After a given experiment, the electrode is returned to its initial state by depletion of the accumulated Cr(VI). This is achieved by cycling it in the above-described manner in a solution that consists only of the pH 3.5, 0.15 M sodium fluoride supporting electrolyte. About 10 cycles are required.

The described preconcentration—depletion cycle in 1 mM Cr(VI) is a necessary part of the preparation of the Pt/PVP electrode. Apparently, the Cr(III) which is formed is retained in part as a crosslinking agent. The procedure provides greater stability and uniformity to the PVP film than would be expected solely on the basis of the protonated PVP properties. As long as the treated electrode is not used outside the range 1.0 to —0.1 V, it has excellent long-term stability.

RESULTS AND DISCUSSION

Experiments were generally done in a buffer prepared by adjusting a 0.15 M sodium fluoride solution to pH 3.5 with dilute hydrochloric acid. Voltammetric experiments at 50 mV s^{-1} are characterized by a Cr(VI) reduction peak at 0.185 V (Fig. 1). The peak currents are proportional to scan rate. The data are consistent with the electrode process involving the reduction of Cr(VI) that has been preconcentrated into the protonated PVP film [19].

Small background peaks, at 0.78 V and 0.42 V, are consistent with the oxidation and reduction of the platinum surface. These processes are suppressed, but not eliminated, by the presence of the PVP film. In this respect, glassy carbon (or graphite) as the substrate material might be better, but unfortunately the resulting PVP films are too thick, which results in a high resistance. Further, the data on a glassy carbon substrate are difficult to reproduce when Cr(VI)/Cr(III) is the test couple.

Also noteworthy is that Cr(III) is not electroactive under the conditions of the experiment; however, in the presence of fluoride, formation of a passivating layer of chromium(III) oxides is minimized or prevented. Therefore, if the Pt/PVP electrode is held positive of 0.9 V, Cr(III) is essentially removed from the positively-charged, protonated electrode surface. This permits design of the cathodic stripping voltammetric experiment in a manner which is free of electrode history effects.

The protonated PVP film acts as a membrane that preferentially absorbs multi-charged anions, including Cr(VI) species, by electrostatic forces augmented by chemical interactions. Moreover, at the modified platinum surface, background currents are significantly lowered. These properties result in an improved signal-to-noise ratio.

The optimum electrode for stripping voltammetry is one which permits the test species to be deposited in a thin layer so that high, narrow peaks are obtained. The internal resistance of the polymer has to be low, and this

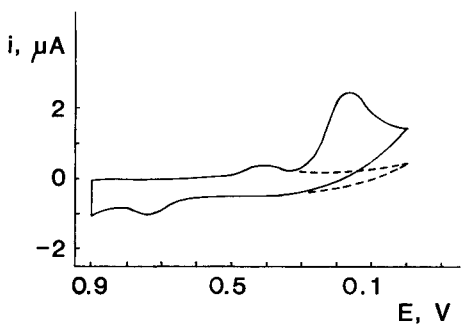

Fig. 1. Cyclic voltammogram of dichromate at Pt/PVP. Concentration, 6×10^{-7} M; electrolyte, 0.15 M NaF at pH 3.5; scan rate, 50 mV s^{-1}; area, 4.5 mm^2; the electrode was held at 0.9 V for 60 s between scans. Dotted line represents background current.

requires, especially in the case of irreversible couples like Cr(VI)/Cr(III), ultra-thin films impregnated by electrolytes.

A technique that is analogous to classical electrochemical stripping methods can therefore be devised as follows. The experiment begins with the Pt/PVP modified electrode held at 0.9 V in a stirred sample which is buffered at pH 3.5. The stirring rate is maintained well below the point of vortex formation. After a prescribed time, the stirring is stopped. Following a 10-s rest, the electrode is scanned from 0.9 to 0 V at 50 mV s^{-1}, and the voltammetric peak current at about 0.2 V is related to concentration by a calibration graph (Fig.2). With a 60-s preconcentration time, the linear range is 10^{-8}—10^{-6} M Cr(VI). The difference between the Cr(VI) cathodic current and the background current (recorded only in supporting electrolyte) is used to quantify Cr(VI). It is noteworthy that sample deaeration is not required. Eight-point working curves over the 10^{-6}—10^{-8} range had the following linear least-squares characteristics: slope, 2.34 μA μM^{-1}; intercept, 0.70 μA; correlation coefficient, 0.9990; relative standard deviation of the slope, 1.7%; relative standard deviation of the intercept, 3.2%; standard error of current estimate, 42 nA; and standard error of estimate of concentration, 1.8 × 10^{-8} M.

At higher concentrations, complex Cr(VI) equilibria [20—22] result in nonlinear response. Samples above 10^{-6} M Cr(VI) either must be determined by an alternative method or diluted into the 10^{-6}—10^{-8} M working range. At concentrations below 10^{-8} M, the variability of the background current causes excessive error. At such concentrations, redox sites in the PVP film are very diluted and probably monomeric Cr(VI) dominates. Strong affinity of these anions toward protonated pyridine sites can be expected, which

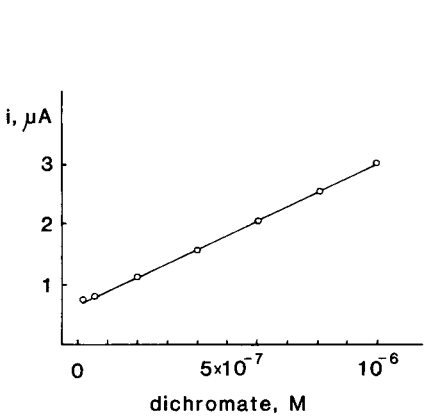

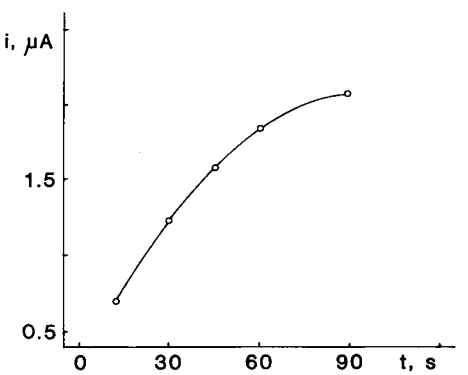

Fig. 2. Working curve for the stripping of Cr(VI) from a Pt/PVP electrode. Preconcentration time, 60 s; area, 4.5 mm^2; electrolyte, 0.15 M NaF at pH 3.5; scan rate, 50 mV s^{-1}.

Fig. 3. Dependence of the stripping peak current on the preconcentration time. Concentration, 5 × 10^{-7} M dichromate; other conditions are the same as in Fig. 2, except that the preconcentration time is varied.

explains the relatively high value of the intercept. The use of differential pulse stripping voltammetry (scan rate, 2 mV s^{-1}; pulse amplitude, 50 mV) increases the sensitivity by sixfold, but the working range is not significantly changed. This observation supports the suggestion that the working range is limited by the chemistry of Cr(VI) rather than the electrochemistry.

It was expected that the quantity of Cr(VI) preconcentrated at the modified surface should be dependent on concentration and the preconcentration time (Fig. 3). It was found that a 60-s preconcentration time is satisfactory for routine determinations. Increasing the preconcentration time to 120 s increases the overall sensitivity and stability, but the current response to concentration is partly nonlinear. The working curves are not extended significantly toward lower concentrations.

When the variation of the characteristics of the modified platinum electrode and of the electrochemical experiment were considered together, the relative standard deviation of the peak current was up to about 10%. This is attributed to variations in the polymer morphology, some formation of platinum oxide under the film, and changes in the ion-transport mechanism inside the film. For example, when the stripping experiment was done with different Pt/PVP electrodes in 1.00×10^{-6} M dichromate solution (in the pH 3.5 electrolyte), the peak currents which were obtained were 3.0, 2.8, 3.1, and 2.7 μA. These results were obtained with a 60-s preconcentration time.

The stability of the Pt/PVP electrode (and the irreversibility of the PVP adsorption at platinum) were tested by multiple measurements of Cr(VI) at the 10^{-6} M level over a period of a few days with the same electrode. Under these conditions, twelve experiments were done with variable intervals between trials. Each of the experiments was repeated at least three times to obtain a representative current. The average of the twelve current values was 3.0 μA, and the relative standard deviation was 6%. The data attest to the stability of Pt/PVP.

The amount of preconcentration and the electrochemistry of the Cr(VI)/Cr(III) couple strongly depend on the pH of the solution. However, pH variation of ± 0.3 about the value 3.5 do not affect experimental current values by more than 2%.

The general trend that the peak current increases as the pH is decreased from 8 to 4 is discussed elsewhere [19]. It reflects the increase in porosity and conductivity of the film caused by proton incursion, changes in the Cr(VI) equilibria, and the dependence of the electron transfer rate on pH [23].

Typical variations in stirring rate or ionic strength (after the supporting electrolyte is added) are not significant. Addition of gelatin (10 mg l^{-1}) did not alter the results.

The system is specific for chromium in the +6 oxidation state. A 1000-fold excess of Cr(III) does not alter the peak current.

The electrochemistry of other cationic and neutral species dissolved in

solution is quenched by the presence of the film. Addition of 1×10^{-6} M iron(III) and 5×10^{-6} M copper(II) to a 1×10^{-6} M dichromate solution did not interfere with the determination of chromium(VI). The film must therefore be free of significant pinholes through which such species would otherwise diffuse.

Among common monovalent anions, iodide can interfere because it will be oxidized during the preconcentration step. However, iodide is not likely to coexist with Cr(VI), especially in acidic medium. Other potential interferences originate from highly charged anions such as hexacyanoferrate(II), or anions such as acetate that can form strong intramolecular hydrogen bonds with pyridine sites of the film. They affect the partition equilibrium of Cr(VI) into the protonated PVP polymer. If such anions are electroactive at 0.2 V or can form insoluble salts with Cr(III) in the film, they will interfere severely.

In conclusion, the present study describes a means for the determination of trace levels of Cr(VI). The application of these systems can expand the scope of stripping voltammetric procedures toward anions that cannot be accumulated by commoner electrolytic methods. Perhaps what is more important is the demonstration of the use of a polymer-modified electrode for an indicator in stripping voltammetry. Among the fundamental requirements, the necessity of preparation of ultra-thin, conductive, and stable films with relatively fast ion-exchange properties should be emphasized. In addition, to prevent memory effects, the electrolysis product must be removed from the film upon completion of the stripping scan.

This work was supported in part by the National Science Foundation.

REFERENCES

1 J. A. Cox and M. Majda, Anal. Chem., 52 (1980) 861.
2 J. A. Cox and M. Majda, Anal. Chim. Acta, 118 (1980) 271.
3 J. F. Price and R. P. Baldwin, Anal. Chem., 52 (1980) 1940.
4 G. T. Cheek and R. F. Nelson, Anal. Lett., A11 (1978) 393.
5 H. Monien, V. Gerlach and P. Jacob, Fresenius Z. Anal. Chem., 306 (1981) 136.
6 K. H. Lubert, M. Schnurrbush and A. Thomas, Anal. Chim. Acta, 144 (1982) 123.
7 N. Oyama and F. C. Anson, J. Electrochem. Soc., 127 (1980) 247, 249.
8 N. Oyama and F. C. Anson, Anal. Chem., 52 (1980) 1192.
9 N. Oyama, T. Shimomura, K. Shigehara and F. C. Anson, J. Electroanal. Chem., 112 (1980) 271.
10 K. Shigehara, N. Oyama and F. C. Anson, Inorg. Chem., 20 (1981) 518.
11 N. Oyama and F. C. Anson, J. Am. Chem. Soc., 101 (1979) 3450.
12 F. Vydra, K. Stulik and E. Julakova, Electrochemical Stripping Analysis, Halsted Press, New York, 1977, p. 250.
13 J. J. Lingane and I. M. Kolthoff, J. Am. Chem. Soc., 62 (1940) 852.
14 Th. Heumann and H. S. Panesar, J. Electrochem. Soc., 110 (1963) 628.
15 J. A. Cox, P. J. Kulesza and M. A. Mbugwa, Anal. Chem., 54 (1982) 787.
16 D. C. Johnson, J. Electrochem. Soc., 119 (1972) 331.
17 A. T. Hubbard, R. A. Osteryoung and F. C. Anson, Anal. Chem., 38 (1968) 692.

18 M. Majda and L. R. Faulkner, private communication, 1982.
19 J. A. Cox and P. J.Kulesza, J. Electroanal. Chem., (1983) in press.
20 J. Y. Tong and E. L. King, J. Am. Chem. Soc., 75 (1953) 6180.
21 W. G. Davies and J. E. Prue, Trans. Faraday Soc., 51 (1955) 1045.
22 P. J. Durrant and B. Durrant, Introduction to Advanced Inorganic Chemistry, Wiley, New York, 1970, p. 1024.
23 R. Knoedler and K. E. Heusler, Electrochim. Acta, 17 (1972) 197.

Analytica Chimica Acta, 154 (1983) 79—86
Elsevier Science Publishers B.V., Amsterdam — Printed in The Netherlands

DETERMINATION OF URANIUM BY ADSORPTIVE STRIPPING VOLTAMMETRY

NGUYEN KHÁC LAM, ROBERT KALVODA* and MILOSLAV KOPANICA

J. Heyrovský Institute of Physical Chemistry and Electrochemistry, Czechoslovak Academy of Sciences, 118 40 Prague (Czechoslovakia)

(Received 27th May 1983)

SUMMARY

A voltammetric method for the determination of uranium in natural waters in the concentration range from 0.4 $\mu g\ l^{-1}$ to 0.2 $mg\ l^{-1}$ is described. The method is based on adsorptive accumulation of the uranium(VI)—pyrocatechol complex on the hanging mercury drop electrode followed by the reduction of the adsorbed complex.

Uranium is readily determined by polarographic methods. For the determination of low amounts of uranium, the measurement of the catalytic current caused by the oxidation of the reduction product of uranium(VI) by nitrate ions and resulting in cyclic re-formation of uranium(VI), is often recommended [1]. When the differential pulse mode is applied in this method, the detection limit approaches 1 $\mu g\ l^{-1}$ [2]. More recently, interest has been turned to adsorptive stripping voltammetry, which can provide very sensitive determinations of compounds with surface-active properties [3]. For adsorptive preconcentration of uranium complexes on the hanging mercury drop electrode (HMDE) followed by reduction of the accumulated compound by a cathodic voltage scan, tributylphosphate, tripropylphosphate [4] or diisopropylphosphate [5] has been used in the appropriate supporting electrolyte. For the determination of uranyl ion after preconcentration, a glassy carbon electrode coated with trioctylphosphine oxide has also been proposed [6—8].

The aim of this paper is to demonstrate a voltammetric method for uranium determination in natural water based on adsorptive stripping voltammetry of the uranium—pyrocatechol complex. The adsorptive properties of this complex were studied earlier by means of oscillographic polarography with alternating current [9].

EXPERIMENTAL

Equipment and reagents

The polarographic analyzers PA-3 and PA-4 (Laboratorní přístroje, Prague, Czechoslovakia) were used in the three-electrode configuration for the

0003-2670/83/$03.00

recording of all modes of polarographic and voltammetric curves: d.c., normal pulse polarography/voltammetry (n.p.p., n.p.v.), differential pulse polarography/voltammetry (d.p.p., d.p.v.), and fast-scan differential pulse polarography/voltammetry where five pulses per second are applied with sampling identical to that in d.p.p.). A static mercury drop electrode (SMDE; Laboratorní přístroje, Prague, Czechoslovakia) served as working electrode either in the dropping mercury electrode (DME) mode or in the hanging mercury drop electrode mode. A silver chloride electrode was used as the reference electrode and a platinum wire as auxiliary electrode. Dissolved oxygen was removed from the test solutions by prepurified nitrogen.

Pyrocatechol (catechol) was purified by recrystallization from toluene. All solutions were prepared from reagent-grade chemicals; twice-distilled water (quartz apparatus) was used throughout.

Procedure for the determination of uranium in natural water

The water sample (ca. 25 ml) was acidified with hydrochloric acid to give a final 4 M HCl concentration. This solution was mixed with a four-fold volume of ethanol and passed through the prepared column. The column was washed with 50 ml of 4 M HCl/ethanol mixture (1:4). After washing, uranium was eluted with 10 ml of 0.1 M HCl. The eluate was neutralized with 0.2 M NaOH, 20 ml of acetate buffer solution (pH 4.7) and 1 ml of 10^{-3} M pyrocatechol were added, and the sample solution was diluted to 50 ml with water. An aliquot (25 ml) of this solution was transferred to the electrolytic cell. After deaeration with purified nitrogen, accumulation on the HMDE (static mercury drop electrode) was done at −0.10 V for a definite period of time in stirred solution. The fast-scan d.p.v. curve was then recorded over the potential range −0.10 to −0.60 V, and the uranium peak was measured at −0.35 V. For the evaluation of results, the method of standard additions was applied with the precautions given above.

The ion-exchange column (12 × 0.6 cm) was filled with Dowex 1-X8 resin in the Cl^- form and washed with 50 ml of 1 M HCl and then with 250 ml of ethanol before use.

RESULTS AND DISCUSSION

Influence of pyrocatechol on polarographic behaviour of uranyl ions

In an acetate buffer (pH 4.6) medium, uranium(VI) yielded a d.c. polarographic wave with the half-wave potential −0.25 V (Ag/AgCl) corresponding to the reduction to uranium(V) [10]. In the presence of pyrocatechol, the half-wave potential of this wave remained constant and the corresponding limiting current increased with increasing reagent concentration; at a 10-fold molar excess of the reagent, the current increased two and half times. Under these conditions, the limiting current increased linearly with increased uranium concentration. Measurements with varied mercury pressure showed that the limiting current depended linearly on the height of the mercury

reservoir. Further it was observed that the limiting current increased with temperature; in the interval 20—50°C the temperature coefficient had the value 2.2%.

Measurements by n.p.p. showed that in the presence of pyrocatechol a rounded maximum appeared on the n.p.p. wave of uranium; the height of this maximum increased with increasing pyrocatechol concentration. The n.p.p. limiting current of the uranium—pyrocatechol complex depended on the initial potential value. In the initial potential interval between +0.20 and 0.0 V, the corresponding limiting current remained constant but decreased sharply when the initial potential was changed from 0 to —0.20 V. It was established that the current corresponding to the maximum on the n.p.p. curve of the uranium—pyrocatechol complex (read at —0.33 V) was reproducible. The current decreased with increasing pulse width. The dependences of this maximum current on uranium concentration, initial potential and temperature were found to be identical with the corresponding dependences of the limiting current.

When d.p.p. was applied for the determination of uranium(VI) in the presence of pyrocatechol, similar results were obtained as with the d.c. mode. The d.p.p. measurement was, however, more sensitive, the detection limit corresponding to 5×10^{-7} mol l^{-1}.

From the results given above, it can be concluded that the limiting current of the uranium—pyrocatechol complex is of an adsorptive nature. If this complex is adsorbed on the surface of the DME at positive potential values (between +0.2 and —0.1 V), then the application of the HMDE should lead to a substantial increase in the sensitivity of a voltammetric determination.

Fast-scan differential pulse voltammetry of uranyl ion in the presence of pyrocatechol

Under conditions where uranium(VI) yielded a d.c. polarographic wave (0.1 M acetate buffer, pH 4.6), fast-scan d.p.v. at the HMDE gave a peak with a peak potential E_p of —0.32 V (Fig. 1). After the addition of pyrocatechol the peak current, i_p, increased. Measurements of the dependence of the peak current on pyrocatechol concentration at varied uranium concentrations showed that the peak current increased up to molar ratios [pyr.]/$[UO_2^{2+}] \leqslant 10$; when this ratio was higher, the peak current remained constant (Fig. 2). If the HMDE was polarized in the direction to positive potentials, the uranium peak current was not enhanced. As expected, an increase of the peak current was observed when the HMDE was kept in stirred solution for a definite time (accumulation time t_{acc}) at a positive potential before scanning. The enhancement of the i_p values depended on the duration of the accumulation period and on the value of the accumulation potential. The peak current remained unchanged when the accumulation potential was varied in the range from +0.20 to 0 V and decreased at more negative values of E_{acc}. With prolonged accumulation times, the current increased and reached a limiting value (Fig. 3). The duration of the accumulation period during

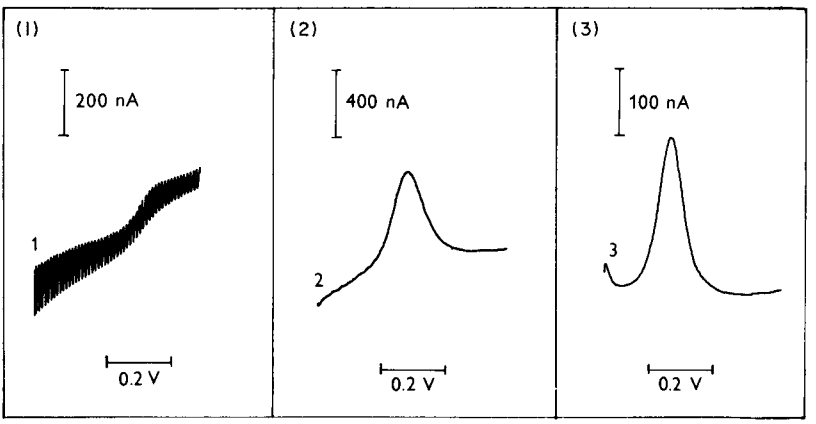

Fig. 1. Polarographic and voltammetric curves of the uranium—pyrocatechol complex. Conditions: 0.05 M acetate buffer, pH 4.6; curves start at —0.10 V (Ag/AgCl). Waves: (1) d.c. polarographic curve (DME), 2×10^{-5} mol l^{-1} UO_2^{2+}, 1×10^{-4} mol l^{-1} pyrocatechol; (2) n.p.v. curve (HMDE), 3×10^{-7} mol l^{-1} UO_2^{2+}, 5×10^{-6} mol l^{-1} pyrocatechol, E_{in} +0.10 V; (3) fast-scan d.p.v. curve (HMDE), 1×10^{-7} mol l^{-1} UO_2^{2+}, 5×10^{-6} mol l^{-1} pyrocatechol.

which the current increased was found to depend on the uranium concentration. In Table 1 are presented the maximum values of the accumulation time during which the peak current increases for different uranium concentrations.

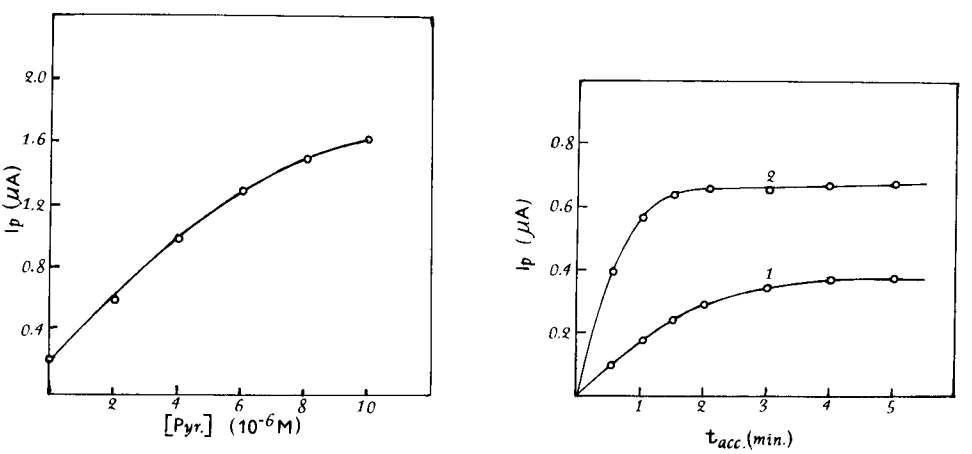

Fig. 2. Dependence of the fast-scan d.p.v. peak current of uranium(VI) on pyrocatechol concentration (0.05 M acetate buffer, pH 4.6, 5×10^{-6} mol l^{-1} UO_2^{2+}).

Fig. 3. Dependence of the fast-scan d.p.v. peak current of the uranium—pyrocatechol complex on accumulation time. Conditions: 0.05 M acetate buffer, pH 4.6, 4×10^{-5} mol l^{-1} pyrocatechol; preconcentration from stirred solution; E_{acc} —0.10 V. Uranyl concentration: (1) 1×10^{-6}; (2) 1×10^{-7} mol l^{-1}.

TABLE 1

Maximum accumulation time for different uranyl ion concentrations in the adsorptive voltammetric determination[a]

UO_2^{2+} conc. (mol l^{-1})	2×10^{-6}	1×10^{-6}	5×10^{-7}	5×10^{-8}	6×10^{-9}
t_{acc} (s)	60	120	300	660	900

[a] Accumulation potential, $E_{acc} = -0.1$ V (Ag/AgCl).

The peak current recorded after an accumulation period increased with increasing pulse amplitude (linearly up to $\Delta E = 25$ mV) and was only slightly influenced by the pulse polarity. When positive pulse polarity was applied, the peak shifted to more negative potentials (from −0.32 to −0.38 V) but with negative pulse polarity, a slight deviation from linearity was observed on the calibration line (i_p vs. $[UO_2^{2+}]$) at higher uranium concentration.

The dependence of the peak current on the uranium concentration was found to be linear over a wide concentration range. For conditions such that the molar concentration ratio $[pyr.]/[UO_2^{2+}] \leqslant 10$ and the accumulation time corresponded to the values given in Table 1, the peak current vs. uranium concentration dependence was linear in the concentration range from 2×10^{-9} to 1×10^{-6} mol l^{-1} uranium(VI).

The results of normal-pulse voltammetry of the uranium—pyrocatechol complex at the HMDE corresponded to those obtained at the DME. However, when adsorptive accumulation was applied in this mode it was found that the maximum accumulation time was 60 s at the 10^{-9} mol l^{-1} uranium concentration level and only 30 s at the 10^{-8} mol l^{-1} level, for an accumulation potential of +0.20 V. Under these conditions, the dependence of the peak current on the uranium concentration was linear in the range 3×10^{-9}—1×10^{-7} mol l^{-1} uranium(VI). These results show that normal-pulse adsorptive voltammetry cannot be applied to the determination of higher amounts of uranium because of the increased amount of adsorbed species on the HMDE.

Fast-scan d.p.v. determination of uranium in the presence of other metal ions

Because of the value of the potential of the fast-scan d.p.v. peak of the uranium—pyrocatechol complex, copper(II) and lead(II) ions can be expected to interfere in the uranium determination. It was found that when no accumulation time was used, copper(II) gave, under the given conditions, a peak with an E_p value of −0.09 V; precise measurement of the height of the uranium peak was then possible up to the molar concentration ratio $[Cu^{2+}]/[UO_2^{2+}] \leqslant 10^3$, but at higher copper concentration the two peaks overlapped. Unfortunately, when the accumulation time was applied, copper as its pyrocatechol complex was also adsorbed and thus the copper peak was enhanced. The determination of uranium under these conditions was therefore possible only up to the molar ratio $[Cu^{2+}]/[UO_2^{2+}] = 10$.

The peak potential of lead(II) in the given medium was at −0.44 V. No adsorption of the lead(II) complex was observed under the given conditions; therefore when the accumulation period was employed, only the uranium peak was enhanced. The enhanced peak could be measured with very good precision up to molar $[Pb^{2+}]/[UO_2^{2+}]$ ratios of 10. If, however, no accumulation was applied, the uranium peak height was lower and the determination of uranium was possible only at lower $[Pb^{2+}]/[UO_2^{2+}]$ ratios.

To eliminate the interfering effect of these two metal ions, the complex-forming activity of a reagent with no adsorption effects was examined. From this angle, advantageous reagents are EDTA (ethylenediaminetetraacetic acid) and DCTA (1,2-diaminocyclohexanetetraacetic acid) which form soluble, stable chelates with heavy metal ions and no chelates with uranium [11]. Neither EDTA nor DCTA affected the adsorption and voltammetric behaviour of the uranium—pyrocatechol complex. In the presence of even a 10^4-fold molar excess of EDTA (or DCTA) over uranium, the uranium peak current was decreased by only 10% compared with the peak current recorded in the absence of the masking reagent. Further, it was established that these reagents were satisfactory for masking copper and lead in the adsorptive voltammetric determination of uranium. In Table 2 are presented the data obtained by adsorptive voltammetric determination of uranium in mixtures containing varying amounts of copper, lead, and cadmium. These results verify that DCTA can be used to mask interfering elements, even when they are present in 100-fold amounts compared to uranium.

Influence of surface-active substances on the adsorptive voltammetric determination of uranium

The presence of surface-active substances, which is likely in samples of natural waters, may influence the adsorption of the uranium—pyrocatechol complex. Therefore their effects on the uranium determination were examined. Gelatine, dodecylsulphate and Triton X-100 were chosen as model sub-

TABLE 2

Determination of uranium in the presence of copper, lead and cadmium by masking with DCTA[a]

Uranium added ($\mu g\ l^{-1}$)	Uranium found ($\mu g\ l^{-1}$)	Interfering element ($mg\ l^{-1}$)			Error (%)
		Pb	Cu	Cd	
11.9	11.9	1.03	0.32	0.56	0
11.9	11.5	1.03	0.32	0.56	−3.0
119.0	116.8	1.03	0.32	0.56	−2.2
119.0	123.1	1.65	0.51	0.90	3.5
238.0	232.3	1.65	0.51	0.90	−2.5
238.0	221.2	3.31	1.02	1.80	−7.0

[a]DCTA/U ≈ 100 (mole ratio).

stances. It was established that these materials had no influence on the results of the described determination when no accumulation was employed. When accumulation was used, the following phenomena were observed. As the concentration of the surfactant was gradually increased, the uranium peak current decreased to about half the value obtained in the absence of the surfactant and then remained practically constant. Examination of the dependence of the peak current on uranium concentration in the presence of these surfactants showed that the linear ranges were shorter than those obtained in the absence of the surfactant, i.e., the calibration line departed from linearity at a lower uranium concentration than in the absence of the surfactant. This effect was observed when the concentration of dodecylsulphate exceeded 4×10^{-4}%, and when the concentration of gelatine or Triton X-100 exceeded 3×10^{-5}%. At these surfactant concentrations, the i_p vs. uranium concentration dependence became non-linear at uranium concentrations of about 2×10^{-7} mol l^{-1} when the accumulation time was 3 min. At longer accumulation times, the linear range failed at lower uranium concentrations, and for shorter accumulation times, the linear dependence covered a wider concentration interval.

The results of these experiments led to the conclusion that experimental data should be evaluated by the method of standard additions. Three additions of the standard solution are necessary to ensure that the measured current value corresponds to the linear part of the i_p vs. uranium concentration dependence. If the i_p values do not increase linearly with the additions of standard solution, the sample solution should be diluted or a shorter accumulation time should be applied.

Application of the adsorptive voltammetry in the analysis of natural and sea water

Because of the high sensitivity of the adsorptive voltammetric determination of uranium, the possibility of applying this method for the determination of uranium in natural waters was tested. The average content of uranium in sea water is usually comparable to that of copper, lead and cadmium, but experiments showed that the direct determination of uranium in sea water was not possible even with masking by DCTA. Uranium was therefore separated from other elements by ion exchange. From hydrochloric acid/ethanol mixtures, uranium is retained by a strongly basic anion exchanger, while the interfering elements are not adsorbed [12]. Uranium is then eluted with 0.1 M HCl. Synthetic sea-water samples were prepared (composition: 0.5 M NaCl, 3×10^{-3} M $NaHCO_3$, 0.02 M K_2SO_4, 0.05 M $MgSO_4$, ca. 10^{-8} M Pb^{2+} and Cd^{2+}, 10^{-6} M Cu^{2+} and 5×10^{-9}—5×10^{-8} M UO_2^{2+}) and uranium was determined by adsorptive voltammetry after separation on Dowex 1-X8 anion exchanger. Under these conditions, good results were obtained: in the concentration range 1—5 $\mu g\ l^{-1}$ uranium, the relative standard deviation (r.s.d.) was 7.60%, and in the range 5—15 $\mu g\ l^{-1}$ uranium the r.s.d. was 3.60%.

Practical utilization of the described method was verified by the analysis

of filtered Atlantic sea water with a reported uranium content of 1.70 $\mu g\ l^{-1}$. From ten determinations, done as described in the Experimental section, the average value of the uranium content was found to be 1.48 $\mu g\ l^{-1}$.

Conclusion

Adsorptive accumulation of the uranium—pyrocatechol complex offers several advantages in the voltammetric determination of uranium. Among the reported electroanalytical methods for uranium, the described method is distinguished by the lowest detection limit and by the short accumulation time even for low uranium concentrations (10^{-9} mol l^{-1}). Because of the relatively positive potential of the measured peak, the effect of interfering elements is minimized. However, for the analysis of samples with complex composition, a rapid and simple anion-exchange separation is recommended.

Uranium can be accumulated on the HMDE under identical conditions as given above in the form of its complex with 8-quinolinol. The corresponding peak appears at a more negative potential (—0.45 V) and the determination is less sensitive [13].

REFERENCES

1 J. V. Collat and J. J. Lingane, J. Am. Chem. Soc., 76 (1954) 4214.
2 R. Keil, Fresenius. Z. Anal. Chem., 292 (1978) 13.
3 R. Kalvoda, Anal. Chim. Acta, 138 (1982) 11.
4 H. Berge and H. Ringstorff, Anal. Chim. Acta, 55 (1971) 113.
5 H. Sohr and L. Liebetran, Fresenius Z. Anal. Chem., 219 (1966) 409.
6 K. H. Lubert, M. Schnurrbusch and A. Thomas, Anal. Chim. Acta, 114 (1982) 123.
7 K. Izutsu, T. Nakamura and T. Oku, Nippon Kagaku Kaishi, 8 (1980) 1656.
8 K. Izutsu, T. Nakamura, R. Takizawa and H. Hanawa, Anal. Chim. Acta, 149 (1983) 147.
9 J. Matysik, Ann. Univ. Mariae Curie-Sklodowska, Sect. AA, 21 (1966) 31.
10 M. A. DeSesa, D. M. Hume, H. C. Glamm and D. D. DeFord, Anal. Chem., 25 (1953) 983.
11 R. Přibil and A. Blažek, Collect. Czech. Chem. Commun., 16 (1951) 567.
12 J. Korkisch and J. Hazan, Talanta, 11 (1964) 1157.
13 N. K. Lam, PhD. Thesis, J. Heyrovský Inst. Phys. Chem. and Electrochem., Czechoslovakian Academy of Sciences, Prague, 1983.

Analytica Chimica Acta, 154 (1983) 87—94
Elsevier Science Publishers B.V., Amsterdam — Printed in The Netherlands

PRECONCENTRATION AND DIFFERENTIAL PULSE VOLTAMMETRY OF BUTYLATED HYDROXYANISOLE AT A CARBON PASTE ELECTRODE

JOSEPH WANG* and BASSAM A. FREIHA
Department of Chemistry, New Mexico State University, Las Cruces, NM 88003 (U.S.A.)
(Received 20th April 1983)

SUMMARY

Butylated hydroxyanisole (BHA) and other tocopherols are shown to accumulate very strongly onto carbon paste, with the surface species retaining their characteristic electroactivity. This accumulation serves as a preconcentration step which improves the voltammetric measurement with respect to the sensitivity and selectivity. After 5-min preconcentration, a detection limit near 2×10^{-8} M BHA is obtained. Enhanced selectivity is achieved if the electrode is transferred into an electrolytic blank solution between the preconcentration and measurement steps. The accumulated analyte can then be quantified in the presence of a 10^3-fold amount of a solution species with similar redox potential. The differential pulse stripping response is evaluated with respect to concentration dependence, reproducibility, preconcentration period, detection limit, and other variables. The preconcentration/medium exchange approach is exploited for selective detection of BHA in a flow injection system. Applicability to various real samples is illustrated.

The determination of antioxidants and tocopherols is of special interest in the food, pharmaceutical, or cosmetic industries. Various voltammetric procedures have been introduced for this purpose utilizing mercury [1], platinum [2] and carbon [3, 4] working electrodes. These procedures are of only moderate sensitivity; the resulting detection limits (micromolar level) are not sufficient when traces of these important compounds have to be determined. In addition, irreproducible voltammetric data may be caused by adsorption of analyte(s) [3].

Recent studies have been initiated to exploit the accumulation of organic compounds at electrode surfaces for enhancing the sensitivity and selectivity of their voltammetric measurement [5—8]. Various organic compounds such as phenanthrenequinone [7], dopamine [9], chlorpromazine [5, 10] and adriamycin [6], have been quantified after their controlled adsorptive accumulation at solid electrodes. Alkaloids, surfactants and other compounds have been accumulated and measured at a static mercury drop electrode [8]. In this report, the spontaneous controlled accumulation of BHA and other similar compounds at carbon paste electrodes is exploited to improve their voltammetric response. Although the extractive/adsorptive accumulation of organic molecules at carbon paste electrodes has been known

0003-2670/83/$3.00

for more than 15 years [11], its analytical utility as a preconcentration step prior to the voltammetric measurement has been reported only recently [5–8]. Increased sensitivity is obtained as a result of the preconcentration step, and a high degree of selectivity is achieved by transferring the electrode into a blank solution between the preconcentration and measurement steps. The effects of various operational parameters on the response for butylated hydroxyanisole are examined in this paper. The potential of this approach to batch and flow systems is illustrated.

EXPERIMENTAL

Apparatus

The working electrode material was carbon paste. Two formulations of the paste were employed, utilizing mineral oil and silicone grease (Dow Corning) as pasting agents. In both cases, the carbon paste was made by thoroughly mixing 2.5 g of graphite powder (Acheson Graphite, Grade 38) with 1.5 g of the pasting agent. The paste was packed into one end of a glass tube (3-mm i.d., 5-mm o.d.); the other end of the paste was connected to a copper wire. A fresh carbon paste surface was used each day. The cell was a Bioanalytical Systems Model VC-2 voltammetric cell. In experiments involving the medium-exchange procedure, a second (measurement) cell was used. The cell was joined to the working electrode, reference electrode (Ag/AgCl, Model RE-1, Bioanalytical Systems) and platinum wire auxiliary electrode through holes in its teflon cover. A magnetic stirrer and a 1.2-cm long stirring bar provided the convective transport during the preconcentration. The flow injection system has been described earlier [12]. The injection valve was a Rheodyne Model 7010 with a 200-μl sample loop. The electrochemical detector was a Bioanalytical Systems Model TL-4 thin-layer cell. Differential pulse voltammograms were recorded with a Princeton Applied Research Model 174 polarographic system and a Houston Omniscribe strip-chart recorder. Instrument settings were as follows: 10 mV s^{-1} scan rate, 25 mV amplitude, 1-s clock time.

Reagents

Deionized water and absolute ethanol (U.S. Industrial Chemical Co.) were used to prepare all solutions. The supporting electrolyte was 0.10 M phosphate buffer (pH 7.4) prepared from a 1:4 mixture of KH_2PO_4 and K_2HPO_4. Submillimolar stock solutions of butylated hydroxyanisole (BHA; reagent grade; Sigma Chemical Co.) were prepared each day by dissolving the compounds in 2 ml of ethanol and making up to 100-ml volume with deionized water. Various real samples were used as discussed below.

Procedure

For the preconcentration step, the carbon paste electrode was immersed in a stirred 10-ml sample solution for a given time period. During this period,

zero potential was applied at the electrode. The stirring was then stopped, and differential pulse measurement of the surface species was made. In experiments involving medium-exchange, the preconcentration proceeded at an open-circuit; the electrode was then removed from the sample solution, rinsed thoroughly with water for 15 s, and re-immersed in a second cell containing the supporting electrolyte solution of choice. The initial potential was then applied, and after the current decay, the voltammogram was recorded. After the potential scan, the electrode was held at +0.75 V for 2 min to clean it from the remaining adsorbable species. Specific details of the flow-injection procedure have been described [12].

RESULTS AND DISCUSSION

The preconcentration of BHA (I) is easily seen from differential pulse voltammograms at a carbon paste electrode which has been immersed in a

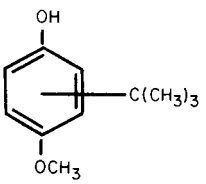

(I)

stirred 3.7×10^{-7} M BHA solution for increasing periods of time (Fig. 1). The peak height increases with increasing preconcentration time, indicating

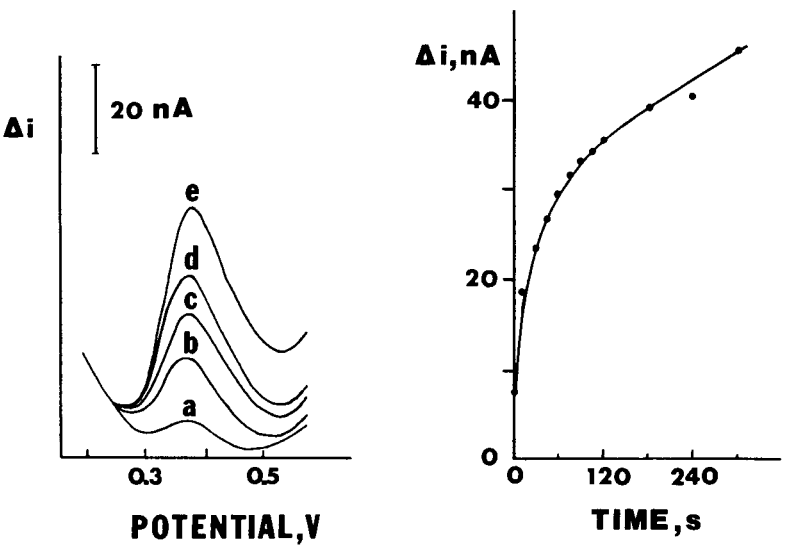

Fig. 1. Effect of preconcentration period on the differential pulse peak current from 3.7×10^{-7} M BHA in 0.1 M phosphate buffer. Preconcentration period: (a) 0, (b) 15, (c) 45, (d) 105, (e) 300 s. Stirring rate, 550 rpm. Carbon (mineral oil) paste electrode.

an enhancement of BHA concentration at the carbon paste. For a 5-min preconcentration period, a 7-fold enhancement of the peak current is observed over that attained by conventional solution-phase pulse voltammetry (compare curves a and e). As a result, submicromolar levels of BHA can be easily quantified; in contrast, the same sample concentration approaches the detection limit of conventional pulse voltammetry (curve a). Also shown in Fig. 1 is the resulting plot of peak current vs. preconcentration period. As this period increases, the peak current rises rapidly at first and then it levels off. Such nonlinear dependence is expected for a preconcentration step of this nature [7, 9]. By holding the electrode at +0.75 V for 2 min the electrode is "cleaned" from the accumulated BHA as indicated from the subsequent differential pulse scan.

The strong accumulation is also indicated from experiments involving the medium-exchange procedure; when the electrode is transferred (between the preconcentration and measurement steps) from the BHA solution to an electrolytic blank solution a well-defined BHA peak is obtained. The advantages of the medium-exchange procedure are illustrated below. Peak currents recorded following preconcentrations at 0.0 V and with open-circuit conditions are similar. For convenience and speed, open-circuit conditions were used in conjunction with the medium-exchange procedure while a 0.0 V potential was used in the direct mode. Both formulations of the carbon paste (with the mineral oil and silicone grease pasting agents) showed similar degrees of accumulation. In contrast, no accumulation was observed when a glassy carbon electrode was used. These data indicate that the accumulation process involves extraction into the paste, rather than adsorption at the electrode surface; various hydrophobic compounds are known to extract into carbon paste electrodes [10]. A similar degree of BHA accumulation was obtained from a 10% ethanol/90% phosphate buffer mixture. No accumulation was observed from a 50% ethanol/50% phosphate buffer mixture. The silicone-grease carbon-paste electrode was used in these experiments because of its greater stability in such mixtures. Another insight into the nature of the accumulation process was achieved by utilizing different compositions of the carbon paste electrode. By increasing the weight percentage of silicone grease from 28% to 44%, a 50% increase in the peak current was observed (conditions: 3 min preconcentration from a 1×10^{-6} M BHA solution, followed by exchange to phosphate buffer, not shown). Similar increase in the signal was observed with chlorpromazine as the analyte [13]. The accumulation of BHA is affected by the mass-transport conditions during the preconcentration period. Peak currents of 9.6, 20.9, 21.5 and 23.0 nA were obtained at stirring rates of 0, 250, 350 and 550 rpm, respectively (conditions: 3×10^{-6} M BHA in a 0.1 M phosphate buffer, carbon (mineral oil) paste electrode, differential pulse measurement after 2-min preconcentration and medium exchange).

Figure 2 illustrates the response to successive standard additions of BHA (2.5×10^{-7} M increments). The well-defined peaks allow convenient measure-

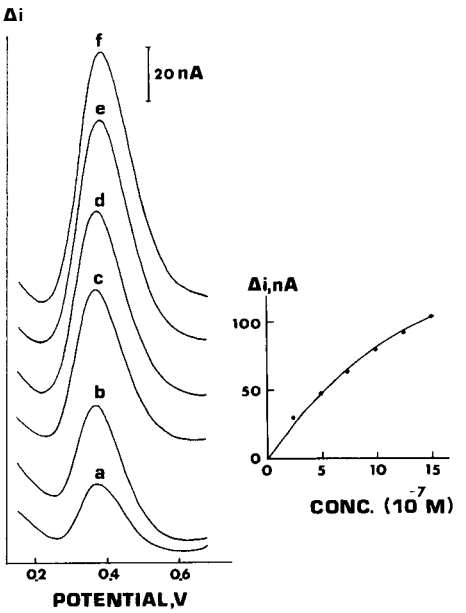

Fig. 2. Differential pulse voltammograms obtained after increasing the BHA concentration in 2.5 × 10^{-7} M steps (a—f). Preconcentration for 2 min with 550 rpm stirring, 0.1 M phosphate buffer. Carbon (mineral oil) paste electrode. The zero current of the individual curves is displaced for clarity.

ment at the submicromolar concentration level. The plot of peak current vs. concentration (also shown in Fig. 2) is nonlinear. Such curvature is expected for a preconcentration step of this nature [6—9]. The quantitative significance lies in the fact that the peak current for a given time and stirring rate is reproducible and related to the bulk concentration. The reproducibility was estimated by eight successive measurements on a 7.5 × 10^{-6} M BHA solution (conditions: 1 min preconcentration with 550 rpm stirring, carbon (mineral oil) paste electrode). The mean peak current was 4.99 nA with a range of 4.80—5.26 nA. The relative standard deviation over the complete series was 3.8%. The precision obtained compares favorably with that reported for other compounds accumulated at solid electrodes [6, 7]. A detection limit near 2 × 10^{-8} M would be expected based on the signal-to-noise characteristics (S/N = 2) of Figs. 1 (curve e) and 2 (curve a). Measurements of a 5 × 10^{-8} M BHA solution confirmed this detectability (not shown). Hence, at low analyte concentration, the preconcentration provides a considerably improved response over that obtained by solution-phase pulse voltammetry.

Enhanced selectivity is another important advantage of the preconcentration approach. This advantage is achieved by transferring the electrode from the complex sample to a blank electrolytic solution between the preconcentration and measurement steps. Thus, the surface-bound species is measured

without interferences from solution phase species. Figure 3 illustrates this improvement in the response of BHA. Curves A(a) and A(b) are the differential pulse responses for a solution containing 1×10^{-6} M BHA and 1×10^{-3} M ascorbic acid recorded with and without medium exchange, respectively. When the measurement is performed in the sample solution, the large ascorbic acid oxidation current masks completely the BHA peak. After exchanging to the blank solution, the surface-bound BHA is quantified without the ascorbic acid interference. This improvement is emphasized by the significant change (25-fold) in the current scale. Thus, micromolar levels of BHA can be quantified even when a 10^3-fold concentration of a species with similar redox potentials is present initially. Figure 3B illustrates the same advantage as applied to real samples. The soft drink mix (Kool-Aid) contained a significant concentration of ascorbic acid (and other constituents) and micro levels of BHA. In the direct mode (curve b), large currents from macro solution constituents swamp the peak current of the surface-bound species. After

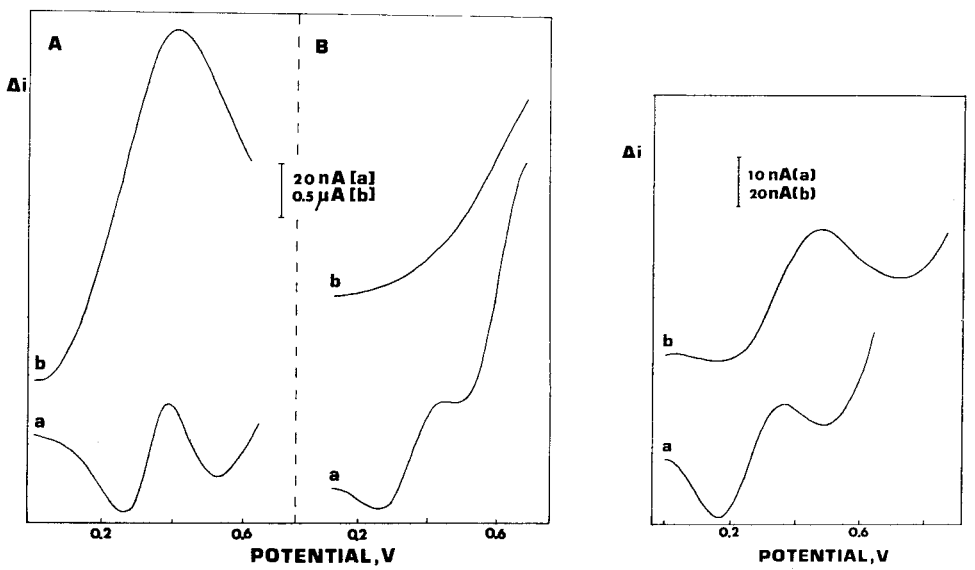

Fig. 3. Differential pulse voltammograms: (a) with and (b) without medium exchange after the preconcentration step. Samples: (A) 1×10^{-6} M BHA and 1×10^{-3} M ascorbic acid in 0.1 M phosphate buffer; (B) Kool-Aid soft drink mix. Solution prepared by dissolving 0.1 g of the mix in 0.2 ml of ethanol and diluting to 10 ml. Exchange solution, 0.1 M phosphate buffer. Preconcentration: (A) 3 and (B) 5 min; 550 rpm stirring. Carbon (mineral oil) electrode.

Fig. 4. Differential pulse response for (a) One-A-Day multivitamin and (b) Mazola corn oil samples. Preconcentration for 2 min at 550 rpm stirring; measurement after medium exchange to a phosphate buffer solution. Carbon (silicone grease) paste electrode. The multivitamin tablet and 1.0 g of the corn oil were diluted in 100 ml of ethanol; 2 ml of the multivitamin solution or 1 ml of the oil solution was dissolved with phosphate buffer to 10 ml to prepare the sample. Exchange solution, 0.1 M phosphate buffer.

medium exchange to a phosphate buffer solution (curve a), the BHA peak is detected.

Figure 4 demonstrates the feasibility of measuring other tocopherols, such as vitamin E, in real samples using the preconcentration/medium-exchange approach. Curves (a) and (b) are the responses recorded in the phosphate buffer solution after preconcentration from multivitamin and corn oil samples, respectively. Because the medium-exchange procedure is utilized, the accumulation of the tocopherols is obvious. No accumulation was observed when butylated hydroxytoluene (BHT) was tested. This can be used to improve the selectivity toward BHA in the presence of BHT. For example, addition of 3×10^{-6} M BHT to a solution containing 3×10^{-6} M BHA did not affect the response following preconcentration/medium exchange.

The preconcentration approach can be exploited as a selective detection mode for flow injection systems, based on a recently developed manifold procedure [12]. Compared to conventional amperometric detection for flow injection systems, this procedure provides remarkable selectivity toward the accumulated analyte, as a result of combining its intimate contact with the electrode surface with the medium-exchange procedure. For this purpose, the preconcentration step is started as the sample plug arrives in the detector and terminated after it has passed through. Then, the stripping step is done while the carrier (blank) solution passes through the detector, i.e., medium exchange is obtained. The preconcentration/medium-exchange flow-injection manifold was applied for selective and sensitive measurements of BHA (Fig. 5). Curves A (a—d) represent the response after successive injections of

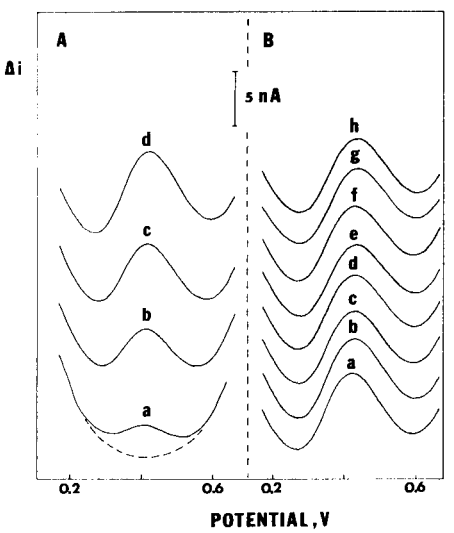

Fig. 5. Differential pulse voltammograms for injections of BHA solutions. A(a—d): BHA solutions of ascending concentrations, $1—4 \times 10^{-6}$ M. B(a—f): Repeated injections of a 4×10^{-6} M BHA solution; (g, h) after addition of 1×10^{-4} M ascorbic acid to the BHA solution. Carbon (silicone grease) paste electrode. Carrier solution, 0.1 M phosphate buffer. Preconcentration, 1 min at 0.0 V; "cleaning", 1 min at +0.7 V. Flow rate, 0.4 ml min^{-1}. The zero current of the individual curves is displaced for clarity.

BHA solutions of ascending concentrations (1—4 × 10^{-6} M). Linear response is obtained (after correcting for the blank response, dotted line). Least-squares treatment of these data yielded the equation I(nA) = (2.37 ± 0.02) C(10^{-6} M) + 0.61 ± 0.06 nA with S_{yx} = 0.051 nA and r = 0.999. Curves B (a–h) illustrate the precision and selectivity of the flow-injection procedure. For the series of eight successive injections of a 4 × 10^{-6} M BHA solution, a mean peak current of 8.55 nA was found, with a range of 8.1—9.2 nA and a relative standard deviation of 4.9%. Curves (a—f) of this series were recorded with the BHA as single analyte in the sample; curves g and h were obtained after addition of 1 × 10^{-4} M ascorbic acid to the same solution. These data demonstrate again that excess of solution phase species does not affect the determination of BHA.

REFERENCES

1 L. I. Smith, L. J. Spillane and I. M. Kolthoff, Anal. Chem., 64 (1942) 447.
2 D. Cozzi, G. Raspi and L. Nucci, J. Electroanal. Chem., 12 (1966) 36.
3 S. S. Atuma and J. Lindquist, Analyst, 98 (1973) 886.
4 H. D. McBride and D. H. Evans, Anal. Chem., 45 (1973) 446.
5 J. Wang and B. A. Freiha, Anal. Chim. Acta, 148 (1983) 79.
6 E. N. Chaney and R. P. Baldwin, Anal. Chem., 54 (1982) 2556.
7 H. Y. Cheng, L. Falat and R. L. Li, Anal. Chem., 54 (1982) 1384.
8 R. Kalvoda, Anal. Chim. Acta, 138 (1982) 11.
9 J. W. Siria and R. P. Baldwin, Anal. Lett., 12 (1980) 577.
10 T. B. Jarbawi and W. R. Heineman, Anal. Chim. Acta, 135 (1982) 359.
11 C. A. H. Chambers and J. L. Lee, J. Electroanal. Chem., 14 (1967) 309.
12 J. Wang and B. A. Freiha, Anal. Chem., 55 (1983) 1285.
13 B. A. Freiha, Ph.D. Thesis, New Mexico State University, Las Cruces, NM, 1984.

Analytica Chimica Acta, 154 (1983) 95—104
Elsevier Science Publishers B.V., Amsterdam — Printed in The Netherlands

THE EFFECTS OF COPPER—ZINC AND COPPER—CADMIUM INTERMETALLIC COMPOUNDS IN DIFFERENT SYSTEMS USED FOR ANODIC STRIPPING VOLTAMMETRY

JOHN A. WISE, DARYL A. ROSTON[a] and WILLIAM R. HEINEMAN*
Department of Chemistry, University of Cincinnati, Cincinnati, OH 45221 (U.S.A.)
(Received 13th April 1983)

SUMMARY

The Cu—Zn intermetallic compound resulting from simultaneous deposition of copper and zinc at a hanging mercury drop electrode (HMDE) and at preformed mercury film electrodes (MFE) has been studied. Goals were to determine what conditions can be used to avoid intermetallic compound formation and to reduce errors that result from the method of standard additions. For Cu^{2+} and Zn^{2+} concentrations in the ng ml^{-1} range, the use of shortened preconcentration times in conjunction with a differential pulse stripping waveform and the HMDE show significant reduction in the extent of the interference. The Cu—Cd interference was also characterized at preformed MFE's and at MFE's deposited in situ from 5—300 μg ml^{-1} mercury(II) solutions. No significant interference with the cadmium stripping wave was observed with preformed MFE's, but peak depression was observed when the electrodes were deposited in situ. The degree of interference was found to decrease with both increased mercury(II) concentration and decreased copper(II) concentration. Errors in the standard addition method are minimal when the copper(II) concentration is not significantly altered.

Anodic stripping voltammetry (a.s.v.) is widely used for the determination of trace metals in environmental, biological, and industrial samples. The advantage of this technique is its low detection limit. An inherent difficulty with stripping voltammetry is the interaction between metal atoms within the mercury electrode [1, 2]. A frequently noted example is the interaction of copper and zinc to form Cu—Zn intermetallic species. The Cu—Zn intermetallic compounds are oxidized at or near the same potential as copper, causing errors when Cu^{2+} and Zn^{2+} are quantified simultaneously by a.s.v. [3—5]. Copper and cadmium have been reported to exhibit a similar interaction, with the presence of copper causing a depression of the cadmium stripping wave [6, 7]. However, the nature of this interference is still in doubt.

One approach to the alleviation of this problem involved the use of excess of gallium to form preferentially the Cu—Ga intermetallic species, which has

[a]Present address: Department of Chemistry, Northern Illinois University, DeKalb, IL 60115, U.S.A.

0003-2670/83/$03.00

a higher formation constant than that of the Cu--Zn compounds [3]. Another approach involves the use of a twin-electrode thin-layer cell, in which the two elemental species forming the intermetallic compound are deposited at two different working electrodes [8].

Because Cu, Cd, and Zn are among the metals most frequently determined by a.s.v. and are invariably found in environmental and biological samples, an accurate assessment of the magnitude of the interferences observed between pairs of these metals with different a.s.v. systems is desirable. Numerous reports have characterized the Cu--Zn intermetallic compound formation in terms of formation constants and solubility products [9—11]. However, uncertainties associated with estimations of amalgam concentrations achieved with "typical" a.s.v. conditions make the use of such constants inconvenient for routine determinations. Also, because several experimental conditions have been used to study intermetallic interferences, the use of reported data to assess the extent of interference with a given a.s.v. system is unreliable.

This paper describes studies of the effects of parameters such as electrode geometry, electrode volume, and metal ion concentration on interferences caused by intermetallic compound formation. Differences in electrode geometry were studied by direct comparison of a hanging mercury drop electrode (HMDE) and two types of mercury film electrodes (MFE), the preformed and in situ deposited types on both glassy carbon and wax-impregnated graphite substrates. Electrode volume was studied using preformed MFE's of different film thickness and by using various concentrations of mercury(II) ions in experiments with in situ deposited MFEs.

EXPERIMENTAL

Apparatus

A conventional electrochemical cell containing 10 ml of standard solution was used in all experiments. The HMDE (PARC, Princeton, NJ) had a volume of 4.3×10^{-4} ml. All working electrodes were used in conjunction with a saturated calomel reference electrode and a platinum wire auxiliary electrode. Mass transport during deposition was enhanced by magnetic stirring with a magnetic stirrer, powered by a variable transformer.

All linear potential ramp a.s.v. experiments were done with a potentiostat (Model DCV-4; Bioanalytical Systems, West Lafayette, IN). A PAR 174A polarographic analyzer was used for differential pulse a.s.v. experiments. The potentiostat used for stripping coulometry was of conventional operational amplifier design. An X-Y recorder (Houston Instrument Omnigraphic 2000) recorded all voltammetric measurements.

Reagents

Standard solutions of Cu^{2+}, Cd^{2+}, and Zn^{2+} were prepared by appropriate dilutions of atomic absorption standards (Fisher Scientific Co.). Supporting

electrolyte was a 0.1 M sodium acetate—0.01 M nitric acid buffer solution, pH 5.5. The supporting electrolyte was preelectrolyzed for about 240 h at —1.5 V over a mercury pool electrode. Standard solutions of mercury for in situ MFE's were prepared from triply distilled mercury and Ultrex nitric acid (J. T. Baker) and diluted with supporting electrolyte.

Procedures

Electrode and cell preparation. Electrochemical cells were stored in dilute nitric acid to minimize contamination. Wax-impregnated graphite electrodes were made from POCO FXI spectroscopic graphite rods in the manner reported previously [12]. The glassy carbon electrodes were obtained from Bioanalytical Systems. The MFE substrates were polished with fine alumina powder each day. Preformed mercury film electrodes were deposited at —0.7 V from a 0.006 M $Hg(NO_3)_2$—0.5 M KNO_3 solution that had been purged with nitrogen for 15 min. The rate of stirring was adjusted until the current was 1 mA. To obtain different film thicknesses, deposition times were varied from 15 s to 20 min. After film deposition, the electrodes were carefully rinsed with distilled deionized water and immersed in supporting electrolyte solution. In situ MFE's of different film thicknesses were formed by altering the added mercury(II) ion concentration, while keeping a constant deposition time of 300 s.

Estimation of film thickness. Stripping coulometry was used to estimate the film thickness achieved with the different deposition periods. After deposition of the film, stirring was stopped. After 60 s, the potential was stepped from —0.7 V to +0.7 V, causing oxidation of the deposited mercury. The resulting current response was integrated. Charge accumulated was then equated to a quantity of mercury and then to a film thickness, assuming a uniformly thick deposit. The amount of mercury comprising the preformed films varied from 0.039×10^{-6} to 1.25×10^{-6} mol.

Anodic stripping voltammetry. Solutions used for a.s.v. experiments were purged with nitrogen for 15 min before use. In each experiment, deposition was done at —1.3 V for Cu—Zn and —1.1 V for Cu—Cd while the solution was stirred; after a 30-s quiescent period, the positive scan was started. A 15-mV s^{-1} scan rate was used for linear potential sweep a.s.v. with preformed MFE's and a 40-mV s^{-1} scan rate with in situ deposited MFE's. Pertinent PAR 174A parameters were as follows: current range, variable (depending on experimental conditions); clock time, 0.5 s; modulation amplitude, 25 mV. The length of the deposition period was varied, depending on the experimental system under study. Linear potential sweep a.s.v. experiments were done with a 300-s deposition period. Deposition periods of 90 s were used for differential pulse a.s.v. experiments.

RESULTS AND DISCUSSION

Copper and zinc

The effect of the Cu—Zn interference on stripping voltammetry is illustrated in Fig. 1. When zinc ions from a 470 ng ml^{-1} solution are deposited at a preformed MFE for 300 s, the subsequent positive scan produces a well defined zinc stripping wave. If the same experiment is repeated with 210 ng ml^{-1} Cu^{2+} in the sample, a severely depressed zinc wave is recorded along with an enhanced copper wave. This well known problem, caused by the formation of Cu—Zn intermetallic compound(s), can be avoided in determinations of copper ions by depositing at potentials that are not so negative as to cause deposition of zinc ions.

The peak stripping current for zinc for a solution containing 2 μg ml^{-1} each of Zn^{2+} and Cu^{2+}, is smaller than expected because the intermetallic interference is most severe when nearly equimolar amounts of Cu^{2+} and Zn^{2+} are present. When enough zinc ion is added to change the Cu^{2+}/Zn^{2+} ratio from 1:1 to 1:2, a stripping current for Zn closer to the expected value is obtained. Hence, the Cu^{2+}/Zn^{2+} ratio influences the magnitude of the interference. Standard-addition experiments for 2.0 μg ml^{-1} Zn^{2+} solution yielded a

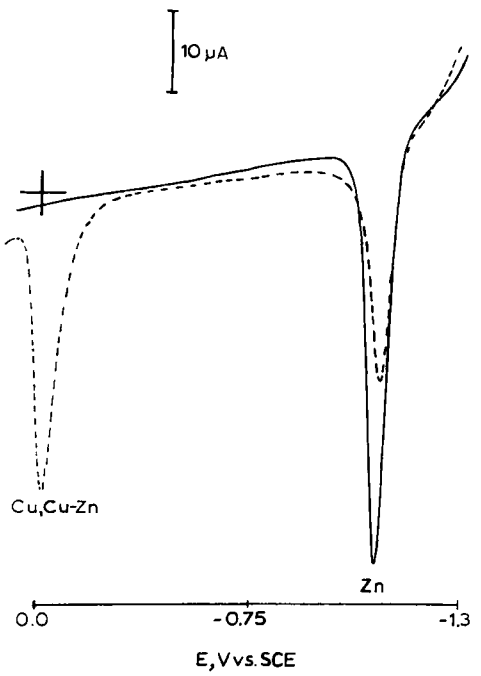

Fig. 1. Effect of codeposition of Cu^{2+} and Zn^{2+} on anodic stripping voltammograms; (———) stripping voltammogram recorded after a 300 s deposition from a 470 ng ml^{-1} Zn^{2+} solution at an MFE; (— — —) stripping voltammogram obtained with same experimental conditions after addition of 213 ng ml^{-1} Cu^{2+}. Linear sweep scan rate, 15 mV s^{-1}.

concentration of 2.03 μg ml^{-1} with no Cu^{2+} present and 0.35 μg ml^{-1} with 2 μg ml^{-1} Cu^{2+} present. Thus, formation of the intermetallic compound impedes quantitation of Zn^{2+} in the presence of Cu^{2+}. Similar effects have been shown previously [3, 4].

Investigation of parameters for the alleviation of Cu—Zn interferences at MFE's. Several papers have reported the use of MFE's in a.s.v. Numerous advantages accrue from the use of MFE's, e.g., increased sensitivity and resolution [6]. Resolution is an important characteristic when Cu^{2+}, Pb^{2+}, Cd^{2+}, and Zn^{2+} are determined simultaneously because the cadmium and lead stripping waves can overlap. Various film thicknesses have been advocated in the literature. Florence [13] has demonstrated the advantages of in situ deposition of mercury films, which results in film thicknesses less than 100 nm. Copeland and Skogerboe [14] recommended the use of films several hundred nanometers thick. Christie and Osteryoung [15] showed that many of the advantages that result from the use of MFE's are retained with films as thick as 1000 nm.

Because of the widespread use of the MFE for stripping voltammetry and the severity of the Cu—Zn interferences often observed when MFE's are used, the effectiveness of varying film thickness to mitigate or eliminate intermetallic interferences was evaluated. Stripping voltammetric experiments were performed with mercury films of four different thicknesses (35 nm, 350 nm, 550 nm and 1150 nm) on wax-impregnated graphite. With films of each thickness, stripping voltammetry was applied to 48, 470, and 930 ng ml^{-1} Zn^{2+} solution. For each zinc concentration, the Cu^{2+} concentration was changed from 0 to about 1000 ng ml^{-1}. The deposition period was 300 s. The metal ion concentrations and deposition period used in the experiments are based on a survey of a.s.v. applications literature and represent typical conditions. Figure 2 shows the effects of Cu^{2+} concentration on the peak current of the zinc stripping wave when 35 and 1150 nm films were used. Although the zinc stripping wave is depressed less when the thicker film is used, the interference is still pronounced. Also, the interference is strongly dependent on the Cu^{2+}/Zn^{2+} ratio in both cases.

In addition to the film thickness study, the effectiveness of using a decreased preconcentration time in conjunction with differential pulse voltammetry to minimize Cu—Zn interferences by minimizing the concentrations of copper and zinc ions in the film was evaluated. In the literature, the preconcentration used with differential pulse a.s.v. is generally less than the preconcentration used with linear potential sweep a.s.v. A series of stripping experiments were completed with the same experimental conditions used for the data summarized in Fig. 2 except that a 90-s deposition time was used. Results are shown in Fig. 3. Although the shorter deposition period decreased the magnitude of the depression for the zinc wave, the interference was still pronounced and dependent on the Cu^{2+}/Zn^{2+} ratio.

Investigation of Cu—Zn interferences at a HMDE. Because the MFE has a higher surface-to-volume ratio than the HMDE, it has been generally assumed

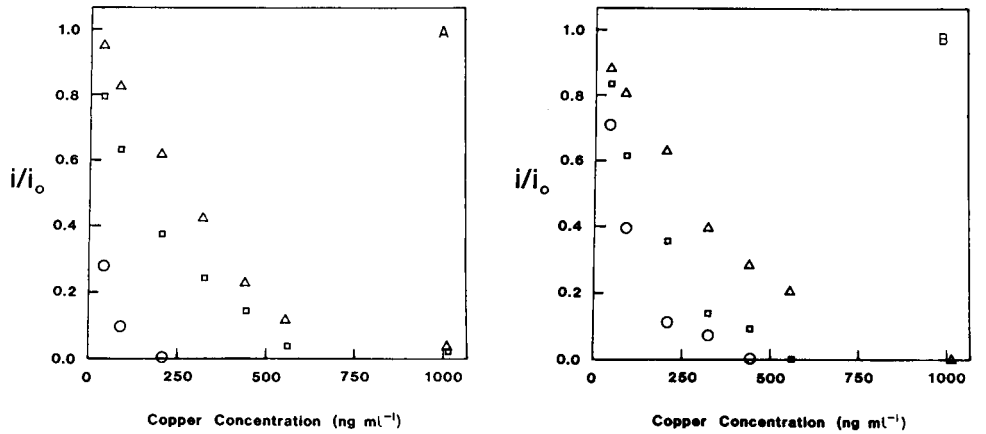

Fig. 2. Intermetallic interferences for Cu^{2+} and Zn^{2+} for mercury film thicknesses of (A) 35 nm and (B) 1150 nm. Zn^{2+} concentrations (ng ml^{-1}): (○) 48; (□) 470; (△) 930. Preconcentration period, 300 s; linear sweep scan rate, 15 mV s^{-1}. i/i_0 is the ratio of the zinc stripping currents after (i) and before (i_0) addition of Cu^{2+}.

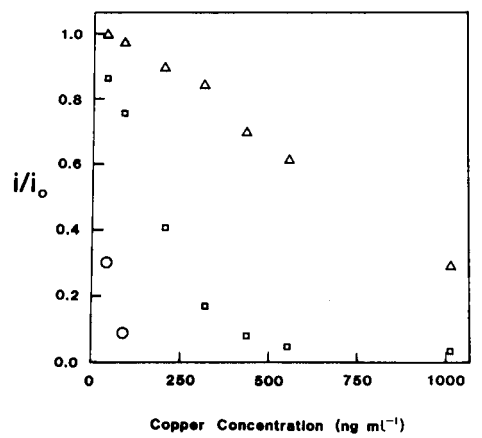

Fig. 3. Intermetallic interferences for Cu^{2+} and Zn^{2+} using the differential pulse waveform for the anodic scan. Film thickness, 350 nm. Preconcentration period, 90 s; differential pulse scan rate, 5 mV s^{-1}. Other conditions as in Fig. 2.

that intermetallic interferences are more pronounced at MFE's [3, 10]. Some authors have [3, 5, 10], and other authors have not [16, 17], reported evidence for Cu—Zn interference during determinations by a.s.v. at the HMDE. In contrast, Cu—Zn interferences have been detected whenever the MFE has been used, regardless of the experimental conditions [3, 4, 10, 18, 19].

To provide a direct comparison of the severity of the Cu—Zn problem at the different electrodes, a.s.v. conditions identical to those used in obtaining Figs. 2 and 3 were repeated with a HMDE rather than a MFE. Results are

shown in Fig. 4. When the HMDE was used, the zinc stripping peak was not depressed as the Cu^{2+} level was increased. Only when excessive preconcentration from samples of very high concentration was attempted was any depression of the zinc stripping wave observed.

Copper and cadmium

Evidence suggesting the existence of a Cu—Cd intermetallic compound is not as convincing as that for the Cu—Zn compounds. Some studies have noted a depression of the cadmium stripping wave in the presence of copper [6, 7]. The formation of a Cu—Cd intermetallic compound was a logical and accepted explanation of these results. Other groups, however, were unable to detect a Cu—Cd intermetallic compound [4, 20]. From the available literature and this work, it appears that the Cu—Cd interference is minimal or nonexistent when a HMDE is used. For this reason, evaluation of this interference is centered on the effect observed with mercury film electrodes.

Investigation of Cu—Cd interference at preformed MFE's. Pre-formed MFE's were prepared with film thicknesses of 550, 350, 200, 70, 35, and 17.5 nm on both wax-impregnated graphite (WIG) and glassy carbon (GC) substrates. Figure 5 shows results obtained with a 35-nm film deposited on a GCE by the procedure described earlier. Comparing this behavior with that observed in the Cu—Zn case (Fig. 2), there is no observable depression of the cadmium stripping wave when the copper ion concentration is increased. Similar results were obtained with electrodes of other film thicknesses. As long as the films were uniformly deposited, the peak stripping current for cadmium remained constant within normal experimental error. Depressions in the cadmium stripping current were observed, however, when the mercury films were not uniform. The major sources of these problems were: (1) disruption of the electrode surface by gas bubbles which impeded the deposition of mercury; (2) damage to the film during transfer from the deposition cell to the measurement cell; and (3) incomplete film formation caused by poor surface preparation of the substrate electrode. The symptoms observed were, most notably, a large positive shift in the solvent breakdown potential with the first addition of Cu^{2+}, multiple stripping waves, or the appearance of a

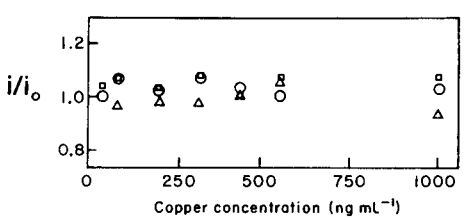

Fig. 4. Investigation of Cu—Zn interferences at a HMDE. Conditions as in Fig. 2.

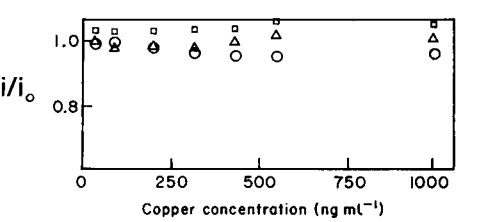

Fig. 5. Investigation of Cu—Cd interferences at a 35-nm MFE. Conditions as in Fig. 2, with cadmium solutions of the same concentrations as given for zinc.

shoulder on the cadmium wave. The most reproducible results were obtained with preformed films with thicknesses greater than 200 nm.

Cu—Cd interference at in situ MFE's. When the MFE is deposited in situ, a depression in the cadmium wave is readily observed. With this procedure, the formation of the mercury film and the deposition and preconcentration of analyte species occurs simultaneously. The resultant films are typically less than 10 nm thick. The results obtained at a WIGE when the Hg^{2+} concentration was 125 μg ml^{-1} can be seen in Fig. 6. Again, all conditions were the same as used in the preformed MFE experiments. As the concentration of Cu^{2+} is increased, the measured cadmium stripping current is decreased. The depression appears to depend only on the Cu^{2+} concentration and not on the Cu/Cd ratio (compare Figs. 2 and 6). This is in agreement with the observations of Florence [7]. The thickness of the mercury film is a factor in the degree of suppression observed in the cadmium wave with in situ electrodes also. As the concentration of Hg^{2+} is decreased, the peak stripping current for cadmium is also decreased (Fig. 7).

From these results, it appears that the interference is caused by a surface phenomenon. One possibility is that the solubility of copper in mercury may be exceeded at parts of the electrode surface during the in situ deposition process (even when the total Cu/Hg solubility ratio is not exceeded) resulting in the direct plating of copper and cadmium onto copper surfaces. This was first postulated by Ostapczuk and Kublik [20], and the results here support their findings. In the competition for electroactive sites on the electrode surface during the deposition step, there are likely to be areas where only copper deposits and/or where it exceeds its solubility in mercury. As the concentration of Hg^{2+} is decreased, it is logical to conclude that the probability of this occurring is increased so that the suppression would increase as the Hg^{2+} concentration is decreased. It also appears that this suppression can be alleviated by raising the Hg^{2+}/Cu^{2+} ratio either by increasing the Hg^{2+} concentration or by diluting the sample.

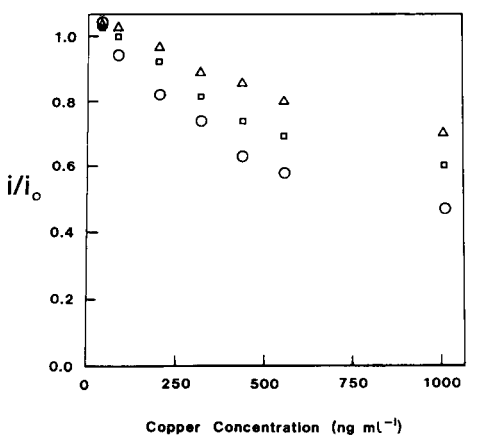

Fig. 6. Investigation of Cu—Cd interferences at a MFE deposited in situ from 125 μg ml^{-1} Hg^{2+} on a wax-impregnated graphite electrode. Linear sweep scan rate, 40 mV s^{-1}. Other conditions as in Fig. 2.

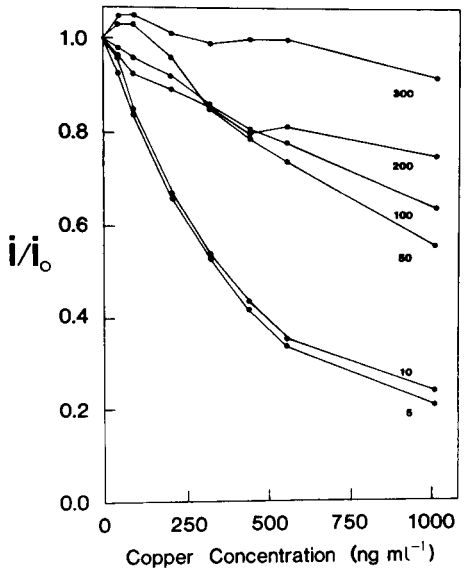

Fig. 7. Effect of Hg^{2+} concentration on the Cu—Cd interferences observed at in situ deposited MFE's. The Hg^{2+} concentrations were 5—300 μg ml^{-1} as indicated on the curves. Cadmium concentration, 470 ng ml^{-1}; preconcentration period, 300 s; linear sweep scan rate, 40 mV s^{-1}. i/i_0 as in Fig. 2.

This postulate is further supported by the fact that a linear calibration plot is obtained for Cd^{2+} even at higher Cu^{2+} concentrations and lower Hg^{2+} concentrations for which the observed depression is relatively large. For five Cd^{2+} concentrations between 150 and 2100 ng ml^{-1} at a fixed Cu^{2+} concentration of 380 ng ml^{-1}, the least-squares equation of peak stripping current vs. concentration was I (μA) = $(0.0577 \pm 0.0005)C^0_{Cd^{2+}}$ (ng ml^{-1}) + (2.40 ± 0.54) μA with a standard error S_{yx} = 0.8 μA and correlation coefficient r = 0.9999. These results are representative of a wide range of Cu^{2+}/Cd^{2+} ratios and were evaluated over a large variety of Cu^{2+} concentrations and film thicknesses. This behavior again differs from that exhibited by copper and zinc.

CONCLUSIONS

Several conclusions can be drawn concerning simultaneous quantitation of Cu^{2+} and Cd^{2+} by a.s.v. Because the relative concentrations of Cu^{2+} and Zn^{2+} determine the magnitude of the effect on the zinc stripping wave, errors with the standard addition method will occur when the addition produces significant change in the Cu^{2+}/Zn^{2+} ratio. Interferences are difficult to avoid when a MFE is used.

For mixtures of Cu^{2+} and Cd^{2+}, the interference is not detectable at the HMDE or at the MFE when uniform, preformed films are used. However, the

interference is detectable when the electrode is deposited in situ, although the effect is less pronounced than for Cu^{2+} and Zn^{2+}. Also, the depression of the cadmium stripping wave is independent of the Cu^{2+}/Cd^{2+} ratio. Finally, the quantitation of Cd^{2+} concentrations by the method of standard additions with in situ deposited electrodes will remain valid if the Cu^{2+} concentration is not drastically altered.

The authors acknowledge helpful discussions with T. H. Ridgway and support from the National Science Foundation (CHE79-11872). J.A.W. and D.A.R. acknowledge support in the form of summer fellowships from University of Cincinnati University Research Council.

REFERENCES

1 F. Vydra, K. Stulik and E. Julakova, Electrochemical Stripping Analysis, Halsted Press, New York, 1976, p. 61.
2 E. Barendrecht, in A. J. Bard (Ed.), Electroanalytical Chemistry, Vol. 2, Dekker, New York, 1967, p. 77.
3 T. R. Copeland, R. A. Osteryoung and R. K. Skogerboe, Anal. Chem., 46 (1974) 2093.
4 S. T. Crosum, J. A. Dean and J. R. Stokely, Anal. Chim. Acta, 75 (1975) 421.
5 B. Lazar, A. Nishri and S. Ben-Yaakov, J. Electroanal. Chem., 125 (1981) 295.
6 G. E. Batley and T. M. Florence, J. Electroanal. Chem., 55 (1974) 23.
7 T. M. Florence, J. Electroanal. Chem., 35 (1972) 237.
8 D. A. Roston, E. E. Brooks and W. R. Heineman, Anal. Chem., 51 (1979) 1728.
9 A. G. Stronberg and V. E. Gorodovykh, Zh. Neorg. Khim., 8 (1963) 2355.
10 M. S. Shuman and G. P. Woodward, Anal. Chem., 48 (1976) 1979.
11 M. Kozlovsky and A. Zebreva, in P. Zuman and L. Meites (Eds.), Progress in Polarography, Vol. 3, Wiley-Interscience, New York, 1972.
12 T. P. DeAngelis, R. E. Bond, E. E. Brooks and W. R. Heineman, Anal. Chem., 49 (1977) 1792.
13 T. M. Florence, J. Electroanal. Chem., 27 (1977) 273.
14 T. R. Copeland and R. K. Skogerboe, Anal. Chem., 46 (1974) 1257A.
15 J. H. Christie and R. A. Osteryoung, Anal. Chem., 46 (1974) 351.
16 Y. K. Chau and K. Lum-Shue-Cham, Water Res., 8 (1974) 383.
17 A. H. I. Ben-Bassat, J. M. Blinderman, A. Saloman and E. Wakshal, Anal. Chem., 47 (1975) 534.
18 D. Jagner and L. Kryger, Anal. Chim. Acta, 80 (1975) 255.
19 J. Gardiner and M. J. Stiff, Water Res., 9 (1975) 517.
20 P. Ostapczuk and Z. Kublik, J. Electroanal. Chem., 83 (1977) 1.

Analytica Chimica Acta, 154 (1983) 105—119
Elsevier Science Publishers B.V., Amsterdam — Printed in The Netherlands

ELECTROCHEMICAL REDUCTION AND DETERMINATION OF CIMETIDINE AT NANOMOLAR TO MICROMOLAR LEVELS OF CONCENTRATION

ANDREW WEBBER, MUMTAZ SHAH and JANET OSTERYOUNG*

Department of Chemistry, State University of New York at Buffalo, Buffalo, NY 14214 (U.S.A.)

(Received 28th April 1983)

SUMMARY

The electrochemical reduction of cimetidine, an H_2-antagonist of histamine used in the treatment of duodenal and gastric ulcers, has been examined by using a variety of electrochemical techniques. Reduction in 0.1 M HCl occurs at −0.8 to −1.1 V vs. SCE depending on the experimental conditions. Square-wave and cyclic voltammetry were found to be the best techniques for the determination of cimetidine whereas sampled-d.c., normal pulse, and differential pulse polarography were not useful. The detection limit for the determination depends on the condition employed but can be as low as 1 ng ml^{-1} (4 nM). A linear calibration plot is obtained up to 2 $\mu g\ ml^{-1}$ and calibration curves can be used at higher concentrations. The high sensitivity is due to reactant adsorption. The electrode process appears to involve a 4-electron reduction of the cyano group in cimetidine. The major metabolites of cimetidine can also be determined by this method.

Cimetidine (I) is a substituted imidazole which acts as an H_2-antagonist of histamine and is used for the treatment of gastric and duodenal ulcers. Clinical monitoring of cimetidine and its metabolites is required to optimize

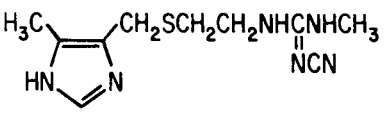

(I)

therapy and to minimize side effects [1, 2]. In addition, analytical information is required in pharmacological studies of this drug. The commonest method for determination of cimetidine involves extraction from the sample, concentration by evaporating the solvent, and separation by high-performance liquid chromatography (h.p.l.c.) with u.v. detection [2—11]. The detection limit of the h.p.l.c.—u.v. method is difficult to estimate because it depends on the method employed and whether urine, blood or serum samples are used. Ziemniak et al. [9] appear to have attained the lowest detection limit (0.05 $\mu g\ ml^{-1}$ corresponding to 0.25 $\mu g\ ml^{-1}$ in the concentrated extract actually assayed). In one report [12] amperometric detection was employed using an electrochemical thin-layer transducer with a carbon paste electrode at +1.05 V; no further details were given. However, there are no reports in

0003-2670/83/$03.00

the literature which discuss the electrochemistry of this compound. This is of some interest from both analytical and mechanistic points of view. From the analytical perspective, the voltammetric characteristics of the compound may provide the basis for a determination either directly or along with h.p.l.c. Further, knowledge of the voltammetric behavior of the compound might provide valuable insights into the mode of action of the compound and the metabolites to be expected. This paper discusses the reduction of cimetidine at mercury electrodes using square-wave voltammetry.

EXPERIMENTAL

Reagents and solutions

Reagent-grade hydrochloric acid (Fischer), guanidine hydrochloride (Baker), imidazole and histamine (Eastman-Kodak), agmatine sulfate (99%, Aldrich), L-histidine hydrochloride monohydrate (Sigma) and cimetidine (*N''*-cyano-*N*-methyl-*N'*-{2-[[(5-methyl-1H-imidazol-4-yl)methyl]thio]ethyl}-guanidine), cimetidine sulfoxide, SK&F 92374 (*N''*-cyano-*N*-methyl-*N'*[(1H-imidazole-4-yl)propyl]guanidine), impromidine (SK&F 92676; Smith, Kline & French) were used as received.

Stock solutions (0.1 and 1.0 mg ml^{-1}) of cimetidine stored in a refrigerator were used. All experiments were done at ambient temperature using purified water (Millipore Milli-Q system). All solutions were deoxygenated by passing purified argon saturated with water through them.

The density of cimetidine was estimated by placing a known weight of the free base in a volumetric flask and filling with cyclohexane, in which cimetidine is insoluble. Reweighing and correction for the density of cyclohexane at room temperature (25.9°C) gave the volume of the solid cimetidine.

Instrumentation

The technique of rapid-scanning square-wave voltammetry has been described in detail elsewhere [13]. Two different square-wave systems were used in these experiments. The first, the one-drop square-wave analyzer (ODSWA), was designed in this laboratory. This is a small analog instrument which operates at 25-mV square-wave amplitude (one-half peak-to-peak) and 30-Hz square-wave frequency. The second, a more flexible system based on a Digital Equipment Corporation PDP 8/e computer with associated interface and analog electronics, was used for all polarography and voltammetry, and has also been described in more detail elsewhere [14]. For cyclic voltammetry, an IBM instrument similar to the Model 225 was used with a Houston Instruments Model 2000 X-Y recorder.

An EG & G Princeton Applied Research Model 303 static mercury drop electrode was used throughout. The drop area was 0.0182 cm. All potentials were measured and are reported vs. a saturated calomel electrode placed in a reference bridge containing 0.1 M KCl separated from the cell by a Vycor tip.

RESULTS AND DISCUSSION

Square-wave voltammetry was used to study the reduction of cimetidine over a range of pH values from 1 to 9 in the following systems: 0.1 M hydrochloric acid (pH 1.1), succinic acid (pH 2.35), acetic acid (pH 4.2), potassium oxalate (pH 6.2), sodium hydrogenphosphate (pH 6—7) and succinic acid (pH 6.2—9) with sodium hydroxide added to attain the desired pH value. The low pH of 0.1 M hydrochloric acid was found to be the best. At higher pH values the reduction peak was ill-defined and poorly separated from the background discharge. Figure 1(a) shows the net square-wave current for 0.1 M hydrochloric acid with and without 0.4 μg ml^{-1} (1.6 μM) cimetidine present. Failure of these two curves to meet at potentials negative of the peak potential suggests that the reactant, cimetidine, or the reduction product(s) (or both) are adsorbed on the electrode and thus change the charging current, and perhaps the current caused by reduction of hydrogen ion, from that characteristic of the supporting electrolyte alone. The background current was therefore estimated by drawing a line tangential to the voltammogram on either side of the peak, as shown. Currents referred to below are measured with respect to this interpolated baseline. The peak currents obtained from square-wave voltammograms of cimetidine solutions from 0.2 to 70 μg ml^{-1} are clearly not proportional to the cimetidine concentration (Fig. 2), except for the initial portion of the plot.

Adsorption phenomena

The fact that the ratio of peak current to concentration decreases with increasing concentration of cimetidine is consistent with a process that is limited by the adsorption of the reactant, cimetidine. As the concentration is increased above a certain level, the electrode surface becomes saturated with the adsorbed cimetidine; further additions have little effect, because

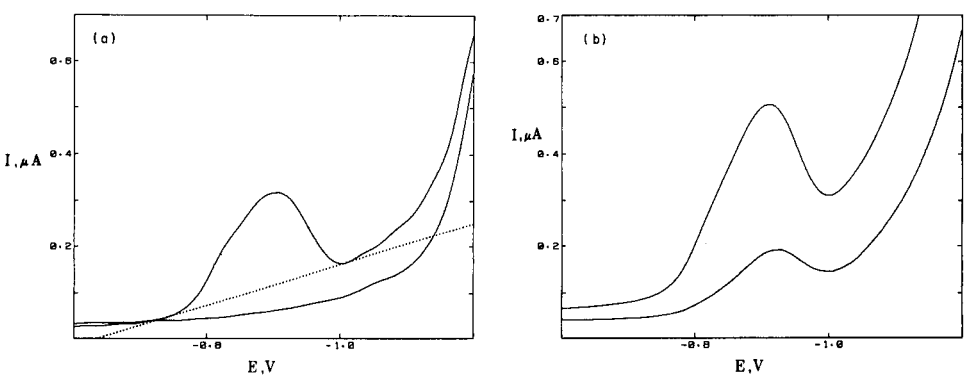

Fig. 1. Square-wave voltammograms with E_{in} = —0.6 V, t_d = 10 s, E_{sw} = 25 mV, f = 30 Hz, ΔE_s = 5 mV. (a) Net currents; lower solid line, background of 0.1 M HCl; upper solid line, with 0.40 μg ml^{-1} cimetidine present; points, base-line from which I_p was measured. (b) Separate forward (upper curve) and reverse (lower curve) currents of 0.40 μg ml^{-1} cimetidine.

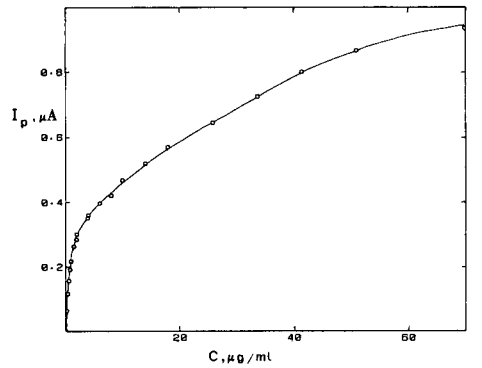

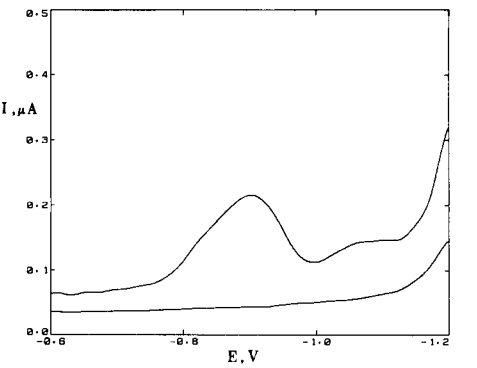

Fig. 2. Square-wave peak current vs. concentration of cimetidine. Experimental parameters as for Fig. 1.

Fig. 3. Square-wave voltammogram of 0.40 μg ml^{-1} both with (lower curve) and without (upper curve) 0.00071% Triton X-100 present. Experimental parameters as for Fig. 1.

the amount of cimetidine arriving at the electrode during the potential scan is minimal for concentrations at the μM level, although this obviously has an effect at higher concentrations. This behavior was observed in a recent paper [15] on the reduction of the acid-decomposition product of NADH; some similarities between the behavior of these two completely unrelated compounds are evident. Figure 3 shows square-wave voltammograms of 0.40 μg ml^{-1} (1.6 μM) cimetidine in 0.1 M hydrochloric acid with and without 0.00071% Triton X-100 present. It is clear that even a small amount of the surfactant completely desorbs the cimetidine from the surface of the mercury drop and no reduction peak is observed. Further evidence for adsorption is that the peak current depends on the delay time before the potential waveform is applied to the electrode; the longer the delay time, the more cimetidine is adsorbed and the larger the peak current. Figure 4 shows a plot of the peak currents observed for solutions containing various concentrations of cimetidine against the square root of the time from the formation of the drop to the time that the potential scan reaches the peak potential. This time, t_p, is a function of the delay time (t_d), the scan rate (given by the step height, ΔE_s = 5 mV, multiplied by the frequency, f), the initial potential (E_{in}) and the peak potential (E_p) and is given by

$$t_p = t_d + |(E_p - E_{in})|/\Delta E_s f \quad (1)$$

The plots for the dilute solutions are linear whereas deviations from linearity occur at higher concentrations. Most significantly, the deviations occur at shorter times as the concentration increases. Table 1 gives the results of a least-squares fit for the initial, linear portion of the data (dashed lines of Fig. 4). A plot of the slopes of the I_p vs. $t_p^{1/2}$ plots ("slope" of Table 1) against the concentration of cimetidine is linear with a slope of 85.7 ± 1.4 nA

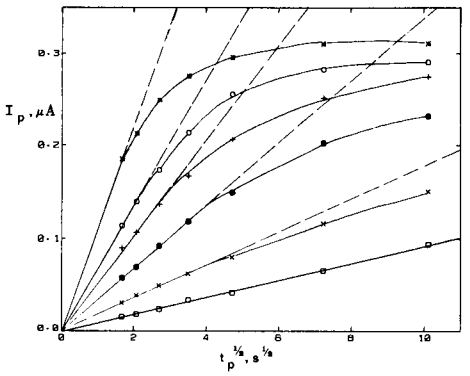

Fig. 4. Square-wave peak currents vs. $t_p^{1/2}$ at different cimetidine concentrations: (□) 0.10; (×) 0.20; (•) 0.40; (+) 0.60; (○) 0.79; (*) 1.27 μg ml^{-1}. Dashed lines correspond to a linear fit to the first portion of each curve. Experimental parameters as for Fig. 1.

ml μg^{-1} s$^{-1/2}$ (0.340 ± 0.006 A M^{-1} s$^{-1/2}$), (x-intercept 0.002 ± 0.001 μg ml^{-1}, correlation coefficient 0.9994). The excellent correlation coefficients and the near-zero intercepts of this and the data in Table 1 show that I_p is proportional to the product $Ct_p^{1/2}$, so long as neither is too large. The plots of peak current vs. concentration at different values of t_p are similar to Fig. 4. The dependence of I_p on $t_p^{1/2}$ is that for diffusion-controlled adsorption of the reactant during time t_p prior to its reduction. From the x-intercept of plots of I_p vs. concentration of cimetidine, the detection limit for this method was estimated to be 0.02 μg ml^{-1} (twice the x-intercept for t_d = 50 s). However, as will be seen, the response depends on a number of other factors which permit this detection limit to be lowered further.

TABLE 1

Dependence of square-wave peak current on accumulation time (t_p) and concentration of cimetidine

Conc. (μg ml^{-1})	Slope[a] (nA s$^{-1/2}$)	σ_s[b] (nA s$^{-1/2}$)	Intercept[c] (nA)	σ_I[d] (nA)	Correlation coefficient	Number of delay times[e]
0.1	9.24	0.14	0.6	0.7	0.9993	8
0.2	17.9	0.4	0.6	0.8	0.9994	5
0.4	33.8	0.3	0.2	0.8	0.99990	5
0.6	51.1	1.8	1.6	3.5	0.9990	4
0.8	64.9	2.1	1.8	4.0	0.9990	4
1.3[f]	110.6	—	0	—	—	2

[a]Slope of the plot of I_p vs. $t_p^{1/2}$ over the initial linear portion. These slopes are proportional to the concentration of cimetidine (see text). [b]Standard deviation of the slope. [c]Intercept of the plot of I_p vs. $t_p^{1/2}$. [d]Standard deviation of the intercept. [e]Number of points to which linear regression was applied. This decreases as the concentration increases because the portion of the plot that is linear diminishes. [f]Only the first point and the origin were used to obtain the slope and intercept.

Forced convection during the delay time should, for example, increase the sensitivity by increasing the rate of transport of cimetidine to the electrode surface. This pre-accumulation on the electrode surface, although non-faradaic, is the same in principle as that employed in stripping voltammetry. If this method were to be used for detection in a flow system (e.g., h.p.l.c.) then the flow of eluent past the electrode would provide an enhancement in the peak current similar to that observed when the cell contents are stirred by either a mechanical stirrer or by purging. If forced convection is employed, then obviously it must be reproducible, as should be the case for the constant flow of eluent from an h.p.l.c. system.

Optimization of square-wave parameters

In all the preceding work, the square-wave amplitude was 25 mV and the frequency was 30 Hz (this frequency averages out noise at 60 Hz). Varying the amplitude from 5 to 100 mV showed that there is no simple relationship between I_p and the amplitude; one merely observes that I_p increases as the amplitude increases, although further increase in the amplitude above the 25 mV employed in this work resulted in only slight enhancement of the peak current. With this amplitude, and a delay time of 10 s, the effect of the square-wave frequency, f, on the response was examined for a 0.40 μg ml^{-1} solution of cimetidine. Even at the highest frequencies no peak was seen in the reverse current portion of the curve (Fig. 1b); this indicates clearly that the overall process is irreversible. A plot of I_p vs. f is linear with a slope of 3.34 ± 0.04 nA s with intercept 18 ± 5 nA, r = 0.9996 (N = 7), $\partial \log I_p / \partial \log f$ = 0.90 ± 0.01, r = 0.99991. The positive intercept of the plot of I_p vs. f occurs because these experiments were not done at constant t_p. Peak current varies with $t_p^{1/2}$ which, in turn, depends on both f and the peak potential (this, as will be seen, is also a function of f). To correct for this, $t_p^{1/2}$ was calculated for each value of f and $I_p/t_p^{1/2}$ was plotted against f. The slope of this plot was 1.05 ± 0.01 nA s$^{1/2}$, r = 0.9997 (N = 8). More to the point, the intercept is only 1.6 ± 1.1 nA s$^{-1/2}$ and the slope of the log ($I_p/t_p^{1/2}$) vs. log f plot is 1.00 ± 0.01 (r = 0.9996). This dependence of I_p on f is also in agreement with the reduction of surface-bound species.

The best way to represent the sensitivity of the method is as $I_p/CAft_p^{1/2}$ which is 0.145 μA ml s$^{1/2}$ μg^{-1} cm^{-2} (0.575 A s$^{1/2}$ M^{-1} cm^{-2}). From the above, one expects that the lowest detection limit would be attained when long delay times, forced convection, and high frequencies are employed. In practice, owing to the greater noise at higher frequencies, the best results were obtained at a frequency of 30 Hz (when the current is sampled every 1/60 s). When a 100-s delay time with purging was followed by a 5-s delay period with no purging, for concentrations over the range 1.8—14 ng ml^{-1} (7.1—56 nM), the least-squares fit to the data gave a line having a slope of 4.76 ± 0.08 nA ml ng^{-1} with an intercept of —0.9 ± 0.5 nA, r = 0.9995 (N = 6). The detection limit was estimated from plots such as these to be twice the x-intercept (S/N ratio of 2). This would give a detection limit of 0.3 ng ml^{-1}.

However, in view of the noise level in the actual voltammograms, a limit of 1 ng ml^{-1} (4 nM) is considered to be more realistic. The sensitivity, as given by $I_p/CAft_p^{1/2}$ for this mode, is then 0.847 μA ml $s^{1/2}$ μg^{-1} cm^{-2} (i.e., nearly six times that when no purging is employed).

The peak potential is independent of concentration, initial delay time and initial potential but shifts to more negative potentials as the frequency increases. Peak potential vs. log f is linear with a slope of 110 ± 3 mV with intercept = —762 mV, r = 0.998 (N = 8). The peak current is a measure of the amount of cimetidine adsorbed on the electrode surface at the initial potential during time t_p (Eqn. 1). If long delay times and high sweep rates are chosen, then the relative variation in $t_p^{1/2}$ as the value of E_{in} is changed becomes negligible. Figure 5 shows the variation in I_p with E_{in} for 0.40 μg ml^{-1} cimetidine with t_d = 20 s and f = 180 Hz. At 180 Hz, E_p = —1.005 V, so that the change in $t_p^{1/2}$ with E_{in} going from 0.0 to —0.6 V is only 1.6%. The adsorption appears to be fairly independent of potential from —0.4 to —0.6 V (this is actually an assumption for the correction term in Eqn. 1) but to decrease as the potential becomes more positive than this.

Saturation of the electrode surface

The use of long delay times or forced convection to enhance sensitivity must be regarded with a certain amount of caution to avoid saturation of the electrode surface with adsorbed cimetidine. The point at which this begins to have an effect, i.e., when large values of $Ct_p^{1/2}$ cause the plots to deviate from linearity, is approximately 2.5 μg $s^{1/2}$ ml^{-1} (9.9 μM $s^{1/2}$) (Fig. 4). Determinations are, of course, possible by means of calibration curves over the whole range of concentration of cimetidine. However, it would seem preferable to

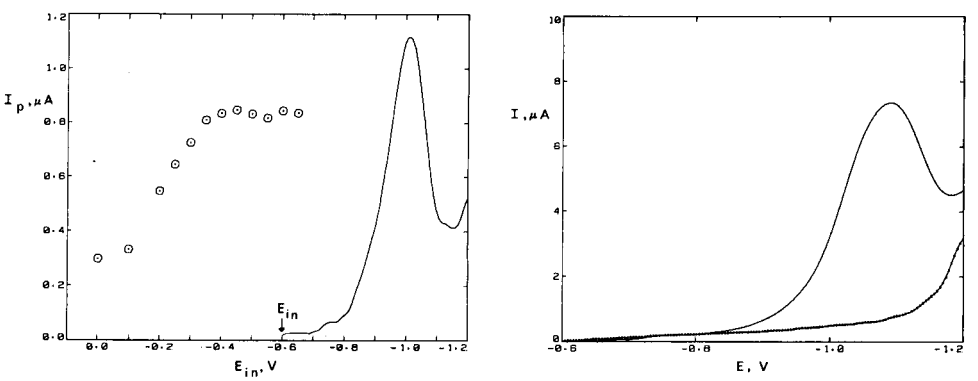

Fig. 5. Square-wave peak currents vs. E_{in} for 0.40 μg ml^{-1} cimetidine. t_d = 20 s, E_{sw} = 25 mV, f = 180 Hz, ΔE_s = 5 mV. The voltammogram obtained when E_{in} was —0.6 V is shown to the right.

Fig. 6. Normal-pulse polarogram of 0.40 μg ml^{-1} cimetidine. Drop time 10 s, pulse width 10 ms, current sampling time 1.67 ms, E_{in} —0.6 V. Line with points is the background polarogram.

limit determinations to the linear portion of the calibration both for simplicity and because this is where the greatest sensitivity (I_p/C ratio) is attained. For this reason, the method of standard additions is recommended, as, if saturation were to occur, it would be readily apparent; non-linear plots of peak current against concentration of added cimetidine would result. In addition, the peak potential is independent of concentration at low concentration but shifts to more negative values when saturation begins to occur. Moreover, as long as the product $Ct_p^{1/2} < 2.5$ μg $s^{1/2}$ ml^{-1}, then saturation should not occur. A simpler way to use this concept, because $I_p/CAt_p^{1/2}$ is 4.71 μA ml μg^{-1} cm^{-2} $s^{-1/2}$ (f = 30 Hz), is that saturation begins to occur when the peak current becomes greater than 11.8 μA cm^{-2} (here 0.215 μA, see Fig. 4). Thus it is easy to determine if the electrode is saturated with cimetidine; the phenomenon is, one may say, unmistakable. In such an event, one merely dilutes the sample or chooses a smaller value for t_p.

Other electrochemical techniques

Partly because commercial instrumentation for square-wave voltammetry is only just becoming available (despite its proven advantages over many conventional techniques for examination of irreversible systems), solutions of cimetidine in 0.1 M HCl were examined by sampled-d.c., normal-pulse and differential-pulse polarography and cyclic staircase voltammetry (a digital form of cyclic voltammetry, which it approaches when small step heights (5 mV) are used, as in this study). Unless otherwise stated, the concentration of cimetidine was 0.40 μg ml^{-1} (1.6 μM).

Sampled d.c. polarography. Even after background subtraction, and using a drop time of 10 s, only a shoulder on the background hydrogen discharge was seen, and this is not useful for analytical purposes. This is not surprising in view of the low concentration employed.

Normal-pulse polarography. Normal-pulse polarograms of cimetidine exhibit pronounced maxima at short pulse times (Fig. 6) but at the relatively long pulse time of commercial instruments (typically 50 ms) the maxima are relatively small. Thus this technique is insensitive (compared to square-wave voltammetry) when such pulse times are employed. This behavior is, of course, exactly what is expected for reactant adsorption. Conceivably, one could envisage a method based upon the height of the maximum at short pulse times but this would require very careful calibration and probably give non-linear current—concentration plots. In addition, all the polarographic techniques are much slower than voltammetric ones. This may be important if the detector is to be used with a flow system. Shorter delay times speed up the determination but decrease the sensitivity, as the peak current is proportional to the square root of the delay time: $\partial \log I_p/\partial \log t_d = 0.52 \pm 0.02$, r = 0.9995, $\partial I_p/\partial t_d^{1/2} = 2.2 \pm 0.1$ μA $s^{-1/2}$, intercept —0.06 ± 0.11 nA, 10-ms pulse width, r = 0.9993 (N = 4).

Differential pulse polarography. No response at all is observed with this method. This is reasonable because when the potential approaches the peak

potential of cimetidine, the adsorbed material is reduced as soon as it arrives at the electrode even before the pulse is applied. Thus, no film of adsorbed cimetidine is built up during the delay time (here 10 s) and, as the amount of material arriving at the electrode surface by diffusion during the pulse application is minimal at these concentrations, no response is observed. This is in contrast to the case for reversible processes where differential pulse polarography has been found to be extremely sensitive for the detection of surface-bound species (e.g., Brown and Anson [16] for the comparison of d.p.p. and cyclic voltammetry). This is because, if the process is reversible, the reduction of the material during the delay time does not remove it from the electrode (assuming that the reduced form is also adsorbed on the electrode surface). It is presumed that this is generally true for irreversible processes (see, e.g., [15]).

Cyclic staircase (cyclic voltammetry). This method appears to give results essentially similar to those of square-wave voltammetry. The peak for the reduction of an adsorbed species in cyclic voltammetry is expected to have a form similar to that for square-wave voltammetry in that the current should decay to the level of the charging current (much higher in the case of cyclic voltammetry) after the peak rather than become diffusion-limited. For this reason, it is valid in this case to use the same system of measurement as employed for square-wave data (Fig. 7). Thus I_p was again found to be proportional to $t_p^{1/2}$; at 0.40 μg ml^{-1} cimetidine, f = 30 Hz, I_p vs. $t_p^{1/2}$ gives a slope of 30.5 ± 0.8 nA s$^{-1/2}$, intercept 3.5 ± 2.4 nA, r = 0.998 (N = 7). The peak current, when normalized to unit $t_p^{1/2}$ in the same manner as was done for the square-wave data, is also proportional to the frequency employed. The plot of $I_p/t_p^{1/2}$ vs. f for a 0.40 μg ml^{-1} cimetidine solution gives a slope of 1.02 ± 0.01 nA s$^{1/2}$ with intercept 1.6 ± 0.8 nA s$^{-1/2}$, r = 0.9998 (N = 9). The

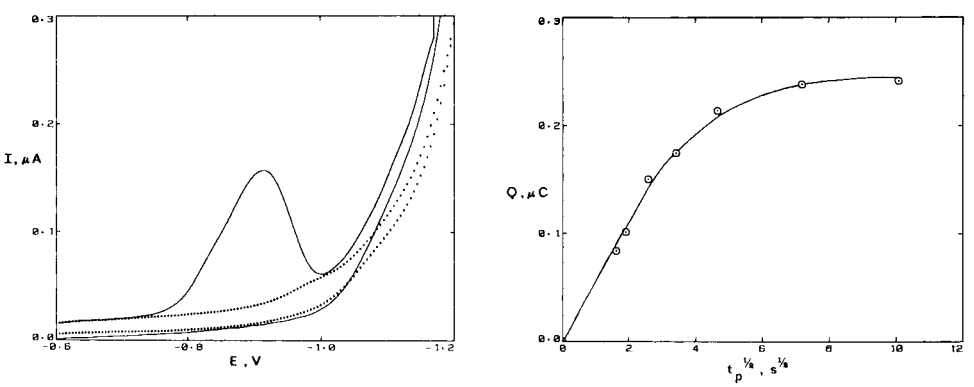

Fig. 7. Cyclic voltammograms of 0.40 μg ml^{-1} cimetidine (solid curve) for E_{in} = −0.6 V, t_d = 10 s, f = 30 Hz, ΔE_s = 5 mV (i.e., effective sweep rate is 150 mV s^{-1}). Points are the background voltammogram.

Fig. 8. Plot of charge under the cyclic staircase peak of 0.99 μg ml^{-1} cimetidine vs. $t_p^{1/2}$. Experimental parameters as for Fig. 7.

peak current is then again proportional to $Cft_p^{1/2}$. The sensitivity, as given by $I_p/CAft_p^{1/2}$, is 0.141 μA ml $s^{1/2}$ μg^{-1} cm^{-2} (35.5 mA $s^{1/2}$ cm^{-2} M^{-1}). Because at short step heights cyclic staircase approximates cyclic voltammetry [17], this can be rewritten as $I_p/CA\nu t_p^{1/2}$ (ν is the sweep rate, i.e., $f \times$ step height) and the sensitivity then becomes 28.2 μA $s^{1/2}$ ml μg^{-1} V^{-1} cm^{-2} (7.10 A $s^{1/2}$ M^{-1} V^{-1} cm^{-2}).

Unfortunately, the charging currents for cyclic staircase are much higher than those in the differential technique of square-wave voltammetry. Thus measurement of the peak current is more difficult. This is probably why the I_p/C plot for cyclic staircase (t_d = 10 s, f = 30 Hz, ΔE_s = 5 mV and ν = 150 mV s^{-1}) gives a poorer correlation coefficient than does the similar plot for square-wave voltammetry. Over the concentration range 0.1—0.8 μg ml^{-1}, I_p vs. C has a slope of 244 ± 7 nA ml μg^{-1}, intercept 1.3 ± 3.3 nA, r = 0.998 (N = 6). Background subtraction gave essentially similar results: slope 253 ± 7 nA ml μg^{-1}, intercept 3.5 ± 3.3 nA, r = 0.998, (N = 6). Partly for this reason, square-wave voltammetry is superior to cyclic voltammetry for the determination of cimetidine. Cyclic voltammetry or linear sweep voltammetry may, however, be used if equipment for square wave-voltammetry is unavailable.

In addition to cyclic staircase, conventional cyclic voltammograms were recorded on various solutions of cimetidine. In all cases the I vs. E curves were very similar. The ratio of the peak current of cyclic voltammetry to that of cyclic staircase was 0.97. The same ratio for the charge under the peaks was 0.95. Thus the techniques are, under these conditions (step height of 5 mV, frequencies of 40—120 Hz), comparable as expected [17].

Estimation of n

Cyclic voltammetry and cyclic staircase were applied on 0.99 μg ml^{-1} cimetidine solutions with various initial delay times. The data of Fig. 4 suggested that full coverage of the electrode occurs, at this concentration, when $t_p^{1/2}$ is 7 $s^{1/2}$ or greater. Figure 8 is a plot of the charge under the cyclic staircase peaks for each value of $t_p^{1/2}$. As is evident, and expected, the charge increases linearly with $t_p^{1/2}$ initially and then levels out when $t_p^{1/2}$ is greater than 7 $s^{1/2}$. This maximum charge is 0.241 μC. The corresponding charge under the cyclic voltammetry peak (t_p = 50 s) was found to be 0.225 μC. From this value, $n\Gamma_{max} = Q_{max}/FA = 1.28 \times 10^{-10}$ eq cm^{-2}. The projected area of cimetidine estimated from molecular models is 195 $Å^2$. Thus the maximum surface concentration from cimetidine adsorbed in the planar position is 0.85×10^{-10} mol cm^{-2}, which would imply n = 1.5.

An alternative approach for estimating n uses the relation between surface coverage, Γ, and time for diffusion-controlled adsorption:

$$\Gamma = 1.128\, C\, (Dt_p)^{1/2} + CDt_p/r \qquad (2)$$

where r is the electrode radius (cm). Equation (2) is that derived by Phillips [18] for spherical electrodes and is used in place of Koryta's equation as

employed by Laviron [19] where the constant term is 0.74. The second term can be neglected under these circumstances [20]. (Parenthetically, we disagree with the claim of Laviron [19] that the amount of material arriving at the electrode can be ignored if ν is about 0.2 V s^{-1} and t_d is 10 s. This is evident from the need to correct the I_p vs. f plots for the different t_p values. Hence we use t_p, not t_d, in the following equations. Valenta and Krznaric [20] estimate that sweep rates of 10 V s^{-1} or higher are required to ignore the difference between t_p and t_d.)

Making use of the fact that $Q = nFA\Gamma$, Eqn. (2) becomes

$$nD^{1/2} = Q/1.128\ FACt_p^{1/2} \tag{3}$$

A least-squares fit to a plot of Q vs. C for cyclic staircase voltammetry (t_d = 10 s, t_p = 12 s, at 0.15 V s^{-1}, C = 0.1—0.8 μg ml^{-1}) gave a line with a slope of 0.214 ± 0.007 μC ml μg^{-1} with intercept —0.2 ± 0.3 nC, r = 0.9990 (N = 6). This gives a value for $nD^{1/2}$ of 7.88 × 10^{-3} cm $s^{-1/2}$. The diffusion coefficient can be estimated from a modified form of the Stokes—Einstein relationship [21]: $D = k/(V_m)^{1/3}$, where k for aqueous solutions at 25°C is 3.31 × 10^{-5} cm s^{-1} [21] and V_m is the molecular mass of cimetidine (252) divided by its density. The density of cimetidine was estimated to be 1.23 g cm^{-3} as described in the experimental section. This gives a value of 5.6 × 10^{-6} cm^2 s^{-1} for D, and substituting this into Eqn. (3), a value of 3.3 for n.

Estimation of αn_a *from voltammetric data*

The peak current for the irreversible reduction of an adsorbed species [19] is given by

$$I_p = n\alpha n_a F^2 A\nu\Gamma/2.718\ RT \tag{4}$$

or, using $Q = nFA\Gamma$,

$$I_p/Q = \alpha n_a F\nu/2.718\ RT \tag{5}$$

Data obtained at 0.40 μg ml^{-1}, 0.2 V s^{-1} and t_p = 1 to 250 s gave a value for αn_a of 0.52 ± 0.07. A completely different way to estimate this is from either the peak width, δ (the difference between the potentials at $I_p/2$), or from the shift in peak potential with sweep rate. The corresponding equations for the irreversible reduction of an adsorbed species [19] are

$$\delta = 62.5/\alpha n_a \text{ mV} \tag{6}$$

$$E_p = E^{\circ\prime} - (RT/\alpha n_a F)\ln(\alpha n_a F\nu/RTk_c^{\theta}) \tag{7}$$

where k_c^{θ} is the apparent standard rate constant. (Note that Eqn. 6 is incorrectly printed in ref. 19). Then

$$\partial E_p/\partial \log \nu = 59.2/\alpha n_a \text{ mV} \tag{8}$$

The peak potential, while independent of concentration, delay time and the initial potential, varies linearly with log f: slope = $\partial E_p/\partial \log f$ = —93 ± 2 mV,

intercept = −798 mV, r = 0.9990 (N = 8). The peak potential is virtually identical to that determined by square-wave voltammetry at the higher frequencies employed.

The values of αn_a from these methods are 0.54, from the peak width, and 0.64 (or 0.54 if square-wave data are used) from $\partial E_p/\partial \log \nu$. The use of staircase voltammetry, as opposed to cyclic voltammetry, has been shown to give identical results for the peak potentials and peak widths, even for irreversible systems [17]. In view of the errors involved, the four values of αn_a are in excellent agreement.

Electrode process

Cimetidine (I) is a substituted imidazole with a pK_a of 7.09 (information supplied by Smith, Kline and French Laboratories), close to that of imidazole itself (6.95), so that at pH 1 no dissociation of the ring NH group occurs. Protonation of the other ring nitrogen with subsequent reduction of the iminium group is conceivable but, as imidazole is electroinactive under these conditions, this mechanism seems very unlikely. Moreover, histidine hydrochloride (II) and histamine (III) also show no response in the potential range of interest (concentrations from 1.1 μM to 3 mM were used). Another possible reduction process is that of a protonated amine or imine group in the side chain. Because guanidine hydrochloride (IV) (6.9 μM to 4.7 mM), agmatine sulfate (V) (9.8 μM to 2.7 mM) and impromidine (VI) (5.6 μM to 0.16 mM) are not electroactive at the potential of cimetidine reduction, it seems that the amine, imine and imidazole groups are not responsible for the electroactivity of cimetidine. The thiol linkage would certainly not be reduced at this potential; reduction of such groups usually requires a medium with a greater cathodic potential range (e.g., *N*,*N*-dimethylformamide) [22].

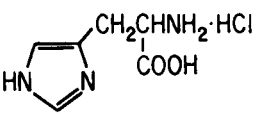

(II)

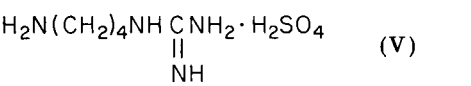

(V)

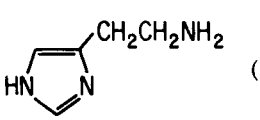

(III)

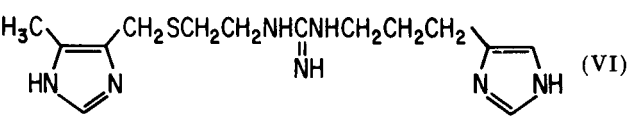

(VI)

(IV)

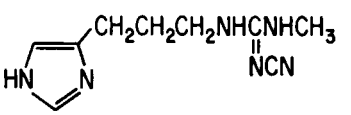

(VII)

Moreover, (VI) contains every functional group of cimetidine except the cyano group in the side chain, yet is electroinactive. However, SK & F compound 92374 (VII) and cimetidine sulfoxide show voltammetric responses similar to those of cimetidine. Thus, the electrode process can be attributed to the cyano group in cimetidine.

The reduction of cyanoamines [23] and cyano groups in general [24] in

acidic media usually involves a $4e^-/4H^+$ (two-step) reduction to the amine. The value of n (3.3) estimated above from Q vs. C data supports a 4-electron process whereas the values of αn_a suggest that n_a is 2. These values are thus consistent with a 2-electron rate-determining step in conjunction with another, faster 2-electron process, as expected. The suggested product is N''-aminomethyl-N-methyl-N'-{2-[[(5-methyl-1H-imidazol-4-yl)methyl]thio]ethyl}-guanidine. Since reaction mechanisms established under conditions of bulk electrolysis are often found to be quite different from those that apply to electroanalytical work, because of the different time-scales and concentrations employed by these techniques, no attempt was made to produce the product coulometrically.

Biological Samples

The demonstrated susceptibility of this method of determination to the presence of surfactants could pose serious problems for the direct voltammetric determination of cimetidine in samples of biological origin. Separation by h.p.l.c. would presumably avoid not only this problem, but also the problem of interference of other compounds in the sample, at the cost of a more complex procedure. To test the method as an accurate analytical procedure, urine samples collected from two laboratory staff members were mixed 1:1 with 0.1 M hydrochloric acid and the square-wave voltammograms were recorded. The sample was spiked with a known quantity of cimetidine and the voltammogram was rerun. The results, given in Table 2, show that the method gives accurate determinations for spiked urine samples. Thus, such samples do not appear to contain surfactants or other interfering compounds. Serum, however, contains surfactants that have the same effect as Triton X-100 on the reduction peak of adsorbed cimetidine. Treatment of the serum with 1 M perchloric acid and filtration through a Rainin h.p.l.c. sample filtration apparatus [25] somewhat alleviated this problem but the wave of cimetidine in 0.1 M HCl was still reduced on addition of this treated serum to the cell. Thus, determinations on serum samples appear to require either a more elaborate pre-treatment method to remove the surfactants in serum or h.p.l.c. separation.

TABLE 2

Determination of cimetidine in urine samples[a]

Cimetidine conc. (μg ml^{-1})		Ratio
Added	Found	
0.50	0.48	0.96
1.0	0.99	0.99
1.5	1.48	0.99

[a] E_{in} = −0.55 V, ΔE_s = 5 mV, E_{sw} = 25 mV, f = 30 Hz, t_d = 1 s.

The major metabolite of cimetidine [1, 9] is cimetidine sulfoxide, which is voltammetrically similar to cimetidine itself and thus direct determinations of unmetabolized cimetidine in biological samples cannot be successful. In addition, the metabolite hydroxymethyl cimetidine would also be expected to interfere, although the minor metabolite [9] guanylurea cimetidine, having no cyano group, probably would not affect determinations. Thus, use of h.p.l.c. to separate cimetidine from its metabolites is required, as is presently used in clinical laboratories. Urine samples, which contain very high levels of cimetidine (e.g., 1 mg ml^{-1}), can be determined adequately with the u.v.—h.p.l.c. method. The higher sensitivity of the electrochemical method should be useful for serum samples where the concentrations are much lower. In addition, it may prove of value in research on the concentration and effect of cimetidine in the cerebrospinal fluid where levels appear to be even less than in serum samples [26].

This work was supported by the National Science Foundation under Grant No. CHE-7917543. The authors thank Marek Wojciechowski, John O'Dea, and John Ziemniak for helpful discussions, Smith, Kline & French Laboratories for samples of cimetidine, and John Ziemniak for samples of cimetidine sulfoxide, impromidine, and SK&F 92374.

REFERENCES

1 J. E. McGuigan, Gastroenterology, 80 (1981) 181.
2 D. A. Chiarmonte and J. J. Schentag, Ther. Drug Monit., 1 (1979) 545.
3 D. R. P. Guay, H. N. Bockbrader and G. P. Matzke, J. Chromatogr., 228 (1982) 398.
4 R. M. Lee and P. M. Osborne, J. Chromatogr., 146 (1978) 354.
5 W. C. Randolph, V. L. Osborne, S. S. Walkenstein and A. P. Intoccia, J. Pharm. Sci., 66 (1977) 1148.
6 N-E. Larsen, P. Hesselfeldt, S. J. Rune and E. F. Hvidberg, J. Chromatogr., 163 (1979) 57.
7 S. J. Soldin, D. R. Fingold, P. C. Fenje and W. A. Mahon, Ther. Drug Monit., 1 (1979) 371.
8 M. G. Kunitani, D. A. Johnson, R. A. Upton and S. Riegelman, J. Chromatogr., 224 (1981) 156.
9 J. A. Ziemniak, D. A. Chiarmonte and J. J. Schentag, Clin. Chem., 27 (1981) 272.
10 B. Lorenzo and D. E. Drayer, J. Lab. Clin. Med., 97 (1981) 545.
11 J. Fleitman, G. Torosian and J. H. Perrin, J. Chromatogr., 229 (1982) 255.
12 I. M. Wiener and L. Roth, J. Pharmacol. Exp. Ther., 216 (1981) 516.
13 J. H. Christie, J. A. Turner and R. A. Osteryoung, Anal. Chem., 49 (1977) 1899.
14 T. R. Brumleve, J. J. O'Dea, R. A. Osteryoung and J. Osteryoung, Anal. Chem., 53 (1981) 702.
15 A. Webber, M. Shah and J. Osteryoung, Anal. Chim. Acta, submitted.
16 A. P. Brown and F. C. Anson, Anal. Chem., 49 (1977) 1589.
17 J. H. Christie and P. J. Lingane, J. Electroanal. Chem., 10 (1965) 176.
18 S. L. Phillips, J. Electroanal. Chem., 12 (1966) 294.
19 E. Laviron, J. Electroanal. Chem., 52 (1974) 355.
20 P. Valenta and D. Krznaric, J. Electroanal. Chem., 75 (1977) 437.
21 L. Meites, Polarographic Techniques, 2nd edn., Wiley-Interscience, New York, 1965, p. 145.

22 R. Gerdil, J. Chem. Soc., B, (1966) 1071.
23 Y. Hatta, N. Yui, T. Nonaka and K. Odo, Nippon Kagaku Kaishi, 12 (1974) 2277; Chem. Abstr., 82, 104821c.
24 L. Eberson, in M. M. Baizer (Ed.), Organic Electrochemistry, M. Dekker, New York, 1973, p. 423.
25 R. Richterich, Clinical Chemistry. Theory and Practice, Academic Press, New York, 1969, p. 99.
26 J. J. Schentag, F. B. Cerra, G. Calleri, E. DeGlopper, J. Q. Rose and H. Bernhard, Lancet, (1979) 177.

Analytica Chimica Acta, 154 (1983) 121—131
Elsevier Science Publishers B.V., Amsterdam — Printed in The Netherlands

OPTIMIZATION OF THE OPERATIONAL PARAMETERS OF THE SUPPORTED MERCURY DROP ELECTRODE DETECTOR IN HIGH-PERFORMANCE LIQUID CHROMATOGRAPHY

J. B. F. LLOYD

Home Office Forensic Science Laboratory, Priory House, Gooch Street North, Birmingham B5 6QQ (Gt. Britain)

(Received 27th May 1983)

SUMMARY

The pendent (or supported) mercury drop electrode detector for high-performance liquid chromatography is examined with reference to the effects on its performance of solvent flow, the residual current, the flow cell characteristics, the size, shape and stability of the mercury drop, and some other factors. The signal-to-noise ratio varies widely with respect to these factors, whose optimization is discussed. Under the optimized conditions, picogram levels of organic nitro and nitrate compounds can be detected.

In general, the detection limits obtained from the high-performance liquid chromatography (h.p.l.c.) of electroreducible compounds with polarographic detection, e.g., the work reviewed by Rucki [1] and by Štulík and Pacáková [2], have remained in excess of 1-ng levels. Recently, much smaller amounts have been selectively and reproducibly detected at semi-permanent mercury drop electrodes, either at a hanging mercury drop electrode or preferably a modification of it (the "pendent" or supported mercury drop electrode) [3]. For eighteen organic nitro and nitrate compounds typical of explosives compositions, the detection limits, given 20-μl sample volumes, are now 2—20 pg [4]. Even with heavily contaminated handswab samples, after a modest degree of clean up, the electrode performance remains satisfactorily constant throughout a chromatogram [5]. In any case, the electrode may be renewed instantly when this is necessary. Thus, the electrode possesses important advantages over the thin-layer and pool mercury electrodes that also have been used for reductive mode detection.

Necessarily, if the sensitivity of the detector is to be fully exploited, the dependence of its performance on, e.g., solvent flow effects, the size of the electrode drop and its physical stability, the residual current, and the flow-cell dimensions must be taken into consideration in the choice of experimental conditions. These factors are illustrated and discussed from an empirical viewpoint in this paper.

EXPERIMENTAL

Chromatographic conditions

Full details have been given before [3]. In brief, the chromatograms were run on 15 cm × 4.5 mm columns of ODS-Hypersil, 3 μm, in phosphate buffer (pH 3.0, 0.025 M)/methanol (86:100, v/v) with a flow of 1.0 ml min^{-1} at ambient temperatures. The eluent reservoir was kept under reflux (atmospheric pressure) to effect its deoxygenation. All the eluent lines were of stainless steel. The pump was an Altex model 102 except where stated otherwise.

Detection

An EG & G Princeton Applied Research (PAR) model 310 polarographic detector was used in conjunction with their 174A control unit. Around the valve body of the detector, but insulated from it with polyethylene foam, was wrapped a screen of copper foil, which was earthed through the back panel of the detector. The detector was seated on foamed polyethylene to insulate it from mechanical vibration transmitted through the bench top.

For most of the work a modified flow cell was used (Fig. 1); details of the original cell may be found in Samuelsson and Osteryoung's paper [6]. The hole in the cell body through which the mercury capillary passes was drilled out, so that the distance between the capillary tip and the eluent outlet jet could be varied. A piece of 0.127-mm polytetrafluoroethylene sleeving was introduced between the capillary and the cell body. This held the two parts sufficiently firmly together that they were not shifted with respect to one another by the drop displacement knocker, but the position of the cell on the capillary could be adjusted manually to fix the tip—jet separation. The bore of the eluent outlet jet, originally 0.5 mm, was distorted to a flared shape with a steel needle to give a new outlet diameter of 0.8 mm. This tapered to the original bore at a depth of 1.0 mm (Fig. 1). For the stainless steel connection between the end of the column and the base of the flow cell, with which the polytetrafluoroethylene connection of the original cell was entirely replaced, thin walled tubing (0.51-mm outer diameter, 0.25-mm inner diameter) was used. The use of stouter tubing would impede both the operation of the drop displacement knocker and any adjustments to be made to the cell. The electrode drops were dispensed with the control unit set at "small", which gave a drop size of 1.6 mg (mean of 100 drops). Larger drops were formed by means of a succession of pulses at this setting. The quoted drop sizes are the number of pulses used to form the drop. In general, the electrode potential was maintained at −1.0 V vs. Ag/AgCl (d.c. mode).

The measurements and observations on the electrode drop were made at magnifications in the range ×15 to ×30 with a microscope fitted with a calibrated eyepiece graticule.

The signal from the control unit was presented to a variable range strip-chart recorder, which could be used to expand the displayed read-out up to

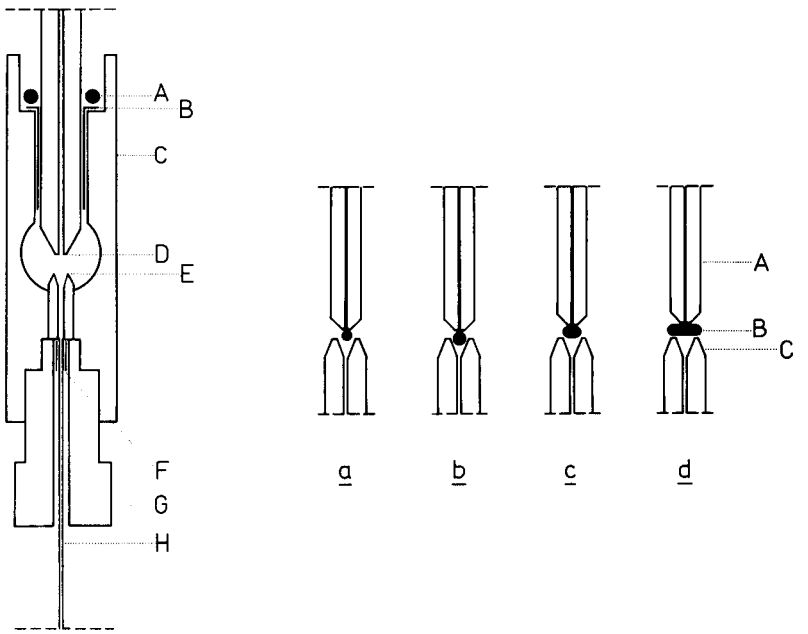

Fig. 1. Cross-sectional diagram of the modified PAR flow cell: (A) O-ring; (B) polytetrafluoroethylene sleeving, which surrounds the mercury capillary and is serated and folded back at its upper end to enable the O-ring to secure it in position; (C) cell body; (D) mercury capillary tip; (E) eluent outlet jet; (F) piece of polytetrafluoroethylene tubing (1.59-mm outer diameter) holding the eluent capillary in position; (G) Omnifit end-fitting; (H) stainless steel capillary eluent line (0.51-mm outer diameter, 0.25-mm internal diameter). The distance between the cut-off points (broken lines) is 6 cm.

Fig. 2. Variation of the shape of the mercury drop with its size. (A) The mercury capillary; (B) the electrode drop; (C) the eluent outlet. The tip—jet separation was 0.4 mm, the outlet jet diameter 0.8 mm, and the eluent flow 1 ml min^{-1}. The drop size was increased in increments of 1.6 mg from (a) (1.6 mg drop) to (d) (6.4 mg), i.e., sizes ×1 to ×4.

0.2 nA full scale. The quoted noise levels are peak-to-peak values recorded with a time constant setting of 0.3 s on the control unit and taken over a period of 20 s.

RESULTS AND DISCUSSION

Drop stability and shape

The flow cell, modified for use in the present work (Fig. 1), was designed for h.p.l.c. detection with a dropping mercury electrode although its applicability to a hanging mercury drop mode of detection was suggested by the manufacturer and has been implemented [7, 8]. However, the latter technique requires the formation of a mercury drop that will remain suspended at the end of a capillary tip for the full duration of a chromatogram.

Even with moderately sized drops, this is often not possible with the original cell. Drops that have remained in place for several minutes tend to fall spontaneously. In the modified cell, the flared eluent jet and a reduced tip—jet separation provide support for the drop if its diameter is similar to the tip—jet separation. With an appropriately adjusted cell, an infinite drop life may be obtained without impediment to the deliberate dislodgement of the drop when necessary.

As the diameter of the drop increases beyond the tip—jet separation, the drop shape distorts. This is shown in Fig. 2, which is drawn from microscopy observations. At (a) in Fig. 2, the smallest drop dispensed by the unit (1.6 mg) is just entering the jet orifice at this particular separation (0.4 mm). A second 1.6-mg increment (b) gives a drop of which approximately half has entered the orifice, but with negligible distortion. With further increments (c and d), the drop shape flattens, which reduces the mercury surface exposed within the orifice. If the drop size is further increased the drop is blown away by the eluent flow, but the first four drops under the conditions of Fig. 2, for example, remain in place for extended periods of time (up to 90 min at a flow rate of 1 ml min^{-1}).

The drop shape also depends on the eluent flow rate. When this is reduced from the value of 1 ml min^{-1} mostly used, a distorted drop such as that at Fig. 2(c) assumes a more closely spherical shape as its support by the eluent flow decreases.

Noise sources

The electrode is susceptible to mechanical vibration, which is readily dampened (see Experimental). The instrumentation at high sensitivities (e.g., 2 nA full scale recorder deflection) gave a response when a person walked passed or operated it. This effect is suppressed by the earthed screen installed around the valve body of the detector.

The only other prominent noise is due to eluent flow pulsation derived from the reciprocating pump. The pulsation of the baseline of a chromatogram is in the region of 0.1—0.5% of, but not closely correlated with, the residual current (see below). Hence, usually it is visible only when high residual currents are encountered because of either the presence of oxygen in the eluent or large drop sizes. The noise appears as a series of regular spikes, the direction of which may vary with drop size. An example from an incompletely deoxygenated eluent is shown in Fig. 3. Negative spikes were detectable with the smallest drop size (A, Fig. 3) and became increasingly prominent as the drop size increased to $\times 12$ (C, Fig. 3). The residual currents are given in the caption to the Figure. Each spike corresponds to, but slightly lags behind (1—2 s), negative spikes monitored at the pressure transducer of the pump (uppermost traces, Fig. 3). These correspond to a fall in pressure, and hence in flow rate, of 0.5%. When the drop size was incremented beyond this point to $\times 13$ (D, Fig. 3), the spikes on the baseline suddenly inverted and intensified, and with a further increment (E, Fig. 3) there appeared a massive random noise.

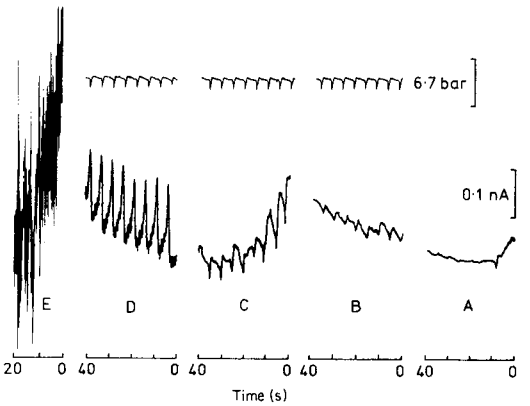

Fig. 3. Variation of noise levels of chromatogram baselines with electrode drop size. In increments of 1.6 mg, the drop sizes were: (A) X 1; (B) X 6; (C) X 12; (D) X 13; (E) X 14. The respective residual currents were 6.2, 41, 90, 89 and 80 nA. Traces of oxygen were present in the eluent. The tip—jet separation in the flow cell was 0.9 mm, and the outlet jet diameter 0.8 mm. The uppermost traces (B, C, D) show the pressure fluctuation monitored at the pump, where the total pressure was 300 bar. Further h.p.l.c. conditions are given under Experimental.

In general, it was found that the peak inversion is associated with drops that are becoming increasingly flattened as their size increases relative to the tip—jet separation. The intense noise exhibited at the upper limit of drop size is due to a state of vibration induced in the drop by the eluent flow. A similar effect has been noted in flow injection analysis with a hanging mercury drop electrode [9].

In accordance with the relationships governing the performance of hydrodynamic voltammetric electrodes [2, 10, 11], it is taken that the negative spikes seen with smaller drop sizes are due to the reduced rate of transport of electroactive material to the electrode surface in the reduced eluent flow associated with the negative pressure spikes. The effect is offset in the region where the drop is flattening whilst its size increases: in a negative pressure spike the area of the drop on which the eluent directly impinges increases because the reduced solvent flow permits the drop to descend into the jet orifice. Consequently, the rate of any (area-dependent) electron transfer process will be increased. Which of these counteracting effects predominates is finely balanced, and whether or not the baseline spikes will be inverted, or even reinverted, with different combinations of electrode dimensions and enlarged drops is not readily predicted (an example of reinverted spikes may be found in Fig. 4). However, with smaller drops the spikes when they can be seen are always of the form shown in Fig. 3(A—C). Clearly, the type and extent of pump-derived noise will vary between pumps, but the same factors will be involved. No noise of this sort could be seen in some experiments made with a high-frequency reciprocating pump (Applied Chromatography Systems), whereas a typical single piston reciprocating

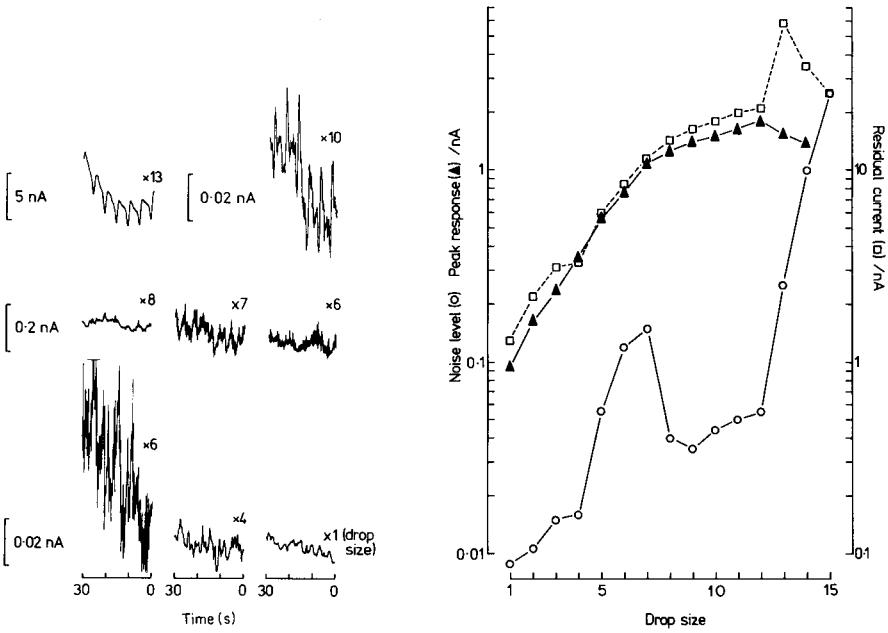

Fig. 4. Variation of noise levels of chromatogram baselines with electrode drop size in a well-deoxygenated eluent. The electrode drops were dispensed in the indicated increments (×1 to ×13) of 1.6 mg, and gave respective residual currents of 1.3, 4.2, 8.6, 11.5, 14.7, 18.0 and 58 nA. The tip—jet separation in the flow cell was 0.95 mm, and the outlet jet diameter was 0.8 mm. Further conditions are as given under Experimental.

Fig. 5. The effect of electrode drop size on: (○) noise level; (▲) peak response to 50 pg of *m*-dinitrobenzene; (□) residual current. The electrode drop size is in increments of 1.6 mg. The tip—jet separation in the flow cell was 0.95 mm, and the outlet diameter was 0.8 mm.

pump is reported [8] to give, with a hanging drop electrode, a fivefold increase in noise level relative to a dual piston pump similar to the one used in the present work. Even so, provided that the residual current from the eluent is small, the noise from an effectively dampened pump should approach negligible proportions.

An example of the variation in noise level with drop size for a well-deoxygenated eluent is shown in Fig. 4. Against the random background noise from the rest of the instrumentation, no clearly defined pump noise is visible below a drop size of ×10, with the exception of the ×7 drop. In these instances, the spikes have a first-derivative appearance. Negative spikes appear with the largest drop. The overall noise level does not increase regularly with drop size. A rapid increase at the ×6 and ×7 points is followed by a considerable decrease. This period of high noise corresponds to the stage at which the drop is flattening and withdrawing from the jet orifice. The effect is generally encountered, but more readily seen with tip—jet separa-

tions >0.5 mm, where the changes that occur as the drop size increases are less abrupt.

The variation of noise with drop size from the same series of experiments as in Fig. 4 is plotted in Fig. 5 (lowest plot), where the peak and the subsequent minimum in the region X 5 to X 8 are clearly apparent.

Dependence of the response to chromatography peaks on eluent flow rate

Because the shape of the electrode drop can be affected by the eluent flow, the response characteristics of the electrode to chromatographic peaks will be affected correspondingly. This is shown in Fig. 6, where the peak area from constant amounts of cyclo-1,3,5-trimethylene-2,4,6-trinitramine (the explosives component RDX) is plotted against flow rate for an essentially spherical drop (X 2; tip-jet, 0.35 mm) and a flattened drop (X 3; 0.35 mm). For the spherical drop (plot A, Fig. 6) the response increases with flow rate in a sigmoidal curve. At the flattened drop (plot B) a similar dependence may be present, but is obscured by the higher variability of the results. The initial flow-rate increment (0.2 to 0.4 ml min^{-1}) gives a sharply increased response that is constant with further increments except for one significantly high value at 0.8 ml min^{-1}. In this series, the respective width and the depth (from the capillary tip) of the drop was observed to vary from 1.15 mm and 0.55 mm (at 0.2 ml min^{-1}) to 1.3 mm and 0.4 mm (at 1.2 ml min^{-1}). No significant changes could be seen in the spherical drop. Probably other changes in behaviour would occur with more extreme variations in flow rate and flow-cell configuration; but because in practice chromatographic requirements dictate the flow rate, and leave slight latitude for its variation to an extent that the performance of the detector can be significantly varied, no further examination of flow rate effects was made.

Dependence of residual current and signal-to-noise ratio on drop and cell dimensions

Included in Fig. 5 are plots of the variation with drop size of the residual current and of the peak height response from 50-pg injections of *m*-dinitrobenzene. Over most of the range of drop size, the two sets of data are closely correlated, as expected if the residual current is due mainly to traces of reducible compounds remaining in the eluent. These residual currents are a substantial improvement over those reported for a hanging drop electrode used in conjunction with an electrochemical scrubber [7]. The improvement is probably due to the very high efficiency with which an eluent can be deoxygenated if it is kept under reflux [3, 12]. The current varies only slightly from the values given (Fig. 5) for an electrode potential of −1.0 V vs. Ag/AgCl when the potential is varied in the range 0 to −1.1 V. Beyond −1.1 V the current rapidly increases.

For a spherical drop under laminar flow conditions, a faradaic current should increase linearly with the area of the drop or, correspondingly, with the two-thirds power of its mass. Such plots for the residual current

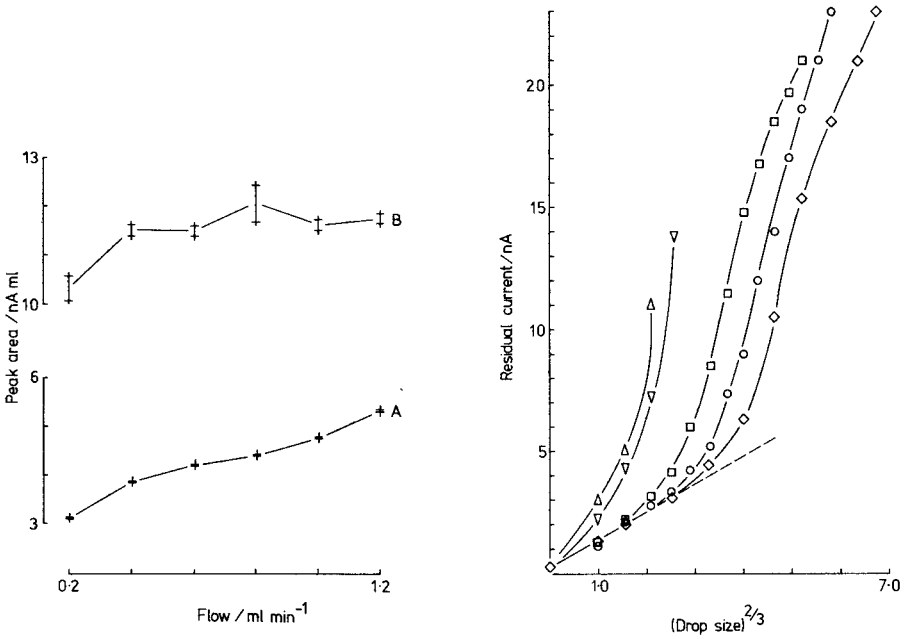

Fig. 6. Variation of peak area (peak height × width at half peak height) of 10-ng injections of cyclo-1,3,5-trimethylene-2,4,6-trinitramine with eluent flow rate. The tip—jet separation was 0.35 mm, the electrode drop sizes were × 2 (A) and × 3 (B). Each result was duplicated, as shown.

Fig. 7. Variation of residual current with electrode drop size (1.6 mg increments) and with the flow-cell configuration. The respective tip—jet separations and the outlet diameters were: (△) 0.25 and 0.8 mm; (▽) 0.4 and 0.8 mm; (□) 0.95 and 0.8 mm; (○) 1.3 and 0.5 mm; (◇) 1.2 and 0.8 mm. Other conditions are given under Experimental.

observed with an unmodified flow cell (tip—jet distance, 1.3 mm), and with a modified cell (tip—jet distance varied between 0.25 and 1.2 mm) are shown in Fig. 7. Evidently, for the smaller drop sizes relative to the tip—jet separation, the results can be represented in this way. With larger drops the residual current rapidly increases, presumably because of the increased linear flow rate and turbulence in the increasingly restricted space between the drop and the wall of the jet and because of the increased surface area relative to the mass of aspherical drops. For the same reasons, with a given (large) drop the current increases as the tip—jet separation is reduced, whereas the current is reduced as the jet outlet diameter is increased as in the modified relative to the unmodified cell results shown (Fig. 7) for similar separations. From Fig. 5, peak response will vary similarly.

The signal-to-noise ratios for 50-pg peaks of *m*-dinitrobenzene are plotted as a function of drop size in various flow-cell configurations in Fig. 8. An initial maximum in the region of 20 is apparent in each plot. When the tip—jet separation is sufficient to enable larger drops to be accommodated

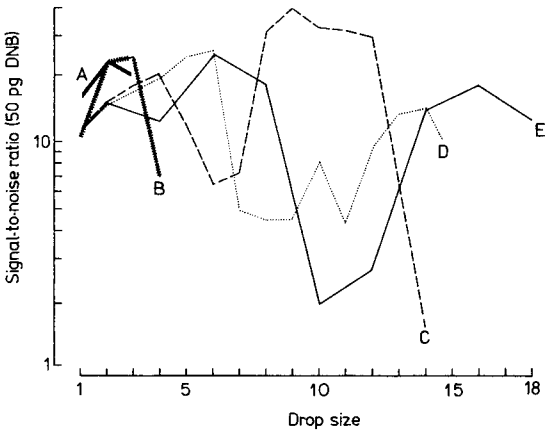

Fig. 8. Variation in signal-to-noise ratio of a chromatographic peak (50 pg of *m*-dinitrobenzene) with electrode drop size (1.6 mg increments) for different flow-cell configurations. The respective tip—jet separations and outlet jet diameters were: (A) 0.25 and 0.8 mm; (B) 0.4 and 0.8 mm; (C) 0.95 and 0.8 mm; (D) 1.3 and 0.5 mm; (E) 1.2 and 0.8 mm. Other conditions are given under Experimental.

(plots C, D, E; Fig. 8) a second maximum appears, which reaches 40 in the case of the 0.95-mm separation with a X 9 drop. Clearly, the theoretical result that, in general, signal-to-noise ratios from voltammetric detectors increase as the electrode area decreases [11] requires qualification in the case of the supported mercury drop electrode, where the effective area is a function of the flow rate. The second maxima in the plots result from the reduction in the noise level immediately after the initial flattening as the drop is enlarged. The effect occurs with an unmodified cell (plot E, Fig. 8) but cannot be exploited usefully because of the instability of large drops at the cylindrical orifice. With an unmodified cell used with a dropping mercury electrode, results have been reported [6] that are optimal with a tip—jet separation of 1 mm and with drops corresponding to the X 1, X 2 and X 4 sizes of the present work. The reduced separations used in the supported mercury drop electrode give, with a dropping electrode, high noise levels. Presumably this is because of an increased turbulence associated with the renewal of each drop.

Baseline drift

Once the chromatographic system has been adequately deoxygenated, which requires ca. 1.5 h from cold for the detection of ng-quantities of nitro compounds and correspondingly longer periods to reduce the residual current to a level appropriate for pg-detection (for this it is convenient to run the chromatograph overnight), the baseline rapidly stabilizes after the formation of a new drop [3]. If a steadily rising baseline occurs, the deposition of trace metal impurities from the eluent, which reduces the over-

potential of hydrogen at the electrode [13], is indicated. This may happen, e.g., after the installation of new pipework. The effect can be minimized by the use of a large electrode drop, because the rate of the drift tends to increase less rapidly with drop size than does the response of the electrode to chromatographic peaks. Possibly this is due to the greater dilution of the deposited impurities in the larger mercury drops. Sometimes the drift may be reduced by a purge of the system with a cation complexant [14], or by treating new parts with nitric acid, but on occasions these treatments aggravate the problem. Generally, an effective cure is to leave the chromatograph running for several days, otherwise the source of the nuisance must be traced and replaced.

As its size increases, the drop becomes accessible to impurities in the electrolyte by which the flow cell is surrounded, even though the drop can be seen to be entirely enveloped by the eluent if this either differs in refractive index from the electrolyte or has been deliberately coloured. For example, with a tip—jet separation of 0.9 mm and a $\times 2$ drop, the residual current remained at 2.8 nA when air was blown through the previously deoxygenated electrolyte. With a $\times 13$ drop, however, the current increased from 68 nA to 360 nA.

Oxygen diffuses into the eluent stream from the electrolyte if a polytetrafluoroethylene rather than a stainless steel capillary eluent line is used within the electrolyte reservoir. This can be prevented if the electrolyte is deoxygenated, but oxygen must be removed simultaneously from the plastic by transfer to the eluent and to the purging electrolyte, which may take up to an hour to do. When both a steel eluent line and a restricted drop size are in use, no oxygen from the electrolyte can reach the drop. Thus, under these conditions, whether or not the electrolyte is deoxygenated is unimportant, in contrast to some recent results [15] from a dropping electrode in the original PAR cell, and to earlier results in the present series [3].

Conclusion

The factors discussed provide a basis on which the performance of the supported mercury drop electrode may be optimized. Given that adequate precautions are taken to exclude traces of electroreducible contaminants from the eluent, residual currents on the order of 1 nA per mg of mercury may be obtained for the smaller drop sizes in a conventional h.p.l.c. solvent at electrode potentials in the region of -1.0 V vs. Ag/AgCl. If the drop size is optimal with respect to the flow-cell configuration, i.e., just before or beyond the point of flattening of the drop, the superimposed noise will be less than 0.5% of the residual current. This requires a detection limit ($\times 3$ signal-to-noise) of 4 pg for a compound typically giving an h.p.l.c. peak of ca. 4 nA ng^{-1} per mg drop size, such as *m*-dinitrobenzene. Actual similar values have been reported already [4]; the two- to three-fold improvement achieved over the original results [3] is due to the application of the detailed considerations presented here.

REFERENCES

1 R. J. Rucki, Talanta, 27 (1980) 147.
2 K. Štulík and V. Pacáková, J. Electroanal. Chem., 129 (1981) 1.
3 J. B. F. Lloyd, J. Chromatogr., 257 (1983) 227.
4 J. B. F. Lloyd, Proc. Int. Symp. Analysis and Detection of Explosives, FBI Academy, Quantico, U.S.A., 1983, in press.
5 J. B. F. Lloyd, J. Chromatogr., 261 (1983) 391.
6 R. Samuelsson and J. Osteryoung, Anal. Chim. Acta, 123 (1981) 97.
7 H. B. Hanekamp, W. H. Voogt, P. Bos and R. W. Frei, Anal. Chim. Acta, 118 (1980) 81.
8 B. Persson and L. Rosén, Anal. Chim. Acta, 123 (1981) 115.
9 E. O. Martins and G. Johansson, Anal. Chim. Acta, 140 (1982) 29.
10 H. B. Hanekamp and H. G. de Jong, Anal. Chim. Acta, 135 (1982) 351.
11 H. B. Hanekamp and H. J. van Nieuwkerk, Anal. Chim. Acta, 121 (1980) 13.
12 J. N. Brown, M. Hewins, J. H. M. van der Linden and R. J. Lynch, J. Chromatogr., 204 (1981) 115.
13 K. Bratin, P. T. Kissinger and C. S. Bruntlett J. Liq. Chromatogr., 4 (1981) 1777.
14 S. G. Weber and W. C. Purdy, Ind. Eng. Chem. Prod. Res. Dev., 20 (1981) 593.
15 J. Y. Lewis, J. P. Zodda, E. Deutsch and W. R. Heineman, Anal. Chem., 55 (1983) 708.

Analytica Chimica Acta, 154 (1983) 133—142
Elsevier Science Publishers B.V., Amsterdam — Printed in The Netherlands

CHLORIDE-ASSISTED ELECTROCHEMICAL DETECTION OF *CIS*-DICHLORODIAMMINEPLATINUM(II) AFTER LIQUID CHROMATOGRAPHY

WILLIAM N. RICHMOND and RICHARD P. BALDWIN*
Department of Chemistry, University of Louisville, Louisville, KY 40292 (U.S.A.)
(Received 1st April 1983)

SUMMARY

The cancer chemotherapy agent, *cis*-dichlorodiammineplatinum(II), is quantified voltammetrically by means of its chloride-assisted oxidation at platinum electrodes. The presence of chloride in the solution is required to lower the potential for the oxidation to a practically useful range, the amount of the decrease being directly dependent on the chloride concentration used. In the presence of 0.10 M chloride, the oxidation occurred at +0.56 V vs. SCE and, with differential pulse voltammetry, gave a detection limit of 1 μg ml^{-1}. When used in conjunction with liquid chromatography, a detection limit of 0.05 μg ml^{-1} was obtained with a linear range of response up to 10 μg ml^{-1}. The presence of chloride also had an analogous effect on the oxidation of the aquated derivatives of the platinum complex.

Numerous heavy metal coordination complexes, particularly many involving the platinum group metals, have been found to possess significant antitumor activity toward a variety of human cancers. Of these compounds, *cis*-dichlorodiammineplatinum(II), or cisplatin, was the first to be introduced into wide clinical use and has been by far the most intensely studied. In particular, this drug, administered intravenously both alone and in combination with other antineoplastic agents, has proven to be effective in the treatment of testicular, ovarian, and urinary bladder carcinomas, osteosarcoma, and tumors of the head and neck [1, 2]. Additionally, several new complexes of platinum, palladium, and other heavy metals have been formulated and are currently being evaluated for increased anticancer activity and reduced toxic side effects compared to cisplatin [3—6].

Plasma levels, tissue distribution, and excretion of cisplatin have been investigated via several analytical approaches. Most commonly, instrumental methods involving atomic absorption [7—9], x-ray fluorescence [10], and the use of radioactively labeled platinum [11] have been employed. As each of these techniques by itself constitutes a method of elemental analysis only, they are inherently capable of quantifying only the total platinum content of the selected samples and provide no immediate information concerning the molecular form in which it is present. This is an especially important

0003-2670/83/$03.00

consideration for cisplatin because substitution of one or more of its chloride ligands has been shown to occur under intracellular conditions and it is these aquated forms which are believed to be the active antitumor species [12, 13]. Accordingly, a quantitative approach has been described [14—16] based on the liquid chromatographic separation of the various platinum-containing species with on-line spectrophotometric detection at 280 nm or electrothermal atomic absorption detection of manually collected chromatographic fractions. Because of the modest molar absorptivity of cisplatin the spectrophotometric approach was useful only for cisplatin concentrations greater than 1 $\mu g\ ml^{-1}$; the more cumbersome atomic absorption approach had a detection limit of 0.04 $\mu g\ ml^{-1}$.

In recent years, the use of electrochemical detection techniques after liquid chromatographic separations has been shown to be advantageous for numerous applications involving easily oxidized or reduced analytes [17]. The particular advantages of such combined liquid chromatography/electrochemical detection (l.c.e.c.) include high sensitivity, simplicity of detector hardware and operation, and a unique selectivity toward electroactive compounds as determined by the applied electrode potential.

The electrochemical behavior of cisplatin and several analogous platinum(II) complexes has previously been characterized by Hubbard and coworkers [18, 19]. In these studies, it was reported that cisplatin, as well as numerous other platinum(II) complexes containing simple monodentate ligands, is oxidized at relatively high positive potentials at platinum electrodes; the resulting Pt(II)—Pt(IV) oxidation waves are generally broad and indistinct, with the precise oxidation potential depending slightly on the nature of the ligands. Additionally, it was observed that the presence of free halide ion in solution served to catalyze the oxidation, lowering the potential required by 200—500 mV. In an alternative approach utilizing reduction at a dropping mercury electrode, Vrana et al. [20] have shown that cisplatin can be converted to the diethyldithiocarbamate complex, extracted into chloroform, and then quantified as the ethylenediamine complex by differential pulse polarography at −1.65 V vs. SCE. A detection limit of 0.010 $\mu g\ ml^{-1}$ in urine samples was claimed; however, extensive sample derivatization and work-up procedures were required.

Initial efforts directed toward the application of l.c.e.c. for the determination of cisplatin have been reported [21, 22]. These studies used both oxidative l.c.e.c. at glassy carbon electrodes and reductive l.c.e.c. at mercury or mercury-coated gold electrodes. The latter approach was shown to be especially successful, permitting operation at a detector potential of 0.0 V vs. Ag/AgCl and yielding a detection limit of 0.10 $\mu g\ ml^{-1}$ for cisplatin in untreated urine samples [21]. In this paper, the oxidation of cisplatin and its hydrated derivatives at platinum electrodes is further investigated for use in the determination of these compounds. In particular, a new on-line l.c.e.c. approach is described for quantifying individual cisplatin species based on their halide-catalyzed oxidation following liquid chromatographic separation.

EXPERIMENTAL

Reagents

Cisplatin was obtained in 99.99% purity (Aldrich Chemical Co.). Unless otherwise stated, standard solutions of cisplatin were also 0.10 M in potassium chloride. Aqueous solution containing mixtures of the aquated derivatives were prepared from cisplatin by incubation in water at 30°C for 2 h according to the procedure of Riley et al. [15]. Other chemicals were reagent grade and were used as received without further purification. All solutions were prepared with deionized water.

Procedures

Electrochemistry. Cyclic voltammetry was done with a Bioanalytical Systems (West Lafayette, IN) Model CV-1B potentiostat and a Houston Instruments Model 2000B X-Y recorder; the potential scan rate was always 10 mV s^{-1}. For differential pulse experiments, a Princeton Applied Research Model 364 polarographic system was used with a pulse amplitude of 50 mV and a scan rate of 2 mV s^{-1}. The working electrode consisted of a 1-cm length of 20-gauge Pt wire, loosely coiled and sealed into glass tubing. Before each run, this electrode was cleaned by repeated heating to incandescence in a methane—oxygen flame and quenching in concentrated perchloric acid. The reference electrode for all voltammetry was a $Hg/HgSO_4$ (saturated) electrode (+0.40 V vs. SCE), and the counter electrode was a Pt wire. All potentials were converted and are reported with respect to the SCE.

Chromatography. The liquid chromatograph used was a modular system consisting of a Waters Associates Model M-6000 A pump, a Rheodyne Model 7125 sample injector with a 20-μl sample loop, a Waters Model 440 u.v.—visible absorbance detector, and a Bioanalytical Systems Model LC-3 amperometric detector. The working electrode for the l.c.e.c. experiments was a Bioanalytical Systems Model TL-10A Pt electrode which was cleaned daily by polishing with alumina. The reference electrode was a Ag/AgCl electrode (—0.045 V vs. SCE).

The 30-cm, 10-μm octadecylsilane column (Regis Chemical Co., Morton Grove, IL) used was pretreated with hexadecyltrimethylammonium chloride (HTAC) by passing 75 ml of 2.7×10^{-3} M HTAC through at a flow rate of 1 ml min^{-1}. The mobile phase always contained 1×10^{-3} M HTAC. The complete separation procedure is described by Riley et al. [15]. The flow rate used for all the chromatography was 2.3 ml min^{-1}.

Serum samples. Blood serum samples used were prepared by mixing equal volumes of whole human blood and acetonitrile and filtering the supernatant liquid first through medium porosity (Whatman 1) qualitative filter paper and then through a 0.3-μm glass filter. Doped serum samples were prepared by adding an appropriate volume of a 500-mg l^{-1} cisplatin solution in 0.1 M KCl to this filtrate. Serum samples were then injected directly onto the chromatographic column without further treatment.

RESULTS AND DISCUSSION

The electrochemistry of cisplatin

Because l.c.e.c. in the oxidative mode is preferentially conducted at some type of carbon electrode, the electrochemical behavior of cisplatin was first investigated by cyclic voltammetry at glassy carbon and carbon paste electrodes. Similar results were obtained with both of these electrode materials. When the cyclic scan was limited to potentials more positive than 0.0 V vs. SCE, the cisplatin oxidation wave occurred only at very high positive potentials ($E_p \geqslant +1.2$ V vs. SCE) at which there is an extremely large background. Furthermore, the wave was quite broad and indistinct in shape. Thus, the prospects for quantifying the compound with optimum sensitivity and selectivity by oxidative l.c.e.c. at carbon electrodes appeared slight. In fact, a recently reported application of such an approach demonstrated that, although the method was of some potential use, detector voltages on the order of +1.2 to +1.4 V vs. Ag/AgCl were required [22]. Interestingly, when the cyclic voltammetric scan was allowed to extend into the negative potential region as well, additional cisplatin activity was observed. This included both a broad region of cathodic activity between 0.0 and —0.5 V and a new anodic wave at +0.65 V which appeared only after first scanning over the negative region and apparently is related to some cisplatin reduction product. The former cathodic activity formed the basis for the recently cited applications of reductive l.c.e.c. for cisplatin determination [21, 22].

Accordingly, the oxidation of cisplatin was subsequently observed by using cyclic voltammetry at a platinum electrode (Fig. 1, curve A). Again, an unusually broad anodic wave was observed, but this time shifted to a somewhat lower potential of approximately +0.9 V vs. SCE. This corresponds closely with the behavior reported by Cushing and Hubbard [18]. However, the background current observed in this case remained substantial even though the peak potential of the oxidation was decreased. Thus, the development of

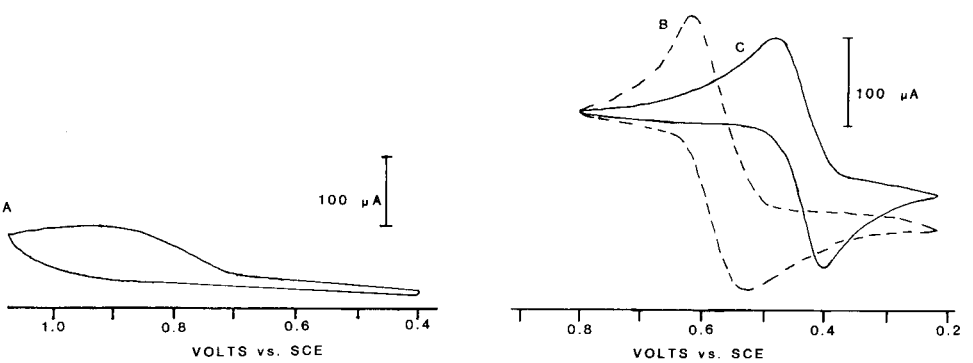

Fig. 1. Cyclic voltammograms of a 500 µg ml^{-1} cisplatin solution at a Pt electrode: (A) no Cl^- present; (B) 0.010 M Cl^-; (C) 1.0 M Cl^-. Total electrolyte concentration was maintained at 1.0 M by the addition of $NaNO_3$; anodic current is plotted in the upward direction.

a useful quantitative method for cisplatin based on its direct oxidation at platinum electrodes was also considered unlikely.

Finally, the electrochemical oxidation of cisplatin was evaluated again by using a platinum working electrode but this time in a solution containing potassium chloride. Cushing and Hubbard [18] reported the occurrence of a chloride-catalyzed oxidation reaction for the complex which was described as follows

$$cis\text{-}Pt(NH_3)_2Cl_2 + Cl^- + H_2O \rightarrow cis\text{-}Pt(NH_3)_2Cl_2(H_2O)Cl^+ + 2e^- \quad (1)$$

The peak potential for this oxidation was reported to be shifted toward considerably lower potentials, the magnitude of the shift depending on the chloride concentration utilized. Present observations confirmed this and are summarized in Fig. 1 (curves B and C) and Table 1. In fact, the cisplatin oxidation was found to be sufficiently sensitive to the presence of chloride that leakage of chloride through the frit of a single-junction calomel electrode over a period of 5—10 min was sufficient to produce the catalytic effect. Therefore, in all subsequent work, a $Hg/HgSO_4$ reference electrode was employed in order to circumvent this potential interference. It can be seen that chloride is extremely effective in decreasing the potential required for cisplatin oxidation; a chloride concentration of 0.10 M or greater was sufficient to decrease the potential required for the process to a value sufficiently low so as to fall well within the useful range for l.c.e.c. In addition, the cisplatin oxidation also appeared to be much more reversible in the presence of chloride, with the waves more distinctly peak-shaped and a pronounced reduction wave appearing on the reverse potential scan. Both bromide and iodide were also investigated in terms of the catalytic effect which these ions analogously might exert on cisplatin oxidation. Bromide exhibited an effect that was similar to that shown by chloride; but, because of the onset of the direct oxidation of iodide at relatively cathodic potentials, it was not possible to observe its catalytic capabilities.

The extent to which this catalytic effect enhances the potential of electrochemical techniques for applications involving the detection and quantitation

TABLE 1

Electrode potential for oxidation of cisplatin as a function of chloride concentration[a]

Concentration (M)	E_{pa} (V vs. SCE)	i_{pa} (μA)	Concentration M	E_{pa} (V vs. SCE)	i_{pa} (μA)
0	+0.90	39	2×10^{-2}	+0.60	208
1×10^{-3}	+0.68	133	5×10^{-2}	+0.60	208
2×10^{-3}	+0.64	181	1×10^{-1}	+0.58	236
5×10^{-3}	+0.62	173	2×10^{-1}	+0.56	153
1×10^{-2}	+0.61	212	1.0	+0.48	188

[a]By cyclic voltammetry; total electrolyte concentration, 1.0 M by addition of $NaNO_3$.

of cisplatin can be simply illustrated by comparison of the differential pulse voltammograms (d.p.v.) of the compound both in the absence and in the presence of chloride (Fig. 2). In the former case, the cisplatin oxidation produced only a broad wave with a "peak" that was difficult to locate and began to merge with the background at an analyte concentration of 100 μg ml^{-1}. But, in the presence of 0.10 M chloride, the oxidation by d.p.v. gave a sharp peak at +0.52 V vs. SCE. In this case, the detection limit (i.e., signal/noise = 2) was less than 1.0 μg ml^{-1}.

The aquated forms of the complex, prepared by the procedure given in the Experimental section, were found to exhibit similar electrochemical behavior to that of cisplatin. Thus, as shown in Fig. 3, the *cis*-diaquodiammine species showed a readily discernible anodic wave only in the presence of chloride. However, unlike the parent complex, the oxidation of the aquated compound was not reversible under the conditions employed. Because of this apparent difference in the electrochemical behavior of the two compounds, the possibility that rapid re-formation of cisplatin might be occurring at the higher chloride concentrations was discounted.

Liquid chromatography with electrochemical detection

Considering the preceding experimental observations, the most favorable conditions for the oxidative l.c.e.c. of cisplatin and its related compounds required the presence of chloride in the chromatographic stream. Although the presence of halide ion in the mobile phase is not a recommended operating procedure for high-performance liquid chromatographic instrumentation, it was found acceptable to add the requisite chloride concentration directly to the mobile phase before entering the chromatograph; no degradation of

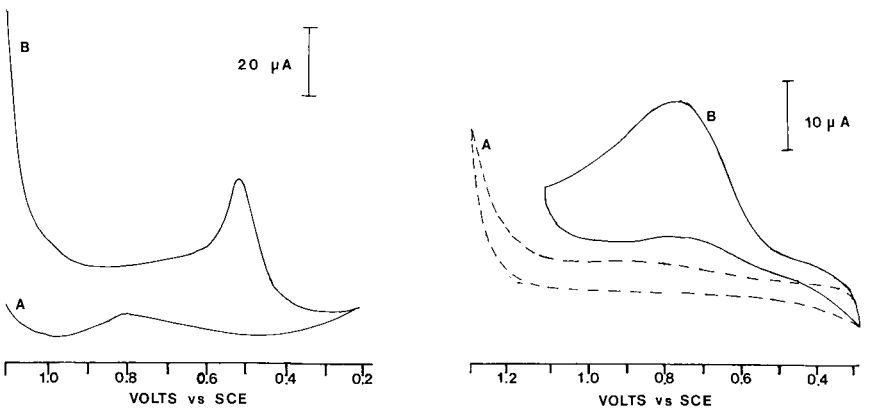

Fig. 2. Differential pulse voltammograms of cisplatin at a Pt electrode: (A) 100 μg ml^{-1}, no Cl^- present; (B) 10 μg ml^{-1}, 0.10 M Cl^-. Total electrolyte concentration was maintained at 1.0 M by the addition of $NaNO_3$; anodic current is plotted in the upward direction.

Fig. 3. Cyclic voltammograms of $Pt(Cl)_2(H_2O)_2$ at a Pt electrode. Electrolyte: (A) 0.10 M $NaNO_3$; (B) 0.15 M NaCl; anodic current is plotted in the upward direction.

performance was observed as long as the chloride-containing mobile phase was never allowed to stand in contact with the chromatographic system and was thoroughly washed off the system immediately after use. It would, of course, also be possible to add the chloride to the mobile phase after the column and immediately before the electrochemical detector. The chromatography was conducted on an octadecylsilane column using the solvent-generated anion-exchange technique previously reported by Riley et al. [15] to be effective for the separation of various Pt complexes. Accordingly, prior to use, the column was treated with HTAC; and the mobile phase consisted of HTAC and sufficient potassium chloride or sodium nitrate to bring the electrolyte concentration to 0.10 M. Under these conditions, the aquated platinum complexes were nearly unretained while cisplatin had a retention time of approximately 3 min.

Chromatograms obtained for a 10 μg ml^{-1} cisplatin solution using a 0.10 M chloride-containing mobile phase are shown in Fig. 4. The potential of the electrochemical detector employed was +0.75 V vs. Ag/AgCl, and the u.v. detection was done at 254 nm. The greatly enhanced response of the l.c.e.c. detector towards cisplatin is readily apparent. The interdependence of detector potential required for cisplatin response and chloride concentration is shown by the hydrodynamic voltammograms recorded for cisplatin sample with chloride concentrations of 0, 0.01 and 0.10 M in the mobile phase. These are shown in Fig. 5. As expected on the basis of the cyclic voltammo-

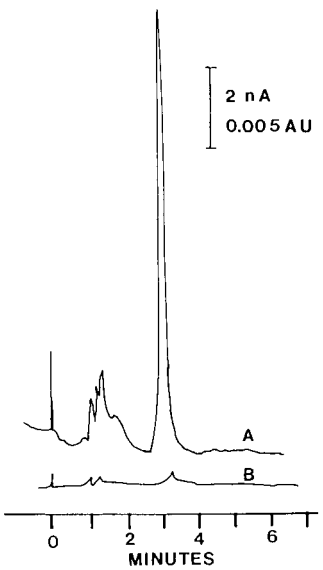

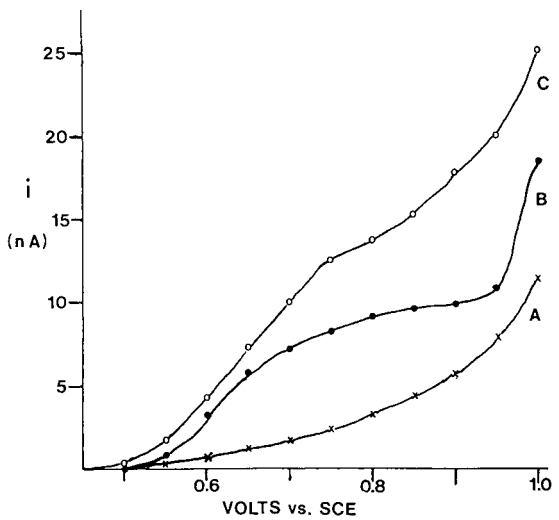

Fig. 4. Chromatograms of 10 μg ml^{-1} cisplatin solution: (A) l.c.e.c. at +0.90 V vs. SCE; (B) l.c.—u.v. at 254 nm.

Fig. 5. Hydrodynamic voltammograms for a 10 μg ml^{-1} cisplatin solution: (A) no Cl^- present in mobile phase; (B) 0.010 M Cl^-; (C) 0.10 M Cl^-.

grams reported above, greater l.c.e.c. current levels can be obtained at lower potentials as the chloride concentration is increased. When the electrode potential was maintained at +0.90 V vs. SCE and a 0.10 M chloride concentration was employed, response to cisplatin was linear over the range 0.05—10 μg ml^{-1}. The regression equation for six concentrations over this range gave a slope of 4.5 and an intercept of 0.0487 with a standard deviation of 0.16 nA; the correlation coefficient was 1.000. Under these conditions, the detection limit was of the order of 0.05 μg ml^{-1}. Once again, an analogous response enhancement over detection via either u.v. absorption at 254 nm or the ordinary electrochemical approach was also obtained for the aquated cisplatin derivatives when a significant chloride concentration was maintained in the aqueous mobile phase.

As Bannister et al. [21] have previously noted, the extension of quantitative procedures for cisplatin to the determination of the compound in actual physiological samples can be severely limited by the presence of co-eluting interferences which either absorb at the detector wavelength used or, for l.c.e.c., undergo electrolysis at the applied detector potential. The practical utility of any quantitative approach is thus directly related to its selectivity or, conversely, to its ability to function independent of intricate or time-consuming sample treatment steps preliminary to the actual concentration measurement. With this in mind, the application of l.c.e.c. to blood serum samples doped with cisplatin was also examined. An optimized chromatogram obtained for a serum sample containing cisplatin (10 μg ml^{-1}) is shown in Fig. 6. Two experimental conditions were altered to enhance the selectivity of the approach. First, a detector potential of +0.80 V vs. Ag/AgCl was used in place of the higher potential employed earlier. Second, the mobile phase composition (0.010 M NaCl, 0.005 M citric acid, and 0.001 M HTAC brought to pH 7 with sodium hydroxide) was altered somewhat over that used above in order to increase the retention of the cisplatin and thereby prevent the co-elution of the analyte with the oxidizable but relatively weakly retained serum components. However, while selectivity was improved considerably, both the decrease in electrode potential and the decrease in chloride concentration also served to diminish somewhat the maximum sensitivity that could be achieved. As a result, the peak current observed for the 10-μg ml^{-1} cisplatin standard in Fig. 4 was considerably greater than that observed for a 10 μg ml^{-1} serum sample observed in Fig. 6. Under these conditions, a detection limit of about 1.0 μg ml^{-1} of serum was achieved. At the 10 μg ml^{-1} level, the reproducibility of the measurement, as characterized by the relative standard deviation of the peak current, was 11.7% for five successive serum injections over the course of 2—3 h of continuous chromatography. Sample preparation was as described under Experimental, consisting essentially of filtration of the doped serum and direct injection.

Both pre- and post-column derivatization reactions have been commonly employed to enhance the capabilities of most liquid chromatographic detection methods. The l.c.e.c. method has been no exception in this regard;

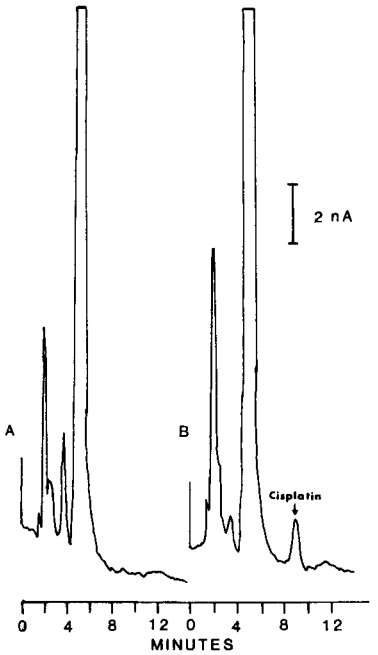

Fig. 6. Chromatograms of blood serum using l.c.e.c. at +0.80 V vs. Ag/AgCl: (A) serum blank; (B) serum doped with 10 μg ml^{-1} cisplatin.

several examples of reactions involving the formation of easily oxidized or reduced derivatives have been reported [23]. The l.c.e.c. method described for cisplatin in this paper is analogous to such derivatizations in its approach; however, there are some important differences involved. Principally, the post-column reaction used for cisplatin does not involve the actual formation of a new, more easily electrolyzed platinum species. Rather, the process entails simply the inclusion in the eluent stream of a suitable quantity of chloride ion as an "electro-catalyst" capable of providing an alternative, low-potential oxidation pathway for cisplatin. Thus, experimental considerations involving reaction time, yield, temperature, etc., which are normally of critical importance for derivatization procedures actually done on-line, do not present severe problems here. Furthermore, the measurement approach demonstrated for cisplatin in this work clearly possesses adequate sensitivity to be of use in monitoring the levels of the drug in patients undergoing chemotherapy and in fact closely approaches that of the previously suggested h.p.l.c.-atomic absorption and l.c.e.c. techniques. Compared to other recently reported l.c.e.c. methods for cisplatin [21, 22], only the reductive approach using mercury electrodes possesses a superior detection limit. This approach, however, also possesses the potential for use in quantifying aquated cisplatin metabolites. Applications of this method for use in the clinical laboratory and extension to new cisplatin analogs are continuing in this laboratory.

This research was supported by American Cancer Society Institutional Research grant IN-111G. The work was presented in part at the 1983 Pittsburgh Conference on Analytical Chemistry and Applied Spectroscopy, Atlantic City, NJ, March, 1983.

REFERENCES

1 M. Rozencweig, D. D. Von Hoff, M. Slavik and F. M. Muggia, Ann. Int. Med., 86 (1977) 803.
2 F. M. Muggia, M. Rozencweig, V. H. Bono and E. M. Jacobs, Jr., Cancer Treat. Rep., 63 (1979) 1431 ff.
3 M. J. Cleare, Coord. Chem. Rev., 12 (1974) 349.
4 R. D. Graham and D. R. Williams, J. Inorg. Nucl. Chem., 41 (1979) 1245.
5 A. W. Prestayko, W. T. Bradner, J. B. Huftalen, W. C. Rose, J. E. Schurig, M. J. Cleare, P. C. Hydes and S. T. Crooke, Cancer Treat. Rep., 63 (1979) 1503.
6 W. C. Rose, J. E. Schurig, J. B. Huftalen and W. T. Bradner, Cancer Treat. Rep., 66 (1982) 135.
7 S. J. Bannister, Y. Chang, L. A. Sternson, A. J. Repta, Clin. Chem., 24 (1978) 877.
8 T. F. Patton, K. J. Himmelstein, R. Belt, S. J. Bannister, L. A. Sternson and A. J. Repta, Cancer Treat. Rep., 62 (1978) 1359.
9 R. J. Belt, K. J. Himmelstein, T. F. Patton, S. J. Bannister, L. A. Sternson and A. J. Repta, Cancer Treat. Rep., 63 (1979) 1515.
10 S. J. Bannister, L. A. Sternson, A. J. Repta and G. W. James, Clin. Chem., 23 (1977) 2258.
11 R. C. DeConti, B. R. Toftness, R. C. Lange and W. A. Creasy, Cancer Res., 33 (1973) 1310.
12 B. Rosenberg, Cancer Treat. Rep., 63 (1979) 1433.
13 J. D. Blachley and J. B. Hill, Ann. Int. Med., 95 (1981) 628.
14 Y. Chang, L. A. Sternson and A. J. Repta, Anal. Lett., Part B, 11 (1978) 449.
15 C. M. Riley, L. A. Sternson and A. J. Repta, J. Chromatogr., 217 (1981) 405.
16 C. M. Riley, L. A. Sternson, A. J. Repta and R. W. Siegler, J. Chromatogr., 229 (1982) 373.
17 P. T. Kissinger, Anal. Chem., 49 (1977) 447A.
18 J. P. Cushing and A. T. Hubbard, J. Electroanal. Chem., 23 (1969) 183.
19 R. F. Lane and A. T. Hubbard, J. Phys. Chem., 79 (1975) 808.
20 O. Vrana, V. Kleinwachter and V. Brabec, Talanta, 30 (1983) 288.
21 S. J. Bannister, L. A. Sternson and A. J. Repta, J. Chromatogr., 273 (1983) 301.
22 I. S. Krull, X.-D. Ding, S. Braverman, C. Selavka, F. Hochberg and L. A. Sternson, J. Chromatogr. Sci., 21 (1983) 166.
23 L. R. Snyder and J. J. Kirkland, Introduction to Modern Liquid Chromatography, 2nd edn., Wiley-Interscience, New York, 1979, pp. 740—746.

Analytica Chimica Acta, 154 (1983) 143—152
Elsevier Science Publishers B.V., Amsterdam — Printed in The Netherlands

BIOGENIC INTERNAL STANDARDS FOR DUAL-LABEL RADIOCHEMICAL DETECTION OF METABOLITES IN LIQUID CHROMATOGRAPHY

LAWRENCE C. THOMAS* and TERRY L. RAMUS
Department of Chemistry, Oregon State University, Corvallis, OR 97331-4003 (U.S.A.)
(Received 7th May 1983)

SUMMARY

Dual-label radiochemical methods for liquid chromatography are described. Two sets of compounds are used, each set with a different isotopic label. The procedures decrease quantitative uncertainties by as much as 30% for samples in which chemical reactions have altered a test compound in compared biological systems. This advantage is especially useful in toxicologic metabolism studies. Determinations or comparisons of several conjugated and unconjugated metabolites are achieved by extraction and high-performance liquid chromatography based on these procedures. Quantitative procedures that include an internal standard, biologically generated by rats exposed to radiolabeled compounds, are used. By means of these internal standards, metabolite concentrations are compared for test organisms, and results are obtained for metabolites common to both organisms. Effects of impurities, isotope exchange, or chemical kinetics are also evaluated utilizing a modification of the technique.

Radiochemical detection methods for liquid chromatography are popular in biological experiments, mainly because radioactivity can offer low detection limits and improved selectivity. Recent work, including examples of quantitative measurements of peptides and metabolites, has been reviewed by Roberts [1]. Concurrent elution of standards and analytes has been used with simultaneous ultraviolet absorbance and radioactivity detection [1]. Similarly, co-elution chromatography of more than one radioactive substance has also been studied [2—6].

In metabolism studies, radiolabeled substances may be needed as internal standards [1]. However, simple internal standard procedures may not be adequate because different metabolites of the same compound may be extracted with different efficiencies and uncertainties [7]. In such cases, the use of multiple internal standards represents a reasonable alternative. The best internal standards are the metabolite compounds themselves, labeled to give appropriate specificity of detection.

To effect dual-label procedures, differently labeled compounds may be used in metabolism studies. For example, a ^{3}H-labeled internal standard could be used for each metabolite [1], and would co-elute with the respective ^{14}C-metabolite. However, such mixed pure standards may be costly or

0003-2670/83/$03.00

unavailable and biologically generated metabolites can be used instead.

In this study, h.p.l.c. is used with biogenic internal standards for dual-label procedures. Two methods are used, each with co-elution chromatographic separations and radioactivity detection. One method utilizes a solution of radiolabeled metabolites that have been biologically generated. In this case, the internal standard is added to samples before extraction. The other method uses a solution of two radiolabeled forms of the same compound with concurrent dosage into the organism. Their respective metabolites each serve as mutual internal standards for quantitative comparisons to evaluate effects of impurities on metabolism experiments. In this second procedure, both radiolabeled forms of each metabolite are generated simultaneously within the same organism.

These new dual-label methods allow compensation for difficulties caused by variations in extraction efficiencies, losses during concentration of extracts, unavailability of appropriate reference compounds, and uncertainties in specific activities of radiolabeled dosage compounds. Furthermore, the dual-label biogenic internal standard methods allow one to evaluate effects of impurities in dosage compounds, isotope exchange, and kinetic differences on quantitative comparisons of metabolites in biological experiments. These effects should be evaluated before extensive metabolism experiments are attempted.

THEORY

The mass of each labeled metabolite, M, can be calculated [1] from its corrected activity, A, for an eluate as

$$M = (A V_t)/(E V_{ss} S) \quad (1)$$

where E is the extraction/concentration efficiency for the metabolite, S is the specific activity of the labeled component of interest, V_t is the volume of the concentrated extract, and V_{ss} is the volume of the subsample used for h.p.l.c.

Metabolite determinations: dual label

The use of pure internal standards for chromatography of radiolabeled substances is well-established [1], but pure standard compounds often are expensive or unavailable. In the absence of pure standards, a fixed known volume, V_a, of a biologically generated internal standard containing several compounds can be used instead. Prior to extraction, one can add H-labeled standards to solutions that contain the same, but C-labeled, compounds of unknown concentrations. If the extraction/concentration efficiencies are equivalent for the two extractable isomers of each component then $E_C = A_H V_t A_{sH}^{-1} V_{ss}^{-1} = E_H$ where A_H and A_{sH} are corrected activities for the H-labeled component in volumes V_{ss} and V_a, respectively. This equivalence is a reasonable assumption when isotope exchange is negligible and the two forms of

the metabolite are chemically alike and are not entrapped or bound by tissue.

This procedure is similar to using several radiolabeled internal standards and conventional radiotracer calculations and requires the same liquid scintillation counting procedures. Thus, the mass of each C-labeled component in the sample can be determined by using subsample activity data from the chromatogram, A_C and A_H, the total H-label activity in volume V_a for the biogenic internal standard stock solution, A_{sH}, and the analyte specific activity, S_C, as

$$M_C = (A_C A_{sH})/(S_C A_H) \tag{2}$$

Single metabolite comparisons: the R *ratio*

Often in biological experiments the absolute masses of analytes are less important than their relative concentrations, e.g., in comparisons of the same metabolites in control vs. test organisms [8]. Such comparisons are suitable for the use of biologically generated multiple internal standards. To use such standards, one adds a fixed volume of homogeneous biogenic internal standard to each sample which is extracted.

Using the same dosage solution of C-radiolabeled compound to expose two sets of organisms, 1 and 2, requires $S_{2C} = S_{1C}$. Similarly, adding equal volumes of the biogenic internal standard taken from the same stock solution for each sample, infers $A_{1sH}A_{2sH}^{-1} = 1$. Also, if $V_{1t} = V_{2t}$ and $V_{1ss} = V_{2ss}$ by experimental design, a ratio of masses, R, can be defined for each component such that for two experimental groups, e.g., 1 and 2,

$$R_{12} = (A_{1C}A_{2H})/(A_{2C}A_{1H}) = M_1/M_2 \tag{3}$$

where M_1 and M_2 are masses (Eqn. 2) of the component of interest for groups 1 and 2.

This R ratio method is useful for studies of metabolism. For example, the mass of accumulated metabolite can be hypothesized to be the same for two groups, 1 vs. 2 (i.e., $R_{12} = 1$ if the hypothesis is valid) and R_{12} can be tested statistically. This procedure can be extended to several metabolites to characterize several metabolic pathways. However, such multiparametric extensions are more amenable to the Q ratio method discussed below.

Multiple metabolite comparisons: the Q *ratio*

In biological experiments, relative magnitudes of several intrasample parameters are often more important than their absolute magnitudes. In such cases, relative intragroup data can be compared to corresponding data for another group, e.g., control vs. test groups [9]. For these comparisons, an extension of the dual-label co-elution method can be formulated for groups 1 vs. 2 and metabolites i vs. j, such that

$$Q_{12} = [(A_{1Ci}A_{1Hj})/(A_{1Cj}A_{1Hi})]/[(A_{2Ci}A_{2Hj})/(A_{2Cj}A_{2Hi})] \tag{4}$$

where subscripts C and H indicate the measured nuclide, subscripts i and j indicate two separated metabolites, and subscripts 1 and 2 indicate the groups from which the subsample was taken. If $Q_{12} = 1$, as tested statistically, then the relative magnitudes of the compared metabolites do not differ significantly. Thus, by using several i, j pairs one can evaluate a metabolic profile representing several modes of metabolism.

Impurity effects on metabolism experiments: the U *ratio*

Unfortunately, despite attempted purifications, toxicologic experiments must sometimes be performed with impure dosage compounds [9]. Thus, dosage impurities may affect results in metabolism studies. Furthermore, isotope exchange or perturbations of reaction kinetics caused by isotopic composition may affect metabolism results [1].

To evaluate potential interferences, a U ratio can be defined for C- vs. H-labeled metabolites, when $V_{Ct} = V_{Ht}$ and $V_{Ca} = V_{Ha}$ with no uncertainty in the volume equalities if the respective volumes are identical subsamples of the same solutions. Separated metabolites, i vs. j, can be compared when the metabolites are derived from the same solution of radiolabeled compounds, and an intrasample comparison

$$U_{ij} = (A_{Ci}A_{Hj})/(A_{Cj}A_{Hi}) \tag{5}$$

can be made. If there has been no isotope exchange nor differences in kinetics, then $U_{ij} = 1$; that is, the relative isotopic composition for each of the metabolites remains constant. However, if there are kinetic differences, isotope exchange, or impurities present from which the components are comprised, then U_{ij} may be significantly different than unity. One can test U_{ij} statistically for each i, j pair.

Similarly, one can compare intersample metabolite levels between experimental groups, e.g., 1 vs. 2, by ratioing H- and C-activities for the respective metabolites from the groups. Thus, differences between the groups can be tested statistically for each metabolite.

EXPERIMENTAL

Reagents and apparatus

Methanol and ethyl acetate were Mallinckrodt ChromAR, and all other organic solvents were of pesticide quality. Labeled compounds (^3H and ^{14}C) were obtained from commercial sources. Dilutions were made with water that was filtered through activated charcoal and distilled in an all-glass apparatus, or with methanol. Corn oil used for intraperitoneal injections was U.S.P. quality. All other chemicals were reagent grade.

A high-performance liquid chromatograph (Spectra-Physics Model 3500) was used with a stainless-steel column, 4 mm i.d. × 50 cm, packed with 10-μm LiChrosorb RP-18 (E-M Laboratories) reverse-phase liquid chromatographic column material. Eluted fractions were collected in glass vials by a

fraction collector. Radioactivities of the fractions were measured using Aquasol (New England Nuclear) cocktail and a liquid scintillation counter (Packard Model 3003). Laboratory glassware was treated with a solution of dimethylchlorosilane in petroleum ether.

Test animals

Sprague-Dawley rats weighing about 200 g were used. Rainbow trout, weighing about 150 g, were obtained from a commercial fish farm. Shrimp were obtained from Puget Sound, Washington. Both aquatic species were maintained in fiberglass tanks without food for one week prior to exposures.

Procedures

Rat urine extracts. Ethyl acetate extracts were prepared from urine collected from rats which had been injected intraperitoneally with purified radiolabeled (^{14}C or ^{3}H) naphthalene dissolved in corn oil. Urine was collected from animals held in silanized plastic rodent urine collection cages. The urine was saturated with sodium chloride and extracted four times with volumes of ethyl acetate equal to the urine volume. These extracts were combined and evaporated to dryness under a stream of nitrogen at ambient temperature. The residue was dissolved in methanol to yield measured radioactivities for stock solutions of about 6×10^5 counts min^{-1} ml^{-1} (cpm ml^{-1}) for ^{3}H or 3×10^4 cpm ml^{-1} for ^{14}C.

For test animals exposed to a ^{14}C-labeled compound, the internal standard was prepared from rats exposed to a ^{3}H-labeled compound. A ^{3}H-labeled internal standard is preferred because low levels of ^{14}C-labeled metabolites can be measured by liquid scintillation counting. Without interference from ^{3}H-labeled metabolites. Interference of ^{14}C-energies on ^{3}H energies was corrected by conventional methods [1].

Internal standards. The rat urine extracts were used as internal standards by adding a fixed volume of the extract, (e.g., 100 μl) to sample solutions or homogenates to be extracted. Alternatively, extracts of metabolites from incubations of radiolabeled compounds with cellular or subcellular matter (e.g., microsomes) can be used. This alternative is useful when there is a need to control metabolite conjugation.

Extraction/concentration. The tissue extraction procedure included: (a) homogenization of ca. 2 g of tissue with 5 ml of water in a Potter-Elvehjem tissue grinder with a teflon pestle, (b) addition of 100 μl, V_a, of the internal standard, (c) transfer of the homogenate to a 50-ml centrifuge tube, (d) addition of 5 ml of acetone to precipitate proteins, (e) addition of 0.2 g of sodium chloride crystals to the mixture, and (f) sequential extraction with two 12.5-ml portions of ethyl acetate (rotated for 10 min on a test-tube rotator). These extracts were concentrated just to dryness at ambient temperature under a stream of nitrogen, and the residues were dissolved in methanol to volume V_t for subsequent processing.

Chromatography. After 10-min equilibrations of the column with the

TABLE 1

Advantages and imprecisions for dual-label methods

Eqn. No. (see text)	Advantages[a]	Relative uncertainty[b] in comparisons (%)
(1)	1	14—55[c]
(2)	3	15—46[d]
(3)	2—7	13—30[d,e]
(4)	2—8	18—45[d,e]
(5)	2—4, 6—9	12—25[e]

[a]1. No internal standard required. 2. Specific activities not required. 3. Internal standards compensate for extraction/concentration efficiency. 4. Activities or imprecisions for internal standards not required. 5. Compensates for intersample variations in extraction/concentration efficiency. 6. Comparisons incorporated into equation. 7. Comparison may be tested statistically to evaluate if ratio = 1. 8. Compensates for intragroup variations in extraction/concentration. 9. Can be used to evaluate effects of impurities, isotope effects, or differences in kinetics. [b]For activities ranging from 100 to 400 cpm, comparisons by ratios. [c]Extraction/concentration relative uncertainties ranging from 4% to 33%. [d]Extraction/concentration efficiencies ranging from 50% to 100%. [e]Can be evaluated statistically because comparisons are included in equations.

buffer (5×10^{-4} mol l^{-1} phosphate, pH 4.6), 100-μl sample aliquots, V_{ss}, were applied to the h.p.l.c. column. The flow rate was 1.0 ml min^{-1} and the column was maintained at 40 ± 1°C. The metabolites were eluted by a linear gradient ranging from the aqueous buffer to 100% methanol over either a 30- or 60-min period. Eluate fractions were collected every 30 s, scintillation cocktail was added, and radioactive decays were counted.

Purifications. Radioactive compounds, when purified by h.p.l.c., were collected as the eluate fraction corresponding to the retention time of the compound of interest [7]. Aliquots of this collected eluate were again separated by h.p.l.c. as above and the radioactivities of the resulting fractions were counted for confirmation of purity. These purified substances were then used as test compounds.

RESULTS

Table 1 gives typical values for relative uncertainties obtained for Eqns. (1—5). Advantages for each method are also listed, consistent with their theoretical bases. The R ratio, Q ratio, and U ratio are direct comparisons, while M and M_C data are compared after mass determinations with concomitant propagation of imprecisions. Using dual-label instead of single-label methods may reduce comparison uncertainties by as much as 30%, and using the R ratio instead of masses can decrease uncertainties for comparisons by as much as 25% (see Table 1). The Q ratio includes more variables than the R ratio and therefore has greater uncertainty.

Figure 1 shows a chromatogram with dual-label radiochemical detection for naphthalene metabolites extracted from a fish and with a rat urine extract as a biogenic internal standard. More than 80 determinations using similar separations of fish metabolites and using Eqns. (1—4) were done. Statistical imprecisions for those results were consistent with the values given in Table 1.

Use of the U ratio showed that variations in apparent metabolite profiles were caused by trace impurities in the dosage compounds. In these experiments, shrimp were exposed to either purified or unpurified (see Fig. 2) solutions of both ^{14}C-labeled and ^{3}H-labeled naphthalene in the fish-tank water for 4 h. The thoraces of the shrimp were extracted, concentrated, and separated by h.p.l.c. The resultant chromatograms from dual-label detection were similar for both groups (see Fig. 3).

However, evaluation of the data showed large differences between the groups. Computation of U ratios for each component gave U_{ij} values, for all pairs of intrasample metabolites resulting from the purified dosage compounds (see Fig. 3a), which varied only between 0.8 and 1.5. The corres-

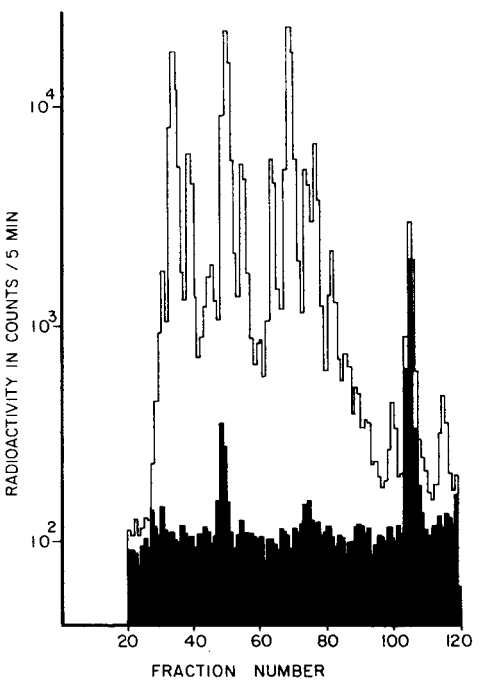

Fig. 1. Dual-label co-elution chromatogram of ^{3}H-labeled naphthalene metabolites from rat urine extract with ^{14}C-labeled metabolites: co-extracted after addition of the ^{3}H internal standard to livers taken from rainbow trout which had been administered ^{14}C-labeled naphthalene. 30-s fractions eluted by 60-min linear gradient from 5×10^{-4} M phosphate, pH 4.6, to methanol over a RP-18 column. Shaded area indicates ^{14}C.

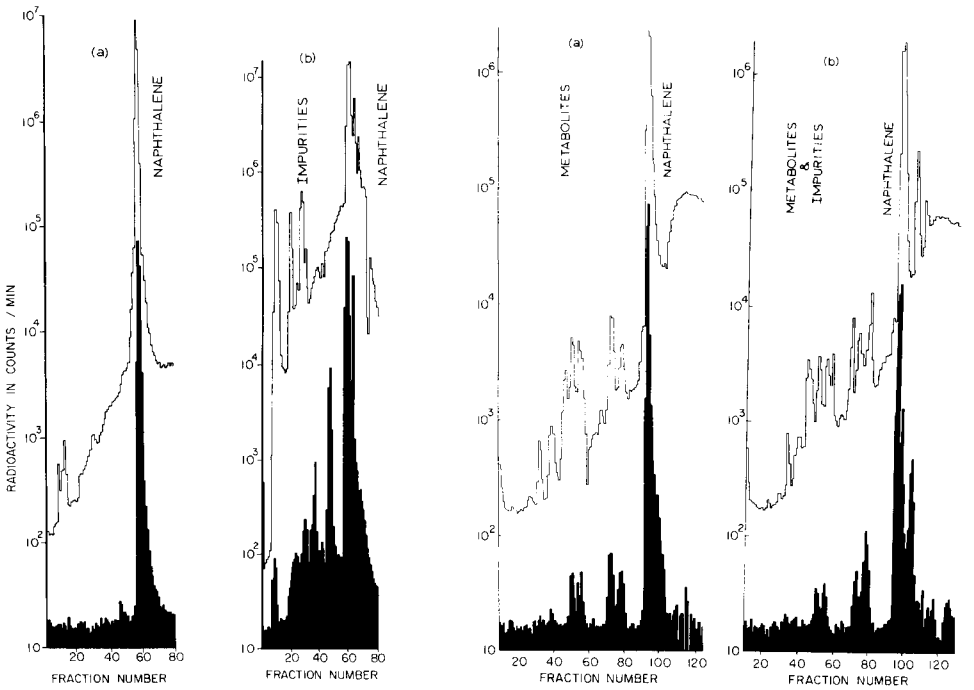

Fig. 2. Dual-label co-elution chromatogram of ^{14}C- and ^{3}H-labeled naphthalene: (a) after purification by h.p.l.c. 30-s fractions eluted by a 30-min linear gradient from 5×10^{-4} M phosphate, pH 4.6, to methanol over a RP-18 h.p.l.c. column, (b) as received from commercial sources. Shaded area indicates ^{14}C.

Fig. 3. Dual-label co-elution chromatogram of ^{14}C- and ^{3}H-labeled metabolites and naphthalene: (a) co-extracted from thoraces of shrimp which had been exposed to a purified ^{14}C- and ^{3}H-naphthalene mixture, (b) co-extracted from thoraces of shrimp which had been exposed to an unpurified ^{14}C- and ^{3}H-naphthalene mixture. 30-s fractions eluted by a 60-min linear gradient from phosphate to methanol as in Fig. 2. Shaded area indicates ^{14}C.

ponding intrasample U ratios resulting from the unpurified dosage compounds (see Fig. 3b) varied widely, ranging (ordered to yield ratios greater than 1) between 1.8 and 12. Similar results were obtained using other subsamples of the organisms.

DISCUSSION

Methods using Eqns. (2—4), like other internal standard procedures [1], compensate for variations in extraction/concentration efficiencies of extractable metabolites on a case-by-case basis. A distinct advantage of using biogenic internal standards is that pure chemical standards for each component are not required because the internal standards are generated by a reference organism. However, the biogenic internal standard stock solution must have a constant concentration of each component, the co-eluted sub-

stances should be chemically alike, and isotope exchange should be negligible.

When the ratio methods are used, structural identities of the individual metabolites need not be established for the biogenic internal standard solution. For instance, metabolites formed by metabolic pathways for aromatic hydrocarbons among marine organisms are essentially the same as the corresponding metabolites in mammals [8]. Thus, urine extracts from mammals can prove to be good internal standards for metabolites from marine organisms [7, 8]. However, caution is needed because some compounds may not be well resolved by the chromatography and thereby complicate data interpretations.

Biogenic internal standards are useful for quantifying metabolites. For example, an aliquot of a homogeneous extract containing several ^{3}H-metabolites from a reference organism (e.g., rat urine extract) can be added to samples from test organisms exposed to ^{14}C-labeled xenobiotics, e.g., bile from marine organisms [7]. Each mixture is then extracted and concentrated, and the metabolites are separated by h.p.l.c., with fractions collected and ^{3}H and ^{14}C counted. The resulting dual-label chromatograms are similar to those shown in Fig. 1. The net ^{3}H and ^{14}C activities for each eluted component are calculated with compensation for counting inefficiencies, quenching, and apparent energy overlap [1, 7] and then used for mass computations, e.g., Eqn. 2. The dual-label chromatograms for each bile sample are thereby related through the biogenic internal standard and the specific activities need not be known precisely if the half-lives are long relative to the duration of the experiment.

For the same experiment, the R ratio of net activities (Eqn. 3), could be used for comparisons, instead of mass determinations. The R ratio would reduce uncertainties (see Table 1) and $R_{12} = 1$ only if the mass of metabolite in bile sample 1 is the same as the mass of the corresponding metabolite in bile sample 2. Similarly, Q_{12} could be calculated for several metabolites and the Q ratio of net activities (Eqn. 4) equals unity if the ratio of masses for metabolites i vs. j are the same in both samples 1 and 2. This equality may indicate identical routes and biological activity for metabolism of a test compound.

Impurity evaluations should be done before extensive metabolism experiments are initiated. For these, the U ratio can yield important chemical information. For example, if $U_{ij} \neq 1$ for in vivo studies using purified compounds, then isotope exchange kinetic effects should be suspected. If, however, $U_{ij} = 1$ for the metabolites of a purified dosage compound but $U_{ij} \neq 1$ for the unpurified substance, then effects of impurities upon metabolite profiles may be proven.

The data for shrimp (i.e., $U_{ij} \approx 1$ for the purified solution) showed that there were no significant differences in the metabolism of the ^{3}H- and ^{14}C-labeled naphthalene, despite the vulnerability of ^{3}H to isotope exchange. Therefore, the result that $U_{ij} \neq 1$ for the unpurified solutions suggests that small amounts of impurities affected results in those metabolism studies.

Such a proof might be very difficult without this method.

The described co-elution chromatographic procedures with radiochemical detection and biogenic internal standards have wide potential applicability, especially for a variety of biological samples in which structural identifications are difficult to obtain because of the absence of pure radiolabeled standard compounds. Thus, metabolites from several organisms can be correlated with metabolites of both known and unknown structure present in the internal standard. Moreover, determinations of the individual metabolites in the internal standard is not required. However, one must be aware of the assumptions involved such as the components being chemically alike and be wary of overlapping eluate fractions. Furthermore, the procedure for determining effects of impurities, isotope exchange or kinetic differences should be used as a routine preliminary test to avoid invalid results in metabolism experiments.

These dual-label co-elution methods can be easily adapted to other separation methods, such as thin-layer chromatography and electrophoresis.

This work was funded in part by the American Chemical Society Petroleum Research Foundation Grant No. 13933G3.

REFERENCES

1 T. R. Roberts, Radiochromatography, Elsevier, Amsterdam, 1978.
2 E. Albanese and D. Goodman, Anal. Biochem., 80 (1977) 60.
3 E. I. Gruenstein and A. L. Pollard, Anal. Biochem., 76 (1976) 452.
4 J. A. Hunt, Anal. Biochem., 23 (1968) 289.
5 R. C. Desrosiers, K. H. Friderici and F. M. Rottman, Biochemistry, 14 (1975) 4367.
6 L. Schutte and E. B. Koenders, J. Chromatogr., 76 (1973) 13.
7 L. C. Thomas, W. D. MacLeod and D. C. Malins, in Natl. Bur. Stand. Spec. Publ. No. 519, National Bureau of Standards, Gaithersburg, MD, 1979.
8 J. R. Bend and M. O. James, in Biochemical and Biophysical Perspectives in Marine Biology, Academic Press, New York, 1980.
9 T. A. Loomis, Essentials of Toxicology, Lea and Febiger, Philadelphia, PA, 1978.

Analytica Chimica Acta, 154 (1983) 153—158
Elsevier Science Publishers B.V., Amsterdam — Printed in The Netherlands

THE USE OF A MICELLAR MOBILE PHASE IN THE HIGH-PERFORMANCE LIQUID CHROMATOGRAPHIC SEPARATION OF HYDROXYBENZENE DERIVATIVES

EDMONDO PRAMAURO and EZIO PELIZZETTI*

Istituto di Chimica Analitica, Università di Torino, 10125 Torino (Italy)

(Received 11th April 1983)

SUMMARY

When aqueous micellar solutions are used as mobile phases in liquid chromatography, retention of solutes depends on the concentration of the micellar surfactant, and relevant information about the partition coefficient and related association constants between solutes and micelles can be calculated from the chromatographic results. The chromatographic parameters of a series of phenols and hydroxyphenols (1,2- and 1,4-diols) eluted with sodium dodecyl sulfate micelles were measured. The association constants evaluated were in good agreement with those obtained by other techniques.

The effects of micellar systems on solubilization processes, chemical equilibria and reactivity have been shown to be useful in a wide variety of analytical techniques [1]. The use of aggregate-forming amphiphiles in liquid chromatography was investigated by Armstrong and Terrill [2] and the separation of some aromatic compounds by means of sodium dodecyl sulfate (SDS) micelles in the mobile phase was reported [3—5]. The use of enhanced fluorescence and micelle-stabilized room-temperature phosphorescence was recently proposed for detecting of polynuclear aromatic hydrocarbons eluted in micellar (pseudophase) liquid chromatography [6, 7].

A theoretical model for the chromatographic behavior of the micellar systems has been described [5]. This model allows the evaluation of association constants between solutes and micelles from the measurement of elution parameters.

In previous papers from this laboratory [8, 9], the partition data for a series of substituted phenols were collected by measuring the changes in acid—base equilibria in the presence of SDS micelles. In later work, the association constants of many benzenediol derivatives were determined from kinetic evaluation of their oxidation to quinones in micellar media.

In the present work, the partition data of phenols, quinols and catechols obtained from chromatographic elution with SDS are compared with data from previously reported techniques. The model is applied successfully to the compounds tested.

0003-2670/83/$03.00

EXPERIMENTAL

The compounds investigated, listed in Table 1 and purchased from Merck, K&K, Aldrich, Fluka and C. Erba, were purified by recrystallization. Sodium dodecyl sulfate (Merck) was recrystallized from water—methanol. Doubly-distilled water was used.

Mobile phases were prepared by dissolving the surfactant in water and filtering through a 0.45-μm cellulose membrane filter (Millipore). Each solute was dissolved in SDS before the runs; 3—10 μl of the sample solution at a concentration in the range 1×10^{-3}—1×10^{-2} M was injected. All the solutes were eluted at a flow rate of 2.5 ml min^{-1} and their absorbance was monitored at 280 nm. The runs were done at room temperature (24 $\pm$ 1°C).

A Perkin-Elmer S-2 chromatograph, equipped with a u.v.—visible LC-55-B detector and a Perkin-Elmer 56 chart recorder, was used. A μ-Bondapak C-18 reversed-phase column (30 cm long, 3.9 mm i.d.; Waters) was used throughout the work.

TABLE 1

Variation of capacity factors, expressed as $(V_e - V_m)/V_m$, of the test compounds with surfactant concentration

Compound	Total SDS concentration in the mobile phase (M)			
	0.06	0.10	0.14	0.20
	$(V_e - V_m)/V_m$			
Phenols				
1. Benzene-1-ol	5.12_5	4.06	3.31	2.69
2. 4-Methylbenzene-1-ol	9.62_5	6.75	5.06	3.81
3. 4-Ethylbenzene-1-ol	14.25	9.19	6.56	4.75
4. 4-n-Propylbenzene-1-ol	19.31	12.12_5	8.44	5.94
5. 4-t-Butylbenzene-1-ol	21.75	13.19	9.06	6.37_5
6. 3,5-Dimethylbenzene-1-ol	13.87_5	9.00	6.37_5	4.62
7. 2,4,5-Trimethylbenzene-1-ol	18.37_5	11.37_5	7.81	5.56
8. 2,3,5,6-Tetramethylbenzene-1-ol	24.00	14.62_5	9.94	6.94
Catechols				
9. Benzene-1,2-diol	3.67	3.13	2.70	2.21
10. 4-Methylbenzene-1,2-diol	7.18	5.37	4.16	3.18
11. 4-Cyanobenzene-1,2-diol	3.25	2.77	2.39	1.93
12. 3-i-Propylbenzene-1,2-diol	15.19	10.00	7.12	5.10
13. 4-t-Butylbenzene-1,2-diol	18.81	11.79	8.14	5.77
Quinols				
14. 2-Methylbenzene-1,4-diol	1.85	1.54	1.42	1.18
15. 2-Chlorobenzene-1,4-diol	2.58	2.09	1.79	1.48
16. 2-Phenylbenzene-1,4-diol	7.05	4.51	3.31_5	2.46
17. 2-t-Butylbenzene-1,4-diol	9.63	6.17	4.44	3.16
18. 2,3,5-Trimethylbenzene-1,4-diol	4.44	3.45	2.69	2.13

RESULTS AND DISCUSSION

As previously reported [5], the elution parameters of the solutes depend on the surfactant concentration in the mobile phase and on the partition coefficient between the three phases involved, according to the equation

$$V_s/(V_e - V_m) = [1/P_{SW}] + [(P_{MW} - 1)/P_{SW}]\bar{v}\, C_m \quad (1)$$

where V_s is the volume of the stationary phase, V_e is the elution volume and V_m the volume of the mobile phase, taken as the void volume; $\bar{v}$ (0.862 ml g^{-1}) is the partial specific volume of SDS [10] and C_m is the concentration of micellized surfactant in g ml^{-1} ($C_m = C_{tot}$ — c.m.c.). The critical micelle concentration (c.m.c.) of SDS is taken as 8×10^{-3} M [11]. The partition coefficients of solutes between the micellar and aqueous pseudophases and between the stationary and aqueous phases are designated as P_{MW} and P_{SW}, respectively.

The retention times and elution volumes of the compounds tested were measured at different SDS concentrations (0.02—0.20 M) in the mobile phase. For the more hydrophobic derivatives, the data were collected starting from a higher surfactant concentration (0.06 M). The void volume of the column was 2.0 ± 0.05 ml; it was measured by eluting an aqueous solution of potassium iodide and monitoring the absorbance of iodide at

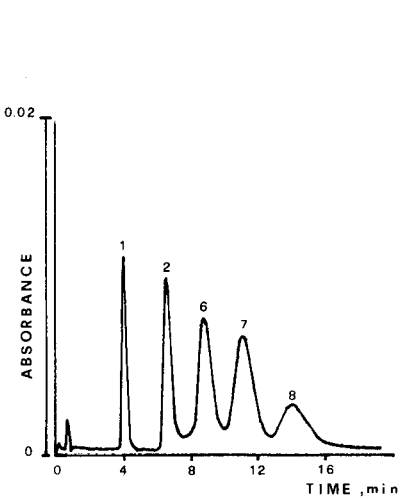

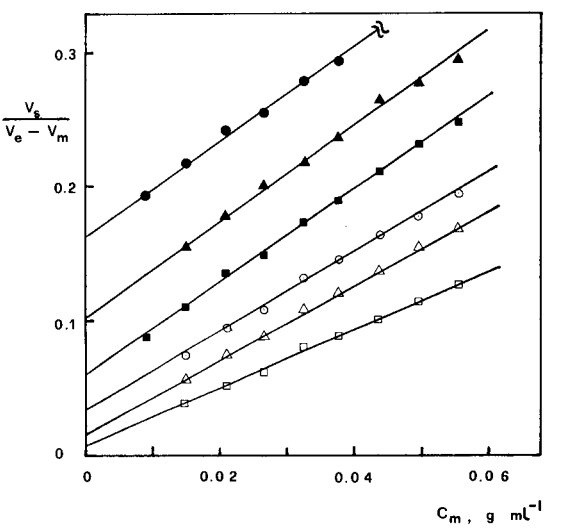

Fig. 1. Characteristic separation pattern of polymethylphenols. Total SDS concentration, 0.09 M; flow rate, 2.5 ml min^{-1}; detector wavelength, 280 nm. Numbers on peaks correspond to listing in Table 1.

Fig. 2. Plots of chromatographic parameter, $V_s/(V_e - V_m)$, of some compounds as a function of micellar SDS concentration (C_m): (•) benzene-1,2-diol; (▲) benzene-1-ol; (■) 4-methylbenzene-1,2-diol; (⊙) 4-methylphenol; (△) 4-ethylphenol; (□) 4-n-propylphenol.

250 nm. The total volume V_t was calculated from the column size as 3.58 ml.

As expected, an increase in the concentration of the micellar phase causes decreased retention for all the solutes tested. Table 1 lists the variation of the capacity factors with surfactant concentration.

Figure 1 shows the elution pattern of some polymethylphenols. Electrostatic interactions between solutes and micelles and between solutes and adsorbed monomer present on the stationary phase can be excluded on the basis of the pH of surfactant mobile phases (between 5.7 and 6.3) and the pK_a values of the investigated compounds [9]. Only hydrophobic interactions can account for the differences in the measured partition coefficients.

The chromatographic parameter $V_s/(V_e - V_m)$ was calculated for the solutes examined at each SDS concentration and the data are collected in Table 2.

Plots of this ratio against C_m, according to Eqn. 1, were satisfactorily linear for all the investigated compounds; the plots for compounds 1, 2, 3, 4, 9 and 10 are shown in Fig. 2.

For each solute, P_{MW} was calculated from the slope and the intercept by linear regression. The relative standard deviation of the slopes was less than 8%, in agreement with recently published work [12]. In the case of the more

TABLE 2

Variation of the chromatographic parameter $V_s/V_e - V_m$ of the test compounds with concentration of SDS micelles (C_m)

Compound[a]	Concentration of micellar surfactant (mg ml^{-1})									
	3.5	9.2	15.0	20.8	26.5	32.3	38.1	43.8	49.6	55.4
	$V_s/(V_e - V_m)$									
Phenols										
1	—	—	0.154	0.176	0.194	0.222	0.238	0.263	0.275	0.294
2	—	—	0.078	0.095	0.108	0.131	0.144	0.161	0.178	0.192
3	—	—	0.055	0.072	0.086	0.101	0.120	0.136	0.152	0.166
4	—	—	0.039	0.052	0.062	0.079	0.089	0.103	0.116	0.127
5	—	—	0.036	0.049	0.060	0.072	0.087	0.099	0.112$_5$	0.124
6	—	—	0.057	0.074	0.088	0.105	0.124	0.139	0.154	0.171
7	—	—	0.043	0.058	0.069	0.084	0.101	0.114	0.128	0.142
8	—	—	0.033	0.045	0.054	0.066	0.079	0.090	0.102	0.114
Catechols										
9	0.165	0.192	0.215	0.239	0.252	0.280	0.292	0.314	0.338	0.357
10	0.065	0.089	0.110	0.133	0.147	0.174	0.190	0.208	0.230	0.248
11	—	—	0.243	0.270	0.285	0.305	0.330	0.371		0.409
12	—	—	0.052	0.067	0.079	0.099	0.111	0.127		0.155
13	—	—	0.042	0.056	0.067	0.085	0.097	0.111		0.137
Quinols										
14	0.338	0.389	0.427	0.474	0.512	0.533	0.556	0.581	0.608	0.671
15	0.215	0.268	0.306	0.347	0.378	0.414	0.442	0.474	0.512	0.533
16	0.042	0.079	0.112	0.147	0.175	0.208	0.239	0.268	0.292	0.321
17	—	—	0.082	0.108	0.128	0.157	0.178	0.205		0.250
18	—	—	0.178	0.209	0.229	0.264	0.294	0.321		0.371

[a]See Table 1.

TABLE 3

Partition coefficients and association constants

Compound[a]	P_{SW}	P_{MW}	K_{MW} (l mol^{-1})	K_{MW} (l mol^{-1})[b]
1	9.7	40.2	10.2	8 ± 2 9.9[c]
2	28.6	95.0	24.4	24 ± 3
3	75.8	245.0	63.5	65 ± 10
4	174.2	450.0	116.7	140 ± 20
5	389.0	995.0	258.4	280 ± 30
6	69.4	229.6	59.5	64 ± 7
7	179.2	513.6	133.3	125 ± 15
8	454.5	1060.0	275.3	270 ± 30
9	6.3	27.4	6.9	4[d]
10	17.6	72.4	18.6	10[d]
11	5.6	28.1	7.1	5[d]
12	75.2	225.0	58.3	37[d]
13	156.2	431.0	111.8	75[d]
Hydroquinone	1.7	14.5	3.5[e]	3[d]
14	3.0	21.1	5.2	6[d]
15	4.7	34.0	8.6	7[d]
16	32.4	202.0	52.2	85[d]
17	50.2	244.4	63.3	65[d]
18	9.4	53.8	13.7	12[d]

[a]See Table 1. [b]From ref. 9. [c]From ref. 12. [d]Kinetic method. [e]From ref. 5.

hydrophobic compounds, having P_{MW} and P_{SW} in the range 300—400, the interaction with the C-18 stationary phase is quite strong and the relative standard deviation becomes large. The calculated partition coefficients P_{MW} are related to the association constants K_{MW} through the equation [13]

$$K_{MW} = (P_{MW} - 1)\,\overline{V} \qquad (2)$$

where $\overline{V}$ is the partial molar volume of the surfactant. For SDS, $\overline{V}$ = 0.26 M^{-1} was assumed [14]. The calculated partition coefficients P_{MW} and P_{SW}, and the related binding constants K_{MW}, are reported in Table 3, together with the previously determined data. The agreement is satisfactory for phenols where spectrophotometric methods were used for independent determination of K_{MW}. Slight differences can, however, be observed between the chromatographic and kinetic data for quinols and catechols.

Conclusions

The binding parameters between the compounds investigated and SDS micelles were successfully evaluated by using micellar liquid chromatographic measurements. The uncertainty in P_{MW} values for compounds exhibiting larger partition coefficients can be overcome by using less hydrophobic

stationary phases which allow the reduction of the P_{SW} terms. Elution studies for the more hydrophobic hydroxyaromatic compounds on other commercially available columns, as well as the separation of many solutes previously investigated in micellar media, are now in progress.

The benefits and limitations of this technique have been reported already [5, 12]. A useful improvement in the separation can be achieved [7, 12] by introducing the electrostatic interactions between charged solutes and ionic micelles, effects not operating in the present tests at pH 5.7—6.3. In fact, charge effects modify not only the partition coefficient P_{MW} but also the interaction with the stationary phase in a complex way because the increase in polarity of the solutes reduces the P_{SW} term, while the adsorption of surfactant monomers on this phase can introduce a partial ionic character with an additional repulsive or attractive mechanisms. By operating at an appropriate pH, so that some solutes are present in ionized form, and by using anionic or cationic surfactant in the mobile phase, the elution parameters can be widely changed and selectivity can be enhanced. The effects of these parameters on a series of aromatic acids is now under investigation.

This work was supported by the Progetto Finalizzato Chimica Fine e Secondaria, C.N.R. (Rome).

REFERENCES

1 W. L. Hinze, in K. L. Mittal (Ed.), Solution Chemistry of Surfactants, Vol. 1, Plenum Press, New York, 1979, p. 79.
2 D. W. Armstrong and R. Q. Terrill, Anal. Chem., 51 (1979) 2160.
3 D. W. Armstrong and M. McNeely, Anal. Lett., 12 (1979) 1285.
4 D. W. Armstrong and S. J. Henry, J. Liq. Chromatogr., 3 (1980) 657.
5 D. W. Armstrong and F. Nome, Anal. Chem., 53 (1981) 1662.
6 D. W. Armstrong, W. L. Hinze, K. H. Bui and H. N. Singh, Anal. Lett., 14 (1981) 1659.
7 R. Weinberger, P. Yarmchuk and L. J. Cline Love, Anal. Chem., 54 (1982) 1552.
8 E. Pramauro and E. Pelizzetti, Anal. Chim. Acta, 126 (1981) 253.
9 E. Pramauro and E. Pelizzetti, Ann. Chim. (Rome), 72 (1982) 117.
10 P. Mukerjee, J. Phys. Chem., 66 (1962) 1733.
11 P. H. Elworthy and K. J. Mysels, J. Colloid Interface Sci., 21 (1966) 331.
12 P. Yarmchuk, R. Weinberger, R. F. Hirsch and L. J. Cline Love, Anal. Chem., 54 (1982) 2233.
13 I. V. Berezin, K. Martinek and A. K. Yatsimirskii, Russ. Chem. Rev. (Engl. Transl.), 42 (1973) 787.
14 J. M. Corkill, J. F. Goodman and T. Walker, J. Chem. Soc. Faraday Trans. I, 63 (1967) 768.

Analytica Chimica Acta, 154 (1983) 159—171
Elsevier Science Publishers B.V., Amsterdam — Printed in The Netherlands

INVESTIGATION OF THE ADSORPTION OF FERROIN-TYPE LIGANDS AND METAL CHELATES ON ACTIVATED CARBONS FOR APPLICATIONS IN REAGENT PURIFICATION AND TRACE METAL ENRICHMENT AND DETERMINATION

DONALD J. HUTCHINSON and ALFRED A. SCHILT*
Department of Chemistry, Northern Illinois University, DeKalb, IL 60115 (U.S.A.)
(Received 23rd May 1983)

SUMMARY

A representative group of ferroin-type ligands and various activated carbons were screened for possible use in trace metal separations. Selected as most promising, 2,2'-dipyridylketone-2-pyridylhydrazone (DPPH) and Norit A were investigated more extensively with special attention to pK_a values and ionic charges of DPPH species, isotherms and Langmuir parameters for the adsorption of DPPH and its chelates on Norit A, and to conditions and procedures optimal for analytical separations and recoveries of trace metal ions. The results provide evidence of two types of sites on Norit A for adsorption of DPPH and its chelates. These are interpreted in terms of Langmuir parameters and ionic charge types of the adsorbates. Practical applications are demonstrated for removing iron, cobalt, nickel and copper ions from various reagents and for preconcentrating trace amounts of these metal ions prior to their quantitation. Metal ion concentrations remaining unextracted are less than 10^{-7} M, 100-fold or higher enrichments are feasible, and recoveries of the metal ions by desorption from Norit A average 99%, with 2—5% relative standard deviations for their determinations.

Trace metal determinations can be enhanced in sensitivity by several orders of magnitude simply by concentrating the analyte species prior to their quantitation when sufficiently large samples are available. Commonly referred to as preconcentration, the enrichment process consists of either stripping the major components from the minor ones (e.g., volatilization of the solvent) or extraction of the analyte into a second phase of less volume than the original. In general, preconcentration techniques have utilized liquid—liquid extraction, electrodeposition, coprecipitation, ion-exchange or adsorption processes. A recent innovation is the use of solid-phase extractants which incorporate immobilized ligands to take up metal ions from solution by chelation [1—3]. Another type of solid-phase extractant is exemplified by activated carbon which can quantitatively adsorb trace amounts of certain metal chelates from solution [4, 5]. Solid extractants or adsorbents other than active carbons have been investigated also, including Amberlite XAD-2 [2, 6] and silica [7].

Of the two types of solid-phase extractants for trace metal ions, that

0003-2670/83/$03.00

based upon chelation in solution followed by sorption of the chelate by the solid appears to be most practical for preconcentration purposes. Chelation tends to be much slower and less efficient if the ligands are immobilized in the solid than if they are free to diffuse and react in solution. Not only is less time required for the separation but less chelation reagent and cheaper adsorbent can be utilized.

This paper reports the results of our investigation of the adsorption of ferroin-type ligands and chelates on activated carbon, more particularly the adsorption of 2,2′-dipyridylketone-2-pyridylhydrazone (DPPH) and some of its metal chelates on Norit A, the solution conditions most favorable for trace metal collection, and some practical applications in chemical analysis and reagent purification.

EXPERIMENTAL

Materials

Norit A (American Norit Co., Jacksonville, Florida) was treated to remove trace metal impurities. A 100-g sample was stirred in contact with 500 ml of hot 6 M hydrochloric acid for two hours, collected by suction filtration, washed with distilled water, and subjected repeatedly to the same series of steps until sensitive colorimetric tests indicated the absence of iron in the acidic filtrate. After washing the iron-free Norit A with distilled water to remove traces of retained hydrochloric acid, it was washed with 250 ml of 95% ethanol and dried overnight at 85°C. The other activated carbons, Norit 211, Nuchar, coconut charcoal, Darco G-60 and Darco KB (ICI Americas, Wilmington, DE), were used as received.

The 2,2′-dipyridylketone-2-pyridylhydrazone (DPPH), also referred to as di-2-pyridylglyoxal-2-pyridylhydrazone or 2,2′-pyridil-2-pyridylhydrazone (and incorrectly as 2,2′-dipyridyl-2-pyridylhydrazone), was prepared according to the procedure reported by Case [8]. The method described by Lions and Martin [9] was followed, to prepare 2-pyridylaldehyde-2-pyridylhydrazone (PAPH). All other ferroin-type compounds were obtained from the G. Frederick Smith Chemical Co. (Columbus, OH). Aqueous solutions of DPPH and other chelation reagents were prepared by dissolving a weighed amount in an equimolar amount of 1.0 M hydrochloric acid followed by dilution with distilled water to the exact desired concentration.

Reagent-grade chemicals were employed in preparation of all solutions. The 10% (w/v) hydroxylammonium chloride, used as a reductant, was prepared iron-free by treatment with PDT and XAD-2 [2]. Stock solutions of metal ions were prepared using primary standards or reagent-grade salts and standardized when necessary by the same method as that used for their determination in subsequent studies.

Apparatus and instruments

A Cary Model 14 recording spectrophotometer was used to measure absorption spectra, and a Beckman Model DU spectrophotometer was

employed for absorbance measurements at single wavelengths. Atomic absorption measurements were made with a Beckman Model DB-G spectrophotometer equipped with a Beckman Model 1301 atomic absorption accessory and a laminar flow burner. Flame emission measurements were taken with a GCA/McPherson Model 700 recording spectrophotometer and Model 703 flame spectrometry module equipped with a Beckman Model 4020 total consumption burner. Differential pulse polarograms were obtained using a Princeton Applied Research Model 364 polarographic analyzer. Measurements of pH were made with a Corning Model 7 pH meter and combination glass-saturated calomel electrode. Solutions were agitated at constant temperature (25°C) with a Blue M Electric Co. Model MSB-1122A-1 constant temperature shaker bath.

Determination of acidity and formation constants

A series of solutions containing identical concentration of DPPH, different hydrogen ion concentrations, and approximately the same ionic strength (0.01 M) was prepared. For solutions of pH above 7, to provide adequate solubility for DPPH, ethanol was introduced at several different concentrations (4, 10 and 20% by volume) so that any solvent effect corrections could be made by extrapolation to 0% ethanol. Ultraviolet spectra of the solutions were recorded and interpreted to determine pK_a values for DPPH. A similar procedure was followed to determine protonation constants for the iron(II) chelate of DPPH, except that visible absorption spectra were recorded.

The stoichiometry of formation and the stability constant of the iron(II)—DPPH chelate were evaluated as a function of pH using spectrophotometry and the mole ratio method [10].

Adsorption isotherms

Various weighed amounts (0.02—2.0 g) of iron-free Norit A were added to a series of 150-ml glass-stoppered conical flasks, each containing exactly 50 ml of a solution of known pH and concentration of solute under investigation. The flasks were tightly stoppered, sealed with paraffin, and agitated in a water-bath at 25°C for 4 h to assure attainment of equilibrium, after which portions of the solutions were analyzed spectrophotometrically to determine solute concentrations.

Solutions for study of DPPH adsorption were 2.00 mM in DPPH for pH 1.0 (0.10 M in HCl) and pH 4.5 (0.10 M in sodium acetate with acetic acid added to adjust pH to the desired level). A more dilute solution, 8.00×10^{-6} M DPPH, was necessary for measurements at pH 7.6 (0.1 M ammonium acetate) because of limited solubility at higher pH. To assure reproducible pH values, each solution was measured and adjusted to the desired pH by addition of small amounts of hydrochloric acid or sodium hydroxide.

Iron(II)—DPPH chelate solutions were prepared for the adsorption study by first mixing 10.0 ml of 0.100 M iron(II) ammonium sulfate, 10 ml of 10% hydroxylammonium chloride, and 10.0 ml of 0.200 M DPPH in a 1-l

volumetric flask. Either 3 ml of 1 M hydrochloric acid (to obtain a solution of pH 2.5) or 30 ml of pH 5.75 buffer (1 M sodium acetate with sufficient acetic acid to give the desired pH) or 100 ml of 6 M ammonia and 400 ml of ethanol was then added, followed by sufficient distilled water to dilute the contents to volume.

Adsorption of metal ions on DPPH-impregnated Norit A

A slurry of 30 g of Norit A in 500 ml of 0.0063 M DPPH (acidified to pH 1.1 with hydrochloric acid) was stirred for two hours before collecting the DPPH-impregnated Norit A by filtration. After washing with distilled water the solid was air-dried. Weighed amounts (typically 0.05—1.00 g) of the DPPH-impregnated Norit A were agitated with 50.0 ml of 1.00×10^{-4} M solutions of various metal ions, adjusted to a pH of either 3 or 5 by addition of either hydrochloric acid or sodium acetate, for 4 h at 25°C. The concentration of the metal ion in solution was then determined: lead by differential pulse polarography; lithium, manganese and chromium by flame emission; and magnesium by atomic absorption spectrometry. Spectrophotometric methods were employed to determine vanadium [11], aluminum [12], mercury [13], cobalt [14], zinc [15], cadmium [16], nickel [17], copper [18], and iron [19].

Removal of metal ions from reagents and solutions

To investigate the recovery of small amounts of iron, cobalt, nickel, copper, zinc and cadmium ions from aqueous solutions of various pH by treatment with DPPH followed by adsorption of the metal chelates on Norit A, 100 ml of 2.50×10^{-4} M metal ion (chloride, nitrate or sulfate salt) was treated with 2.0 ml of 0.01 M DPPH, adjusted to the desired pH by addition of hydrochloric acid or ammonia, and stirred for 5 min in contact with 0.5 g of Norit A. The concentration of metal ion remaining in solution was determined spectrophotometrically using additional DPPH as chromogenic reagent and 4.00-cm absorption cells.

Solutions of various reagents, commonly used in trace metal determination, were prepared to contain 1 mg l^{-1} each of iron, copper, cobalt and nickel. A 250-ml sample of each reagent solution and 2 ml of 0.01 M DPPH were mixed well to effect metal ion chelation and then stirred with 0.5 g of Norit A for 1 min to adsorb the metal chelate. After filtration the reagent solution was tested for the presence of the metal ions added by using DPPH as chromogenic reagent and 10-cm absorption cells to allow detection of any trace metal concentration as low as 10^{-7} M.

Recommended procedure for trace metal enrichment

Trace quantities of iron, cobalt, nickel and copper (sample size 100—2000 ml) are complexed with DPPH and collected on Norit A by the procedure described above. If the sample solution is either strongly acidic or basic, its pH is adjusted to between 5 and 8 after addition of DPPH prior

to treatment with 0.5 g of Norit A. After collection by filtration, the Norit A is washed with distilled water, transferred to a beaker, and stirred in contact with 3 ml of 1 M hydrochloric acid for 5 min while heating near boiling to extract the metal ion content. After filtration and quantitative collection of the acid solution together with two 1-ml portions of distilled water used to rinse the Norit A, the extraction procedure is repeated a second time. The extract and wash solutions, combined in a 10-ml volumetric flask, are diluted to volume with distilled water. Separate aliquots of this solution can be taken for the determination of each of the metals sought.

To test the recovery efficiency of this method, separate solutions containing metal ions of only one kind were subjected to the above procedure. Thus, the recovery of each could be evaluated separately, and each metal ion could be determined spectrophotometrically without interference by using DPPH as the chromogenic reagent.

RESULTS AND DISCUSSION

Selection of active carbon and ligand

Six different activated carbons were examined. They showed only minor differences when tested as adsorbents for various iron(II) chelates. Norit A, Darco G-60 and Darco KB exhibited lower levels of acid-extractable iron impurities (12—17 $\mu g\ g^{-1}$ iron) than did Norit 211, Nuchar or coconut charcoal ($\geqslant 45\ \mu g\ g^{-1}$ iron). All except Nuchar were readily wetted and dispersed by water. Adsorption of iron(II) chelates was rapid except for Nuchar and coconut charcoal. Approximate adsorption capacities for iron(II) chelates were somewhat lower for Darco G-60 (1.1 mol g^{-1}) than for the others (1.9 mol g^{-1}). Norit A was selected for subsequent use and further study, primarily because of its lower iron content.

Thirteen different ferroin-type ligands, selected as representative of the many available, were tested for applicability in conjunction with Norit A to remove metal ions from aqueous solutions. The iron(II) chelates were employed in these tests because of their intense color and ease of detection. The most surprising result was that some of the iron(II) chelates were rapidly destroyed when contacted with Norit A; these were chelates with 2,2'-bipyridine, 1,10-phenanthroline, 5-nitro-1,10-phenanthroline, 3-(2-pyridyl)-5,6-diphenyl-1,2,4-triazine (PDT), 3-(2-pyridyl)-5,6-bis(4-phenylsulfonic acid)-1,2,4-triazine disodium salt (PDTS), 2,4,6-tripyridyl-1,3,5-triazine (TPTZ), and 3-(4-phenyl-2-pyridyl)-5,6-diphenyl-1,2,4-triazine-trisulfonic acid trisodium salt (PPDTS). No free ligand but all of the iron(II) was detectable in the supernatant liquid after treatment with Norit A. This is surprising because iron(II) chelates of this type are known to be very slow in undergoing ligand-exchange reactions [20]. It appears likely that the chelate is first adsorbed but so greatly weakened in the process by very strong attraction between the bound ligands and the activated carbon surface that complete dissociation of the iron(II) from the chelate results. The iron(II)

chelates of the other ligands tested remained intact on adsorption as evidenced by the fact that both iron and the ligands were quantitatively removed from the Norit A unchanged by extraction into methanol. Thus the following ligands showed promise for our purpose: 4,7-diphenyl-1,10-phenanthroline, 5-amino-1,10-phenanthroline, 5-phenyl-1,10-phenanthroline, 2,6-bis(2'-pyridyl)pyridine, pyridine-2-aldehyde-2-pyridylhydrazone (PAPH), and DPPH. From this group, DPPH was selected for further study, because it forms intensely colored complexes with a greater variety of metal ions than the others and qualitative tests revealed that these are strongly adsorbed by Norit A.

Spectrophotometric studies

To identify the particular solute species involved in adsorption, especially their ionic charges, the acidity constants of the various protonated species of DPPH and of the iron(II)—DPPH chelate were evaluated. Also the metal-to-ligand ratio of the iron(II)—DPPH chelate was determined as a function of pH.

The acidity constants (pK_a values) found for DPPH and the iron(II)—DPPH chelate are listed in Table 1, together with spectral data pertinent to their elucidation. The various protonation equilibria were easily distin-

TABLE 1

Acidity constants and spectrophotometry of DPPH and $Fe(DPPH)_2$

Equilibrium[a]	Spectral isosbestic points		pK_a
	pH range	Wavelength (nm)	
$LH_3^{2+} \rightleftharpoons LH_2^+ + H^+$	2.2—4.3	234 250 276 299 347	3.14
$LH_2^+ \rightleftharpoons LH + H^+$	4.7—7.0	287 346	5.75
$LH \rightleftharpoons L^- + H^+$	8—12	400 (460)[b]	9.36
$[Fe(HL)_2]^{2+} \rightleftharpoons [Fe(HL)(L^-)]^+ + H^+$	2.6—6.0	487 551	5.25
$(Fe(HL)(L^-)]^+ \rightleftharpoons [Fe(L^-)_2]^0 + H^+$	6.0—9.1	516 584 637	7.47

[a]Symbol LH represents DPPH in molecular form (with its imino proton not yet ionized).
[b]Wavelength of absorption band that grows with increasing pH, up to pH 10.5.

guished one from another by the separate and distinctly different sets of isosbestic points associated with each equilibrium-pair.

Plots of absorbance versus mole ratio of metal to ligand, with ligand concentration held constant, indicated that iron(II) forms a bis-chelate with DPPH over the pH range examined (pH 2.50—9.80). At pH 2.5 and 6.2, the mole ratio plots showed essentially no curvature near the stoichiometric point, indicating a high formation constant for the iron(II) chelate. At pH 9.80 the plot was sufficiently curved to allow calculation of the formation constant; data treatment yielded a conditional formation constant of 1.9×10^{10} at pH 9.80.

It is concluded from these results that the iron(II) chelate of DPPH exists in aqueous solution predominantly as a dipositive ion at a pH below 5.3, as a monopositive cation between pH 5.3 and 7.5, and as an uncharged species above pH 7.5. Interestingly, the acidity of the imino-proton of DPPH is greatly enhanced when the ligand binds to iron(II); its pK_a changes from 9.36 to 5.25, probably as a consequence of the dipositive charge on the chelate favoring loss of the positively charged proton. It is also interesting that loss of the imino-proton of the second bound DPPH ligand is also enhanced sufficiently to allow measurement of its pK_a as well.

Adsorption isotherms

Isotherms obtained for the adsorption of DPPH on Norit A at 25°C from aqueous solutions of different pH are shown in Fig. 1; those for the iron(II) chelate appear on Fig. 3. Their most remarkable feature is the presence of two distinct plateaux rather than just one, as most commonly observed for Langmuir behavior. Apparently there are two different kinds of adsorption sites on Norit A that can be occupied independently of one another by the same adsorbate species. For such a system the Langmuir equa-

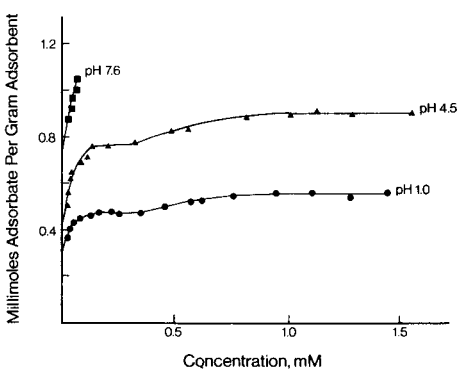

Fig. 1. Adsorption isotherms for DPPH on Norit A at 25°C and different pH values.

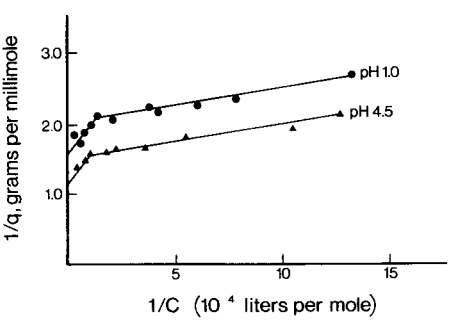

Fig. 2. Langmuir treatment of adsorption isotherms for DPPH on Norit A at 25°C.

tion can be written as follows

$$q = [b_1K_1C/(1 + K_1C)] + [b_2K_2C/(1 + K_2C)]$$

where C is the molar concentration of the solute in solution at equilibrium, q represents the moles of adsorbed solute per gram of adsorbent, and q is determined by the sum of two adsorption processes, each characterized by a different equilibrium constant (K_1 and K_2) and a different maximum number (b_1 and b_2) of moles adsorbable per gram of adsorbent. A plot of $1/q$ versus $1/C$ for such a system should exhibit two linear regions, one at low and the other at high values of C, dependent upon the value of K_1 relative to that of K_2. Thus, if K_1 is one or more orders of magnitude greater than K_2, graphical treatment of the isotherm data should yield the parameters K_1 and b_1, as well as K_2 and b_2. Such is the case for the data at hand, as evidenced by Figs. 2 and 4. Numerical results obtained from the plots of $1/q$ versus $1/C$ are listed in Tables 2 and 3. The effects of pH on the adsorption parameters are of particular interest as they afford some insights as to possible adsorption mechanisms, discussed below.

The existence of two different types of adsorption sites on activated carbons is reasonable, since the surfaces possess two distinct structural features [21, 22]: graphite-like basal planes and polar group-populated edges. Adsorption on the basal planes is believed to involve van der Waal's forces, in

TABLE 2

Langmuir parameters for the adsorption of DPPH on Norit A

pH	Adsorption site	b (10^{-4} mol g^{-1})		K (l mol^{-1})
		Isotherm	Langmuir	
1.01	Primary	4.76	4.95	1.05×10^5
	Secondary	1.04	1.04	4×10^3
4.54	Primary	8.10	8.16	0.85×10^5
	Secondary	1.19	1.30	3×10^3

TABLE 3

Langmuir parameters of the adsorption of the iron(II)—DPPH complex on Norit A

pH	Adsorption site	b (10^{-4} mol g^{-1})		K (l mol^{-1})
		Isotherm	Langmuir	
2.50	Primary	2.18	2.31	1.04×10^5
	Secondary	0.79	1.01	1×10^4
5.75	Primary	2.77	2.79	2.18×10^5
	Secondary	0.51	0.78	3×10^4
>11[a]	—	1.30	1.50	1.05×10^4

[a]Solution 0.6 M NH_4OH in 40% (v/v) ethanol.

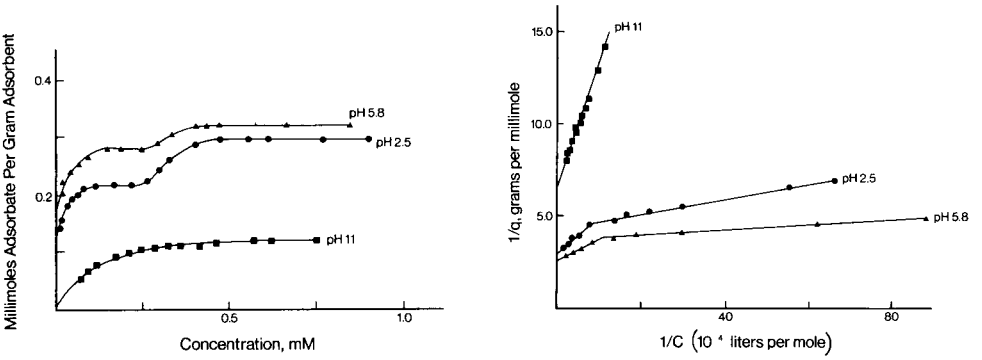

Fig. 3. Adsorption isotherms for the iron(II) chelate of DPPH on Norit A at 25°C and different pH values (pH 11 solution is 0.6 M NH_3 in 40% (v/v) ethanol).

Fig. 4. Langmuir treatment of adsorption isotherms for the iron(II) chelate of DPPH on Norit A at 25°C.

particular π-electron interactions between adsorbent and adsorbate. Carbonyl, hydroxyl and carboxyl functional groups at the edges of the basal planes constitute polar adsorption sites where interactions with charged or polar solutes should be favourable. Both DPPH and its iron(II) chelate possess considerable π-electron character conducive for adsorption at basal planes; also, their polar nature and ionic charge (dependent on pH) facilitate adsorption at basal plane edges.

The effect of pH on the Langmuir parameters for DPPH is greatest for the b value of the primary sites. As the pH is changed from 1 to 7, the formal charge on DPPH changes from +2 to 0 (see Table 1) and the capacity of Norit A for the solute (as measured by the value of b for the primary site) increases approximately two-fold. Unfortunately, the solubility of DPPH also approaches a minimum near pH 7, so that sufficient data to evaluate the Langmuir parameters in that region could not be obtained. Nevertheless, the trend is clear, indicating that either more primary sites become available or that the uncharged species are more efficiently (if not more strongly) accommodated with increasing pH. Further studies are needed to elucidate this and to distinguish which of the two postulated sites is the primary one, i.e., first to be occupied. A tentative conclusion of the present study is that the primary sites are those that reside on the basal planes. These should be more numerous than the edge-sites, and they should be occupied most efficiently by uncharged molecules that are planar and aromatic. It should be noted that DPPH exists predominantly uncharged in solutions of pH between 5.7 and 9.4 (see Table 1). Additional support for identifying the primary sites is provided by a comparison of the Langmuir K values obtained for the iron(II) chelate of DPPH on Norit A with that for a similar but simpler system. Previous study has shown that adsorption of the iron(II) chelate of PDT on XAD-2, a copolymer of divinylbenzene

and polystyrene, involves primarily a π-electron overlap mechanism characterized by a K value of 4.9×10^5 at pH 3 [2]. It is not unreasonable to conclude from this that a similar mechanism applies to the adsorption of the iron(II) chelate of DPPH on the primary sites of Norit A, since these exhibit a K value of the same order of magnitude (10^5) at pH 3. Thus, the primary sites for adsorption of aromatic compounds on activated carbons are probably those that reside on the graphite-like basal planes, and the secondary sites probably involve polar interactions between adsorbates and polar substituents located at the edges of the graphite planes.

The Langmuir parameters for adsorption of the iron(II) chelate of DPPH on Norit A were found to be only slightly affected by an increase in pH from 2.5 to 5.75. Solubility of the complex decreases with increasing pH, so an ethanol—water system was necessary for the evaluation of the parameters at higher pH. The combined effect of pH and ethanol, in this case, produced a more normal single-plateau adsorption isotherm, with a K parameter more closely approximating that of secondary than that of primary sites. The major cause of diminished adsorption affinity is probably due more to the presence of ethanol and solvation effects than to the high pH, because higher pH should favor, not discourage, adsorption. In aqueous solutions of pH 7 and above the iron(II) chelate of DPPH exists predominantly as an uncharged species (see Table 1) and thus should be more strongly attracted by π-electron interactions at basal graphite planes than if it existed as a charged and hence more strongly solvated species. Further study, particularly of the effects of solvent, might shed more light on this matter.

Adsorption of metal ions on DPPH—Norit A

Equilibrium measurements at 25°C were made to determine the extent of adsorption of various metal ions from aqueous solutions of pH 3 and 5 on DPPH-impregnated Norit A. To favor utilization of primary sites the Norit A was impregnated with DPPH to a level of 0.21 mmol g^{-1}, approximately 20% of its total capacity (0.93 mmol of DPPH per g of Norit A) at pH 5. Values found for the Langmuir parameters K and b are compiled in Table 4.

The b value for each metal ion is appreciably greater at pH 5 than at pH 3, indicating that the number of sites available increases with increasing pH over the range examined. Values of K for copper(I) and copper(II) remain essentially unchanged while those of the other metal ions show two to ten-fold increases with the change in pH. Investigations at higher pH were impractical because of risk of hydrous metal oxide formation and precipitation. The trend in K values for the different metal ions apparently parallels that of the formation constants usually observed for ferroin-type complexes [20].

It is of interest to compare the maximum number of moles of metal ion adsorbed (b values) with the number of moles of DPPH present per g of Norit A (0.21 mmol g^{-1}). For iron(II), cobalt(II), nickel(II), zinc(II) and cadmium(II), approximately one metal ion is sorbed at pH 5 for every

TABLE 4

Langmuir parameters of the adsorption of metal ions by DPPH-impregnated Norit A

M^{n+}	pH 3		pH 5	
	b (10^{-5} mol g^{-1})	K (10^{4} mol l^{-1})	b (10^{-5} mol g^{-1})	K (10^{4} mol l^{-1})
Li(I)	—	—	0.00	0.00
Mg(II)	—	—	0.00	0.00
Al(III)	—	—	0.00	0.00
Cr(III)	0.00	0.00	0.00	0.00
V(IV)	0.00	0.00	0.00	0.00
Mn(II)	0.00	0.00	0.00	0.00
Fe(III)	1.24	0.89	—	—
Fe(II)	1.19	0.79	6.58	1.57
Co(II)	1.15	0.66	6.58	6.82
Ni(II)	1.24	0.42	6.45	4.92
Cu(I)	2.67	2.96	10.3	2.83
Cu(II)	2.75	4.84	10.5	4.88
Zn(II)	2.47	0.41	5.62	1.35
Cd(II)	2.43	0.17	5.71	0.72

3.2—3.7 sorbed ligands. For copper(I) or copper(II) the approximate ratio is one metal ion per two sorbed ligands. Based on an expected coordination stoichiometry of one metal ion per two ligands, these results indicate that copper ions are more efficiently sorbed than the other ions, presumably because the sorbed DPPH is more accessible to them. A similar conclusion was made concerning the adsorption of copper ions on PDT-impregnated XAD-2 [2].

Applications

Two applications of DPPH in conjunction with Norit A were investigated: one for purification of reagents to minimize blanks in trace metal determinations and the other for enrichment of trace metals to enhance the sensitivity of their quantitation. These applications require procedures that are quantitative, rapid, simple and conserving of reagents. It was found that for DPPH and Norit A these requirements are achieved best if the chelation step precedes rather than accompanies the sorption process. Chelation of metal ions with DPPH followed by adsorption of the chelates on Norit A proved faster overall and more conserving of DPPH than the simpler single-step procedure involving treatment of metal ion solutions with DPPH-impregnated Norit A. Both approaches afforded quantitative recovery.

The results compiled in Table 5 indicate that the two-step procedure (chelation followed by adsorption) achieves quantitative removal of trace amounts of iron(II), cobalt(II), nickel(II), copper(I) and copper(II) from aqueous solutions of widely differing pH. Extraction of either zinc or

TABLE 5

Percent removal of metal ions from aqueous solution by complexation with DPPH followed by adsorption onto Norit A as a function of pH

M^{n+}	Portion removed (%) vs. pH				
	2.0	3.5	5.0	6.5	8.0
Fe(II)	34	100	100	100	100
Co(II)	46	100	100	100	100
Ni(II)	5	45	100	100	100
Cu(I)	98	100	100	100	100
Cu(II)	86	100	100	100	100
Cd(II)	0	0	71	79	97
Zn(II)	6	8	46	81	92

cadmium is more favorable at high pH and presumably quantitative if multiple extractions were employed.

Quantitative removal of trace amounts of iron(II), cobalt(II), nickel(II), copper(I) and copper(II) from 1 M solutions of the following reagents proved practical by the two-step procedure: ammonium perchlorate, hydroxylammonium chloride, sodium acetate, sodium citrate, and potassium chloride. Sensitive tests indicated these metals to be absent at the 10^{-7} M level from the treated solutions. Similar success was achieved in the purification of 0.1 M solutions of the nitrate salts of zinc, lead, aluminum, chromium and manganese. Efficient removal requires that the solution pH be between 3 and 11. The hydroxylammonium chloride, for example, was too acidic and required adjustment to pH 3.5 by addition of concentrated ammonia solution.

Before applying DPPH and Norit A to preconcentrate or enrich trace metals prior to their quantitation it was necessary to find an effective means of recovering the adsorbed metal ions or chelates from Norit A. Methanol, ethanol, or anhydrous acetic acid were found to extract the chelates; however, multiple extractions proved necessary for quantitative recovery. A faster method proved to be heating with 1 M hydrochloric acid to decompose the complexes. On testing this procedure, the results compiled in Table 6

TABLE 6

Determination and recovery of metal ions from known solutions employing chelation with DPPH, adsorption on Norit A, and desorption with hydrochloric acid

M^{n+}	Concentration ($mg\ l^{-1}$)		Recovery (%)	Replicates	RSD (%)
	Initial	Found			
Fe(II)	0.228	0.221	97.1	3	5
Cu(I)	0.254	0.252	99.5	3	2
Co(II)	0.218	0.217	99.5	3	2
Ni(II)	0.235	0.238	101.2	3	3

were obtained. All of the recoveries proved practical and quantitative within experimental error. The relative standard deviations observed are typical of photometric procedures. Some complications may arise when the recovered metal ions are determined spectrophotometrically, because the hot hydrochloric acid treatment liberates DPPH as well as the metal ions. The DPPH may interfere with the determination of certain metal ions if a spectrophotometric reagent other than DPPH were to be utilized. However, use of DPPH as the chromogenic reagent is limited in practice to simultaneous determinations of only iron(II) and cobalt(II) in the presence of copper, nickel, manganese, and zinc [23]. Other methods are necessary if either copper or nickel is to be determined in the presence of zinc, manganese, iron, cobalt, or one another. An attractive alternative, worthy of investigation, would be direct determination of the metals in Norit A by either graphite-furnace atomic absorption or x-ray fluorescence spectrometry.

REFERENCES

1 A. Sugii, N. Ogawa, I. Yukikazu and H. Yamamura, Talanta, 28 (1981) 551.
2 J. L. Lundgren and A. A. Schilt, Anal. Chem., 49 (1977) 974.
3 J. R. Jezorek and H. Freiser, Anal. Chem., 51 (1979) 368.
4 B. M. Vanderborght and R. E. Van Grieken, Anal. Chem., 49 (1977) 311.
5 E. Piperaki, H. Berndt and E. Jackwerth, Anal. Chim. Acta, 100 (1978) 589.
6 T. D. Harris and A. M. Williams, Anal. Chem., 53 (1981) 1727.
7 F. Vydra and V. Maricoa, Talanta, 10 (1963) 339.
8 F. H. Case, J. Chem. Eng. Data, 21 (1976) 124.
9 F. Lions and K. V. Martin, J. Am. Chem. Soc., 80 (1958) 3858.
10 C. D. Chriswell and A. A. Schilt, Anal. Chem., 47 (1975) 1623.
11 G. Charlot and D. Bezier, Quantitative Inorganic Analysis, Wiley, New York, 1964, p. 627.
12 A. Classen, L. Hastings and J. Visser, Anal. Chim. Acta, 10 (1954) 379.
13 S. Shibata in H. A. Flaschka and A. J. Barnard (Eds.), Chelates in Analytical Chemistry, Vol. 4, M. Dekker, New York, 1972, p. 80.
14 G. S. Vasilikitois, T. Kouimtris, C. Apostolopoulou and A. Voulgaropoulos, Anal. Chim. Acta, 70 (1974) 319.
15 H. Alexaki-Tzivanidou, Microchem. J., 22 (1977) 388.
16 H. Alexaki-Tzivanidou, G. Kouneis and B. Elezoglou, Microchem. J., 23 (1978) 329.
17 H. Alexaki-Tzivanidou and G. S. Vasilikiotis, Microchem. J., 26 (1981) 1.
18 A. A. Schilt, P. C. Quinn and C. L. Johnson, Talanta, 26 (1979) 273.
19 G. L. Traister and A. A. Schilt, Anal. Chem., 48 (1976) 1216.
20 A. A. Schilt, Analytical Applications of 1,10-Phenanthroline and Related Compounds, Pergamon Press, New York, 1969.
21 J. Mattson, H. B. Mark, W. J. Malbin and J. C. Crittendon, J. Colloid Interfacial Sci., 31 (1969) 116.
22 S. Miller, Environ. Sci. Technol., 8 (1980) 910.
23 M. R. DiTusa, Ph.D. Thesis, Northern Illinois University, DeKalb, IL, 1982.

Analytica Chimica Acta, 154 (1983) 173—180
Elsevier Science Publishers B.V., Amsterdam — Printed in The Netherlands

THERMAL-DESORPTION GAS CHROMATOGRAPHIC PROCEDURE FOR SCREENING COAL FLY ASH FOR VOLATILE ORGANIC COMPOUNDS

C. E. HIGGINS, W. H. GRIEST*, J. E. CATON and S. H. HARMON

Analytical Chemistry Division, Oak Ridge National Laboratory, Oak Ridge, TN 37830 (U.S.A.)

(Received 27th May 1983)

SUMMARY

Thermal desorption of coal fly ash in a flowing stream of helium liberates volatile compounds which are collected on Tenax resin. A chemical "fingerprint" of these components collected from the fly ash is obtained by using thermal desorption of the material collected on the Tenax resin and capillary-column gas chromatography. Compounds ranging in volatility from that of benzene (b.p. 80°C) through C_1-phenanthrene (b.p. ca. 360°C) are detected, but recoveries of components only through naphthalene (b.p. 218°C) are suitable for quantitative work. The method provides chemical information on volatile organic compounds complementary to that achieved by procedures based on solvent extraction.

Relatively little is known of the organic compounds associated with the fly ash emitted by coal-fired electric power generating plants. Most of the reported data [1—4] have been based on solvent extraction. However, those procedures are time-consuming, and the steps in which solvent volume is reduced can cause selective losses of the more volatile constituents from the extract.

More direct methods have been reported [5, 6] for the collection and quantitative measurement of organic compounds in atmospheric particulate matter. Portions of air filters have been subjected to thermal desorption, the compounds liberated being collected either on precolumns or directly on a gas chromatographic (g.c.) column for separation and measurement. The procedures were more facile than solvent extraction and results, even for less volatile compounds, were similar to those achieved by solvent extraction. However, the range of species determined was not significantly extended from those found in solvent extracts. Profiles for volatile organic compounds in solid and semisolid waste materials have also been established qualitatively by g.c. [7] with a dynamic headspace sampling procedure.

This paper reports the development of a thermal desorption procedure for the collection, separation and quantitation of volatile organic compounds from coal fly ash or other finely divided particulate matter. The results are comple-

mentary to those obtained by solvent extractions and extend the range of species which can be measured.

EXPERIMENTAL

Materials

Samples. The fly ash samples used in this study were collected at an eastern U.S. power plant by another contractor. Fly ash aerosol from the post-electrostatic precipitator ductwork was aspirated through an insulated teflon bag held above the dewpoint of sulfuric acid. Other details of collection are reported elsewhere [8].

Materials and treatments. Tenax (150 g, 35—60 mesh; Applied Sciences Laboratories, State College, PA 16801) was extracted at least three times with 2 l each of water, water—methanol, methanol, and ether, then was Soxhlet-extracted for 48 h with n-pentane (Burdick and Jackson Laboratories, Muskegon, MI 49442). Residual pentane was removed with a helium purge; the Tenax was then thermally conditioned in a flow-through bomb placed in an oven programmed to heat at 1°C/min up to 250°C with a two-day hold at 250°C. Throughout the heat treatment, a helium flow was maintained at 300 ml min^{-1} per liter of Tenax.

Quartz wool (ca. 400 ml) was extracted for 15 min twice each with 600 ml of boiling acetone, methanol, and dichloromethane. It was then dried and heated at 800°C in air in a furnace for 8—16 h. Quartz wool, Tenax and pyrex desorption tubes were all checked for contamination by using thermal desorption—gas chromatography (t.d.—g.c.).

Procedures

Volatile organic material from fly ash was desorbed by heating the fly ash in a tube furnace at 300°C in a stream of helium. The sample (ca. 0.3 g) was transferred to a pyrex tube (10-mm i.d., 13-mm o.d., 33 cm) plugged in the middle with 4 cm of preconditioned quartz wool. The tube was connected to a helium tank, the fly ash was tapped into a plug on the quartz wool, and the tube was placed in an 18-cm tube furnace (E. H. Sargent & Co., Chicago, IL) at room temperature. A Tenax trap (ca. 230 mg of purified Tenax held in place with quartz wool in a 9-mm o.d. × 5-mm i.d. × 11-cm pyrex desorption tube) was inserted, tapered end first, into the exit end of the furnace tube and held tightly in place with a 3-cm × 1.8-cm o.d. teflon sleeve. It was positioned so that the front (inlet) end of the trap was just outside the furnace. The temperature at this point reached a maximum of 110°C. With a helium flow of 60 ml min^{-1}, the fly ash was heated rapidly from room temperature to 300°C and kept at that temperature for at least 1 h (total time 1.5 h). The trap was removed for immediate separation and quantitation by t.d.—g.c.

A Perkin-Elmer Model 3920 gas chromatograph was used. The Tenax trap was heated in the injection port of the g.c. for 18 min at 250°C at a helium

flow rate of 6—8 ml min^{-1} and desorbed organics were frozen out (liquid nitrogen) in a stainless steel cryoloop (0.5-mm i.d.) at the front of a 25-m Quadrex fused-silica bonded-phase capillary column (007 methyl silicone, 0.25 μm; 0.24-mm i.d.). The Tenax trap was removed and the inlet pressure was reduced from 34—40 psig to 12 psig, which provided a carrier gas flow rate of 1 ml min^{-1} at room temperature. At a 19.5 min run time, the liquid nitrogen was removed, the oven temperature was raised to 30°C, kept there for 16 min, and then programmed at 4° min^{-1} to 250°C where it was held for an additional hour. Components were detected by flame ionization and their peak areas were integrated by a PDP8/e computer. External standards were used for calibration. Known weights of standard compounds in carbon disulfide solution were applied by microliter syringe to the Tenax, desorbed, and separated by using the same program as for the fly ash to determine their response factors.

Experiments to estimate the recovery of the procedure used thermally treated fly ash. Fly ash was heated at 300°C overnight in the tube furnace. Little volatile organic material then remained on the fly ash. The sample and equipment were cooled to room temperature. Aliquots (2 μl) of a carbon disulfide solution containing approximately 0.5 μg of each standard compound (aliphatic hydrocarbons, aromatic hydrocarbons, and oxygenated compounds) were applied throughout the middle of the fly ash sample from a microliter syringe. The sample was flushed for 20 min with helium at room temperature to remove the carbon disulfide before the 90-min thermal desorption routine was conducted. The collected standards were separated and quantified as described above and results were compared with those for standards added directly to the Tenax trap to calculate recoveries.

Gas chromatography—mass spectrometry (g.c.—m.s.). A Hewlett-Packard Model 5985 instrument with a column and temperature program similar to that described above was used for g.c.—m.s. studies. Spectra were recorded at 70-eV ionizing voltage in the electron impact mode.

RESULTS AND DISCUSSION

Figure 1 shows the chromatographic profiles of the compounds thermally liberated from three coal fly ashes and collected on Tenax. It is evident that considerable chemical information can be obtained by the procedure, and that a distinctive volatile chemical "fingerprint" can be generated for each fly ash sample. In Fig. 1, profile C is that of fly ash sample No. 484, which contains solvent-extractable mutagenic activity [9]. It is interesting to note that the t.d.—g.c. profile of this sample is more complex than those of the other two ash samples. Whether or not the species visualized by t.d.—g.c. relate to bacterial mutagenicity in solvent extracts remains to be established. Fisher et al. [10] have observed that the mutagenic activity extractable from fly ash is decreased when the fly ash is heated above ca. 150°C in a sealed tube. It is not yet known if heating fly ash in the present dynamic system causes the decomposition of mutagens.

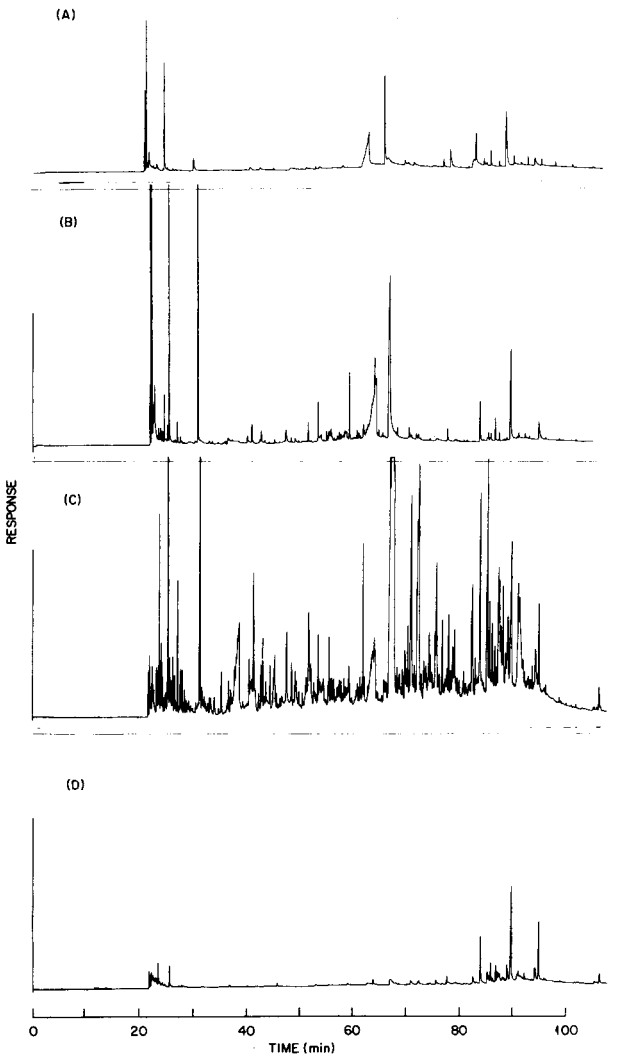

Fig. 1. Thermal-desorption g.c. profiles of compounds thermally collected from fly ashes: (A) 481; (B) 483; (C) 484; (D) a blank.

A wide range of species is detected in the fly ash samples. Table 1 lists the compounds tentatively identified by g.c. retention time and/or g.c.—m.s. in the sample from fly ash No. 484. Nineteen aliphatic hydrocarbons from tridecane through tetracosane, benzene, C_1—C_4 benzenes, naphthalene, biphenyl, C_1—C_4 naphthalenes, siloxanes, and phthalates are some of the major species detected. Phenanthrene, alkylated phenanthrenes, higher aliphatic hydrocarbons, and other siloxanes also were observed but are not confidently identified as originating from the fly ash sample because they were also found, but at lower levels, in the blank. Many of these compounds have been reported [11] in coal-combustion effluents.

TABLE 1

Characterization by g.c.—m.s. of compounds collected on Tenax from thermal desorption of fly ash No. 484

t_R (min)[a]	Apparent molecular ion (m/z)	Tentative identification
25.5	78	Benzene[b]
31.4	92	Toluene[b]
38.7	96	Furanaldehyde
40.6	106	Ethylbenzene[b]
41.4	106	*m*- and/or *p*-Xylene[b]
43.1	106	*o*-Xylene[b]
46.3	268	Unknown
47.6	106	Benzaldehyde[b]
48.5	120	n-Propylbenzene[b]
49.9	120	1,3,5-Trimethylbenzene[b]
51.7	120	C_3-Benzene
53.4	120	1,2,3-Trimethylbenzene[b]
55.5	296	Octamethylcyclotetrasiloxane
58.3	98	Unsaturated hydrocarbon
61.3	134	C_4-Benzene
61.9	128	Naphthalene[b]
64.1	112	Hydrocarbon
65.7	146	C_1-Tetrahydronaphthalene
67.0	142	2-Methylnaphthalene[b]
~67[c]	142	1-Methylnaphthalene
~67[c]	148	Oxygenated hydrocarbon
~67[c]		Phthalate
68.2	184	n-Tridecane[b]
70.3	154	Biphenyl[b]
71.0	156	C_2-Naphthalene
71.0	162	C_2-Benzofuranone
71.5	156	C_2-Naphthalene[b]
	164	Oxygenated hydrocarbon
72.0	162	C_2-Benzofuranone
72.1	198	n-Tetradecane[b]
72.5		Dimethylphthalate[b]
73.3	178	Oxygenated hydrocarbon
73.6	168	C_1-Acenaphthene/biphenyl[d]
	176	Oxygenated hydrocarbon
74.3	168	C_1-Acenaphthene/biphenyl[d]
	170	C_3-Naphthalene
	176	Oxygenated hydrocarbon
75.4	212	n-Pentadecane[b]
75.7	176	Oxygenated hydrocarbon
	170	C_3-Naphthalene
76.8	176	Oxygenated hydrocarbon
78.0	222	Diethylphthalate[b]
78.3	190	Oxygenated hydrocarbon
79.1	226	n-Hexadecane[b]

TABLE 1 (continued)

t_R (min)[a]	Apparent molecular ion (m/z)	Tentative identification
79.6	190	Oxygenated hydrocarbon
80.8	180	Fluorenone
81.2	184	C_4-Naphthalene
82.2	240	n-Heptadecane[b]
83.6	178	Phenanthrene[b]

[a]Retention time on 25-m methyl silicone column described in Experimental. Blank space indicates co-elution of components. [b]Identification supported by g.c. retention time comparison with authentic standards. [c]Poor chromatographic resolution prevented accurate measurement of retention time. [d]Either C_1-acenaphthene or C_1-biphenyl, indistinguishable by m.s.

Of particular interest is the tentative identification of oxygenated polycyclic aromatic hydrocarbons (PAH) such as fluorenone. It is speculated that the species corresponding to molecular ions of m/z 112, 162, 172, 176, 190, and 212 may represent oxygenated PAH such as C_2-benzofuranone (m/z 162). The present hypothesized identification is based on the losses of 28 (possibly CO) and 44 (possibly CO_2) mass units in the mass spectra of these compounds. Although high-resolution m.s. will be required for confirmation of these species as oxygenated PAH, the observation [9] of strong carbonyl bands in the infrared spectra of solvent extracts from this ash is consistent with the presence of oxygenated compounds. Also, some oxygenated PAH have been reported [11] in combustion effluents, including those from coal.

Considerable difficulties were experienced in generating g.c.—m.s. total ion current chromatograms which resembled the t.d.—g.c. profiles. No such problems were encountered with samples containing predominantly aromatic and aliphatic hydrocarbons, suggesting that the compounds released from fly ash are polar (oxygenated) in nature. Less volatile compounds with similar mass spectral fragmentation characteristics were also observed in the g.c.—m.s. responses for the extracts. This finding suggests that these species, if present, are native to the fly ash, and not artificially formed by the thermal desorption of the ash or during the t.d.—g.c. procedure. However, fluorenone has been identified [12] as a non-photochemical degradation product of fluorene applied to fly ash, and the artificial formation of such oxygenated species may be difficult to distinguish from in-situ formation separate from the analytical procedure.

The recovery of authentic standards applied to thermally stripped fly ash samples was investigated to define the range of compounds that can be quantified. Table 2 lists the recoveries of standards applied to fly ash samples Nos. 483 and 484. The results for fly ash No. 484 suggest that under the conditions of this study, compounds with boiling points approximately

TABLE 2

Data for recovery of standards applied to fly ash samples and for quantitation of selected compounds in fly ash No. 484

Compound	Recovery (%)		Found in 484[a] ($\mu g\ g^{-1}$)
	No. 484	No. 483	
Benzene	83	99	2.6 ± 0.24 (9.3)
Toluene	97	86	1.4 ±0.06 (4.2)
m-Xylene	87	48	0.54 ± 0.02 (4.2)
Benzaldehyde	64	5	0.56 ± 0.06 (9.8)
1,3,5-Trimethylbenzene	84	26	0.06 ± 0.02 (33)
Acetophenone	48	0.4	—
Naphthalene	84	8	0.39 ± 0.07 (17)
2-Methylnaphthalene	43	0	—
n-Tetradecane	49	0	—
Dimethylphthalate	9	0	—
n-Hexadecane	28	0	—
2-Methylphenanthrene	3	0	—
Ethylbenzene	—	—	0.14 ± 0.01 (7.1)
o-Xylene	—	—	0.22 ± 0.04 (16)
n-Propylbenzene	—	—	0.13 ± 0.01 (7.7)
C_4-Benzene	—	—	0.09 ± 0.02 (22)

[a]Average of three runs ±1 s.d. with % r.s.d. in parentheses.

equal to or lower than that of naphthalene (b.p. 218°C) can be determined with reasonable confidence. However, more volatile but polar species such as acetophenone may not be recovered as well. Decomposition of these species is likely; a second thermal desorption of the fly ash sample recovered less than 10% of any component. However, no new peaks representing degradation products appeared on the profiles. The much lower recoveries for fly ash No. 483 are consistent with its much greater sorptivity [13]. We have found this fly ash sample to be 10^2—10^3 times more sorptive than any other fly ash sample tested here. Recoveries of compounds by this procedure apparently are mediated by the surface activity of the fly ash sample. Studies [13] of the sorptivity of different fly ash samples suggest that most fly ashes should behave more like No. 484 than No. 483.

Samples of fly ash No. 484 were processed in triplicate over a two-day period to establish the reproducibility of the procedure. Results included in Table 2 indicate surprisingly good precision considering the low concentration levels of the components and the two desorption steps required. Compounds with boiling points above naphthalene were not quantified because of their apparently lower recoveries from the ash. However, they can be quantified by using conventional extraction procedures. Although no quantitative data are available in the literature for comparison with these results, the concentrations are consistent with the levels of extracted compounds determined [1, 14] in this ash and in other fly ash samples.

Conclusions

Thermal desorption allows the facile separation and detection of volatile compounds which would not be easily determined by using solvent-extraction procedures. It thus provides information complementary to the latter. Because it aids in the visualization of some of the components which are better determined by the more time-consuming extraction procedures, it also appears to have considerable value as a rapid screening tool prior to more detailed procedures.

The authors acknowledge M. V. Buchanan and G. Olerich for conducting the g.c.—m.s. studies. This research was sponsored by Electric Power Research Institute, under Interagency Agreement DOE No. RTS 77-58 and EPRI No. RP 1057-1 under Union Carbide Corporation contract W-7405-eng-26 with the U.S. Dept. of Energy.

REFERENCES

1 W. H. Griest and M. R. Guerin, Identification and Quantification of Polynuclear Organic Matter on Particulates from a Coal-Fired Power Plant, EA-1092, The Electric Power Research Institute, Palo Alto, CA, 1979.
2 R. L. Bennett, K. T. Knapp, P. W. Jones, J. E. Wilkerson and P. E. Strup, in P. W. Jones and P. Leber (Eds.), Polynuclear Aromatic Hydrocarbons, Ann Arbor Science Publ., Ann Arbor, MI, 1979, p. 419.
3 S. G. Zelenski, G. T. Hunt and N. Pangaro, in A. Bjorseth and A. J. Dennis (Eds.), Polynuclear Aromatic Hydrocarbons: Chemistry and Biological Effects, Battelle Press, Columbus, OH, 1980, p. 589.
4 L. Sucre, W. Jennings, G. L. Fisher, O. G. Raabe and J. Olechno, in Trace Organic Analysis: A New Frontier in Analytical Chemistry, N.B.S. Spec. Publ. No. 519, Natl. Bur. Stand., Washington, DC, 1979, p. 109.
5 H. P. Burchfield, E. E. Green, R. J. Wheeler and S. M. Billedeau, J. Chromatogr., 99 (1974) 697.
6 E. Wauters, P. Sandra and M. Verzele, J. Chromatogr., 170 (1979) 125.
7 R. S. Brazell and M. P. Maskarinec, J. High Res. Chromatogr. Commun., 4 (1981) 404.
8 R. I. Mitchell and W. C. Baytos, Collection and Analysis of Fly Ash from Stack Gas Emissions, Rep. U.S. E.P.A. Contract No. 68-03-1371 to W. Pepelco, U.S. Environmental Protection Agency, Health Effects Research Laboratory, Cincinnati, OH, February, 1979.
9 W. H. Griest, J. E. Caton, T. K. Rao, S. H. Harmon, L. B. Yeatts, Jr. and G. M. Henderson, Int. J. Environ. Anal. Chem., 12 (1982) 241.
10 G. L. Fisher, C. E. Chrisp and O. G. Raabe, Science, 204 (1979) 879.
11 G. A. Junk and C. S. Ford, Chemosphere, 9 (1980) 187.
12 W. A. Korfmacher, G. Mamantov, E. L. Wehry, D. F. S. Natusch and T. Mauney, Environ. Sci. Technol., 15 (1981) 1370.
13 W. H. Griest and J. E. Caton, in M. Cooke and A. J. Dennis (Eds.), Chemical Analysis and Biological Fate: Polynuclear Aromatic Hydrocarbons, Battelle Press, Columbus, OH, 1981, p. 719.
14 W. H. Griest, J. E. Caton and B. A. Tomkins, Identification and Quantification of Polynuclear Organic Matter (POM) in Energy-Related Materials, Interim Rep. Research Project RP 1057-1, submitted to the Electric Power Research Institute, Palo Alto, CA, June, 1982.

Analytica Chimica Acta, 154 (1983) 181—189
Elsevier Science Publishers B.V., Amsterdam — Printed in The Netherlands

PATTERN RECOGNITION APPLIED TO VAPOUR-PHASE INFRARED SPECTRA

L. DOMOKOS, I. FRANK and G. MATOLCSY

Department of General and Analytical Chemistry, Technical University, Budapest (Hungary)

G. JALSOVSZKY*

Central Research Institute for Chemistry, Hungarian Academy of Sciences, H-1025 Budapest (Hungary)

(Received 23rd February 1983)

SUMMARY

Various supervised and unsupervised pattern recognition methods are compared, to study the effect of data reduction and preprocessing scale transformations on recognition ability. Data were taken from a collection of 2300 vapour-phase infrared spectra. The basis of chemical classification was the presence or absence of carboxy, amino, alcoholic hydroxy, nitro, ester and phenyl groups, respectively.

Pattern recognition methods, such as binary linear separation or learning machine [1—7], *K*NN [6, 8—10], hierarchal clustering [11, 12] and maximum likelihood [6], have been applied to the interpretation of infrared spectra, to separate chemical classes of organic compounds. The aim of the present study was to compare the performance of various supervised and unsupervised pattern recognition methods and to examine the effect of data reduction and preprocessing scale transformations on recognition ability. Because vapour-phase infrared data were used the expectation was that, in the absence of intermolecular interactions, the separation of categories would be better than in previous investigations.

DATA

Data were taken from a collection of 2300 vapour spectra (EPA library) which is included in the standard software of Nicolet 7199 F.t.i.r. systems. On the basis of the presence or absence of five functional groups (carboxy, amino, alcoholic hydroxy, nitro and ester) and of aromatic and non-aromatic character, 385 compounds were selected from the collection as model compounds for the training set. The distribution of these compounds in the categories is shown in Table 1.

The model compounds were selected from a list prepared by a program which runs library searches on the basis of Wiswesser line notation (WLN)

0003-2670/83/$03.00

TABLE 1

The distribution of categories in the training set

Chemical property	Aromatic	Non-aromatic	Total
Carboxy	27	50	77
Alcohol	39	41	80
Ester	39	41	80
Nitro	62	8	70
Amine	53	25	78
	220	165	385

or any substring thereof. The Nicolet-1180 computer of the F.t.i.r. system was used and the selected spectra were retrieved from the library, decoded and converted into an appropriate external format by a BASIC program. The converted spectra were stored in a disk file. The contents of this file were transferred through an RS-232 channel to a PDP-11/34 computer which was used to write the file on magnetic tape. (The programs run on Nicolet-1180 are available from one of the authors (G. J.) on request.)

The library spectra contain 460 data points in the 455—3996 cm^{-1} region, and the intensity range is 0—1.0 absorbance units. By summing four adjacent points, 115 intensity data were obtained, i.e., the spectra were represented in the pattern recognition models as a point in a 115-dimensional Euclidean space. (Although there may be better methods available for this "preliminary dimension reduction", the application of this simple method is justified by the experience that no relevant information is lost.)

METHODS

The calculations, except for the predictions on the complete library, were done by the ALFI pattern recognition program system developed at the Technical University in FORTRAN-IV. The methods are well known from the literature [13—16], thus only a brief description of the algorithm used is given below.

Feature selection and dimension reduction

Fisher weighting (FISHER). Pattern vector components are selected on the basis of their Fisher ratios (i.e., the square of difference between category means divided by the sum of category variances) and the components with the smallest Fisher ratios are eliminated.

Variance weighting (VARI). Vector components are selected on the basis of the ratio of interclass and intraclass variances for each vector component.

Weight vector threshold (TLURED). Pattern vector components which have the smallest absolute values in the trained weight vector are eliminated.

Scale transformations

Autoscaling (AUTO). Vector components are scaled by subtracting the component mean and dividing by the component standard deviation, producing components with zero mean and unit variance.

Logarithmic scaling (LOG). The logarithm of components is taken.

Range scaling (RANGE). The components are scaled into the 0—1 range.

Binary encoding (BIN). The vector components are 0 or 1 depending on whether the component is below or above a given threshold.

Autoscaled binary encoding (BINAUT). The autoscaled vector components are transformed to 0 or 1 depending on whether the scaled value is negative or positive.

Pattern recognition training and clustering methods

Binary linear separation (TLU). Pattern vectors are separated into two categories by a hyperplane with a normal vector determined by a negative feedback training. After training, the unknown patterns are classified according to the sign of the scalar product of the normal vector of the plane with the pattern vector, i.e. according to the "side" of the hyperplane to which the unknown "point" falls. The method is applicable only to two, linearly separable categories.

Multicategory linear separation (MULTI). Pattern vectors are separated by hyperplanes, equal in number to the number of categories. The training and classification of unknown patterns is similar to the TLU method, except that patterns are classified on the basis of the maximum of scalar product of pattern vector and normal vectors.

SIMCA method. Categories are described by principal component models determined separately for each category on the basis of the training set. Patterns are classified into the category for which the principal component model (domain) best reproduces the data, and each pattern is given a probability concerning each category.

Non-hierarchal k*-mean clustering (KMEAN).* The n-dimensional points (patterns) are clustered on the basis of their Euclidean distances. The number of the clusters required and their centroids are given as input, but after each iteration step new centroids are calculated as the centres of gravity of the clusters. The iteration process is terminated when no further change takes place in clustering.

Karhunen—Loeve projection (KLM). This is a linear mapping of the n-dimensional vectors onto an orthogonal space of lower dimension defined by the most significant principal component vectors. In this work two principal components were used.

Prediction on the complete library

By means of the normal vectors determined from the selected training set by TLU, predictions were made on the original data set consisting of all 2300 spectra. This was done by a BASIC program (TLU2) run on the

Nicolet 1180 computer. The program classifies the spectra on the basis of the normal vector and the compounds on the basis of WLN. The results can be given as a 2 × 2 matrix which contains the number of correctly and incorrectly classified spectra in the positive (present) and negative (absent) cases, respectively. The performance of normal vectors was characterized by their overall and average predictive abilities and by transinformation, all calculated by means of well known relationships [13].

RESULTS AND DISCUSSION

First the effect of feature selection (VARI, FISHER and TLURED) was investigated on the recognition ability of the TLU method. The percentage of correctly classified spectra was taken as the measure of the goodness of feature selection/reduction. The number of selected features (i.e., the dimension of the reduced patterns) was 115, 20, 10 and 5. Because of the strong similarity between the results of the VARI and FISHER methods, only the results of the latter are shown here.

Table 2 contains the percentages of correctly classified spectra with FISHER and TLURED feature selection. Although the latter seems to be superior, the differences are not decisive. It is interesting to note that the drastic reduction of dimension from 115 to 20 hardly affects the quality of classification, which decreases significantly for dimensions 10 and 5 only. This can be seen in Fig. 1(a—e), where the percentages of correctly classified spectra are plotted against the dimension of pattern vectors. The solid line pertains to TLURED, the dotted to the FISHER method. The advantage of feature reduction is obvious, because only 10—20 dimensions are required

TABLE 2

Effect of the TLURED and FISHER feature selection methods on the recognition ability of TLU training

Chemical class properties	Method	Dimension of selected patterns			
		115	20	10	5
Carboxy/	TLURED	99	98	98	98
not carboxy	FISHER	99	98	78	74
Alcohol/	TLURED	98	99	99	98
not alcohol	FISHER	98	96	87	85
Ester/	TLURED	99	100	97	93
not ester	FISHER	99	97	87	84
Nitro/	TLURED	99	99	96	89
not nitro	FISHER	99	95	93	90
Amine/	TLURED	98	98	97	88
not amine	FISHER	96	95	89	85
Aromatic/	TLURED	96	93	81	74
not aromatic	FISHER	96	90	82	73

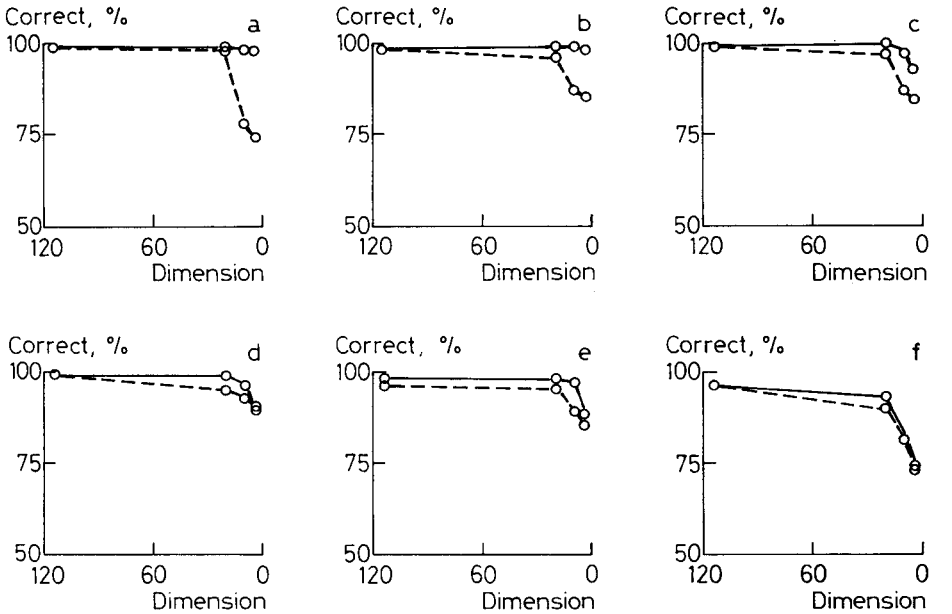

Fig. 1. Percentage of correctly classified spectra as a function of the dimension of the pattern: (a) carboxy; (b) alcohol; (c) ester; (d) nitro; (e) amine; (f) aromatic. Feature selection: (—) TLURED; (---) FISHER.

instead of 115, without any significant loss in classification ability but with an enormous gain in computer time.

Clearly, the reduced features are different in the six classification problems corresponding to different chemical groups. The connection between the characteristic infrared absorption bands of these groups [18] and the features selected by the TLURED and FISHER techniques was studied.

When the first five most significant features in the TLU's were investigated, it was observed that at least one of them coincides with one of the characteristic absorptions of the group in question (see Table 3). However, some of the most significant features have virtually no relationship with the characteristic frequencies of the given category. Closer inspection shows that the corresponding elements of the normal vector are negative numbers, and thus these features are required for negative classification rather than for an affirmative answer. However, under these conditions, these features are equally characteristic of the other spectra of the training set and of the spectra included in the category in question.

Because the training set was selected according to the categories investigated and not randomly taken from the library, the spectra which do not belong to a given category always belong to another category studied here. Therefore, some of the negative features in one normal vector must be the same, and indeed are the same, as the positive features in another normal vector.

TABLE 3

The most significant features remaining after TLURED and FISHER feature selection and the characteristic group frequencies
(region corresponding to the features is ±15 cm^{-1})

Group	Feature selection	Most significant features					Group frequencies [18]
Carboxylic acid	TLU	779	1211	1797	2877	3587	ν_{OH}: 3550—3500, $\nu_{C=O}$: 1800—1740,
	FIS	563	594	1766	1797	3587	ν_{CH}: 3000—2840
Alcohol	TLU	1427	1643	1736	3556	3649	ν_{OH}: 3650—3590
	FIS	1736	1766	1797	3649	3679	
Ester	TLU	1241	1396	1519	1797	3587	$\nu_{C=O}$: 1750—1735, ν_{C-O}: 1330—1050
	FIS	532	1211	1232	1736	1766	
Nitro	TLU	1334	1365	1550	1612	3556	$\nu_{a NO_2}$: 1570—1540, $\nu_{s NO_2}$: 1390—1310
	FIS	1334	1365	1550	1581	2939	
Amine	TLU	748	1211	1427	1643	3648	ν_{NH_2}: 3500—3300, β_{NH_2}: 1650—1550,
	FIS	779	1643	1766	3402	3433	γ_{NH_2}: 850—700
Phenyl	TLU	1488	1539	3062	3093	3617	ν_{CH}: 3080—3030, ν_{CC}: 1525—1475
	FIS	1519	2877	2908	2939	2970	

Next, the effect of scale transformations on TLU training ability was studied. The 20-dimensional patterns obtained by TLURED was used and the training was done on the original, logarithmed, autoscaled and range-scaled patterns. The training algorithm was TLU for the five two-category cases, but the case of five different categories was also investigated by MULTI and SIMCA. The results are given in Table 4, which shows that there is no preprocessing scale transformation that is significantly superior to the others. A similar conclusion has been reached in a study of orthogonal preprocessing transformations [17].

It is a basic assumption in pattern recognition that chemically similar compounds have similar pattern vectors, i.e., their pattern vectors are close to one another in terms of the similarity or distance measure applied. Unfortunately, the validity of this fundamental assumption is very difficult to

TABLE 4

The effect of scale transformations on 20-dimensional patterns

Scale transformation	Chemical properties						
	Carboxy/ not carboxy	Alcohol/ not alcohol	Ester/ not ester	Amine/ not amine	Arom./ not arom.	Carboxy, alcohol, ester, amine, aromatic	
	TLU	TLU	TLU	TLU	TLU	MULTI	SIMCA
Original	99	98	98	99	98	94	85
Logarithmic	80	83	81	83	82	94	75
Auto-scaling	99	97	97	100	97	94	93
Range scaling	98	98	99	98	96	96	84
Binary	98	93	95	93	89	95	72
Auto-scaled binary	99	97	98	97	98	91	92

check because of the high dimension of the patterns. One possible way of treating this problem is to seek clusters of pattern vectors in the pattern space and study whether these natural clusters agree with the chemical categories. This is possible by means of cluster analysis [13, 15, 16, 19, 20]. Another possibility is to project the multidimensional patterns onto a 3- or 2-dimensional space and check visually whether the projected points cluster according to the given chemical properties. For such projections, the Karhunen—Loeve transformation is often recommended; this projects the patterns onto the space of principal component vectors obtained from the correlation matrix of the patterns.

Cluster analysis was done here by the k-mean method. Five classes were expected, corresponding to carboxy, alcohol, ester, nitro and amino groups (the spectra in the model were selected so that these categories were mutually exclusive). Table 5 shows the effect of feature selection on clustering in the case of the original, binary-encoded and autoscaled binary-encoded patterns, whereas Table 6 shows the effect of various scale transformations applied to the 20-dimensional patterns before cluster analysis. According to the results, the autoscaled binary patterns are almost always the best, but otherwise there are no significant differences.

The Karhunen—Loeve transformation was examined with two principal components. The 2-dimensional projections obtained are shown in Fig. 2. These figures indicate that autoscaling is of fundamental importance in this method.

TABLE 5

The effect of feature selection on clustering

Chemical property	Dimension											
	115			20			10			5		
	ORIG	BIN	BINAUT	ORIG	BIN	BINAUT	ORIG	BIN	BINAUT	ORIG	BIN	BINAUT
Carboxy	90	73	100	77	90	100	93	80	97	94	94	93
Alcohol	73	90	90	80	97	90	100	93	87	30	54	40
Ester	87	80	77	73	100	90	80	100	90	63	97	90
Nitro	97	87	97	77	93	93	93	87	80	20	20	80
Amine	70	63	80	78	70	77	60	60	63	90	77	38

TABLE 6

The effect of scale transformations on clustering (20-dimensional patterns)

Chemical property	Transformation					
	ORIG	LOG	RANGE	AUTO	BIN	BINAUT
Carboxy	77	70	76	90	90	100
Alcohol	80	53	80	90	97	97
Ester	73	22	70	87	100	92
Nitro	77	35	78	80	93	94
Amine	78	10	78	70	70	79

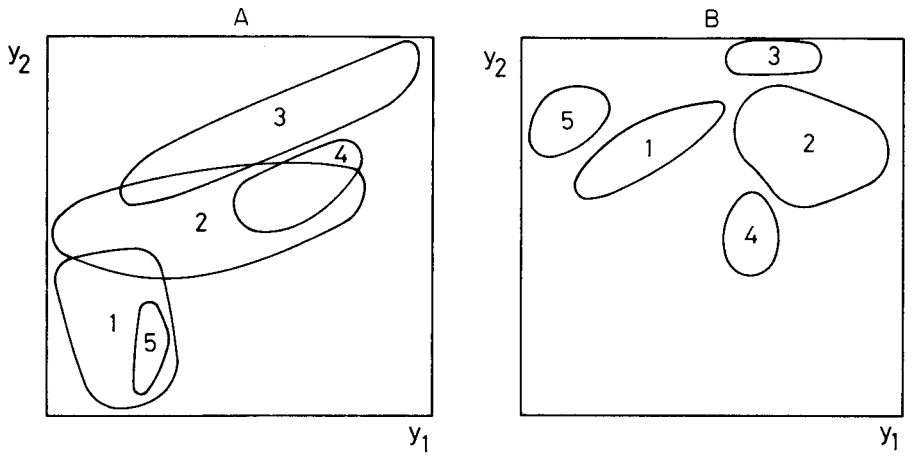

Fig. 2. Karhunen—Loeve mapping from 20-dimensional patterns obtained by FISHER reduction: A, untransformed data; B, autoscaling transformation applied. (1) Carboxy; (2) alcohol; (3) ester; (4) nitro; (5) amine.

Both cluster analysis and Karhunen—Loeve transformation suggest that in the classification problems studied here the low-dimensional patterns obtained by feature extraction permit a fairly good clustering according to chemical properties. It should be noted, however, that the categories investigated here are relatively simple, and in complicated cases more complex research is necessary to establish the most appropriate preprocessing transformation and feature selection method.

The predictive abilities of four TLU vectors (carboxy, amine, nitro and phenyl) were also investigated for the complete library of 2300 spectra. From the results, given in Table 7, it can be seen that most of the misclassifications are of the type in which the classifier gives a positive answer

TABLE 7

Predictions on the complete library

Group	Classified as		Predictive ability			Trans-information (bit)
	positive	negative	Individual (%)	Overall (%)	Average (%)	
Carboxy	132	4	97	66	81	0.35
not carboxy	779	1385	64			
Amine	121	32	79	71	75	0.19
not amine	625	1522	71			
Nitro	110	7	94	97	96	0.74
not nitro	64	2119	97			
Phenyl	888	11	99	64	70	0.21
not phenyl	826	575	41			

although the true category is negative. This must arise from the fact that the training set is not truly representative of the complete library, which is a direct consequence of the way of selecting the training set (only monofunctional, relatively simple compounds were selected to form a model of mutually exclusive categories).

Despite this, the prediction of nitro group can be said to be excellent, and that of carboxy group quite good. Even the two other classifiers are useful, as can be seen from their significantly non-zero transinformation property.

The authors are indebted to Dr. P. Bruck and Gy. Feller for creating the software and hardware link between the Nicolet 1180 and the PDP computers.

REFERENCES

1 P. C. Jurs, B. R. Kowalski, T. L. Isenhour and C. N. Reilley, Anal. Chem., 41 (1969) 1945.
2 R. W. Liddell III and P. C. Jurs, Appl. Spectrosc., 27 (1973) 371.
3 J. B. Justice and T. L. Isenhour, Anal. Chem., 46 (1974) 223.
4 D. R. Preuss and P. C. Jurs, Anal. Chem., 46 (1974) 520.
5 R. W. Liddell III and P. C. Jurs, Anal. Chem., 46 (1974) 2126.
6 H. B. Woodruff, S. R. Lowry, G. L. Ritter and T. L. Isenhour, Anal. Chem., 47 (1975) 2027.
7 H. B. Woodruff, G. L. Ritter, S. R. Lowry and T. L. Isenhour, Appl. Spectrosc., 30 (1976) 213.
8 L. N. Drozdow—Tichomirow, Opt. Spectrosc., 27 (1968) 77.
9 C. D. Baer and C. W. Brown, Appl. Spectrosc., 31 (1977) 524.
10 M. F. Delaney, P. C. Denzer, R. M. Barnes and P. C. Uden, Anal. Lett., 12 (1979) 963.
11 M. Penca, J. Zupan and D. Hadzi, Anal. Chim. Acta, 95 (1977) 3.
12 F. H. Heite, P. F. Dupuis, H. A. van't Klooster and A. Dijkstra, Anal. Chim. Acta, 103 (1978) 313.
13 K. Varmuza, Pattern Recognition in Chemistry, Springer-Verlag, Berlin, 1980.
14 P. C. Jurs and T. L. Isenhour, Chemical Applications of Pattern Recognition, Wiley, New York, 1975.
15 W. Meisel, Computer-Oriented Approach to Pattern Recognition, Academic Press, New York, 1972.
16 M. R. Anderberg, Cluster Analysis for Applications, Academic Press, New York, 1973.
17 L. Domokos and I. Frank, Anal. Chim. Acta, 133 (1981) 261.
18 E. Pretsch, T. Clerc, J. Seibl and W. Simon, Tabellen zur Strukturaufklärung organischer Verbindungen, Springer-Verlag, Berlin, Heidelberg, New York, 1976.
19 B. Everitt, Cluster Analysis, Heinemann, London, 1977.
20 J. Zupan, Clustering of Large Data Sets, Research Studies Press (Wiley), Chichester, 1982.

Analytica Chimica Acta, 154 (1983) 191—201
Elsevier Science Publishers B.V., Amsterdam — Printed in The Netherlands

DATA ANALYSIS IN GAS—LIQUID CHROMATOGRAPHY OF BENZENE DERIVATIVES

R. FELLOUS, L. LIZZANI-CUVELIER* and R. LUFT

Laboratoire de Chimie Organique, Institut Polytechnique Méditerranéen, Université de Nice, Parc Valrose, F-06034 Nice Cedex (France)

D. LAFAYE DE MICHEAUX

Laboratoire de Signaux et Systèmes, E.R.A. 835, 41, bd. Napoléon III, F-06200 Nice (France)

(Received 4th October 1982)

SUMMARY

With the final aim of predicting chromatographic retention data, a population of mono- and poly-functional benzenes was subjected to diverse methods of multivariate analysis. Numerical taxonomic aggregation indicated three clusters of stationary phases, the polyfluorinated ones behaving very differently from the polar or non-polar phases. Factor analysis was largely successful for the g.l.c. data prediction; the method is based on a multiparametric regression model.

Among various other possible uses, data analysis allows the prediction of retention data and also a global evaluation of solvent/solute interactions, without prejudice from the chemical nature of the solvents and solutes under study. Diverse techniques of data analysis have been employed in gas—liquid chromatography (g.l.c.); e.g., principal components analysis (p.c.a.) was used by Weiner and co-workers [1—4]. With the aid of p.c.a., Funke et al. [5] predicted the value of activity coefficients. Other workers [3, 6—10] succeeded in identifying principal components that strongly influence the very complex phenomenon of retention. Still others have pointed out the possibility of classification of solutes [11] and solvents [11—14] by p.c.a. Such solvent classification has also been achieved by means of numerical taxonomic methods [15, 16] and information theory [16, 17]. In practice, all these methods have been tested on the retention data series of either Rohrschneider [18] or McReynolds [19].

The structures of the substances chosen by these authors do not always give the opportunity of identifying separately each of the intramolecular interactions. It seemed that, on account of their structure, substituted benzenes would offer some advantages for a better evaluation of the interactions between the solvent and the solute skeleton on the one hand and between the solvent and the chemical function of the solute on the other hand. Unfortunately, the retention data for aromatic compounds [20—25]

0003-2670/83/$03.00

are not very numerous. For this reason, retention data were determined for 16 monofunctional benzenes (in such a way that the principal chemical functions of organic chemistry were represented), and of 110 difunctional and of 15 trifunctional benzenes. This data collection [26] was then subjected to analysis.

RESULTS AND DISCUSSION

Cluster analysis

Cluster analysis [26], one of the taxonomic methods, is appropriate for arranging phases to show any analogy in their chromatographic behaviour. The aim of this technique is to rank items by means of similarity or dissimilarity indices and by an amalgamation rule.

Figure 1 represents the tree diagram obtained by use of the BMDP 1M cluster analysis program [27]. The absolute value of the correlation coefficient was used for the evaluation of a "similarity" index of the stationary phases (Table 1). Three groups of stationary phase (A, B and C) appear and are easily identified. Within a given group, the correlation of one phase with another is always higher than, or at least identical to, the similarity level of the members of this group. Group A comprises the apolar or nearly apolar stationary phases (Apiezon-L, SE-30, DC-200, PMPE-5R, Apiezon-H and OV-17); the value of the phase correlation is better than 0.9661. The polyfluorinated phases constitute group B (OV-210, QF-1, DCL-5X); the value of the phase correlation is $\geqslant 0.9848$. The polar phases appear in group C (UCON-50 HB-2000, ULB-550X, NPGS, Carbowax 20M, XF-1150, FFAP, PDEAS,

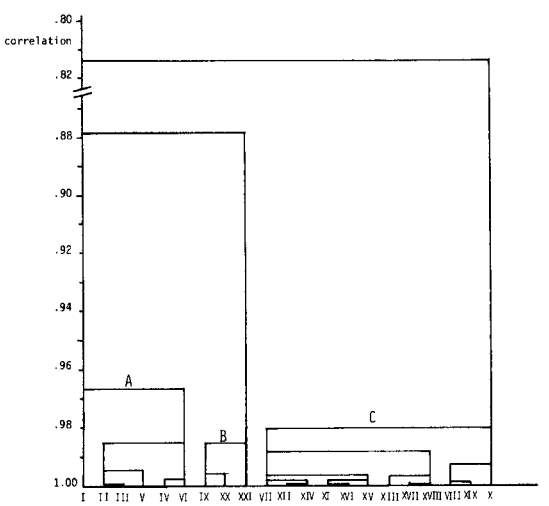

Fig. 1. Tree printed over correlation matrix clustering by the maximum distance method. I—X correspond to the stationary phases listed in Table 1.

TABLE 1

Cluster analysis of stationary phases

Variable (stationary phase)	Abbreviation	Number	Other boundary of cluster	Number of items in cluster	Similarity when cluster formed[a]
Apiezon-L	APIEZ-L	I	X	21	90.91
Silicone SE-30	SE-30	II	VI	5	99.23
Silicone DC-200	DC-200	III	II	2	99.95
Apiezon-H	APIEZ-H	V	II	3	99.70
Polyphenyl ether (5 rings)	PMPE-5R	IV	VI	2	99.86
Silicone OV-17	OV-17	VI	I	6	98.30
Silicone OV-210	OV-210	IX	XXI	3	99.24
Silicone QF-1	QF-1	XX	IX	2	99.77
Silicone DCL-5X	DCL-5X	XXI	I	9	93.90
UCON-50 HB-2000	UP	VII	X	12	99.01
Carbowax 20M	CRB-20M	XII	XIV	2	99.94
Free fatty acid phase	FFAP	XIV	VII	3	99.86
Neopentyl glycol succinate	NPGS	XI	XV	3	99.87
Diethyleneglycol adipate	DEGA	XVI	XI	2	99.97
Phenyldiethanolamine succinate	PDEAS	XV	VII	6	99.79
Silicone XF-1150	XF-1150	XIII	XVIII	3	99.81
Diethyleneglycol succinate	DEGS	XVII	XVIII	2	99.97
Ethyleneglycol succinate	EGS	XVIII	VII	9	99.39
ULB-550X	ULB-550X	VIII	X	3	99.62
Diethyleneglycol sebacate	DEGSEB	XIX	VIII	2	99.92
Silicone OV-225	OV-225	X	I	21	90.91

[a]Relation between correlation and similarity is given by: correlation = (similarity − 50) × 2/100.

DEGA, DEGS, EGS, DEGSEB, OV-225); the value of the phase correlations is $\geqslant 0.9802$.

Within each group, the behaviour of the stationary phases towards solutes is similar, although the chemical structure of these phases could be different. Linear relationships of excellent quality can be worked out for the retention data of two stationary phases of the same group. This is not the case for relationships concerning retention on phases belonging to two different groups. For a given cluster, these linear relationships fit the following model

$$\log t'(\phi Z, \Phi_1, T_1) = \alpha \log t'(\phi Z, \Phi_2, T_2) + \beta$$

where $\log t'$ represents the net retention time, ϕZ the solute, Φ_1 and Φ_2 the stationary phases, and T_1 and T_2 are temperatures. Using Kovats indices, one can find relationships of the same type. As an example, Table 2 shows the correlation of Kovats indices determined by Cook and Raushel [22] at 130°C, and the present retention data. Considering the complexity of the chromatographic phenomena and the mixed mechanisms that coexist, finding such linear relationships between series of retention data obtained under various working conditions is stimulating.

TABLE 2

Correlation of Kovats indices [22] and the present retention data ($I_{\phi-Z}$(Apiezon-L, 130°C) = 425.3 log ($t_{\phi-Z} - t_{CH_4}$) (Apiezon-L, 170°C) + 238.3. r = 0.9994).

ϕ—Z	Experimental Kovats index	log $t'_{\phi-Z}$[a]	Deviation between experimental and predicted value
Z = CH_3	800	1.3226	−0.6
F	680	1.0336	2.3
Cl	886	1.5236	−0.5
Br	986	1.7546	1.7
I	1109	2.0386	3.9
OMe	930	1.6106	6.5
CN	971	1.7356	−5.7
NO_2	1092	2.0056	0.5
NH_2	972	1.7366	−5.1
CHO	969	1.7276	−4.3
CH_2OH	1013	1.8316	−4.1
COMe	1069	1.9396	5.5

[a]This work.

Factor analysis

The BMDP 4M procedure [27] was selected. When applied to log t' values of the present series of retention data for 17 monofunctional benzenes measured on 21 stationary phases, factor analysis on the covariance matrix [28] provided a distribution of solutes and solvents amongst groups of similar characteristics, an identification, inasmuch as possible, of abstract factors with physical ones, and the prediction of retention data.

The products (solutes) or stationary phases (solvents) can be chosen either as the set of variables or as the set of cases. When the stationary phases constitute the set of variables, three abstract factors are needed in order that: (a) 99.8% of the total variance be taken into account; (b) the tendency of the phenomenon under study be restored; (c) the data matrix be reconstituted without too much loss of information.

The total variance is defined by the sum of the diagonal elements of the

TABLE 3

Eigenvalues for factor analysis

Factor	Variance explained by each factor	Cumulative proportion of total variance (%)
1	4.389	96.3
2	0.126	99.1
3	0.031	99.8

covariance matrix; the variance explained by each factor is the eigenvalue for that factor (Table 3). The same three factors also define the size of the factor space whose "3-dimensionality" is confirmed by the rotational technique. For this purpose, the VARIMAX procedure was applied as outlined previously [28]. The unrotated factor loading (i.e., correlations of the principal components with the original variables) (Table 4) of the first three principal components show that the first principal component is not discriminating, although highly representative for all stationary phases. Polar phases are differentiated from apolar and polyfluorinated phases by the second principal component. However, plotting the loadings of factor 2 against those of factor 3 (Fig. 2) shows a distribution of stationary phases over three groups, i.e., apolar group A, polyfluorinated group B, and polar group C.

This result is consistent with the preceding cluster analysis. Factor 2 can be associated in different ways with the polarity of the stationary phase

$$\text{factor } 2 = -0.161 \times 10^{-3}\, P + 0.373 \quad (r = 0.901; n = 18)$$

where P is the polarity factor of McReynolds [29], r is the multiple correlation coefficient, and n is the number of the dependent variables;

TABLE 4

Unrotated factor loadings for principal components

Variable	Factor 1	Factor 2	Factor 3
Apiezon-L	0.9119	0.3521	−0.2060
SE-30	0.9471	0.3014	−0.0823
DC-200	0.9427	0.3064	−0.0971
PMPE-5R	0.9771	0.1980	−0.0581
Apiezon-H	0.9397	0.3185	−0.1221
OV-17	0.9672	0.2370	−0.0762
UCON-50 HB-2000	0.9922	−0.1037	−0.0535
ULB-550X	0.9959	−0.0369	−0.0454
OV-225	0.9988	0.0177	0.0280
NPGS	0.9960	−0.0779	0.0064
Carbowax-20M	0.9897	−0.1325	−0.0124
XF-1150	0.9931	−0.0907	0.0661
FFAP	0.9876	−0.1472	−0.0248
PDEAS	0.9932	−0.1072	−0.0166
DEGA	0.9938	−0.1097	−0.0054
DEGS	0.9913	−0.1175	0.0090
EGS	0.9907	−0.1224	0.0284
DEGSEB	0.9961	−0.0694	−0.0358
OV-210	0.9418	0.2603	0.2075
DCL-5X	0.9596	0.2141	0.1654
QF-1	0.9322	0.2834	0.2182

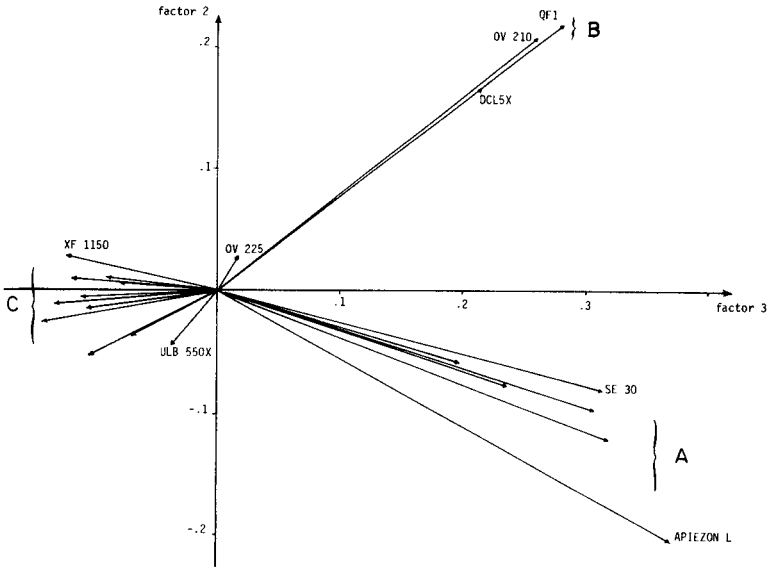

Fig. 2. Unrotated factor loadings.

factor 2 = $-2.452\ Z_1 + 0.083$ ($r = 0.935$; $n = 14$)

where Z_1 is the polarity factor of Wold and Andersson [12];

factor 2 = $-0.056\ X + 0.120$ ($r = 0.944$; $n = 14$)

where X is the polarity factor of Lowry et al. [14].

TABLE 5

Factor scores

Case ϕ—Z	Factor 1	Factor 2	Factor 3
Z = H	−1.734	−0.744	−0.227
CF_3	−1.646	−0.064	1.384
CH_3	−1.215	0.193	−0.665
OMe	−0.232	0.272	−0.409
Br	−0.130	0.692	−1.061
Cl	−0.619	0.433	−0.323
F	−1.569	−0.476	0.605
I	0.440	1.130	−1.869
CHO	0.404	0.290	1.011
SH	0.210	0.201	−1.292
COOMe	0.718	1.070	−0.223
CN	0.651	0.277	1.812
$COCH_3$	0.850	0.860	0.804
NH_2	0.725	−1.037	0.006
NO_2	1.114	0.810	1.181
CH_2OH	1.015	−1.026	−0.333
OH	1.018	−2.880	−0.400

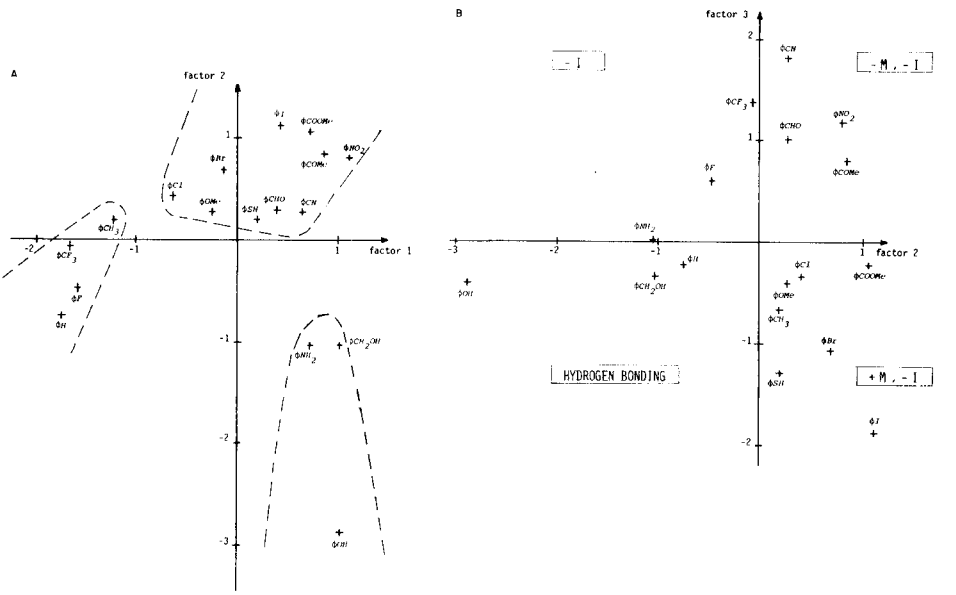

Fig. 3. Factor scores for each case. A, Factor 1, factor 2 plane; B, factor 2, factor 3 plane. For details, see text.

TABLE 6

Application of the relationship $\log t'_{\phi Z,\Phi_i} = a_{\Phi_i} \log t'_{\phi Z,SE\text{-}30} + b_{\Phi_i} \log t'_{\phi Z,OV210} + c_{\Phi_i} \log t'_{\phi Z,DEGS} + d_{\Phi_i}$ to monofunctional benzenes

Φ_i	a_{Φ_i}	b_{Φ_i}	c_{Φ_i}	d_{Φ_i}	r[a]	$\sigma_{e,\Phi}$[b]
Apiezon-L	1.753	−0.268[c]	−0.047[c]	−0.012	0.9916	0.05
DC-200	1.112	−0.025[c]	−0.005[c]	0.149	0.9993	0.01
PMPE-5R	1.158	0.092[c]	0.229	−0.334	0.9953	0.05
Apiezon-H	1.472	−0.029[c]	−0.007[c]	−0.040	0.9926	0.05
OV-17	1.141	0.067[c]	0.127[c]	−0.061	0.9940	0.05
UCON-50 HB-2000	0.410	−0.233[c]	0.808	0.428	0.9967	0.04
ULB-550X	0.536	−0.124[c]	0.614	0.149	0.9968	0.04
OV-225	0.256	0.252	0.541	0.116	0.9988	0.03
NPGS	0.160[c]	0.043[c]	0.782	0.137	0.9984	0.03
Carbowax-20M	0.046[c]	−0.057[c]	0.934	−0.472	0.9960	0.05
XF-1150	−0.315	0.342	0.832	0.336	0.9991	0.02
FFAP	0.122[c]	−0.174[c]	0.980	0.511	0.9979	0.04
PDEAS	0.125[c]	−0.049[c]	0.913	0.123	0.9975	0.04
DEGA	0.085[c]	−0.016[c]	0.901	0.380	0.9982	0.04
EGS	−0.149[c]	0.105[c]	0.975	0.060	0.9994	0.02
DEGSEB	0.375	−0.099[c]	0.754	0.472	0.9975	0.04
QF-1	−0.019[c]	0.935	−0.030[c]	0.339	0.9966	0.03
DCL-5X	0.156[c]	0.879	0.103	−0.712	0.9975	0.03

[a]Multiple correlation coefficient. [b]Standard error of estimate. [c]Fischer's Test > 2%.

In each case (solute), examination of factor scores (Table 5, Fig. 3) leads to the following conclusions. In Fig. 3A, one cluster contains substances with a group that can undergo hydrogen bonding with polar stationary phases and another contains substances showing very short retention times on all phases. Figure 3B shows the influence of the third solute factor. Its action leads to distribution of the products taking into account the electronic effects of their functional group (—I, +I, —M, +M effects and hydrogen bonding).

The same scores may be used as the input in stepwise regression analyses (BMDP 2R program [27]). The following scores were obtained when stepwise regression was applied to factor scores, considered as the dependent variables, and to potential predictors, e.g., physical constants of solutes, considered as the independent variables

factor 1 = —1.977 log p + 5.833 (r = 0.994; n = 17)

TABLE 7

Application of the relationship $\log t'_{\phi Z_1Z_2,\Phi i} = a_{\Phi_i} \log t'_{\phi Z_1Z_2,\text{SE-30}} + b_{\Phi_i} \log t'_{\phi Z_1Z_2,\text{OV210}} + c_{\Phi_i} \log t'_{\phi Z_1Z_2,\text{DEGS}} + d_{\Phi_i}$ to polyfunctional benzenes

Disubstituted benzenes	Φ_i	a_{Φ_i}	b_{Φ_i}	c_{Φ_i}	d_{Φ_i}	r[a]	$\sigma_{e,\Phi}$[b]
Ortho	Carbowax-20M	—0.045[c]	0.029[c]	0.972	—0.016	0.979	0.08
	ULB-550X	0.482	—0.278	0.682	0.363	0.993	0.04
	OV-225	0.221	0.290	0.510	0.062	0.997	0.02
	PDEAS	0.247[c]	0.017[c]	0.813	0.058	0.994	0.04
	Apiezon-L	1.385	—0.139[c]	—0.094[c]	0.221	0.996	0.03
	PMPE-5R	1.066	0.108	0.140	—0.181	0.999	0.02
Meta	Carbowax-20M	0.142[c]	—0.056[c]	1.030	—0.421	0.995	0.04
	ULB-550X	0.811	—0.170[c]	0.510	—0.072	0.995	0.03
	OV-225	0.256	0.269	0.543	—0.056	0.999	0.01
	PDEAS	0.245[c]	0.059[c]	0.851	—0.111	0.998	0.03
	Apiezon-L	1.393	—0.185[c]	—0.039[c]	0.170	0.997	0.02
	PMPE-5R	0.760	0.327[c]	0.253[c]	—0.210	0.976	0.07
Para	Carbowax-20M	—0.026[c]	—0.115[c]	1.117	—0.210	0.995	0.04
	ULB-550X	0.157[c]	—0.085[c]	0.768	0.431	0.985	0.06
	OV-225	0.210	0.244	0.574	0.005	0.999	0.02
	PDEAS	0.263	—0.006[c]	0.872	—0.059	0.996	0.03
	Apiezon-L	1.530	—0.178	—0.120	0.096	0.995	0.03
	PMPE-5R	1.294	0.002[c]	0.119[c]	—0.376	0.995	0.04
Tri-substituted benzenes	Carbowax-20M	—1.460[c]	—1.080	2.832	0.511	0.992	0.06
	ULB-550X	0.987	—0.002[c]	0.247	0.178	0.999	0.01
	OV-225	0.391[c]	0.443	0.293	0.105	0.999	0.02
	PDEAS	0.421	0.178	0.707	—0.084	0.999	0.01
	Apiezon-L	1.631	—0.213	—0.053[c]	0.031	0.998	0.01
	PMPE-5R	0.912	0.036[c]	0.342	—0.080	0.999	0.01

[a—c]See Table 6.

TABLE 8

Equation (1) applied to McReynolds retention data
($I_{RZ,\Phi_i} = a'_{\Phi_i} I_{RZ,SE\text{-}30} + b'_{\Phi_i} I_{RZ,DC1265F} + c'_{\Phi_i} I_{RZ,DEGS} + d'_{\Phi_i}$)[a]

Φ_i	a'_{Φ_i}	b'_{Φ_i}	c'_{Φ_i}	d'_{Φ_i}	r[b]	$\sigma_{e,\Phi}$[c]
Apiezon-L	1.255	−0.010[d]	−0.119[d]	−57.63	0.9814	29.0
Carbowax-20M	0.518	−0.324	0.856	−141.23	0.9986	9.2
DEGA	0.277	−0.178	0.917	−95.89	0.9993	6.7
DEGSEB	0.565	−0.163	0.618	−78.11	0.9988	7.7
Di-2-ethylhexyl sebacate	0.773	−0.061[d]	0.224	−13.70	0.9986	6.9
Diisodecyl phthalate	0.711	0.058[d]	0.198	−22.38	0.9982	8.5
EGS	0.636	−0.186	0.581	−84.18	0.9986	8.4
NPGS	0.372	−0.054[d]	0.679	−81.54	0.9990	7.3
PMPE-5R	0.693	0.199	0.144	−15.41	0.9989	7.2
UCON-50 HB-2000	0.688	−0.292	0.640	−124.63	0.9991	6.6
XF-1150	−0.117[d]	0.359	0.738	−108.30	0.9966	15.5
Tricresyl phosphate	0.589	−0.011[d]	0.423	−54.97	0.9980	9.8

[a]R = tBu, iBu, sBu, nBu, nPent, nHex; Z = OH, CHO, COMe, COOMe, OMe. [b–d]See footnotes a–c, Table 6.

TABLE 9

Equation (1) applied to Rohrschneider's retention data
($I_{RZ,\Phi_i} = a'_{\Phi_i} I_{RZ,DC200} + b'_{\Phi_i} I_{RZ,QF1} + c'_{\Phi_i} I_{RZ,DEGS} + d'_{\Phi_i}$)

Φ_i	a'_{Φ_i}	b'_{Φ_i}	c'_{Φ_i}	d'_{Φ_i}	r[b]	$\sigma_{e,\Phi}$[c]
Squalane	1.144	−0.071[d]	−0.059	−4.013	0.9962	13.4
Apiezon-L	1.110	−0.109[d]	0.012[d]	−5.080	0.9927	18.1
Diethylhexylsebacate	0.866	−0.100[d]	0.185	21.228	0.9957	12.4
Celanese ester NR9	0.842	−0.081[d]	0.202	11.886	0.9965	11.3
Diisodecylphthalate	0.736	0.074[d]	0.160	10.033	0.9965	11.1
DC-710	0.705	0.201	0.121	−11.308	0.9949	14.1
Polypropyleneglycol	0.815	−0.225	0.345	22.350	0.9922	17.3
Acetyltributylcitrate	0.612	0.065[d]	0.297	3.807	0.9947	14.3
Tricresylphosphate	0.562	0.040[d]	0.371	8.969	0.9959	13.1
PMPE	0.639	0.206	0.229	−36.985	0.9911	19.9
Marlophene-87	0.603	−0.140[d]	0.472	19.780	0.9931	17.6
Polypropylenesebacate	0.630	−0.081[d]	0.434	−2.142	0.9973	11.1
Marlophene-814	0.552	−0.174	0.560	19.480	0.9938	17.9
NPGS	0.321	0.040[d]	0.605	5.300	0.9957	16.3
XF-1150	−0.015[d]	0.433	0.543	4.811	0.9961	15.9
Carbowax-20M	0.442	−0.210	0.755	−13.486	0.9923	24.0
Carbowax-4000	0.433	−0.222	0.775	−14.974	0.9931	23.1
Reoplex-400	0.334	−0.106	0.785	−22.634	0.9981	12.5
Ethyleneglycol-cyanoethyl ether	−0.368	0.492	0.953	−64.168	0.9988	13.1
1,2,3-Tris(2-cyano-ethoxy)propane	−0.510	0.462	1.096	−35.029	0.9988	14.3

or factor 1 = 2.237×10^{-2} b.p.— 3.627 ($r = 0.992$; $n = 17$)

factor 2 = $-1.671\ R - 0.016\ \Delta H_v + 1.876$ ($r = 0.999$; $n = 17$)

factor 3 = $0.0718\ \epsilon - 9.418 \log (SR) - 0.721 \log p + 6.936$ ($r = 0.999$; $n = 17$)

It can be seen that for factor 1 the sequence of scores is analogous to that of the boiling points (b.p.) of solutes and also of the logarithm of their vapour pressures (log p). In a similar way, factor 2 seems to be related to the polar substituent constants of the solutes (the resonance constant R of Swain and Lupton [30] and the heat of vaporization, ΔH_v), whereas the third factor can be correlated with the dielectric constant, ϵ, and the logarithm of the electronegativity constant (SR) of functional groups Z.

Regression model

Numerical taxonomic analysis and factor analysis of the present retention data both lead to classification of the stationary phases into three clusters. Therefore, prediction of retention data cannot lead to satisfactory results when undertaken with only two parameters. However, when polyfluorinated phases are listed in a separate category, an appropriate regression model can be obtained

$$x_{Q,\Phi_i} = a_{\Phi_i} x_{Q,\Phi_A} + b_{\Phi_i} x_{Q,\Phi_B} + c_{\Phi_i} x_{Q,\Phi_C} + d_{\Phi_i} \quad (1)$$

where x_{Q,Φ_i} are the dependent variables and represent the retention data of solute Q on phase Φ_i; a_{Φ_i}, b_{Φ_i} and c_{Φ_i} are the regression coefficients, and d_{Φ_i} is the intercept; and x_{Q,Φ_A}, x_{Q,Φ_B}, x_{Q,Φ_C} are the independent variables and represent the retention data of the same solute Q on phases Φ_A, Φ_B and Φ_C corresponding to the best representatives within each phase cluster. These representatives can be selected by multiple regression [26], factor analysis [28] or discriminant analysis [28] among other methods. Each of these methods was tested and SE-30, OV-210 and DEGS were found to be the best independent variables.

Tables 6 and 7 concern such a prediction established with the aid of the present retention data for the series of monofunctional benzenes and of polyfunctional benzenes. Equation (1) seems to be of general applicability; when fitted to the retention data of McReynolds [19] (Table 8) and to those of Rohrschneider [18] (Table 9), good agreement is observed between the initial and predicted matrix data.

REFERENCES

1 P. H. Weiner and D. G. Howery, Can. J. Chem., 50 (1972) 448.
2 P. H. Weiner and D. G. Howery, Anal. Chem., 44 (1972) 1189.
3 P. H. Weiner, C. Dack and D. G. Howery, J. Chromatogr., 69 (1972) 249.
4 D. G. Howery, P. H. Weiner and J. S. Blinder, J. Chromatogr. Sci., 12 (1974) 366.
5 P. T. Funke, E. R. Malinowski, D. E. Martire and L. Z. Pollara, Sep. Sci., 1 (1966) 661.

6 R. B. Selzer and D. G. Howery, J. Chromatogr., 115 (1975) 139.
7 J. H. Kindsvater, P. H. Weiner and T. J. Klingen, Anal. Chem., 46 (1974) 982.
8 D. G. Howery, Anal. Chem., 46 (1974) 829.
9 J. F. K. Huber, E. T. Alderlieste, H. Harren and H. Poppe, Anal. Chem., 45 (1973) 1337.
10 P. H. Weiner and J. F. Parcher, Anal. Chem., 45 (1973) 302.
11 M. Chastrette, J. Chromatogr. Sci., 14 (1976) 357.
12 S. Wold and K. Andersson, J. Chromatogr., 80 (1973) 43.
13 D. H. McCloskey and S. J. Hawkes, J. Chromatogr. Sci., 13 (1975) 1.
14 S. R. Lowry, G. L. Ritter, H. S. Woodruff and T. L. Isenhour, J. Chromatogr. Sci., 14 (1976) 126.
15 D. L. Massart, P. Lenders and M. Lauwereys, J. Chromatogr. Sci., 12 (1974) 617.
16 A. Eskes, F. Dupuis, A. Dijkstra, H. De Clercq and D. L. Massart, Anal. Chem., 47 (1975) 2168.
17 F. Dupuis and A. Dijkstra, Anal. Chem., 47 (1975) 379.
18 L. Rohrschneider, J. Chromatogr., 22 (1966) 6.
19 W. O. McReynolds, Gas Chromatographic Retention Data, Preston Technical Abstracts Company, Evanston, IL, 1966.
20 B. L. Karger, Y. Elmehrik and W. Andrade, J. Chromatogr. Sci., 7 (1969) 209.
21 M. Kremser, M. Jernejcic and L. Premru, J. Chromatogr., 65 (1972) 129.
22 L. E. Cook and F. M. Raushel, J. Chromatogr., 65 (1972) 556.
23 S. D. West and R. C. Hall, J. Chromatogr. Sci., 13 (1975) 5.
24 G. H. E. Nieuwdorp, C. L. De Ligny and N. G. van der Veen, J. Chromatogr., 154 (1978) 133.
25 J. Grzybowski, H. Lamparczyk, A. Nasal and A. Radecki, J. Chromatogr., 196 (1980) 217.
26 R. Fellous, D. Lafaye de Micheaux, L. Lizzani-Cuvelier and R. Luft, J. Chromatogr., 213 (1981) 223.
27 W. J. Dixon, Biomedical Computer Programs, University of California Press, Berkeley, LA, 1981.
28 R. Fellous, D. Lafaye de Micheaux, L. Lizzani-Cuvelier and R. Luft, J. Chromatogr., 248 (1982) 35.
29 W. O. McReynolds, J. Chromatogr. Sci., 8 (1970) 685.
30 Cited in C. Hansch, A. Leo, S. H. Unger, K. H. Kim, D. Nikaitani and E. J. Lien, J. Med. Chem., 11 (1973) 1207.

Analytica Chimica Acta, 154 (1983) 203—209
Elsevier Science Publishers B.V., Amsterdam — Printed in The Netherlands

QUANTITATIVE NMR SPECTROMETRY OF PHASE-TRANSFER CATALYSTS
Part 1. Determination of Extraction Constants and Water of Hydration

RAPHAEL BAR, LILIANA KARPUJ-BAR and YOEL SASSON*
Casali Institute of Applied Chemistry, The Hebrew University, Jerusalem (Israel)
JOCHANAN BLUM*
Department of Organic Chemistry, The Hebrew University, Jerusalem (Israel)
(Received 3rd June 1983)

SUMMARY

Proton magnetic resonance spectrometry was applied for evaluation of the distribution ratios and apparent extraction constants of tetraalkylammonium and tetraalkylphosphonium salts in two liquid-phase systems. Triethylbenzyl- and tetrabutylammonium chloride in dichloromethane and chlorobenzene, respectively, were shown to be salted out in the presence of aqueous sodium hydroxide solutions. ^{1}H-n.m.r. spectrometry was also used to determine the degree of hydration of quaternary onium salts in two-phase systems. The results were compatible with those obtained by the Karl Fischer method.

Phase-transfer catalysis is widely applied in organic and inorganic synthesis [1—3]. However, the lack of simple methods for rapid determination of the distribution of the onium salts between the immiscible layers, often makes mechanistic studies very difficult (see, e.g., [3, 4]). Among the current methods, the most frequently applied are two-phase titration [3], electric conductivity [5], selective ion electrode measurements [4], ultraviolet spectrophotometry [6] and halide radioisotope counting [7, 8]. High-performance liquid chromatography [9] has, so far, been used only to a limited extent.

The present paper is concerned with the application of ^{1}H-n.m.r. for the determination of both distribution ratios and apparent extraction constants of some typical phase-transfer catalysts as well as the determination of co-extracted water of hydration of the onium salts in the organic layer.

EXPERIMENTAL

Reagents and equipment

The various quaternary ammonium and phosphonium salts (Fluka or Aldrich Chemicals Co.) were of highest grade available and were used without further purification. Dichloromethane, chloroform, chlorobenzene and *o*-dichlorobenzene were purified by standard methods [10] prior to use.

0003-2670/83/$03.00

The ^{1}H-n.m.r. spectra were taken on a Bruker FT HW-300 instrument. Deuterochloroform was used as solvent for the measurements listed in Table 1. All other n.m.r. measurements were done in non-deuterated solvents using 1% TMS as internal reference and a capillary with D_2O for external lock.

Procedures

System equilibration and onium salt determination. A water-saturated organic solution (5 ml) containing either an ammonium or phosphonium salt (0.1 M) and durene (0.05 M) (internal standard), was stirred vigorously for

TABLE 1

300-MHz ^{1}H-n.m.r. data for some quaternary onium salts in deuterochloroform

Compound	Chemical shift, δ (ppm)
Tetraethylammonium bromide	1.395 (12, t, J = 7.4 Hz), 3.489 (8, q, J = 7.4 Hz)
Tetrapropylammonium bromide	1.063 (12, t, J = 6.8 Hz), 1.781 (8, m), 3.364 (8, br t, J = 8.4 Hz)
Triethylbenzylammonium bromide	1.476 (9, t, J = 6.7 Hz), 3.448 (6, q, J = 6.7 Hz), 4.796 (2, s), 7.509 (5, m)
Methyltributylammonium bromide	1.012 (9, t, J = 7.4 Hz), 1.455 (6, m), 1.697 (6, m), 3.322 (3, s), 3.473 (6, br t, J = 9.0 Hz)
Ethyltributylammonium bromide	1.017 (9, t, J = 7.4 Hz), 1.451 (6, m), 1.697 (6, m), 3.337 (6, br t, J = 9.0 Hz), 3.553 (2, q, J = 7.4 Hz)
Tetrabutylammonium chloride	1.013 (12, t, J = 7.2 Hz), 1.464 (8, m), 1.691 (8, m), 3.375 (8, br t, J = 8.4 Hz)
Tetrabutylammonium bromide	1.016 (12, t, J = 7.2 Hz), 1.469 (8, m), 1.692 (8, m), 3.357 (8, br t, J = 8.4 Hz)
Tetrabutylammonium iodide	1.022 (12, t, J = 7.2 Hz), 1.490 (8, m), 1.706 (8, m), 3.379 (8, br t, J = 8.4 Hz)
Tetrabutylammonium hydrogensulfate	0.986 (12, t, J = 7.4 Hz), 1.453 (8, m), 1.643 (8, m), 3.284 (8, br t, J = 8.4 Hz), 9.843 (1, s)
Tetrabutylphosphonium bromide	0.984 (12, t, J = 7.0 Hz), 1.546 (16, m), 2.459 (8, m).
Tetrapentylammonium bromide	0.940 (12, t, J = 7.0 Hz), 1.398 (16, m), 1.692 (8, m), 3.336 (8, br t, J = 8.6 Hz)
Tetrahexylammonium chloride	0.899 (12, t, J = 7.0 Hz), 1.344 (24, m), 1.692 (8, m), 3.387 (8, br t, J = 8.6 Hz)
Tetrahexylammonium bromide	0.898 (12, t, J = 6.9 Hz), 1.345 (24, m), 1.689 (8, m), 3.351 (8, br t, J = 9.0 Hz)
Tetrahexylammonium hydrogensulfate	0.866 (12, t, J = 7.0 Hz), 1.328 (24, m), 1.656 (8, m), 3.298 (8, br t, J = 8.4 Hz), 9.840 (1, s)
Tetraheptylammonium bromide	0.889 (12, t, J = 6.8 Hz), 1.292 (16, m), 1.377 (16, m), 1.684 (8, m), 3.346 (8, br t, J = 8.4 Hz)
Tetraoctylammonium bromide	0.884 (12, t, J = 6.9 Hz), 1.279 (40, m), 1.688 (8, m), 3.375 (8, br t, J = 8.4 Hz)
Tetradodecylammonium bromide	0.883 (12, t, J = 6.7 Hz), 1.261 (72, m), 1.684 (8, m), 3.378 (8, br t, J = 8.0 Hz).

1 h at constant temperature (±0.5°C) with an equal volume of an aqueous solution (pre-saturated with the organic solvent) of the appropriate inorganic compound. The n.m.r. spectrum of the organic layer was recorded both prior to mixing and after equilibration of the two phases. The concentration of the onium salt was then calculated from the peak integrals.

Systems in which the aqueous phase contained sodium hydroxide were stirred only for 15 min to avoid Hofmann degradation of the quaternary ammonium salts.

Determination of water content of the organic layer. The water signal was identified either by addition of D_2O or anhydrous magnesium sulfate to the n.m.r. tube. Comparative results were obtained with the aid of the Karl Fischer reagent (electrometric end-point determination).

RESULTS AND DISCUSSION

Distribution ratios and apparent extraction constants

The 300-MHz ^{1}H-n.m.r. spectra of common phase-transfer catalysts (see Table 1) have distinguishable resonance bands that can be integrated with great accuracy. The best signals for this purpose are generally the high-field CH_3 triplets.

Two important extraction parameters of the onium salts [11] can be deduced from these spectra: (i) the distribution ratio between the organic and aqueous phases, D, which is defined as $D = [Q^+X^-]_o/[Q^+]_w$; and the extraction constant, K_{ex}, defined as $K_{ex} = [Q^+X^-]_o/[Q^+]_w[X^-]_w$, where $[Q^+X^-]_o$, $[Q^+]_w$ and $[X^-]_w$ are the concentrations of the phase-transfer catalyst ion pair, of the onium cation and of the counter anion in the respective immiscible layers.

The data for several quaternary ammonium and phosphonium salts are given in Table 2. Very few D and K_{ex} values have so far been reported for onium salts in two-phase water—organic liquid systems at room temperature. Among those studied is that of tetrabutylammonium bromide in dichloromethane–water which was found by titrimetric analysis to be $K_{ex} = 47\ M^{-1}$ [12]. This value is in good agreement with the present result ($K_{ex} = 44.8\ M^{-1}$). It should be noted that the present calculations are based on the average of at least three measurements with standard deviation of $\leqslant 1.8\%$.

As expected, the extractability proved to depend on the nature of both the cation and the anion. Figure 1 shows the variations in distribution of some symmetric tetraalkylammonium bromides between chloroform and water. Substitution of the ammonium ion by the corresponding phosphonium ion increases the lipophilicity of the phase-transfer catalyst. For one and the same ammonium cation with different counter anions, the hydrophilicity decreases in the order $Br > Cl > HSO_4$ (Table 2).

Under phase-transfer conditions, the rates of many reactions can be increased by applying a fairly concentrated sodium hydroxide solution as the aqueous phase [1—3]. This fact was interpreted in terms of a salting-out

TABLE 2

Distribution ratios (D) and apparent extraction constants (K'_{ex}) of quaternary onium salts in two liquid phase systems at 25°C[a]

Quaternary salt	Solvent	D	K'_{ex} (M^{-1})
Tetrabutylammonium hydrogensulfate	chloroform	6×10^{-4}	6×10^{-2}
Methyltributylammonium bromide	chloroform	0.101	1.15
Ethyltributylammonium bromide	chloroform	0.111	1.24
Tetrabutylammonium bromide	chloroform	1.67	44.8
Tetrapentylammonium bromide	chloroform	4.05	205
Tetrabutylphosphonium bromide	chloroform	6.14	439
Tetrahexylammonium bromide	chloroform	∞	∞
Tetrabutylammonium chloride	dichloromethane	4×10^{-2}	0.8
Tetrahexylammonium chloride	dichloromethane	10.9	2.59×10^{3}
Tetrahexylammonium hydrogensulfate	*o*-dichlorobenzene	3.59	330

[a]Initial salt concentrations: 0.1 M in chloroform and 0.05 M in dichloromethane and *o*-dichlorobenzene.

effect. With the aid of proton magnetic resonance, the extent of this effect can be evaluated quantitatively. Figure 2 demonstrates the changes in content of the widely applied triethylbenzylammonium chloride, $[TEBA]^+[Cl]^-$, in dichloromethane on variation of the concentration of sodium hydroxide in the aqueous phase. A typical salting-out effect occurs when the hydroxide ion concentration exceeds 20%. It should be noted, however, that these

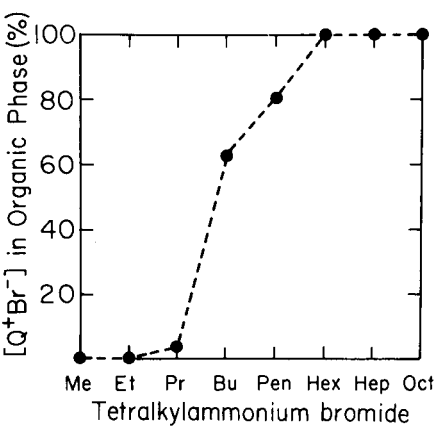

Fig. 1. Dependence of the extractability of tetra-n-alkylammonium bromides on the chain length of the alkyl groups in a water—chloroform system. Initial onium salt concentration 0.1 M, temperature 25°C.

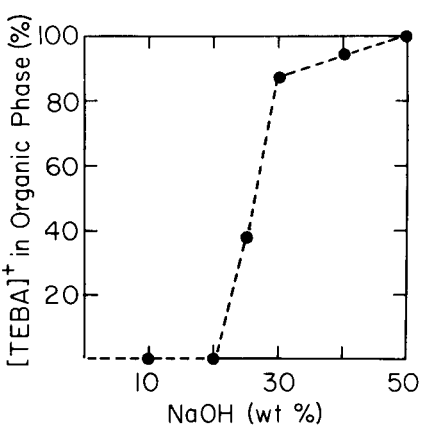

Fig. 2. Percentage of triethylbenzylammonium cation in dichloromethane after equilibration with aqueous sodium hydroxide solutions. Initial ammonium ion concentration 0.1 M; temperature 25°C.

measurements give the assay of the total tetraalkylammonium salt and do not differentiate between the ammonium—chloride and —hydroxide ion-pairs. The latter, however, has been assumed to be present only in minor quantities, if at all [2].

A similar sodium hydroxide-assisted salting-out effect was found in the tetrabutylammonium chloride/water—chlorobenzene system (Fig. 3).

Degree of hydration of quaternary onium salts

The ^{1}H-n.m.r. technique was also found to be useful for determination of the water co-extracted with the quaternary onium salt. As shown in Table 3, the values for chloroform-extracted water are similar to those obtained from the Karl Fischer method. These data, and the reported value for the solubility of water in chloroform (1.5 g l^{-1} at 22°C [13]), make it possible to calculate the degree of salt hydration in this solvent. The limited hydration that generally takes place in chloroform can be rationalized by the competitive complexation of the onium salt with the chloroform via hydrogen bonding [14]. Solvent that cannot form hydrogen bonds with the phase-transfer catalyst promotes indeed a higher degree of hydration. Thus, for example, tetrabutylammonium chloride that is hydrated in chloroform to an extent of 0.72 (0.50 according to the studies of Frolo et al. [15]) attracts 2.29 mol of water per mole of the salt in nitrobenzene [15]. Even the lipophilic tetrahexylphosphonium chloride is hydrated to a high extent (3.4) in non-hydrogen-bonding chlorobenzene [16].

As the degree of hydration reflects the extractability of the ion-pair, tetrabutylammonium formate [17] would be expected to co-extract the highest number of water molecules. This effect is, however, masked by the strong

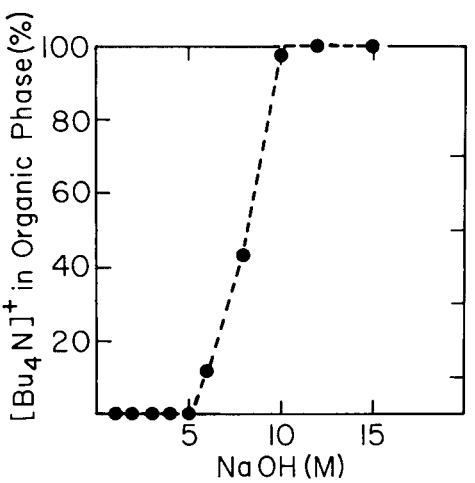

Fig. 3. Percentage of tetrabutylammonium cation in chlorobenzene after equilibration with aqueous sodium hydroxide solution. Initial ammonium ion concentration 0.1 M; temperature 25°C.

TABLE 3

Water of hydration of quaternary onium salts distributed between chloroform and aqueous solutions of the corresponding inorganic or carboxylic salts[a]

Quaternary salt	$(C_4H_9)_4N^+Cl^-$	$(C_4H_9)_4N^+HSO_4^-$	$(C_4H_9)N^+HCO_2^-$	$(C_6H_{13})_4N^+Cl^-$
Aqueous salt	KCl	$NaHSO_4$	NaOCHO	KCl
D	13.1	6.14	1.21	∞
$[H_2O]/[Q^+X^-]$ from n.m.r. measurements	1.63	1.41[b]	2.23	1.34
$[H_2O]/[Q^+X^-]$ by Karl Fischer method	1.65	1.45	2.30	1.41
Degree of hydration	0.72	0.45	0.71	0.51
δ_{H_2O} (ppm)	2.592	4.723	3.043	2.588

[a]Initial concentration of ammonium salt in chloroform 0.1 M; concentration of inorganic salt in water 4 M; system temperature 20°C. [b]The contribution of the hydrogensulfate proton to the n.m.r. signal was subtracted from the integral.

interaction of the formate with the chloroform. Thus the degree of hydration is only 0.71.

Finally the chemical shift of the extracted water can be regarded as a qualitative indicator for the degree of association of water molecules with the onium ion-pair. Owing to fast proton exchange between the chloroform-soluble water ($\delta \sim 1.6$ ppm at 33°C [18]) and the water of salt hydration at equilibrium $[H_2O]_{CHCl_3} \rightleftharpoons [H_2O]_{Q^+X^-}$, the observed resonance peak is shifted downfield. Thus, the respective signal of hydrated tetrabutylammonium formate, which interacts with water more strongly than the corresponding chloride, appears at a lower field (see Table 3). The large chemical shift of hydrated tetrabutylammonium hydrogensulfate (4.723 ppm) is the mean value of chloroform-soluble water, of the acidic sulfate proton (9.843 ppm) and of the water associated with the quaternary ammonium salt.

We are grateful to the U.S.—Israel Binational Science Foundation (BSF) for financial support of this study.

REFERENCES

1 C. M. Starks and C. Liotta, Phase Transfer Catalysis. Principles and Applications, Academic Press, New York, 1978.
2 E. V. Dehmlow and S. S. Dehmlow, Phase Transfer Catalysis, Verlag Chemie, Weinheim, 1980.
3 A. Brändström, Preparative Ion-Pair Extraction, Apotekarsocieteten and Hässle, Läkemedel, 1976.
4 E. Gordon and R. E. Kutina, J. Am. Chem. Soc., 99 (1977) 3903.
5 M. A. Manvelyan, G. L. Neugodova and L. I. Boguslavskii, Sov. Electrochem., 12 (1976) 310.
6 T. Kenjo, S. Brown, E. Held and R. M. Diamond, J. Phys. Chem., 76 (1972) 1775.
7 C. M. Starks and R. M. Owens, J. Am. Chem. Soc., 95 (1973) 3613.
8 H. J. James, G. P. Carmack and H. Freiser, Anal. Chem., 44 (1972) 853.

9 V. T. Wee and J. M. Kennedy, Anal. Chem., 54 (1982) 1631.
10 D. D. Penin, W. L. F. Armarego and D. R. Perrin, Purification of Laboratory Chemicals, Pergamon Press, Oxford, 1966.
11 A. Brändström, Pure Appl. Chem., 54 (1982) 1769.
12 A. Brändström, Adv. Phys. Org. Chem., 15 (1977) 267.
13 T. V. Healy, J. Inorg. Nucl. Chem., 19 (1961) 328.
14 R. M. Venable and T. D. Doyle, J. Assoc. Off. Anal. Chem., 60 (1977) 52.
15 Yu, G. Frolo, V. V. Sergievskii, A. V. Ochkin and A. P. Zuev, Sov. Radiochem., 14 (1971) 664; Chem. Abstr., 78 (1973) 8479u.
16 D. Landini, A. M. Maia and F. Montanari, J. Chem. Soc. Chem. Commun., (1975) 950.
17 R. Bar, L. Karpuj-Bar, Y. Sasson and J. Blum, Anal. Chim. Acta, 154 (1983) 313.
18 Y. L.-H. Shaw, S. M. Wang and N. C. Li, J. Phys. Chem., 77 (1973) 236.

Analytica Chimica Acta, 154 (1983) 211—218
Elsevier Science Publishers B.V., Amsterdam — Printed in The Netherlands

DETERMINATION OF ISOTOPE COMPOSITION IN PROTIC SOLVENTS BY COBALT-59 NUCLEAR MAGNETIC RESONANCE SPECTROMETRY

S. H. PETERSON and R. G. BRYANT*

Chemistry Department, University of Minnesota, 207 Pleasant St. S.E., Minneapolis, MN 55455 (U.S.A.)

J. G. RUSSELL

Chemistry Department, California State University, 6000 J. Street, Sacramento, CA 95819 (U.S.A.)

(Received 29th May 1983)

SUMMARY

The very large chemical shift range provided by cobalt-59 yields well resolved lines for each of the nineteen isotopic species in the series of complexes ranging from $Co(NH_3)_6^{3+}$ to $Co(ND_3)_6^{3+}$ and each of the thirteen isotopic species in the similar series of tris(ethylenediamine)cobalt(III) complexes. The relative intensity distribution of these n.m.r. signals at equilibrium is related directly to the proton isotope composition of the solvent. This n.m.r. method of quantifying the isotope composition is examined with respect to the equilibrium isotope effect and the application to determinations in aqueous and non-aqueous solvents.

Though there are several methods in common use for determining the H/D isotope ratio in liquids, some types of environment still present unique problems. Nuclear magnetic resonance (n.m.r.) methods provide a direct means for determinations of isotope composition in systems such as optically opaque samples, in heterogeneous samples in which there may be differences inside and outside a support medium, and in mixed solvent systems in which volatilization during the measurement may alter the isotopic composition of the sample. The n.m.r. chemical shift range for the heavier nuclides is larger in general than that for protons. Cobalt-59 is well known to have n.m.r. chemical shifts that span the parts per thousand range [1]. At a cobalt-59 resonance frequency of 70.8 MHz, there is sufficient resolution that each isotopic isomer is resolved in the cobalt-59 spectra of symmetrical cobalt(III) ammine complexes. In a preliminary note [2] it has been shown that cobalt-59 n.m.r. provides a faithful report of the solvent isotopic composition based on determination of the equilibrium isotope distribution obtained by analysis of the multiline cobalt-59 n.m.r. spectrum. This report offers a more complete description of the experiments; it includes the consequences of the equilibrium isotope effects. The method is applied to several systems of rather different nature to explore its general utility.

0003-2670/83/$03.00

EXPERIMENTAL

Cobalt-59 n.m.r. spectra were recorded using a Nicolet NT-300 n.m.r. spectrometer with the standard data acquisition routines in conjunction with the 12-mm midrange broadband probe. Hexaamminecobalt(III) chloride and perchlorate, and tris(ethylenediamine)cobalt(III) chloride and perchlorate were prepared by standard methods [3, 4]. Stock solutions were prepared by weight using deionized water and 99.8% deuterium oxide. Glassware was dried in an oven, and in the cases of the most dilute proton samples, pre-equilibrated with deuterium oxide vapor prior to use in sample preparation in order to avoid contamination by adsorbed water. Nonaqueous solvents were dried over type 4A molecular sieves for at least a week before use, to minimize water contamination. Sample volumes were generally 5.0 ml and were made directly in the 12-mm n.m.r. tubes from stock solutions and sealed tightly to avoid contamination by water vapor. The chemical shift scales are unreferenced.

RESULTS AND DISCUSSION

The method

The cobalt-59 n.m.r. spectrum is shown in Fig. 1 for a solution of tris-(ethylenediamine)cobalt(III) chloride taken at three values of the solvent

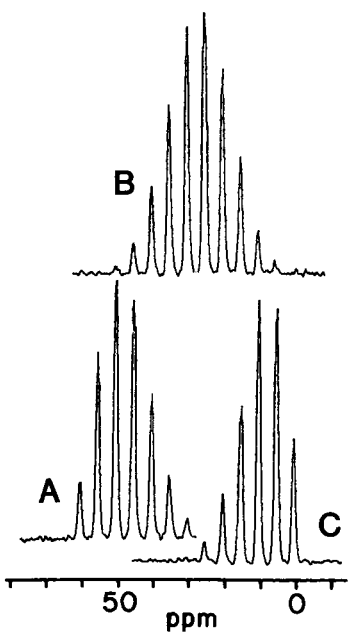

Fig. 1. The cobalt-59 n.m.r. spectra recorded at 71.77 MHz for aqueous 0.08 M solutions of tris(ethylenediamine)cobalt(III) chloride at equilibrium with three solvent isotope compositions for which X_H is (A) 0.824, (B) 0.498, and (C) 0.184.

isotope composition. The chemical shift of 5.0 ppm between each isotopic isomer is clearly observable, and among the three spectra, all 13 lines are shown ranging from the H_{12} to the D_{12} isotopic isomer. Similar spectra with a total of nineteen lines have been reported for the hexaamminecobalt(III) ion for which the chemical shift between each isotopic isomer is 5.6 ppm [2]. The absolute intensity of the lines in these spectra is related to a number of spectrometer characteristics and the cobalt concentration. The relative intensities of the individual isomer lines, however, are coupled to the isotope composition in the solvent by the binomial distribution provided that the proton exchange between the cobalt complex and the solvent system has reached equilibrium. That is, the relative fractional intensity of a particular isotopic isomer line, I_y, is related directly to the isotope composition by the equation

$$I_y = [n!/y!(n-y)!]p_H^y(1-p_H)^{(n-y)} \quad (1)$$

where n is the maximum number of protons in the metal complex (18 for the hexaamminecobalt(III) ion and 12 for the tris(ethylenediamine)cobalt-(III) ion) and p_H is the probability of finding a proton in the solvent, i.e., the concentration of exchangeable protons divided by the sum of the concentrations of the exchangeable protons and deuterons. If p_H is known, the relative intensities of the isotopic isomer lines can be calculated. If the relative intensities are known, the more common case of analytical interest, then the p_H can be extracted from the data and p_H is a direct measure of the isotopic composition of the solvent.

The precise relation between the isotopic composition of the cobalt complex and the composition of the solvent must also include equilibrium isotope effects, which can be measured in calibration spectra. Two examples are shown in Fig. 2 for which the mole fraction of protons obtained from the n.m.r. spectra is plotted vs. the stoichiometric mole fraction of protons in the test sample for a series of compositions. Two features are readily apparent. First, both the tris(ethylenediamine)cobalt(III) chloride and the hexaamminecobalt(III) chloride respond directly to the isotopic composition of the solvent. Secondly, in both cases, the calibration line expected, which is a straight line with unit slope, is not observed; rather a curve is found with a maximum deviation from the expected line very near 0.5 mole fraction of protons. As will be shown, this curvature is a consequence of the equilibrium isotope effects. The procedure summarized in Fig. 2 is simply to take the intensity distribution observed in the cobalt(III) spectrum obtained from observations on a small concentration of complex added to the test sample, iteratively fit n.m.r. line intensities to the binomial distribution to extract a p_H, relate the p_H to the proton mole fraction, and then deduce the final solution mole fraction from the calibration data summarized in Fig. 2 which is ultimately based on gravimetric synthesis of the samples. Inspection of Fig. 2 demonstrates that the measurement is not a sensitive function of the concentration of the cobalt complex used, though the contribution of the

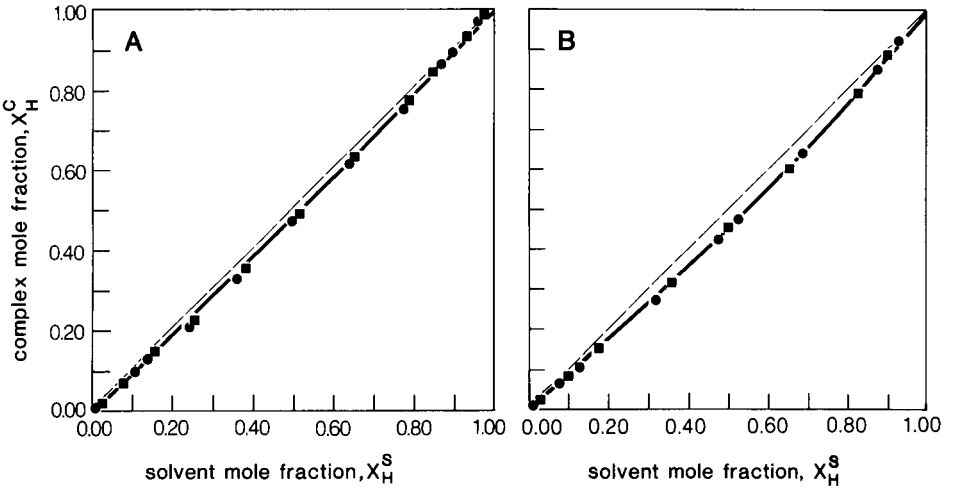

Fig. 2. Plots of the proton mole fraction determined from the cobalt-59 n.m.r. spectrum vs. the solvent mole fraction determined gravimetrically for: (A) hexaamminecobalt(III); (B) tris(ethylenediamine)cobalt(III). The dashed lines show the unit slope. The solid lines were calculated from Eqn. 3: (•) 10 mM metal complex; (▪) 100 mM complex.

exchangeable protons from the cobalt complex must be included as a correction.

Consequences of the equilibrium isotope effect

The source of the curvature in Fig. 2 can be understood in terms of the equilibrium isotope effect. Assuming that the hydrogen/deuterium ratio in the cobalt complex, R_c, is linearly related to that in the bulk solution [5], R_s,

$$R_c = (H/D)_{complex} = f(H/D)_{soln} = fR_s \quad (2)$$

This assumption is strongly supported by the data shown in Fig. 3. The expression for the mole fraction of protons in the complex then becomes

$$(X_H)_{complex} = R_c/(1 + R_c) = fR_s/(1 + fR_s) = R_s/(f^{-1} + R_s) \quad (3)$$

At very large values of R_c or R_s, the fractionation factor, f, divides out and X_H in the complex approaches that in the solvent. At the opposite extreme, linear behavior also results with slope equal to f which is close to unity. Differentiation of Eqn. 3 with respect to f indicates that the maximum deviation from unit slope is expected to occur at values of R_s close to unity as long as f is on the order of unity, which it is. Maximum deviation from the ideal calibration line is therefore expected at a mole fraction of 0.5 as observed in Fig. 2.

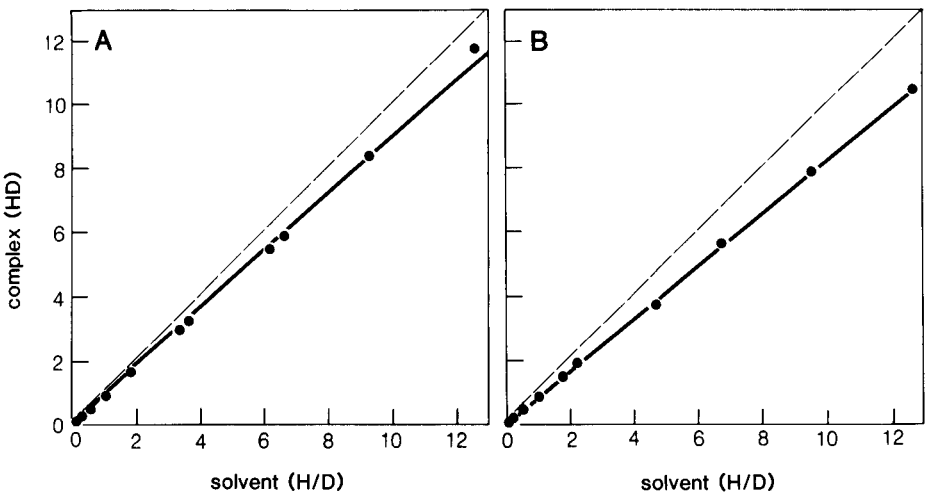

Fig. 3. Plots of the hydrogen/deuterium ratios in the metal complex vs. that in the solvent determined for: (A) hexaamminecobalt(III); (B) tris(ethylenediamine)cobalt(III) in various solvent isotope compositions. The dashed line shows unit slope.

Mixed solvent systems

A useful application of this type of measurement is likely to be to mixed solvent systems. An important consideration in this case is the rate at which the cobalt complexes approach equilibrium with the residual protic solvent component in the solution. In pure aqueous systems, the rate constants for proton exchange are large [6] and though proton exchange may be suppressed in strong acid solutions [7], the exchange rates are sufficient at neutral pH to pose no problem in achieving equilibrium in several minutes. In nonaqueous systems, however, the presence of bases to facilitate proton exchange is minimized and the acid—base properties of both the residual water and the metal complex may be altered as well. A nonequilibrium distribution of line intensities is easy to spot as the cobalt spectrum is often rather unsymmetrical (Fig. 4), and of course the intensity pattern is then not binomial. Inspection of Fig. 4 suggests that the cobalt spectrum provides a very efficient means for the study of the proton exchange mechanism. In a study of the application of this n.m.r. method in the analysis of the isotopic composition of traces of water in nonaqueous solvents, it was found that the addition of a proton exchange catalyst is very useful for routine work. The particular catalyst will depend on the solvent system under study. In investigating the determination of the isotope composition of water in water—DMSO mixtures, we found that the addition of approximately equimolar concentrations of triethylamine and the cobalt complex provides efficient catalysis of the proton exchange at the nitrogen atoms to achieve equilibrium in minutes. In nonaqueous solvents, the solubility of the charged cobalt complex may be a problem, but some flexibility is provided in the

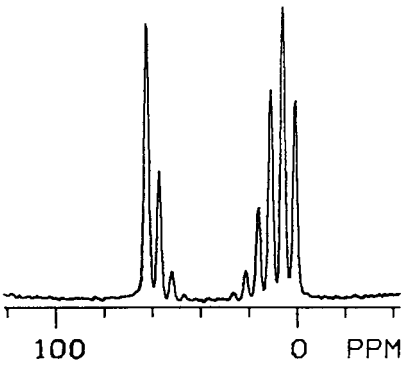

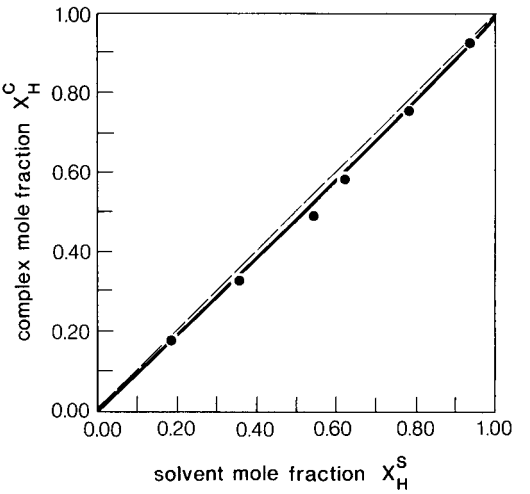

Fig. 4. The cobalt-59 n.m.r. spectrum obtained three hours after preparation at 71.77 MHz for a 15 mM solution of tris(ethylenediamine)cobalt(III) perchlorate prepared by taking 5.00 ml of DMSO that was 0.25 M in pyridine and adding 50 μl of water having a proton mole fraction of 0.051.

Fig. 5. Plot of the proton mole fraction determined from the cobalt-59 n.m.r. spectrum for 15 mM tris(ethylenediamine)cobalt(III) perchlorate vs. the solvent mole fraction in the water component determined gravimetrically in DMSO. The total water content was 1% by volume. The dashed line shows unit slope and the solid line was calculated from Eqn. 3.

choice of the anion. In these experiments the perchlorate salt was used to improve solubility. The results of a DMSO study are summarized in Fig. 5 for which the water concentration was 1% by volume.

Similar results were obtained for water in acetonitrile [8]. In the acetonitrile solutions, however, high base concentrations may cause loss of resolution because of conjugate base formation which will lower the symmetry of the cobalt complex and broaden the spectrum through the nuclear electric quadrupole relaxation mechanism. An example is shown in Fig. 6. In the top spectrum, the base concentration is high and in the bottom spectrum, the base is neutralized by bubbling hydrochloric acid gas through the sample. This observation points to a general limitation on the use of symmetrical cobalt complexes for this purpose.

General considerations

The examples described above were chosen to demonstrate the basic principles of the method. The approach should be generally applicable when the isotopic composition of a system with exchangeable protons is required. For example, by equilibrating a solvent such as D_2O with an insoluble polymer containing OH functions, it is possible to determine the number of OH groups without dissolving the polymer [8]. Similar experiments should

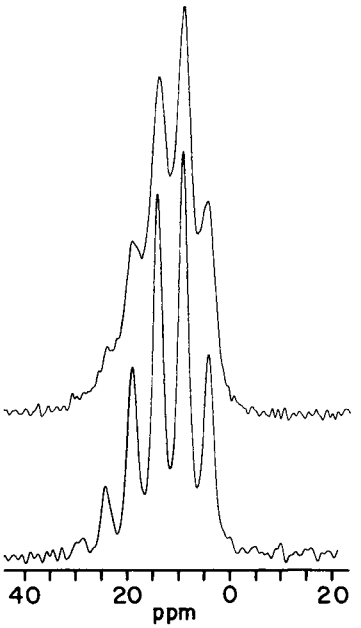

Fig. 6. The cobalt-59 n.m.r. spectrum obtained at 71.77 MHz for 15 mM tris(ethylenediamine)cobalt(III) perchlorate in acetonitrile containing 1% water by volume with a proton mole fraction of 0.051. The solution yielding the top spectrum contained 14.3 mM triethylamine and the spectrum was obtained immediately after sample preparation. The bottom spectrum was obtained after passing hydrogen chloride through the sample.

work for such diverse systems as surfaces, zeolites, or other porous materials. There is no reason why the method should be limited to cobalt(III) complexes.

The difficulty with the use of the highly charged cation in solvents of low dielectric constant has been pointed out. It is difficult to change the charge on the cobalt complex without also lowering the symmetry of the metal complex and inducing intolerably large line broadening to the n.m.r. spectrum. The general requirement of the metal complex is that the central metal ions have very large chemical shifts so that individual resonances can be resolved for each isotopic isomer. The complex is likely to be more useful the more exchangeable protons it has, so that the problem is significantly overdetermined.

In summary, the availability of high-field n.m.r. spectra of the heavy nuclides provides an interesting and useful means of obtaining the isotopic composition of solvent systems in cases for which other methods may fail.

This work was supported by the University of Minnesota and the National Institutes of Health (GM25757). The authors thank Professor Maurice Kreevoy for several helpful discussions concerning this work and Dr. Carl Polnaszek for aid in programming.

REFERENCES

1 R. K. Harris and B. A. Mann, NMR and the Periodic Table, Academic Press, New York, 1978.
2 J. G. Russell and R. G. Bryant, Anal. Chim. Acta, 151 (1983) 227.
3 J. Bjerrum and J. P. McReynolds, Inorg. Synth., 2 (1946) 217.
4 J. B. Work, Inorg. Synth., 2 (1946) 221.
5 L. Melander and W. H. Saunders, Jr., Reaction Rates of Isotopic Molecules, Wiley, New York, 1980, pp. 203—205.
6 R. G. Wilkins, The Study of Kinetics and Mechanisms of Reactions of Transition Metal Complexes, Allyn and Bacon, Boston, MA, 1974, p. 207.
7 F. Basolo and R. G. Pearson, Mechanisms of Inorganic Reactions, A Study of Metal Complexes in Solution, Wiley, New York, 1967, Ch. 3.
8 S. H. Peterson, M. S. Thesis, University of Minnesota, Minneapolis, MN, 1983.

Analytica Chimica Acta, 154 (1983) 219—226
Elsevier Science Publishers B.V., Amsterdam — Printed in The Netherlands

SIMULTANEOUS MULTIELEMENT DETERMINATION IN MICROLITER SAMPLES BY RAPID-SCANNING SPECTROMETRY COUPLED TO A MICROWAVE-INDUCED PLASMA

MANTAY ZEREZGHI, KEVIN J. MULLIGAN and JOSEPH A. CARUSO*
Department of Chemistry, University of Cincinnati, Cincinnati, OH 45221 (U.S.A.)
(Received 1st April 1983)

SUMMARY

A modified electrothermal atomizer is coupled to a helium microwave-induced plasma (m.i.p.) for atomic emission spectrometry. For preliminary evaluation, this arrangement was coupled to a monochromator to quantify single elements in microliter samples. Detection limits range from 3 to 25 pg for Cd, Fe, Pb, Mn and Au and linear dynamic ranges are 2—4 orders of magnitude. The monochromator, fitted with a rapid scanning galvanometer mirror, is also used as a multielement detector. A spectral window of ca. 40 nm is rapidly scanned (10 Hz) across the exit slit and five elements from one solution are determined in rapid sequence. In the multielement mode, the detection limits are in the range 50—250 pg, as might be expected, owing to the decreased duty cycle. However, there is a significant improvement when compared to an earlier report from this laboratory. By narrowing the spectral coverage and taking data more rapidly this drawback is minimized.

The ability to quantify multiple elements simultaneously is desirable because of the potential time-savings, reduced costs, and reduced sample amounts required compared to single-element detection. Multielement determination by emission spectrometry (e.s.) can be done with multichannel detectors (polychromators), which provide good stability, wide spectral coverage, high sample throughput, and convenience, but lack flexibility and are expensive. Monochromators are versatile, but require a separate run for each element to be quantified.

Another approach to simultaneous multielement determination is to use sequential slew-scanning spectrometers equipped with computer-controlled stepper motor-driven grating(s) which can be rapidly slewed between spectral lines. Such devices have been used with direct solution nebulization with the inductively coupled plasma (i.c.p.) and gas chromatographic introduction to the i.c.p. (g.c.-i.c.p.) [1—3]. In i.c.p.e.s. with solution nebulization the analyte must be introduced continuously while the grating is slewed to the appropriate wavelength. In g.c.-i.c.p., the components that contain the various elements to be quantified have to be well separated in time to allow for the slewing of the grating. This virtually eliminates the use of slew-scanning spectrometers with pulse sample introduction systems such as an electrothermal atomizer where the analyte residence time may be less than 2 s.

0003-2670/83/$03.00

An alternative method of multielement quantification involves introducing a galvanometer-driven oscillating mirror into the optical path of a monochromator. Movement of this mirror scans a given spectral region across the exit slit. Rapid repetition of this scan and coupling with a suitable data acquisition system can provide information similar to that obtained by simultaneous observation (polychromator) of the different elemental lines within this spectral region. Earlier reports showed that such a rapid-scanning spectrometer has potential as a multielement detector when used in conjunction with electrothermal atomizers or gas chromatography and microwave induced plasmas [4, 5]. This work addresses some of the shortcomings associated with the earlier work through redesign of the instrument. The goals were to improve the levels of detection and extend the linear dynamic range.

This study describes the results that were obtained when a modified commercially available graphite-furnace atomizer was used for sample introduction to a helium m.i.p. coupled to a rapid scanning spectrometer for simultaneous quantification of trace metals by atomic emission spectrometry. Both single-element and multi-element studies are presented.

EXPERIMENTAL

Equipment and software

A Spex model 1870 0.5-m spectrometer with a stepper motor-driven grating (Compudrive option, Spex) was equipped with a rapid-scanning galvanometer fitted with a flat mirror. The grating is blazed at 300 nm and ruled at 600 grooves mm^{-1}. A diagram of the microcomputer-controlled rapid scanning spectrometer has been given [5]. A pulse of 5 V and 50-ms duration prompts a signal generator (Exact Electronics model 126C VC8 sweep generator) to produce a uniform voltage ramp which is converted to a current by the AX-200 driver amplifier (General Scanning, Inc.). This current is responsible for moving the galvanometer (General Scanning, model GS-306).

The microcomputer is based on an Intel 8080A. The prototype [6] was built by W. S. Woodward, further developed by T. H. Ridgway, and has been described [5]. Experimental input/output was provided by a 12-bit digital-to-analog converter and a 12-bit analog-to-digital converter (ADC) which accepted signals in the range of ±10 V. Nominal conversion time for the ADC was 15 μs/point; in practice, at least 25 μs/point for rapid scanning and 20 μs/point for single-channel utilization were required. A programmable-gain amplifier converted the photomultiplier current to voltage [2]. For the rapid scanning experiment, it was necessary to incorporate the ADC on a card that allowed direct memory access. With the direct memory access, it was possible to acquire, digitize and store data in random access without involvement of the CPU. Data-processing subroutines could be run parallel to and independent of data acquisition [5].

Available memory is allocated as shown in the earlier Fig. 2 [5]. Buffers 1

and 2 of the direct memory access are temporary storage locations for 12-byte data points taken during successive scans in a "ping-pong" fashion. The desired information is transferred to a semipermanent buffer while the galvanometer-driven mirror settles between scans and while data are being loaded into the temporary buffer. Data for a given experiment are accumulated as a three-byte summation (summed over the number of scans) in a semipermanent buffer which allows results to be carried over between experiments. Subtraction of these three-byte sums from separate experiments serves as a means of background correction. These three-byte binary data are ultimately converted to floating point representation so that data reduction and display can be handled in BASIC.

The Beenakker cavity that was used to couple the radiation from the generator to form the helium m.i.p. was constructed from copper stock. Details of the cavity, plasma formation, and other associated hardware have been described [7].

Sample introduction

The power supply/electrothermal atomizer were the Varian Model 63 carbon rod atomizer, with the modifications described below. The corrugated metal strips located at the base between the support blocks were removed to provide room for a small glass dome to surround the atomizer (minidome). The minidome shown in Fig. 1 had a total volume of about 15 ml and was made of quartz. It was made in two pieces to facilitate changing the cup atomizers easily. The graphite cups (Varian model 99100244) were cut to a height which accommodated a 10-μl volume, and were pyrolytically coated by heating in a 10% methane in helium mixture. It was observed that these smaller cups led to greater reproducibility. Viton O-rings on the outside and graphite washers on the inside provided a seal between the side holes of the dome and the electrodes. An auxiliary helium flow was needed to maintain the plasma when the sample introduction port was opened. A teflon sleeve served as a coupler between the dome and the plasma containment tube (4.7 mm o.d., 2.7 mm i.d., 6 cm long).

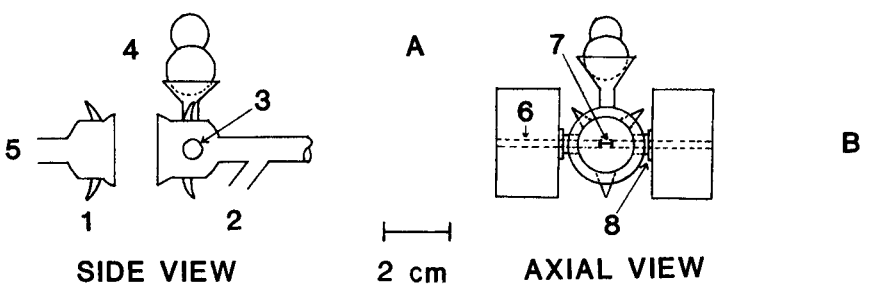

Fig. 1. (A) Minidome; (B) minidome fitted between the support blocks of the electrothermal atomizer. (1) Hooks (three on each piece); (2) inlet for auxiliary helium; (3) side-arms for inserting electrodes; (4) sample introduction port; (5) main helium inlet; (6) electrodes; (7) minicup; (8) graphite couplers.

Reagents. Standards were prepared in 2% nitric acid from 1000 mg l^{-1} stock solutions daily (Spex).

RESULTS AND DISCUSSION

Single-channel measurements

To evaluate the performance of the minidome and the m.i.p., single channel experiments were done without rapid scanning by setting the galvanometer mirror at 45° from the entrance beam. The optics were configured for *f*/5.5. This increased the throughput while providing sufficient resolution. Entrance and exit slits were set at 30 μm wide, 2 mm high, and the wavelength of interest was located by maximizing the signal from hollow-cathode lamps. Samples (5 μl) were pipetted into the cup. Then, the sample was slowly desolvated for 20 s with the sample introduction port open and the auxiliary helium flow on. The auxiliary flow was cut off, the sample introduction port was closed, and another 40 s was allowed for the plasma to restabilize. An ash step of 10 s was needed to remove the acid completely. The cup was then quickly heated to about 2000°C for 1.5 s. It was observed that the analyte was removed from the cup before 1 s had elapsed. The ADC was triggered at the end of the ash cycle. A 2% nitric acid blank was atomized and the resulting signal was stored in the background buffer. Subsequently, the sample was atomized and the results were stored in a separate buffer. The two sets of data were subtracted and the difference was smoothed.

Effects of flow rate and power

Figure 2A shows the effect that varying the flow rate has on the background-subtracted signals. At flow rates between 300 and 600 ml min^{-1} there is no significant change; at flow rates above 300 ml min^{-1} there is a sharp decline in signal and at flow rates in excess of 600 ml min^{-1} there is a gradual decrease. A compromise flow rate of 400 ml min^{-1} was used.

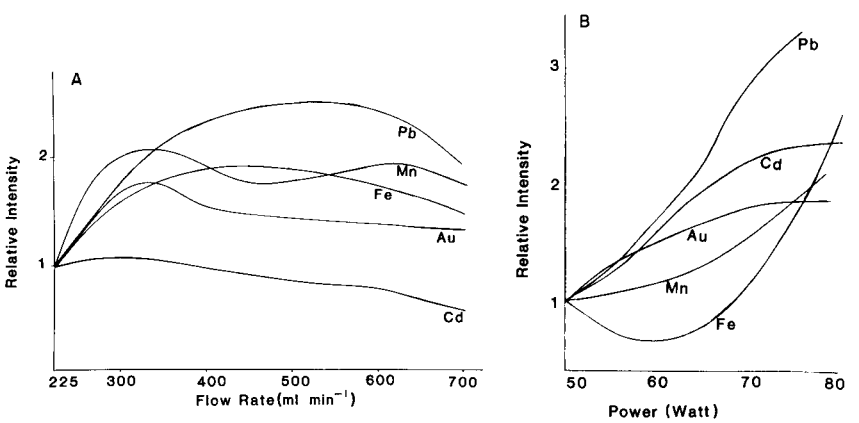

Fig. 2. Effect of (A) flow rate and (B) microwave forward power on signal intensity.

Figure 2B shows the dependence of signal intensity on microwave forward power. A significant increase in signal intensity was observed for all elements except iron as the power was increased from 50 to 80 W; iron showed a decrease at 60 W. However, better signal-to-noise ratios were obtained at about 70 W, and this forward power was chosen for this study.

Figure 3 shows a typical time vs. intensity signal for cadmium. Similar signals were obtained for other elements. The elements vaporized as expected: cadmium, gold, and lead appeared within the first 0.2 s of the onset of the atomization cycle and were completely removed within 0.5 s. Two other elements, iron and manganese, appeared between 0.5 and 0.9 s. These observations are consistent with the volatilities of these elements. Visual observation also showed that the data acquisition was completed before the cup reached its maximum temperature. Peak areas were used for quantification. Linear dynamic ranges of 2—4 orders of magnitude were obtained, and are comparable to literature values for m.i.p-a.e.s. [8, 9]. Table 1 compares the detection limits of the present system with others reported.

Multielement measurements

For rapid-scanning experiments, the grating was set to a wavelength corresponding to the midpoint of the scan. The mirror was scanned at 10 Hz, 50 ms

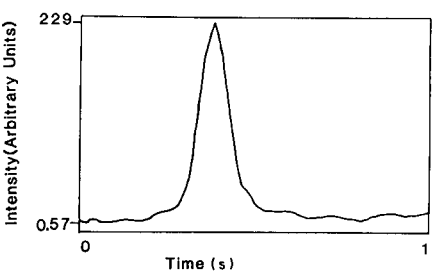

Fig. 3. Cadmium emission signal as a function of time.

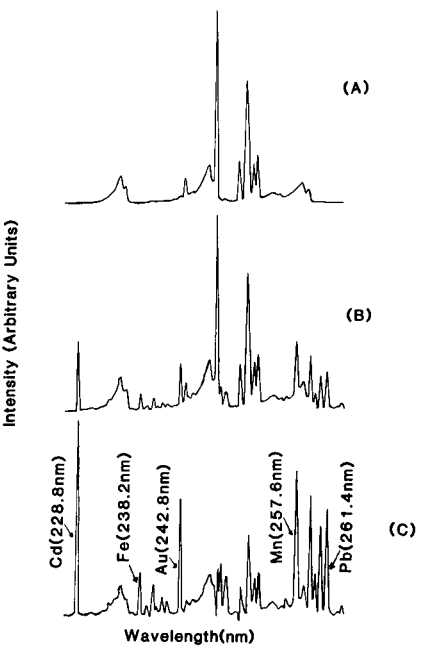

Fig. 4. Rapid-scanning spectra: (A) atomization of 2% nitric acid blank; (B) atomization of a mixture of Cd, Fe, Au, Mn, Pb in 2% nitric acid; (C) B — A. The general scale in C is expanded 2.5 ×.

TABLE 1

Comparison of detection limits

Element	Wavelength (nm)	Detection limits (pg)[a]			Rapid scan
		Single channel	Ar-m.i.p.[b]	He-m.i.p.[c]	
Cd I	228.8	3.0	1750	—	50
Fe II	238.2	10.0	—	—	200
Fe II	260.0	—	4500	—	—
Au I	242.8	10.0	—	—	200
Pb I	261.4	25.0	—	—	250
Pb I	283.3	—	—	7	—
Mn II	257.6	5.0	350	1.0	200

[a]Detection limits are defined as the amount of analyte that produces a signal 2.5 times the background signal. [b]With a Perkin-Elmer HGA-2000, data taken from [9]. [c]With a minidome, data taken from [8].

per scan, and 50-ms delay between scans (this time was needed by the mirror to come to the rest position). After the necessary parameters had been set, the amplitude of the ramp (which determined the width of the spectral window to be monitored), the number of scans (typically 30), and the time per point (25 μs) were specified. The computer then waits for the ash cycle clock of the electrothermal atomizer to reach the end of the cycle. At the end of this cycle, it triggers the ADC. Sample desolvation and atomization were identical to those for single-channel measurements. A spectrum obtained by atomizing 2% nitric acid was used as the blank and subtracted from all subsequent spectra.

Figure 4 shows typical emission spectra that were obtained over a window of 36 nm. Typical calibration plots are shown in Fig. 5. The slopes for the lines are 1.01 ± 0.05, 1.05 ± 0.06 and 1.01 ± 0.06 for Cd, Au and Fe, respectively. The linear dynamic ranges are 2—3 orders of magnitude, which is a significant improvement when compared to earlier reports [4]. This may be attributed to improvements in the optics, the advantages associated with

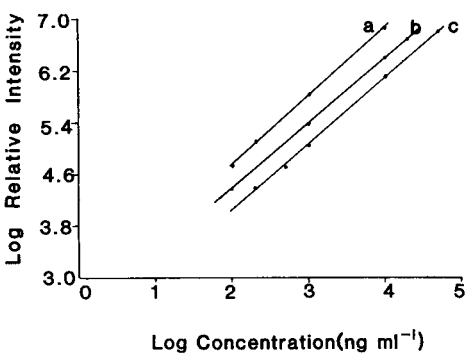

Fig. 5. Calibration plots for selected elements: (a) Au (b) Cd (c) Fe.

axial viewing in the Beenakker cavity, and the more efficient analyte transfer that was achieved by the miniature dome. Table 1 includes the detection limits of the rapid-scanning experiments with those of the single-channel work. As expected, the results for rapid scanning are at least an order of magnitude poorer than those for single channel work. This is not surprising, because the duty cycle for rapid scanning is typically 0.005 of the duty cycle for a single-channel measurement. For example, if the cadmium line is considered, the computer took 20 points across the cadmium peak at 25 μs/point. As the cadmium residence time is 0.3 s, data were taken during 3 scans only (10 Hz scan rate) giving a duty cycle of 1500 μs which is 1/200 of that of the single-channel experiment. By taking data at a rate of 50 μs/point, the signal was halved. When spectral coverage was narrowed to about 12 nm, the rapid-scanning results approached those of the single-channel studies.

Interferences

The m.i.p., because of its low power, is more prone to interferences than the i.c.p. The stability and excitation efficiency are affected when excessive amounts of foreign material are introduced into the plasma gas stream [10]. Figure 6 shows the effect of adding various amounts of sodium chloride or nitrate on 10-ng amounts of the elements studied. A modest enhancement of 2—3-fold was observed for a sodium nitrate concentration of 100—500 mg l^{-1} (Fig. 6A). No significant change was observed at 1000 mg l^{-1}. However, varied and significant enhancements were observed with sodium chloride (Fig. 6B), 10-fold for manganese and 5-fold for iron. This is consistent with earlier reports by other workers. The present observations seem in accord

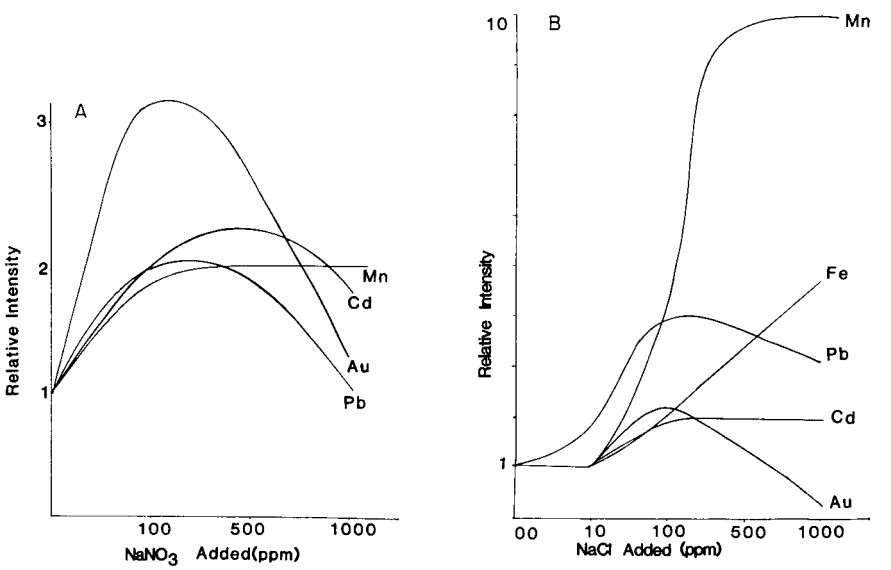

Fig. 6. The effects of adding various amounts of (A) sodium nitrate and (B) sodium chloride on the intensity of the analyte signals.

with the enhancement mechanism by sodium chloride proposed by Kawaguchi et al. [11] who suggested a two-process phenomenon: first, the excess of chloride stabilizes the metal during the desolvation and ashing stages, thus minimizing analyte loss; secondly, ionic lines would be expected to be more intense in the presence of chloride according to the reactions: $MCl \rightarrow M^+ + Cl + e^-$; $He_m + MCl \rightarrow He + M^+ + Cl + e^-$; $M^+ \rightarrow M^{+*}$, where He_m represents metastable helium. Some term this "mechanistic enhancement." Effects from stabilization would be expected to be similar, but mechanistic effects will favor ionic lines (Mn, Fe) as opposed to atomic lines (Cd, Au, Pb), as suggested by these reactions; this is what is observed.

The authors are grateful to NIOSH for support of this work with grant number OH-00739.

REFERENCES

1 M. A. Eckhoff, J. P. McCarthy and J. A. Caruso, Anal. Chem., 54 (1982) 165.
2 J. P. McCarthy, M. E. Jackson, T. H. Ridgway and J. A. Caruso, Anal. Chem., 53 (1981) 1512.
3 M. A. Floyd, V. A. Fassel, R. K. Winge and J. M. Katzenberger, Anal. Chem., 50 (1980) 431.
4 O. Rose, Jr., W. R. Heineman and J. A. Caruso, Analyst, 103 (1978) 113.
5 K. J. Mulligan, M. Zerezghi and J. A. Caruso, Spectrochim. Acta, Part B, 38 (1983) 369.
6 W. S. Woodward and C. N. Reilley, Pure Appl. Chem., 50 (1978) 785.
7 K. J. Mulligan, J. A. Caruso and F. L. Fricke, Analyst, 105 (1980) 1060.
8 C. I. M. Beenakker, P. W. J. M. Boumans and P. J. Rommers, Philips Tech. Rev., 39 (1980) 65.
9 A. Aziz, J. A. C. Broekaert and F. Lies, Spectrochim. Acta, Part B, 37 (1982) 381.
10 A. T. Zander and G. M. Heiftje, Appl. Spectrosc., 35 (1981) 357.
11 M. Kawaguchi, I. Atsuya and B. L. Vallee, Anal. Chem., 49 (1977) 266.

Analytica Chimica Acta, 154 (1983) 227—234
Elsevier Science Publishers B.V., Amsterdam — Printed in The Netherlands

DETERMINATION OF BORON, BERYLLIUM AND LITHIUM IN COAL ASH AND GEOLOGICAL MATERIALS BY SPARK OPTICAL EMISSION SPECTROMETRY

JOHN C. MILLS

The Broken Hill Proprietary Company Ltd., Central Research Laboratories, P.O. Box 188, Wallsend 2287 (Australia)

(Received 16th May 1983)

SUMMARY

A method is described for the accurate and precise determination of boron, beryllium and lithium in coal ash and geological materials by a point-to-plane high-voltage spark optical emission spectrometric technique. A 200-mg sample is crushed and blended with graphite, copper oxide internal standard and cellulose powders, and briquetted. Synthetic calibration standards are prepared from spectrographically pure materials blended into graphite. Corrections are made for spectral interference by iron and silicon on boron. Accurate results are presented for certified reference materials. The precision of the method, about 5%, is superior to that obtained by d.c. arc optical emission.

Boron has been classified among the "elements of greatest concern" to environmental quality and health [1], in relation to its release during coal utilization and waste disposal. Boron in certain concentrations may have severe toxic effects on plant life [2, 3]. Boron is also of geochemical interest as an indicator of marine paleoenvironments of coal [4], sediments and sedimentary rocks [5]. Analyses for boron in coal and geological materials have generally been done [6—8] by d.c. arc optical emission spectrometry (o.e.s.) which has good sensitivity but poor accuracy (±15 to 40% relative) and poor precision (5—13% relative standard deviation). Nevertheless, o.e.s. was preferred to the slower and more skill-dependent chemical and spectrophotometric methods [9]. An improved optical emission method was sought in this work by using the inherently more precise high-voltage spark excitation, for which the instrumentation is widely available especially in laboratories associated with metallurgical industries and research. Recently, determination of boron by inductively-coupled plasma (i.c.p.) emission spectrometry has been reported [10] but i.c.p. instruments are not yet very widely available.

Two other elements of low atomic number and with high sensitivity in o.e.s. were included in this study. Beryllium, which is classified as an "element of concern, but with negligible concentrations in coal and coal residues" [1], was included both to demonstrate the wider applicability of the method

0003-2670/83/$03.00

and to check the results obtained by a recently developed atomic absorption spectrometric (a.a.s.) technique for the determination of twelve elements by the direct analysis of pulverised whole coal samples in an electrothermal furnace atomizer [3]. Lithium was included to provide a useful extension of the method to materials in which the lithium content is of interest, e.g., confirmation of the mineral lithiophorite in manganese ores, for which existing methods [11] were unsuitable because of the use of lithium tetraborate fusion procedures. In this context, the proposed method fills the gap in elemental coverage created by the commonly used spectrochemical fluxing elements boron, lithium and lanthanum.

EXPERIMENTAL

Instrumentation

The spectrometer was a Jarrell-Ash 2-m direct reader model 66-105 with dispersion 0.42 nm mm^{-1}, wavelength ranges 175—210 and 220—420 nm, vacuum <1 Pa, entrance slit 25 μm. The excitation stand was fitted with a hinged plate over the spark chamber.

An auxiliary spectrometer, a Techtron Sirospec 0.5-m grating monochromator with dispersion 3.3 nm mm^{-1} and wavelength range 250—850 nm, was fitted as an extra channel to the direct reader, and used for lithium. Analytical discharge light was conveyed to the 150-μm entrance slit by a quartz optical fibre (Schott type UV, 1 m × 3 mm diameter). A cut-off filter transmitting only wavelengths exceeding 530 nm was inserted between the optical fibre and the entrance slit to eliminate high-order spectral interference on alkali lines.

Other parameters were: Labtest high-voltage spark source operated at 4.8 kV, 0.25 μF, 70 μH, 0.7 ohms, 100 Hz; Ringsdorff graphite counter electrodes grade RW-003 (<0.01 $\mu g\ g^{-1}$ boron), 6.15 mm diameter, ASTM C5A tip; excitation using 5-mm gap, nitrogen 7.5 l min^{-1} gas flow, preflush 5 s, prespark 2.5 s, integration 10 s; Labtest CRT-1000 control and readout system. The analytical line parameters were as shown in Table 1.

Internal standard

Incorporation of an internal standard element during sample preparation is almost universal practice in o.e.s. to obtain improved precision in spite of source variations. Oxides of five elements of very low concentration in coals and with lines already installed in the spectrometer were tested (Cu, Y, Mo, Cd, Ta) for reproducibility and signal-to-background ratio; of these, Cu and Cd were suitable. Copper was selected because virtually all direct-reading spectrometers contain a copper line which is sensitive and comparatively free of interference, copper oxide is nontoxic and inexpensive, and the coals themselves contained only a few $\mu g\ g^{-1}$ of copper which is readily and routinely determined by other techniques.

An internal standard mixture was prepared by blending 0.5 g of spectro-

TABLE 1

Analytical line parameters

Element	Line (nm)	Exit slit (μm)	Attenuator (1—20)	Photomultiplier tube	Limit of detection (μg g^{-1})	
					A[a]	B[b]
B	249.67	50	3	EMI9783A	3	0.3
Be	313.04	75	16	R306	0.1	0.01
Li	670.7	150	14	R446UR	3	0.3
Cu[c]	327.40	50	12	EMI9661A	—	—
Fe[d]	259.84	50	7	R154	—	—
Si[d]	288.16	75	10	R154	—	—

[a]In coal ash and silicates. [b]On a whole coal basis, assuming 10% ash. [c]Internal standard. [d]Interfering element.

graphically pure copper oxide and 9.5 g of Ringsdorff low-boron grade RW-A graphite for 60 s in a 100-cm^3 Siebtechnik rotary swing mill with tungsten carbide elements. The quantity of copper oxide added to each sample for analysis is 1.25% of the sample mass.

Sample preparation

Coal ash was prepared at 815°C in accordance with Australian Standard AS1038 [12], cooled rapidly in a desiccator to minimize errors resulting from absorption of moisture and carbon dioxide, and weighed within 30 min of removal from the furnace. Coal mineral matter, prepared by low-temperature (ca. 150°C) radio-frequency oxygen plasma ashing, was equilibrated with the laboratory atmosphere and a concurrent moisture determination was done as specified in AS1038 to allow calculation of the results to a dry basis. Mineral and geological samples were crushed to −76 μm and dried at 105°C for 2 h before weighing. Certified reference materials (CRM) were pre-treated according to certificate instructions.

The sample briquette was prepared by weighing 0.200 g of sample, 1.450 g of low-boron grade RW-A Ringsdorff graphite, 0.0500 g of internal standard mixture and 0.300 g of Whatman CF11 chromatographic cellulose powder into a polystyrene vial with cap, shaking by hand for 10 s to mix, transferring to a 10-cm^3 Siebtechnik rotary swing mill with tungsten carbide elements, milling for 300 s, and briquetting the resultant powder in a 19-mm mould at 45 kN for 20 s. Briquettes were stored in a desiccator over magnesium perchlorate. In order to avoid mill memory cross-contamination effects, the mill elements were cleaned before each sample or standard by wiping with a paper towel soaked in ethanol, milling 1 g of a cleaning powder (90-mesh Al_2O_3 and graphite powder, 20:1) for 30 s, and wiping again with a paper towel soaked in ethanol. It was necessary to add cellulose as a binding agent because the low-boron grades of spectrographic graphite were not alone capable of forming self-supporting briquettes.

Avoidance of contamination in procedures for boron and lithium is

difficult when lithium borate and carbonate are widely used in the laboratory for fusion of materials prior to chemical or spectroscopic analyses. It was necessary to clean the working area thoroughly, to use only apparatus and vessels that had been reserved and kept free of lithium borate dust or contact, and to isolate the B/Li task from other laboratory operations. The milling step is not rapid, because of these precautions, but it is vital to ensure a very fine sample particle size for complete excitation in the spark, and to achieve thorough mixing of the powders.

Calibration

Experience at these laboratories has shown that oxide mixtures blended in graphite were satisfactory for preparation of calibration standards for trace analysis of coal by x.r.f. [13], and a similar scheme was implemented in this work. A trace element mixture was prepared by finely pulverizing and blending spectrographically pure lithium tetraborate, lithium carbonate and beryllium oxide with Ringsdorff low-boron grade RW-A graphite in a 100-cm^3 tungsten carbide rotary swing mill; the pure chemicals were pretreated at 350°, 105° and 950°C, respectively, to remove moisture and assure stoichiometry. A second trace mixture prepared by pulverizing and blending lithium tetraborate and graphite only was used to cover high boron ranges (>300 $\mu g\ g^{-1}$). A synthetic mineral matter was prepared by pulverizing and blending five pure oxides.

Calibration standards for coal ash and silicates were prepared by weighing appropriate quantities of trace mixtures, low-boron graphite, synthetic mineral matter, internal standard mixture and cellulose. Calibration ranges were from zero up to 2010 $\mu g\ g^{-1}$ boron, 139 $\mu g\ g^{-1}$ lithium and 54 $\mu g\ g^{-1}$ beryllium. These standards were three times the mass of the samples in briquettes of 25-mm diameter, in order to obtain 4 sparks per fresh surface compared with 1 or 2 on the smaller sample briquette, and to conserve chemicals and effort by retaining the same calibration briquettes for many batches of work. Each one-third of each standard was milled separately, and the three millings were combined, shaken by hand for 20 s to mix and briquetted in a 25-mm diameter mould at 45 kN for 20 s. The synthetic mineral matter was replaced by individual pure oxides to make standards for calibration of spectral interferences.

Measurement

Duplicate sparks were made on all standards and samples, with additional sparks as necessary to achieve reproducibility. Each spark was made with a freshly shaped counter electrode, and on a clean spot on the briquette which was resurfaced by rubbing on P600 SiC abrasive paper on a clean flat surface followed by wiping on clean tissue paper to remove surface dust. When lithium was determined, the spark chamber was wiped clean between excitations with tissue paper moistened with ethanol, paying particular attention to the window over the optical fibre. Data were collected as intensity ratios to the internal standard.

Spectral interference correction

No interferences were observed in this work for beryllium and lithium, provided that the cut-off filter was used for the latter. Only the two boron lines at 249.67 nm and 249.78 nm have adequate sensitivity for the point-to-plane high-voltage spark excitation technique, and both suffer iron interference. The extent of the interference is shown in the profile scans in Fig. 1, obtained with our spectrometer. The 249.67-nm boron line is preferred because of the lower iron interference, and the extent of the interference was minimized by carefully adjusting the alignment of the boron slit using the refractor plate so that boron was run slightly off-profile (by 0.006 nm). Minor interference from SiO band emission in silicate base materials has been reported [6], and was confirmed in this work.

The interference correction for silicon was calculated from the intensity ratios of standards which contained no boron or iron, and the interference correction for iron from silicon-corrected intensity ratios of standards which contained no boron. The corrections were first applied to the calibration standards before plotting the boron calibration curve. Calibration curves for silicon and iron were also drawn, and the concentrations of the interfering elements found in the samples and CRMs were applied to obtain the final boron concentration corrected for interference. The correction equations were as follows for the off-profile alignment: 1% Fe_2O_3 = 3.4 $\mu g\ g^{-1}$ B; 1% SiO_2 = 0.22 $\mu g\ g^{-1}$ B.

RESULTS AND DISCUSSION

The procedure has been developed and applied during the course of projects related to the trace element analysis of a wide range of Australian coals, coke

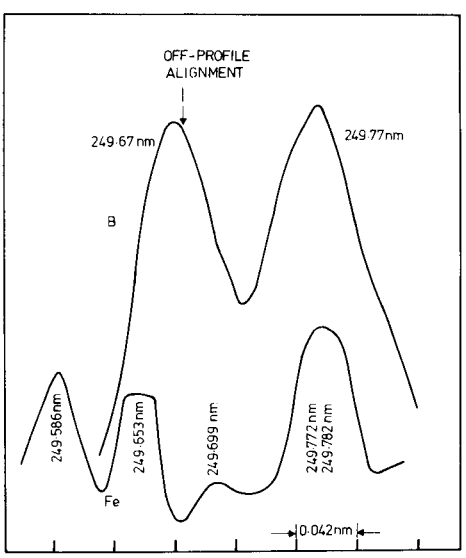

Fig. 1. Iron interference on the boron doublet.

and ash. Boron has been of principal interest, while beryllium and lithium have been determined less frequently. Detection limits at the 95% confidence level (twice the standard deviation of the background at zero analyte concentration) are shown in Table 1. The sensitivity is excellent for coal and coke analyses, and all results obtained to date for Australian bituminous coals have been more than five times higher than the detection limits.

The desired improvement in precision over d.c. arc methods has been achieved, the overall relative standard deviation being about 5%. The means and standard deviations (s) are presented in Table 2 for replicate preparations of the ash of a Wongawilli bituminous coal analysed in many batches over two years, and of the Canadian syenite rock standard SY2.

The accuracy of the method has been demonstrated by analysis of certified reference materials; the results are presented in Table 3. None of the CRMs has certified values for B, Be and Li. Values for comparison have been taken from the literature [14—18]; many are called "recommended values", having been derived from a number of independent analyses and may be considered reliable, while there is less certainty about the remainder which are indicated in brackets in the table. Where disagreement or duplication occurs for the silicate rock standards, the figures from the more recent compilation by Abbey [14], are preferred to those from Flanagan [15], and information values from the certificates are preferred to any literature value. Results for the Coal Standard NBS 1632a were obtained by analysing the low temperature mineral matter and calculating back to a dry coal basis. The accuracy of the described method is good for boron and beryllium. The lithium results are a little less satisfactory, partly because they represent only two determinations by this method and also because there are fewer reliable values in the literature. It is possible that the disagreement shown for lithium in the USGS Standard G2 was caused by contamination. Boron and lithium results are not

TABLE 2

Precision obtained from replicate preparations

Sample	Element	Number of replicates	In coal ash or silicates ($\mu g\ g^{-1}$)		Whole coal basis ($\mu g\ g^{-1}$)	
			Mean	s	Mean	s
BHP-SC143[a]	B	31	133	6	25	1.1
	Be	13	12	0.7	2.2	0.13
	Li	5	46	5	9	0.9
CCRMP-SY2[b]	B	14	86	5	—	—
	Be	10	21	1.0	—	—
	Li	4	95	2	—	—

[a]Ash of Wongawilli bituminous coal, 18.5% ash. [b]Canadian certified reference materials project, syenite rock SY-2.

TABLE 3

Trace element concentrations in certified reference materials[a]

CRM	B ($\mu g\ g^{-1}$)		Be ($\mu g\ g^{-1}$)		Li ($\mu g\ g^{-1}$)	
	This work	Lit.	This work	Lit.	This work	Lit.
Coal						
NBS 1632a	55	53	1.7	(1.6)	35	36
Ash						
NBS 1633a	44	39	12	(12)	100	
Silicates						
CCRMP-SY2	86	(86)	21	23	95	90
USGS-DTS1	na[b]	<5	1.6		2	(2)
USGS-G2	4	2	2.2	2.6	45	37
USGS-GSP1	<3	<3	2.0	(1.5)	34	34
CRPG-GR	—[c]	(9)	5.8	5.5	—[c]	55
CRPG-GA	—[c]	20	3.7	3.6	—[c]	90
NBS 278	21	(25)	1.4		na	
NBS 688	<3	0.9	1.2		na	

[a]Literature values in brackets are uncertain. [b]na = not analysed. [c]Sample previously contaminated in the author's laboratory.

presented for the two CRPG Standards GR and GA because these particular samples were contaminated with lithium tetraborate during a crushing procedure many years earlier.

Extension of the method to minerals other than silicates involves preparation of a similar suite of calibration standards using the same trace mixtures but a different synthetic matrix mixture broadly matching the major mineral composition. It is also necessary to check potential interferences with a few synthetic standards of appropriately varied matrix composition.

This work was supported in part by the National Energy Research, Development and Demonstration Council, Australian Government Department of National Development and Energy, through Grant No. 80/0220. Appreciation is expressed to the Broken Hill Proprietary Company Ltd., for permission to publish the work.

REFERENCES

1 U.S. National Research Council, Trace Element Geochemistry of Coal Resource Development related to Environmental Quality and Health, PECH Report, U.S. National Committee for Geochemistry, National Academy Press, Washington, DC, 1980.
2 E. S. Gladney, L. E. Wangen, D. B. Curtis and E. T. Jurney, Environ. Sci. Technol., 12 (1978) 1084.
3 K. J. Doolan, J. C. Mills and K. E. Turner, BHP Tech. Bull., 24 (1980) 17.
4 D. J. Swaine, Geol. Surv. Queensl., Rep. No. 62 (1970) 41.

5 E. L. Couch, Am. Assoc. Petrol. Geol. Bull., 55 (1971) 1829.
6 L. S. Dale, Appl. Spectrosc., 33 (1979) 404.
7 H. J. Gluskoter, R. R. Ruch, W. G. Miller, R. A. Cahill, G. B. Dreher and J. K. Kuhn, Ill. State Geol. Surv., Circular 499 (1977).
8 G. Thompson and D. C. Bankston, Spectrochim. Acta, Part B, 24 (1969) 335.
9 E. N. Pollock, in S. P. Babu (Ed.), Trace Elements in Fuel, American Chemical Society, Washington, DC, 1975, p. 23.
10 J. W. Owens, E. S. Gladney and D. Knab, Anal. Chim. Acta, 135 (1982) 169.
11 J. C. Mills, A. C. Knott and C. B. Belcher, in I. M. Varentsov and Gy. Grasselly (Eds.), Geology and Geochemistry of Manganese, Vol. 1, Akademiai Kiado, Budapest, 1980, p. 443.
12 Standards Association of Australia, AS 1038, Part 3: Proximate Analysis of Hard Coal, Standards Association of Australia, Sydney, 1979.
13 J. C. Mills, K. E. Turner, P. W. Roller and C. B. Belcher, X-ray Spectrom., 10 (1981) 131.
14 S. Abbey, Geol. Surv. Canada, Paper 77-34; X-ray Spectrom., 7 (1978) 99.
15 F. J. Flanagan, Geochim. Cosmochim. Acta, 37 (1973) 1189.
16 E. S. Gladney, Anal. Chim. Acta, 118 (1980) 385.
17 C. C. Graham, M. D. Glascock, J. J. Carni, J. R. Vogt and T. G. Spalding, Anal. Chem., 54 (1982) 1623.
18 A. C. Knott, K. J. Doolan and K. E. Turner, Part 3, Final Rep., NERDDP Grant 78-3031, June, 1981.

Analytica Chimica Acta, 154 (1983) 235—249
Elsevier Science Publishers B.V., Amsterdam — Printed in The Netherlands

A COMPARISON OF METHODS FOR THE DETERMINATION OF LEAD IN POTABLE WATERS BY ELECTROTHERMAL ATOMIC ABSORPTION SPECTROMETRY WITH LANTHANUM MATRIX MODIFICATION AND STANDARD ADDITION PROCEDURES

I. J. FLETCHER

South Staffordshire Waterworks Company, Green Lane, Walsall, West Midlands WS2 7PD (Gt. Britain)

(Received 1st February 1983)

SUMMARY

The determination of lead by electrothermal atomic absorption spectrometry was investigated for 30 different borehole and surface water samples by using direct, standard addition and lanthanum matrix modification procedures. In the direct method, suppressive interference was evident for most samples. In some cases suppression could be directly related to the constitution of the sample. Nitric acid and lanthanum (as the chloride or nitrate) were added to samples to overcome interferences in the direct determination. Source waters that exhibited severe suppression were used to optimize the concentrations of lanthanum and nitric acid (0.05% and 0.4%, respectively) required to effect full recovery of lead. The optimized procedure was evaluated during routine operation over a 6-month period with quality control samples and was shown to satisfy the required performance criteria for the determination of lead in potable waters. The method was superior to manual and automated standard addition procedures.

The determination of lead in potable waters has become of increasing interest following current concern over the effect of the total body lead burden on human health. Lead concentrations in surface and potable waters are typically less than 20 $\mu g\ l^{-1}$; however, where water has been in contact with lead plumbing, substantially higher levels may occur. The World Health Organisation [1] recommends a limit of 100 $\mu g\ l^{-1}$ lead in drinking water with a maximum of 300 $\mu g\ l^{-1}$ after 16 h contact with the pipes. The E.E.C. directive [2] specifies a maximum admissible concentration of 50 $\mu g\ l^{-1}$ lead in running water. Recognizing these limits and the expected range of lead concentrations in water, the Water Research Centre (W.R.C.) [3] proposed a set of analytical performance characteristics for the determination of lead in potable waters: concentration range, 0—100 $\mu g\ l^{-1}$; total standard deviation, 1.5 $\mu g\ l^{-1}$ (or 5% of the concentration); bias, 5 $\mu g\ l^{-1}$ (or 10% of the concentration) and limit of detection, 5 $\mu g\ l^{-1}$.

The direct determination of lead by flame atomic absorption spectrophotometry (a.a.s.) is not capable of achieving these performance criteria. In order that the required limit of detection can be achieved, pre-concen-

0003-2670/83/$03.00

tration techniques such as evaporation, chelation and liquid—liquid extraction or ion-exchange have been employed. Whilst such methods can meet the performance criteria, they suffer the disadvantage of being more time-consuming, requiring greater technical skill and in some cases being subject to interference and bias. The use of electrothermal a.a.s. is advantageous because it renders pre-concentration unnecessary and, with the availability of autosamplers, involves a minimum of operator time. Unfortunately, for the determination of lead, the method can suffer from severe suppressive interference that is dependent upon the major ion composition of the matrix. Several researchers [3—7] have reported the interference effects to be complex, unpredictable and variable from one atomizer to another. Although standard addition procedures can be used to eliminate errors caused by suppressive interferences, they also increase the complexity of the determination, increase the time required, and generally suffer from poorer precision. Consequently, much research has been expended in finding a method that eliminates the suppressive interference but still allows the direct determination of lead. The addition of chemical releasing agents such as ascorbic acid [8] and EDTA [9], matrix modifiers such as ammonium nitrate [10, 11] and mineral acids [5, 12] and graphite-coating elements such as lanthanum [6, 7, 13], tantalum [10] and molybdenum [5, 13] have been claimed to minimize suppressive interferences. Lanthanum coating of graphite tubes combined with lanthanum and nitric acid addition to samples has recently been reported as satisfying the performance criteria for the determination of lead in 14 drinking waters [6]. This paper reports further research into this method using 30 different ground and surface waters of the South Staffordshire Waterworks Company. The concentrations of lanthanum and nitric acid used were optimized to effect the release of lead from sources that still exhibited bias and the methods were compared to both automated and manual standard addition procedures. Additionally, the use of lanthanum as the chloride and nitrate salts was compared.

EXPERIMENTAL

Reagents and apparatus

The following reagents were used: nitric acid (1.42 s.g., UltraR; Hopkin and Williams), lanthanum chloride heptahydrate and lanthanum nitrate hexahydrate (both atomic absorption grade), lead standard, 1000 mg l^{-1}, in 0.1 M perchloric acid (Hopkin and Williams). Distilled water was used unless otherwise stated.

A Perkin-Elmer HGA-500 fitted with a non-pyrolytically coated graphite furnace tube was used in conjunction with a Perkin-Elmer 5000 atomic absorption spectrometer with deuterium arc background correction. Argon was used as a purge gas for the furnace. All pipetting of samples into the furnace was done automatically by an AS-40 autosampler. Results were printed out on a PRS-10 printer and the shape of the atomization peaks was monitored on a Perkin-Elmer 56 flatbed recorder.

Instrumental parameters

The spectrometer was set up according to the manufacturer's recommendations. Measurements were taken at 283.3 nm with simultaneous background correction in the peak height mode, which was found to be more precise than peak-area measurements. The operating parameters of the furnace (Table 1) were determined as follows. A sample volume of 20 μl with 20 μl of diluent, lanthanum or standard, necessitated a drying time of 45 s to prevent sputtering. The ashing temperature was optimized using a number of different sources of variable composition. A temperature of 600°C for 20 s minimized background absorption during atomization without causing a deterioration in sensitivity (Fig. 1). Ashing temperatures up to 700°C could be tolerated before the sensitivity of lead absorption during atomization was affected (Fig. 2). For atomization, the HGA-500 has the option of using maximum power heating with temperature overshoot being prevented by the use of optical temperature control. This has the advantage that lower atomization temperatures may be used without loss of sensitivity, thus lengthening tube life and potentially providing a means of atomizing more volatile metals prior to the matrix. When this facility was used, the optimum atomization temperature for lead was found to be 1300°C as opposed to 2600°C using normal voltage control of temperature (Fig. 3).

The precision of the different atomization methods was investigated by analyzing 5 randomly arranged aliquots of a series of standard solutions (Table 2). No significant variation in precision between the two principal atomization methods was recorded; however, the use of a 5-s ramp in place of the usual 1-s ramp for voltage control atomization did yield poorer results. Another feature of the HGA-500 is the ability to control the flow of argon passing internally through the graphite tube. Interrupting the gas flow during atomization provides greater sensitivity and is also a convenient means of controlling the linearity of the calibration graph (Fig. 4). The use of this facility at 283.3 nm for a 50 μg l^{-1} standard gave an absorbance of 0.4 to 0.45. At 217 nm sensitivity could be further increased 2—3 times but this was considered to be too sensitive for routine application. The effect

TABLE 1

Furnace operating parameters

Stage	Step	Temp. (°C)	Ramp time (s)	Hold time (s)	Internal gas flow (ml min^{-1})
Drying	1	90	4	1	300
	2	110	10	35	300
Ashing	3	450	4	1	300
	4	600	10	15	300
Atomisation	5	1300	0	10	0
Cleaning	6	2500	1	4	300

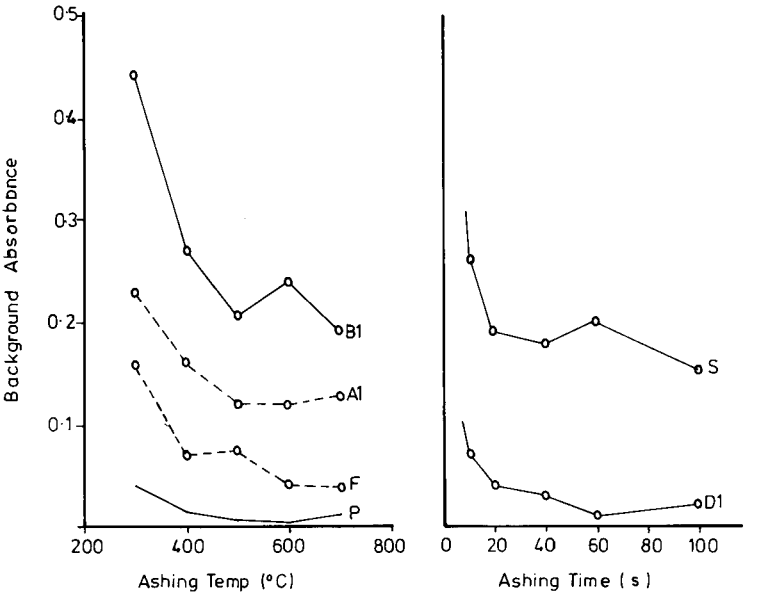

Fig. 1. Effect of ashing temperature and time on background absorbance during atomization of various source waters (see Table 4 for identity).

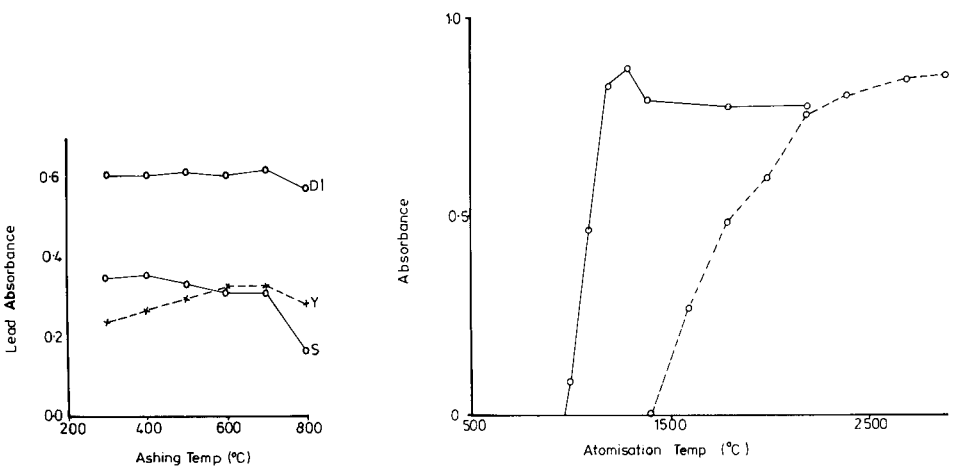

Fig. 2. Effect of ashing temperature on lead absorbance during atomization for spiked samples (see Table 4 for identity).

Fig. 3. Optimization of lead atomization temperature: (—) maximum power heating; (---) voltage-controlled heating.

on precision of using an internal gas flow rate of 60 ml min^{-1} to extend the linear range to 100 $\mu g\ l^{-1}$ was investigated for both atomization methods with standard solutions. No significant variation in precision was recorded.

TABLE 2

Precision (within-batch standard deviation, 4 degrees of freedom) for different atomization methods (expressed as $\mu g\ l^{-1}$)

Lead standard ($\mu g\ l^{-1}$)	Atomization at 1300°C Maximum power heating	Atomization at 2600°C Voltage control heating	
	No ramp	Ramp 1 s	Ramp 5 s
0 (blank)	0.13	0.06	0.10
5	0.00	0.09	0.50
10	0.11	0.18	0.54
20	0.57	0.91	1.48
50	0.59	1.48	1.70

Procedures

The use of the furnace programme in Table 1 necessitated the use of two standard solutions for operation in the concentration range 0—100 $\mu g\ l^{-1}$. On the autosampler a first standard (S1) of 50 $\mu g\ l^{-1}$ was used to calibrate the linear range and a second standard (S2) of 100 $\mu g\ l^{-1}$ was used to calibrate the non-linear region of the graph. All determinations were done in duplicate and the spectrometer was typically recalibrated with a blank and two standards after every 8—10 samples.

For determinations with lanthanum matrix modification, unless stated otherwise, new graphite furnace tubes were pre-conditioned with 5 firings of 20 μl of a 0.5% (w/v) lanthanum solution as either the chloride or nitrate.

Source water samples were stored in 250-ml polythene bottles and acidified with 1 ml of nitric acid (0.4% v/v). Low concentration lead standard solutions were prepared daily by dilution from a 10 mg l^{-1} stock standard, also in 0.4% nitric acid. Initially, samples of each of the source waters (in 0.4% nitric acid) were spiked at 20 and 40 $\mu g\ l^{-1}$ by the addition of 50 and 100 μl,

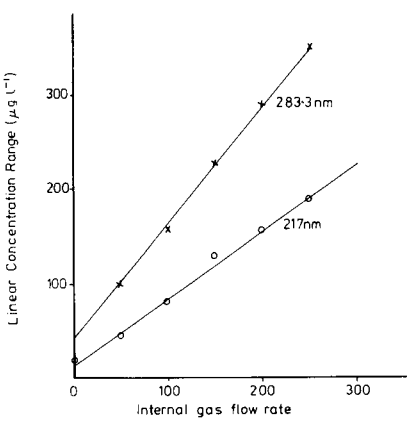

Fig. 4. Linear calibration range as a function of internal gas flow rate (ml min^{-1}) at 283.3 nm and 217 nm.

respectively, of a 10 mg l^{-1} standard to 25 ml of sample in a volumetric flask. The lead recoveries were investigated for all of these by five methods: (1) direct determination; (2) 0.01% lanthanum addition (as the chloride) before direct determination [6]; (3) automated standard addition with no lanthanum addition by means of the AS-40 autosampler (on 20-μl injections of sample and diluent, the spectrometer zeroes, then on 20-μl injections of sample and a 40 μg l^{-1} standard, it calibrates automatically, and on injection of 40 μl of diluent, the negative reading corresponds to the lead concentration in the sample); (4) manual standard addition with no lanthanum addition (samples spiked at 20 μg l^{-1} are treated as unknowns, the 40 μg l^{-1} spiked sample being utilized as a standard addition); (5) manual standard addition with 0.01% lanthanum addition (as chloride).

RESULTS AND DISCUSSION

Direct determination

The results are presented in Table 3. Without lanthanum addition, suppressive interference was evident for the majority of the source waters. Suppression was typically of the order of 20% with the exception of source waters K, S and E1 where substantially higher suppressions were recorded. Examination of the major ion concentrations for these waters revealed unusual facets of their composition that could be related to this suppression (Table 4). Source K had a sulphate concentration (398 mg l^{-1}) which was present principally as calcium sulphate [from a probable combinations analysis, (Table 5)] and resulted in a suppression in lead recovery of 70%. Similar interference ascribed to sulphate has been reported in a number of other studies [5, 10, 12, 15]. Source S contained a high chloride level (320 mg l^{-1}, as the sodium salt) and gave rise to a suppression of 41%. Chloride has also been widely reported to interfere in lead determinations [4, 5, 10, 11, 15]. Three mechanisms for its action have been identified. One is a high background absorption from the volatilization of sodium chloride. This is not thought to be a problem in this study because background absorption resulting from the use of lanthanum chloride (up to 766 mg l^{-1} chloride) did not result in any suppression. Another is the formation of lead chloride molecules which volatilize between 800 and 1000°C. In this study the use of maximum power heating should render this effect negligible. Finally, the formation of metal chloride crystals, which may occlude lead atoms, appears to be the most likely cause of suppression for source water S. Source water E1 had a less distinctive matrix but it seems likely that suppression is again related to the presence of various sulphate salts (Table 5). In this case, occlusion of lead in metal sulphate crystals may be the cause of suppression.

It is interesting to note that sample B1, which is similar to E1 except for its calcium carbonate concentration, does not show the same degree of suppression. A correlation analysis using all the sources did not reveal any

TABLE 3

Percentage suppression for the determination of lead (40 $\mu g\ l^{-1}$) for various lanthanum matrix modifications and standard addition procedures (all in 0.4% nitric acid)

Sample	Source[a]	Lanthanum pretreatment				Standard addition		
		None	0.01% (as Cl^-)	0.05% (as Cl^-)	0.05% (as NO_3^-)	Auto-mated	Manual	Manual (+La)
A	S + GW	−20	3	2	1	3	1	−7
B	S	−8	−4	−10	−4	−3	8	−13
C	S	−22	−8	−10	2	−3	4	−6
D	T.S.	−21	0	−1	−2	15	−3	−11
E	T.S.	−2	−1	−1	6	14	17	−1
F	T.S.	−28	−2	−5	−6	−6	−18	7
G	BH	−28	5	−6	−3	12	−15	9
H	BH	−12	2	−3	3	20	4	−13
I	BH	−26	−2	2	2	13	15	−5
J	BH	−2	−3	0	7	−1	24	−22
K	BH	−70	−27	4	0	37	−7	−7
L	BH	−18	−4	2	−1	21	6	10
M	BH	−20	−3	2	−3	18	−1	−2
N	BH	−16	−5	−3	−5	13	−4	−10
O	BH	−24	−8	−5	1	−1	−5	−1
P	BH	−14	−8	2	−3	−21	18	−6
Q	BH	−17	−9	5	6	27	3	6
R	BH	−18	−6	5	9	11	−10	−2
S	BH	−41	−34	−23	−17	39	15	45
T	BH	6	−8	−6	−3	−23	25	−10
U	S	−12	0	−6	−9	10	−3	8
V	BH	−22	−6	−8	−11	23	−7	−15
W	BH	−24	−5	−2	1	−6	11	17
X	BH	−21	−6	−8	−9	12	3	21
Y	BH	−14	−4	−4	−6	24	15	−4
Z	BH	−6	−2	−1	−7	—	−9	9
A1	BH	−11	−2	3	−7	20	−16	3
B1	BH	−16	5	4	−7	9	−12	−10
C1	BH	−15	6	2	−5	−4	−4	−6
D1	BH	−23	−4	2	4	—	−18	4
E1	BH	−54	−7	3	4	−13	0	15
Mean		−19.9	−4.8	−2.0(−1.3)[b]	−2.2(−1.7)[b]	8.8	1.3	0.2
Stand. Dev.		14.6	7.8	6.0(4.5)[b]	5.7(5.0)[b]	15.3	11.8	12.9
t value		7.48	3.37	1.83(1.6)[b]	2.12(1.9)[b]	3.15	0.60	0.0
Significance		Yes	Yes	No	No	Yes	No	No

[a]S, Surface water; T.S., treated surface water; GW, ground water; BH, borehole water.
[b]Values in parentheses exclude source S.

significant relationship between suppression and chloride, sulphate or hardness concentration. These findings support the results of other studies that the mechanisms of interference are complex; they cannot generally be related to the presence of a given species, but are specific to individual sample matrices.

Lanthanum addition at 0.01%

The use of only 0.01% lanthanum as recommended by Bertenshaw et al. [6] eliminated suppression for the majority of samples (Table 3). However, source K still exhibited a suppression of 27% and source S one of 34%. The bias for the remaining samples was within the recommended guidelines of 10%.

TABLE 4

Major ion concentrations (mg l^{-1}) in the source waters analyzed

Sample	ALK[a]	EC[a]	TH[a]	Ca^{2+}	Mg^{2+}	Na^{+}	K^{+}	Cl^{-}	SO_4^{2-}	NO_3^{-}
A	139	500	264	76	15	14	5	30	80	7
B	115	430	218	62	15	8	6	19	76	3
C	63	310	114	48	8	14	3	21	45	3
D	131	510	270	78	14	10	5	29	89	7
E	117	430	219	61	16	12	6	18	80	1
F	86	350	143	46	7	—	—	24	—	3
G	158	540	268	90	10	20	3	33	65	10
H	151	540	298	106	5	8	3	29	69	12
I	64	450	200	68	7	15	5	31	73	12
J	147	510	272	103	3	12	3	147	59	13
K	140	910	532	182	19	23	5	22	398	1
L	159	560	278	103	5	18	4	29	65	12
M	111	510	277	104	4	17	4	32	89	13
N	144	560	264	98	4	33	4	59	63	9
O	109	720	177	61	3	76	4	115	63	1
P	76	320	130	44	4	13	4	23	29	5
Q	77	510	192	63	9	24	7	51	64	9
R	86	430	162	55	6	24	6	39	47	5
S	214	1130	112	30	9	273	3	320	66	<1
T	124	490	242	87	3	11	3	25	59	10
U	12	70	22	7	2	4	<1	9	8	<1
V	164	660	252	80	12	56	4	96	58	2
W	125	690	293	104	8	29	3	99	64	10
X	138	630	258	93	4	34	2	75	59	6
Y	213	490	259	69	20	8	5	14	28	3
Z	207	560	267	92	9	15	3	26	37	3
A1	122	480	224	88	7	30	7	42	74	8
B1	151	740	320	115	8	35	5	59	104	13
C1	91	350	159	57	3	10	2	20	40	6
D1	252	830	392	106	31	50	10	74	149	<1
E1	109	690	274	57	32	45	9	78	136	<1

[a]ALK = alkalinity; TH = total hardness; EC = electrical conductivity (μS cm^{-1}).

Overall, the method showed an average negative bias of only 4.8%; however, the t value of 3.37 indicates that this bias is significantly different from zero at the $P = 0.01$ level ($t = 2.75$). For a method to be routinely applied, it is important that it should be valid for all of the water sources to be analyzed routinely. Consequently, lanthanum addition at 0.01% was judged to be unsatisfactory for routine use, but it was considered that further adjustment of lanthanum and nitric acid concentrations could yield satisfactory results.

Standard addition procedures

The automated standard addition procedure exhibited both poor precision and a positive bias that was significant at the $P = 0.01$ level ($t = 3.15$). Poor

TABLE 5

Probable combinations formed upon drying of source waters K, S and E1, based upon solubility considerations

Compound	Concentration (mg l^{-1})		
	K	S	E1
Calcium carbonate	152	78	106
Calcium sulphate	424	—	16
Magnesium carbonate	—	27	—
Magnesium sulphate	87	—	134
Sodium carbonate	—	121	—
Sodium sulphate	28	95	32
Sodium chloride	—	478	89
Sodium nitrate	—	0.6	—
Potassium chloride	1.5	—	18
Potassium nitrate	3.6	—	—

precision can be related to three factors. First, for automated standard addition all measurements must be taken on the linear portion of the calibration graph. To achieve this, it is necessary to reduce the sensitivity, in this case by increasing the internal gas flow rate during atomization. Secondly, the variance of each result depends upon the variance of three separate determinations. Finally, for samples exhibiting a suppressive interference the calibration slope will be less and will consequently result in a greater variance in the final result; the higher the suppression the greater the variance. The positive bias found for the procedure is tentatively ascribed to differences in the matrix composition between the diluent and sample.

Manual standard addition procedures showed no bias but poor precision was again evident due to the second and third factors listed above. Manual standard addition with matrix modification using 0.01% lanthanum showed slightly better precision than without matrix modification, because of the reduction in the error resulting from the calibration slope. Both procedures showed significantly better precision than automated standard addition.

However, neither the manual nor automated standard addition procedures investigated satisfied the required performance criteria. The precision of the techniques was 2—3 times worse than direct analysis. One of the claimed advantages of standard addition, the elimination of bias, is thus shown not to be universally true, and it is evident that standard addition procedures do not represent, as is widely believed, a satisfactory approach to the routine determination of lead in potable waters.

Optimization of lanthanum matrix modification

The three source waters, K, S and E1, that had resulted in particularly severe suppressive interference were used to investigate the effect of varying the nitric acid and lanthanum concentrations on lead recovery. Nitric acid concentrations of 0.1, 0.4 and 1.0% (v/v) and lanthanum concentrations of

0.005, 0.01, 0.025, 0.05 and 0.10% (w/v) were used. Lanthanum was investigated as its nitrate and chloride. It was considered that the nitrate salt could yield better results than the chloride because of decreased background absorption, increased partial pressure of oxygen during ashing (which has been reported [16] to affect the appearance temperature of lead during atomization), and decreased need for nitric acid to remove unwanted chloride during ashing. A new graphite tube was used for each batch of tests at a given acid concentration. The tube was preconditioned with lanthanum at the same concentration as that to be used in the tests.

The benefits of lanthanum addition are clearly illustrated in Fig. 5a which shows the average recoveries for the three source waters. The addition of small amounts of lanthanum gave large increases in recovery up to a concentration of 0.05%; further increases in lanthanum concentration afforded no further improvement. The results suggest that there is little difference between the use of lanthanum as either the chloride or nitrate. The effect of nitric acid concentration on the average lead recovery for the three sources is illustrated in Fig. 5b. Whilst not as dramatic as the effect of lanthanum, a steady improvement in recovery is evident with increasing acid concentration. Again there is no evidence of any difference between lanthanum nitrate and chloride except at low acid concentrations. For an acid concentration of 0.1% significantly poorer recoveries were recorded using lanthanum chloride; this may be explained by there being insufficient nitric acid to react with the excess of chloride to form hydrogen chloride which can then be removed during ashing. The use of the chloride also suffers from the disadvantage that

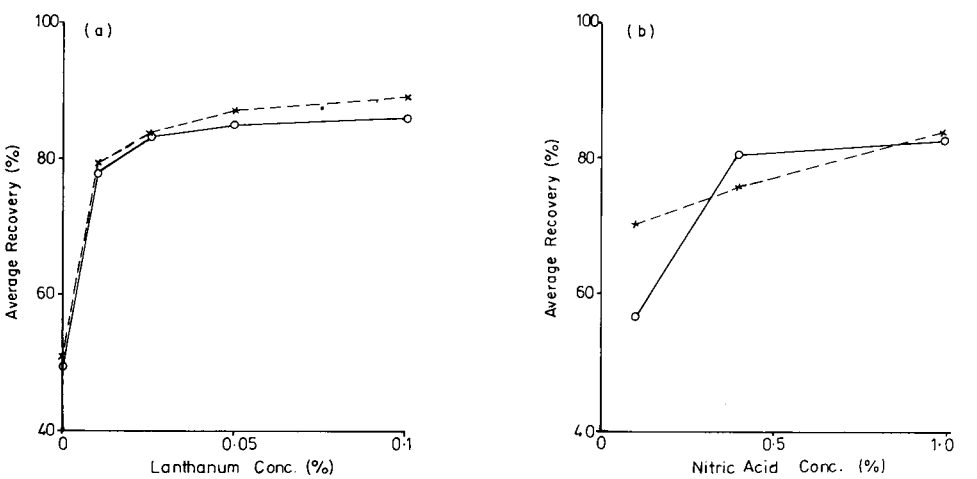

Fig. 5. Effect of reagent additions on the recovery of lead (40 $\mu g\ l^{-1}$) added to source waters K, S and E1. a, lanthanum addition: (×) as nitrate; (○) as chloride; each result is the mean of 9 for acidities of 0.1—1.0% (v/v). b, nitric acid addition for all lanthanum concentrations; (×, ○) as in a; each result is the mean of 18.

at 0.1% and above or combined with matrices with high chloride concentrations background interference may cause problems. The use of lanthanum nitrate, whilst suffering from none of the above drawbacks, is restricted by reagent contamination. The UltraR-grade reagent used for these tests was found to contain 2.37 μg Pb g^{-1}, resulting in a background lead concentration of 3.7 μg l^{-1} for a lanthanum addition of 0.05%. However, this did not result in any bias in the determinations, because equal quantities were used in both the samples and blanks. It is possible to clean up lanthanum nitrate stock solution by adding ammonium pyrrolidinedithiocarbamate to complex the lead and then extracting with freons.

Examination of the results for the individual sources highlighted the differing effects of the addition of lanthanum and nitric acid on different sample matrices (Fig. 6). For source water K, composed predominantly of calcium and magnesium sulphates, lead was released by the addition of lanthanum at concentrations down to 0.02% (Fig. 6a). The addition of nitric acid was also important, 0.4% being necessary to achieve full recovery. Similar results were obtained for source water E1 (Fig. 6b), which was again composed predominantly of sulphate salts, albeit at a lower concentration than source K; full recovery could be obtained with 0.01% lanthanum and 0.4% nitric acid. The results for source water S, which was composed primarily of sodium chloride, were of a completely different character (Fig. 6c). Lanthanum addition up to 0.1% was found to have no significant impact on lead recovery. However, the addition of 1.0% nitric acid improved recovery by 20%, through the mechanism discussed previously, but was not sufficient to yield full recovery. This last result contradicts the findings of Bertenshaw et al. [15], working on a different atomizer (IL-555) and using a different atomization method, with 0.05% lanthanum and 1% nitric acid. They reported full recovery for a sample containing 1150 mg l^{-1} chloride and 760 mg

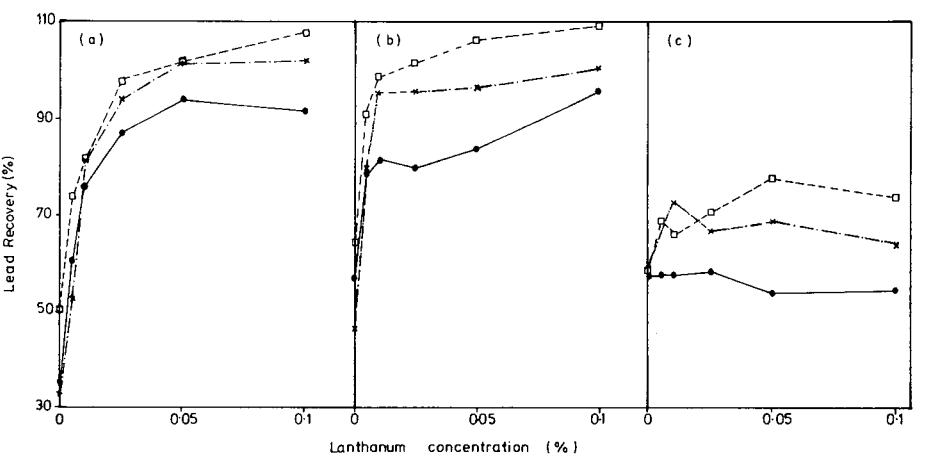

Fig. 6. The effect of lanthanum addition (as nitrate) on lead recovery (spiked at 40 μg l^{-1}) for various nitric acid concentrations: (a) source K (predominantly calcium sulphate); (b) source E1 (mixed sulphates); (c) source S (predominantly sodium chloride). Nitric acid: (•) 0.1%; (×) 0.4%; (□) 1.0%.

l^{-1} sodium. It is interesting to note that whilst chloride in the sample matrix, as either the calcium or in this case the sodium salt, is frequently related to suppression in the lead determination the addition of lanthanum chloride does not have this adverse effect. These observations again support the view that it is the total matrix composition that is important in defining the degree of suppression and not the concentration of individual species. Additionally, the fact that specific compounds rather than individual species are related to the suppression suggests that it is the type and mechanism of crystalline salt formation during drying that is important in determining the degree of suppression. During drying, the occlusion of lead atoms in a crystalline salt that is subsequently not completely volatilized during atomization may account for the suppression. It has been proposed that the beneficial action of lanthanum may be due to its disruptive action during salt formation [15].

Three different atomization methods were investigated to see if the recovery for source S could be further improved. The furnace programme remained the same, except for: (A) voltage-controlled atomization at 2600°C, ramp time 1 s, hold time 9 s; (B) ramped voltage-controlled atomization at 2300°C, ramp time 3 s, hold time 7 s; (C) maximum power heating atomization at 1300°C, ramp time 0 s, hold time 10 s. (Maximum power heating is thought to correspond to a heating rate of ca. 2000°C s^{-1}, resulting in an actual ramp time of 0.65 s.) Recoveries for sources K and E1 were also investigated by the three methods. The results are presented in Table 6. Voltage-controlled atomization at 2600°C with a ramp time of 1 s yielded full recovery for K and E1 and gave a recovery for source S that, at 90%, was just within the bias guidelines. Lowering the atomization temperature to 2300°C and introducing a ramp time of 3 s resulted in a large positive bias for K and E1 and an apparent 99% recovery for source S.

The cause of this bias was resolved by examination of the atomization traces for both standards and samples. For pure standards, the use of a 3-s ramp time resulted in twin atomization peaks because of the selective volatilization of the principal lead compounds present after drying. For samples, the matrix is more complex and the various atomization peaks, although detectable, were not fully resolved and hence resulted in a positive bias up to 20%. The apparent 99% recovery for source S is, therefore, not a

TABLE 6

Lead recoveries at the 40 $\mu g\ l^{-1}$ level for different atomization methods (A—C)

Source water	Lead recovery (%)		
	A	B	C
S	90	99	82
E1	101	116	103
K	99	121	102

TABLE 7

Performance of the optimized method for source water E1 spiked at various lead concentrations

Lead added ($\mu g\ l^{-1}$)	Standard deviation		
	Within-batch	Between-batch	Total
0	0.23	0.00	0.23
5	0.48	0.00	0.48
20	0.95	0.40	1.03
50	0.91	0.96	1.32
100	3.34	1.43	3.64

true result but can be ascribed to the bias of the technique. The findings indicate that ramped atomization is unsatisfactory for the determination of lead and that caution is needed in the interpretation of recovery tests. The use of maximum power heating with atomization at 1300°C showed no advantages over conventional voltage-controlled heating at 2600°C for these samples.

Method performance

The performance of the optimized lanthanum pre-treatment method (0.05% lanthanum, 0.4% nitric acid with maximum power atomization at 1300°C) was evaluated by analyzing samples of source water E1 spiked at 0, 5, 20, 50 and 100 $\mu g\ l^{-1}$ on 5 successive days. On each day, five randomly arranged aliquots at each concentration were injected. An analysis of variance was performed on the results to determine the within-batch, between-batch and total standard deviations [17]. The results are presented in Table 7. The total standard deviations do not exceed 1.5 $\mu g\ l^{-1}$ or 5% of the concentration and therefore satisfy the W.R.C. performance requirements. The limit of detection (4.65 × blank) is 1.07 $\mu g\ l^{-1}$ and is well within the required limit of 5 $\mu g\ l^{-1}$.

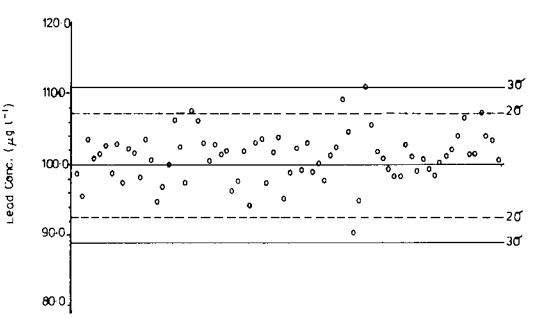

Fig. 7. Quality control chart for routine lead determination (Sept. '81—Feb. '82) for source water E1 spiked at 100 $\mu g\ l^{-1}$.

The bias of the optimized method (0.05% lanthanum chloride or nitrate with 0.4% nitric acid) was investigated for all of the water sources (Table 3). With the exception of source water S, which has been discussed above, all of the samples satisfied the requirement that the bias must not exceed ±10%. No significant difference was recorded between the use of lanthanum chloride or nitrate and the mean bias of −1.3% and −1.7%, respectively, was not significantly different from zero at the $P = 0.05$ level.

The optimized method has been in routine use in this laboratory for 6 months. Since the determination has been shown to be prone to suppressive interferences, it is considered important that quality control samples, prepared from a water known to cause suppressive interferences, are run with all batches of samples. For routine analysis, source water E1 spiked at 0 and 100 $\mu g\ l^{-1}$ has been used as a quality control. The results for the 100 $\mu g\ l^{-1}$ quality control samples are presented in Fig. 7; for 74 analyses a mean of 101 $\mu g\ l^{-1}$ and a standard deviation of 3.58 $\mu g\ l^{-1}$ were recorded. These results are in close agreement with those found by analysis of variance and serve to confirm the accuracy and precision of the method.

Conclusions

The direct determination of lead by electrothermal a.a.s. is prone to severe suppressive interference. The mechanisms causing suppression are recognised as being complex and often specific to a given sample matrix composition. In this study, calcium sulphate and sodium chloride matrices were particularly identified as resulting in severe suppression. For the source waters investigated, the addition of lanthanum was shown to be effective in eliminating suppression attributable to calcium sulphate but not sodium chloride. The addition of nitric acid was shown to reduce suppression caused by sodium chloride.

Matrix modification with 0.05% lanthanum and 0.4% nitric acid eliminated interferences for all but one of the 31 source waters examined and offers an approach for the direct routine determination of lead in potable waters by electrothermal a.a.s. Long-term evaluation of the method using quality control samples has shown it to be accurate and precise. Yet, it is recommended that the method should be applied with caution; the recovery of lead from source waters of unusual composition should be checked prior to routine use and quality control samples should be run with all measurements.

Standard addition procedures are unsatisfactory for the routine determination of lead in potable waters. Both manual and automated standard addition suffered from significantly poorer precision than direct measurements. Additionally, the automated procedure was found to be prone to a positive bias.

The author thanks the Directors of the South Staffordshire Waterworks Company for permission to publish this paper, and Dr. M. Richards, Head of the Water Quality Department for his interest.

REFERENCES

1 World Health Organisation, European Standards for Drinking Water, 2nd edn., WHO, Geneva, 1970.
2 Commission of the European Communities, Council Directive Relating to the Quality of Water Intended for Human Consumption; 80/778/EEC, Off. J. Eur. Communities, L229/11 (1980).
3 L. Ranson and B. Orpwood, An Evaluation of an Electrothermal Device for the Determination of Lead and Cadmium in Potable Water, Water Research Centre Tech. Rep. No. 49, 1977.
4 J. G. T. Regan and J. Warren, Analyst, 101 (1976) 220.
5 D. J. Hodges, Analyst, 102 (1977) 66.
6 M. P. Bertenshaw, D. Gelsthorpe and K. C. Wheatstone, Analyst, 106 (1981) 23.
7 K. C. Thompson, K. Wagstaff and K. C. Wheatstone, Analyst, 102 (1977) 310.
8 J. G. T. Regan and J. Warren, Analyst, 193 (1978) 447.
9 F. Dolinsek and J. Stupar, Analyst, 98 (1973) 841.
10 M. C. Halliday, C. Houghton and J. M. Ottaway, Anal. Chim. Acta, 119 (1980) 67.
11 V. B. Stein, E. Canellli and A. M. Richards, Int. J. Environ. Anal. Chem., 8 (1980) 99.
12 L. R. Hageman, J. A. Nichols, P. Visanadham and R. Woodriff, Anal. Chem., 51 (1979) 1406.
13 J. E. Poldoski, Anal. Chem., 52 (1980) 1147.
14 W. Frech and A. Cedergren, Anal. Chim. Acta, 88 (1977) 57.
15 M. P. Bertenshaw, D. Gelsthorpe and K. C. Wheatstone, Analyst, 107 (1982) 163.
16 S. G. Salmon, R. H. Davis and J. A. Holcombe, Anal. Chem., 53 (1981) 324.
17 R. V. Cheeseman and A. L. Wilson, Manual on Analytical Quality Control for the Water Industry, Water Research Centre Tech. Rep. No. 66, 1978.

Analytica Chimica Acta, 154 (1983) 251—257
Elsevier Science Publishers B.V., Amsterdam — Printed in The Netherlands

DETERMINATION OF ZINC(II) IONS WITH A REACTOR CONTAINING IMMOBILIZED CARBOXYPEPTIDASE A IN A FLOW SYSTEM

LARS RISINGER, LARS ÖGREN[a] and GILLIS JOHANSSON*

Department of Analytical Chemistry, University of Lund, P.O. Box 740, S-220 07 Lund (Sweden)

(Received 5th July 1983)

SUMMARY

Zinc(II) was determined in the range 2—20 × 10^{-7} M through its activation of immobilized, metal-free carboxypeptidase A. The activity was assessed by injection of hippuryl-L-phenylalanine and the decomposition product was determined by high-performance liquid chromatography. Cadmium(II) and mercury(II) depressed the zinc response of the method although there was excess of metal-free enzyme in the reactor. Regeneration was made by pumping a 1,10-phenanthroline solution through the reactor between successive samples.

Townshend and coworkers [1—3] pioneered the use of metalloenzymes for trace metal determinations by using alkaline phosphatase for the determination of zinc and polyphenol oxidase for the determination of copper. The first step of the method involves removal of the metal from the enzyme by a strong complexing agent. The apoenzyme formed is then brought into contact with the sample so that metal ions can be taken up and bound to the active site. Only enzyme molecules containing a metal ion will be active and the trace metal content can therefore be evaluated from a measurement of the enzyme activity.

The limit of detection will depend on the stability constant of the enzyme—metal ion complex and the selectivity will reflect the degree to which other ions will produce enzyme activity when they replace the natural occupant of the binding site. The binding strength, the degree of selectivity and the interference from inhibitors varies from one enzyme to another. Around 120 zinc metalloenzymes are known [4] and the metal-binding properties have been studied for quite a number of these. The present work on carboxypeptidase A is part of a program in this laboratory to improve methods for zinc determination. Carboxypeptidase A is very stable both as a metalloenzyme and as an apoenzyme [4—6]. It can catalyze either a peptidase reaction involving removal of a terminal amino acid or an esterase reaction involving breakage of a terminal ester bond. The peptidase reaction can take place with zinc,

---

[a]Present address: AB Draco, P.O. Box 1707, S-221 07 Lund, Sweden.

0003-2670/83/$03.00

cobalt, nickel and manganese ions, whereas the esterase activity can be evoked also by cadmium, mercury, rhodium and lead. The latter metals inhibit the peptidase activity when bound at the active site [7, 8]. A selective and sensitive enzymatic method for zinc(II) determination was described by Lehky and Stein [9]. They utilized the zinc activation of aminopeptidase and monitored the reaction spectrophotometrically.

EXPERIMENTAL

Enzyme reactors

Carboxypeptidase A from bovine pancreas (Sigma Cat. No. C-0386) was coupled with glutaraldehyde to porous glass CPG-10 (pore diameter 72.9 nm, 140—170 mesh; Electronucleonics). The enzyme (100 mg g^{-1} of alkylamino-glass) was dissolved in a buffer (0.5 M sodium chloride, 0.05 M sodium phosphate, pH 7.0) and reacted overnight at 4°C with the activated glass. About 60% of the enzyme remained on the glass when it had been washed with buffer and water.

The enzyme glass was used to fill three reactors of different sizes (I: i.d. 2.5 mm, length 4.1 mm, volume 20 μl. II: i.d. 2.7 mm, length 17.8 mm, volume 100 μl. III: i.d. 2.7 mm, length 28.4 mm, volume 160 μl). The reactors were made of teflon with screw fittings for the connecting tubes and the enzyme-glass was held in place with two polypropylene nets.

Apparatus and reagents

The flow injection manifold (Fig. 1) consisted of a peristaltic pump (Ismatec, type mp-ge), a six-way rotary valve (Altex, model 202), a Růžička—Hansen-type injector with a bypass loop for flow injection analysis (f.i.a.) [10] and a loop injector (Rheodyne, model 7125, 10 μl) used for introduction of samples into a h.p.l.c. system.

The metal ions were first removed from the immobilized enzyme with an apoenzyme regeneration solution (3 min, 1 ml min^{-1}) followed by water (4 min, 1 ml min^{-1}). The sample, normally 0.5 ml, was then introduced via the f.i.a. injection loop. It was transported through the reactor with water as carrier (1 ml min^{-1}). The activity of the enzyme reactor was assessed by

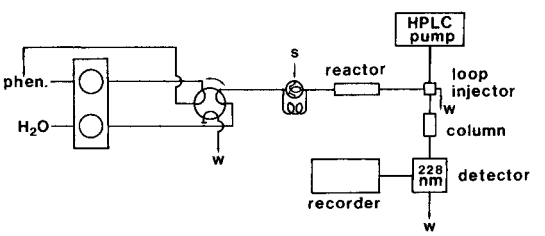

Fig. 1. Flow injection manifold for zinc determination based on a reactor containing carboxypeptidase A, in the measurement mode. The product assay is made with a h.p.l.c. system connected to the outlet of the reactor. The regeneration solution can be switched on-line with the first valve. W = Waste, S = sample or substrate injection.

introduction of 0.5 ml of substrate solution via the f.i.a. injection loop. This volume was large enough to give a steady-state product concentration in the h.p.l.c. loop injector. When this occurred, 30 s after injection for a flow rate of 1 ml min^{-1}, a 10-μl sample was switched into the h.p.l.c. system for measurement. The i.d. of the teflon tubing in the f.i.a. system was always 0.3 mm.

The substrate solution was 10 mM hippuryl-L-phenylalanine (Sigma H-6875) in 50 mM Tris—HCl buffer (Tris[hydroxymethyl]aminomethane, Sigma T-1378), pH 7.5. Active carboxypeptidase A cleaves the substrate into L-phenylalanine and hippurylic acid. The recommended regeneration solution is 10 mM 1,10-phenanthroline.

The h.p.l.c. product separation was done on a C-18 stationary phase (Spherisorb ODS, 5 μm, column i.d. 4 mm, length 90 mm) with a mobile phase of 50 mM Tris—HCl buffer, pH 7.5, containing 1% ethanol. The substrate is completely absorbed by the column; the two product peaks are almost separated, and emerge from the column after 4 min. The molar absorptivity of hippurylic acid at 228 nm is 240 times greater than that of L-phenylalanine. The recorded signal therefore represents essentially the amount of hippurylic acid in spite of a small peak overlap. The substrate itself absorbs radiation at the same wavelengths as hippurylic acid which rules out the possibility of detection without separation.

The substrate from successive injections accumulates on the columns and gradually changes its properties. The peak height for standard injections of hippurylic acid increased by 0.22% for each injection (10 mM substrate) into the chromatographic system. The column was regenerated with 100% ethanol after about 15 injections.

Decontamination and sample preparation

Concentrated Tris—HCl buffers (0.25 M) were purified electrolytically for 50 h over a stirred mercury pool kept at −1.4 V vs. SCE by potentiostatic control. The buffers were diluted with water before use. Purification by passing through a column (i.d. 10 mm, length 400 mm) of Chelex-100 (BioRad Laboratories) was equally effective. The apoenzyme regeneration solutions were sometimes purified by extraction with Freon 112 (trichlorotrifluoroethane). Any effect was only marginal and this step was therefore often omitted.

All glass and plastic materials were washed in 2 M nitric acid (pro analysi) for 48 h or more before thorough washing in water. The water was purified by reverse osmosis, ion exchange and carbon adsorption (Milli-Q, Millipore).

Stock solutions of the metal ions were made by weighing appropriate amounts of the nitrates to prepare 0.1 M solutions which were then diluted to 10^{-4} M secondary standards. Sample solutions were prepared fresh just before use by further dilutions of the secondary standards with 50 mM Tris—HCl containing 2×10^{-5} M alanine. The amino acid was added to decrease zinc adsorption on the walls of the apparatus.

RESULTS

Figure 2 shows the calibration curves obtained for zinc, cadmium and mercury when one metal at a time was present in the sample. The response is linear with respect to the zinc concentration except below 0.1 nmol. A fully active 100-μl enzyme reactor produces 5 mM hippurylic acid when fresh. Its maximum output decreases slightly with time because of slow deactivation of the enzyme. As the substrate concentration was 10 mM, the reactor conversion will be at most 50% for reactor II when excess of zinc is added and at most 8% within the range shown in Fig. 2. A linear relation between the amount of zinc and the amount of product is expected if mass transfer effects in the reactor can be neglected and the conversion is less than 10% [11]. The chromatographic system has a linear response up to 2 mM hippurylic acid with peak height measurements and up to the maximum output of the reactor with peak integration. The system has thus been designed to give a linear response.

The lower limit of detection, 0.1 nmol, is determined by the impurities remaining in the water and in the reagents. The sensitivity of the detection system is not a limiting factor and it could have been increased substantially. The responses of the 100- and 160-μl reactors were almost equal but slightly greater than that of the 20-μl reactor. The 100-μl reactor was selected because its substrate conversion was low enough to give a linear response over the range used ($0—12 \times 10^{-10}$ mol zinc) and because its capacity exceeded that needed for zinc alone by a factor of six.

The apoenzyme regeneration conditions were established from a series of runs with a standard amount of zinc in the reactor. The regeneration time was increased successively and the remaining peptidase activity was determined each time from a standard substrate injection (Fig. 3). An almost constant level, which is significantly different from zero, seems to be reached for each reagent. There is little difference between 8-quinolinol and 1,10-phenanthro-

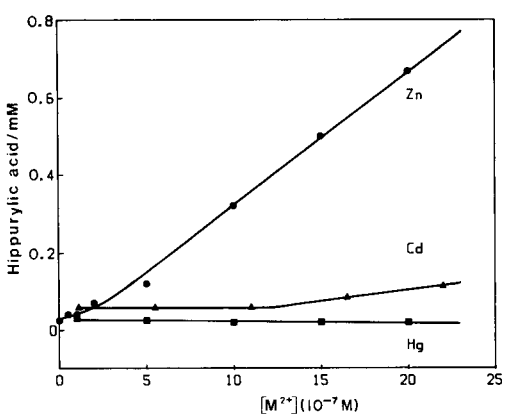

Fig. 2. Calibration graphs for zinc, cadmium and mercury (Reactor II, 100-μl volume, 0.5-ml samples).

line, although equilibrium data [7] indicate that the former should have been superior. The remaining peptidase activity is probably due to the inability of the chelating agents completely to remove the zinc. Impurities in the water or the reagent will also show up as a remaining peptidase activity. A procedure involving regeneration with 10 mM 1,10-phenanthroline for 3 min was selected.

Vallee [4] states that cadmium, mercury, rhodium, lead and copper are unable to activate the peptidase reaction of the enzyme. Figure 2 confirms that there is no activity with mercury and only a slight activity with cadmium. When zinc and cadmium are both present simultaneously in the same sample, however, the response is substantially less than that expected from the amount of zinc alone (Fig. 4). Cadmium seems to inhibit the zinc metalloenzyme and to depress the overall peptidase activity. Substitution between zinc and cadmium has been studied before [8], when it was shown that a considerable time is required for equilibrium to be achieved. Because the contact time in the enzyme reactor is very short, only slight interference had been expected in the present experimental arrangement. Mercury depressed the response to about the same degree as cadmium when it was present in the zinc sample solution.

Addition of alanine to the dilute samples increased the reproducibility of the measurements substantially. The zinc—amino acid complex (pK = 10.5 [8]) is not strong enough to compete with the enzyme—zinc complex but the complexation is sufficient to prevent zinc losses by adsorption. The enzyme takes up zinc at almost the same rate from the amino acid complex as from a solution of zinc aquo ions [12]. The rate of uptake from tris-, tetra- or higher dentate ligands decreases by orders of magnitude in the mentioned order. Addition of an amino acid to the sample might also serve a

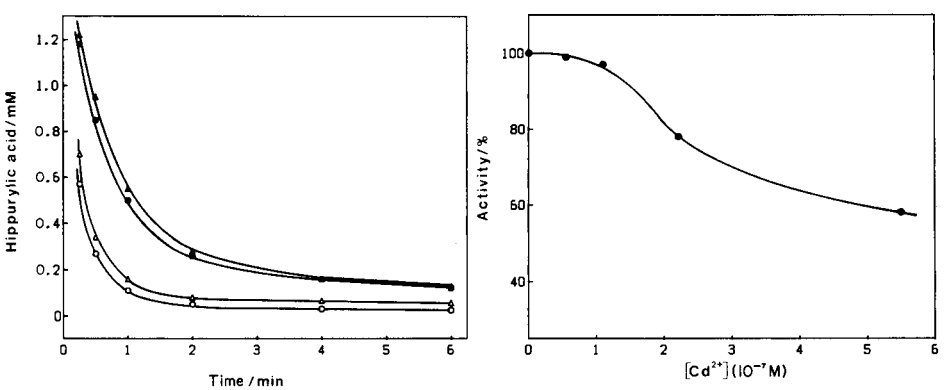

Fig. 3. Peptidase activity after various regeneration times (Reactor II, 100 μl, 1 ml min^{-1}) with solutions of 8-quinolinol or 1,10-phenanthroline. 8-Quinolinol: (▲) 1 mM, (△) 10 mM. 1,10-Phenanthroline: (●) 1 mM, (○) 10 mM.

Fig. 4. Depression of the zinc response when various amounts of cadmium were also present (0.5-ml sample, 2.0 × 10^{-6} M zinc.)

second purpose, mediating zinc transfer between multidentate ligands and the enzyme site.

The response obtained with a standard amount of zinc depended on the flow rate and the reactor size (20—35% decrease with increasing flow rate from 0.25 to 1.00 ml min^{-1} for reactors I—III). It was not possible to evaluate the completeness of the metal uptake from the data obtained. One effect behind the changed response is probably that differences in flow rate will affect the distribution of the metal both along the reactor and inwards towards the center of the enzyme-treated porous glass. If the internal mass transfer resistance is of importance in the reactor kinetics, such a redistribution will affect the rate of product formation [13].

DISCUSSION

The most important advantage of the present method compared to those described before [1, 2, 9] derives from the use of an immobilized enzyme in a flow system. The enzyme can be converted to the apoenzyme on-line by just turning a valve, and the number of steps to be undertaken in the sampling and activity measurement are also fewer. The chromatographic step makes the method slower (5 samples h^{-1}) than it would have been with a more direct method of product determination and it also increases the amount of equipment necessary.

The interferences from inhibiting metal ions were expected to be less than those actually observed for two reasons. The available data [7, 8] indicate that several hours were necessary for complete interchange in the steady state. If the zinc is bound to an enzyme site first, it should not be replaced by cadmium to any significant degree during the short time of the experiment. The second reason is that the reactors contain an excess of apoenzyme sites compared to the total metal ion content. It should make little difference if a few of the metalloenzyme molecules contain cadmium because of its slow turnover. The observation that even small amounts of cadmium or mercury depress the response for zinc may indicate that the interfering metal ions are bound at a second site of a zinc metalloenzyme with a resulting inhibition of its peptidase activity. The way the active sites are distributed within the reactor may also be of importance for the response. The carboxypeptidase A thus seems to be less selective in practice than the aminopeptidase used by Lekhy and Stein [9].

The sensitivity of the method can be adjusted by changing the sample volume. The linearity of the response curve shows that it should make no difference if a certain amount of zinc is present in a smaller or larger sample volume as long as the binding strength of the apoenzyme is sufficient to remove the metal ions from the sample solution. The sensitivity of the present method using carboxypeptidase A seems to be about the same as that of the reported aminopeptidase method. It was impossible in both cases to obtain a completely inactive apoenzyme. It might be possible to increase the sensi-

tivity by using a stronger chelating agent during the regeneration. EDTA alone is out of the question for kinetic reasons but an approach based on multidentate and mediating ligands together may show some promise.

The authors thank Mr. I. Csiky for valuable comments on the h.p.l.c. method and the Swedish Natural Research Council for financial support.

REFERENCES

1 A. Townshend and A. Vaughan, Talanta, 16 (1969) 929.
2 A. Townshend and A. Vaughan, Talanta, 17 (1970) 289.
3 J. V. Stone and A. Townshend, J. Chem. Soc. Chem. Commun., (1972) 502; J. Chem. Soc., Dalton Trans., (1973) 495.
4 B. L. Vallee, Carlsberg Res. Commun., 45 (1980) 423.
5 P. Campbell and N. T. Nashed, J. Am. Chem. Soc., 104 (1982) 5221.
6 J. E. Coleman and B. L. Vallee, J. Biol. Chem., 235 (1960) 390.
7 T. L. Coombs, J.-P. Felber and B. L. Vallee, Biochemistry, 1 (1962) 899.
8 J. E. Coleman and B. L. Vallee, J. Biol. Chem., 236 (1961) 2244.
9 P. Lehky and E. A. Stein, Anal. Chim. Acta, 70 (1974) 85.
10 J. Růžička and E. H. Hansen, Anal. Chim. Acta, 114 (1980) 19.
11 L. Ögren, Thesis, University of Lund, Lund, Sweden, 1981.
12 E. J. Billo, J. Inorg. Biochem., 10 (1979) 331.
13 G. Johansson, L. Ögren and B. Olsson, Anal. Chim. Acta, 145 (1983) 71.

Analytica Chimica Acta, 154 (1983) 259—265
Elsevier Science Publishers B.V., Amsterdam — Printed in The Netherlands

SIMULTANEOUS DETERMINATION OF IRON AND TITANIUM IN SILICATE ROCKS BY USING DIANTIPYRINYLMETHANE WITH DUAL-WAVELENGTH SPECTROPHOTOMETRY

CHAN-HUAN CHUNG

The Laboratory of Anhui Geological Bureau of China, Hafei, Anhui (People's Republic of China)

(Received 11th April 1983)

SUMMARY

The simultaneous determination of iron(III) and titanium(IV) with diantipyrinylmethane (DAPM) based on dual-wavelength spectrophotometry is described. The absorbances at 388 nm, 470, and 514.9 (A_{388}, A_{470}, and $A_{514.9}$, respectively) are measured and a ratio k (= $A_{388}/A_{514.9}$) of 3.64 is introduced to allow simultaneous determinations of iron and titanium. The apparent molar absorptivities obtained by using the differences in absorbance, $A_{388}-A_{514.9}$, for titanium and $A_{470} \times k - A_{388}$ for iron, are 1.41×10^4 and 1.13×10^4 l mol^{-1} cm^{-1}, respectively. The calibration graphs are linear up to 20 mg l^{-1} iron(III) oxide and 5 mg l^{-1} titanium(IV) oxide. The proposed method was applied successfully to the determination of iron and titanium in silicate rocks. The protonation equilibria of DAPM were also studied; K_{a1} and K_{a2} are estimated as $10^{1.10}$ and $10^{0.75}$, respectively.

Diantipyrinylmethane (DAPM), which forms a yellow complex with titanium, was first introduced for the determination of titanium in the presence of iron, fluoride, and phosphate by Minin [1]. Jeffery and Gregory [2] used DAPM for the determination of titanium in rocks; the major interference by iron(III) can be reduced by adding ascorbic acid. Therefore, DAPM has been extensively used for the determination of titanium in rocks and minerals [3].

In the work described here, the protonation reaction of DAPM and the equilibria of complex formation of the iron(III)—DAPM and titanium(IV)—DAPM systems were investigated by using conventional spectrophotometry. Methods were developed for simultaneously determining titanium and iron in rocks by using dual-wavelength techniques. The reagent is readily available, the procedure is simple and rapid, and the results are accurate. The recommended procedure is useful for silicate rocks.

EXPERIMENTAL

Apparatus and reagents

A Hitachi 220-A double beam spectrophotometer and a Hitachi 557 dual-wavelength spectrophotometer with 10-mm silica cells were used for the measurements of absorbance.

0003-2670/83/$03.00

All solutions were prepared from analytical reagent-grade chemicals and distilled water.

Diantipyrinylmethane solution. DAPM (5 g) was dissolved in 100 ml of 1.7 M (mol dm^{-3}) hydrochloric acid.

Standard titanium solution. A solution of titanium(IV) oxide (0.1 mg ml^{-1} TiO_2) was prepared by dissolving titanium potassium oxalate in dilute sulfuric acid, heating the solution, and diluting with water.

Standard iron(III) solution. A solution of iron(III) oxide (0.2 mg ml^{-1} Fe_2O_3) was prepared by dissolving iron(III) oxide in hydrochloric acid and diluting with water.

Procedures

Recommended general procedure. Take aliquots of a sample solution containing not more than 0.5 mg of titanium(IV) oxide and 2 mg of iron(III) oxide in 100-ml volumetric flasks. Add 2.5 ml of 2 M hydrochloric acid and 15 ml of 5% (w/v) DAPM solution, while swirling the flask, and allow to stand for about 30 min. Measure the absorbances of this solution at 388 nm, 470 nm, and 514.9 nm using the double-beam spectrophotometer.

Preparation of calibration curves. Transfer five solutions covering the range 0.1—0.5 mg of titanium(IV) oxide to five 100-ml volumetric flasks, and five solutions covering the range 0.4—2.0 mg of iron(III) oxide to another five 100-ml flasks. Add 2.5 ml of 2 M hydrochloric acid, and 15 ml of 5% (w/v) DAPM solution to each flask, dilute to the mark with water, and mix thoroughly. After 30 min, measure the absorbances at 388, 470, and 514.9 nm using the double beam spectrophotometer. Prepare the calibration curve for titanium(IV) oxide by plotting the difference in absorbance, $A_{388} - A_{514.9}$, and that for iron(III) oxide by plotting the difference in absorbance, $A_{470} \times k - A_{388}$ (see Results and Discussion).

Analysis of samples. Prepare the rock samples in the usual way by fusion with sodium carbonate. After leaching the sodium carbonate melt, remove silica as its gelatinous precipitate. Transfer 5-ml aliquots of the filtered solution to 100-ml volumetric flasks, add 15 ml of 5% (w/v) DAPM solution, dilute to the mark with water, and mix thoroughly. Measure the absorbances in the same way as for the preparation of the calibration graph.

RESULTS AND DISCUSSION

Protonation of DAPM and ion-pair formation with iron and titanium species

Sandell and Onishi [4] indicated that DAPM is protonated through the carbonyl groups with one or two H^+ to form colorless DAPM cations (RH^+, RH_2^{2+}) in acidic media. This cation forms ion-pairs with the anionic complexes of Cl^-, Br^-, I^-, and SCN^- with various metals.

The absorption spectra of DAPM solution at various acid concentrations were studied (Fig. 1). Increasing acidity decreases the absorbance at 265.5 nm and yields maximum absorption at 237 nm, indicating that the $DAPMH_n^{n+}$

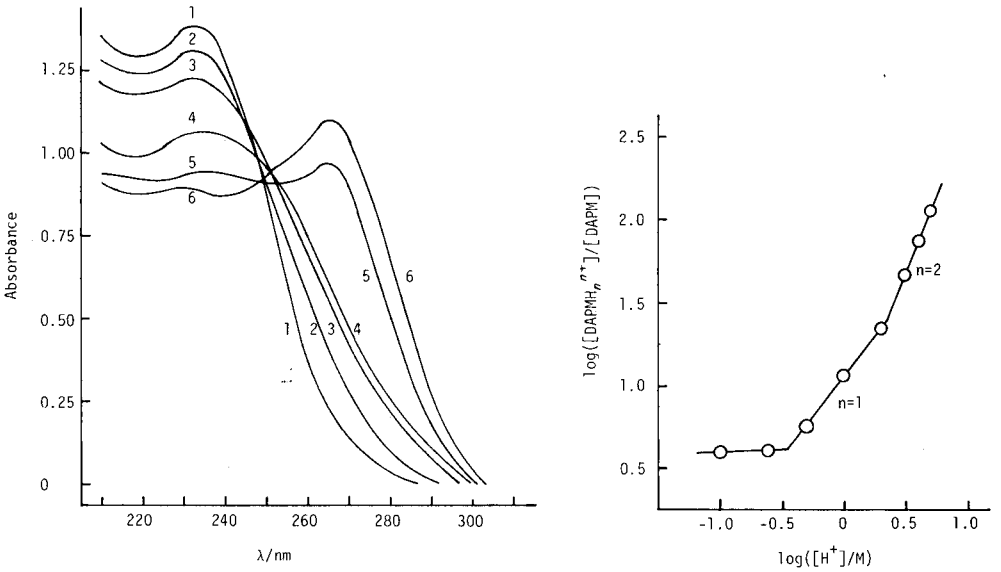

Fig. 1. Absorption spectra for 0.0025% DAPM at various acidities with hydrochloric acid: (1) 4.8 M; (2) 2 M; (3) 1 M; (4) 0.5 M; (5) 0.005 M; (6) 0.00075 M.

Fig. 2. Plots of $\log([DAPMH_n^{n+}]/[DAPM])$ against $\log[H^+]$ at 0.0025% DAPM.

cation is formed. In 7 M hydrochloric acid the absorbances at 237 nm and 265.5 nm are 1.34 and zero, respectively. The protonation equilibrium is described by

$$DAPM + nH^+ \rightleftharpoons DAPMH_n^{n+};\ K_a = [DAPMH_n^{n+}]/[DAPM][H^+]^n$$

$$\text{or } \log[DAPMH_n^{n+}]/[DAPM] = \log K_a + n\log[H^+] \quad (1)$$

The left-hand side of Eqn. 1 can be evaluated from the absorption spectra of solutions with different acidities. The logarithmic plot is shown in Fig. 2. It was then calculated that the first protonation constant is $10^{1.10}$ and the second constant is $10^{0.75}$.

Diantipyrinylmethane forms a yellow complex with titanium(IV) and a red-brown one with iron(III) in acidic media. The formation of ion-pairs was examined by the slope-ratio method [5].

The equilibrium reaction in acidic solutions is described by

$$mM + nR \rightleftharpoons M_mR_n;\ K = [M_mR_n]/[M]^m[R]^n$$

$$\text{or } \log[M_mR_n] = \log K + m\log[M] + n\log[R] \quad (2)$$

where M and R refer to metal complex ions and DAPM ions, respectively. When the reagent R is in large excess, a plot of $\log[M_mR_n]$ against $\log[M]$ gives the m and K values; when the metal ion is in large excess, a plot of $\log[M_mR_n]$ against $\log[R]$ gives the n and K values. Experimental results

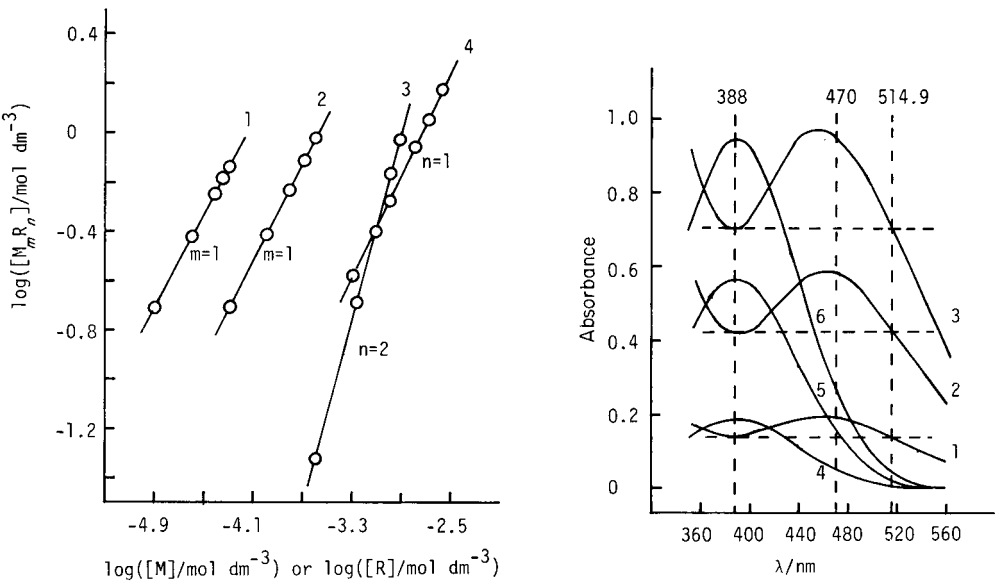

Fig. 3. Plots of $\log[M_mR_n]$ against $\log[M]$ or $\log[R]$: (1) for titanium in excess of R; (2) for iron in excess of R; (3) in excess of titanium; (4) in excess of iron.

Fig. 4. Absorption spectra for the iron(III)—DAPM and titanium(IV)—DAPM complexes. Iron(III) oxide concentration: (1) 0.4; (2) 1.2; (3) 2.0 mg/100 ml. Titanium(IV) oxide concentration: (4) 0.1; (5) 0.3; (6) 0.5 mg/100 ml.

(Fig. 3) indicate the equilibria

$$DAPMH^+ + FeCl_4^- \rightleftharpoons DAPMH \cdot FeCl_4$$

$$2DAPMH^+ + Ti(OH)_2Cl_4^{2-} \rightleftharpoons (DAPMH)_2 \cdot Ti(OH)_2Cl_4$$

with the corresponding equilibrium constants, $\log K$(Fe—DAPM) = 5.00 and $\log K$(Ti—DAPM) = 11.4.

Absorption spectra and simultaneous determination of iron and titanium

The absorption spectra of the ion-pairs are shown in Fig. 4. A strong yellow color is obtained with titanium(IV) in hydrochloric acid media, and the wavelength of maximum absorption is 388 nm. The red-brown complex formed with iron(III) has strong absorption over the range 540—360 nm, with maximum absorption at 456 nm, and so seriously interferes with the determination of titanium(IV). Ordinarily, in rock analysis, the interference from iron(III) on titanium(IV) can be avoided by prior reduction to iron(II) with ascorbic acid, but titanium(IV) also seriously interferes in the determination of iron with DAPM.

The dual-wavelength technique based on measurements at different wavelengths where one of the two species gives the same absorbance was therefore applied to the determination of titanium(IV). When the acidity of the

solution and the amount of DAPM were controlled, it was possible to determine titanium(IV) in the presence of a comparable amount of iron(III) by using the dual-wavelength method at 388 nm and 514.9 nm, at which the Fe—DAPM ion-pair has the same absorbance. The difference in absorbance between 388 nm and 514.9 nm gives the concentration of titanium(IV); the apparent molar absorptivity corresponding to the difference in these absorbances is 1.41×10^4 l mol^{-1} cm^{-1}.

For the determination of iron(III), the dual-wavelength technique with k coefficient method is applied. The ratio k is defined as the ratio of the absorbance at 388 nm and 470 nm, i.e., $k = A_{388}/A_{470}$. Therefore, in a way similar to the determination of titanium mentioned above, the difference between the absorbance at 470 nm multiplied by k and the absorbance at 388 nm, $A_{470} \times k - A_{388}$, gives the concentration of iron(III). The difference in absorbance gives an apparent molar absorptivity of 1.13×10^4 l mol^{-1} cm^{-1}, the sensitivity being comparable to that of the 1,10-phenanthroline method.

A procedure for the analysis of rocks calls for the development of the color of both the iron— and titanium—DAPM ion-pairs. In the double-beam spectrophotometer, the absorbance is measured successively at the wavelengths 388, 470 and 514.9 nm, and is recorded by a printer. The dual wavelength spectrophotometer can also be used. Thus, mutual interference between iron(III) and titanium(IV) can be removed.

Effects of acidity and of DAPM concentration, and stability

In the analysis of rocks, titanium was determined spectrophotometrically in 2 M hydrochloric acid solution with DAPM, because the interference by iron(III) is decreased at higher acidities. The colored solutions of the titanium—DAPM ion-pair formed in the acidity range 0.2—4 M are very stable. Although DAPM is slowly crystallized from an acidic solution of less than 0.2 M, the color intensity of the solution remains unchanged. When the pH exceeds 2, the color intensity reduces slightly because of the titanium ion hydrolysis.

The color intensity for iron(III) decreases with increasing acidity and the acidity dependence increases with decreasing DAPM concentrations (Fig. 5, lines A, B, and C). Lines a, b, and c show the difference in the absorbances at 470 and 388 nm, $A_{470} - A_{388}$. With a DAPM concentration of 0.75 g/100 ml these differences are independent of acid concentration in the range 0.3—0.4 M. The acidity of the solution need not be closely controlled. Thus, it is possible to determine iron and titanium in the 0.3—0.4 M range of acidity.

The effect of the DAPM concentration on the Fe—DAPM absorbance in 0.3 M acid solution is shown in Fig. 6. The absorbance at 470 nm increases with an increase in DAPM concentration, whereas the difference in the absorbances at 388 nm and 470 nm (curve B) is independent of the DAPM concentration if it exceeds 0.6 g/100 ml. For the most accurate determination of iron and titanium, addition of 15 ml of 5% (w/v) DAPM solution is generally satisfactory.

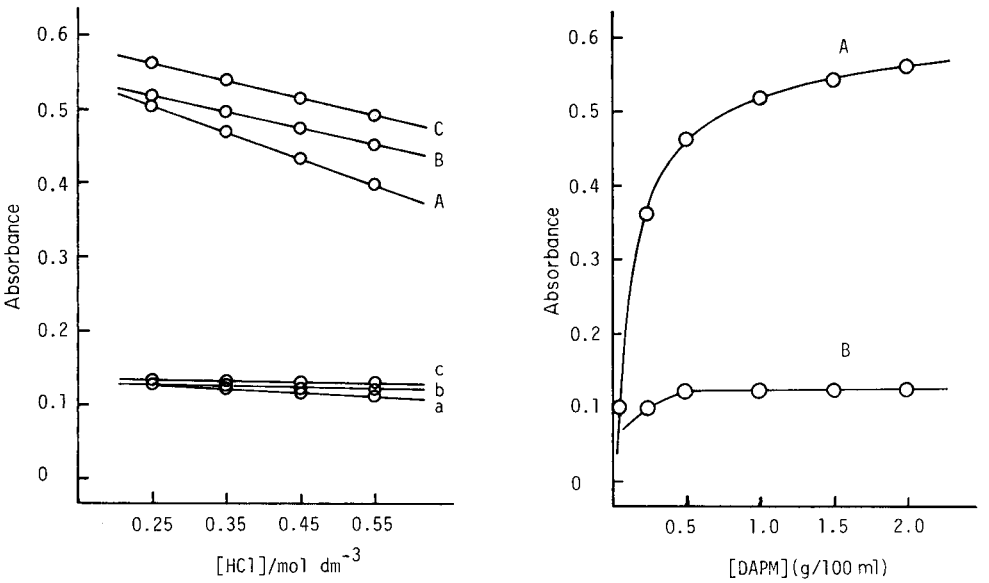

Fig. 5. Dependences of absorbance on acidities and the DAPM concentration. DAPM concentration: (A) 0.6; (B) 0.75; (C) 1.6 g/100 ml. Lines (a—c) are the differences in absorbance, $A_{470} - A_{388}$, corresponding to (A), (B), and (C), respectively.

Fig. 6. Dependences of absorbance for iron on the DAPM concentration at 0.3 M hydrochloric acid: (A) absorbance at 470 nm; (B) the difference in absorbance $A_{470} - A_{388}$.

The color intensities for iron and titanium do not change in at least six days. Under the conditions recommended in the procedure, the calibration graphs are linear up to 2 mg of iron(III) oxide and 0.5 mg of titanium(IV) oxide in the 100-ml solution.

TABLE 1

Results obtained for some rock samples

Sample	TiO_2 (%)		Fe_2O_3 (%)	
	Conventional method[a]	This work	Conventional method[b]	This work
1	0.63	0.63	6.71	6.70
2	0.72	0.72	5.54	5.54
3	0.71	0.71	4.90	4.93
4	0.61	0.61	5.88	5.75
5	0.59	0.60	4.48	4.50
6	0.56	0.56	3.24	3.20
7	0.71	0.70	4.92	4.93
8	0.50	0.51	4.86	4.85
9	0.68	0.68	6.51	6.66
10	0.62	0.61	6.18	6.28

[a]Given in refs. 2 and 3. [b]The method based on 1,10-phenanthroline.

Interference from other metals and application to rocks

No interferences were found from Ca, Mg, Al, P (as PO_4^{3-}), and Si (as SiO_3^{2-}) at levels up to 10 mg/100 ml; Mn, Sr, Pb, Zn, Cd, Ni, Sn(IV), Cu, and F^- up to 1 mg/100 ml; Au(III), Bi, Co, Be, Mo(VI), V(V), and Cr(VI) up to 0.1 mg/100 ml; Ir, Os, Pd, Pt, Rh, and Tl(III) up to 0.01 mg/100 ml, for titanium. In the determination of iron, only a slight increase in absorbance was observed for the yellow chromate ion or for gold and silver which precipitated to make the solution turbid. However, in rock analyses, these elements are ordinarily very rare.

Some results obtained by application of the proposed method to silicate rocks are shown in Table 1, together with the results obtained by using conventional methods. It is evident that the developed procedure is a valuable method for simultaneous determination of iron and titanium in rocks.

The author is indebted to Professor Y. Yamamoto of Hiroshima University, Japan, for his advice and encouragement, and also thanks Dr. E. Iwamoto for revising the English text and helpful criticism.

REFERENCES

1 A. A. Minin, Uch. Zap. Permsk. Gos. Univ., 7 (1955) 206.
2 P. G. Jeffery and G. R. E. Gregory, Analyst, 90 (1965) 177.
3 Geological Editorial Office of China, Rock and Mineral Analysis, Peking, China, 1974, p. 55.
4 E. B. Sandell and H. Onishi, Photometric Determination of Traces of Metals: General Aspects, Wiley, New York, 1978, p. 654.
5 A. E. Harvey, Jr. and D. L. Manning, J. Am. Chem. Soc., 72 (1950) 4488.

Analytica Chimica Acta, 154 (1983) 267—275
Elsevier Science Publishers B.V., Amsterdam — Printed in The Netherlands

ZUM EXTRAKTIONSVERHALTEN VON LIGANDEN DES CMAB-CHINOLIN-8-OL-TYPS UND DIE PHOTOMETRISCHE BESTIMMUNG VON MAGNESIUM MIT CMAS-CHINOLIN-8-OL

G. RÖBISCH* und A. RERICHA

Sektion Chemie/Biologie der Pädagogischen Hochschule "Karl Liebknecht" Potsdam, DDR-1500 Potsdam (D.D.R.)

(Eingegangen den 26. April 1983)

SUMMARY

(The extraction behaviour of ligands of the CMAB-quinolin-8-ol type and spectrophotometric determination of magnesium with CMAS-quinolin-8-ol)

The extraction behaviour of ligands analogous to CMAB-quinolin-8-ol and their complexes with Mg, Ca, Sr, Ba, Al, In, Pb, Bi, Mn, Co was studied. In forming complexes, these ligands, like quinolin-8-ol, are monobasic and bidentate, not tridentate as previously suggested. As extractants, they are superior to quinolin-8-ol because of their better hydrophobicity. A highly selective extraction—spectrophotometric determination of traces of magnesium (>24 $\mu g\ l^{-1}$) is possible with CMAS-quinolin-8-ol, 7-[1-(2-carbomethoxyanilino)-1-(2-hydroxyphenyl)-methyl]-quinolin-8-ol, in toluene.

ZUSAMMENFASSUNG

Es wird über das Extraktionsverhalten von Reagenzien des CMAB-Chinolin-8-ol-Typs und ihrer Komplexe mit Mg, Ca, Sr, Ba, Al, In, Pb, Bi, Mn, Co berichtet. Bei der Bildung von Komplexen reagieren diese Liganden, wie Chinolin-8-ol, einbasisch und zweizähnig, nicht dreizähnig, wie bisher allgemein angenommen wurde. Als Extraktionsmittel sind sie dem Chinolin-8-ol wegen ihrer größeren Hydrophobizität überlegen. Eine hochselektive extraktionsphotometrische Bestimmungsmethode für Magnesiumspuren (24 $\mu g\ l^{-1}$) mit CMAS-Oxin/Toluen wurde entwickelt.

Mit dem Ziel, die Selektivität von Chinolin-8-ol (Oxin, HOx) sowie die Extrahierbarkeit von Oxinaten der Art $[M(II)Ox_2(H_2O)_2]^0$ zu verbessern, führten Umland und Meckenstock [1] die "einbasisch dreizähnigen" Liganden des CMAB-Oxin-Typs in die Analytik ein. Über die extraktionsphotometrische Bestimmung von Magnesium [2—4], Blei [5], Bismut [6] mit CMAB-Oxin, 7-[α-(*o*-Carbomethoxyanilino)-benzyl]-chinolin-8-ol, und über die Acidität von zehn Vertretern dieses Typs [7] wurde berichtet. Leveque und Rosset [8] untersuchten das Extraktionsverhalten von Eu(II), Eu(III), Zn und Sr mit CMAB-Oxin/Chloroform, Bhatt und Mitarbeiter [9] die Komplexbildung von Zn mit AB-Oxin im Einphasensystem Wasser/Dioxan. Wir führten Untersuchungen zum bisher ungeklärten komplexchemischen Verhalten dieser Reagenziengruppe am Beispiel des CMAB-, CMAP- und CMAS-Oxin im Verteilungssystem Wasser/Toluen durch.

0003-2670/83/$03.00

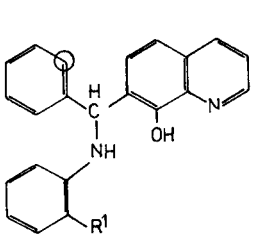

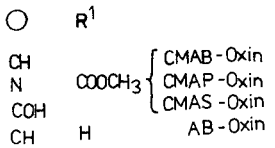

EXPERIMENTELLER TEIL

Gearbeitet wurde mit 2.10^{-4} M Lösungen von $MgSO_4 \cdot 7H_2O$, $CaCl_2 \cdot 6H_2O$, $SrCl_2 \cdot 6H_2O$, $BaCl_2 \cdot 2H_2O$, $Al_2(SO_4)_3 \cdot 18H_2O$, $In_2(SO_4)_3$, $Pb(NO_3)_2$, $BiONO_3$, $MnSO_4 \cdot 7H_2O$, $Co(NO_3)_2 \cdot 6H_2O$ in 10^{-1} M H_2SO_4. Der Hilfskomplexbildner wurde als 10^{-1} M Kaliumnatriumtartratlösung zugesetzt. Als Reagenzlösungen dienten 5.10^{-3} M Lösungen von CMAB-Oxin und CMAP-Oxin bzw. eine 10^{-3} M Lösung von CMAS-Oxin in Toluen.

Die Einstellung des pH-Wertes erfolgte unter Verwendung einer kombinierten Glaselektrode. Zur Messung der Extinktion standen ein Specord bzw. ein VSU-2P (beide VEB Carl Zeiß Jena) zur Verfügung.

In einem Becherglas wird das Gemisch aus 5 ml Metallsalzlösung und 2 ml Tartratlösung nach Zusatz von Wasser bidest. mit Natronlauge bzw. Salzsäure auf den gewünschten pH-Wert gebracht und dann in einen Schütteltrichter überführt. Zur wäßrigen Phase (20 ml) setzt man 20 ml toluenische Reagenslösung zu und schüttelt 10 Min. Nach Abtrennung der organischen Phase wird diese scharf zentrifugiert und dann die Extinktion gegen eine entsprechende Blindlösung gemessen.

Der praktische molare Extinktionskoeffizient (ϵ_{prakt}) ergibt sich aus der Differenz zwischen den Extinktionen der Komplexlösungen und der Blindlösungen unter den angegebenen Meßbedingungen.

Das stöchiometrische Verhältnis M:L im extrahierten Komplex ermittelten wir graphisch aus dem Anstieg der Geraden im lg D/pH-Diagramm (D = Verteilungskoeffizient des Metalls).

ERGEBNISSE

Die Elektronenspektren

Die Spektren der Liganden und der untersuchten Komplexe zeigen im visuellen und nahen UV-Bereich im wesentlichen eine Bande, die, vergleicht man mit den Oxin- und Oxinatspektren, dort der ^1L_a-Bande entspricht (Abb.1). Bei Komplexbildung ist die beobachtete Rotverschiebung dieser Bande im allgemeinen ausreichend, sodaß bei ihrer analytisch—photometrischen Nutzung Empfindlichkeitsverluste durch die Eigenabsorption des Reagenses nicht auftreten.

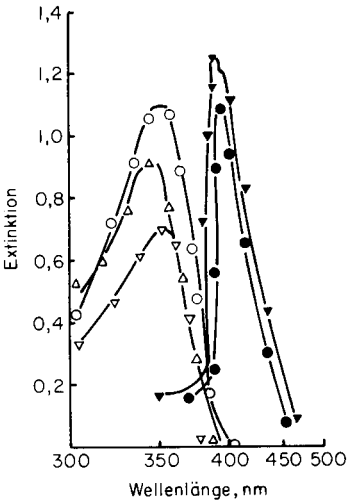

Abb. 1. Elektronenspektren in Toluen: (○) $1{,}5.10^{-4}$ M CMAB-Oxin; (△) $1{,}25.10^{-4}$ M CMAS-Oxin; (▽) 1.10^{-4} M CMAP-Oxin; (●) $1{,}5.10^{-4}$ M $Mg(CMAB\text{-}Oxin)_2$; (▼) $1{,}5.10^{-4}$ M $Mg(CMAP\text{-}Oxin)_2$. (l = 1 cm, gemessen gegen Toluen.)

Das Extraktionsverhalten

Die Extraktionskonstante bzw. ihr negativer, dekadischer Logarithmus

$$pK_{ex} = pML_n + n\,pH - pM - n\,pHL$$

ist komplexer Natur und wird bestimmt durch die Verteilungskonstanten des Komplexes und des Liganden sowie durch die Stabilitätskonstante des Komplexes und die Säurekonstante des Liganden. Zur Kennzeichnung der Lage der Extraktionskurven haben wir den Quotienten pK_{ex}/n verwendet (Tabelle 1). pK_{ex}/n ist der pH-Wert hälftiger Extraktion bei der fiktiven Ligandkonzentration von 1 mol l^{-1}.

In Übereinstimmung mit der gegenüber dem Grundkörper Oxin geringeren Basizität der Liganden vom CMAB-Oxin-Typ [7] liegt der sigmoide Ast ihrer Extraktionskurven bei niedrigeren pH-Werten als bei der entsprechenden Kurve des Oxins, und das pH-abhängige Extraktionsmaximum ist deutlich breiter (Abb. 2). Das ist beim analytischen Arbeiten von Vorteil. Der von der Erfahrung abweichende Verlauf der Extraktionskurven für CMAB- und CMAP-Oxin im alkalischen Bereich ist bisher nicht geklärt.

Der größeren Stabilität der Kobaltkomplexe entsprechend, sind ihre pK_{ex}/n-Werte deutlich kleiner als die der analogen Magnesiumkomplexe (Tab. 1, Abb. 3). Bezogen auf ein und dasselbe Kation steigen sie immer in der Reihe CMAS < CMAP < CMAB (Tab. 1), was in dieser Richtung auf abnehmende Komplexstabilität hinweist. In Einklang damit steht, daß zur Erzielung der maximalen Extraktion beim CMAB- und CMAP-Oxin hundertfacher, beim CMAS-Oxin nur zwanzigfacher Ligandüberschuß erforderlich ist.

TABELLE 1

Ermittelte Extraktionsparameter (im System Wasser/Toluen)

	λ (nm)	ϵ_{prakt} ($l\ mol^{-1}\ cm^{-1}$)	pH_{max}	pK_{ex}/n
Oxin	320	7500	8,5 ± 2,5	—
CMAB-Oxin	350	7200	8,0 ± 6,0	—
CMAP-Oxin	350	7000	8,7 ± 4,7	—
CMAS-Oxin	340	7400	6,7 ± 3,7	—
$Mg(CMAB)_2$	394	7340	12,8 ± 0,1	9,7
$Mg(CMAP)_2$	395	8000	11,4 ± 0,1	8,1
$Mg(CMAS)_2$	378	7275	11,0 ± 0,3	6,7
$[Z^+.Mg(CMAB)_3^-]$[a]	410	6680	10,8 ± 0,6	7,4
$Ca(CMAS)_2$	380	9500	13,2 ± 0,1	9,0
$Sr(CMAS)_2$	380	5200	13,2 ± 0,1	9,3
$Ba(CMAS)_2$	364	4200	13,7 ± 0,1	9,9
Al/CMAS	380	nicht extrahierbar		
In/CMAS	372	9100	12,8 ± 0,2	6,9
$Pb(CMAS)_2$	375	7800	9,2 ± 1,2	2,8
		9200	10,8 ± 0,0	
Bi/CMAS	378	20800	8,2 ± 1,2	—0,3
$Mn(CMAS)_2$	375	8400	8,0	3,5
$Co(CMAB)_2$	430	8140	8,7 ± 1,0	4,3
$Co(CMAP)_2$	400	7340	11,1 ± 0,2	
	400	6000	8,2 ± 1,2	3,4
$Co(CMAS)_2$	390	8400	7,5 ± 0,6	2,1

[a]Z = Zephiramin

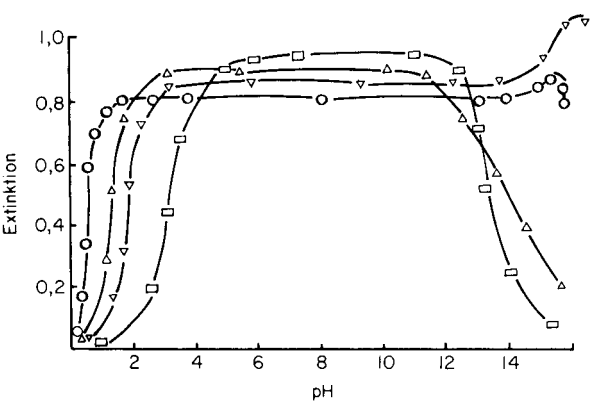

Abb. 2. Extraktionskurven der Liganden ($1{,}25.10^{-4}$ M) im System Wasser/Toluen. (l = 1 cm; gemessen am Absorptionsmaximum gegen Blindlösung.) (○) CMAB-Oxin; (△) CMAS-Oxin; (▽) CMAP-Oxin; (□) Oxin.

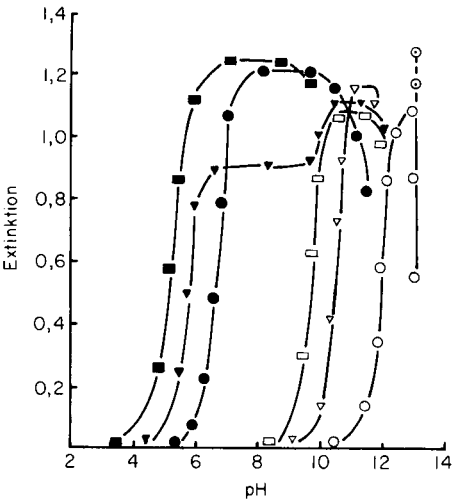

Abb. 3. Extraktionskurven der Mg-Komplexe (leere Symbole) und Co(II)-Komplexe (volle Symbole): (○) CMAB-Oxin; (▽) CMAP-Oxin; (□) CMAS-Oxin. $Mg(CMAB)_2$ in (○) Toluen und in (⊙) Chloroform. $c_M = 5.10^{-5}$ M; $c_{CMAB,CMAP} = 5.10^{-3}$ M; $c_{CMAS} = 1.10^{-3}$ M; $l = 3$ cm; gemessen am Absorptionsmaximum gegen Blindlösung.

Die ungewöhnliche Form der Extraktionskurve des $Co(CMAP\text{-}Oxin)_2$ (Abb. 3) deutet auf das Vorliegen von zwei verschiedenen Komplexen hin. Wir prüften daher auch bei pH 11 die Stöchiometrie (nach der Molverhältnismethode), erhielten aber, so wie bei pH 6, die Zusammensetzung 1:2. Bemerkenswert ist der völlig unterschiedliche Verlauf der Extraktionskurve des $Mg(CMAB\text{-}Oxin)_2$ in den Lösungsmitteln Chloroform und Toluen bei pH 13. In Chloroform wird der unerwartete Anstieg der Extraktionskurve nach dem Extraktionsmaximum (pH 12,8) auf Redoxreaktionen am Liganden zurückgeführt [2]. Analog wurde das so beim Bismut gefunden [6].

Während für Magnesium die Extraktionsverhältnisse relativ eindeutig sind, ist beim Kobalt die mögliche Überlagerung eines Redoxgleichgewichtes [10, 11] bzw. die Bildung von Polymeren [12] zu beachten. Da Co(III) kinetisch sehr träge ist, unsere Extraktion aber bei Zimmertemperatur schnell verläuft, muß in der wäßrigen Phase Co(II) vorliegen und auch als solches extrahiert werden. Das wird bestätigt durch die gefundene Stöchiometrie. Der Zusatz von Wasserstoffperoxid zur wäßrigen Phase verändert das Extraktionsverhalten nicht, wohl aber das Spektrum. Redoxprozesse laufen offensichtlich vorzugsweise am Liganden ab. Verhindert wird die Extraktion (unter unseren Arbeitsbedingungen) bei gleichzeitiger Anwesenheit von Wasserstoffperoxid und Ammoniak bei pH 8. Luftsauerstoff und Ammoniak verhindern die Extraktion partiell, wie schon von Umland und Meckenstock [10] auch für das CMAB-Oxin beobachtet. Es bestätigt sich damit, daß starke N-Donatoren die Oxydation von Co(II) zu Co(III) begünstigen. Dieser Sachverhalt kann zur extraktiven Trennung von Kobalt und Nickel genutzt

werden [10]. Im Gegensatz dazu wird bei Anwesenheit von starken O-Donatoren die Geschwindigkeit der Oxydation von Co(II) zu Co(III) durch Luftsauerstoff während der Extraktion mit Oxin oder 7-Dodecenylquinolin-8-ol (Kelex-100; Ashland, U.S.A.) in Toluen deutlich verringert [13].

Eklatante, bisher nicht eindeutig geklärte Unterschiede bestehen für $Co(CMAP\text{-}Oxin)_2$ und $Co(CMAB\text{-}Oxin)_2$ bei der Rückextraktion von Kobalt in eine wäßrige Phase. Während die Rückextraktion des $Co(CMAP\text{-}Oxin)_2$ bei pH < 3 zu 85% möglich ist, unterbleibt sie für $Co(CMAB\text{-}Oxin)_2$. Auch $Ga(CMAB\text{-}Oxin)_3$ ist in einem chloroformischen Extrakt stabil beim Schütteln dieses Extraktes selbst mit 1,5 M Schwefelsäure [14].

Da innerhalb der untersuchten Ligandengruppe die CMAS-Oxinate die jeweils niedrigsten pK_{ex}/n-Werte haben, was vor allem bei schwachen Komplexbildnern, wie etwa der Erdalkaligruppe, wegen der Verschiebung der Extraktionskurven zu niedrigeren pH-Werten Vorzüge bringt, untersuchten wir die Extraktion speziell dieser Gruppe mit CMAS-Oxin/Toluen. Die Extraktionskurven der Erdalkaliionen (Abb. 4) zeigen auch hier die Sonderstellung des Magnesiums gegenüber seinen höheren Homologen. Es ist danach mit CMAS-Oxin möglich, Magnesium aus einer Erdalkalimatrix zu separieren. Diese Möglichkeit setzt sich aber innerhalb der Gruppe Ca/Sr/Ba nicht fort. Der deutlich geringere praktische Extinktionskoeffizient der Strontium- und Bariumkomplexe weist auf einen niedrigen Extraktionsgrad hin.

Die Extraktion von Blei mit CMAS-Oxin (Abb. 5) erfolgt bei einem um zwei Einheiten tieferen pH-Wert als bei Verwendung von CMAB-Oxin [1, 5].

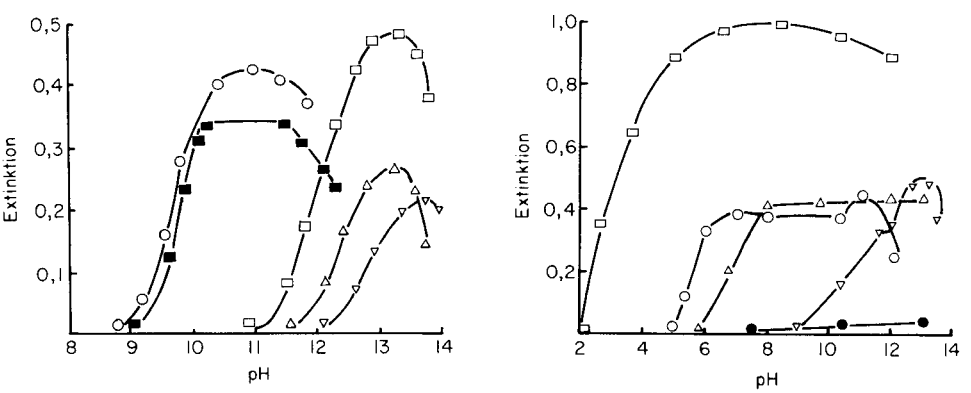

Abb. 4. Extraktionskurven der CMAS-Oxin-Komplexe von: (○) Mg; (□) Ca; (△) Sr; (▽) Ba. (■) $[Mg(CMAB\text{-}Oxin)_3]^-$ in Gegenwart von Zephiramin. $c_Z = 1{,}25.10^{-3}$ M; $c_M = 5.10^{-5}$ M, $c_{CMAS} = 1.10^{-3}$ M; $l = 1$ cm; gemessen am Absorptionsmaximum gegen Blindlösung.

Abb. 5. Extraktionskurven der CMAS-Oxin-Komplexe von: (○) Pb; (△) Mn(II); (●) Al; (▽) In; (□) Bi; bei 20-fachem Ligandüberschuß. $c_M = 5.10^{-5}$ M; $l = 1$ cm; gemessen beim Absorptionsmaximum gegen Blindlösung.

Analytisch günstig ist, daß das Extraktionsmaximum über mehrere pH-Einheiten reicht. Dem Blei im wesentlichen analog verhält sich Mangan(II). Aluminium wird mit CMAS-Oxin, wie auch mit CMAB-Oxin [2—4], nicht extrahiert (Abb. 5). Es ist noch nicht klar, ob dieses Phänomen vordringlich durch sterische Hinderung oder durch kinetische Trägheit verursacht wird. Die glatte Extraktion von Indium und Bismut mit CMAS-Oxin (Abb. 5) macht erneut deutlich, daß das ursprünglich postulierte Selektivitätsverhalten der Reagenzien vom CMAB-Oxin-Typ gegenüber Kationen der Ladung 2+ bzw. $\geqslant 3+$ [1] nicht generalisiert werden darf [5, 6, 8].

Bei Indium und Bismut lassen sich aus den Extraktionskurven keine unmittelbaren Schlüsse auf die Stöchiometrie der extrahierten Komplexe ziehen. Sehr auffällig ist für Bi(III) der vergleichsweise [6] sehr hohe praktische Extinktionskoeffizient. Dieser Sachverhalt und die potentiell günstige Möglichkeit der Bi/Pb-Trennung lassen CMAS-Oxin als effektives Reagens für die photometrische Bismut-Bestimmung erscheinen.

So wie Oxin mit Mg, Zn, Cd, Mn, Ni, nich Cu [15], sowie Oxin-5-sulfosäure mit Mn [16] und V(V) [17], bildet CMAB-Oxin mit Magnesium bei Anwesenheit des Tensids Zephiramin (Z^+) ein Tris-(CMAB-Oxinato)-Magnesiat, das als Ionenassoziat extrahiert wird (Abb. 4). Es verbessert sich deutlich die pH-Abhängigkeit der Extraktion, die Lichtabsorption nicht (Tab. 1). Die Zusammensetzung der extrahierten Spezies ist nach der Linearisierung der Extraktionskurve, der Molverhältnismethode und nach Job $Z^+[Mg(CMAB)_3]^-$.

Koordinationsverhalten der Liganden vom CMAB-Oxin-Typ

Durch Substitution der Wassermoleküle in den Transoktaederpositionen des wasserhaltigen Magnesiumoxinats $[MgOx_2(H_2O)_2]^0$ mittels geeigneter Zusätze zum Extraktionssystem wie Butylcellosolve [18], Methanol, *n*-Butylamin [19], Isopentanol, Ethanolamin [20], Pyridin [21] oder durch Extraktion in ein koordinativ aktives Lösungsmittel wie MIBK [22, 23] gelang es, die Stabilität des Komplexes in der organischen Phase zu erwirken. Da das $[Mg(CMAB\text{-}Oxin)_2]^0$ diese gewünschte Stabilität auch ohne Zusätze zeigte, lag der Gedanke nahe, daß die zusätzlichen potentiellen Haftatome (O, N) im Substituenten des Oxins das Koordinationsoktaeder vervollständigten, die Liganden vom CMAB-Oxin-Typ also einbasisch dreizähnig seien [1].

Bei Abwesenheit der Carbomethoxygruppe, im AB-Oxin, wurden bei Extraktionsexperimenten mit Magnesium im wesentlichen dem CMAB-Oxin analoge (zum Teil bessere) Extraktionsparameter gefunden [1]. Das machte die Koordination des Carbonylsauerstoffs im CMAB-Oxin unwahrscheinlich. Es blieb noch der Anilinostickstoff. Wir konnten jedoch durch IR-, ^{1}H-NMR-, ^{13}C-NMR-, magnetische und EPR-Untersuchungen [24] an festen Komplexen des CMAP-Oxins (hier war mit dem Pyridyl-stickstoff ein weiteres potentielles Haftatom im Substituenten) mit Mg, Cu(II), VO^{2+}, Mn(II) und Co(II) zeigen, daß die im Substituenten vorhandenen potentiellen Haftatome

(O, N, N) unwirksam sind und nur die klassische Oxingruppierung (O, N) koordinativ aktiv ist, so wie beim unsubstituierten Oxin. Die unkomplizierte Bildung des Tris-(CMAB-Oxinato)-magnesiats steht damit in Übereinstimmung, ebenso die Bildung von Self-Addukten, wie sie von Leveque und Rosset [8] mit CMAB-Oxin (HL) beim Europium als $Eu(II)L_2(HL)_2$ und Strontium als $SrL_2(HL)$, unter analogen Bedingungen aber nicht beim ZnL_2 und $Eu(III)L_3$, beobachtet wurden.

In den von uns bisher untersuchten Fällen reagieren also die Liganden vom CMAB-Oxin-Typ einbasisch und nur zweizähnig. Die gegenüber dem Oxin deutlich besseren Extraktionseigenschaften der Liganden vom CMAB-Oxin-Typ dürften daher auf einen Hydrophobizitätseffekt zurückzuführen sein, der von den übergroßen hydrophoben Liganden verursacht wird und bewirkt, daß die Extraktion trotz der Anwesenheit von Koordinationswasser gut möglich ist, und nicht auf einen Koordinationseffekt.

Erste orientierende HPLC-Untersuchungen ergaben steigende Hydrophobizität für die Liganden in der Reihe Oxin $\approx$ AS-Oxin $<$ CMAS-Oxin $<$ 3,4-Dichlor-AB-Oxin $\ll$ AB-, CMAB-, CMAP-Oxin, für die Magnesiumkomplexe $[MgL_2(H_2O)_2]_0$ in der Reihe Oxinat $\ll$ CMAP-, CMAS-, CMAB-Oxinat.

Die extraktionsphotometrische Bestimmung von Magnesium mit CMAS-Oxin

Das Verfahren haben wir nach den im experimentellen Teil angegebenen Arbeitsbedingungen bei pH 10,7 ± 0,5 (Glycocollpuffer), λ = 378 nm, l = 1 cm und mindestens zehnfachem Ligandüberschuß getestet [25]: Arbeitsbereich 7—70 nmol ml^{-1}; Verfahrenskonstante 137,01 nmol ml^{-1}; Extinktionskoeffizient 7300 l mol^{-1} cm^{-1}; Standardabweichung ± 1,45 nmol ml^{-1}; Rel. Standardabweichung ± (2,2 — 21,6)%.

Die Selektivität ist sehr hoch und entspricht der mit CMAB-Oxin erreichbaren [2, 3]. Bei Anwesenheit von KCN und Tartrat bzw. Citrat stören z.B. die Alkalielemente, Ca, Sr, Ba, Cu, Zn, Cd, Hg, Al, In, Tl, Co, Ni nicht (geprüft wurde bis zum 1000-fachen Überschuß). Mangan(II) muß durch Vorextraktion mit DDTC entfernt werden, große Mengen Pb und Bi werden mitextrahiert. Magnesium kann dann durch Rückextraktion in eine wäßrige Phase bei pH 8 von ihnen abgetrennt werden.

Nutzt man die (bei der Testung des Grundverfahrens nicht eingesetzte) auf das 7-fache mögliche anreichernde Extraktion, liegt die untere Arbeitsbereichsgrenze bei 24 $\mu g\ l^{-1}$ Magnesium.

Die Magnesiumbestimmung mit CMAS-Oxin ist weniger pH-anfällig und in bezug auf das Reagens kostengünstiger als die mit CMAB-Oxin, Empfindlichkeit sowie Selektivität sind in beiden Fällen gleich, der zufällige Fehler ist bei Verwendung von CMAS-Oxin größer.

LITERATUR

1 F. Umland und K.-U. Meckenstock, Fresenius Z. Anal. Chem., 177 (1960) 244.
2 F. Umland, B. K. Poddar und K.-U. Meckenstock, Fresenius Z. Anal. Chem., 185 (1962) 362.

3 G. Röbisch, Z. Chem., 11 (1971) 353.
4 A. Hofer und R. Heidinger, Fresenius Z. Anal. Chem., 230 (1967) 95.
5 G. Röbisch, Anal. Chim. Acta, 47 (1969) 539.
6 G. Röbisch, Anal. Chim. Acta, 48 (1969) 161.
7 G. Röbisch und W. Schefter, Z. Chem., 15 (1975) 445.
8 A. Leveque und R. Rosset, C. R. Acad. Sci. Paris, Ser. C, 273 (1971) 1073.
9 Y. N. Bhatt, K. K. Patel, K. I. Shah und R. S. Patel, Curr. Sci., 45 (1976) 218.
10 F. Umland und K.-U. Meckenstock, Z. Anal. Chem., 190 (1962) 186.
11 S. Oki, Anal. Chim. Acta, 50 (1970) 465.
12 E. Sekido und K. Fujita, Bull. Chem. Soc. Jpn., 49 (1976) 3073.
13 P. Guesnet, I. L. Sabot und D. Bauer, J. Inorg. Nucl. Chem., 42 (1980) 1459.
14 E. Uhlemann, Privatmitteilung.
15 S. Noriki und M. Nishimura, Anal. Chim. Acta, 72 (1974) 339; 94 (1977) 57.
16 M. Sugawara und T. Kambara, Bull. Chem. Soc. Jpn., 46 (1973) 3789.
17 T. Kambara und M. Sugawara, Bull. Chem. Soc. Jpn., 46 (1973) 500.
18 C. L. Luke und M. E. Campbell, Anal. Chem., 26 (1954) 1778.
19 F. Umland und W. Hoffmann, Anal. Chim. Acta, 17 (1957) 234.
20 S. I. Jankowski und H. Freiser, Anal. Chem., 33 (1961) 776.
21 S. Nakaya und M. Nishimura, Jpn. Analyst, 22 (1973) 733.
22 H. Goto und Y. Kakita, J. Chem. Soc. Jpn., Pure Chem. Sect., 80 (1959) 1448.
23 M. Suzuki, M. Yamagisawa und T. Takeuchi, Talanta, 12 (1965) 989.
24 R. Stoesser, A. Rericha und G. Röbisch, Z. Chem., 21 (1981) 332.
25 G. Gottschalk, Statistik in der quantitativen Analyse, F. Enke Verlag, Stuttgart, 1962.

Analytica Chimica Acta, 154 (1983) 277—286
Elsevier Science Publishers B.V., Amsterdam — Printed in The Netherlands

EXTRACTION OF SMALL AMOUNTS OF DIALKYLPHOSPHORODITHIOATES WITH TETRAPHENYLARSONIUM CATION FROM AQUEOUS MEDIUM

V. DREVENKAR*, Z. FRÖBE and B. ŠTENGL

Institute for Medical Research and Occupational Health, YU-41000 Zagreb (Yugoslavia)

Z. ŠTEFANAC

Laboratory of Analytical Chemistry, Faculty of Science, University of Zagreb, YU-41000 Zagreb (Yugoslavia)

(Received 26th January 1983)

SUMMARY

The extraction behaviour of ion-pairs formed by dialkylphosphorodithioates with tetraphenylarsonium cation was examined for the dichloromethane—water system. The mole ratio method, with spectrophotometric and conductimetric measurements of the organic phase, showed the mole ratio of the ion-pair to be 1:1. Dissociation of the ion-pairs occurred at concentrations in the aqueous phase lower than 10^{-4} mol dm^{-3} for the dimethyl compound and 6×10^{-4} mol dm^{-3} for the diethyl analogue. Under favourable experimental conditions, dialkylphosphorodithioates can be collected from aqueous solutions at concentrations not exceeding 1 μg cm^{-3} (ca. 5×10^{-6} mol dm^{-3}), with extraction efficiencies of 86—95%. Dialkylphosphorothioates are extracted much less efficiently; diethylphosphate and inorganic phosphate are not extracted.

Most organic pollutants including organophosphorus pesticides and their degradation products are present in very low concentrations in aquatic environments. Therefore a useful method for their determination has to include not only a sensitive mode of detection but also a reliable procedure for their collection from larger volumes of water samples. For this purpose the extraction of organophosphorus pesticides with different organic solvents [1—5] or adsorption on an appropriate adsorbent [5—11] is most often used.

Hydrolysis of organophosphorus pesticides in natural water occurs relatively rapidly and results in ionic hydrophilic derivatives, generally considered as non-toxic. However, because of their persistence these various degradation products account for the greater part of water pollution caused by organophosphorus pesticides. Therefore attention has also been given to the development of accumulation procedures, based on adsorption, for the simultaneous determination of dialkylphosphorus anions originating from parent organophosphorus pesticides [12, 13].

The determination of ionic dialkylphosphates and dialkylphosphorothioates

0003-2670/83/$03.00

in large volumes of aqueous media by means of Amberlite XAD-4 resin [12] was found to suffer from considerable difficulties in desorption of dialkylphosphorodithioates [14]. This problem arose during extended studies concerning the persistence of organophosphorus pesticides in aquatic environments [5, 6]. The amazingly fast degradation of malathion in one of the rivers (Sava) monitored was at first tentatively ascribed to the bacteriological profile of the river water. Thorough investigations in model systems with definite types of bacteria demonstrated the need for reliable determinations not only of malathion but of its degradation products [14]. The collection of dimethylphosphorodithioate thus became essential, and new approaches were needed because of the failure of the adsorption method. Preliminary experiments on various extraction procedures showed that extraction with tetraphenylarsonium cation was the most promising for the purpose in mind. These extractions were therefore studied in detail.

EXPERIMENTAL

Reagents

Standard organophosphorus compounds *O,O*-dimethylphosphorothioate potassium salt (DMTPK; lot no. 5058), *O,O*-diethylphosphorothioate potassium salt (DETPK; lot no. 4223), *O,O*-dimethylphosphorodithioate potassium salt (DMDTPK; lot no. 5057) and *O,O*-diethylphosphorodithioate potassium salt (DEDTPK; lot no. 4224) were received from the United States Environmental Protection Agency Repository (Research Triangle Park, NC, U.S.A.). Other chemicals used were tetraphenylarsonium chloride ($(Ph_4As)Cl$; Fluka) and tris(hydroxymethyl)aminomethane (Tris; Kemika, Yugoslavia). An ethereal solution of diazomethane (10 ± 5 mg cm^{-3}) was prepared by the usual distillation procedure from *N*-methyl-*N*-nitroso-*p*-toluenesulphonamide (Merck-Schuchardt).

Apparatus

The tetraphenylarsonium species were measured spectrophotometrically with a Varian-Techtron u.v.-visible spectrophotometer, model 635, with 1-cm quartz cells. Infrared spectra were obtained with a Perkin-Elmer i.r. spectrophotometer, model 167. Conductivity was measured with a Radiometer conductivity meter model CDM3, equipped with a PP1042 cell.

A Varian 1400 gas chromatograph equipped with an alkali flame ionization detector (Rb_2SO_4) was used. The 1.5 m × 2 mm i.d. glass column was packed with 80—100-mesh Chromosorb W-AW/DMCS coated with 20% (w/w) Triton X-305 liquid phase. The operating conditions were: injector 200°C, column 155°C, detector 235°C, nitrogen carrier-gas flow 33, air flow 230, hydrogen flow 34 cm^3 min^{-1}.

Procedures

Extractions of dialkylphosphorodithioate and dialkylphosphorothioate ion-pairs with tetraphenylarsonium cation were best done from aqueous solutions adjusted to pH 8—9 by addition of a 5×10^{-2} mol dm^{-3} Tris buffer solution. A 50.0-cm^3 aliquot of the aqueous solution containing the dialkylphosphorodithioate or dialkylphosphorothioate salt and tetraphenylarsonium chloride in a mole ratio within the range (1:2)—(1:8) was transferred to a separatory funnel. The sample was extracted with 5.0 cm^3 of dichloromethane by shaking the mixture in an automatic shaker for 5 min. The organic layer was separated and the extraction repeated with another 5.0-cm^3 portion of dichloromethane. The extracts were combined and diluted to 10.0 cm^3 with dichloromethane. Modifications to this general procedure for definite aims are specified in the relevant figure captions.

The concentration of tetraphenylarsonium species was determined by measuring the absorbance of the aqueous phase at 264 nm and of the dichloromethane extract at 265 nm. Standard solutions for quantitative work were prepared by direct weighing and dissolving of tetraphenylarsonium chloride in water at pH 8 or in dichloromethane. Absorbance was proportional to the concentration of $(Ph_4As)Cl$ in water as well as in dichloromethane in the range 9×10^{-6}—3×10^{-3} mol dm^{-3}. Values of $\epsilon_{264} = 3100$ dm^3 mol^{-1} cm^{-1} in water and $\epsilon_{265} = 3550$ in dichloromethane were obtained and were not affected by the presence of dialkylphosphorodithioate or dialkylphosphorothioate salts. For conductivity measurements in the organic phase the extracts were dried overnight on anhydrous sodium sulphate.

For gas chromatography of dialkylphosphates, dialkylphosphorothioates and dialkylphosphorodithioates in the dichloromethane extracts, an aliquot of the extract was methylated with diazomethane; after 10 min, the excess of diazomethane was removed under a stream of nitrogen.

All extracts containing the $(Ph_4As)(DMDTP)$ ion-pair were collected after u.v. and conductivity measurements and evaporated under a stream of nitrogen to 0.5 cm^3. Precipitated crystals were recrystallized from ethanol, air-dried and thoroughly powdered. Infrared spectra for characterization of the isolated crude ion-pair were recorded in KBr pellets.

RESULTS AND DISCUSSION

Dialkylphosphoric acid esters are frequently extracted with petroleum ether [1], benzene [2, 3], hexane [3], chloroform [3, 4], dichloromethane [4] or with mixtures of solvents [4, 5]. In preliminary tests on dialkylphosphorothioates and dialkylphosphorodithioates, the expected negligible extraction (<1%) was obtained with benzene, hexane, chloroform and dichloromethane. In these experiments, the addition of tetraphenylarsonium salt to the aqueous phase notably improved the efficiency of extraction with chloroform and dichloromethane at concentrations of the mentioned anions not exceeding 1 μg cm^{-3} in water.

These preliminary results emphasized the need for a sensitive and selective method of quantifying the dialkylphosphoric moieties. Gas chromatography is usually preferred for the final step in the determinations [12, 13]. Under the conditions worked out here for the gas chromatographic stage, dichloromethane gave a narrow and well separated solvent peak, whereas chloroform did not. On that account, dichloromethane was chosen for further investigations.

Comprehensive data can be found in the literature concerning the extraction behaviour of tetraphenylarsonium salts with numerous inorganic anions in the chloroform—water [15—18] but not in the dichloromethane—water system. Therefore the main characteristics of tetraphenylarsonium chloride were first checked and then the properties and extraction behaviour of the cation associated with dialkylphosphorodithioate and dialkylphosphorothioate anions were examined more thoroughly.

Extraction behaviour of tetraphenylarsonium chloride in the dichloromethane—water system

The independence of the distribution ratio from the pH value of the aqueous phase was proven for tetraphenylarsonium chloride in the dichloromethane—water system within the pH range 4—9 of direct interest, in agreement with the data obtained with chloroform as the organic phase [15, 17]. The value of the distribution ratio between dichloromethane and aqueous solution was determined under analogous conditions as described for chloroform [16] except that the temperature was kept at 22.8 ± 0.3°C. The resulting mean value of four simultaneous determinations, $D = 0.38 \pm 0.01$, exceeded the chloroform values in previous work, 0.16 [16] and 0.18 [15], more than twofold. This rather high distribution ratio was explained from the results of a series of extractions done under the conditions described in the experimental part with initial amounts of $(Ph_4As)Cl$ increasing from 9.253×10^{-6} to 3.044×10^{-3} mol dm^{-3} (Fig. 1a). The steep nonlinear increase at concentrations exceeding 1.3×10^{-3} mol dm^{-3} was interpreted as

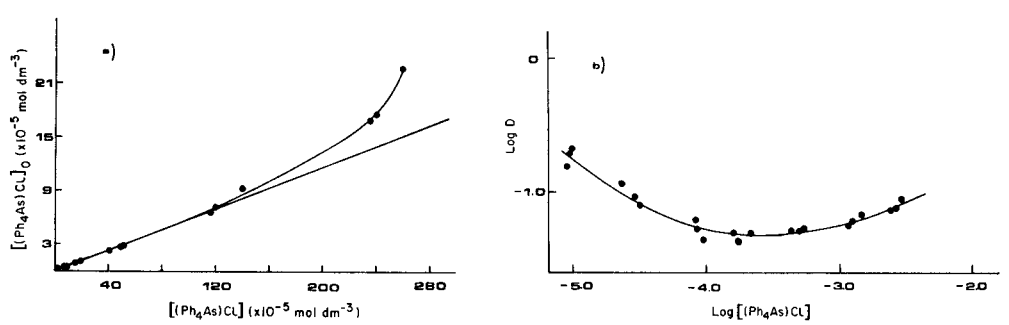

Fig. 1. (a) Plot of the $(Ph_4As)Cl$ concentration in the extract against the concentration of the quaternary salt in the aqueous phase of ionic strength 0.15 (Na_2SO_4). (b) Logarithmic plot of the $(Ph_4As)Cl$ distribution ratio against the total concentration of the quaternary salt in the water—dichloromethane system.

a consequence of polymer formation and the increase of the distribution ratio at concentrations lower than 1×10^{-4} mol dm^{-3} (Fig. 1b) as issuing from the dissociation of $(Ph_4As)Cl$ in dichloromethane, in accordance with the reasons assigned by earlier workers [17, 18].

Extraction behaviour of dialkylphosphorodithioate ion-pairs with tetraphenylarsonium cation

The cation-to-anion ratios of the ion-pairs formed by tetraphenylarsonium cation and four different anions were determined by the mole ratio method. The results obtained by extraction from aqueous solutions containing gradually increasing mole ratios of the cation with respect to dialkylphosphorothioate and dialkylphosphorodithioate anions are presented in Figs. 2 and 3, respectively.

Different characteristics of the extracted species of dialkylphosphorothioates compared with one another and particularly with dialkylphosphorodithioates are obvious from the curves showing the dependence of the absorbance of extracts on the cation-to-anion mole ratio. The continuous increase over the entire investigated range for diethylphosphorothioate indicates the simultaneous formation of ion-pairs with diverse mole ratios in the extract, whereas the more distinct single steps for the dimethyl analogue emphasize their successive appearance. In the case of dialkylphosphorodithioates, u.v. measurements of the organic phase proved the formation of ion-pairs with a 1:1 stoichiometric proportion. Intersections of the straight lines correspond to a mole ratio of 1.02 for dimethyl- and of 1.13 for diethylphosphorodithioate.

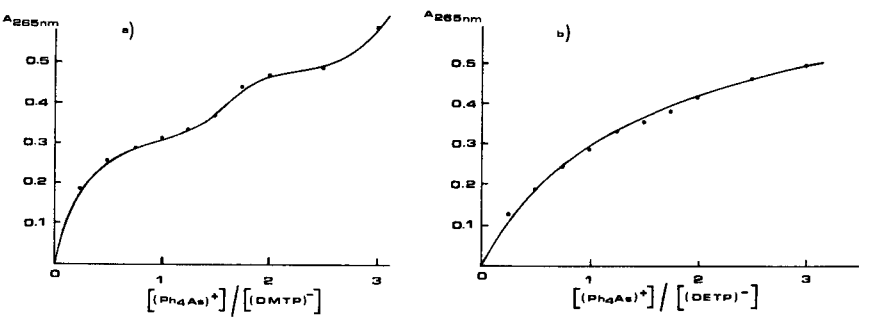

Fig. 2. Plots of the absorbance of the organic phase against the ratio of tetraphenylarsonium to dialkylphosphorothioate. (a) Samples were 20.0 cm^3 of an aqueous 5.50×10^{-4} mol dm^{-3} solution of *O,O*-dimethylphosphorothioate potassium salt (DMTPK) and 0—6.0 cm^3 of an aqueous 5.08×10^{-3} mol dm^{-3} solution of $(Ph_4As)Cl$ diluted to 50.0 cm^3; reference solutions were identical except that buffer replaced DMTPK. (b) Sample and reference were prepared with volumes of solutions analogously to series (a) but with a 1.98×10^{-4} mol dm^{-3} solution of *O,O*-diethylphosphorothioate potassium salt (DETPK) and 1.98×10^{-3} mol dm^{-3} $(Ph_4As)Cl$. All solutions were adjusted with Tris buffer pH 8.0 which was also used to dilute the samples to the given volume.

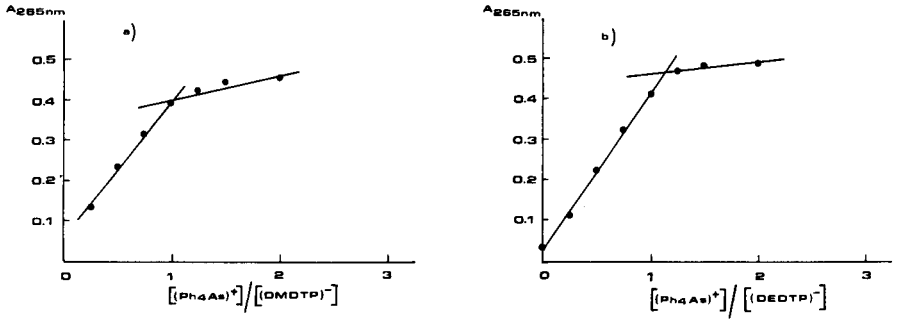

Fig. 3. Plots of the absorbance of the organic phase against the ratio of tetraphenylarsonium to dialkylphosphorodithioate. (a) Samples were 40.0 cm^3 of aqueous 3.63 × 10^{-5} mol dm^{-3} *O,O*-dimethylphosphorodithioate potassium salt (DMDTPK) and 0—4.0 cm^3 of 7.26 × 10^{-4} mol dm^{-3} $(Ph_4As)Cl$ diluted to 50.0 cm^3; reference solutions were identical except that DMDTPK was replaced by buffer. (b) Samples were 20.0 cm^3 of 6.61 × 10^{-5} mol dm^{-3} *O,O*-diethylphosphorodithioate potassium salt (DEDTPK) and 0—4.0 cm^3 of 6.61 × 10^{-4} mol dm^{-3} $(Ph_4As)Cl$ diluted to 50.0 cm^3; reference solutions were the same except that DEDTPK was replaced by buffer. All solutions were adjusted and diluted with Tris buffer pH 8.0.

These findings were confirmed by conductivity measurements. In one series, the extracts were obtained by extraction from aqueous solutions containing a constant concentration of tetraphenylarsonium cation and increasing concentrations of dimethylphosphorodithioate whereas in the other a constant concentration of diethyl analogue was accompanied by increasing cation concentrations (Fig. 4). Conductivity of the organic phase increased in both cases linearly up to the point corresponding to the 1:1 mole ratio in the aqueous solution and remained constant thereafter, regardless of the excess of counter-ion. The conformity of these two series of measurements done with the extracts of aqueous solutions prepared in the inverse manner leads to the assumption that the conductivity of the organic phase is due to the presence of ionic species originating from dissociation of dialkylphosphorodithioate associates with tetraphenylarsonium cation.

According to the theory developed by Gibson and Weatherburn [17], if dissociation of ion-pairs in the organic phase is negligible, the distribution ratio of quaternary salt should increase as the square-root function of the initial concentration in the aqueous solution. To check if the investigated ion-pairs obey this prediction, the logarithm of the dichloromethane—water distribution ratios of tetraphenylarsonium chloride and ion-pairs of dialkylphosphorodithioates, as well as that of diethylphosphorothioate, were plotted against the logarithms of the initial concentrations in the aqueous phase. As shown in Fig. 5, tetraphenylarsonium chloride, like the ion-pairs studied here, satisfies the predicted linear relationship only at high concentrations. The significant discrepancy from the theoretically expected linear dependence observed in the low concentration range, approximately below 10^{-4} mol dm^{-3} in aqueous solution, indicates that dissociation of ion-pairs occurs in

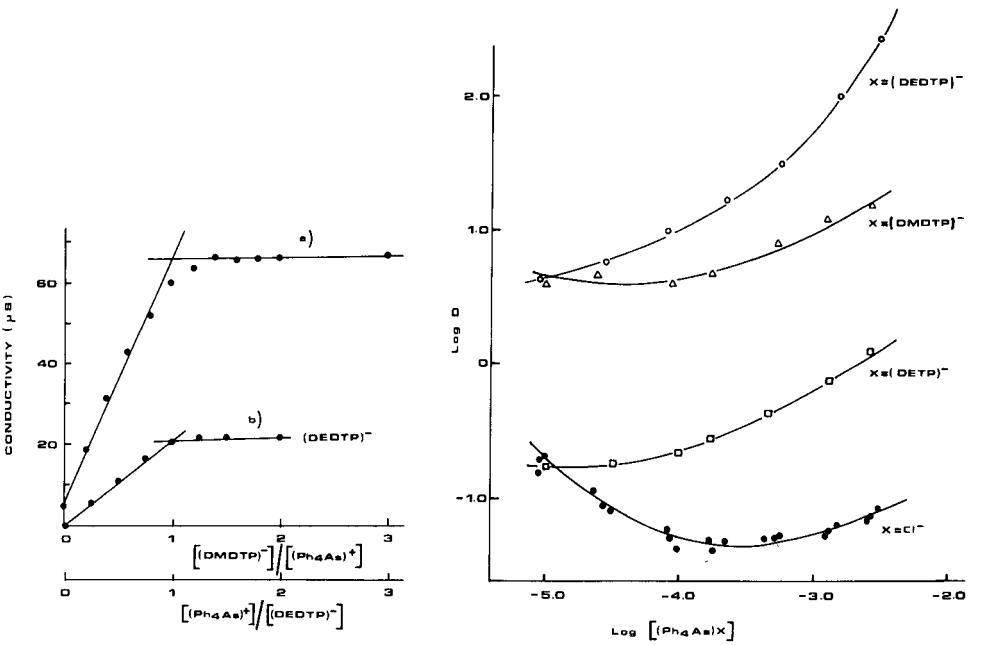

Fig. 4. Plots of the conductivity of the organic phase against the ratio of concentrations in the aqueous phase. (a) Anion-to-cation ratio: 30.0 cm^3 of 1.59×10^{-4} mol dm^{-3} $(Ph_4As)Cl$ and 0—15.0 cm^3 of 9.56×10^{-4} mol dm^{-3} *O,O*-dimethylphosphorodithioate potassium salt (DMDTPK) diluted to 50.0 cm^3. (b) Cation-to-anion ratio: 20.0 cm^3 of 6.61×10^{-5} mol dm^{-3} *O,O*-diethylphosphorodithioate potassium salt (DEDTPK) and 0—4.0 cm^3 of 6.61×10^{-4} mol dm^{-3} $(Ph_4As)Cl$ diluted to 50.0 cm^3. All solutions were adjusted and diluted with Tris buffer pH 8.0 before extraction.

Fig. 5. Plots of the logarithmic distribution ratio against the logarithm of initial salt concentration $(Ph_4As)X$ in the aqueous phase of ionic strength 0.15 (Na_2SO_4): (○) $DEDTP^-$; (△) $DMDTP^-$; (□) $DETP^-$; (●) Cl^-.

dichloromethane. Similar results were reported previously for some triphenylmethylarsonium salts in the chloroform—water system [17].

The extraction behaviour reported here calls for some further comment. In accordance with the values of the distribution ratio, the extraction recoveries follow the sequence: DEDTP>DMDTP>DETP, the distribution ratios of the more lipophilic dialkylphosphorodithioates being at least one order of magnitude higher than the values obtained by extraction of diethylphosphorothioate. Analogously with the adsorption onto the XAD-4 resin [12], the extraction is favoured not only by higher p*K* value but also by increased aliphatic character and sulphur content of the anion.

Characterization of the $(Ph_4As)(DMDTP)$ ion-pair by i.r. spectrophotometry

For characterization of $(Ph_4As)(DMDTP)$ ion-pair isolated from dichloromethane extracts, the i.r. spectrum of the crude ion-pair was compared with the i.r. spectra of pure standard compounds, tetraphenylarsonium chloride

and dimethylphosphorodithioate (potassium salt) recorded separately and as a mechanical mixture with a 1:1 mole ratio. The absorption bands in the i.r. spectra were assigned in the usual manner [19, 20]. The spectrum of the isolated (Ph_4As)(DMDTP) ion-pair showed the absorption bands characteristic of both compounds, with some obvious differences ascribed to ion-pair formation (Fig. 6), e.g., the shifts of the bands at about 1200 cm^{-1} and 1020 cm^{-1} corresponding to P—O—CH_3 vibrations, ν_{P-O} and ν_{C-O}, respectively, as well as the appearance of a broad band at 1600 cm^{-1} assigned to the phenyl nucleus conjugated with unsaturated groups or groups having lone-pair electrons.

Optimal conditions for the extractions

The extraction behaviour of the ion-pairs with the tetraphenylarsonium cation were further investigated, with the aim of improving the collection of dimethylphosphorodithioate from aqueous media. The dependence of extraction recovery on the pH value of the aqueous phase, on the cation-to-anion mole ratio and on the concentration of the ion-pair in water was therefore examined systematically.

At pH values higher than 4.25, the distribution ratio of the ion-pair in the dichloromethane—water system did not depend on the acidity of the aqueous phase. The distribution ratio also remained constant under neutral and slightly alkaline conditions (pH 7.25—8.90).

Spectrophotometric measurements allowed only the tetraphenylarsonium cation in the ion-pair to be quantified. Therefore, the dependence of the DMDTP recovery on the pH of the aqueous phase was also determined by gas chromatography. The concentration of DMDTP in water was 5.66×10^{-6} mol dm^{-3} and the mole ratio of tetraphenylarsonium cation to DMDTP

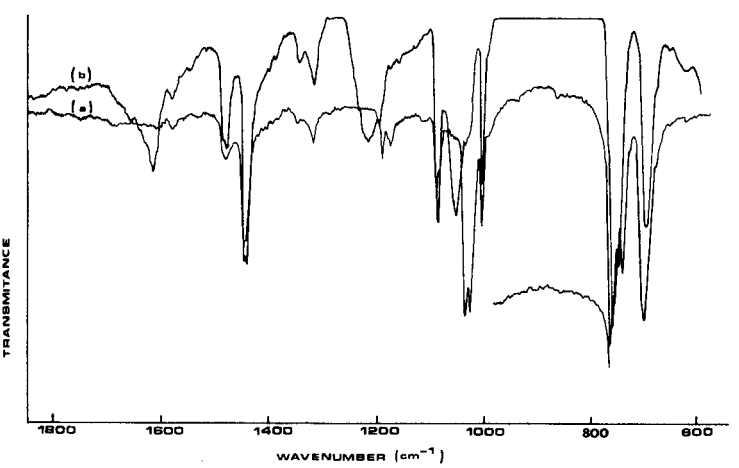

Fig. 6. Infrared spectra: (a) crude, mechanically prepared mixture of (Ph_4As)Cl and *O,O*-dimethylphosphorodithioate, potassium salt, in 1:1 mole ratio; (b) ion-pair of $(Ph_4As)^+$ with *O,O*-dimethylphosphorodithioate isolated in crude form from the extracts.

TABLE 1

Extraction recoveries of dialkyl phosphates, phosphorothioates and phosphorodithioates as ion-pairs with tetraphenylarsonium cation from water in dichloromethane

Compound	Concentration in water		Extraction recovery (%)[a]
	$\mu g\ cm^{-3}$	(10^{-6} mol dm^{-3})	
$(DEDTP)^-$	1.05	4.685	95
$(DMDTP)^-$	1.11	5.660	86
$(DETP)^-$	1.09	5.238	33
$(DMTP)^-$	1.0	5.608	9
$(DEP)^-$	1.02	5.310	not detected
PO_4^{3-}	3.22	19.634	<1

[a]Mean value of 5—7 simultaneously-run experiments.

in water was 8:1. The extraction recovery under these conditions at pH 8—9 was about 90% (±7%). The dependence of the DMDTP concentration in the dichloromethane extract on its initial concentration in a water sample of pH 8 was investigated in the concentration range 1.6668×10^{-8}—6.844×10^{-6} mol dm^{-3}. The samples with concentrations higher than 8.555×10^{-7} mol dm^{-3} were subjected to gas chromatography after methylation of a 0.1—1.0-cm^3 aliquot of the extract. In the lower concentration range, the whole extract was evaporated under a stream of nitrogen to 2 cm^3 and then methylated.

The relationships between the sample-to-standard peak height ratio and the DMDTP concentration in the ranges of 8.555×10^{-7}—6.844×10^{-8} mol dm^{-3} and 5.003×10^{-7}—1.668×10^{-8} mol dm^{-3} were linear. The slope of the second straight line was lower, which is very likely due to the evaporation before gas chromatography affecting the efficacy of the entire sample treatment procedure. Besides, it is realistic to suppose that the extraction efficiency decreases at very low concentrations.

For investigation of the dependence of the extraction efficiency of DMDTP from aqueous solution at pH 8, on the mole ratio of tetraphenylarsonium to DMDTP, the initial concentration of DMDTP in water was 5.66×10^{-6} mol dm^{-3}. The gas chromatographic results showed that DMDTP could not be extracted with dichloromethane in the absence of tetraphenylarsonium cation in accordance with the results of conductivity measurements. The extraction recovery increased with increasing concentration of tetraphenylarsonium and reached a maximum of 86% at cation-to-anion mole ratios higher than 2; increasing the mole ratio from 2 to 8 gave no further changes in the extraction recoveries.

Table 1 shows the extraction recoveries of some organophosphates obtained under the established optimum conditions. As expected, on the basis of distribution ratios, dialkylphosphorodithioates were extracted considerably more efficiently than phosphorothioates while diethylphosphate was

not extracted at all. Further, the recoveries of diethylphosphorothioate and diethylphosphorodithioate were slightly higher than those of the corresponding dimethyl analogues and the recovery of inorganic phosphates remained poor even at relatively high concentrations.

These results indicate that extraction with tetraphenylarsonium cation is applicable as a collection procedure for dialkylphosphorodithioates present in aqueous medium in low concentrations.

REFERENCES

1 H. Lenon, L. Curry, A. Miller and D. Patulski, Pest. Monit. J., 6 (1972) 188.
2 G. H. Boone, J. Ass. Off. Anal. Chem., 48 (1965) 748.
3 J. Askew, J. H. Růžička and B. B. Wheals, Analyst, 94 (1969) 275.
4 J. W. Eichelberger and J. J. Lichtenberg, Environ. Sci. Technol., 5 (1971) 541.
5 V. Drevenkar, K. Fink, M. Stipčević and B. Štengl, Arh. Hig. Rada, 26 (1975) 297.
6 V. Drevenkar, K. Fink, M. Stipčević and B. Tkalčević, Arh. Hig. Rada, 27 (1976) 297.
7 R. J. Maguire and E. J. Hale, J. Agric. Food Chem., 28 (1980) 372.
8 G. G. Volpe and V. N. Mallet, Int. J. Environ. Anal. Chem., 8 (1980) 291.
9 J. E. Woodrow and J. N. Seiber, Anal. Chem., 50 (1978) 1229.
10 V. Leoni, G. Puccetti, R. J. Colombo and A. M. D'Ovidio, J. Chromatogr., 125 (1976) 399.
11 G. Goretti, A. Lagana, B. M. Petronio and M. V. Russo, Ann. Chim., 69 (1979) 457.
12 C. G. Daughton, D. G. Crosby, R. L. Garnas and D. P. H. Hsieh, J. Agric. Food Chem., 24 (1976) 236.
13 J. J. Richard and J. S. Fritz, J. Chromatogr. Sci., 18 (1980) 35.
14 V. Drevenkar, Ž. Vasilić, B. Štengl, B. Tkalčević and B. Stilinović, in Concerted Action "Analysis of Organic Micropollutants in Water", COST Project 64 b bis, Activity Report 1978—1981, Proc. First European Symp., Berlin, 1979, Vol. 2, Commission of the European Communities, Bruxelles, 1982, p. 341.
15 R. Bock and G. M. Beilstein, Fresenius Z. Anal. Chem., 192 (1963) 44.
16 N. A. Gibson and D. C. Weatherburn, Anal. Chim. Acta, 58 (1972) 159.
17 N. A. Gibson and D. C. Weatherburn, Anal. Chim. Acta, 58 (1972) 149.
18 J. S. Fok, Z. Z. Hugus and E. B. Sandell, Anal. Chim. Acta, 48 (1969) 243.
19 N. B. Colthup, L. B. Daly and S. E. Wiberley, Introduction to Infrared and Raman Spectroscopy, 2nd edn., Academic Press, New York, 1975, p. 342.
20 L. J. Bellamy, The Infrared Spectra of Complex Molecules, Wiley, New York, 1966, pp. 64—68, 311—327.

Analytica Chimica Acta, 154 (1983) 287—293
Elsevier Science Publishers B.V., Amsterdam — Printed in The Netherlands

INVESTIGATION OF THE PROTONATION OF TRIETHYLENETETRAMINE BY MEANS OF A GLASS ELECTRODE

JAMES I. WATTERS*, PAULA C. DUNNIGAN[a] and SAMI Y. KALLINEY[b]
Department of Chemistry, The Ohio State University, Columbus, OH 43210 (U.S.A.)
(Received 12th October 1982)

SUMMARY

A quantitative study by means of a glass pH electrode was made of the successive protonation of triethylenetetramine(trien), in the pH range 2.0—12.0 at 25°C for unit ionic strength (KNO_3). The successive acidity constants of fully protonated H_4trien^{4+} were found to be $10^{-3.97}$, $10^{-7.12}$, $10^{-9.49}$ and $10^{-10.14}$.

The results obtained in four previous studies of the protonation constants of triethylenetetramine(trien) [1—4] are summarized in Table 1. In all of these studies, the acidity constants of H_4trien^{4+}, the fully protonated form of trien, were determined by the simultaneous solution of Bjerrum's formation functions for the mean number of bound hydrogen ions as discussed previously [5]. Evaluation of these data reveals that sufficiently different experimental conditions were used so that no reliable comparison can be made among these studies or with the present study. The average values for the stepwise acidity constants reported in the two studies made under conditions closest to those of the present study are approximately 3.9, 7.0, 9.3 and 10.0 [1, 2]. The present study was done in order to obtain accurate values of the acidity constants in solutions having the ionic strength adjusted to exactly 1 M with KNO_3 at 25°C, for use in the indirect study of trien complexes of several metal ions by means of a mercury electrode.

When hydrogen ions dissociate successively from a polyvalent acidic cation, such as the fully protonated amine, H_4trien^{4+}, the successive acidity constants decrease in magnitude largely because of the decrease in the repulsive positive ionic charge. There is also a statistical factor which depends on the number of filled and vacant sites [6]. The remainder of the bond energy can be considered as the intrinsic bond energy. The differences in successive pK values are indicated under the headings, Δ_{21}, Δ_{32} and Δ_{43} in Table 1 along with their mean values. These values, corrected for the statistical effect, are listed as Δ^*_{ij}. The effective statistical factor in K_{a1} is prob-

[a]Present address: B. F. Goodrich Chemical Group, 6100 Oak Tree Boulevard, Cleveland, OH 44131, U.S.A.
[b]Present address: Schering Corporation, 60 Orange Street, Bloomfield, NJ 07003, U.S.A.

0003-2670/83/$03.00

TABLE 1

Acidity constants of H_4trien^{4+} reported by various authors

pK_{a1}	Δ^{a}_{21}	pK_{a2}	Δ_{32}	pK_{a3}	Δ_{43}	pK_{a4}	Conditions	Ref.
3.32	3.35	6.67	2.53	9.20	0.72	9.92	0.1 M KCl, 20°C	[1]
3.85	3.15	7.00	2.25	9.25	0.67	9.92	0.5 M KCl, 20°C	
3.89	3.12	7.01	2.35	9.36	0.63	9.99	1.00 M KNO_3 + 0.100 M $BaCl_2$, 30°C	[2]
3.25	3.30	6.55	2.53	9.08	0.72	9.80	0.1 M $NaClO_4$, 25°C	[3]
3.37	3.25	6.62	2.47	9.09	0.60	9.69	0.1 M KCl, 26°C	[4]
Mean Δ_{ji}	3.23		2.43		0.67			
Mean Δ^{*}_{ji}	3.05[b]		2.36[b]		0.00[b]			

[a] Δ_{ji} is the difference, $pK_j - pK_i$ where $j = n$ and $i = n - 1$. [b] Δ^{*}_{ji} is Δ_{ji} minus the statistical effect.

ably 2/1 instead of a purely theoretical 4/1, because the protons probably dissociate from the internal secondary amines which have two adjacent protonated amines separated by only an ethylene group while terminal amines have only one. Furthermore, the product has a lower charge density. In either case, there is only one vacant amine site after this dissociation.

Because of the charge effect, it is highly probable that the next proton to dissociate from H_3trien^{3+} will be one of the two adjacent ones separated by only an ethylene group. This reduces the probability of dissociation in K_{a2} from the purely theoretical 3 to an effective 2. Two sites become available for protonation in half the resulting structures of H_2trien^{2+} which contain two terminally bonded protons, and one site becomes available in half the structures which contain only one terminally bonded proton. Hence, the weighted mean statistical probability of the association of a third proton is 1.5 and the statistical factor in K_{a2} is 1.33, so that the statistical effect in K_{a1}/K_{a2} is 1.50. Subtracting log 1.50 (or 0.18) from $\Delta_{21} = 3.23$ (Table 1) yields $\Delta^{*}_{21} = 3.05$, which is the statistics-free value of $pK_2 - pK_1$. In arriving at this value, we have introduced the principle that intermediate structures containing avoidable adjacent protons are highly improbable and will be excluded from statistical consideration. The probability of a proton dissociating from both H_2trien^{2+} structures is 2. After the dissociation of the next proton, 3/4 of the structures contain only one terminally bonded proton and 1/4 contain only one internally bonded proton. In the former case, there are two sites for proton association so that the probability of association is 2. In the latter case, there is only one suitable site so that the probability of association is 1, and the weighted probability of association in K_{a3} is 1.75. Hence, the statistical factor on K_{a3} is 1.14, the statistical effect in K_{a2}/K_{a3} is 1.17, and Δ^{*}_{32} has a value of 2.36.

In $Htrien^{+}$ there is only one proton to dissociate and the four neutral sites are equivalent. Hence, the statistical factor in K_{a4} is 1/4 and the statistical effect in $K_{a3}/K_{a4} = 4.56$, having a log of 0.66 which is very close to the mean

value given in Table 1. Thus, Δ^*_{43} is practically zero. It follows that, except for the statistical effect, K_{a3} and K_{a4} are practically equal. This result supports our statistics and also indicates that the charge effect between nonadjacent protonated amines is negligible.

The mathematical treatment of data for the successive protonation of a polyacidic base in terms of $\bar{n}_H$, the mean number of hydrogen ions bound by the polyacidic base, has been described [5]. Throughout this paper, the symbol C, followed by a subscript formula, indicates the concentrations of the added species; f' and f'' indicate the activity coefficients of H^+ and OH^-, respectively. Formulae enclosed in brackets indicate concentrations and those enclosed in parentheses indicate activities.

The data obtained in the titrations of H_4trien^{4+} with potassium hydroxide were used to calculate the constants by using a modified form of the MINI QUAD program [7]; in this procedure, the equilibrium constants which are finally chosen are those which yield the minimum value of the summation, $T(\text{calculated})^2 - T(\text{observed})^2$, where the T's indicate calculated and added concentrations, respectively, of one or more species. Thus, this method is an application of the Gauss—Newton method of least squares. The data obtained in the titration of trien with nitric acid were used to compute the constants by means of a graphic slope—intercept treatment of the equation

$$\bar{n}_H + (\bar{n}_H - 1)(H^+)\beta_1 + (\bar{n}_H - 2)(H^+)^2\beta_2 + (\bar{n}_H - 3)(H^+)^3\beta_3 + (\bar{n}_H - 4)(H^+)^4\beta_4 = 0 \quad (1)$$

As an illustration, at $\bar{n}_H$ values appreciably below 1.0, it was assumed that H_3trien^{3+} and H_4trien^{4+} were absent so that the β_3 and β_4 terms could be dropped. The equation was then rearranged to the form

$$\bar{n}_H/(2 - \bar{n}_H)(H^+)^2 = \beta_2 + [\beta_1/(H^+)]\,[(1 - \bar{n}_H)/(2 - \bar{n}_H)] \quad (2)$$

Plotting $\bar{n}_H/[(2 - \bar{n}_H)(H^+)^2]$ versus $[1 - \bar{n}_H]/[(2 - \bar{n}_H)(H^+)]$ yielded a straight line having a slope equal to β_1 and an intercept equal to β_2. Equation (1) was then rearranged with β_1 and β_2 as knowns, and β_3 and β_4 were evaluated by a similar slope—intercept treatment. Results obtained in this way agreed with those obtained by manual solution of simultaneous equations by means of an electronic computer.

EXPERIMENTAL

For the titrations with nitric acid, triethylenetetramine was purified by distilling it over sodium metal under vacuum (0.1 mm Hg). A jacketed 3-ft. fractionating column filled with glass helices and heated by a spiral coil of resistance wire was connected above the distillation flask by means of ground-glass connections. The first 25% fraction was discarded. The following perfectly colorless 50% fraction (b.p. 115°C) was collected. A stock solution, about 0.1 M, was standardized and stored in a polyethylene container under a nitrogen atmosphere. For the titrations of H_4trien^{4+} with

potassium hydroxide solutions, technical-grade trien was purified as described by Reilley and Sheldon [8]. Trien was precipitated as trien·$4HNO_3$ and dried at 105°C for 2 h. Sufficient product to prepare a 0.1 M solution and sufficient potassium nitrate to make the ionic strength 1.0 M were added. In the ionic strength calculations, the charge on H_4trien^{4+} was treated as four single positive charges rather than one 4+ charge because the charge is dispersed over four amines. A sufficient extra concentration of potassium nitrate was included to compensate for the hydrogen ion neutralized during the titration.

Commercial glass and saturated calomel electrodes were used. The reference electrodes were immersed in 1.0 M potassium nitrate and electrical contact to the solution titrated was made with a 3% agar-agar bridge containing 1.0 M potassium nitrate. A Beckman Research Model pH meter and a Corning Model 12 pH meter were used.

RESULTS

The conversion of hydrogen ion activities to molarities, needed in mass-balance equations, was achieved by measuring the pH of a series of solutions of known hydrogen ion concentration in a solution having a relatively high constant ionic strength. Dividing the measured hydrogen ion activity by its known concentration yielded the effective activity coefficient which, for practical purposes, can be treated as a conversion factor quite independently of its theoretically complex nature. Typical data and results are given in Table 2. Above a pH of about 2.1, the mean value of f' is 0.84 ± 0.02. Below this pH, the value decreases fairly regularly from 0.82 to 0.78; presumably because of the liquid-junction potential caused by the increased acidity.

Typical data obtained during the titration of H_4trien^{4+} with potassium hydroxide and the titration of trien with nitric acid are given in Tables 3 and 4, respectively, and a graph of data obtained in the latter titration is shown in Fig. 1. For comparison of the data from the two studies and to simplify calculations of the hybrid acidity constants, the values of the pH at half

TABLE 2

Activity coefficients of hydrogen ion
(50.00 ml of a solution 0.0206 M in HNO_3 and 0.9794 M in KNO_3 titrated with a solution 0.0645 M in KOH and 1.00 M in KNO_3 at 25°C)

pH	KOH (ml)	(H^+) X 10^2 [a]	$[H^+]$ X 10^2	f' [b]	pH	KOH (ml)	(H^+) X 10^2 [a]	$[H^+]$ X 10^2	f' [b]
1.792	0.00	1.61	2.06	0.78	2.124	6.08	0.75	0.90	0.83
1.846	1.24	1.43	1.80	0.79	2.216	7.18	0.61	0.71	0.86
1.884	2.11	1.31	1.62	0.81	2.306	8.01	0.49	0.58	0.84
1.929	3.04	1.18	1.44	0.82	2.446	9.05	0.36	0.42	0.86
1.987	4.06	1.03	1.25	0.82	2.642	10.06	0.23	0.27	0.85
2.049	5.04	0.89	1.08	0.82	2.996	11.05	0.10	0.12	0.83

[a] (H^+) = antilog (—pH). [b] f' is activity coefficient of H^+.

TABLE 3

The titration of H_4trien^{4+} with potassium hydroxide solution
(30.00 ml of solution containing 0.03320 M H_4trien^{4+} titrated with 0.08645 M KOH; T = 25°C, μ = 1.00 with KNO_3 in both solutions)

V (ml)	pH	b[a]	$\bar{n}_H$[b]	$\bar{n}^*_H$[c]	pH*[d]
5.02	3.854	0.4357	3.647	3.500	3.985
6.02	4.002	0.5225	3.481		
11.05	5.193	0.9596	3.041	3.000	5.560
12.05	5.891	1.046	2.954		
17.10	7.103	1.484	2.516	2.500	7.129
18.03	7.237	1.565	2.435		
23.01	8.255	1.9972	2.003	2.000	8.264
24.01	8.533	2.0840	1.916		
28.06	9.186	2.436	1.565	1.500	9.253
29.15	9.285	2.530	1.470		
34.00	9.655	2.951	1.046	1.000	9.684
35.05	9.712	3.0388	0.954		
40.09	10.113	3.480	0.509	0.500	10.124
41.14	10.211	3.571	0.431		
45.05	10.691	3.910	0.000		

[a] $b = C_{KOH}/C_{H_4trien^{4+}}$. [b] $\bar{n}_H = (C_{H^+} - [H^+])/C_{trien}$. [c] Interpolated pH at integral and half integral values of $\bar{n}_H$, indicated by *. [d] Compare values in Table 4.

TABLE 4

The titration of trien with nitric acid
(100.33 ml of solution containing 0.02793 M trien titrated with 0.1092 M HNO_3; μ = 1.0 with KNO_3 in both solutions, T = 25°)

V (ml)	pH	a[a]	$\bar{n}_H$[b]	$\bar{n}^*_H$[c]	pH*[c]
11.72	10.32	0.457	0.457	0.500	10.292
12.72	10.292	0.496	0.505		
13.72	10.250	0.535	0.543		
36.72	9.403	1.431	1.432		
37.72	9.360	1.470	1.471	1.500	9.326
38.72	9.316	1.509	1.510		
63.80	7.135	2.486	2.486		
64.72	7.074	2.522	2.522	2.500	7.117
65.72	7.007	2.561	2.560		
66.72	6.931	2.600	2.600		
88.72	4.027	3.457	3.450		
89.72	3.964	3.496	3.487	3.500	3.941
90.72	3.898	3.535	3.525		
91.72	3.830	3.574	3.562		

[a] $a = C_{HNO_3}/C_{trien}$. [b] $\bar{n}_H = (C_{HNO_3} - [H^+])/C_{trien}$. [c] Interpolated pH at half integral $\bar{n}_H$ indicated by *. Compare values in Table 3.

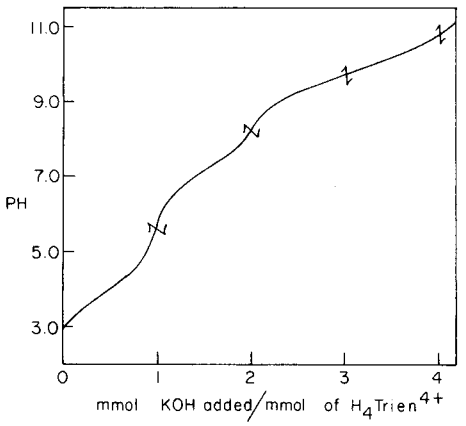

Fig. 1. Titration of 45.00 ml of a solution 0.01107 M in H_4trien^{4+} and 0.96 M in KNO_3 with a solution 0.08645 M in KOH and 1 M in KNO_3 to maintain unit ionic strength.

integer values were obtained by interpolating between the closest points indicated by asterisks in columns 5 and 6. Comparison of these calculated values of pH* in the two tables shows that the agreement is excellent at $\bar{n}$ = 2.5 and 3.5, particularly when it is considered that all of the reagents and instrumentation were completely different. The close agreement of these results, with one exception, constitutes strong evidence that both the trien and the trien·$4HNO_3$ reagents were of high purity. However, the fact that, in titration with potassium hydroxide, the pH was slightly lower at $\bar{n}_H$ = 1.5 (where b = 2.5) and 0.17 units lower at $\bar{n}_H$ = 0.5 (where b = 3.5) than in the titration with nitric acid suggested some contamination of the potassium hydroxide solution by CO_2, or a weak acid extracted from plastic components of the apparatus. Additional evidence for contamination was the fact that the experimental value of Δ_{32} was only 0.50 compared to the theoretical value of 0.66. This is appreciably below the values obtained in the cited studies [1—4] and also, that obtained in the present titrations of trien with nitric acid. Another consideration was the fact that errors such as those related to the concentration of titrant and the evaluation of the equivalence point, increase with the volume of titrant. This effect can become particularly significant past the second equivalence point. Consequently, optimum accuracy can be predicted for values of b less than 2 in Table 3 and for values of a less than 2 in Table 4. Hence, the calculation of the various pK_a values manually by the simultaneous solution of equations at half integer values of $\bar{n}_H$ are based on these data and are presented in Table 5. In every case, the results agree within 0.02 units with those obtained in the original calculations. This supports the accuracy of these constants and the reliability of the calculations which involve completely different procedures. The values obtained for pK_a with the MINIQUAD program and manually were 3.97 and 3.96, respectively. Their difference of 0.01 is less than the standard deviation of 0.02 obtained in the MINIQUAD procedure. The preferred

TABLE 5

Successive acidity constants of H_4trien^{4+}

Source of data	Method of calc.	pK_{a1}	Δ_{21}	pK_{a2}	Δ_{32}	pK_{a3}	Δ_{43}	pK_{a4}
Table 3	MINIQUAD	3.97 ± 0.02	3.15	7.12 ± 0.01	2.33	9.45 ± 0.01	0.50	9.95 ± 0.01
Table 4	Graph	4.04	3.11	7.15	2.33	9.48	0.67	10.15
Tables 3, 4	Manual	3.96	3.16	7.12	2.37	9.49	0.66	10.13
Chosen values		3.97 ± 0.02	3.15	7.12 ± 0.01	2.37	9.49 ± 0.01	0.65	10.14 ± 0.01

value for pK_{a1} is 3.97 ± 0.02. This value and those for pK_{a2}, pK_{a3} and pK_{a4} are given in Table 5. Both procedures yielded the same value of 7.12 for pK_{a2} so this value, along with the MINIQUAD standard deviation of ±0.01, was chosen. The original calculations of pK_{a3} and pK_{a4}, based on the data in Table 4, were made graphically. The values of pK_{a3} obtained graphically and manually, were 9.48 and 9.49, respectively, for which the value 9.49 ± 0.01 was chosen. The values of pK_{a4} were 10.15 and 10.13 or a mean value of 10.14 ± 0.01. The calculation of pK_{a3} and pK_{a4} as the unknown at points in the vicinity of the half integer values of $\bar{n}_H$ = 0.50 and 1.50, respectively, also yielded standard deviations for pK_{a3} and pK_{a4} amounting to less than ±0.01. Combining these pK_a values yields the following values for the overall constants for the successive protonation of trien: $\beta_1 = 10^{10.14 \pm 0.01}$, $\beta_2 = 10^{19.23 \pm 0.02}$, $\beta_3 = 10^{26.75 \pm 0.03}$, $\beta_4 = 10^{30.72 \pm 0.05}$.

REFERENCES

1 G. Schwarzenbach, Helv. Chim. Acta, 33 (1950) 974.
2 H. B. Jonassen, R. B. LeBlanc, A. W. Meibohm and R. M. Rogan, J. Am. Chem. Soc., 72 (1950) 2430.
3 D. W. Margerum, D. B. Rorabacher and J. F. G. Clarke, Jr., Inorg. Chem., 2 (1963) 667.
4 R. L. Pecsok, R. A. Garber and L. D. Shields, Inorg. Chem., 4 (1965) 447.
5 J. I. Watters, P. E. Sturrock and R. E. Simonaitis, Inorg. Chem., 2 (1963) 765.
6 J. Bjerrum, Metal Ammine Formation in Aqueous Solutions, P. Haase, Copenhagen, 1941.
7 A. Sabatini, A. Vacca and P. Gans, Talanta, 21 (1974) 53.
8 C. N. Reilley and M. V. Sheldon, Talanta, 1 (1958) 127.

Analytica Chimica Acta, 154 (1983) 295—300
Elsevier Science Publishers B.V., Amsterdam — Printed in The Netherlands

Short Communication

AUTOMATION OF A GRAPHITE-FURNACE ATOMIC ABSORPTION SPECTROMETRY SYSTEM WITH A Z80-BASED MICROCOMPUTER[b]

ROGER GUEVREMONT* and JOHN WHITMAN[a]

Atlantic Research Laboratory, National Research Council, 1411 Oxford Street, Halifax, Nova Scotia B3H 3Z1, and Seimac Ltd., Bedford, Nova Scotia (Canada)

(Received 23rd February 1983)

Summary. A microprocessor was used to control the operation of an atomic absorption spectrometer and a graphite-furnace atomizer. The system allows complete and flexible control of the graphite furnace heating program and active feedback with an optical temperature sensor, control of purge gas flows, and control of an autosampler. With microprocessor control, the graphite furnace can be heated from 0 to 2500°C in about 3 s with little or no overshoot. Reproducibility data for cadmium in oyster tissue gave relative standard deviations between 1.3 and 3.3% with microprocessor control and between 2.1 and 7.8% without control. Digitized data may be plotted and stored on disk.

Availability of inexpensive microprocessor hardware has led to many improvements in atomic absorption spectrometry (a.a.s.). Computers have simplified data acquisition and storage [1, 2], especially in laboratories with several instruments and large sample throughput [3, 4]. Automatic data acquisition has made sophisticated data processing [5—7] and signal enhancement [8] possible. The computer can take an active role in management of experiments; this can include simple start and stop instructions, automated sample preparation [9] and introduction [10], and active real-time feedback and multichannel acquisition during a dynamic experiment [11, 12]. Finally, the computer can be a vital tool for acquisition of information during unique experiments [13, 14]. Beyond simple data acquisition, most such work has been done by manufacturers of a.a.s. instrumentation [11].

This communication describes the development of a system that uses the active feedback and data acquisition roles of a Z80 microprocessor system for graphite-furnace a.a.s.

Operation of the system

Parameters that control heating of the graphite furnace and acquisition of the a.a.s. data are stored on disk in a "method" file. In addition to the parameters in the method file, the operator has control over the system through a series of "operator requested" routines for such operations as redefinition of the axes for an X-Y display. All possible selections from the menu are

[a]Present address: Bedford Institute of Oceanography, Dartmouth, Nova Scotia, Canada.
[b]NRCC No. 22526.

0003-2670/83/$03.00

displayed. Selection from each part of the menu requires only a single keystroke. Software listings or copies on floppy disks are available from Seimac Ltd., 1378 Bedford Highway, Bedford, N.S., Canada, B4A 1E2.

Instrumentation

The Perkin-Elmer model 503 atomic absorption spectrometer used was not modified electronically. Slightly improved sensitivity was achieved by removing a half-silvered window on the detector side of the spectrometer. Deuterium background corrections were used in all work; hence optical components required for the double-beam operating mode were removed. A Perkin-Elmer model HGA-2200 graphite-furnace atomizer was used with minor electronic modifications. A switch allowed reconnection of all original circuits to their unaltered state (e.g., for routine maintenance or servicing).

The computer used was a Cromemco Z80-based microprocessor with 64 kB memory and dual single-density floppy-disk drives. The Cromemco CDOS (disk operating system) version 2.17, Fortran version 3.21, and relocatable assembler version 2.15 were used in all work described here. The computer also included several S-100 interface boards: a serial/parallel interface (Cromemco TU-ART) an 8-bit A/D—D/A board (Cromemco D + 7A), a 12-bit programmable gain A/D board (California Data Corp. AD-100), a 12-bit D/A board (TecMar) and an optically isolated parallel input/output board (Cromemco 4PIO). All analog inputs and outputs except those to the X-Y plotter were through the 12-bit A/D and D/A boards. All boards were used as described in the manufacturers' literature.

The hardware connections between the interface boards of the microprocessor and the atomic absorption unit were kept as simple as possible. Figure 1 shows the system design. The following sections describe the hardware and software approach to automated operation of the system.

Automated operation

Absorbance data. Absorbance data were obtained both from the analog output and by digital processing of signals from the hollow-cathode and deuterium lamps monitored at test points TP 2103 and TP 2104 on the Demodulating Signal Separator board of the PE 503.

Temperature measurement. Although several methods have been used to measure temperatures of furnace walls and gases [11, 15—17], the approach described here is a hybrid of power measurements and optical pyrometry. Furnace temperature was monitored with a current/voltage measurement (internal to the HGA-2200), and by an external infrared (i.r.) detector. The current/voltage feedback function (analog temperature meter of the HGA-2200 control panel) operated below a user-selected threshold; the i.r. detection system was operated above the threshold.

Infrared measurements were made with a one-stage, lead-sulphide, thermoelectrically cooled detector (Infrared Industries, Waltham, MA). A water-cooled brass heat sink was used to maximize detector stability. Although a

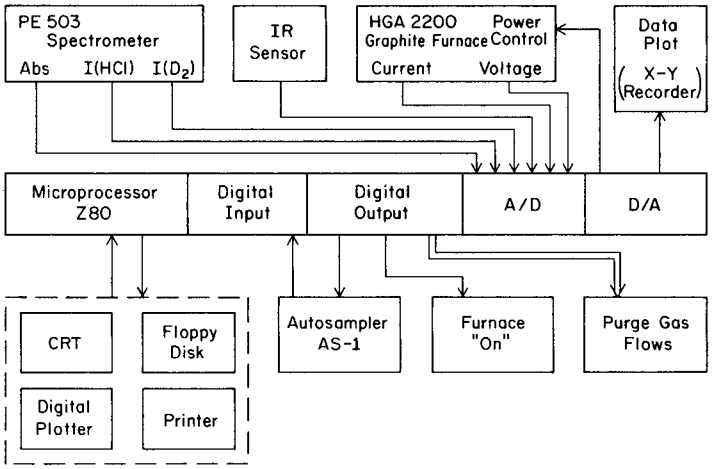

Fig. 1. Automatic control and data acquisition for graphite furnace atomic absorption spectrometry by means of a Z80 microprocessor.

cooled PbS i.r. detector can easily be configured to measure temperatures below 25°C, a compromise operating point was necessary to allow measurements above 2500°C. In the present configuration, a cross-over temperature of 200°C was used most frequently. The detector was used in the d.c. mode. Stability and reproducibility of the PbS infrared detection system were checked by optical pyrometry and, below 1800°C, with a 6% rhodium/30% rhodium in platinum thermocouple. The thermocouple was fused to the inside wall at the center of the graphite furnace by carefully increasing the target temperature of 3-s heating pulses by 5°C increments until the thermocouple melted and cooled into a cone shape and remained bonded to the graphite.

When the furnace was heated repeatedly (>16 cycles) under computer control, in a manner similar to that in a standard additions experiment, the standard deviation of the set temperature as measured by thermocouple, was 10°C at 1450°C and 8°C at 1770°C. Repeated (27) heatings done intermittently over five days showed a standard deviation of 19°C at 1350°C and 23°C at 1750°C. All electrical power, gas, and cooling water supplies were shut down between measurements. Experience has shown that thermocouple reliability deteriorates after more than 20 heatings above 1750°C. The short-term stability of the i.r. detector was studied while it was subjected to intense i.r. radiation. Infrared and thermocouple measurements agreed within 10°C during continuous (10 s duration) measurements at 1750°C. Continuous or intermittent radiation at furnace temperatures up to 2500°C induced no detectable drift or bias in the i.r. detector.

Temperature calibration. The furnace temperature was calculated by comparison of detector signals with tabular data previously stored in computer memory. This table can be edited in several ways by the user, including

additions, deletions, and changes to individual response values. The response table can be recalibrated manually or automatically in 15 min if the i.r. sensor is changed or physically moved.

Plot of output data. Use of a low-quality X-Y plotter and 8-bit D/A control to the plotter resulted in no loss of information. The scales of the plot are chosen by the user and the data can be replotted as often as necessary with altered parameters in the method file, and with various menu selected options (absorbance or background vs. temperature, temperature vs. time, etc.)

Gas flow control. Solenoid-actuated gas valves in the HGA-2200 are controlled by relays through the Cromemco 4PIO board. The software includes an option to operate two additional gas flows, again through the 4PIO board. Therefore, gases including air or hydrogen can be metered to the furnace during any step of the heating program.

Autosampler control. In automated sampling, a signal is sent to the autosampler (Perkin-Elmer AS-1), which then injects the sample into the furnace. The computer detects the signal from the AS-1 indicating the end of the injection, and initiates the HGA heating program. Alternatively, the furnace heating program can be started simultaneously with the start of the AS-1, with the first steps of the program below the boiling temperature of the sample. A sample can be introduced to a warm graphite furnace if this is necessary to improve the reproducibility of drop deposition. Mandatory cooling steps are run before any further sample introduction. If additional time is required for cooling, more cooling steps can easily be added to the furnace heating program.

Temperature programming. A d.c. signal is applied through resistor R123 of the original HGA-2200 circuit to control the furnace temperature. The signal voltage must range from +15 V which will place the furnace effectively in the off state, to +5 V or lower, where maximum power is applied to the graphite furnace. A 12-bit D/A conversion was required to provide the needed resolution. Temperature control voltage is adjusted to minimize the difference between the programmed temperature and the temperature sensed by the i.r. detector. The detector is calibrated by an independent procedure.

Safety features. It was considered important that none of the automatic shut-down features of the graphite furnace be disabled and that the system remain fail-safe. The temperature alarm circuit sends a signal to the computer if a problem arises, and the computer output is altered to permit the furnace to cool down. The furnace cools down if the computer stops processing for any reason.

All furnace heating programs are part of a method data file; the furnace cannot be heated unless a method has been entered. A method contains up to 30 user-selected steps. Mandatory extra steps 31 and 32 return argon gas flows to their normal values and provide a period of cooling to reduce the possibility of sample injection into a hot furnace.

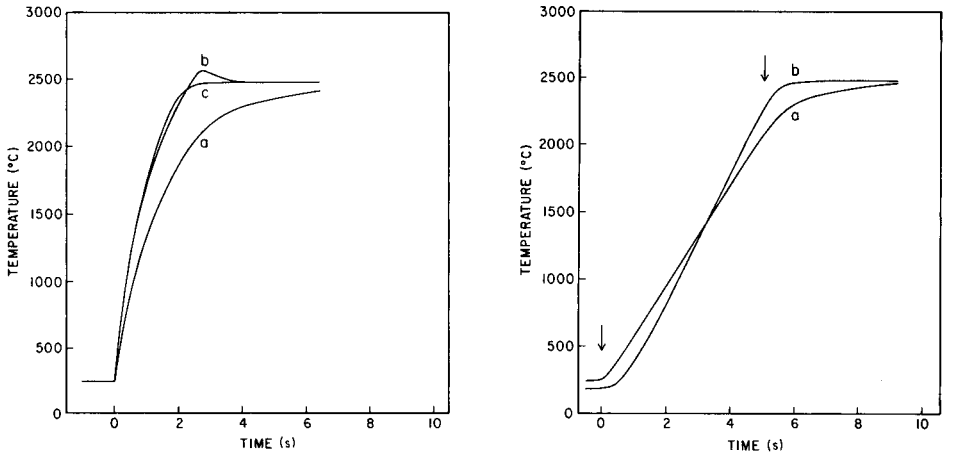

Fig. 2. Furnace temperature during a step from 250 to 2500°C: (a) with the unmodified HGA-2200; (b) with the unmodified HGA-2200 and MAX TEMP; and (c) with the computer-controlled HGA-2200.

Fig. 3. Furnace temperature during a 5 s ramp from 250 to 2500°C: (a) with the unmodified HGA-2200; and (b) with the computer-controlled HGA-2200. Arrows indicate the expected start and end of the ramp.

Application

Figure 2 shows the more rapid response of the furnace temperature with computer control relative to the unmodified furnace. Once the target temperature was reached with computer control, a deviation less than 10°C was observed within the next 1 s, and much less during the following 6-s period. The control function was designed to apply the maximum power necessary to reach the target with the minimum oscillation before stabilization. The time needed to reach 2500°C is a function of the total current available from the HGA-2200 power supply.

Figure 3 compares temperature profiles observed when heating the graphite furnace in accord with a 5-s ramp from 250 to 2500°C with and without computer control. The onset of heating is apparently very rapid without computer control, but the ramp tails off badly above 2200°C. Computer control provides a linear ramp of about 5-s duration and rapid approach to the target temperature at the end of the ramp.

Reproducibility data were obtained for cadmium in unspiked and spiked digests of NBS oyster tissue (SRM 1566) and of a homogenized lobster hepatopancreas sample. Twenty consecutive injections for four different samples gave relative standard deviations that ranged from 1.3 to 3.3% with computer control and from 2.1 to 7.8% without control, the highest deviation being for the unspiked lobster tissue. Spurious signals are virtually eliminated by computer control. Triplicate digestions with standard addition experiments were performed on NBS oyster tissue to quantify cadmium and

lead, and five similar procedures were applied to the homogenized lobster tissue. The oyster was found to contain 3.63 ± 0.12 $\mu g\ g^{-1}$ Cd and 0.46 ± 0.07 $\mu g\ g^{-1}$ Pb, and the lobster hepatopancreas 21.0 ± 2.1 $\mu g\ g^{-1}$ Cd and 0.41 ± 0.07 $\mu g\ g^{-1}$ Pb.

The computer-controlled system has been used routinely to quantify components in sea water and marine samples.

Helpful discussion and comments from L. Ramaley, Dalhousie University, and F. G. Mason are gratefully acknowledged. Work was carried out by Seimac under contracts 31028-2-2850, 31028-1-2251, 080-077/0-6309, and 081-015/1-6303.

REFERENCES

1 L. E. Holboke, Chem. Biomed. Environ. Instrum., 11 (1981) 27.
2 D. C. McDonald and R. S. Neil, Anal. Chim. Acta, 138 (1982) 145.
3 M. R. Harris and N. W. Lepp, Analyst, 106 (1981) 283.
4 W. Brunner, Spez. Ber. Kernforschungsanlage Juelich, Juel-Spez-, 46 (1979) 32.
5 J. H. Kalivas and B. R. Kowalski, Anal. Chem., 54 (1982) 560.
6 K. Eckschlager and V. Stepanek, Anal. Chem., 54 (1982) 1115A.
7 P. J. Whiteside, T. J. Stockdale and W. J. Price, Spectrochim. Acta, Part B, 35 (1980) 795.
8 M. Suzuki, K. Ohta and T. Yamakita, Anal. Chim. Acta, 133 (1981) 209.
9 M. E. Ruddel and S. W. McClean, Anal. Chem., 53 (1981) 1946.
10 T. Uchida, I. Kojima and C. Iida, Analyst, 106 (1981) 206.
11 M. W. Routh, P. S. Doidge, J. Chidzey and B. Frary, Am. Lab., 14 (6) (1982) 80.
12 D. A. Katskov, I. G. Burtseva, I. L. Grinshtein and L. P. Kruglikova, Zh. Anal. Khim., 35 (1980) 2289.
13 J. M. Harnly and T. C. O'Haver, Anal. Chem., 53 (1981) 1291.
14 H. Koizumi, H. Sawakabu and M. Koga, Anal. Chem., 54 (1982) 1029.
15 R. E. Sturgeon and C. L. Chakrabarti, Spectrochim. Acta, Part B, 32 (1977) 231.
16 M. J. Adams and G. F. Kirkbright, Anal. Chim. Acta, 84 (1976) 79.
17 W. Slavin, S. A. Myers and D. C. Manning, Anal. Chim. Acta, 117 (1980) 267.

Analytica Chimica Acta, 154 (1983) 301—306
Elsevier Science Publishers B.V., Amsterdam — Printed in The Netherlands

Short Communication

DECREASED MOLYBDENUM EMISSION IN A CARBON ARC CAUSED BY ZIRCONIUM CARBIDE FORMATION ON THE SAMPLE ELECTRODE[a]

J. C. BURRIDGE* and I. J. HEWITT

Department of Spectrochemistry, The Macaulay Institute for Soil Research, Craigiebuckler, Aberdeen AB9 2QJ (Gt. Britain)

(Received 3rd March 1983)

Summary. The presence of about 10% zirconium (as oxide) in alumina samples obtained by the ignition of aluminium 8-quinolinolate (precipitated as a trace-element collector) greatly decreased the intensity of molybdenum emission when the alumina was analysed by means of a cathode-layer carbon arc. Retention of the molybdenum on the sample electrode was confirmed with radioactive molybdenum-99. A prominent crystalline residue on the cathode, identified as ZrC by x-ray powder diffraction, was probably responsible for the decreased emission. Thus, zirconium crucibles cannot be used for the sodium carbonate fusion of samples in a spectrochemical procedure for determining traces of molybdenum in soils and plants.

The recent availability of high-purity zirconium crucibles led to an investigation of their suitability as an alternative to platinum crucibles for the sodium carbonate fusion of ashed plant materials. Such fusion is an essential stage in the spectrochemical procedure of Mitchell and Scott [1], as applied here and elsewhere for many years, for the determination of molybdenum and other trace elements in relation to agricultural problems. The method uses 8-quinolinol, tannic acid and thionalide to co-precipitate trace elements with aluminium from a hydrochloric acid sample solution buffered to pH 5.2 with ammonium acetate.

There were two main reasons for seeking an alternative to platinum for the crucibles. First, difficulty has been experienced in obtaining platinum crucibles of sufficient purity at a reasonable cost; a fusion blank should contain, for example, less than 0.1 μg of silver, and comparable amounts of several other elements. Secondly, the ease with which platinum forms alloys, e.g., with iron, makes it difficult to maintain high-purity platinum crucibles in that condition when they are used for samples having a wide range of heavy-metal contents. Crucibles made from boron nitride or vitreous carbon were also tested, but although their purity was adequate, their working life was short.

Experimental

The zirconium crucible used for sodium carbonate fusions was squat, with a capacity of about 25 ml and a wall thickness of nearly 1 mm (Specialized Component Manufacturers, Brookmans Park, Herts., England). A stock solution of $Zr(NO_3)_4 \cdot 5H_2O$ was used to precipitate controlled weights of zirconium.

The spectrographic determination of molybdenum (and other trace elements) in alumina using the cathode-layer carbon arc, after preconcentration by precipitation with mixed organic reagents, has been fully described [1—3]. A Hilger and Watts E1 Large Quartz spectrograph was used. The anode and cathode were both of carbon, grade SG305 (Morganite, no longer available); 1 part of alumina was mixed in an agate mortar with 2 parts of pure carbon and tightly packed by hand using a steel tamper into a cavity (1-mm diameter, 8-mm depth) in the cathode (2.8-mm outer diameter). The anode was an unpointed 5.5-mm diameter rod. The samples were arced to completion (in about 180 s) at 9 A with a continuously adjusted, constant inter-electrode gap of 10 mm. The arc was free-burning in air; the open-circuit line voltage was 300 V. Molybdenum was determined from the intensity of the Mo 317.02-nm line, with internal standard Fe 319.69 nm or Fe 330.60 nm.

Precipitates were also analysed, without ignition to alumina, by treatment with nitric acid (67%, w/w) to destroy organic matter followed by dissolution in 0.06 M hydrochloric acid. The molybdenum content of such solutions was determined by inductively-coupled plasma emission spectrometry (i.c.p.e.s.) with a Radyne SC15 1.5-kW source and a Techtron AA4 monochromator, at the Mo 379.83-nm line. In addition, spectrophotometric determinations of molybdenum were made by measuring the absorbance of the green dithiol complex [4] after extraction into iso-amyl acetate.

Molybdenum-99 ($t_{1/2}$ = 67 h) was used as tracer, activity being measured by liquid or crystal scintillation counters as appropriate. X-ray powder diffraction was used to identify ZrC with a Debye—Scherrer camera (114.8-mm diameter) and cobalt K_α radiation.

Results

Initial tests confirmed the high purity of the zirconium crucible, but its shape and size caused some difficulty in raising it to a high enough temperature to give fluid sodium carbonate fusions. A glass-blower's torch with a coal gas/oxygen flame gave the most satisfactory control of temperature and effective fusions.

The existence of a serious problem in the spectrographic determination of molybdenum was indicated by very low results for a soil known to contain about 20 μg Mo g^{-1}. After fusion of 100 mg of finely milled soil in the zirconium crucible, and concentration of the trace elements in alumina by co-precipitation [1], spectrography showed a molybdenum content of less than 5 μg g^{-1}. Results for cobalt were satisfactory but those for titanium and

vanadium also appeared somewhat low; this effect was not investigated further.

Visual examination of the spectra showed that the ignited alumina precipitates, obtained after sodium carbonate fusion in the zirconium crucible, contained large but variable amounts of zirconium. When the alumina contained significant amounts of zirconium, the Fe 330.60-nm line was used as internal standard for molybdenum because the Zr 319.70-nm line interfered with the Fe 319.69-nm line normally used. The amounts of zirconium in the precipitates were not determined, but zirconium was probably precipitated quantitatively by 8-quinolinol from the acetate-buffered solution [5]. Precipitation of molybdenum together with various known amounts of zirconium showed that 5 mg of zirconium in the sample solution caused severe depression of molybdenum emission, and that as little as 0.5 mg of zirconium had a marked effect (Table 1). Ignited precipitates increased in weight by about twice the weight of zirconium added to the sample solutions, probably because the zirconium was present as a hydrated oxide.

Two methods were used to confirm that molybdenum was fully precipitated by the organic reagents in the presence of 5 mg of zirconium. Firstly, the molybdenum in unignited precipitates was determined by i.c.p.e.s. Secondly, the ^{99}Mo was used to measure molybdenum remaining in the filtrate after precipitation (Table 2). The method of standard additions was applied in i.c.p.e.s., with small corrections for the interference of the Fe 379.85-nm line on the Mo 379.83-nm line and for an enhanced general background emission when the solutions contained zirconium. The i.c.p.e.s. results showed that zirconium did not have any significant effect on the precipitation of molybdenum, and the ^{99}Mo activity measurements suggested that zirconium might have reduced the small loss of molybdenum in the filtrate. Other experiments with ^{99}Mo showed that the precipitation of

TABLE 1

Effect of zirconium in sample solution on molybdenum determined spectrographically in the ignited alumina precipitates

Sample solution content[a]		Ignited precipitate weight[b] (mg)	Spectrographic Mo determination		
Mo (μg)	Zr (mg)		in ppt.[b] (μg g^{-1})	recovery[b] (μg)	(%)
5	0	34; 30	136; 154	4.6; 4.6	92
5	0.05	32; 30	132; 151	4.3; 4.5	88
5	0.5	35; 33	56; 57	2.0; 1.9	39
5	5	45; 41	<5; <5	<0.2; <0.2	<4
10	0	30	295	8.9	89
10	5	42	<5	<0.2	<2

[a] All solutions in Tables 1—3 also contained about 1.4 mg of iron and 12 mg of aluminium.
[b] Independently precipitated duplicates.

TABLE 2

Effect of zirconium on the precipitation of molybdenum from acetate-buffered solution at pH 5.2 by 8-quinolinol, tannic acid and thionalide

Sample solution content		Mo found		Sample solution content		Mo found	
Mo (μg)	Zr (mg)	in ppt.[a] (μg)	in filtrate[b] (% of total Mo)	Mo (μg)	Zr (mg)	in ppt.[a] (μg)	in filtrate[b] (% of total Mo)
20	0	21	—	50	0	—	4.5
20	5	17	—	50	5	—	0.2
100	0	99	—	100	0	—	2.0
100	5	104	—	100	5	—	0.2
5	0	—	3.2	200	0	—	0.2
5	5	—	0.2	200	5	—	0.2

[a]By i.c.p.e.s. [b]By ^{99}Mo activity.

molybdenum was complete within 15 min. All precipitates examined in this study, however, were allowed to stand overnight before being filtered, as recommended [1]. It was also established that the co-precipitation of molybdenum and zirconium from the same solution was not necessary for the subsequent depression of molybdenum emission in the arc. When molybdenum and zirconium were precipitated separately, and their precipitates dried and mixed thoroughly before ignition to alumina, decreased emission again occurred, comparable to that shown in Table 1.

Use of ^{99}Mo proved that molybdenum was not lost by volatilization during the ignition of precipitates to alumina. Measurements of the ^{99}Mo activity remaining on the cathodes after arcing for 180 s (i.e., to completion, the stage at which emission from the arc decreased sharply) proved that a significant amount of molybdenum was retained in residues on the electrode (Table 3). Such measurements also revealed a significant residue of molybdenum on the electrode in the absence of zirconium.

Alumina samples derived from solutions that contained 5 mg of zirconium

TABLE 3

Effect of zirconium on the retention of molybdenum on the cathode after arcing alumina samples for 180 s

Sample solution content		Retained ^{99}Mo activity in residue after arcing (%)		Sample solution content		Retained ^{99}Mo activity in residue after arcing (%)	
Mo (μg)	Zr (mg)	β-counter	γ-counter	Mo (μg)	Zr (mg)	β-counter	γ-counter
5	0	24	13	50	0	18	16
5	0.05	32	20	50	5	58	58
5	0.5	55	46	200	0	24	17
5	5	100	100	200	5	71	71

left an obvious deposit, apparently crystalline, on the tip of the cathode after arcing. One of these deposits was examined by x-ray powder diffraction. The line pattern obtained could be attributed almost entirely to zirconium carbide, the pattern being virtually identical to that on the JCPDS (Joint Committee for Powder Diffraction Standards) reference card 19-1487, all lines being very strong and sharp, including the back-scattered reflections. The *a* parameter was measured as 4.688 Å. Other much weaker lines could be attributed to ZrO_2; there was no indication of zirconium nitride being present.

Discussion

These results clearly show that zirconium crucibles cannot be used instead of platinum crucibles for the sodium carbonate fusion of samples in the spectrochemical procedure developed by Mitchell and Scott [1—3] for trace elements in plants and soils. In addition to the specific effect reported here for molybdenum, other difficulties were encountered. The spectrochemical procedure was developed to concentrate trace elements from the original samples, and to simplify the matrix for arcing. Typically, the trace elements from a 20-g sample are collected in a 40-mg alumina precipitate, giving a concentration factor of 500. The large, variable amounts of zirconium derived from the crucible not only decreased this concentration factor, but also considerably altered the matrix. Furthermore, line interferences from the complex zirconium spectrum disturbed the spectrographic measurements. Finally, the oxide or nitride scale formed on the crucible was a serious source of contamination of other samples, in which zirconium was present at the 100 $\mu g\ g^{-1}$ level.

No other workers seem to have reported such a severe decrease in the emission intensity from a trace element by a matrix component, in a cathode-layer carbon arc. The physical conditions in the sample electrode during arcing are not yet understood sufficiently to justify any detailed physicochemical explanation of the effect. The reduction of ZrO_2 to ZrC by carbon and the conversion of ZrC to ZrN by nitrogen, at high temperature, are both established reactions [6]. The present conditions, however, favour the formation of ZrC rather than ZrN; their different *a* parameters enable them to be easily distinguished. Under very similar arc conditions, but with samples consisting of mixed zirconium and iron oxides, Strock [7] stated that the "ZrC is transformed to the still more stable silver-colored nitride", when referring to the refractory residue on the cathode. The nitride, however, is generally described as yellow [8], and in the absence of specific crystallographic evidence, the identification given earlier [7, 9] must now be open to question.

Molybdenum and zirconium both form interstitial carbides [10], and the mixed carbide (Zr, Mo)C is very likely to be a solid solution [11]. The melting point of ZrC is so high, around 3420°C, that little vaporization from the cathode could occur. The molybdenum retained on the cathode in the absence of zirconium (Table 3) is probably present as its carbide, but the μg-amounts

present were too small to allow its identification by x-ray powder diffraction. It is suggested that the most likely reason for the decreased molybdenum emission, when a relatively large amount of zirconium is present, is the simultaneous formation of molybdenum and zirconium carbides from their oxides, and the development of a coherent, crystalline solid solution of the trace amounts of molybdenum in the more abundant zirconium carbide. Similar processes could explain the decreased titanium and vanadium emissions, as these elements also form interstitial carbides.

A further implication of the results given in Table 1 is that application of the cathode-layer carbon arc to the semi-quantitative analysis of rocks and soils [12] will need to be re-assessed for molybdenum determinations. If ZrC is formed when such materials are arced, there would appear to be a considerable risk of low molybdenum results, for the zirconium:molybdenum ratio will often exceed 100:1.

The authors acknowledge the help given by A. H. Knight and H. Shepherd in supervising the experiments with ^{99}Mo and making the activity measurements; by B. L. Sharp and Jamshid Manzoori in providing i.c.p.e.s. facilities; and by M. J. Wilson in the identification of ZrC by x-ray diffraction.

REFERENCES

1 R. L. Mitchell and R. O. Scott, J. Soc. Chem. Ind., 66 (1947) 330.
2 R. L. Mitchell, The Spectrochemical Analysis of Soils, Plants and Related Materials, Tech. Commun. No. 44A, Commonwealth Agricultural Bureaux, Farnham Royal, Bucks., England, 1964.
3 R. O. Scott, R. L. Mitchell, D. Purves and R. C. Voss, Consultative Committee for Development of Spectrochemical Work, Bull. No. 2, The Macaulay Institute for Soil Research, Aberdeen, 1971.
4 N. J. Marshall, Econ. Geol., 59 (1964) 142.
5 R. G. W. Hollingshead, Oxine and its derivatives, Vol. 2, Butterworths, London, 1954, p. 557.
6 J. W. Mellor, A Comprehensive Treatise on Inorganic and Theoretical Chemistry, Vol. 7, Longman, Green and Co., London, 1947.
7 L. W. Strock, Am. Soc. Test. Mat., Bull., March, 1941, p. 37.
8 J. W. Mellor, A Comprehensive Treatise on Inorganic and Theoretical Chemistry, Vol. 8, Suppl. I, Nitrogen (Part 1), Longmans, London, 1964, p. 177.
9 L. W. Strock and S. Drexler, J. Opt. Soc. Am., 31 (1941) 167.
10 A. F. Wells, Structural Inorganic Chemistry, 4th edn., Oxford University Press, Oxford, England, 1975.
11 O. Kubaschewski (Ed.), Zirconium: Physico-chemical Properties of its Compounds and Alloys, Atomic Energy Review: Special Issue No. 6, International Atomic Energy Agency, Vienna, 1976.
12 R. L. Mitchell, J. Soc. Chem. Ind., 59 (1940) 210.

Analytica Chimica Acta, 154 (1983) 307—312
Elsevier Science Publishers B.V., Amsterdam — Printed in The Netherlands

Short Communication

EXTRACTION OF GOLD AND MERCURY FROM SEA WATER WITH BISMUTH DIETHYLDITHIOCARBAMATE PRIOR TO NEUTRON ACTIVATION—γ-SPECTROMETRY

J. C. YU, J. M. LO and C. M. WAI*
Department of Chemistry, University of Idaho, Moscow, ID 83843 (U.S.A.)
(Received 4th May 1983)

Summary. Gold and mercury in sea water can be selectively extracted by bismuth diethyldithiocarbamate into chloroform at pH ≤ 1. The matrix species and many other trace elements in the system are effectively removed during extraction. When neutron activation—γ-spectrometry is used, the detection limits for gold and mercury are 0.001 and 0.01 μg l^{-1}, respectively. The relative precision is 9% for gold and 13% for mercury.

Neutron activation is one of the most sensitive techniques for trace elements. However, its direct application for quantifying trace elements in a complex system such as sea water is generally difficult because of matrix interferences. Separation procedures are often used before or after neutron irradiation to eliminate such interferences. Diethyldithiocarbamate (DDTC) has been widely used for trace metal extraction. In sea water, common matrix species which do not complex with DDTC are eliminated during the extraction. This communication describes a bismuth diethyldithiocarbamate extraction method which is highly selective for preconcentration of gold and mercury from sea water prior to neutron activation. The $Bi(DDTC)_3$ was chosen because bismuth captures neutrons to form a pure β-emitter which does not interfere with the γ-spectrometry and because the extraction constant of bismuth is small compared with that of gold and mercury, but is greater than most of the common trace metals found in the environment [1—4]. Therefore, under proper conditions, Au and Hg can be selectively extracted by $Bi(DDTC)_3$ into an organic phase. In principle, this method can be applied to any natural water system. Sea water is used as an example because of its complex matrix and low metal concentrations.

Experimental

Reagents. The reagent, $Bi(DDTC)_3$, was prepared by reacting an excess of bismuth(III) with NaDDTC as described earlier [5]. The extracting solution contained 100 μg ml^{-1} $Bi(DDTC)_3$ in chloroform. Chloroform and nitric acid were Baker Analyzed reagent and Baker Ultrex grade, respectively. The mercury stock solution was prepared by dissolving mercury(II) oxide

0003-2670/83/$03.00

(Baker Analyzed) in 0.5 M HNO_3. The gold standard was prepared in accordance with the Environmental Protection Agency's (EPA) recommended procedure [6]. A purified Bi^{3+} stock solution was prepared by extracting a bismuth nitrate solution with $Bi(DDTC)_3$ in chloroform to remove traces of Au and Hg.

Samples. Surface sea-water samples were collected from two different locations in the Seattle area. The first sampling site was on the southwest corner of Discovery Park in western Seattle and the second site was behind the Pike Place Market near downtown Seattle. The salinities of the samples were 27‰ and 18‰, respectively. The samples were filtered through 0.45-μm membrane filters, acidified to pH <1 immediately after collection, and stored in precleaned polyethylene bottles. All containers used in this study were washed with nitric acid, rinsed with deionized water, and stored in a class-100 clean hood equipped with a vertical laminar flow HEPA filter.

Extraction procedures. Concentrated nitric acid was added to reduce the pH of the sea-water sample to about 0.5. The sample was then shaken with chloroform to remove bromine. For each sample, 15 ml of the pretreated sea water was placed in a 20-ml Beckman polyvial with a fast turn cap. In some experiments, the water samples were spiked with 100 $\mu g\ ml^{-1}$ bismuth(III) to suppress the extraction of copper. To each water sample, 1.5 ml of the $Bi(DDTC)_3$ extraction solution was added. The mixture was shaken vigorously for 5 min and the phases were allowed to separate. Most of the aqueous phase was drained from the vial and discarded. The chloroform phase was washed with deionized water several times to remove sodium ions. After washing, 1 ml of the chloroform solution was pipetted into a 2/5-dram polyethylene vial. The solution was evaporated to dryness at room temperature before heat-sealing of the vial for neutron irradiation. This procedure gives a preconcentration factor of 10 for Au and Hg. Standards consisted of 1 ml of solutions containing suitable concentrations of Au and Hg sealed in 2/5-dram polyethylene vials.

Sample irradiation and counting. All samples and standards were irradiated for 3 h in a 1 MW TRIGA nuclear reactor at a steady flux of 6×10^{12} n $cm^{-2}\ s^{-1}$. After irradiation, the samples were cooled for 10—20 h before counting. A simple transfer procedure was used to avoid ^{24}Na and other radioactivities produced in the plastic material of the irradiated vials. To each vial approximately 1 ml of a 1 M HNO_3 solution was injected by means of a 5-ml disposable syringe. After shaking for about 1 min, the acid solution was transferred with the same syringe into a new 2/5 dram vial for γ-counting. Less than 1% of Au and Hg activities were found to remain in the irradiated vial after this sample transfer. Standards were also transferred to new vials with disposable syringes.

Each sample was counted for 2000 s in a large-volume ORTEC Ge(Li) detector with a resolution (FWHM) of about 2.3 keV at the 1332-keV ^{60}Co peak. The peaks used were the 77.6-keV peak for mercury and the 411.8 keV peak for gold. The detector output was fed to a Nuclear Data

4096-channel pulse-height analyzer. Peak heights were converted to elemental concentrations by using the SPAN program in an IBM 370 computer.

Results and discussion

The extraction constants ($(1/n)\log K$) of Au and Hg are 27.2 and 20.3, respectively, i.e., very much larger than that of bismuth [3,7]. Therefore, Au and Hg can be easily extracted by $Bi(DDTC)_3$. In addition to Au and Hg, palladium and platinum also have high extraction constants and may be extracted by $Bi(DDTC)_3$ [8, 9]. However, both the latter are much less sensitive than Au and Hg in neutron activation, and they should not interfere in this procedure. Most of the common trace metals in the environment such as Cd, Ni, Pb, Zn, etc., are not significantly extracted by $Bi(DDTC)_3$ because of their relatively small extraction constants [1—4]. Copper can be partially extracted because its extraction constant is only slightly lower than that of bismuth. Based on the K values given earlier [3], the distribution ratio of copper between the organic phase (o) and the aqueous phase (w) can be expressed by the following equation

$$[Cu(DDTC)_2]_o/[Cu^{2+}]_w = 0.159\,([Bi(DDTC)_3]_o/[Bi^{3+}]_w)^{2/3}$$

Under the present experimental conditions, i.e. 100 μg ml^{-1} (1.53×10^{-4} M) $Bi(DDTC)_3$ and 1×10^{-10} M bismuth(III) (average Bi in sea water), 99.95% of copper could be extracted into the organic phase. The presence of a large ^{64}Cu peak could interfere indirectly with the ^{197}Hg count by producing a high background radiation. The extraction of copper can be suppressed to about 7% by adding 100 μg ml^{-1} Bi^{3+} (4.79×10^{-4} M) to the aqueous phase. Experiments done under this specific condition showed that about 10% of Cu^{2+} was extracted from a synthetic sea-water sample with 2 μg ml^{-1} copper. When Au and Hg are quantified in water samples with high concentrations of copper, this Bi^{3+} addition technique is obviously useful.

Extraction of Au and Hg from sea water with $Bi(DDTC)_3$ in chloroform is very rapid. Normally, 2—3 min of vigorous shaking is sufficient to reach equilibrium. To ensure quantitative extraction, 5 min of shaking was applied in each experiment. The effects of pH on the extraction of Au and Hg with $Bi(DDTC)_3$ are shown in Fig. 1. In the pH range 0.3—1.0, nearly total extraction of Au and Hg was observed. Extraction at pH <0.3 is not practical because of the accelerated decomposition of metal—DDTC complexes in acid. At pH >1, the extraction efficiency decreased; at pH 2, only about 50% of the Au and Hg were recovered. In most experiments, extractions were done at a pH near 0.5.

The percentage recoveries of Au and Hg were evaluated with the sea water collected from Discovery Park. The sea water was spiked with 0.1 μg l^{-1} gold and 1.0 μg l^{-1} mercury and taken through the procedure given. The levels of Au and Hg in the natural sea water were also quantified by the same procedure. After subtraction of the natural levels from the spiked samples, the recoveries were calculated to be 99 ± 3% for gold and 95 ± 5% for

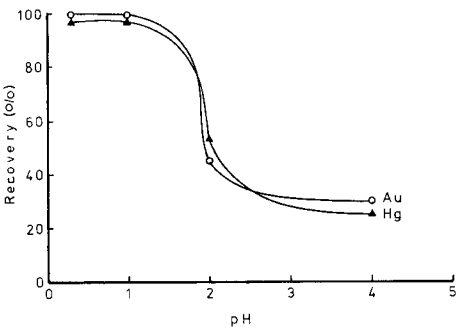

Fig. 1. Dependence on pH of the extraction of Au and Hg by $Bi(DDTC)_3$ into chloroform.

mercury based on five replicate measurements. The relative standard deviation of the method was 9% for Au and 13% for Hg based on ten separate samples. The accuracy could not be thoroughly evaluated because no standard samples were available. However, the errors were always less than 10% for the spiked samples. The calibration ranges were 0.01—10 $\mu g\ l^{-1}$ for Au and 0.05—50 $\mu g\ l^{-1}$ for Hg. Linear calibration graphs were obtained with $r^2 = 0.99$ and 0.97, respectively, based on least-squares fits of five different concentrations.

Figure 2 shows a typical γ-spectrum of a sea-water sample collected from Discovery Park. The sample was spiked with 100 $\mu g\ ml^{-1}$ Bi^{3+} and then extracted with the $Bi(DDTC)_3$ in chloroform as described above. The possible interference of the 78-keV Hg x-ray from ^{198}Au on the 77.6-keV ^{197}Hg peak is insignificant when the Hg/Au ratio in a sample exceeds 1.5,

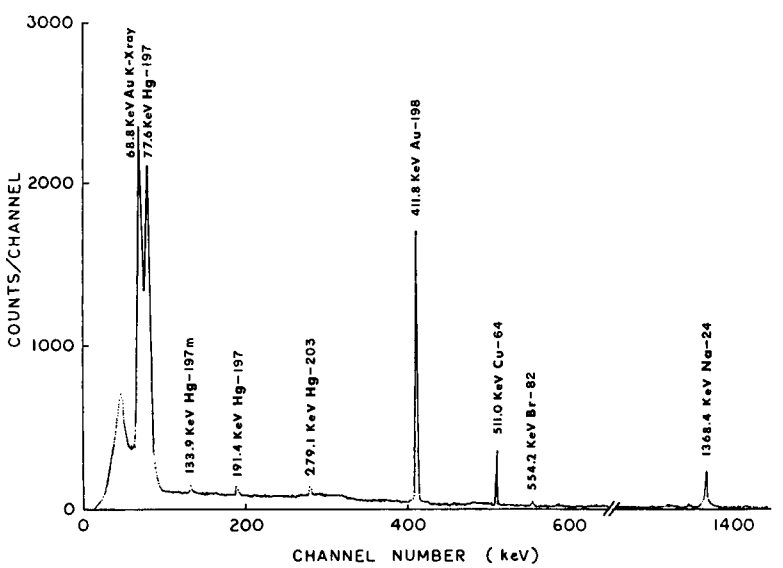

Fig. 2. Gamma spectrum of a preconcentrated sea-water sample collected from western Seattle.

which is the case for the sea-water samples studied [10]. It is clear from the spectrum that sodium and bromide in the sea water were essentially all removed by this extraction and the small ^{64}Cu annihilation peak had no significant effect on the background radiation. The detection limits for gold and mercury by the proposed method were estimated from a synthetic sea-water blank to be 0.001 $\mu g\ l^{-1}$ gold and 0.01 $\mu g\ l^{-1}$ mercury based on two standard deviations from the background. Because the γ-peak height depends on the preconcentration factor, the irradiation time, and the counting time, it is possible further to improve the detection limits by increasing these factors.

Lo et al. [10] reported an extraction procedure with $Pb(DDTC)_2$ for trace metal determination by neutron activation [10]. The extraction constant of $Pb(DDTC)_2$ is much smaller than that of $Bi(DDTC)_3$. As a result, metals like Cd, Cu, and Ni can also be extracted with Au and Hg by $Pb(DDTC)_2$. Furthermore, the extraction with $Pb(DDTC)_2$ is best done at pH 2—3. At this pH range, losses of Au and Hg to container walls during extraction are a potential problem for accurate determination of low levels of these metals [11, 12]. The proposed $Bi(DDTC)_3$ extraction is done at a pH of about 0.5 where losses of Au and Hg to container walls should be a minimum. Extraction at a low pH also has the advantage of suppressing naturally occurring complexation capacity which may interfere with the trace metal extraction in certain systems. For the determination of low levels of Au and Hg, this method has several advantages over the $Pb(DDTC)_2$ extraction method reported earlier.

The concentrations of Au and Hg in the sea-water samples determined by this extraction method were as follows: Discovery Park, Au 0.021 ± 0.002 and Hg 0.13 ± 0.02 $\mu g\ l^{-1}$; Pike Place market, Au 0.017 ± 0.002 and Hg 0.88 ± 0.10 $\mu g\ l^{-1}$. The mercury level in water collected from Pike Place market is much higher than the average value reported for open ocean water [13]. This may be the result of contamination by local discharge sources around the market. The gold contents in both samples are in good agreement with the average value for sea water [13].

Neutron irradiations were done at the Washington State University Nuclear Radiation Center under the Reactor Sharing Program supported by DOE.

REFERENCES

1 J. Stary and K. Kratzer, Anal. Chim. Acta, 40 (1968) 93.
2 A. Wyttenbach and S. Bajo, Anal. Chem., 47 (1975) 2.
3 S. J. Yeh, J. M. Lo and L. H. Shen, Anal. Chem., 52 (1980) 528.
4 L. H. Shen, S. J. Yeh and J. M. Lo, Anal. Chem., 52 (1980) 1882.
5 A. Wyttenbach and S. Bajo, Anal. Chem., 47 (1975) 1813.
6 U.S. Environmental Protection Agency, Methods for Chemical Analysis of Water and Wastes, Cincinnati, OH, 1979.
7 H. Chermette, J. F. Colonat and J. Tousset, Anal. Chim. Acta, 88 (1977) 331.
8 J. T. Pyle and W. D. Jacobs, Anal. Chem., 36 (1964) 1796.

9 G. B. Briscoe and S. Humphries, Talanta, 16 (1969) 1403.
10 J. M. Lo, J. C. Wei and S. J. Yeh, Anal. Chem., 49 (1977) 1146.
11 R. M. Rosain and C. M. Wai, Anal. Chim. Acta, 65 (1973) 279.
12 H. V. Weiss and M. G. Lai, Anal. Chim. Acta, 28 (1963) 242.
13 J. P. Riley and G. Skirrow, Chemical Oceanography, Vol. 3, 2nd edn., Academic Press, London, 1975, p. 376.

Analytica Chimica Acta, 154 (1983) 313—317
Elsevier Science Publishers B.V., Amsterdam — Printed in The Netherlands

Short Communication

QUANTITATIVE NMR SPECTROMETRY OF PHASE-TRANSFER CATALYSTS
Part 2. Formate Selective Extraction Constants

RAPHAEL BAR, LILIANA KARPUJ-BAR and YOEL SASSON*
Casali Institute of Applied Chemistry, The Hebrew University, Jerusalem (Israel)
JOCHANAN BLUM*
Department of Organic Chemistry, The Hebrew University, Jerusalem (Israel)

(Received 3rd June 1983)

Summary. Selective extraction constants ($K_{ex(s)}$) of aqueous sodium formate in the presence of organic solvents and tetraalkylammonium salts were obtained by 300-MHz n.m.r. measurements; data are given for two-phase liquid systems containing chloroform and tetra-butyl-, -hexyl-, -heptyl-, -octyl-, and -dodecylammonium bromides. The values decrease with an increase in the alkyl chain length. The dependence of $K_{ex(s)}$ on formate concentration was studied in a water—dichloromethane system. Bromide, chloride and sulfate ions were found to have greater affinities than formate for the extracting quaternary ammonium cations.

The application of ^{1}H-n.m.r. spectrometry for determination of distribution ratios and apparent extraction constants of quaternary onium salts in two-phase liquid systems has been described [1]. These data are usually insufficient for kinetic studies of phase-transfer processes because the reactions depend on the relative extractability of both anions present in the aqueous layer [2]. However, if one of these anions contains hydrogen atoms (e.g., carboxylates), then it should be possible to deduce the selective extraction constants, $K_{ex(s)}$, from a single n.m.r. measurement. This technique was therefore studied in the hope of overcoming the difficulties which are associated with the current ion-selective electrode method, i.e., high dilution, the need for special water-insoluble tetraalkylammonium salts and low precision [3].

This communication is concerned with the use of ^{1}H-n.m.r. for the evaluation of selective extraction constants of formate in dichloromethane and chloroform in the presence of competing anions, some of which interfere with the standard titrations of formate [4]. Previous $K_{ex(s)}$ measurements of formate were limited to two particular cases in which the solvent was 1-decanol and the accompanying anion chloride [5] or iodide [6].

0003-2670/83/$03.00

Experimental

Tetrabutylammonium formate. To a vigorously stirred mixture of 10 ml of water and 200 ml of dichloromethane were added 10 g (29.5 mmol) of commercial tetrabutylammonium hydrogensulfate, 1.1 g (27.5 mmol) of sodium hydroxide and 4.0 g (17.7 mmol) of barium formate. When the heavy precipitate of barium sulfate started to separate, 6.0 g (88 mmol) of sodium formate was added (to provide effective salting-out) and the stirring was continued for 30 min. After phase separation, the organic solvent was evaporated and the oily residue dried for 48 h over phosphorus pentoxide at 0.5 torr. The tetrabutylammonium formate (yield 96%) was proved to be pure by the 300 MHz ^{1}H-n.m.r. spectrum: ($CDCl_3$) δ 1.006 (12, t, J = 6.9 Hz), 1.443 (8, m), 1.661 (8, m), 3.306 (8, br t, J = 8.7 Hz), 8.768 (1, s) [7].

Tetrabutylammonium sulfate. This salt was prepared in situ from equimolar quantities of tetrabutylammonium hydrogensulfate and sodium hydroxide. The sodium sulfate, so formed, was taken into account in computation of the apparent extraction constants.

Extraction procedure. A solution that was 0.05 M in the tetraalkylammonium salt and 0.025 M in durene (internal standard) in either water-saturated dichloromethane or chloroform was prepared. A volume of 5 ml of this solution was added to 5 ml of aqueous sodium formate (saturated with the organic solvent) and stirred vigorously for 1 h at constant temperature (±0.5°C). Longer periods of stirring had no effect on the ion distribution.

Results and discussion

Extraction of carboxylate salts from aqueous solutions is often accompanied by phase transfer of their corresponding conjugate acids [8] which are formed either by hydrolysis or by protonation. An example of a system in which this phenomenon occurs is illustrated in Table 1. The total formyl content of the organic phase after equilibration is shown to be considerably higher than expected from stoichiometric extraction of the formate by the ammonium salt. Because the formic acid in this case resulted mainly by hydrogensulfate protonation of the sodium formate, $HSO_4^- + HCOO^- \rightarrow HCOOH + SO_4^{2-}$, it was essential to take care that all extraction experiments were done under practically neutral conditions.

TABLE 1

Extraction of aqueous formate into 1,2-dichlorobenzene by tetrahexylammonium hydrogensulfate at 25°C[a]

Initial NaOCHO conc. in water (M)	0	1	2.5	4	5
Extracted $(C_6H_{13})_4N^+$ (%)	78.2	80.1	83.9	87.7	92.7
$[HCOO^-]/[(C_6H_{13})_4N^+]$ ratio in organic phase		1.70	1.62	1.53	1.29

[a]Initial concentration of the ammonium salt 0.05 M.

Although the chemical shifts of the formyl protons of pure tetrabutylammonium formate and formic acid differ by 0.55 ppm (see Table 2), the n.m.r. spectrum of solutions containing both species show only one formyl signal. This can be interpreted in terms of rapid proton exchange. Thus, in phase-transfer systems in which formic acid and formate are co-extracted, the magnitude of the chemical shift of the signal between 8.0 and 8.6 ppm is a qualitative measure for the relative amount of each species.

The formate selective extraction constant derived from the following equilibrium

$$(Fm^-)_w + (Q^+X^-)_o \rightleftharpoons (Q^+Fm^-)_o + (X^-)_w \quad (1)$$

where Fm^- is the formate anion and Q^+X^- the ion-pair of the extracting quaternary ammonium salt, is given by

$$K_{ex(s)} = [Q^+Fm^-]_o[X^-]_w/[Q^+X^-]_o[Fm^-]_w \quad (2)$$

If the ammonium salts are partitioned between the two liquid phases, $K_{ex(s)}$ can be expressed also by the ratio of the apparent extraction constants [8]:

$$K_{ex(s)} = K'_{ex}(Q^+Fm^-)/K'_{ex}(Q^+X^-)$$

where $K'_{ex}(Q^+Fm^-) = [Q^+Fm^-]_o/[Q^+]_w[Fm^-]_w$ and $K'_{ex}(Q^+X^-) = [Q^+X^-]_o/[Q^+]_w[X^-]_w$.

As the total ammonium ion concentration in the organic phase ($[Q^+Fm^-]_o + [Q^+X^-]_o$) and the organic formate $[Q^+Fm^-]_o$ (which equals $[X^-]_w$ in the present systems) can be derived from the ^{1}H-n.m.r. spectrum, and because $[Fm^-]_w$ is practically identical with the initial formate concentration in the aqueous phase, $K_{ex(s)}$ can be calculated.

The experimental data for formate in the presence of some symmetric tetraalkylammonium bromides are summarized in Table 3. As expected, the affinity of the quaternary cation for bromide is much higher than for formate. The decrease in $K_{ex(s)}$ with the increase in length of the alkyl chain seems to reflect the tendency for accommodation of the lipophilic cation with the lipophilic bromide rather than with the hydrophilic formate ion.

TABLE 2

^{1}H-n.m.r. data for mixtures of formic acid and tetrabutylammonium formate in dichloromethane at 20°C

X[$(C_4H_9)_4NOCHO$][a]	δ_{HCOO^-} (ppm)	δ_{OH} (ppm)
0	8.060	10.674
0.2	8.391	9.269
0.5	8.463	7.372
1	8.614	—

[a]Molar fraction with respect to formyl compound at a total constant concentration of 0.625 M.

TABLE 3

Formate $K_{ex(s)}$ data for a water—chloroform system containing tetraalkylammonium bromides, R_4NBr[a]

R	n-C_4H_9	n-C_6H_{13}	n-C_7H_{15}	n-C_8H_{17}	n-$C_{12}H_{25}$
$K_{ex(s)}$	1.27×10^{-3}	0.58×10^{-3}	0.34×10^{-3}	0.22×10^{-3}	0.28×10^{-3}

[a]Initial bromide and formate concentration 0.05 and 7 M, respectively; system temperature 20°C.

The dependence of $K_{ex(s)}$ on formate concentration in the presence of three different ammonium salts is shown in Table 4. In a system containing tetrabutylammonium chloride in water-dichloromethane $K_{ex(s)}$ is higher for an aqueous 1 M than a 2.5 M formate solution. This decrease in the selectivity constant can be explained by the great difference in the variation of $K'_{ex}(Q^+Fm^-)$ and $K'_{ex}(Q^+Cl^-)$ which together characterize the two-phase system better than $K_{ex(s)}$ alone. While the value of $K'_{ex}((C_4H_9)_4N^+Fm^-)$ hardly changes, $K'_{ex}((C_4H_9)_4N^+Cl^-)$ increases from 1.29 to 7.28 M^{-1} (i.e., tetrabutylammonium chloride is "salted-out" to a greater extent than the quaternary ammonium formate). However, when the extractant is tetrahexylammonium chloride, the higher lipophilicity of the cation forces the ion-pair to be mainly in the organic phase; the salting-out becomes less dependent on formate concentration and consequently $K_{ex(s)}$ changes moderately.

As for tetrabutylammonium chloride, the presence of the corresponding sulfate also leads to an inverse correlation between the $K_{ex(s)}$ values and formate concentration. In this system the formate selective extraction constant is given by

TABLE 4

Extraction constants and formate selective extraction constants for a dichloromethane—aqueous sodium formate system in the presence of various quaternary ammonium salts at 20°C

Ammonium salt[a]	Formate conc. (M)	$K'_{ex}(Q^+Fm^-)$ (M^{-1})	$K'_{ex}(Q^+X^-)$ (M^{-1})	$K_{ex(s)}$ ($\times 10^{-3}$)
$[(C_4H_9)_4N]Cl$	1	2.12×10^{-2}	1.29	16.4
$[(C_4H_9)_4N]Cl$	2.5	3.11×10^{-2}	7.28	4.27
$[(C_4H_9)_4N]Cl$	4	0.368	61.4	0.599
$[(C_6H_{13})_4N]Cl$	1	2.24	114	19.6
$[(C_6H_{13})_4N]Cl$	2.5	1.30	58.8	22.1
$[(C_6H_{13})_4N]Cl$	4	1.11	45.1	24.6
$[(C_4H_9)_4N]_2SO_4$	1	—[b]	—	—[b]
$[(C_4H_9)_4N]_2SO_4$	2.5	0.158	5.98	4.18
$[(C_4H_9)_4N]_2SO_4$	4	0.874	6430	0.119

[a]Initial concentration 0.05 M. [b]No formate was detected in the organic layer.

$$K_{ex(s)} = [Q^+Fm^-]_o^2[SO_4^{2-}]_w/[Q_2^{2+}SO_4^{2-}]_o[Fm^-]_w^2 = [K'_{ex}(Q^+Fm^-)]^2/K'_{ex}(Q_2^{2+}SO_4^{2-})$$

Table 4 indicates that in spite of the double negative charge on the sulfate ion, it is extracted to a greater extent than the formate (cf. [8]). Unfortunately, as no direct measurements of formate—sulfate selective extraction constants in two liquid-phase systems have yet been reported it remains uncertain if the effect is common to other quaternary ammonium sulfates. However, tetrabutylammonium sulfate was found to behave abnormally also in the presence of chloride [8]: while the extractability of tetrahexylammonium sulfate was larger than that of the corresponding chloride, the tetrabutylammonium salts showed the opposite effect.

We are grateful to the U.S.—Israel Binational Science Foundation (BSF) for financial support of this study.

REFERENCES

1 R. Bar, L. Karpuj-Bar, Y. Sasson and J. Blum, Anal. Chim. Acta, 154 (1983) 203.
2 F. Montanari, D. Landini and F. Rolla, Topics in Current Chemistry, 101 (1982) 147.
3 J. E. Gordon and R. E. Kutina, J. Am. Chem. Soc., 99 (1977) 3903.
4 F. P. Treadwell and W. T. Hall, Analytical Chemistry, Vol. II, 9th edn., Wiley, New York, 1942, p. 561.
5 C. J. Coetzee and H. Freiser, Anal. Chem., 41 (1969) 1129.
6 H. J. James, G. P. Carmack and H. Freiser, Anal. Chem., 44 (1972) 853.
7 R. Bar, Y. Sasson and J. Blum, Reactive Polymers, (1983) in press.
8 A. Brändström, Adv. Phys. Org. Chem., 15 (1977) 267.

Analytica Chimica Acta, 154 (1983) 319—322
Elsevier Science Publishers B.V., Amsterdam — Printed in The Netherlands

Short Communication

DETERMINATION OF BROMIDE IN SUSPENDED PARTICULATE MATTER BY HIGH-PERFORMANCE LIQUID CHROMATOGRAPHY WITH U.V. DETECTION

TOSHIKAZU KAMIURA*, YOSHIAKI MORI and MASANOBU TANAKA

Department of Environmental Medicine, Osaka City Institute of Public Health and Environmental Sciences, 8-34, Tojo-cho, Tennoji-ku, Osaka 543 (Japan)

(Received 10th February 1983)

Summary. High-performance liquid chromatography on a Zipax SAX column with u.v. detection at 200 nm gives precise results for bromide. Chloride, bromate, nitrite, nitrate, iodide, thiocyanate and various cations do not interfere; prior treatment with activated charcoal removes interfering organic compounds. Calibration graphs are linear over the range 0—50 mg l^{-1} bromide in aqueous extracts of the particulates; the limit of detection is 10 ng of bromide. The relative standard deviations at the 0.5 and 1.0 mg l^{-1} levels are 2.3 and 1.0%, respectively.

Bromide has been used as a secondary marker element to estimate the contribution of motor vehicles to the total suspended particulate matter [1—4]. The bromide has usually been measured by instrumental neutron activation analysis, proton-induced x-ray emission or x-ray fluorescence spectrometry. None of these techniques is very convenient for routine determinations of trace bromide in particulate matter containing many different compounds.

Ion chromatography with a conductivity detector has been recently used for the determination of trace anions including bromide [5—10]. High-performance liquid chromatography (h.p.l.c.) with u.v. detection is also suitable for various inorganic anions [10—14]. These methods do not seem to have been applied to determine bromide in particulate matter, possibly because of the interference of some compounds, particularly nitrate or organic compounds, present at relatively high concentrations.

This communication reports the application of the u.v. method to the determination of bromide in suspended particulate by h.p.l.c.

Experimental

Apparatus and reagents. Aqueous extracts of the particulate matter were examined with a Shimadzu-Dupont LC-3 chromatograph (500 × 2.1-mm Zipax SAX column with a 50 × 4.0-mm Zipax SAX guard column) with a u.v. detector, which was used at 200 nm. The mobile phase was water containing 300 mg l^{-1} magnesium as sulfate at a flow rate of 1.5 ml min^{-1}. The column was used at room temperature.

0003-2670/83/$03.00

Activated charcoal for column chromatography was used to remove the organic compounds from the extracts of the particulates. A column (20 mm high, 9.8-mm diameter) was prepared by introducing a suspension of the activated charcoal in methanol into a glass tube and washing with 75 ml of water.

All chemicals were of analytical grade. A stock solution of bromide (1000 mg l^{-1}) was prepared from potassium bromide; working standards were prepared by suitable dilution immediately before use.

Procedures. The suspended particulate matter (collected on a quartz fiber filter during a 24-h period with a high-volume air sampler) was extracted with 100 ml of hot water. After cooling, the extract was filtered through Toyo filter paper No. 5c. An aliquot (10 ml) of the filtered sample solution was introduced into the activated charcoal column, which was washed with 40 ml of deionized-distilled water. The effluent was evaporated to a few ml at 55°C. A 100-μl aliquot was injected into the h.p.l.c. column by microsyringe. Peak heights were related to those of known amounts of bromide. Standard additions were normally used.

Results and discussion

Although mixtures of nitrite and nitrate were completely separated on elution with a solution containing some copper sulfate, separation of bromide and nitrate was only partial [12]. When the mobile phase was changed to a solution containing magnesium sulfate, bromide and nitrate were completely separated, as were bromate and nitrite (Fig. 1).

Effect of other elements and organic compounds. Many ions give significant u.v. absorption in the same region as that of bromide [12, 15, 16], hence separation of bromide from complex matrices is essential. Chloride, sulfate, and iodide do not absorb around 200 nm, and thiocyanate is not eluted within a reasonable time under the conditions used. Elution data were obtained for some cations having relatively significant absorptions near 200 nm; the retention times were 54 s for Ni^{2+}, Co^{2+} and Mn^{2+}, 60 s for Cr^{3+}, Zn^{2+} and Pb^{2+}, 66 s for Cu^{2+}, and 102 s for Fe^{3+}. Thus none of these interferes with the u.v. determination of bromide, which is eluted at ca. 3.5 min.

The elution of three typical organic compounds was examined. The retention times for ethyl acetate, chloroform and cresol were 1.2, 1.9 and 5.6 min, respectively. Thus organic substances are likely to show some interference in the u.v. detection of bromide by the h.p.l.c. method, but their concentrations should be low in air particulate matter and they can be removed easily by prior treatment with activated charcoal.

Calibration graph for bromide. A linear relationship was obtained for 0—50 mg l^{-1} bromide. The limit of detection was 10 ng of bromide (signal/noise = 2). Relative standard deviations (n = 10) of 2.3 and 1.0% were obtained for 0.5 and 1.0 mg l^{-1} bromide, respectively.

Application to the determination of bromide in suspended particulate matter. Bromide alone was significantly adsorbed on activated charcoal,

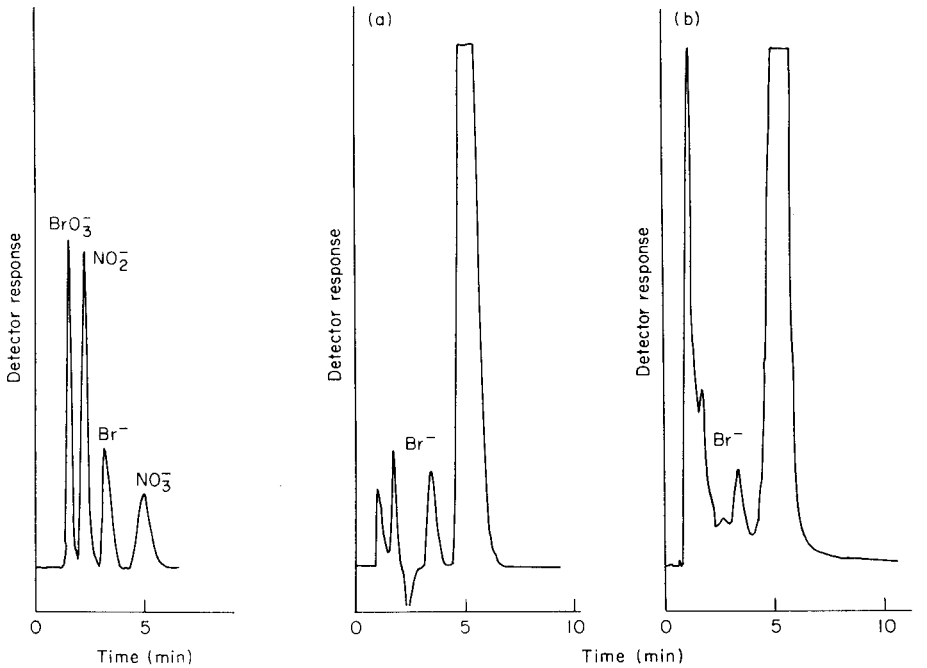

Fig. 1. Chromatogram of a mixture of bromate (2900 ng), nitrite (200 ng), bromide (250 ng) and nitrate (110 ng).

Fig. 2. Determination of bromide in an aqueous extract of particulates with (a) and without (b) passage through activated charcoal.

but recoveries were good when nitrate, sulfate or chloride in relatively large amounts was also present and the column was washed with water (Table 1).

The method proposed was applied to the measurement of bromide in aqueous extracts of suspended particulate matter. Figure 2(b) shows a

TABLE 1

Effect of some anions on the recovery of bromide (10 μg)

Ratio of anion to bromide	Recovery [a] (%) from solutions of		
	nitrate	sulfate	chloride
—	36	36	36
10	69	70	58
50	83	79	71
100	97	85	83
500	100	87	91

[a] Average of three determinations.

TABLE 2

Bromide in water extracts of suspended particulate matter collected in Osaka City during 1982–1983 for 48-h periods

Time	Dec. 8	Dec. 10	Jan. 7	Jan. 9	Feb. 1
Br^- found (mg l^{-1})	0.60	1.16	0.23	0.71	0.81

chromatogram without treatment by activated charcoal; as the concentration of bromide is low compared to that of other contaminants, the bromide peak appears on the shoulder of other peaks from cations and organic compounds. These peaks are reduced by the activated charcoal treatment (Fig. 2a) so that the bromide peak is cleanly separated.

In a typical example, four standard additions of bromide to aliquots of an aqueous extract gave a linear plot, extrapolation of which indicated a bromide concentration of 0.60 mg l^{-1} in the original extract. The results of the determination of bromide in suspended particulates are shown in Table 2.

In conclusion, the proposed method gives precise and apparently accurate results for the determination of bromide in suspended particulate matter, with freedom from many interferences. The method may also be applicable to wastewaters and foodstuffs, which contain many compounds.

The authors are grateful to Mr M. Oka and Dr. T. Hotta who have given assistance in various ways.

REFERENCES

1 E. S. Gladney, W. H. Zoller and G. E. Gordon, Environ. Sci. Technol., 8 (1974) 551.
2 J. J. Paciga, T. M. Roberts and R. E. Jervis, Environ. Sci. Technol., 9 (1975) 1141.
3 G. S. Kowalczyk, C. E. Chroquette and G. E. Gordon., Atmos. Environ., 12 (1977) 1143.
4 R. K. Stevens, T. G. Dzubay, R. W. Shaw, Jr., W. A. McClenny, C. W. Lewis and W. E. Wilson., Environ. Sci. Technol., 14 (1980) 1491.
5 D. T. Gjerde, J. S. Fritz and G. Schmuckler, J. Chromatogr., 186 (1979) 509.
6 D. T. Gjerde, G. Schmuckler and J. S. Fritz, J. Chromatogr., 187 (1980) 35.
7 I. Molnar, H. Knauer and D. Wilk, J. Chromatogr., 201 (1980) 225.
8 T. S. Stevens, J. C. Davis and H. Small, Anal. Chem., 53 (1981) 1488.
9 J. Crowther and J. McBride, Analyst, 106 (1981) 702.
10 M. J. van Os, J. Slanina, C. L. de Ligny, W. E. Hammers and J. Agterdenbos, Anal. Chim. Acta, 144 (1982) 73.
11 R. G. Gerritse, J. Chromatogr., 171 (1979) 527.
12 T. Kamiura and M. Tanaka, Anal. Chim. Acta, 110 (1979) 117.
13 U. Leuenberger, R. Gauch, K. Rieder and E. Baumgartner, J. Chromatogr., 202 (1980) 461.
14 J. P. de Kleijn, Analyst., 107 (1982) 223.
15 F. A. J. Armstrong, Anal. Chem., 35 (1963) 1214.
16 R. Bastian, R. Weberling and F. Palilla, Anal. Chem., 28 (1956) 459; 29 (1957) 1795.

Analytica Chimica Acta, 154 (1983) 323—327
Elsevier Science Publishers B.V., Amsterdam — Printed in The Netherlands

Short Communication

IN SITU ELECTRODE MODIFICATION FOR DIRECT DIFFERENTIAL PULSE POLAROGRAPHY OF 2,6-DIAMINOPURINE AND ITS METABOLITE, 2,6-DIAMINO-8-PURINOL

EDITH SZURLEY and ANNA BRAJTER-TOTH*[a]

Department of Chemistry, University of Maine at Orono, Orono, ME 04469 (U.S.A.)

(Received 13th December 1982)

Summary. Preferential adsorption of allopurinol (1H-pyrazolo-[3,4-d]-pyrimidin-4-ol) at graphite electrodes from pH 7.0 phosphate buffer solutions of 2,6-diaminopurine and 2,6-diamino-8-purinol allowed in situ electrode modification. Modified electrodes were applied to the simultaneous determination of 2,6-diaminopurine and 2,6-diamino-8-purinol in phosphate buffer at pH 7.0. Differential pulse polarography allowed both compounds to be quantified in the concentration range 1×10^{-6}—5×10^{-4} M. The relative standard deviation of the peak current is about 10%. Calibration curve characteristics are C (μM) = 0.0094 ± 0.0002 I (μA) + 0.22 ± 0.07 μA, with r = 0.9985 and C (μM) = 0.0065 ± 0.0001 I (μA) + 0.03 ± 0.04 μA with r = 0.9990 for 2,6-diamino-8-purinol and 2,6-diaminopurine, respectively.

2,6-Diaminopurine is one of a large class of compounds, analogs of natural purines, which show pharmacological properties as antimetabolites of nucleic acid metabolism. 2,6-Diaminopurine has been shown to act as a growth inhibitor of bacteria and mammalian cells [1]. It is a known substrate of xanthine oxidase, an enzyme involved in the metabolism of natural purines [2], and is metabolized in the presence of this enzyme to 2,6-diamino-8-purinol [3]. It was shown recently in this laboratory that 2,6-diamino-8-purinol is an intermediate in the electrochemical oxidation of 2,6-diaminopurine.

It is important to be able to determine biologically active compounds in the presence of their metabolites under physiological conditions using a method which does not require time-consuming separations. In the case of mixtures of 2,6-diaminopurine and 2,6-diamino-8-purinol, spectroscopic methods are not successful because of the great similarity between the ultraviolet (u.v.) spectra of the two compounds [4]. However, electrochemical methods are well suited to this determination. Both 2,6-diaminopurine and 2,6-diamino-8-purinol are electroactive, and the potentials at which the compounds can be oxidized at a pyrolytic graphite electrode at pH 7.0 in phosphate buffer are separated by 300 mV, allowing easy distinction between them. A serious limitation to the development of an electroanalytical method

[a]Present address: Department of Chemistry, University of Florida, Gainesville, FL 32611, U.S.A.

0003-2670/83/$03.00

is the adsorption of both compounds at graphite electrodes. This effect leads to curved calibration graphs and poor precision. This communication describes the determination of 2,6-diaminopurine in the presence of its metabolite, 2,6-diamino-8-purinol, in phosphate buffer at physiological pH.

Experimental

An IBM EC-225 Voltammetric Analyzer was used for all electrochemical experiments with a Houston 2000 X-Y recorder. Rough pyrolytic graphite of 2.25 mm^2 area (Pfizer) sealed in glass was used as the working electrode. Rough pyrolytic graphite was chosen because of the well defined oxidation peaks of purines at this surface [5]. Platinum foil served as a counter electrode and all potentials were recorded and reported against a saturated calomel electrode (SCE). The solutions were deaerated with nitrogen, which was also passed over solutions during measurements.

2,6-Diaminopurine and allopurinol (Sigma Chemical Co., St. Louis, MO) and 2,6-diamino-8-purinol (Aldrich) were used as obtained. All buffers were prepared from reagent-grade chemicals and the ionic strength of the buffer was maintained at 0.5 M.

Differential pulse polarographic parameters giving the best sensitivity and resolution were: 40 mV pulse amplitude, 5 mV s^{-1} sweep rate, timer 0.3 s. To ensure reproducible and clean electrode surfaces for each determination, rough pyrolytic graphite was resurfaced before each experiment by polishing on a silicon carbide polishing paper (Buehler) of 600 grit. After being polished, electrodes were rinsed with deionized water, and the remaining graphite particles were removed from the electrode surface by wiping with tissue.

Results and discussion

A cyclic voltammogram for a mixture of 2,6-diaminopurine and 2,6-diamino-8-purinol is shown in Fig. 1. The voltammogram is quite complex, but characteristic peaks of 2,6-diaminopurine and 2,6-diamino-8-purinol are well resolved even at very low concentration ratios of 2,6-diaminopurine to 2,6-diamino-8-purinol. Peak currents of the first 2,6-diamino-8-purinol (I_a) and the primary 2,6-diaminopurine peak (III_a) vary nonlinearly with concentration. These results and the linear dependence of peak (I_a) and (III_a) current on scan rate at low concentrations show that adsorption is a serious limitation to the development of an electrochemical method for the determination of both compounds alone and in mixtures.

Dryhurst and De [6] have shown that allopurinol (1H-pyrazolo-[3,4-d]-pyrimidin-4-ol) is strongly adsorbed on rough pyrolytic graphite electrodes at potentials from 0.0 to 1.0 V in buffers of varying pH and composition. In saturated solutions, allopurinol displaces uric acid from the electrode surface [6]. Preferential adsorption of allopurinol in the presence of other compounds adsorbing on graphite in the same potential range (0.0—1.0 V) could be of general analytical utility. Addition of allopurinol to solutions of less strongly adsorbed analytes should prevent or largely diminish their adsorption.

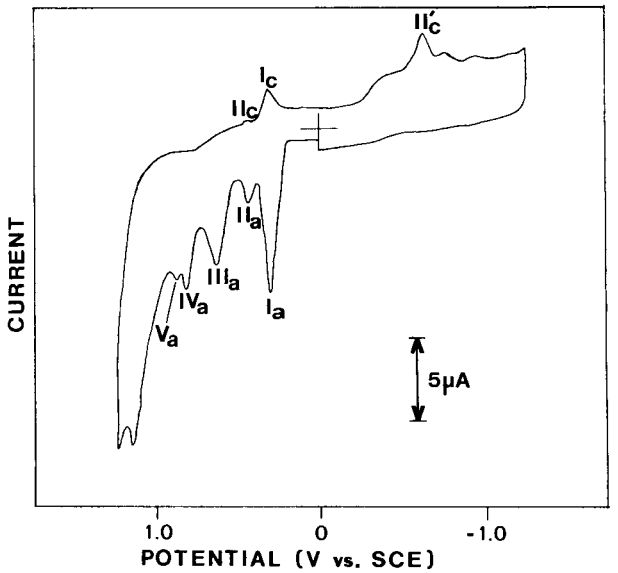

Fig. 1. Cyclic voltammogram of a solution 0.1 mM in 2,6-diaminopurine and 0.1 mM in 2,6-diamino-8-purinol in phosphate buffer pH 7.0, ionic strength 0.5 M. Scan rate 100 mV s^{-1}. Peaks I_a/I_c and II_a/II_c correspond respectively to the oxidation (a) and reduction (c) of 2,6-diamino-8-purinol. Peaks III_a—V_a are 2,6-diaminopurine oxidation peaks.

To ensure electrode modification by adsorption and to avoid variations in the concentration of allopurinol, solutions saturated with allopurinol should be used. At graphite electrodes in the pH range 1—14, allopurinol shows a single oxidation peak. This peak occurs at very positive potentials (1.0 V) close to the background oxidation and does not pose an interference problem.

The effect of addition of 2 mM allopurinol (saturated solutions) on the cyclic voltammograms of mixtures of 2,6-diaminopurine and 2,6-diamino-8-purinol in pH 7.0 phosphate buffer is a decrease in all peak currents. The peaks become broader and the reduction peaks I_c and II_c (Fig. 1) can no longer be detected. Plots of peak current vs. concentration for 2,6-diamino-8-purinol become linear over the concentration range for which nonlinear behavior was observed in the absence of allopurinol. Least-squares data are summarized in Table 1. Although the calibration plots are linear, the standard errors of estimate for the cyclic voltammetric data reflect substantial scatter about the best-fit line, because of the usual problem of establishing the baseline.

To improve performance characteristics, differential pulse polarography (d.p.p.) was used [7]. Data in Fig. 2 show that d.p.p. gives improved resolution relative to cyclic voltammetry for mixtures of 2,6-diaminopurine and 2,6-diamino-8-purinol in which the latter compound is present in a large excess.

TABLE 1

Least-squares statistics for mixtures of 2,6-diaminopurine and 2,6-diamino-8-purinol saturated with allopurinol[a]

Method	Peak	No. of points	Slope ± s (μA μM^{-1})	Intercept ± s (μA)	Std. error (μA)	Corr. coeff.
C.v.	I_a[b]	3	0.021 ± 0.002	0.4 ± 0.6	0.6	0.9954
	III_a[c]	3	0.022 ± 0.006	−1 ± 2	1.6	0.9658
D.p.p.	I_a[b]	6	0.0094 ± 0.0002	0.22 ± 0.07	0.1	0.9985
	III_a[c]	6	0.0065 ± 0.0001	0.03 ± 0.04	0.06	0.9990

[a]Working curves were obtained for different concentration ratios with a fixed total concentration. [b]First oxidation peak of 2,6-diamino-8-purinol (peak I_a, Fig. 3). [c]First oxidation peak of 2,6-diaminopurine (peak III_a, Fig. 3).

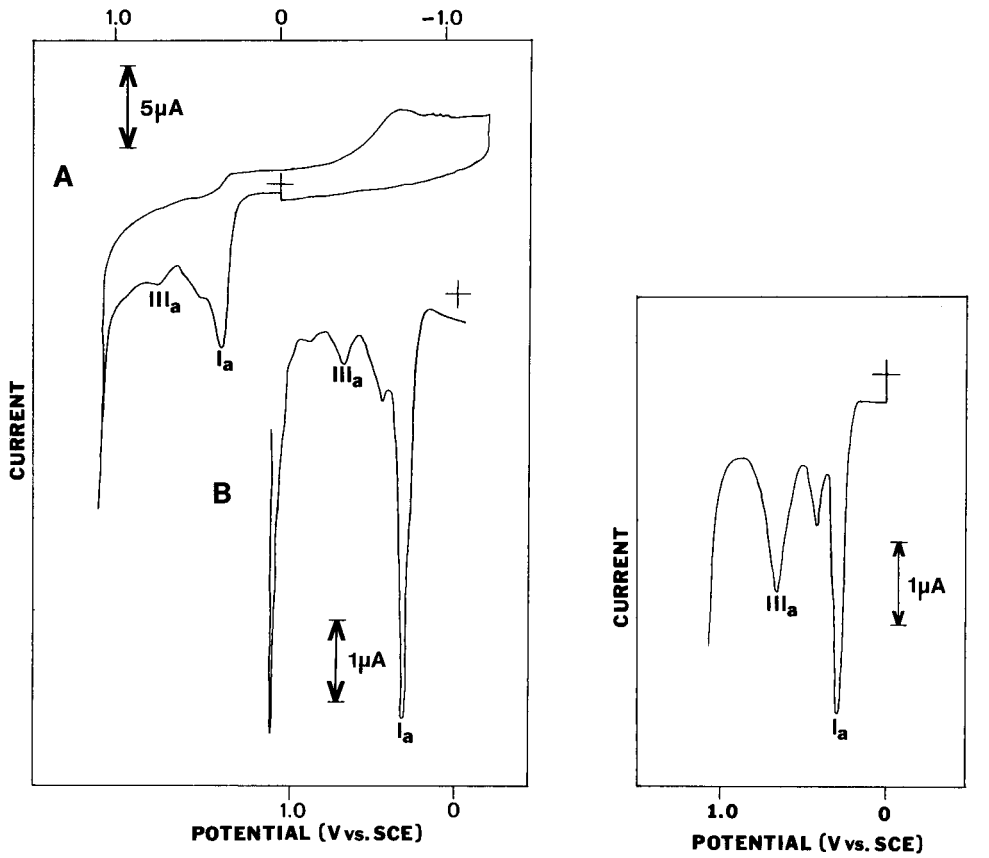

Fig. 2. Cyclic voltammetry (A) and differential pulse polarography (B) of 0.05 mM 2,6-diaminopurine and 0.45 mM 2,6-diamino-8-purinol with 2 mM allopurinol in solution. Phosphate buffer pH 7.0, ionic strength 0.5 M. (A) Scan rate 100 mV s^{-1}; (B) pulse amplitude 40 mV, scan rate 5 mV s^{-1}. Numbered peaks refer to the same processes as in Fig. 1.

Fig. 3. Differential pulse polarography of 0.25 mM, 2,6-diaminopurine, 0.25 mM 2,6-diamino-8-purinol mixture with 2 mM allopurinol. Phosphate buffer pH 7.0, ionic strength 0.5 M. Pulse amplitude 40 mV, scan rate 5 mV s^{-1}. Numbered peaks refer to the same processes as in Fig. 1. Peaks I_a and III_a were used to obtain the results given in Table 1.

Solutions of 2,6-diaminopurine and 2,6-diamino-8-purinol in phosphate buffer at pH 7.0 give d.p.p. peak currents that vary nonlinearly with concentration. However, as with cyclic voltammetry, selective adsorption of allopurinol should improve response by eliminating adsorption of the compound of interest and by producing a new surface which does not change in the potential range of interest. Figure 3 shows d.p.p. responses when 2 mM allopurinol (saturated solution) is added to mixtures of 2,6-diaminopurine and 2,6-diamino-8-purinol. Well separated d.p.p. peaks are observed at 40 mV pulse amplitude which gives the best sensitivity and peak resolution. Least-squares statistics for 2,6-diamino-8-purinol and 2,6-diaminopurine are shown in Table 1. It can be seen (curve parameters for peak III_a) that improved linearity is observed for 2,6-diaminopurine relative to that obtained with cyclic voltammetry. It is probable that better defined baselines in d.p.p. are responsible for the observed linearity. The linear working curves extend from 1×10^{-6} to 5×10^{-4} M total concentration in solutions of the two compounds.

This work was supported in part by the Faculty Research Fund at the University of Maine at Orono and by Research Corporation. Support by an NSF grant PRM 8203534 is also acknowledged.

REFERENCES

1 P. Langen, Antimetabolites of Nucleic Acid Metabolism, Gordon and Breach, New York, 1975.
2 Davidson, The Biochemistry of the Nucleic Acids, Academic Press, New York, 1976.
3 J. B. Wyngaarden, J. Biol. Chem., 224 (1957) 453.
4 S. F. Mason, J. Chem. Soc., (1954) 2071.
5 J. L. Owens, H. A. Marsh, Jr. and G. Dryhurst, J. Electroanal. Chem., 91 (1978) 231.
6 G. Dryhurst and P. K. De, Anal. Chim. Acta, 58 (1972) 183.
7 A. J. Bard and L. R. Faulkner, Electrochemical Methods, Fundamentals and Applications, Wiley, New York, 1980.

Analytica Chimica Acta, 154 (1983) 329—334
Elsevier Science Publishers B.V., Amsterdam — Printed in The Netherlands

Short Communication

INVESTIGATION OF THE MERCURY(II) COMPLEX WITH TRIETHYLENETETRAMINE BY MEANS OF GLASS AND MERCURY ELECTRODES

PAULA C. DUNNIGAN[a] and JAMES I. WATTERS*
Department of Chemistry, The Ohio State University, Columbus, OH 43210 (U.S.A.)
(Received 15th October 1982)

Summary. A comprehensive study by means of a mercury pool and a glass pH electrode was made of the equilibria involved in aqueous solutions containing varied concentrations of mercury(II) and triethylenetetramine, in the pH range 2.0—12.0 at 25°C with potassium nitrate used to adjust the ionic strength to unity. Only the 1:1 complex, Hg(II) trien^{2+}, having a stability constant of $10^{24.53 \pm 0.10}$ was found in the entire pH range using the entirely independent Bjerrum and Leden methods.

The present communication is the third of a series concerned with the stability of the complexes of triethylenetetramine [1, 2]. This study was undertaken in order to obtain precise and reliable values for the stability constant of the mercury(II) triethylenetetramine complex and to resolve inconsistencies in the literature. Previous investigations of the complexes formed between the mercury(II) ion and trien have been limited to two studies. Schwarzenbach [3] used pH measurements to study the system and reported evidence indicating the formation of both Hgtrien^{2+} and HgHtrien^{3+}. He used potassium chloride and potassium bromide to adjust the ionic strength; both these anions form mercury(II) complexes. After correcting for the stability of the mercury(II) halide complexes, he reported values of 25.2_6 and 26.3_5 for log $\beta^{Hg}_{Hgtrien}$ in the presence of 0.5 M KCl and 0.5 M KBr, respectively, at 20°C. He found it necessary also to postulate the formation of a singly protonated complex having values of 20.9 and 23.6, respectively, for log $\beta^{Hg}_{HgHtrien}$ in the presence of the two halides. The poor agreement of the values in the presence of these halides led him to conclude that a mixed complex containing the halide ion as well as the trien must actually have been formed.

Later, Reilley and Schmid [4] investigated the mercury(II)—trien system using a mercury electrode. They measured the potential of a solution containing 0.001 M mercury(II) and 0.002 M trien as a function of pH while

[a]Present address: B. F. Goodrich Chemical Group, 6100 Oak Tree Boulevard, Cleveland, OH 44131, U.S.A.

0003-2670/83/$03.00

keeping the ionic strength at 0.1 M (KNO_3) and the temperature at 25°C. They obtained a value of 25.0 for log β_{1100}, by calculating the concentration of free mercury(II) from the potential measurement at pH > 11 where all the uncomplexed trien was assumed not to be protonated. There is no indication in that paper of the value of the formal potential of the Hg^{2+}/Hg electrode but, in other papers utilizing this same technique [5, 6], Reilley and his co-workers used a value of 0.612 V vs. SCE which is consistent with published standard potentials. The use of the standard potential would yield a somewhat too high value for the stability constant.

In the present study the concentration of aquo-mercury(II) was calculated by the following rearranged form of the Nernst equation, which is valid if the reaction is reversible in the Nernstian sense:

$$[Hg^{2+}] = \text{antilog}[(E_2^f - E_m)S/2] \tag{1}$$

where E_2^f is the formal potential for the $[Hg^{2+}]/[Hg^0]$ electrode having the value 0.5822 V (vs. SCE) at unit ionic strength (KNO_3) at 25°C and E_m is the measured potential of the mercury pool vs. SCE, in equilibrium with a solution containing Hg(I) and Hg(II) ions; S indicates 2.303 RT/F having the value 0.05916 V at 25°C.

Because about 99% of the uncomplexed mercury ions are present in the univalent form, one must take into consideration the following equilibrium which was evaluated earlier [1]: $Hg^{2+} + Hg^0 \rightleftharpoons Hg_2^{2+}$ with $K = [Hg_2^{2+}]/[Hg^{2+}]\cdot[Hg^0] = 98.8$ at $\mu = 1$ and 25°C. As the pH decreases below 3.0, the concentration of aquo-Hg(II) and aquo-Hg(I) both increase and the latter rapidly becomes the predominant species. Throughout this communication, the symbols C_{Hg}, C_T, C_H and C_{OH} will indicate the added total concentrations of mercury ions, trien, a strong acid (nitric acid), and a strong base (potassium hydroxide), respectively. Brackets will be used to indicate actual concentrations and parentheses will be used to indicate activities. The total concentration expressed as moles per liter of $[Hg_2^{2+}] + [Hg^{2+}]$ remains constant even though Hg^{2+} is reduced to Hg_2^{2+} by free mercury.

For clarity and simplicity, Leden's functions will be written assuming that only the 1:1 complex of mercury(II) exists. Substituting β_{11} and K into the equation for the conservation of mercury ions, as either Hg(II) or Hg(I), dividing through by $[Hg^{2+}]$ and rearranging yields the following Leden functions which have a unique form because of the Hg(II)—Hg(I)—Hg(0) equilibrium:

$$F_0 = (C_{Hg}/[Hg^{2+}]) - (K + 1) = \beta_{11}[\text{trien}] \tag{2}$$

$$F_1 = F_0/[\text{trien}] = \beta_{11} \tag{3}$$

Here β_{11} indicates the stability constant of the 1:1 complex. If only the 1:1 complex is present, F_1 will remain constant when the pH and, hence, the concentration of trien, is varied. If Hg(I) also forms a trien complex, an additional term will appear on the right side of both F_0 and F_1. The latter

possibility was eliminated by the fact that solutions of Hg(I) turned black on addition of free trien because of its disproportionation to form Hg(II) complexes and free mercury. It is well established that amines form stable complexes with Hg(II) and not with Hg(I).

Because no protonated complexes were obtained in the pH range 2.0—12.0, it was also possible to obtain the stability constant, β_{11}, by the classical Bjerrum procedure in which, $[\text{trien}]_{xp}$, the concentration of trien in all forms except the complex was calculated from the pH and the known added concentration of strong acid and not in terms of the total trien concentration as is done in many equilibrium studies. Mass-balance equations for trien and Hg(II) yield the two additional terms, $[Hg^{2+}]$ and $[Hg\ trien^{2+}]$ in β_{11}. The complex is so stable that a pH of about 2.1 is needed in order to obtain a measurable concentration of aquo-Hg(II). At this pH, one must compute the free H^+ concentration by using its activity coefficient, which is 0.82 in this pH range at unit ionic strength (KNO_3) and 25°C [1].

Experimental

The reagents, instruments and general procedures were as described previously [1, 2].

In order to establish the reversibility of the electrode reaction with respect to independent variations of the concentrations of the mercury complex and free trien at different but constant pH, titrations were done by using solutions A and B, which differed in only one variable. The potential and pH were measured during the course of the titration. The first series of titrations was done in the following manner to obtain data for varied concentrations of mercury at fixed concentrations of trien at any chosen pH: in each titration the solution titrated (B) was identical with the titrant (A) except that solution B contained an excess of potassium hydroxide. The titration curves, which are not shown, were then plotted as potential vs. pH. Then the procedure was repeated using increased but identical total concentrations of mercury(II) in both solutions. Points of constant pH were then taken from four of these curves for increasing concentrations of mercury(II) at pH values of 4.0, 5.0, 7.0, 9.0 and 11.0. Then, as shown in Fig. 1, curves of potential vs. the logarithm of concentration of both the uncomplexed mercury and trien were plotted. In the concentration calculations, it was assumed that only the 1:1 complex was formed, and that the reaction between Hg(II) and trien was essentially quantitative. In the first series of titrations (lines 1—5 in Fig. 1), $[\text{trien}]_{xp}$, the concentration of trien except that in complex form, was maintained at 5.00×10^{-2} M while the Hg(II) concentration was varied. The mean slope of a plot of potential vs. $\log[Hg^{2+}]$ was 0.02904 ± 0.00046 V which is close to the theoretical value of 0.02958 V for a mononuclear complex of Hg(II).

In a second series of titrations, both solutions A and B contained 1.00×10^{-4} M Hg(II) but B contained an excess of potassium hydroxide. In successive titrations the concentration of trien in excess of that required for

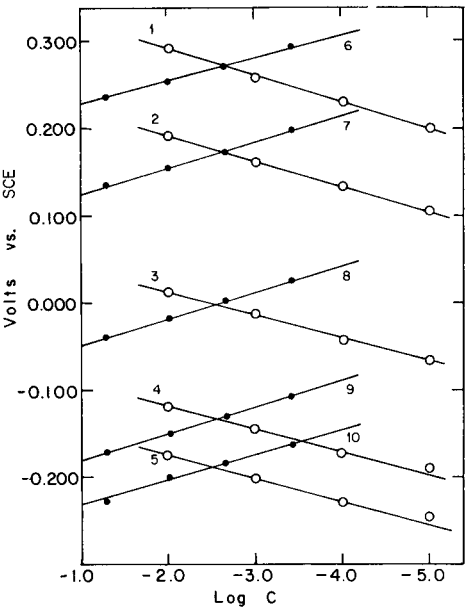

Fig. 1. 1—5: Plots of potential vs. log C_{Hg} with constant $[trien]_{xp}$ = 5.00 × 10^{-2} M; 6—10: plots of potential vs. log$[trien]_{xp}$ with constant C_{Hg} = 1.00 × 10^{-4} M.

1:1 complex formation was varied from 4.17 × 10^{-4} M to 5 × 10^{-2} M (lines 6—10, Fig. 1) for varied pH values. A plot of potential vs. log[trien] had a slope of —0.02988 ± 0.00054 V in good agreement with the theoretical value of —0.02958 V for a mononuclear complex ion containing one trien molecule. The above experiments confirm the essentially reversible electrode behavior of the system with only a 1:1 complex present.

In order to confirm that the complexed trien is not protonated, it is expedient to solve for F_1. If F_1 turns out to be constant with no increasing trend in the relatively more acidic solutions, as will be shown next, it follows that no measurable concentration of the complexed trien is protonated and also F_1 must be equal to β_{11}. In the series of experiments performed to study F_1, a series of solutions containing Hg(II) ion concentrations of 0.0004396—0.00890 M and total trien concentrations of 0.00664—0.00996 M but a greatly varied excess of uncomplexed trien was titrated with a solution containing 0.08645 M KOH and sufficient KNO_3 to maintain the ionic strength at unity throughout the titration.

In a series containing 0.4396 mM Hg(II) and 6.64 mM trien, an essentially constant value of 24.59 ± 0.03 was maintained for log F_1 from pH 2.6—12.0. These data confirm that only the 1:1 complex exists in this pH range and that Schwarzenbach's [3] conclusion that an acidic complex exists is not valid, at least in a solution containing nitrate ion. His conclusions must have been the consequence of his choice of halides, which also form complexes with Hg(II), as the background electrolyte which greatly complicated the equilibria.

The value of F_1 for another series having a concentration of 0.001758 M Hg^{2+} and 0.00996 M trien is also essentially constant, having a mean value of 24.67 ± 0.05. This difference from the previous mean of 24.59 is a reasonable experimental deviation. However, when the mercury(II) ion concentration was increased further by a factor of about 2.5 to 0.00495 M Hg(II) with 0.009960 M trien, a definite decrease in the value of F_1 to a minimum value of about 24.2 (average of 24.56 ± 0.03) was observed at a pH of about 4.0. A further increase in pH to 10.0 resulted in a steady increase in the value of F_1 to 24.59 which is essentially the same as that for the first two series.

In another series containing 0.00890 M Hg(II) and 0.009960 M trien, a similar but somewhat greater decrease in F_1 (average of 24.50 ± 0.03) was observed at an intermediate pH range of 4.0—10.0 followed by an increase close to the previous value. The systematic appearance of these minima, which seem to be appreciably greater than any expected experimental deviation, indicate a slight degree of irreversibility of the electrode reaction at intermediate pH values when the concentration of mercury is increased appreciably above about 2 mM.

Observations in the previous papers [1, 2] had suggested that the concentration of mercury(II) should not be above about 2 mM if an essentially completely reversible electrode behavior is to be obtained. The presence of additional complex species is not a possibility because this would have resulted in an increase in F_1. Furthermore, the effect persisted with greatly varied excesses of trien and cannot be attributed to association of the excess of ligand as a consequence of hydrogen bonding.

The stability constant was also determined by the completely independent Bjerrum method which depends only on the attainment of chemical equilibrium and reliable pH measurements [7]. As a consequence of the very great stability of the mercury(II)—trien complex, a high acidity of close to 0.01 M H^+ was required in order to obtain a measurable extent of dissociation of the complex. This makes the accurate evaluation of the large concentration of free H^+ extremely difficult because it depends on the antilog of the measured pH. Furthermore the activity coefficient of H^+ ions must be accurate. Three sets of conditions involving 8.99×10^{-3} M Hg(II), 0.01509 M trien and 0.086 M HNO_3; 0.1164 M Hg(II), 0.01465 M trien and 0.086 M HNO_3; and 0.01413 M Hg(II), 0.01423 M trien and 0.0874 M HNO_3 yielded average values of $\log \beta_{11}$ of 24.43 ± 0.04, 24.54 ± 0.03 and 24.37 ± 0.01, respectively. The overall average for the three sets was 24.45 ± 0.10, which is in satisfactory agreement with the potentiometrically obtained value of 24.60 ± 0.06. These results constitute strong evidence that protonated complexes do not make a significant contribution even at a pH close to 2.1. The value, 24.55 ± 0.10, is a mean of those obtained by the two completely different methods. The extremely simple equilibrium enhances the possible usefulness of the mercury electrode in the indirect investigation of the stability of the trien complexes of other metal ions which will be discussed in later papers. The present study has shown that the total concentration of Hg(II) must not

exceed 2 mM in order for the electrode behavior to be completely reversible in the Nernstian sense.

REFERENCES

1 J. I. Watters, P. C. Dunnigan and S. Kalliney, Anal. Chim. Acta, 154 (1983) 287.
2 P. C. Dunnigan and J. I. Watters, Anal. Chim. Acta, 153 (1983) 341.
3 G. Schwarzenbach, Helv. Chim. Acta, 33 (1950) 974.
4 C. N. Reilley and R. M. Schmid, J. Elisha Mitchell Sci. Soc., 73 (1957) 229.
5 C. N. Reilley and W. W. Porterfield, Anal. Chem., 28 (1956) 433.
6 C. N. Reilley and R. M. Schmid, Anal. Chem., 30 (1958) 947.
7 J. Bjerrum, Metal Ammine Formation in Aqueous Solutions, P. Haase, Copenhagen, 1941.

Analytica Chimica Acta, 154 (1983) 335—339
Elsevier Science Publishers B.V., Amsterdam — Printed in The Netherlands

Short Communication

DETERMINATION OF NITRITE IN ANIMAL FEED BY SPECTROPHOTOMETRY OR POTENTIOMETRY WITH A NITRITE-SELECTIVE ELECTRODE

HALEEM J. ISSAQ*, GARY M. MUSCHIK and NELSON H. RISSER[a]

Chemical Synthesis and Analysis Laboratory, NCI-Frederick Cancer Research Facility, Frederick, MD 21701 (U.S.A.)

(Received 12th April 1983)

Summary. A method is presented for the extraction and quantitation of nitrite in animal feed. The extracting solution consists of ammonium sulfate at pH 8.5. The recovery of nitrite usually exceeds 90%. Nitrite is quantified with a nitrite-selective electrode or by a modified Griess reaction. The effects of extraction time on recovery are compared for acidic and alkaline extracting solutions.

Nitrite, a meat preservative, may play a significant role in carcinogenesis; the in vivo interaction of nitrite with amines or amides can result in the formation of nitrosamines [1]. The carcinogenicity of nitrosamines in animals has been demonstrated; cancer could be induced at specific sites in animals by nitrosamines and nitrosamides as well as by nitrite administered together with the corresponding amine or amide [1, 2]. Therefore, it is important to determine the nitrite concentration in foods for humans and animals. It is especially important to monitor the amount of nitrite in animal feeds used in bioassay feeding studies.

The Griess reaction [3] has long been used for the determination of nitrite in plant material and animal feed. The modification suggested by Schall and Hatcher [4] for determining nitrate and nitrites in feed was later adopted as the official method for nitrate and nitrite by the Association of Official Analytical Chemists [5]. Although this method is good for the determination of nitrate in feed, it is inadequate for nitrite because of the acidity of the extracting solution. The present study led to two modifications which make the method useful for the determination of nitrite by either spectrophotometry or a nitrite-selective electrode. It also enables nitrate to be quantified with an ion-selective electrode.

Experimental

Materials. Sulfuric acid (97.5%), ammonia liquor (29.6%), hydrochloric acid (37.4%), and the other chemicals used were Baker analyzed (Baker

[a]Present address: Lancaster Laboratories, Lancaster, PA, U.S.A.

Chemical Co.) or certified A.C.S. (Fisher Scientific). Animal feed was from Wayne Feed (Chicago, IL). Deionized water was used for sample and reagent preparation.

Solutions and reagents. Nitrate-nitrogen standard (500 ppm NO_3^--N) was prepared by dissolving 0.7598 g of KNO_3 in 250 ml of water. Nitrite-nitrogen standard (500 ppm NO_2^--N) was prepared by dissolving 0.6162 g of $NaNO_2$ in 250 ml of water. Nitrate extracting solution was prepared by dissolving 50 g of $CdCl_2$ and 50 g of $BaCl_2$ in water and adjusting to pH 1 in 1 l of water. Ammonium chloride buffer solution, pH 9.6, was prepared from 50 g of NH_4Cl in 1 l of water, adjusted with ammonia liquor. Nitrite—nitrate extracting solution was prepared by dissolving 5 g of $(NH_4)_2SO_4$ in water, adjusting to pH 8.5 with dilute ammonia solution, and diluting to 2 l with water. Sulfate buffer stock contained 190 g of Na_2SO_4 in 800 ml of water with 53 ml of sulfuric acid, diluted with water to 1 l. Sulfate buffer for the NO_2 electrode contained 100 ml of sulfate buffer stock diluted to 500 ml with water.

Apparatus. Items used included a double-junction reference electrode (model 90-02-00), a nitrate-selective electrode (model 93-07), a nitrite-selective electrode (model 95-46), all from Orion, an internal reference pH electrode (Broadley-James No. 91693S), a hot-plate stirrer, a digital pH meter (Corning model 112) and a u.v. spectrophotometer (Cary model 17).

Extraction procedure. Experiments were done at room temperature. Samples (5 g) of feed (finely ground) were placed in a 200-ml volumetric flask and 100 ml of the ammonium sulfate extracting solution was added, after which the sample was placed on a shaker. After 30 min, the flask was removed and filled to the mark with deionized water and the feed was allowed to settle. Two 25-ml aliquots were pipetted into 100-ml beakers for quantification by the nitrite-selective electrode.

Spectrophotometric measurement. Aluminum sulfate solution (0.1 M, 50 ml) was added to the volumetric flask and the sample was shaken for 30 s. The mixture was then filtered immediately on a Buchner funnel. Depending on nitrite concentration, between 1 and 10 ml of the filtrate was pipetted into a 50-ml volumetric flask and 5 ml of the sulfanilamide reagent (0.5% in 1 + 1 hydrochloric acid) and 2 ml of the coupling reagent (0.5% *N*-(1-naphthyl)ethylenediamine hydrochloride in water) were added. (It is important that the pH of the solution, after having been diluted to the mark with deionized water, be less than 2; the effect of pH on absorbance of nitrite after the azo dye formed by the above diazotization and coupling is illustrated in Fig. 1.) The absorbance of the solution, after standing for 3 min, was measured at 540 nm. The color is stable for at least 60 min. The concentration of nitrite in feed was quantified by comparing the absorbance obtained with that of a standard aqueous nitrite solution.

Potentiometric measurement. Aliquots (25 ml) of the extracted solution were mixed with 25 ml of sulfate buffer for 30 s. The potential of the nitrite-selective electrode was measured and the results were compared with those from standard aqueous solutions.

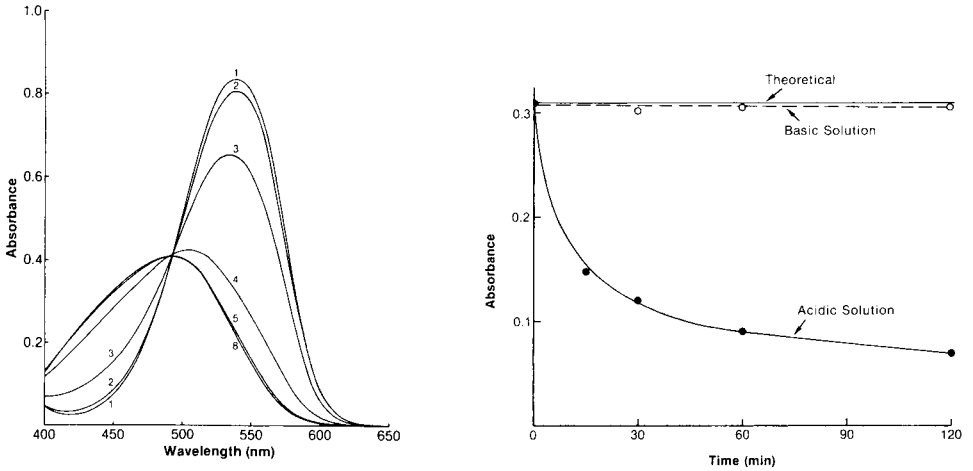

Fig. 1. Effect of pH (given on the spectra) on absorbance of the azo dye formed.

Fig. 2. Effect of time of mixing with $CdCl_2/BaCl_2$ solution at pH 1, and with ammonium sulfate solution at pH 8.5 on the recovery of nitrite from animal feed.

Results and discussion

In this laboratory, the use of $BaCl_2/CdCl_2$ solution at pH 1 for extraction of nitrite from spiked animal feed led to erroneous and inconsistent results; the longer the extraction period, the lower the nitrite concentration. A time study was undertaken in which four 5-g samples of feed were spiked with 500 μg of nitrite (NO_2^--N) after which 100 ml of $BaCl_2/CdCl_2$ solution at pH 1 was added. The four flasks were shaken for 15, 30, 60, and 120 min, respectively. Figure 2 compares the results obtained with results for an aqueous nitrite standard. The results indicated that 70% of the nitrite was lost after 60 min. The official method [5] calls for mixing the feed with the extracting solution for 60 min. Varying recoveries were obtained when the acidic extracting solution was used. When different concentrations of nitrite (164—1643 $\mu g\ g^{-1}$) were added to feed and extracted with the $BaCl_2/CdCl_2$ solution at pH 1, the loss ranged from 94% for 164 $\mu g\ g^{-1}$ nitrite added, to 58% when ten times that concentration was added.

The acidic $BaCl_2/CdCl_2$ solution was therefore replaced by an ammonium sulfate solution of pH 8.5. A basic solution would hinder the reaction of nitrite with the amines or amides. A time study using this basic extracting solution showed (Fig. 2) that there was no significant loss of nitrite from animal feed after 120 min. The difference between the theoretical and experimental values is within 3%. These results clearly show that the loss of nitrite caused by the extractant is much reduced compared to that in acidic solution. The recovery of nitrite with the proposed procedure was better than 90% (Table 1).

Another modification was to substitute aluminum sulfate for sodium

TABLE 1

Comparison of nitrite results obtained for spiked feeds

Nitrite added ($\mu g\ g^{-1}$ feed)	Spectrophotometry		Potentiometry	
	Found (μg)	Recovery (%)	Found (μg)	Recovery (%)
0	0	0	66 (background)	0
164	150	91 ± 2	145[a]	88 ± 4
329	305	93 ± 2	329[a]	100 ± 4
657	622	95 ± 3	591[a]	90 ± 5
1643	1550	94 ± 2	1406[a]	88 ± 4

[a]Corrected for blank response.

hydroxide. Aluminum sulfate gave a clear solution and allowed the use of an i.s.e. for nitrate and nitrite by providing the necessary constant background ionic strength. Recovery for nitrite with the nitrite-selective electrode is also shown in Table 1. Although there are differences in recovery for the spectrophotometric and potentiometric methods, these may be due to interference with the electrode from the feed.

For spiked feeds, absorbance varied linearly with nitrite concentration between 0.1 and 0.6 $\mu g\ g^{-1}$ nitrite-nitrogen; potential of the electrode varied logarithmically with nitrite concentration between 0.2 and 10 $\mu g\ g^{-1}$. Sample-to-sample variations for 0.05—10 ppm nitrite in feeds (triplicates) were less than 4% for spectrophotometric detection and less than 6% for potentiometric detection.

An added advantage for substituting ammonium sulfate for the $BaCl_2$/$CdCl_2$ solution is the elimination of chloride which interferes with the i.s.e. method for nitrate. The addition of ammonium sulfate is a precautionary measure to ensure a basic or neutral extracting solution which prevents the conversion of nitrite to nitrosamines. In subsequent studies, it was found that water gave quantitative and reproducible results.

In conclusion, the method of Schall and Hatcher [4] and the official AOAC method [5] are adequate for nitrate, but not nitrite determination. The methods presented above work well for nitrite whether spectrophotometric or potentiometric detection is used. Both detection methods give useful response from 0.1 to 50 ppm nitrite.

This work was supported by Contract No. NO1-CO-23910 with the National Cancer Institute, Program Resources, Inc., Frederick, MD 21701, U.S.A.

REFERENCES

1 W. Lijinsky, E. Conrad and R. Van de Bogart, Nitroso Compounds: Analysis and Formation, Vol. 3, International Agency for Research on Cancer, Lyon, France, pp. 130—133.
2 P. N. Magee, R. Montesano and R. Preussmann, Chemical Carcinogens, American Chemical Society, Washington, DC, 1976, pp. 491—625.
3 P. Griess, Ber. Deutsch. Chem. Ges., 12 (1879) 426.
4 E. D. Schall and D. W. Hatcher, Sr., J. Assoc. Off. Anal. Chem., 15 (1968) 763.
5 W. Horwitz (Ed.), Methods of Analysis, 13th edn., Association of Official Analytical Chemists, Washington, DC, 1980.

Analytica Chimica Acta, 154 (1983) 341—345
Elsevier Science Publishers B.V., Amsterdam — Printed in The Netherlands

Short Communication

THE DETERMINATION OF URANIUM IN AQUEOUS SAMPLES BY MEANS OF A PULSED-SOURCE FLUORESCENCE SPECTROMETER

A. T. RHYS WILLIAMS*

Perkin-Elmer Ltd., Beaconsfield, Bucks. HP9 1QA (Gt. Britain)

J. N. MILLER

Department of Chemistry, University of Technology, Loughborough LE11 3TU (Gt. Britain)

(Received 7th March 1983)

Summary. Luminescence from aqueous uranyl ions is examined by means of a fluorescence spectrometer with a pulsed xenon light source. Background fluorescence is reduced by using time-based discrimination of the uranyl emission, but interference can still occur from quenchers such as iron(III). Such interferences are reduced by extraction of the uranyl ion into hexane containing tri-n-butyl phosphate, with back-extraction into dilute phosphoric acid before measurement. A detection limit of 5 ng ml^{-1} is found with a linear calibration range of 0—10 μg ml^{-1}.

The determination of uranium is required in several fields. Typical samples include ores, surface and ground water run-off, sea water and urine. In the nuclear power industry, uranium determinations may be needed in relatively concentrated samples containing high levels of acid and/or organic materials. Several luminescence methods for uranium determination have been reported, most of them based on sodium fluoride—lithium fluoride fusion [1—3]. Typically the uranium is first extracted with ethyl acetate from a solution salted with aluminium nitrate and an aliquot of the solute in the organic phase is transferred to a pellet of sodium fluoride containing 2% lithium fluoride. The latter is melted at 1075°C for 15 min and the luminescence of the button, when exposed to u.v. radiation, is measured. The limit of detection is ca. 100 ng of uranium in the button.

Uranyl luminescence is very susceptible to quenching both by organic molecules and by inorganic ions such as iron(III), manganese(II) and chloride [4, 5]. Several methods have been used to minimise such interferences. For example, the uranyl luminescence can be studied after precipitation from a solution containing calcium fluoride followed by calcination [6]. Liquid—liquid extraction systems, including ethyl acetate [1], tributyl phosphate (TBP) in iso-octane [7], and trioctylphosphine oxide (TOPO) in cyclohexane [8] or Varsol [9] have been used to isolate the uranium before the luminescence is measured. A further problem is the substantial background fluorescence from organic sample components and reagents. Since the luminescence

0003-2670/83/$03.00

from an acidic uranyl solution has a lifetime in the sub-millisecond region [10], time discrimination has been used as a means of decreasing the effect of background fluorescence (which has a lifetime of a few nanoseconds), hence improving the detection limit [11—13]. The luminescence lifetime of the uranyl ion varies with the type and concentration of acid, ranging from 2.1 μs in 0.1 M perchloric acid to 187 μs in phosphoric acid [14]. Orthophosphoric acid has been extensively used as an enhancer of the uranyl emission; it may prevent quenching of the excited uranyl ion by hydroxyl ions, though the precise mechanism is not known [15].

The present communication describes the use of a combined extraction—time-resolved luminescence method for uranium determination. The extra selectivity provided by this method minimises both luminescence quenching and luminescence background interferences and permits the determination of uranium at ng ml^{-1} levels.

Experimental

Reagents. All chemicals were of analytical-reagent grade (BDH) unless otherwise stated. Water was distilled and filtered through a 0.45-μm Millipore filter. Uranyl nitrate stock solution (1 μg ml^{-1} uranyl ion) was prepared by dissolving uranyl nitrate in 1 M nitric acid. Aluminium nitrate (90% w/v) and orthophosphoric acid (10% w/v) were shaken for 1 min with 1% (v/v) TBP in hexane and the upper, organic layer was discarded. These precautions were necessary because the aluminium nitrate may contain up to 0.5 ng g^{-1} uranium (as UO_2^{2+}) and the acid also contains measurable amounts of uranium. Extraction with TBP minimised the background luminescence arising from this contamination.

Apparatus. Excitation and emission spectra were recorded at room temperature on a Model LS-5 Luminescence Spectrometer (Perkin-Elmer, Beaconsfield, Bucks.) with a bandpass of 5 nm. Quantitative measurements (excitation wavelength 245 nm, emission wavelength 515 nm) were done with a 15-nm excitation bandpass and a 20-nm emission bandpass. Excitation spectra were fully corrected by using the reference beam of the spectrometer which incorporates a Rhodamine 101 quantum counter and a compensation plate to allow for the wavelength dependence of the beam splitter [16]. Data were recorded using a Model 3600 Data Station (Perkin-Elmer Ltd.) equipped with PECLS II Applications Software. The fluorescence spectrometer has an 8-W pulsed xenon lamp as its light source, pulsed at 50 Hz, the width of each pulse being <10 μs. The microprocessor-controlled detection system allows the signal reaching the sample photomultiplier to be gated. The duration of the gate (t_g) and the delay time between the light source pulse and the opening of the gate (t_d) can be controlled, the permissible values being in multiples of 10 μs in each case, up to a total ($t_d + t_g$) of 13.33 ms. In the fluorescence mode there are two gating periods, one coinciding with each pulse of the light source and the second occurring shortly

before the next pulse. The signal intensity of the second gate is subtracted from that of the first. The effect of this double gating is that fluorescence is observed, but that long-lived phosphorescence is not. As the luminescence lifetime of uranyl ion is 0.1 ms (see below), this emission is observed in both modes.

Procedure. To a 10-ml glass extraction tube containing 2 ml of the aluminium nitrate solution were added 1 ml of the sample or uranium standard (0—10 $\mu g\ ml^{-1}$) and 3 ml of 1% (v/v) TBP in hexane; the tube was sealed with a glass stopper and shaken for 2 min. After separation, 2 ml of the upper (organic) layer was removed and added to 3 ml of the phosphoric acid in a second 10-ml extraction tube. The latter was stoppered and shaken for 2 min. After separation the lower (aqueous) layer was transferred by Pasteur pipette to a 10-mm silica cuvette for measurement.

Results and Discussion

Figure 1 shows the improved signal:background ratio provided by the "phosphorescence" mode of the spectrometer. In this mode, the structured luminescence of uranyl ion, with maximum emission at 515 nm, is clearly seen. In the "fluorescence" mode, the luminescence is heavily masked by a short-lived broad band signal arising from scattered and stray light and fluorescent impurities in the solvents and reagents. A 50 ng ml^{-1} solution of uranium in 10% (w/v) phosphoric acid gave a signal-to-background ratio of 10.4 and 2.3, respectively, in the phosphorescence and fluorescence modes (measured at 515 nm). The variation of the luminescence lifetimes of uranyl ion with phosphoric acid concentration is illustrated in Fig. 2. In contrast to earlier results [11], single exponential decays were obtained in all cases. On the basis of these results, the t_d and t_g values for routine work were set at 30 μs and 250 μs, respectively.

Tri-n-butyl phosphate in hexane was found to be the most efficient

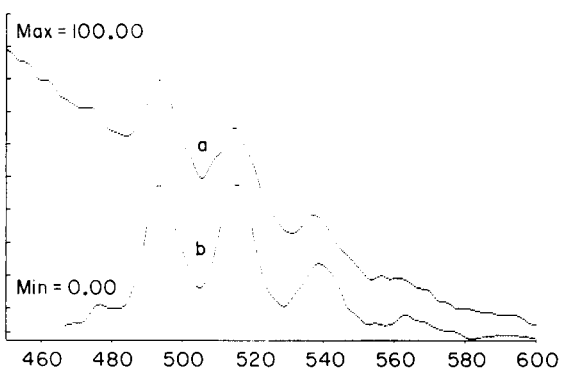

Fig. 1. Comparison of (a) the fluorescence and (b) the phosphorescence mode emission of 50 ng ml^{-1} uranyl ion in 10% (w/v) orthophosphoric acid saturated with 1% (v/v) TBP in hexane; excitation at 245 nm with t_d = 30 μs and t_g = 250 μs for the phosphorescence mode.

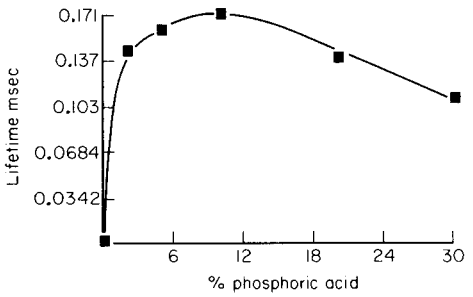

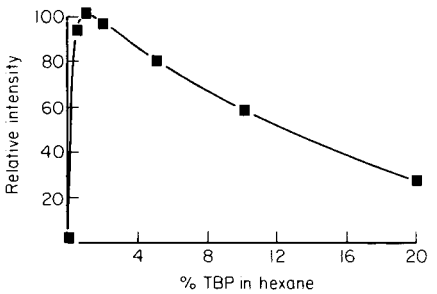

Fig. 2. Variation in lifetime of a 1 μg ml^{-1} uranyl ion solution with orthophosphoric acid concentration.

Fig. 3. Variation in the relative intensity of the uranyl emission in the final aqueous phase with concentration of TBP in hexane.

extraction system, being almost twenty times more efficient than ethyl acetate. Figure 3 shows the variation in the intensity of the extracted uranyl ion with varying TBP concentration in hexane. Greatest intensity was found at 1% (v/v). When combined with 10% (w/v) phosphoric acid for back-extraction, an average efficiency of 81% was achieved for the whole procedure. To construct a calibration graph, eight standards were measured in triplicate. A linear graph with a slope of 0.81, intercept 0.035 and a correlation coefficient of 0.98 was obtained for 0—10 μg UO_2^{2+} ml^{-1}. The relative standard deviation at the 10 ng ml^{-1} level was 8% (6 results), leading to a statistical detection limit of 3 ng ml^{-1}.

Interferences from potential quenchers such as iron(III), manganese(II) and chloride were examined by comparing the intensities of 1 μg UO_2^{2+} ml^{-1} solutions containing 0—500 μg ml^{-1} iron(III), 0—100 μg ml^{-1} manganese(II) and 0—100 μg ml^{-1} chloride. No significant difference was observed for these solutions, indicating that the 1% (v/v) TBP in hexane provided adequate separation of the uranyl ion from these ions. This compares favourably with the 10% (v/v) TBP in iso-octane used by François [7] to obtain a satisfactory differential extraction.

Samples of tap water and Thames river water were spiked with known concentrations of uranyl ion and compared with standard solutions which contained the same concentration. For concentrations ranging from 1 to 100 ng UO_2^{2+} ml^{-1}, no significant difference was observed. Samples below 5 ng ml^{-1} gave irreproducible results, indicating a practical detection limit of 5 ng ml^{-1}. The procedure described is therefore an effective means of determining uranium in the presence of quenchers such as iron(III), manganese(II) and chloride. The detection limit of 5 ng ml^{-1} compares well with the 1 ng ml^{-1} detection limit observed using laser excitation and liquid—liquid extraction [17].

The authors thank P. E. Croft of Robertson Research International Ltd., for advice and Dr. S. A. Winfield for technical assistance.

REFERENCES

1 J. A. S. Adams and W. J. Maeck, Anal. Chem., 26 (1954) 1635.
2 F. A. Centanni, A. M. Ross and M. A. DeSasa, Anal. Chem., 25 (1956) 1651.
3 L. L. Thatcher and F. B. Barker, Anal. Chem., 29 (1957) 1575.
4 J. C. Veselsky and Y. Ratsimandresy, Anal. Chim. Acta, 104 (1979) 345.
5 Y. Yokoyama, M. Mariyasu and S. Ikeda, J. Inorg. Nucl. Chem., 38 (1976) 1329.
6 D. L. Perry, S. M. Klaimer, H. R. Bowman, F. P. Millanovitch, T. Hirchfeld and S. Miller, Anal. Chem., 53 (1981) 1048.
7 C. A. François, Anal. Chem., 30 (1958) 50.
8 C. A. Horton and J. C. White, Anal. Chem., 30 (1958) 1779.
9 R. J. McElhaney, J. D. Caylor, S. H. Cole, T. L. Futrell and V. M. Giles, Report No. Y-2111, NTIS, 1978.
10 D. D. Pant and H. B. Tripathi, J. Luminescence, 8 (1974) 492.
11 R. Kaminski, F. J. Purcell and E. Russavage, Anal. Chem., 53 (1981) 1093.
12 J. C. Robbins and J. D. Kinrade, Can. Pat. No. 1064726, Oct., 1979.
13 E. R. Hinton and L. E. White, Anal. Lett., 14 (1981) 947.
14 M. Mariyasu, Y. Yokoyama and S. Ikeda, J. Inorg. Nucl. Chem., 39 (1977) 2199.
15 H. D. Burrows and T. G. Kemp, Chem. Soc. Rev., 3 (1974) 139.
16 A. T. Rhys Williams, Int. Lab., 11 (1981) 90.
17 P. J. Whitkop, Anal. Chem., 54 (1982) 2475.

Analytica Chimica Acta, 154 (1983) 347—350
Elsevier Science Publishers B.V., Amsterdam — Printed in The Netherlands

Short Communication

PROPERICIAZINE AS A REAGENT FOR THE SPECTROPHOTOMETRIC DETERMINATION OF RUTHENIUM(III)

A. THIMME GOWDA and H. SANKE GOWDA

Department of Post-Graduate Studies and Research in Chemistry, University of Mysore, Manasagangotri, Mysore-570 006 (India)

N. M. MADE GOWDA*

Division of Biochemistry, Department of Human Biological Chemistry and Genetics, The University of Texas Medical Branch, Galveston, TX 77550 (U.S.A.)

(Received 17th June 1983)

Summary. Propericiazine forms an orange-red species with ruthenium(III) immediately in 6—8 M phosphoric or hydrochloric acid or 4.5—5.5 M sulphuric acid. The absorption maximum is at 511 nm and the molar absorptivity is 1.1×10^4 l mol^{-1} cm^{-1}. Beer's Law is obeyed over the range 0.2—9.4 mg l^{-1} (optimum range 0.5—9.0 mg l^{-1}). Interferences are described. The method is used to determine ruthenium in synthetic zinc—magnesium alloy and uranium alloy (fuel) solutions.

Many reagents have been suggested for the spectrophotometric determination of ruthenium. Of these, thiourea [1] is the most popular. Most other reagents require either heating or a long standing time for maximum colour development to take place, or are very sensitive to the reaction medium [2]. Cyano-3[(hydroxy-4-piperidino)-propyl]-10-phenothiazine (propericiazine, PPC) has been used as a spectrophotometric reagent for vanadium [3] and gold [4]. This reagent also forms a coloured complex with ruthenium(III) and is suitable for the determination of microgram amounts of ruthenium in acid solutions in presence of large amounts of other metals including some platinum metals. It is more sensitive than thiourea [1]. This communication describes the use of PPC as a sensitive reagent for the spectrophotometry of ruthenium(III) and includes data for some applications.

Experimental

Ruthenium(III) solution. An aqueous solution was prepared by dissolving 0.985 g of ruthenium(III) chloride (Johnson Matthey Chemicals, London) in 500 ml of 1.0 M hydrochloric acid, and standardized gravimetrically [1]; working solutions were prepared by suitable dilutions.

Propericiazine solution. A 0.2% solution of PPC was prepared in water containing a few drops of hydrochloric acid and stored in an amber bottle in a refrigerator.

All other reagents were of analytical grade. Doubly distilled water was used throughout.

0003-2670/83/$03.00

A Beckman Model DB spectrophotometer with stoppered 10-mm silica cells was used for absorbance measurements.

Procedure. Transfer an aliquot of the sample solution containing 5—235 μg of ruthenium(III) to a 25-ml volumetric flask. Add sufficient acid to give a final concentration of 5 M in sulphuric acid or 7 M in phosphoric or hydrochloric acid, followed by 3.0 ml of 0.2% PPC solution. Dilute the solution to the mark with water, mix thoroughly, and measure the absorbance at 511 nm against a reagent blank prepared in the same way.

Results and discussion

The reagent readily forms an orange-red species with ruthenium(III) at room temperature in acid medium. The sensitivity and stability of the product depend on the nature and concentration of the acid used. The sensitivity in four acid media is in the following order: $H_3PO_4 \approx HCl \approx H_2SO_4 >$ acetic acid. The colour development in acetic acid medium is very slow. Nitric acid cannot be used because it oxidizes PPC. Maximum colour intensity is achieved in 4.5—5.5 M sulphuric acid or 6—8 M phosphoric or hydrochloric acid medium. The reaction is slow at acidities higher than those cited. The oxidation product is stable in 5 M sulphuric acid, 7 M hydrochloric acid, and 7 M phosphoric acid for 100, 120 and 160 min, respectively. Therefore, 7 M phosphoric acid was selected for further studies.

Absorption spectra. The absorption spectra of PPC, ruthenium(III), and the orange-red species in 7 M phosphoric acid medium are shown in Fig. 1.

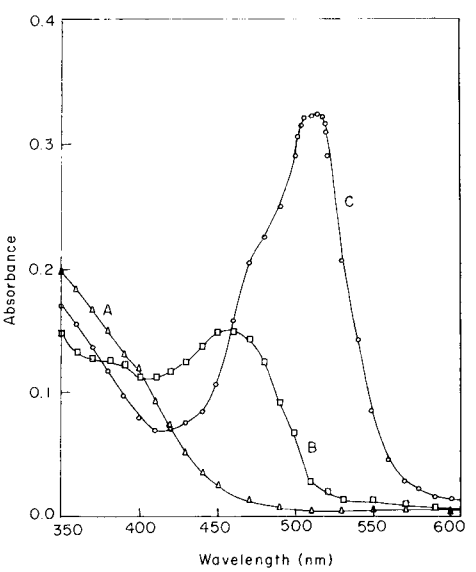

Fig. 1. Absorption spectra: (A) reagent blank vs. water; (B) ruthenium(III) vs. water; (C) orange-red species vs. reagent blank. For B and C, a 3 mg l^{-1} Ru(III) in 7 M phosphoric acid was used.

The spectra of the reagent and ruthenium(III) show no appreciable absorption at the peak wavelength (510—512 nm) for the product.

Effects of reagent concentration, temperature, and order of addition of reactants. The effect of reagent concentration was examined by measuring the absorbance of solutions containing 3 μg ml^{-1} ruthenium(III) and varying amounts of PPC. A 12-fold molar excess of PPC over ruthenium(III) was needed for complete reaction. Addition of more reagent had no effect on the absorbance. An amount of 3 ml of 0.2% reagent solution was used.

The absorbance was not affected by temperature in the range 10—63°C. However, above 63°C, the absorbance gradually decreased with increasing temperature. There was no change in the absorbance reading when the order of addition of reactants was changed.

Calibration, range, sensitivity and precision. Beer's law was obeyed over the concentration range of 0.2—9.4 mg l^{-1} ruthenium(III) with an optimal range of 0.5—9.0 mg l^{-1}. The apparent molar absorptivity was 1.1×10^4 l mol^{-1} cm^{-1} at 511 nm. The standard deviation calculated for ten solutions containing 3 mg l^{-1} ruthenium(III) was 0.0028 mg l^{-1}.

Effect of diverse ions. In order to assess possible quantitative applications of this method, the effects of some ions which often accompany ruthenium were studied by adding different amounts to 75 μg of ruthenium in 25 ml of solution. The colour was developed as outlined in the procedure. Of 32 cations and anions examined, only Os(VIII), Pd(II), Au(III), Ag(I), V(V), Ce(IV), iodide, and thiosulphate caused errors of 2% when present in concentrations at or below 2.5 mg l^{-1}. All other ions studied had tolerance limits (2% error) of 20 mg l^{-1} or higher [e.g., Rh(III), Ir(III), Pt(IV)].

Determination of ruthenium in zinc—magnesium alloy and uranium alloy. The fuel for initial core loading of the experimental Breeder Reactor-II (EBR-II) is an alloy of 95% uranium, 2.5% molybdenum, 2.0% ruthenium and smaller amounts of zirconium, palladium and rhodium. In one phase of the processing system devised for EBR-II, molten zinc and zinc—magnesium alloy are used as solvents in the separation of uranium from ruthenium and other fission products. Synthetic mixtures containing the metal composition corresponding to (i) the uranium alloy (fuel) and (ii) zinc—magnesium alloy were prepared and the ruthenium content (0.8—8 ppm) was quantified. A least-squares fit of concentration found (y) vs. that added (x) gave $y = 0.9996 \pm 1.5 \times 10^{-3} - 0.0003 \pm 0.007$ with standard error (S_{yx}) of 0.0095 and correlation coefficient of 0.99999 for the uranium alloy. Differences between added and found amounts (4.0 and 2.0 ppm) were all less than 0.5% for the zinc—magnesium alloy.

The major advantages of the proposed method are that: (i) maximum colour intensity is attained instantaneously at room temperature, (ii) ruthenium can be determined in presence of several other metal ions including Pt(VI), and (iii) the ruthenium content in important alloys such as zinc—magnesium alloy and uranium alloy can be determined with reasonable accuracy.

The authors thank L. Julou and J. Molle of Rhône—Poulenc Centre, Paris for the generous supply of PPC. One of us (ATG) is grateful to the University Grants Commission, New Delhi, for the award of a Teacher Fellowship under the Faculty Improvement Program.

REFERENCES

1 F. E. Beamish, The Analytical Chemistry of the Noble Metals, Pergamon Press, Oxford, 1966.
2 F. E. Beamish and J. C. Van Loon, Recent Advances in the Analytical Chemistry of Noble Metals, Pergamon Press, Oxford, 1972.
3 H. Sanke Gowda and A. Thimme Gowda, Curr. Sci., 50 (1981) 395.
4 H. Sanke Gowda, A. Thimme Gowda and N. M. Made Gowda, Microchem. J., (1983) in press.

Analytica Chimica Acta, 154 (1983) 351—354
Elsevier Science Publishers B.V., Amsterdam — Printed in The Netherlands

Short Communication

FLUORIMETRIC DETERMINATION OF MEBENDAZOLE AND FLUBENDAZOLE IN PHARMACEUTICAL DOSAGE FORMS AFTER ALKALINE HYDROLYSIS

F. ABDEL FATTAH[a], W. BAEYENS* and P. DE MOERLOOSE

Department of Pharmaceutical Chemistry and Drug Quality Control, Faculty of Pharmaceutical Sciences, State University of Ghent, Harelbekestraat 72, B-9000 Ghent (Belgium)

(Received 21st April 1983)

Summary. The selective and very sensitive fluorimetric determination of mebendazole and flubendazole is based on alkaline hydrolysis and adsorption on Whatman 42 filter paper. Limits of detection are 0.1 $\mu g\ ml^{-1}$ and 0.5 $\mu g\ ml^{-1}$, respectively, with linear response up to 10 $\mu g\ ml^{-1}$ and 50 $\mu g\ ml^{-1}$. The fluorescence produced is very stable (λ_{em} = 460 nm) and the method is applicable to anthelmintic pharmaceutical preparations.

Mebendazole [I; (5-benzoyl-1H-benzimidazol-2-yl)-carbamic acid methyl ester] and its monofluorinated derivative, flubendazole {II; [5-(4-fluorobenzoyl)-1H-benzimidazol-2-yl]-carbamic acid methyl ester}, are frequently used as anthelmintic drugs. Most benzimidazole derivatives show intense

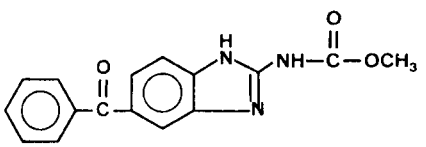

(I)

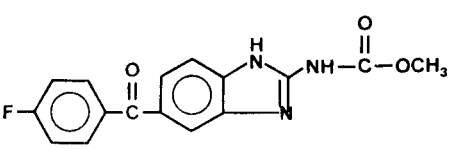

(II)

luminescence characteristics [1—3] (π—π* fluorescence and n—π* phosphorescence). Longworth et al. [4] reported that high fluorescence intensities were observed for benzimidazole and 5,6-dimethylbenzimidazole in various organic solvents. Mebendazole and flubendazole show little or no fluorescence at pH 1—13 in various organic solvents [5], probably because of fluorescence quenching by the carbonyl group. It was thought that the fluorescence behaviour of these compounds might be improved to some extent after hydrolysis with sodium hydroxide. In this communication, practical data are reported for the fluorimetric determination of small amounts of mebendazole and flubendazole, i.e., excitation and emission

[a]Present address: Pharmaceutical Chemistry Department, Faculty of Pharmacy, Assiut University, Assiut, Egypt.

0003-2670/83/$03.00

maxima, relative fluorescence intensities, optimum measuring conditions, linear ranges and detection limits. The proposed method is applied in the analysis of some anthelmintic preparations.

Experimental

Chemicals. Mebendazole and flubendazole, generously donated by Janssen Pharmaceutica (Beerse, Belgium), were used as received. The pharmaceutical formulations (Vermox and Flumoxal tablets and suspensions) were obtained from the same manufacturer.

All reagents and solvents used were of analytical grade. Deionized water was used throughout; its quality was checked by fluorimetric scanning at the highest instrumental sensitivity settings.

Apparatus. Fluorescence was measured by using a PMQ-3 Zeiss densitometer in the fluorescence mode; the instrument was equipped with a mercury lamp and a Spectra-Physics Minigrator. The wavelengths for excitation and emission were 365 nm and 460 nm, respectively. The filter paper (Whatman 42) was fixed between two glass plates on the stage of the scanner. The operating instrumental parameters were as follows: scanning speed 50 mm min^{-1}, peak width 1, slope sensitivity 200, baseline 5, tailing peak 60, and minimum area 200. An Aminco-Bowman t.l.c. scanner was unsatisfactory for measuring the fluorescence emission of the dried spots on a filter paper fixed to a specially made sample holder because of stray light. The reflection mode in the Zeiss scanner is important for accurate measurements.

A Camag u.v. lamp (type 29000) was used at 254 nm and at 366 nm for viewing solutions and solid supports. A Nanomat (Camag) apparatus was used to spot 100—200-nl portions of the solutions.

Procedures. Mebendazole or flubendazole (2—5 mg) was dissolved in 10 ml of 1 M sodium hydroxide and the solution was heated in a boiling water-bath for 45—60 min in order to obtain complete hydrolysis.

In order to obtain emission spectra and quantitative results, the hydrolysates were spotted on Whatman 42 filter paper after dilution with methanol—1 M sodium hydroxide (98 + 2, v/v). Spotting was done in lines 1.5 cm apart; the filter paper was dried under an infrared lamp at 65°C for 5—10 min, allowed to cool to room temperature in a desiccator, attached to clean glass plates with tape, and carefully placed on the stage of the Zeiss scanner. The fluorescence signals were recorded and peak heights measured.

All the results given are based on 5—10 independent samples. The precision of measurements was evaluated by repeated spotting and measurement of the same solution.

Results and discussion

Hydrolysis of compounds I and II with 1 M sodium hydroxide produced yellow solutions. These alkaline solutions did not exhibit fluorescence on excitation at 254 nm or 366 nm, nor did their extracts into various organic solvents fluoresce, even when extraction was done from the neutralized or

acidified hydrolysates. Unexpectedly, when the alkaline solutions were spotted on filter paper and placed under u.v. irradiation, strong bluish-white fluorescence was obtained, and when liquid nitrogen was poured over the spots, a very intense bluish-white fluorescence was followed by a long-lasting greenish phosphorescence. These luminescence phenomena were visible even for nanogram amounts per spot, 1 ng for mebendazole and 5 ng for flubendazole. These observations prompted more detailed investigation on the qualitative and quantitative aspects of the active fluorophors.

The most probable hydrolysis reaction for compounds **I** and **II** is splitting of the carbamate ester group to form an amino group. The resulting compound is very polar and so is likely to be attached strongly to filter paper through hydrogen bonding to the cellulose hydroxyl groups. This semi-rigidity leads to higher fluorescence yields [6]. It was observed that the intense bluish-white fluorescence of the alkaline spot decreased on acidification (1 M HCl), probably because of protonation of the free amino group formed in the hydrolysis.

The methanolic sodium hydroxide solution used for dilution of the hydrolysates provided good spotting properties (low viscosity) and good solvent properties for the fluorophor. Many commercially available solid supports were tested (Schleicher and Schüll No. 604, Schleicher and Schüll No. 589[3], Whatman 1PS, Whatman No. 5 or 42 and Toyo No. 131 filter papers, silica gel 60 t.l.c. plates, silica reversed-phase (RP-18F 254 HPTLC plates, alumina plates and cellulose plates). Whatman 42 filter paper yielded the highest signal-to-background ratio and the most reproducible readings. Preliminary drying of the spotted plates seems to be necessary for obtaining highest fluorescence signals, as the rigidity of the molecules plays an important role in their luminescence. The fluorescence signal increased by about 10% when air-drying was replaced by infrared drying (65°C) for 5—10 min.

Under the above conditions, the reproducibility of the signals was quite good. The peak heights for spots obtained for mebendazole (8 ng/spot) showed a relative standard deviation of 9.5% (n = 19). The fluorescence spectra of the products from both mebendazole and flubendazole (20 μg ml^{-1}) on the filters showed broad emission bands covering 450—500 nm with the maximum at about 460 nm. The calibration graphs for mebendazole and flubendazole were linear from the detection limits of 0.1 and 0.5 μg ml^{-1} up to 10 and 50 μg ml^{-1} in the solution spotted, with correlation coefficients of 0.998 and 0.999, respectively. Table 1 shows the results obtained from the fluorimetric determination of the pharmaceutical preparations.

In contrast to other methods that require preliminary extraction procedures, the proposed method allows direct and rapid estimation of both anthelmintics. No interference was observed from any of the adjuvants in the formulations examined. It is of interest that pure mebendazole in ethanol produced about 1% of the relative fluorescence intensity of the fluorescent derivative resulting from its alkaline hydrolysis. This clearly indicates a possibility of determining the fluorophor if it is present as a decomposition

TABLE 1

Determination of mebendazole and flubendazole in some pharmaceutical preparations by fluorescence scanning on filter paper after alkaline hydrolysis

Compound	Preparation	Average recovery (%)	Standard deviation[a]	Relative standard deviation (%)
Mebendazole	Vermox tablets	99.71	2.34	2.35
	Vermox suspension	100.54	2.32	2.30
Flubendazole	Flumoxal tablets	99.04	2.25	2.27
	Flumoxal suspension	100.56	2.99	2.97

[a] $n \geqslant 6$.

or metabolic product [7]. A full description of the isolation and structure elucidation of the intensely fluorescing mebendazole derivative will be reported in a later paper.

REFERENCES

1 S. Udenfriend, Fluorescence Assay in Biology and Medicine, Vols. I and II, Academic Press, New York, 1962 and 1969.
2 W. Baeyens, Talanta, 24 (1977) 579.
3 W. Baeyens and P. De Moerloose, Anal. Chim. Acta, 110 (1979) 261.
4 J. W. Longworth, R. O. Rahn and R. G. Schulman, J. Chem. Phys., 45 (1966) 2930.
5 F. Abdel Fattah, Doctoral Thesis, State University of Ghent, Ghent, Belgium, 1981.
6 R. T. Parker, R. S. Freedlander and R. B. Dunlap, Anal. Chim. Acta, 120 (1980) 1.
7 K. B. Alton, J. E. Patrick and J. L. McCuire, J. Pharm. Sci., 68 (1979) 880.

Analytica Chimica Acta, 154 (1983) 355—358
Elsevier Science Publishers B.V., Amsterdam — Printed in The Netherlands

Short Communication

POTASSIUM SUPEROXIDE AS A FLUX IN ORE AND ROCK ANALYSIS

ALAN D. WESTLAND and CHIRAN J. KANTIPULY
Department of Chemistry, University of Ottawa, Ottawa, Ontario K1N 9B4 (Canada)

(Received 11th April 1983)

Summary. Potassium superoxide mixed with potassium hydroxide is an effective oxidizing flux for rock and ore samples. Sodium is not added to the sample and potassium may be removed by precipitation with perchloric acid. Traces of cations with various charges, i.e., Ca^{2+}, Eu^{3+}, and Th^{4+}, are not significantly carried down but silver(I) is partially lost to the precipitate.

In a programme of rock analysis for alkaline earth, rare earth, and other elements at sub-mg kg^{-1} levels, it proved necessary to work with large samples and to effect a considerable reduction in the volume of sample solutions in order to achieve the desired concentrations of analyte. This presents no unusual problems when the rock is completely soluble in acids, but if it is necessary to resort to a fusion, the large quantity of added salt introduces the need for additional steps with their attendant uncertainties. If the analyte species are to be separated from the bulk of the salts, there is the problem of ensuring their quantitative behaviour. This generally requires the addition of carriers which is effective when neutron activation is used with radiochemical separations. In the work described here, attempts were made to avoid radiochemical techniques and to remove the bulk of the sample salts that derive from the flux while leaving the trace analytes in solution. While this is normally difficult, if not impossible, in trace analysis, the development of a successful procedure is described below.

Certain rare earth-containing rocks require the use of a strongly alkaline and oxidizing fusion. Sodium peroxide is most commonly recommended as the flux, being particularly effective for the decomposition of ferrosilicon, chromite, iron ores, platiniferous minerals, etc. Occasionally, procedures entailing the use of other peroxides (magnesium peroxide [1] and barium peroxide [2]) have been recommended, but these peroxides do not long survive at elevated temperatures unless they are used in conjunction with alkali.

The separation of sodium salt is not straightforward; it has been shown that in several suggested procedures selectivity was low and applicability was limited to a few particular cases [3–5]. Girardi and Sabbioni [6] succeeded in selectively removing sodium by passing a strongly acidic sample

0003-2670/83/$03.00

solution through a column of hydrated antimony(V) oxide. However, the procedure is not promising for the separation of large quantities of sodium on a repetitive basis because the column cannot be regenerated. It seemed preferable to avoid sodium-containing fluxes altogether.

Potassium superoxide, KO_2, is available commercially and was found to be as effective as sodium peroxide for decomposing various rock samples. It was normally used in admixture with potassium hydroxide, the latter being added in order to reduce the cost of routine analyses. Experiments were conducted to determine the efficiency of separation of the potassium from a selection of analytes at trace levels. The analytes chosen for study were Ag^+, Ca^{2+}, Eu^{3+}, and Th^{4+}.

Experimental

Materials. Carrier-free ^{45}Ca and ^{152}Eu tracers (Amersham Co.) were used; ^{234}Th was isolated from uranyl nitrate by extraction with cupferron [7]. Experiments with milligram quantities of the four analytes were done with aliquots of standard solutions of nitrate or perchlorate salts. The rocks tested were United States Geological Survey No. BCR-1 (a basalt certified for rare earths) and Energy, Mines and Resources, Ottawa, Canadian Certified Reference Materials Project Nos. SY-2 and DL-1a. The former was a lanthanide-containing syenite and the latter was an arkose sandstone certified for uranium and thorium.

Decomposition procedure. The powdered rock or ore is mixed with flux in the ratio of 1 part sample to 3 parts flux by weight. The flux is prepared by grinding a mixture of potassium superoxide (Alpha Ventron) and potassium hydroxide in a 1:3 ratio by weight. The sample/flux mixture is heated to redness in a covered zirconium crucible for 3—5 min. The melt is cooled and dissolved in dilute hydrochloric acid.

A nickel crucible suffered attack as expected but the zirconium crucible showed very little corrosion. The three standard reference materials mentioned above were tested and each was fully decomposed. The relative efficiencies of KO_2—KOH and Na_2O_2 in decomposing silicate materials were not examined. The choice of the KO_2—KOH mixture would be governed by the need to remove the excess of alkali salt from the sample solution; it might also be useful if sodium was to be determined.

Final measurements. A Beckman Model 3133P scintillation counter was used for radiochemical determination of ^{45}Ca and ^{234}Th. Aquasol-2 and Sentiverse were used as cocktails for ^{45}Ca and ^{234}Th, respectively. A γ-ray spectrometer with a NaI(Tl) detector was used to count ^{152}Eu. Thorium was also measured spectrophotometrically with arsenazo-III [8]. Silver was determined turbidimetrically as silver chloride [9].

General procedure for potassium separation. An aliquot that contained between 1 and 10 mg of one of the selected analytes (Ag^+, Ca^{2+}, Eu^{3+}, or Th^{4+}) was added to 3 ml of a solution that contained 225 mg of potassium as nitrate. The solution, contained in a 50-ml beaker, was cooled in ice and

TABLE 1

Percentage of selected cations distributed between potassium perchlorate precipitate and filtrate

Cation	No. of determinations	Amount found (%)	
		Precipitate	Filtrate
Ag^{+}	4	10.9 ± 1.4	89.2 ± 1.4
$^{45}Ca^{2+}$ [a,b]	5	3.6 ± 0.4	96.5 ± 0.7
$^{45}Ca^{2+}$ [b,c]	3	⩽0.8	
$^{152}Eu^{3+}$ [b]	5	⩽0.3	
$^{234}Th^{4+}$ [b]	3	⩽0.3	
Th^{4+} [d]	5		99.9 ± 0.4

[a]Found in first precipitate and filtrate. [b]Radiochemical determination; 2—10 mg of non-radioactive ion was also present in each case. [c]Found after reprecipitation. [d]Determined spectrophotometrically with arsenazo-III.

excess of cold perchloric acid (20%) was added. The precipitate was separated by filtration and washed with more of the acid. Europium-152 in the potassium perchlorate precipitates was determined by counting the solid on a Metricel membrane filter disc at 0.34 MeV. The other ions were determined after dissolution of the precipitates in hot water, as outlined above; these ions were also measured in the filtrates.

Results and discussion

The results are shown in Table 1. In the case of the radioactive ions, experiments similar to those described above were also done with carrier-free tracer quantities. The results of these separations were in general similar to those shown in the table except that the reproducibility was not as good.

With europium and thorium, the separations were efficient and quantitative after a single precipitation. Calcium required a reprecipitation of the potassium perchlorate. Silver caused significant contamination of the precipitate. The behaviour of the four ions follows Goldschmidt's rules which dictate that the contamination of a crystal should be minimal if the radius and/or charge of the foreign ion is dissimilar to that of the ions of the host substance; the crystals of potassium perchlorate are dense and very well formed, which suggests that other ions will also conform to these rules.

The usefulness of KO_2—KOH as a flux was tested by determining thorium in the standard ore DL-1a [8]; the small amount of unprecipitated potassium did not interfere with the determination. In our current work, neutron activation follows the initial sample treatment, and it is essential to achieve quantitative retention of the trace analyte with minimal interference from reagent material; the reagents used here gave acceptably small blank values. Potassium has a lower thermal neutron cross-section than does sodium and the ^{42}K produced by irradiation has a shorter half-life (12.4 h) than ^{24}Na

(15.0 h) and ^{22}Na(2.60 y). The use of the potassium salts is therefore advantageous in various neutron activation methods.

The authors thank the Government of India for a scholarship to C. J. K. Their appreciation is expressed to Professors C. R. Pride of University of Ottawa and D. R. Wiles of Carleton University for making counting facilities available.

REFERENCES

1 W. E. Crutchfield, Ind. Eng. Chem. Anal. Ed., 14 (1942) 57.
2 E. Donath, Dinglers Polytech. J., 263 (1887) 245.
3 M. P. Menon and R. E. Wainerdi, Proc. 1965 Int. Conf. Modern Trends in Activation Analysis, Texas A & M University, TX, U.S.A., 1965, p. 152.
4 W. Bock-Wertmann, Paper SM 91/24, Proc. Int. Conf. Activation Techniques in the Life Sciences, I.A.E.A., Amsterdam, 1967.
5 N. Spronk, Trans. Am. Nucl. Soc., 6 (1963) 398.
6 F. Girardi and E. Sabbioni, J. Radioanal. Chem., 1 (1968) 169.
7 G. A. Cowan, Preparation of Carrier-free ^{234}Th Tracer, in LA-1721, 2nd edn., Los Alamos Scientific Laboratory of Univ. of California, NM, 1954.
8 A. D. Westland and C. J. Kantipuly, Talanta, (1983) in press.
9 E. B. Sandell, Colorimetric Determination of Traces of Metals, 3rd edn., Interscience, New York, 1959.

ANALYTICA CHIMICA ACTA, VOL. 154 (1983)

AUTHOR INDEX

(Continued from inside back cover)

0003-2670/83/$03.00

Printed in The Netherlands

(Continued from outside back cover)

Short Communications

(Continued on page 364)

CONTENTS

(Abstracted, Indexed in: Anal. Abstr.; Biol. Abstr.; Chem. Abstr.; Curr. Contents Phys. Chem. Earth Sci.; Life Sci.; Index Med.; Mass Spectrom. Bull.; Sci. Citation Index; Excerpta Med.)

(Continued on inside back cov